JULY 2021

Ph.D. in Civil Engineering

MUSA EŞİT

REPUBLIC OF TURKEY

GAZİANTEP UNIVERSITY

GRADUATE SCHOOL OF NATURAL & APPLIED SCIENCES

COPULA BASED BIVARIATE DROUGHT FREQUENCY ANALYSIS IN THE CEYHAN BASIN, TURKEY

Ph.D. THESIS

IN

CIVIL ENGINEERING

BY

MUSA EŞİT

JULY 2021

COPULA BASED BIVARIATE DROUGHT FREQUENCY ANALYSIS IN THE CEYHAN BASIN, TURKEY

Ph.D. Thesis

in

Civil Engineering

Gaziantep University

Supervisor

Assoc. Prof. Dr. Mehmet İshak YÜCE

by

Musa EŞİT

July 2021

COPULA BASED BIVARIATE DROUGHT FREQUENCY ANALYSIS IN THE CEYHAN BASIN, TURKEY

Submitted by **Musa EŞİT** in partial fulfillment of the requirements for the degree of Doctor of Philosophy in **Civil Engineering, Gaziantep University** is approved by,

Assoc. Prof. Dr. Mehmet İshak YÜCE
Director of the Graduate School of Natural and Applied Sciences …….....

Prof.Dr. Aytaç GÜVEN
Head of the Department of Civil Engineering …….....

Assoc. Prof. Dr. Mehmet İshak YÜCE
Supervisor, Civil Engineering
Gaziantep University …….....

Graduation Date: 2 August 2021

Examining Committee Members:

Assoc. Prof. Dr. Mehmet İshak YÜCE
Thesis Supervisor, Civil Engineering
Gaziantep University …….....

Prof. Dr. Murat PALA
Civil Engineering
Adıyaman University …….....

Prof. Dr. Mehmet ÜNSAL
Civil Engineering
Kahramanmaraş Sütçü Imam University …….....

Prof. Dr. Mustafa GÜNAL
Civil Engineering
Gaziantep University …….....

Assoc. Prof. Dr. Ali AYTEK
Civil Engineering
Gaziantep Islam Bilim ve Teknoloji Univesity …….....

I hereby declare that all information in this document has been obtained and presented in accordance with academic rules and ethical conduct. I also declare that, as required by these rules and conduct, I have fully cited and referenced all material and results that are not original to this work.

Musa EŞİT

ABSTRACT

COPULA BASED BIVARIATE DROUGHT FREQUENCY ANALYSIS IN THE CEYHAN BASIN, TURKEY

EŞİT, Musa
Ph.D. in Civil Engineering
Supervisor: Assoc. Prof. Dr. Mehmet İshak YÜCE
July 2021
352 pages

Drought is a very costly natural disaster that affects many socio-economic activities from agriculture to public health and threatens the sustainability of environmental systems. In this study, ten notable indices (SPI, SPEI, scPDSI, CZI, MCZI, RAI, RDI**,** DI, PNI and ZI) have been employed to monitor drought events in the Ceyhan Basin, Turkey. The applicability of these indices and their performances corresponding to historical droughts were examined. Secondly, the trends of extreme drought events such as annual maximum drought severity (AMDS) and annual maximum drought duration (AMDD) were investigated. Two extreme events were calculated using the SPI drought index for multiple-time scales (1-, 3-, 6-, 9- and 12-month). Finally, copula functions, which have been used as an effective method in recent years, have been used in the modeling of the joint distribution of drought severity and duration parameters. Different marginal distribution functions were fitted to duration and severity data. The best fit copula is found to construct joint distribution function. After acquiring the best fit copula, the joint and conditional return periods were modeled for each station. Finally, considering drought risk categories (light, moderate, severe and extreme drought), spatial distributions of drought risk return period were constructed.

Keywords: Drought, Climate Change, Drought Indices, Trend, Copula Function, Ceyhan Basin

ÖZET

CEYHAN HAVZASININ KOPULA TEMELLİ İKİ DEĞİŞKENLİ KURAKLIK FREKANS ANALİZİ

EŞİT, Musa
Doktora Tezi, İnşaat Mühendisliği
Danışman: Doç. Dr. Mehmet İshak YÜCE
Temmuz 2021
352 sayfa

Kuraklık, tarımdan halk sağlığına kadar pek çok sosyo-ekonomik faaliyeti etkileyen ve çevresel sistemlerin sürdürülebilirliğini tehdit eden çok maliyetli bir doğal afettir. Bu çalışmada, Ceyhan Havzası'ndaki kuraklık olaylarını izlemek için on önemli kuraklık indisi (SPI, SPEI, scPDSI, CZI, MCZI, RAI, RDI, DI, PNI ve ZI) kullanılmıştır. Bu indislerin uygulanabilirliği ve tarihsel kuraklıklara karşılık gelen performansları incelenmiştir. İkinci olarak, yıllık maksimum kuraklık şiddeti (AMDS) ve yıllık maksimum kuraklık süresi (AMDD) gibi aşırı kuraklık olaylarının trendleri araştırılmıştır. Aşırı kuraklık olayları SPI kuraklık indisi kullanılarak farklı zaman ölçekleri (1-, 3-, 6-, 9- ve 12 ay) için hesaplanmıştır. Son olarak, Kuraklık şiddet ve süre parametrelerinin ortak dağılımının modellemesinde ise, son yıllarda etkili bir metot olarak kullanılan Kopula fonksiyonlarından yararlanılmıştır. Süre ve şiddet verilerine farklı marjinal dağılım fonksiyonları uygulanmıştır. Belirlenen marjinal dağılmalara göre, en uygun kopula fonksiyonları elde edilmiştir. En uygun kopulayı elde ettikten sonra, her istasyon için ortak ve şartlı dönüş süreleri modellenmiştir. Son olarak, kuraklık risk kategorileri (hafif, orta, şiddetli ve aşırı kuraklık) dikkate alınarak kuraklık risk dönüş sürelerinin mekânsal dağılımları oluşturulmuştur.

Anahtar Kelimeler: Kuraklık, İklim Değişikliği, Kuraklık İndisleri, Eğilim, Kopula Fonksiyonu, Ceyhan Havzası

''Dedicated to my family''

ACKNOWLEDGEMENTS

First, I offer my most sincere gratitude to my supervisor Assoc. Prof. Dr. Mehmet İshak Yüce for all his help and guidance in every step of my research. I am very grateful to him for his persistent support, precious advice and productive reviews of my thesis.

I would also like to thank to all those who helped me to reach the successful realization of the thesis, as well as expressing my apology for not mentioning them all by name.

Finally, the greatest thanks to my parents for their endless support and great patience at all times.

TABLE OF CONTENTS

Page

LIST OF TABLES

Page

LIST OF FIGURES

Page

LIST OF SYMBOLS/ABBREVIATIONS

AMDD	Annual Maximum Drought Duration
AMDS	Annual Maximum Drought Severity
IPCC	Intergovernmental Panel on Climate Change
UNEP	United Nations Environment Program
WMO	World Meteorological Organization
UNFCC	United Nations Framework Convention on Climate Change
GCM	Global Circulation Model
MGM	The Turkish General Directorate of Meteorology
SPI	Standard Precipitation Index
SPEI	Standard Precipitation Evaporation Index
scPDSI	Self-Calibrated Palmer Drought Severity Index
CZI	China Z-Index
MCZI	Modified China Z-Index
RAI	Rainfall Anomaly Index
RDI	Reconnaissance Drought Index
DI	Decile Index
PNI	Percent of Normal Index
ZI	Z-score Index
AI	Aridity Index
ET	Evapotranspiration
PET	Potential Evapotranspiration
AET	Actual Evapotranspiration
Di	Water Balance
S	Drought Severity
D	Drought Duration

MK	Mann-Kendall
CMIP5	Coupled Model Intercomparison Project
NCA3	The Third National Climate Assessment
GoF	Goodness of Fit Test
K-S	Kolmogorov-Smirnov
AD	Anderson Darling
AIC	Akaike's Information Criterion
BIC	Bayesian Information Criterion
ML	Maximum likelihood
r	Correlation Coefficient
$\boldsymbol{\tau}$	Kendall Tau
$\boldsymbol{p}$	Spearman Rank Correlation
$\boldsymbol{\psi}$	Digamma Function
Γ	Gamma Function
β	Scale Parameter
$\boldsymbol{\mu}$	Location Parameter
$\boldsymbol{\sigma}$	Standard Deviation
$\boldsymbol{\lambda_u}$	Upper tail dependence
$\boldsymbol{\lambda_L}$	Lower tail dependence
$\boldsymbol{\lambda_u^{CFG}}$	The nonparametric upper tail dependence

CHAPTER ONE

INTRODUCTION

1.1 General

Water is an indispensable resource of life and necessary for the existence of all life. The efficient use and sustainable management of water are critical for humanity. Water scarcity adversely affects all life. Global warming is considered a major reason. Research on climate change clearly reveals that it is taking place all over the world. Millions of years previously, we see that the world climate had a different morphology. Millions of years ago, the average mass of the nuclei in the sun was greater, increasing the pressure and temperature in the outer parts of the sun and causing the nuclear reactions in the sun to generate energy more intensely. If the light of the sun is less than in the early history of the solar system, the world is considered to be cooler since the sun provides the consistency of the temperature on the surface of a planet. If the composition of the atmosphere had not changed, all the waters in the world would freeze (Walker, 1977). The worldwide temperature was only 1-2 degrees Celsius colder than it is now, according to the first pollen records and the first large forest community is seen between the 10200-9400 BC period. In 9400-8300 BC, the average annual temperature was 5 ºC lower than it is currently. While the summer rainfall was relatively moist in Arizona, New Mexico and North America the Colombian plateau had a dry period in 6000- 2000 BC. In tropical Africa pollen records prove that there are several warm and humid environments recorded in the 7500-1500 BC in the center of the South Sahara (Manley, 1953). The historical periods of the world climate are given in Table 1.1.

Table 1.1.1 The historical periods of the World climate (Manley, 1953)

Date (Years)	Region	Climate
9000-6000 B.C.	South Arizona	Warm and drought
7800-6800 B.C.	Europe	Cold and humid, the ice sheets at 6840 left Switzerland.
6800-5600 B.C.	North America and Europe	Mammal animals extinct in cold and drought Arizona.
5600-2500 B.C.	Both two hemisphere	Warm and humid
2500-500 B.C	North Hemisphere	Usually warm and dry
500 B.C-0 A.D	Europe	Cold and humid
330 A.D.	America	Drought in Southeast region
600 A.D	Alaska	Advance of glassier
590-645 A.D.	Near East and England	Severe drought followed by cold winter
673 A.D.	Near East	The Black Sea froze
673-800 A.D.	Mexican	Beginning the humid period
800-801 A.D.	Near East	The Black Sea froze
829 A.D.	Africa	The icing on the Nile
900-1200 A.D.	Iceland	Stagnation in glaciers
1000 A.D.	Africa	The icing on the Nile
1000-1100 A.D.	Utah	snow height 300 m higher than today
1200 A.D.	Alaska	Advance of glassier
1000-1215 A.D.	America	Humidity in West
1220-1290 A.D.	America	Drought in West
1226-1290 A.D.	America	The severe drought in the Southeast region
1300-1330 A.D.	America	Humidity in West
1500-1900 A.D.	Europe	Usually cold and drought
1570-1595 A.D.	America	Between 1573 and 1593 drought in Northwest America
1880-1940 A.D.	Both two hemisphere	11 ºC increase in winter temperatures, 5.2 m drop in ice lakes, falling 40% in arctic ice and 25% in alpine ice

1.2 Drought Definition

Drought is a very costly natural hazard which affects many socio-economic activities from agriculture to public health and threatens the sustainability of environmental systems. Drought, compared to other natural hazards, is a slow onset, creeping and complicated phenomenon (Dubrovsky et al., 2009; Wilhite et al., 2007; WMO, 2006). It is caused by “a period of abnormally dry weather” in consequence of a lack of

precipitation, causing critical moisture deficiency and hydrological imbalances corresponding with water use needs (Mpelasoka et al., 2008). It can occur in any kind of environment (humid, arid and semi-arid) (Wilhite, 2009). The inter-annual uncertainty in precipitation causes drought risk mostly in arid regions because of a higher probability of deficiency or poor distribution of precipitation (Smakhtin and Schipper, 2008). Moreover, this deficiency also influences both groundwater resources and surface water (Hayes et al., 2010), and causes reduced agricultural efficiency (Wang et al., 2019), reduced water quality and supply (Nicolai-Shaw et al., 2017), disturbed wetland habitats and riparian (Mirabbasi et al., 2012; Sheffield et al., 2012), decreased hydro-electric power generation (She and Xia, 2018a), and also diminished opportunities for certain recreational activities (Vicente-Serrano et al., 2012).

According to NOAA (National Center for Environmental Information), drought is a complicated condition that is quite hard to detect, monitor and define. For example, hurricanes, which are another natural hazard, can easily be detected and tracked from its beginning to end. Unlike other natural hazards, drought is identified as an absence of water and is a creeping phenomenon which gradually sneaks up to influence a number of critical industries (NOAA, 2020). Due to difficulty detecting a drought's onset and end, droughts are noted as creeping phenomenon (Tannehill, 1947). According to Tannehill;

> "*We have no good definition of drought. We may say truthfully that we scarcely know a drought when we see one. We welcome the first clear day after a rainy spell. Rainless days continue for a time and we are pleased to have a long spell of such fine weather. It keeps on and we are a little worried. A few days more and we are really in trouble. The first rainless day in a spell of fine weather contributes as much to a drought as the last, but no one knows how serious it will be until the last dry day is gone and the rains have come again . . . we are not sure about it until the crops have withered and died*."

Even though Tannehill's book was released almost seventy years ago, climatologists, scientists, policymakers, and the other major fields concerned with drought are still struggling with identifying the onset of drought and continue to debate. Wilhite and Glantz (1985) examined more than 100 definitions in the literature and many more exist. While studies have been performed to determine an exact definition, a big percentage of definitions may not adequately be accepted by researchers because of

drought characteristics. For instance, drought can be easily misleading when one definition is truly applied from one location to another. Due to affecting climatologic parameters, drought doesn't show some impact. Therefore, drought can occur in both high and low precipitation areas.

Researchers have agreed on just a common definition of drought, e.g. (Beran and Rodier, 1985) noted that "*the chief characteristic of a drought is a decrease of water availability in a particular period over a particular area*". According to (Yevjevich, 1966), a few common acceptance of the unique and objective drought definition has been seen as the primary obstacle in quantifying droughts. The Yevjevich view is accepted as a dominant drought definition. Hence, conflicting drought definitions generally confuse to decide a precise definition by scientists. Some researchers noted that an objective and certain definition of drought can be formed as the basis for more convenient drought administration strategies by individual countries and cities.

Quantifying drought severity is also difficult. Because, it is related to not only the intensity, duration and geographical extent of a specific drought episode but also human activities and the region's water supplies (Wilhite and Glantz, 1985b). Drought events have negative impact on society, environment and economy. For example, although drought can occur in a month, season, or year, its impact on society can continue for several years.

The drought definition may be classified broadly as operational and conceptional (descriptions formulated in common terms).

1.2.1 Operational Definition of Drought

Operational definitions are to quantify the onset, termination, continuations and severity of the drought. These definitions constitute the basis of early warning system estimation. They may be employed to identify drought duration, frequency and severity for a given historical time scale. For example, when focused on agricultural drought, to quantify the soil water depletion, daily rainfall to evapotranspiration (ET) rates which are the most important parameter in climatology, is great of importance and also compare their relationships concerning drought effect on plant behavior (Wilhite, 2000). Considering other parameters including runoff, soil moisture, temperature, etc., may be investigated the drought effect on the meteorological,

hydrological. The probabilities of drought events can be evaluated in terms of these definitions.

1.2.2 Conceptual Definition of Drought

Conceptual definitions are generally dictionary type. They are defined as the boundaries of the terms of drought and they explain extensive descriptions on the drought phenomenon. For example, according to the Random House Dictionary, drought is defined as "an extended period of dry weather, especially one injurious to crops." Another well-known dictionary, American Heritage Dictionary, defines drought as "a long period with no rain, especially during a planting season." Encyclopedia of Climate and Weather describes drought as "an extended period – a season, a year, or several years – of deficient rainfall relative to the statistical multi-year mean for a region." (*Encyclopedia of Climate and Weather*, 2011). These types of definitions cannot be employed to determine the onset, termination or severity of the drought.

1.3 Drought Types

Drought types, considering a disciplinary perspective, are noted in Dracup et al., (1980), where droughts are linked to meteorological, climatological, hydrological, agricultural, atmospheric, water management and socio-economic. In general, due to relating precipitation to meteorological, streamflow to hydrological, soil moisture to agricultural and socio-economic, droughts have been broadly grouped within 4 types of droughts. Figure 1.1 illustrates the relationship between the four types of drought. Drought typically takes three or more months to develop. However, this period may vary particularly based on the initiation of the rainfall deficiency. For example, few can occur during the winter season for a considerable dry period, but if it occurs as predicted more than more, it will affect regions. If the absence of precipitation continues into the growing season, it will lead to a low soil moisture recharge rate in the spring season (Wilhite, 2000).

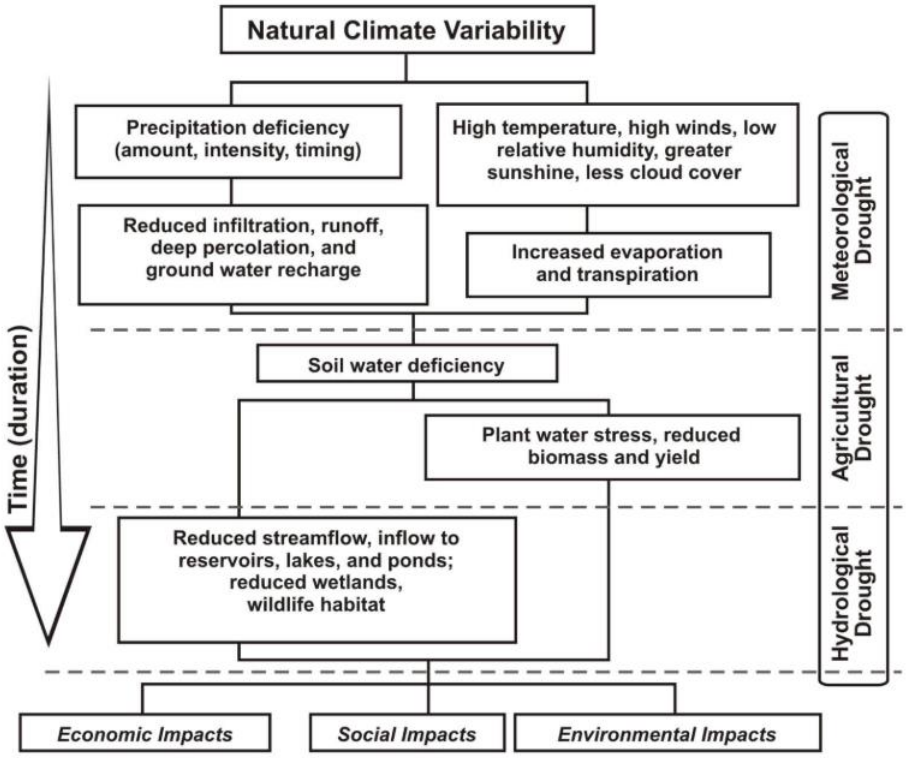

Figure 1.1 The relationship between four types of drought (National Drought Mitigation Centre, 2020)

1.3.1 Meteorological Drought

Meteorological droughts are identified by just considering the degree of dryness and the duration of the dry period. Computation of a dry period is a comparison to some "normal" or "average". (Linsley Jr et al., 1975) reported that it is a "period of more than some particular number of days with precipitation less than some specified small amount." Hence, severity, duration and intensity are great of importance for this drought. Meteorological drought identifications must be taken into consideration as location, region or country because deficiency of precipitation varies from one location to another in term of atmospheric conditions. Some countries have developed specific meteorological drought definitions for application including:

1-) (Britain) "fifteen days, none of which received as much as 0.25 mm" (Great Britain Meteorological Office, 1951)

2-) (United States) "less than 2.5 mm of precipitation in forty-eight hours" (Benton, 1942)

3-) (India) “actual seasonal rainfall is deficient by more than twice the mean deviation” (Ramdas, 1961)

4-) (Bali) “six days without rain” (Chow and 1919-, 1964)

5-) (Libya) “when annual precipitation is less than 180 mm” (Chow and 1919-, 1964)

1.3.2 Hydrological Drought

Hydrological droughts are caused by periods of low rainfall, which have an impact on surface and subsurface hydrology (streamflow, groundwater, lake levels and, reservoir) which differ from meteorological drought (Dracup et al., 1980; Klemes, 1987). Beran and Rodier, (1985) noted that it is associated with low flows and streamflow droughts. Drought is characterized by a lack of water for some reason. For instance, droughts cause low flows to be raised. Low flow analysis is characterized as research aimed at understanding the physical process of lows at a particular point along the stream or river due to the impact of one aspect of drought. When hydrologic droughts are examined with regards to streamflow deficits, their impacts are felt over a season or longer period. According to Linsley Jr et al., (1975), hydrological drought is considered as a “period during which stream flows are inadequate to supply established uses under a given water management system”.

Whipple, (1966) defined drought year, is one in which the total runoff is lower than the long-term average. The severity and frequency of this drought is generally determined at the river watershed scale and low flow frequency has been evaluated for a number of streams. Therefore, if the actual flow is less than a certain threshold for a selected period, the drought can be considered as a hydrologic drought. The influence of hydrological drought in an upstream part of a river may also extend downstream since diminished streamflow may lead to lower groundwater and reservoir levels at downstream parts, while there is no meteorological drought in this part of the watershed. Reductions in groundwater and reservoir levels in downstream parts of the basin can lead to severe impacts on hydroelectric power production, water supplies, recreation, agriculture, transportation and other sectors.

Even though groundwater is a significant source of water, it is discussed rarely in the literature by researchers. Wilhite and Glantz, (1985a) mentioned groundwater levels only once in an overview of drought event definitions as one of the parameters that

must be detected in case of a drought warning. Tate and Gustard (2000) reported in their paper "Drought definition: Hydrological perspective" that just one part is related to groundwater. The impact of drought on the groundwater has occurred in the UK between 1988-1992 (Marsh, 1994). The comprehensive definition related to groundwater is defined by Calow et al (1999): "We use the term 'groundwater drought' to describe a situation where groundwater sources fail as a direct consequence of drought." This description was performed in a project for groundwater drought in Africa that primarily concentrates failure of boreholes and wells. Van Lanen and Peters (2000) expressed a detailed operational description and effects of groundwater droughts after one year. "A groundwater drought occurs if in an aquifer the groundwater heads have fallen below a critical level over a certain period, which results in adverse effects."

1.3.3 Agricultural Drought

Agricultural drought is related to several meteorological drought characteristics due to agricultural influences, including soil water deficits, rainfall deficiencies, differences between potential and actual evapotranspiration (ET) and etc. (Barger and Thom, 1949). Water consumption by a plant is related to its stage of growth, biological characteristics of the specific plant, prevailing weather conditions and the physical and biological features of the soil (Wilhite, 2000). A detailed definition of agricultural drought must consider for crop vulnerability at different stages of the crop cycle. For example, if topsoil moisture is sufficient to meet early development needs, the lack of subsurface moisture in the early stages of growth will have little impact on final crop production. As the weather-sensitive phonological stages indicate differences between crops, the effect of drought is unique on the crop. Maturation periods and planting dates also show a discrepancy between location and crops.

Drought intensity is described by Kulik (1962) as the difference between available water and plant water demand. Kulik suggested that the upper especially 0-2 m of soil is vital to plant growth due to root activities, nutrient supplies and activities of microorganisms that occur in this layer. Hence, a decrease in yield is indicated by the drying of this layer of soil.

1.3.4 Socio-Economic Drought

Socio-economic drought is generally associated with the demand and supply of some economic good or services which incorporate features of meteorological, hydrological and agricultural drought (Kifer and Stewart, 1938). Yevjevich, (1966) reported that space and time processes of demand and supply are the two main processes that must be considered for the definition of drought. Heathcote, (1988) described the agricultural drought is defined as a "water deficit that is harmful to man's agricultural activity. It is caused by a combination of agricultural activities (i.e., demand) and natural events (i.e., supply), resulting in water volumes or quality insufficient for plant and/or animal needs." After the following year, Gibbs et al., (1967) expended this definition as "dependent upon the distribution of plant, animal and human populations, their lifestyle and their use of the land."

Most studies are focused on ecological drought, described as being "dependent upon the distribution of human populations, animal and plant, their lifestyle and their use of the land." (National Drought Mitigation Centre, 2020). Significantly, the view of "ecological drought" includes humans in the equation. Since, in the notion of drought, it is closely associated with various feedbacks between ecosystems and humans.

1.4 Climate Change

1.4.1 The Intergovernmental Panel on Climate Change (IPCC)

The Intergovernmental Panel on Climate Change (IPCC) was established in 1988 by the United Nations Environment Program (UNEP) and the World Meteorological Organization (WMO) to combat climate change. The objectives of the IPCC include researching the scientific aspects of the phenomenon of climate change, identifying possible future risks, adapting to climate change and introducing scientific assessments and reports to address the negative impacts of climate change. The IPCC published its 1st Assessment Report (AR1) in 1990. In 1992, Supplementary Reports was published before the 2nd assessment report. The 2nd Assessment Report (SAR) was published in 1995, and the 3rd Assessment Report (TAR) was published in 2001 and the 4th Assessment Report (AR4) was published in 2007. The 5th Assessment Report-AR5 has added thousands of new scientific works to the findings of climate change. Reports collected under four different headings have been published in 2013 and 2014. The findings of the IPCC, the latest report AR4, have been updated to improve the results in areas where more data and advanced techniques are available, and new

developments are highlighted. In total, 831 scientists from 85 countries took part in three different study groups of the AR5 report. Beginning in April 2016, the 6th Assessment Report-AR6 studies have been started. The group work of AR6 is planned to be completed and published at the end of 2021 and the synthesis report in 2022 (IPCC, 2013, 2007).

Governments approved 1.5ºC Global Warming Special Report prepared by reviewing over 6,000 scientific studies. The IPCC report was prepared by 91 writers and editors from 40 countries on the invitation of the United Nations Framework Convention on Climate Change (UNFCCC) following the adoption of the Paris Agreement in 2015. Panmao Zhai, co-chairman of the IPCC 1st Working Group, said that one of the very clear key messages of this report is that we are already seeing the results of the current global warming of 1 °C as more extreme weather events, rising sea levels and melting of Arctic sea ice and other changes. Jim Skea, co-chairman of the IPCC 3rd Working Group said that keeping global warming at 1.5 °C is possible under the laws of chemistry and physics, but unprecedented changes are needed to achieve this goal. The report, which was announced to the public at a press conference held in Korea's Incheon city on 8 October 2018, is of great importance for limiting global warming to 1.5 ºC, sustainable development and human well-being. The key findings of the Global Warming Special Report of 1.5 ºC are as follows:

- When compared to the pre-industrial period, people caused the earth to warm up by about 1.0 ºC.
- Rising sea levels, extreme weather events, melting Arctic Sea ice, and other impacts are already being felt as a result of the current 1° C global warming.
- If emissions continue to increase in the existing form, global warming will exceed the limit of 1.5ºC sometime between 2030 and 2052.
- Limiting global warming to 1.5ºC means preventing many lasting effects on ecological systems and habitats.
- In order to avoid the limit of 1.5 ºC, global emissions need to be reduced by 45 percent in 2030 compared to 2010, and it needs to be completely reset (net zero) in 2050.
- To be limited to 1.5 °C, fast and comprehensive transformations are needed in agriculture, energy, industry, buildings, transportation and cities (IPCC, 2018).

1.4.2 Effects of Climate Change on the World

The effects of climate change vary regionally. These effects are most commonly seen in Southern Europe, the Mediterranean Basin, the Arctic Region, the Alps, coastal areas, and islands. This change in climate affects many sectors of life as well as the regions. In the agricultural sector, productivity and livestock management are affected, while the fertility of the soil is adversely affected. In forests, due to climate change, decreases in wood species, forest health, and production are observed. In fisheries and water culture, climate change is a stress factor. Also, it is seen that the possible effects of erosion in coastal areas will increase. The energy sector will be directly affected by supply and demand. Production of hydroelectric power plants will decrease by 5% in Northern Europe and 25% in Southern Europe due to the impact of global warming on melting glaciers and precipitation. In addition, increasing temperatures affect human, animal and plant health negatively. As extreme weather events increase, climate-related deaths and diseases will also increase. Climate change reduces the quality and appropriateness of water resources. More than 80% of agricultural land is fed by rain. Food production is also indirectly affected because it depends on the quality of accessible water resources. Aquatic ecosystems, biodiversity and services linked to ecosystems are largely affected by climate change. Swamps, wetlands and deep seas play an important role in ecosystem regulation in terms of carbon content (Tekten, 2016). Figure 1.2 illustrates a schematic framework for anthropogenic drivers, climate change impacts and responses, and their interactions.

The United Nations Educational, Scientific and Cultural Organization and the World Meteorological Organization (UNESCO and WMO) jointly established the IPCC prepared scenarios in 2000 to explore their emissions in the atmospheric environment and published these scenarios under the name of Special Reports on Emission Scenarios-SRES. SRES scenarios have been developed by considering the factors affecting the amount of greenhouse gases and suspensions released to the atmosphere with 4 different scenarios such as A1, A2, B1 and B2. Each scenario is based on the continuous increase of different population, social, economic, technological and environmental developments. SRES projections for the rise of the average surface temperature plot are shown in Figure 1.3.

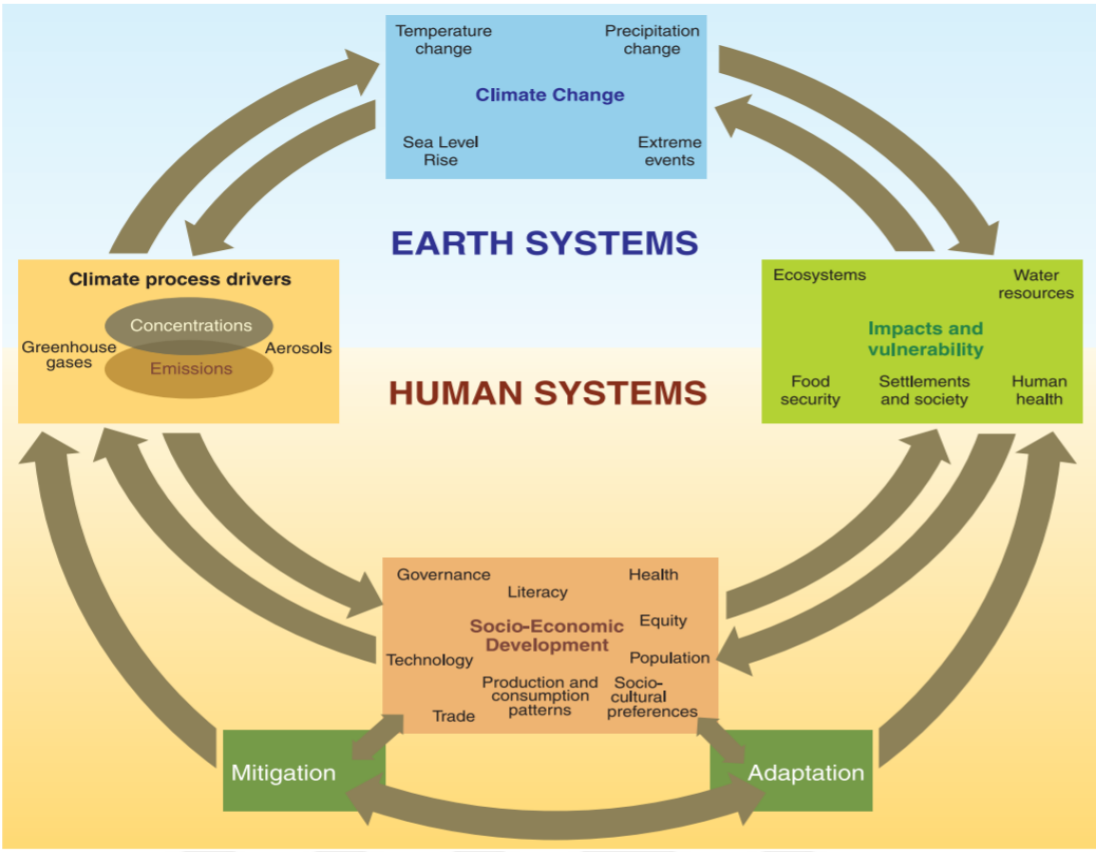

Figure 1.2 A schematic framework standing for anthropogenic drivers, impacts of and answers to climate change, and their joints (IPCC, 2007)

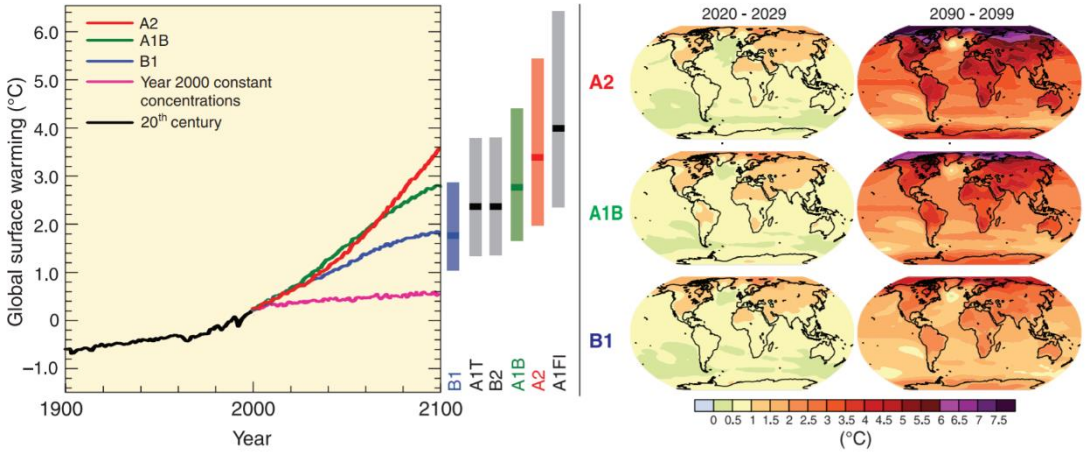

Figure 1.3 Rising global average temperature projections according to different SRES scenarios (IPCC, 2007)

A1 Scenarios: In this scenario adoption, there are few economic differences between regions, but social and cultural development levels are close to each other. This scenario, which represents rapid technological and economic development, is subdivided into three classes. First, A1F1 represents intensive fossil fuel use; secondly,

A1T represents the use of non-fossil source energy resources, and the third A1B represents the balanced use of all energy sources.

B1 Scenarios: This scenario shows similarity when considering the A1 scenarios assumption, but represents a slower increase in the economic, technological field and represents the slowdown after half a century. Besides, it is based on the assumption that the number of substances in the atmosphere will be reduced by accepting more using clean energy resources. In this scenario, where sustainability is important, economic, social and environmental sustainability is important.

B2 scenarios: As a B1 scenario, this scenario is regarded as an essential component of sustainability, acceptance of the rising population is less than A2 scenarios. According to the B1 and A1 scenarios, both greater diversity and rapid technological growth have been accepted. Regional scales are prioritized in this scenario, where social equality and environmental protection are at the forefront (Dabanlı, 2017).
The data used in the digitization of the acceptances of all the types of scenarios described above were included in the scenario by taking them from the centers producing statistical data on a global scale such as the United Nations and the World Bank (Şen et al., 2010).

The greenhouse effect and ozone depletion are the simplest two concepts of climate change. The increase of gases released into the atmosphere and the effect of the sun's rays and ozone depletion cause the earth to become more and more heated. This situation, which appears as global warming, has a wide range of effects on the world climate. Glacial melting increases sea surface temperatures, extraordinary climate events (storm, flood, typhoon, tornado), snow cover, shortening of winter sleep times and sea-level rise can be given as examples of these effects. The only way to prevent this change is to control and limit the emissions of gases that are released by developed countries into the atmosphere (CO_2) and with the derivative greenhouse effect. Together with the developing technologies, the interaction between human and natural environment is continuously increasing in different dimensions. For example, manpower-based systems have now been completely replaced by mechanization in the field of agriculture, and as a result of this mechanization, the emission of carbon and greenhouse gases (CH_4, CO_2, N_2O, HFCs, SF_6 and PFCs) has increased continuously. Increasing numbers of vehicles, building technologies and structural

areas as a whole can be easily seen to have disruptive effects on the natural structure of the climate. The impact of harmful gases, which began to accumulate in the atmosphere, especially after the end of the 19th century, became noticeable in the 1980s and 1990s. As seen in Figure 1.4, global average temperatures tend to increase continuously (Hansen et al., 2010).

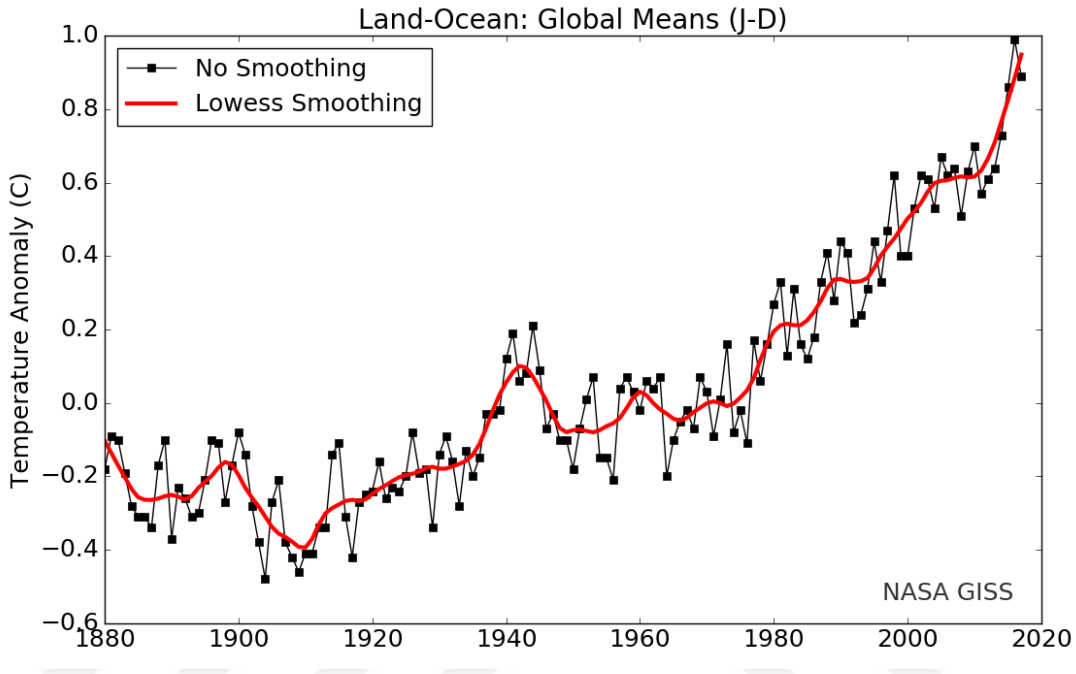

Figure 1.4 Changing global average temperature over years (Hansen et al., 2010)

1.4.3 Effect of Climate Change on Turkey

In Turkey, the adverse effects of climate change have been apparent just like in all countries. Expected impacts due to the geographical conditions are estimated to negatively affect the ecosystem and social life. The most striking example of the expected impacts can be seen in increasing desertification and decreasing water resources. For example, one of the most notable examples of climate change impacts is the decreasing surface areas of the Tuz, Akşehir, and Eber lakes in the Aegean and Central Anatolia regions.

In the fourth evaluation report of the IPCC (IPCC, 2007), according to the outputs of the Global Circulation Model (GCM) conducted for different emission scenarios, there will be significant reductions in precipitation with the rise of temperatures towards the end of the twenty-first century in the Mediterranean Basin, which includes Turkey,

making this region one of the most vulnerable to global climate change. Based on twenty-first-century climate change projections, the Mediterranean region is one of the hot spots in terms of climate change. Simulations with different GCM are largely consistent with each other in the reduction of precipitation across the Mediterranean Basin (Gao et al., 2006). Researchers agreed that almost all models of rainfall on the western coast of Turkey declined in the first half of the 21st century (5-25%) (Hemming et al., 2010). As a result of eighteen GCM for the Middle East Region, the largest decrease in rainfall (over 25%), significantly reduced storm activity over the eastern Mediterranean, will become apparent in southwest Turkey in 2095 (Evans, 2009). A significant decrease in the Euphrates River flows (30-70%) will be seen in the Euphrates Basin as a result of the decrease in precipitation in the late 21st century (Kitoh et al., 2008).

With the help of sensitivity simulations that have examined the effect of the Anatolian peninsula precipitation changes in sea surface water temperature in Turkey (Bozkurt and Sen, 2013). This study revealed that summer and autumn seawater temperatures two times higher than normal increase the precipitation of the Anatolian peninsula (including the welded parts of the Euphrates) in different parts of the region leading to floods. According to a relatively pessimistic scenario based on realized simulation results, at the end of the century, temperatures will rise between 2 °C and 6 °C in Turkey. The highest increase is expected to be in the summer, with only a small increase in the winter. According to this study, the decrease in the snow cover in the Eastern Anatolia Region, which feeds large and significant rivers such as the Euphrates and Tigris, will cause significant seasonal changes in the surface flow. In winter, which is the snow accumulation period, there will be less accumulation and more water will flow. The flow regime in the rivers will change. In the winter months, the flow will rise while falling in the spring months (Bozkurt et al., 2010).

An increase in the need for agricultural irrigation with the increase of drought leads to excessive water withdrawal through uncontrolled underground wells. This situation causes the groundwater level to decrease, thus causing the plant roots to be insufficient to reach the water and eventually to dry. In addition, sea-level changes in coastal water supplies are projected to occur in the sea, and freshwater resources are likely to pose significant problems in the future. Konya plain can be given as the most tangible example. Increasing forest fires is another disaster that can be explained by the increase

in temperatures. Each year, because of fires occurring in the Mediterranean and Aegean regions, hectares of forests are turned to ash. Even though terrorism and other human factors have a significant share in the emergence of fire, wastes such as reflective glass left unconsciously in forest areas can also act as lenses and start the first spark at extreme temperatures. Therefore, the awareness of people and their education in combating climate change are of utmost importance (Dabanlı, 2017).

The Turkish General Directorate of Meteorology (MGM) has developed climate projections with three different global models between the 2016-2099 period to reveal how climate change will affect Turkey in the future. In the study, using the global scale model data sets HadGEM2-ES, MPI-ESM-MR, GFDL-ESM2M, according to the RCP4.5 and RCP8.5 scenarios with a reference period of 1971-2000, 2070, 2071-2099 future periods projection results have been obtained for Turkey. According to the results that obtained from the projections of 3 global models, the average temperature increasing throughout the country for the period 2016-2099 is given as follows:

- According to RCP4.5 scenario, the annual average temperature is expected to increase as 1.5 - 2.6 ° C.
- The average temperature anomaly is foreseen to be between -0.9 and 4.1 ° C in the first half of the century and annual average temperatures increase by an average of 1.4 ° C. In the second half of the century, these values are also predicted an increase between 0.6 and 4.1 ° C and 2.2 ° C, respectively.

RCP4.5 scenarios for annual average temperature between the period of 2016-2099 is shown in Figure 1.5.

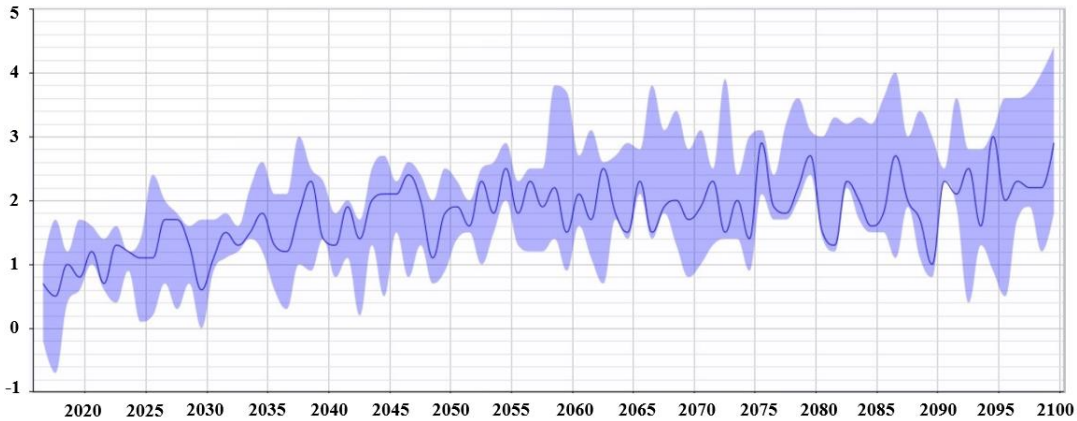

Figure 1.5 According to RCP4.5 scenarios on Turkey for annual average temperature anomaly between the period of 2016-2099

According to RCP8.5 scenarios, Turkey 2016-2099 period (MGM, 2015), the average annual mean temperature is expected to increase between 2.5 and 3.7 ° C. Average temperature anomaly is foreseen to be the range of -0.4 to 3.8 ° C in the first half of the century and annual average temperatures increase by an average of 1.4 ° C. In the second half of the century, these values are also highly expected an increase between 1.6 and 6.6 ° C and 3.8 ° C, respectively (Figure 1.6).

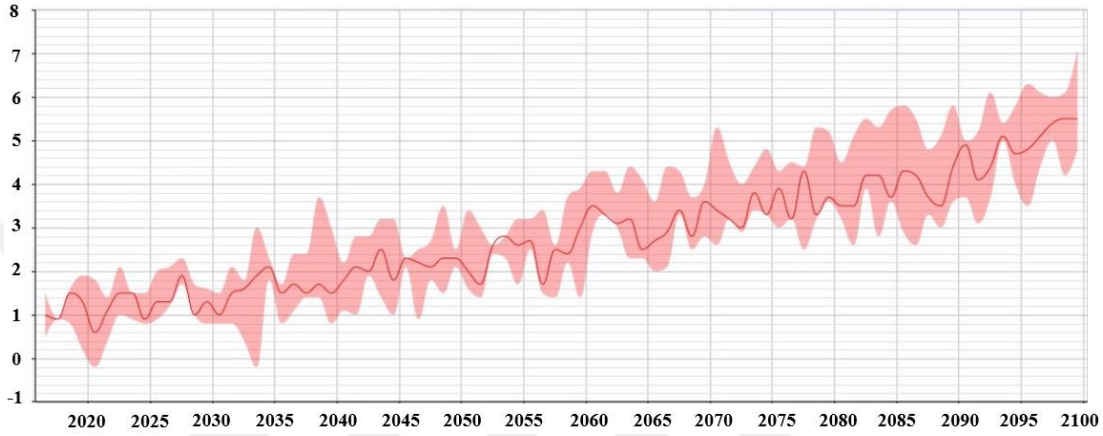

Figure 1.6 According to RCP8.5 scenarios on Turkey for annual average temperature anomaly between the period of 2016-2099

When Annual total precipitation is considered, it is observed that there is not a continuous increase or decrease trend, although a decrease in precipitation is expected in general along with an increase in precipitation irregularities. According to the RCP4.5 scenario, between 2016 and 2099, Turkey's average annual total precipitation anomalies are projected to drop by 3 to 6%. In the first half of the century, the average change in precipitation anomaly is expected to be between 1% and6%, and in the second half of the century, between 5% and 6%. Figure 1.7 indicates the average change in precipitation anomaly between 2016 and 2099.

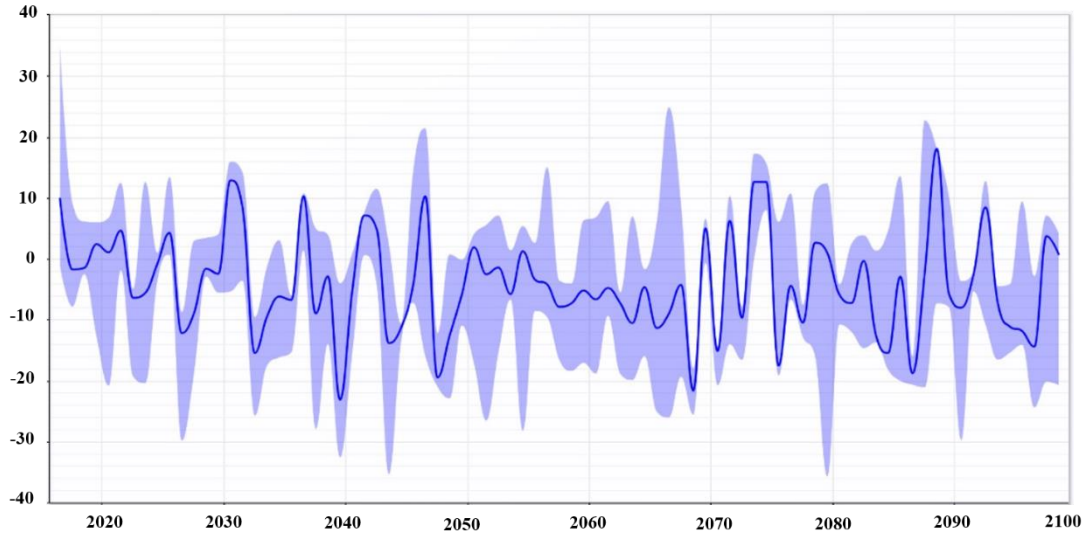

Figure 1.7 According to RCP4.5 scenarios, the average change in precipitation anomaly between 2016-2099 (MGM, 2015)

According to the RCP8.5 scenarios, the average annual total precipitation anomalies of Turkey is estimated to be in the range of -12% to +3% between the years of 2016-2099. In the first half of the century, the average change in precipitation anomaly is expected to be between +5% and -1 %, and between+1 % and -18 % in the second half. Figure 1.8 shows the average change in precipitation anomaly between 2016-2099 (Demircan et al., 2014). Climate projections can be used in future planning, sectoral impact, adaptation and research activities against climate change.

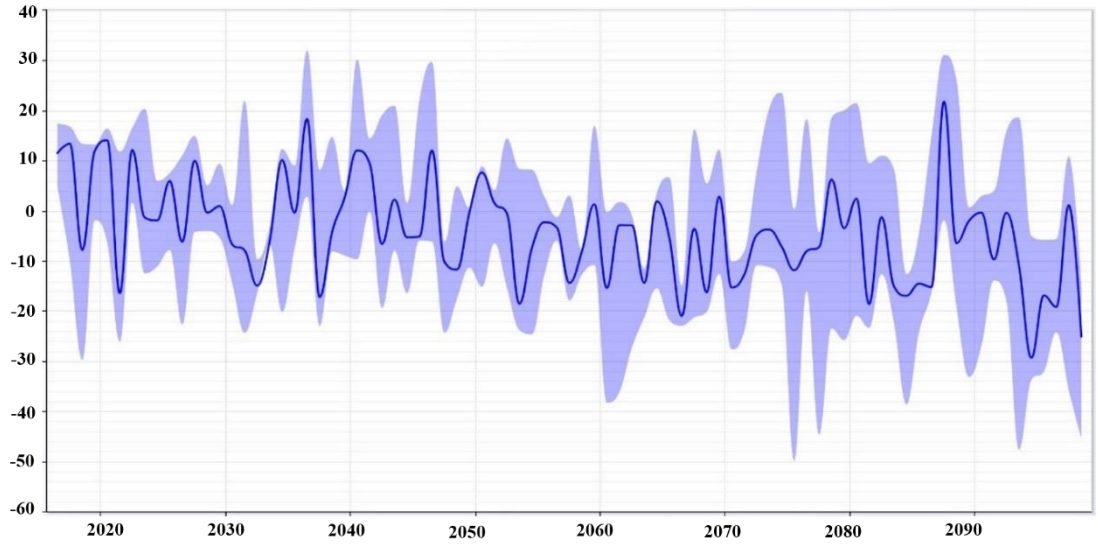

Figure 1.8 According to RCP8.5 scenarios, the average change in precipitation anomaly between 2016-2099 (MGM, 2015)

1.5 Objectives

The main goal of this thesis is to investigate the univariate and bivariate distribution and derive a joint probability distribution of drought in Ceyhan watershed, Turkey. To achieving this purpose, (1) monthly rainfall data from 22 gauging stations located in the Ceyhan watershed are gathered and the Mann-Kendall trend test is employed to determine the homogeneous precipitation basin, (2) the Standard Precipitation Index (SPI) method is used to identify drought variables (severity and duration) and to test their stationary and randomness, Mann-Kendall and Spearman Rho Tests are performed, (3) the best-fit marginal distributions of drought severity and duration are determined respectively, (4) ten types of copulas (i.e., Gumbel copula, Clayton copula, Gaussian copula, Student t copula (t-copula), Frank copula, Joe copula, BB1 copula, BB6 copula, BB7 copula and BB8 copula) are applied to generate two-dimensional joint distributions and (5) consideration with upper and lower tail dependence, the best fit copula for each stationary station, significant probabilistic specifications of droughts are derived.

Chapter one represents the introduction part which defines drought definitions, types and effects of climate change over the World and Turkey. Chapter two is a comprehensive review of literature about trend tests, drought indices and copula theory. Chapter three provides the methodology used. First, any trends and significant tests used in this study are detailed extensively. Second, the most used ten drought

indices are presented. Chapter four represents comprehensive information about the study area and data will be given in detail. The Ceyhan Basin, one of Turkey's most important agricultural basins, has been chosen for both hydro-climatic parameter trend study and drought monitoring. Chapter five; ten drought indices will be discussed in the Ceyhan Basin. These indices include Standard Precipitation Index (SPI), Standard Precipitation Evaporation Index (SPEI), Self-Calibrated Palmer Drought Severity Index (scPDSI), China Z-Index (CZI), modified (CZI), Reconnaissance Drought Index (RDI), Rainfall Anomaly Index (RAI), Decile Index (DI), Percent of Normal Index (PNI) and Z-score Index (ZI), and calculate their performance corresponding with historic drought events. According to statistical test results such as correlation tests including Mann-Kendall, Spearman Rho and Pearson, the most appropriate indices will be investigated. After getting indices, it will be compared in terms of drought categories considering normal, moderate, severity, extreme and wet. Finally, the Ceyhan Basin risk map will be spatially presented. Chapter six; firstly, annual total precipitation will be investigated in terms of statistical tests. Our main concern is to evaluate any changes using the historical data in the Ceyhan Basin. Hence, if the presence of trend is detected, the magnitude of trend, change-point detection will be discussed in detail. Secondly, the trends of extreme drought events such as annual maximum drought severity (AMDS), defined as the largest cumulative severity value for each year, and drought duration (AMDD), are described as the length of maximum drought duration for each year, will be investigated. Chapter seven aims to investigate the distribution of bivariate and derive the joint distribution of the probability of meteorological drought in the Ceyhan Basin, Turkey.

CHAPTER TWO

LITERATURE REVIEW

2.1 Overview

Droughts are a serious threat that impacts human life, health, socioeconomic and ecological systems directly or indirectly at various levels. Long-term drought periods adversely affect including agriculture, forestry, underground, animal husbandry, surface resources, access to adequate and potable water, energy production, especially terrestrial aquatic ecosystems and mountain. Therefore, drought monitoring should be considered following the affected sections considering the use and management of water, absence of precipitation or severity (for example, decrease snowfall, rapid snow melting and increase frequency heavy rains, etc.). Because of the complexity, drought is one of the most dangerous climate threats. Other disasters related to natural hazards such as floods, heat waves and hurricanes are predicted at a certain time. Also, these events are generally documented in the literature.

One of the most important factors that affect drought is changing climate which results in intensity, frequency, duration, spatial extend, climate extreme and timing of weather. Also, climate change has been observed effect on the environment by scientists such as shifting plant and animal ranges, flowering trees sooner and breaking ice on rivers and lakes up earlier. Global temperatures are inevitable that will continue to rise for decades to come. Hence, the importance of drought monitoring with changing parameters related to climate (temperature, precipitation and evapotranspiration) is much considered by the researcher over the world.

In light of the above information, comprehensive trend tests, drought deciles, and copula families are documented. Trend tests aim to identify whether there is any

significant trend in any time series related to climate data such as precipitation, temperature, etc. A suitable drought index for a specific region is important for monitoring and preventing from drought-related disasters. Hence, drought indices are investigated in detail in terms of the skill of their performance. In recent times, copula families have been mostly employed in bivariate drought duration and severity. Copulas are widely used as a method for addressing multivariate hydrological analysis problems. For example, copulas have been employed for flood frequency analysis, rainfall frequency analysis and for predicting groundwater parameters. Therefore, the application of copula-based on drought is presented extensively over the world.

2.2 Trend Tests

Estimation of trends especially in long-term time series of climatological data is of paramount importance. Hydrologic and hydraulic structures have been operated based on the assumptions. If these assumptions aren't well evaluated for reservoirs, dams or designing levees, etc., it is in danger systems and does not serve an appropriate purpose as expected as full efficiency without revision again. Notably, change studies are also crucial because of our need to discover the effect that humans can have on the environment, such as deforestation, urbanization, greenhouse gases, improvements in agricultural practices, etc., which can affect important hydrological cycle perspectives. The main water-related problems have been usually associated with too little water (droughts and low flows) and too much water (floods) (Kundzewicz and Robson, 2000). Detection of trends in observed historical data and their occurrence are great of importance in water resource and management in space and time (Rahmat et al., 2012). Hence, changes in precipitation, temperature, evapotranspiration, flood and especially extreme events have become a very active study area in recent years. Hence, plenty of papers related to changes have been published. A good description of precipitation, temperature trends and variability are necessary for some studies related to climatology, hydrology and agriculture. Long-term trend analysis in precipitation and temperature is especially for the rainfed agricultural place, where both precipitation and temperature may influence irrigation, which is highly crucial (Feng et al., 2016). Trend analysis of hydro-climatologic variables is considered as the central process in investigating the state of the climate location. In addition, a good description of trends in precipitation and temperature is great of importance for better water demand and

supply, water resource management in a watershed, agricultural water use as well as better planning in a basin (Sunday et al., 2014).

For the analyses of hydro-climatologic variability and trends, various parametric (F-test, T-test and linear regression) and non-parametric (Sen's slope estimator, Mann-Kendall, Spearman rho test, Buishand range, Standard homogeneity test (SNHT), Pettitt's test and Bartel's test for randomness, etc.) methods have been studied in the literature. Even though the parametric test is highly powerful, but their performing is limited to normally distributed time series. While most of the climate long-term time series, especially precipitation, temperature and river discharge, don't fit normality requirements, non-parametric methods are usually employed in trend analysis (Burn et al., 2004; Fu et al., 2010; Wang et al., 2012) and also more robust than parametric methods (Sonali and Nagesh Kumar, 2013; Zhang et al., 2006).

The primary driver for probable change is shown as climate change. According to the IPCC report (2012), an increase in heavy rainfall will probably occur in most of the world. Because river flow gives information about the response of some processes including morphologic properties of the basin (elevation, slope), meteorological forcing (precipitation, temperature and evaporation), geologic characteristics (runoff, groundwater) and dams for hydropower production or flood mitigation, it is a crucial part of hydrology (Madsen et al., 2014). Hence, an increase in temperature as well as an increase in precipitation is likely affected on flood frequency. To evaluate these impacts, numerous studies have been presented using projections from climate models. A comprehensive study on trend detection of extreme precipitation and flood have been analysis over Europe by Madsen et al (2014).

According to reviewed studies, all Europe has been shown spatially in Figure 2.1. Turkey has been demonstrated a negative trend considering only both two basins and two stations. However, to make a clear decision about the country, all (26) basin should be considered as well as more than 400 meteorological stations. When focused on Figure 2.1, Turkey doesn't have a highly significant skill about using trend tests (neither positive nor negative) as bordered green color.

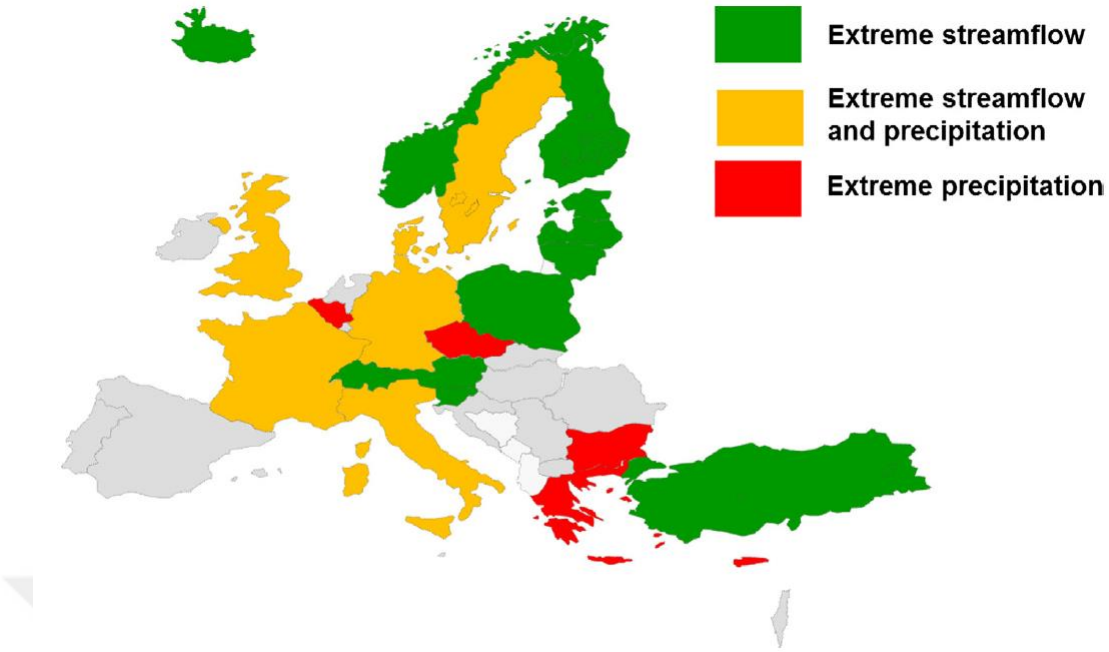

Figure 2.1 Trend analysis with reviewed studies of extreme flow and streamflow (Madsen et al., 2014)

Mahmood et al. (2019) investigated the existence of trend and climate variability from 1951 to 2015 on the Lake Chad Basin, Africa. They concluded that 84% of temperature (α= 0.001) indicates a highly increasing trend and 25-38% precipitation (0.05) shows strong decreasing trends. Surprisingly, some of the regions have shown a decreasing temperature trend at 95% significant level due to protecting natural resources areas. New et al., (2006) analyzed the evidence of daily climatic extremes trends in southern and western Africa. They reported the findings of the analysis of precipitation and daily temperature (minimum and maximum) data from 14 west and south African countries between 1961 and 2000. Results indicate that temperature has statistically significant trends over most of the selected regions and especially the occurrence of extremely cold nights and days has dramatically decreased by -6.0 and -3.7 days/decade, respectively. In addition, the occurrence of extreme hot nights and days considering 95% percentile, over the same period, has significantly increased by 8.6 and 8.2 days/decade, respectively. Several studies have been performed to identify the trend of climate variability over Africa (Fauchereau et al., 2003; Hulme et al., 2001; MAHE et al., 2001; Misra, 2003; Unganai and Mason, 2001), but a few studies have been focused on extreme climate variability due to the lack of available data. Mason et al. (1999) worked on the extreme rainfall at south African station and evaluated that

significantly increase in the intensity of extreme rainfall events for the period of 1931-1960 and 1961-1990 over 70% of the country. Frich et al., (2002) investigated extreme precipitation event in global analysis data from Zambia, Zimbabwe, South Africa and Mozambique. During the second part of the twentieth century, there was an increase in maximum 5-day rainfall.

Due to different climate region and large landmass, spatial and temporal variability precipitation and temperature in China is more complicated. In terms of total precipitation, China had an inconsistent trend. However, there were some significant trends, considering seasonal and regional patterns. For instance, annual total precipitation has significantly increased over western China and the southeastern coast but significantly decreased in northeast China from 1951 through 2000 (Zhai et al., 2005). In the summer season, annual precipitation has no significant trends in West China, While there are highly significant in North China during 1955-2008 (Ye, 2014). Due to the increasing trend after 1990 in China, the temperature has also highly increased (Liu et al., 2004). For instance, the increase rate of temperature in the Altay region is about 0.39 ºC per decade, while the extremely cold days has dramatically decreased by -0.85-day decade^{-1} in the central and eastern Tibetan Plateau (You et al., 2008) and annual mean temperature, during 50 years, has increased by 1.20 ºC in Shanxi province (Li et al., 2011).

Many studies have generally performed on the major watershed in China, such as the Yellow River Basin, Yangtze River Basin, Huai River Basin, Zhujiang River Basin and Haihe River Basin, trend analysis results of precipitation were quite unobvious, while temperature indicated a significantly increasing trend. A significant decrease in precipitation days was evaluated over most of the Yangtze River Basin, whereas rainfall intensity showed a decrease trend during 1960-2005 (Zhang et al., 2014). Precipitation trends showed unobvious trend. For example, the Yellow and Haihe River Basin quantified as drying trend the period of 1959-2008 (B. Wang et al., 2013; W. Wang et al., 2013) and 1959-2008 (Wang et al., 2011), respectively. While the trend of annual maximum precipitation measured as no significant in Huai River Basin during 1960-2011, a decreasing trend was found in the Zhujiang River basin and also detected a longer dry period, compared to the wet period from 1961-2007 (Fischer et al., 2011).

The effect of climate change over China is simulated in the 21st century, using the Abdus Salam International Centre for Theoretical Physics (ICTP) Regional Climate Model version 3 (RegCM3). The distribution of temperature change December-January-February (DJF) and Jun-July-August (JJA) for the middle (2041-2060) and (2081-2100) of the 21st-century modeling in RegCM3. According to the simulation model, significant warming is monitored in both seasonal and periods. The change of precipitation as a percentage, in DJF and JJA the period of the middle of the 21st century and at the end of the century simulated by RegCM3. A general increase is found in DJF in the middle of the century by exceeding 10% over most areas. An increase exceeded 25% is detected in the part of North China, Northwest and Northeast (Gao et al., 2012).

According to the Third National Climate Assessment (NCA3), between 1901 and 2015, annual precipitation changes in the United States have increased about 4%, a bit less than 5% increase during the 1901- 2012 period (Easterling et al., 2017). Seasonally, little change is measured for winter, while more change is detected in the fall season. Regional differences are obvious, because the Great plain, Midwest and Northeast have highly increased changes considering the historical data, whereas, the part of the Southeast and Southwest has slightly decreased. Due to occurring some severe droughts in southwestern and western United States, this slight decrease has been explained across the United States (Barnston and Lyon, 2016). In a seasonal perspective, changes in precipitation are significantly shown differently across the United States. Fall detects most widespread and largest increase 15% in most of the Northern Southeast, Northeast and Great Plains, the smallest increase exhibits 2% over the parts of the Southeast as well as the much of western United States (IPCC, 2013).

The future change projection in seasonal mean precipitation using the CMIP5 (Coupled Model Intercomparison Project) which is a collaborative framework designed to get higher climate change knowledge. The changes are stippled with a highly significant level to be larger than natural variation. In spring and winter, in consequence of climate change, the northern part is projected to be wetter. Because temperature continues to rise, it is going to be too warm to snow in some snow-producing conditions.

According to the Third National Climate Assessment (NCA3), the annual mean temperature in the United States has increased since the beginning of the 20th century. Especially, the temperature raised until approximately 1940, decreased until about 1970, and dramatically accelerated quickly through 2016. The lowest prediction of 0.7 ºC was evaluated by calculating the difference between the average during 1986-2016 and all trend methods were 95% significant level. The highest prediction of 1 ºC was analyzed by fitting linear regression from 1895-2016 (Vose et al., 2017).

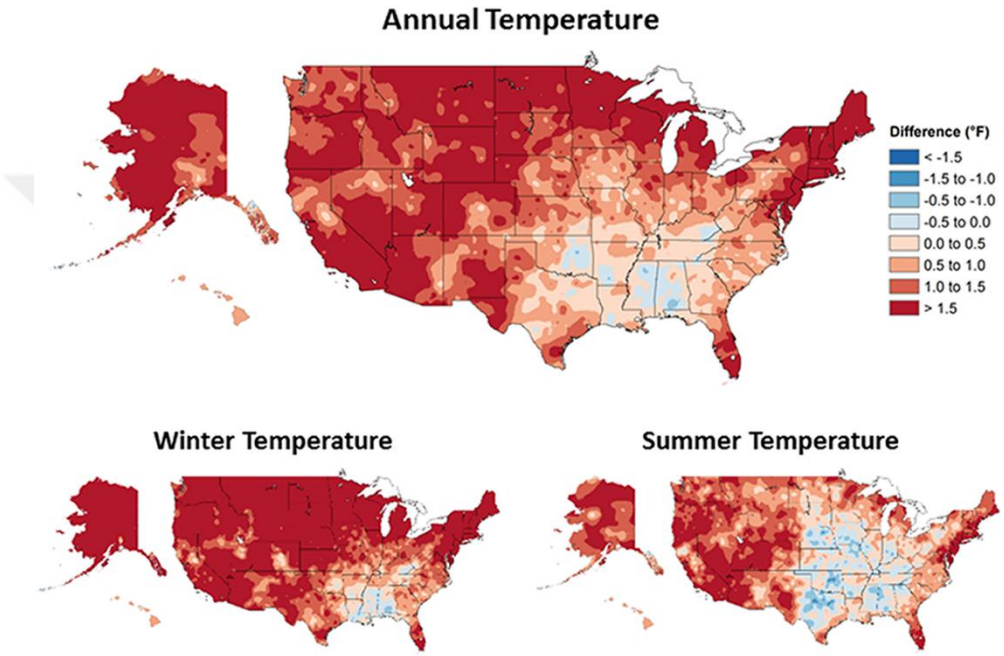

Figure 2.2 Measured changes in annual, winter, and summer temperature (°F) during 1986-2016 over the United States (Vose et al., 2017).

using historical data changes seasonal and annual temperatures from 1986 to 2016. Annual temperature increases at a highly 95% significant level most of the part of the United States. However, a small part of Southern Great Plains and Southeast exhibits cooler. In seasonal view, the greatest warm was evaluated in winter with an increase of 0.8 ºC. In summer, warming is seen lees experiencing especially in the western third of the nation and East Coast, and the cooling is mostly detected in the Great Plains, Midwest and many parts of Southeast (Vose et al., 2017). The future projected using significant trend tests is also demonstrated over the United States in Figure 2.2.

Trend analysis of hydro-climatologic variables is investigated in the state of the various specific climate locations. For example, Azam et al., (2018) have analyzed the

spatial and temporal trend analysis of drought and precipitation in South Korea and used different trend tests such as Mann-Kendall for detecting trends, Theil-Sen's slope estimator with linear regression estimator to exhibit trend magnitude. Trend results have been performed at 55 stations across South Korea during the 1980-2015 periods. According to results, the most substantial precipitation trends were recorded on South Korea's south coast, particularly in late spring, summer, and winter, whereas there was no notable change in annual precipitation. Trend magnitude was significantly decreased from August onward, whereas the increase from January to August. The influence of global warming on the maximum and minimum temperatures of Gombe city in northeastern Nigeria has been shown positively increasing by the Mann-Kendall method (Alhaji et al., 2018). In northern Ethiopia, Asfaw et al. (2018) investigated the precipitation and temperature trend for the Woleka basin. The number of dry years revealed increasing positively, while the mean and minimum temperatures increased with respect to the Mann-Kendall method, no significant trends were observed in maximum temperature values.

Xu et al. (2003) has analyzed monotonic trend and step shifts in precipitation in Japanese and applied both nonparametric Mann-Kendall and Mann-Whitney technologies and parametric t-test. Even though several steps changes taken place in precipitation, there weren't found any significant changes by using historical data. Salehi et al. (2020) has also demonstrated the existence of a trend on a spatial and temporal scale over Iran during 1957-2016. For testing homogeneity, the Standard Normal Homogeneity, the Pettitt-Whitney-Mann and Alexandersson's SNHT, Von Neumann and Buishand's tests were performed and for trend analysis, Sequential Mann-Kendall and classic Mann-Kendall test were used. According to trend test results, homogeneity indicated that most annual and seasonal precipitation were homogeneous and change points were evaluated just at a few stations. Modarres and Sarhadi (2009) have determined trends in maximum and annual 24-hr precipitation considering 145 stations during the 1951-2000 year in Iran and indicated that 50% of stations showed increasing trends in maximum 1-day precipitation, while 67% exhibited decreasing trends in the annual 1-day precipitation. When focused on monthly precipitation and rainy days, Soltani et al. (2012) noted that there was no obvious significant trend in Iran.

When it comes to reviewing literature in Turkey, several studies have been performed on precipitation, temperature, and also extreme variability in Turkey. For example, Keskin et al. (2015) analyzed annual and monthly water level data for Lake Eğirdir in Turkey. Test results revealed that annual water level reduction was determined as approximately 0.026 m by using Mann-Kendall (MK) and Sen's slope (SS) tests. Karabulut et al. (2008) analyzed rainfall and temperature trend in the Samsun region between 1931-2006 timescale that statistically significant trends for temperature data observed the summer season. Partal and Kahya (2006) have determined trends at monthly total and annual mean precipitation data in Turkey using non-parametric tests (Sen's T, Mann-Kendall). For the magnitude of changes, Sen's slope estimator was performed to historical long-term time series. A total of 13 precipitation stations among used 96 meteorological stations, was detected highly statistically significant especially in January, February and September precipitation. A slight decrease in annual mean precipitation was found in southern and most parts of western Turkey, as well as including the coasts of the Black Sea. For temperature variabilities,

Kadioğlu (1997) employed the seasonal Mann-Kendall (S-MK) test to identify temperature trends over Turkey and concluded that there was an increasing trend during the 1939- 1989 period. Türkeş and Erlat (2018) have investigated variability and trends maximum and minimum temperature events of Turkey from 1950 to 2015 and reported that minimum temperature revealed decrease since the mid-1980s, whereas maximum temperature showed an increasing trend starting from the year of 2000. Ay (2020) has analyzed homogeneity and trends in temperature and precipitation time series over the western Black Sea region, Turkey. Monthly total precipitation and mean temperature data were obtained from the province of Zonguldak, Sinop, Kastamonu, Düzce, Bolu, and Bartın of the western Black Sea region in Turkey. For the homogeneity test, the run test was used both variable and for trend analysis, Mann-Kendall, Linear trend and Şen trend test was employed between 1960 and 2017. Results showed that the monthly total precipitation of Düzce and Bolu has homogeneous, while Zonguldak, Sinop and Kastamonu have inhomogeneous. Sinop and Kastamonu revealed highly statistically increasing trends considering the linear trend test, while other regions exhibited no significant trend in both two variables. The monthly mean temperature has no significance for all stations. According to Mann-Kendall trend test results, the existence of trends, both temperature, and precipitation

in all stations, weren't statistically significant. Yavuz and Erdoğan (2012) evaluated the increasing trend in rainfall data, recorded 120 meteorological data over the whole of Turkey especially, in March, April and October from 1975 to 2009.

2.3 Drought Indices

In order to accurately identify and predict drought events such as duration, severity, magnitude, etc., several drought-related indices are offered to date. Palmer drought severity index (PDSI) is the first commonly used index quantified drought impacts under different climate (Palmer, 1965). But, due to some limitations, calibrations and spatial comparability, it is still debated by researchers (Dai, 2013; Mo and Chelliah, 2006; Vicente-Serrano et al., 2009). The standardized precipitation index (SPI), is widely applied under different climate region for describing and comparing drought events (McKee et al., 1993). However, numerous studies have been agreed the rise of global temperature, which causes an increase in water demand because of evapotranspiration (Heim, 2017). Hence, the standardized precipitation evaporation index (SPEI) is developed considering precipitation and potential evapotranspiration (PET) (Vicente-Serrano et al., 2009). The calculation of PET is based on applying the classic Thornthwaite (TH) (Ahmadi and Fooladmand, 2008; Thornthwaite, 1948), which is vulnerable in the arid and semi-arid region (Tabari et al., 2013), and the Penman-Monteith method (PM), that takes more factors leading more reasonable drought trend (Trenberth et al., 2014).

The selection of drought indices is of great importance due to changing climate variability from one region to another. Drought indices are derived for a single region and have the restriction of applying under different climate variability due to understanding the complexity of drought phenomena. Hence, drought indices performance to accurately describe prior drought experiences varies by location. For instance, Several indices applied by national-meteorological organizations are; Modified China-Z index (MCZI) and China-Z index (CZI) by the National Meteorological Center of China (Wu et al., 2001), SPEI and PDSI in the USA (Palmer, 1968), SPI, which gains more popularity in the world and for all kind of climate variability, Decile index (DI) by the National Meteorological Center of Australia (Gibbs et al., 1967), Reconnaissance Drought Index (RDI) in some meteorological organizations of European countries (Tsakiris et al., 2007). Percent of Normal Index

(PNI), Z Index (ZI) and Rainfall Anomaly Index (RAI) are being also used to monitor drought events.

In general, it is critical to develop a good drought index for a specific region in order to monitor and prevent drought-related disasters. Several studies have been performed to detect the most appropriate indexes for many regions and watersheds. Morid et al., (2006) employs seven drought indices including EDI, PDN, SPI, DI, China Z-index, Z-index, and modified CZI for Iran and suggested applying the SPI and EDI for drought monitoring. Okpara and Tarhule (2015) studied on the performance of three indices in the Upper Niger basin, West Africa, and indicated that the SPI is more appropriate than other indices. Vicente-Serrano et al., (2012) analyzed the performance of SPI, SPEI and PDSI at a global scale for 1901-2009 years and recommended that the SPEI has more appropriate in describing drought events.

Barua et al. (2011) calculated five drought indices, namely, PDN, SPI, DI, Aggregated Drought Index (ADI) and Surface Water Supply Index (SWSI) for the Yarra River Basin, Australia. They concluded that ADI performance skill, based on some criteria (transparency, tractability, robustness, sophistication and extendibility), indicates better in monitoring historical drought events. For Iran, Jamshidi et al. (2012) studied the performance of the RDI and SPI meteorological indices to assess drought events. Drought indices for 3- and 6- and 12-month time series were evaluated and then the dry periods for all stations are computed. Resulted showed that the number of extreme drought periods in RDI exhibited much higher than SPI. Hence RDI is more sensitive to capture extreme drought events considering the role of evapotranspiration.

Determining a suitable drought index for a basin or location is important to detect and monitor drought and then estimate correctly future projection. Hence, assessments and comparative drought indices studies have been widely performed for different regions. While SPI is more appropriate for a semi-arid region, its performance skill for the arid region shows inconvenient compared to other indices. For example, Ken River Basin is located in the dry-sub-humid and semi-arid climate region of India. Jain et al., (2015) studied to compare on the performance of six drought indices (SPI, EDI, ZI, CZI, DI and Rainfall Decile based Drought Index (RDDI) based on the occurrence of frequency drought events (severity and duration) at different time scale (1-,3-,6-,9- and 12 month). The study showed that drought indices evaluated for 9-month exhibits highly

correlated to each other. But drought duration calculated using RDDI and RD is inconvenient with other drought indices, Hence, two indices, for Ken River is not appropriate. EDI correlated better performance with other drought indices both the drought duration and severity, especially at 9-month time step. It is discovered to be a more suitable drought indicator for the Ken River Basin in India.

Ntale and Gan (2003) computed the more appropriate drought index among PDSI, SPI and Bhalme-Mooley Index (BMI) over East Africa, where is suited in the dry climate region (Schreck and Semazzi, 2004), considering eight assessment criteria. SPI indicated more performance skills to monitor droughts in East Africa. Because it's applicable and flexibility on different time scales performed relatively consistent power spectra spatially. Correlation between the BMI and PDSI for East Africa is shown in Figure 2.3. According to the figure, while some parts of East Africa (parts of western Kenya and southwestern Tanzania) indicated lower correlation between two indices, higher correlation (greater than 0.8) was found in the eastern parts of Africa.

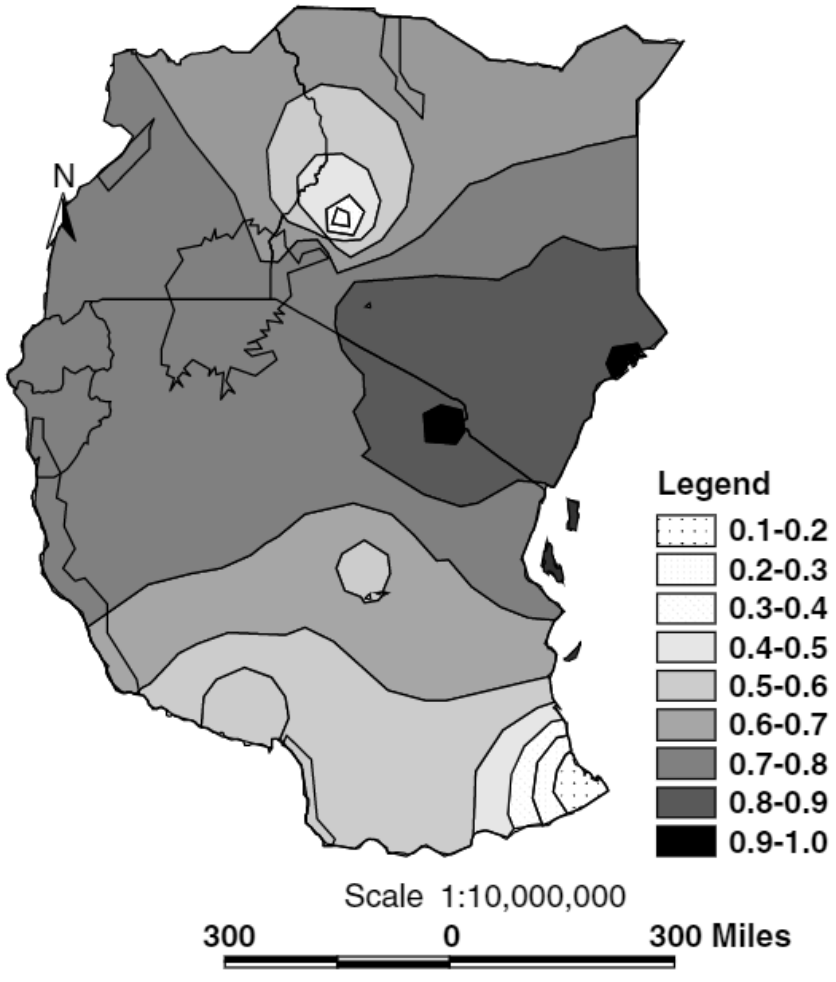

Figure 2.3 The correlation between the BMI and PDSI over East Africa (Ntale and Gan, 2003)

When focused on South Korea, Kwon et al., (2019) analyzed the comparison of two popular drought indices; SPI and Standardized Soil Moisture Index (SSI) to explore both the temporal and spatial characteristics of meteorological and agricultural droughts. Results indicated that SPI is higher frequent droughts and shorter drought duration with comparison to SSI, because of a decrease in the autocorrelation function of the SSI. At a one-month time scale, the high correlation was discovered, and SSI may be more appropriate for detecting drought persistence, while SPI appears to be suitable for defining the onset of drought (Figure 2.3).

Wang et al. (2017) compared to the performance of three drought indices (scPDSI, SPI and SPEI) in the arid region of northwestern China. Three indices were statistically highly correlated with each other, in addition, there wasn't found a statistically significant difference for drought severity during the year of the 1960-2011 period.

The SPI and SPEI correlated well especially, higher correlation were found at 16-36 months. In Greece, Loukas et al., (2003) investigated the use of three indices (RAI, SPI and Z-score) for drought assessment and detecting. Three indices were calculated for historical events of severe wet and dry periods and their advantage and disadvantage was compared for each index for the period 1960-2000. They concluded that all indices had a good agreement and were highly correlated to detect extreme and severe drought severity categories with also comparison to PDSI and Palmer Z-index. They suggested that these indices can be used for operational droughts.

According to Shigang et al. (2011) studies, they evaluated and compared the performance of three drought indices (PDSI, Z-score and Precipitation Anomaly Percentage (PAP) in terms of their credibility. The obtained results, the highest credibility of drought trends was found PAP index followed by PDS and Z-score. Other findings were on realistic that PDSI is more appropriate and Z-score was suitable, applied to one station. Pathak and Dodamani, (2020) assessed several drought indices for various climate locations of Indian River Watershed. Drought indices, namely, Reconnaissance Drought Index (RDI), SPI, and SPEI were employed. A significant increasing trend in temperature and a decreasing trend in precipitation were tested by using Mann-Kendall. SPEI, compared to other indices, showed the highest drought duration and severity. RDI and SPI indicated a good harmony and highly correlated at different time scales, whereas SPEI generally indicated not good agreement with two indices.

A few studies have been performed to detect and monitor various drought indices to any specific basin, location, or whole of Turkey. For example, Danandeh Mehr and Vaheddoost (2020) investigated two indices (SPI and SPEI) across Ankara Province to detect meteorological drought events (trend, drought and severity) at different time scales (3-, 6- and 12 month). They used six stations well disturbed across the Ankara border during observed 46 years of monthly precipitation data. Although two indices indicated five extreme events correctly from 1971 to 2016, temporal disagreement between two indices, especially 6- and 12-month, analyzed. Unlike SPI, SPEI, considering drought events trend, exhibited significantly decreasing.

Another study was applied to Van Lake Basin by Fırat et al. (2018). They evaluated and compared to different drought indices (SPI, PDSI (scPDSI, scPHDI and scWPLM)

and Standard Runoff Index (SRI)) and quantified drought events over the basin. However, the comprehensive studies were performed by Dogan et al., (2012) and computed to detect drought events in semi-arid Konya closed Basin. This study compared DI, PNI, RDDI, SPI, Z-score, CZI and EDI and to select the more appropriate index for Konya Basin, Turkey. EDI was found the best drought with comparison to other drought indices considering at all time scales. CZI and SPI indicated more agreement for capturing droughts for all-time series. They suggested that the application of the EDI index in arid/semi-arid regions could be more preferable and suitable to monitor drought events. Tunalıoğlu and Durdu, (2012) investigated the performance of different well-known indices for identifying future olive crop yield in western Turkey. The crop yield model that employed the best was the scPDSI model in Manisa, Izmir, Aydin and Mugla regions.

2.4 Copulas

Drought characteristics are generally analyzed separately by univariate frequency analysis (Cancelliere and Salas, 2004; Serinaldi et al., 2009). Because of complexity phenomena, using one parameter cannot depict the extensive impact of drought events. Two significant randomly correlated drought characteristics are used generally in literature as severity and duration (Shiau et al., 2012; Shiau and Modarres, 2009). To quantitatively investigate the impact of drought, a convenient method is to employ the stochastic process and the probability theory method (Shiau, 2006; Tosunoglu and Kisi, 2016). However, since drought variables (e.g. severity and duration) are randomly correlated to each other, a substantial correlation between these variables cannot be found in a univariate analysis of drought characteristics. Multivariate analysis characteristic is a better approach for assessing drought characteristics. But, multivariate models are complicated to derive joint distribution functions of drought variables (Mishra and Singh, 2010). For instance, Salas et al. 2005, Kim et al. 2003, Bonaccorso et al. 2003 and Shiau and Shen 2001 have suggested the different theories for identifying the joint distribution of drought variables. However, due to some difficulty mathematical derivations and obtaining their parameters by fitting the observed data, these models are not applicable (Chen et al., 2012).

Bivariate and multivariate distributions using copula functions may overcome the above-stated problems. The copula is an effective method “to assess the dependency and correlation among multiple variables by linking multivariate distribution

depending on their univariate marginal distribution (Sklar, 1959)". In recent years, copulas are widely performed as a method to address multivariate hydrological analysis problems. For example, copulas have been employed for flood frequency analysis (Dong et al., 2019; Durocher et al., 2018; Ismail et al., 2018; Shiau, 2006; Wang, 2016; Zhang and Singh, 2006a), rainfall frequency analysis (Kao and Govindaraju, 2010, 2007; Zhang and Singh, 2006b), drought frequency analysis (Hui-Mean et al., 2019; Kwon and Lall, 2016; Masud et al., 2015; Vazifehkhah et al., 2019; Wang et al., 2019), for predicting groundwater parameters (Bárdossy, 2006) and for estimating streamflow discharge using remote sensing (Chacon-Hurtado et al., 2017). A comprehensive description of theoretical backgrounds for using copulas are demonstrated by Nelsen (2006) and Salvadori et al. (2007).

Shiau et al. (2007) constructed joint probabilities and return period for drought severity and duration using two-dimensional copulas for bivariate drought frequency analysis. Yoo et al. (2016) modeled confidence intervals of bivariate drought frequency curve, after analyzing the model performance of several copula functions. Applying the Copula-GARCH rainfall generation model, 100 realizations of 100-year long monthly precipitation were produced. Ahmadi et al. (2018) applied copula for estimating bivariate frequency analysis of low flow in the Dez River Basin, Iran. Song and Singh (2010a) constructed the joint probability distribution of more than two variables including drought duration, severity and inter-arrival time employing a trivariate Placket copula. In another of their study, they applied various metaelliptical copulas (Gumbel-Hougaard, Clayton, Frank and Ali Mikhail-Haq) to obtain trivariate joint distributions of drought variables (Song and Singh, 2010b).

She and Xia (2018b) evaluated the copula-based drought events determination and risk assessments in Loess Plateau of China, characterized by SPEI during 1950-2014. They concluded that the northwest of LP was much experience large severity and a long duration than the northwest of LP. From the statistical perspective, exponential and Gamma distribution were well fit the drought duration and severity, respectively. The Gumbel copula was more appropriate to construct multivariate distribution function as compared to other copula families as well as considering tail dependence. Drought risk was found to be substantially higher in the northern LP than in other regions, based on the spatial distribution of the joint return period in the various scenarios. Another study-based copula is employed to Yellow River, China by Shiau et al. (2007)

analyzed the hydrological droughts. The observed drought severity indicated highly statistically correlated to the observed drought duration. The marginal distribution of drought characteristics was found bivariate gamma and exponential distribution for severity and duration, respectively. The year of 1919-2002 and 1930-1933 was found as the most severe drought of the Yellow River. When considered China as a whole, it has been suffered many severe droughts affected social life, economy and agriculture. Liu et al. (2016) investigated the meteorological drought return period using copula in China. In this study, SPEI was used to identify drought events (duration, severity and peak) during the year 1961-2013 considering 810 stations. Weibull, Exponential and Pareto were selected to define the marginal distribution of severity, duration and peak, respectively. Gaussian copula and Clayton copula were used to construct the joint distribution of duration-severity-peak and severity-peak, while the Gumbel-Hougaard copula was fitted to construct the multivariate distribution of duration-peak and duration-severity, respectively.

Reddy and Singh (2014) used meta-heuristic methods to estimate copula parameters and methodology was applied to the arid region in Texas, USA. First, SPI was performed to define drought characteristics and copula was applied to quantify multivariate drought risks. Here, to estimate copula parameters accurately, particle swarm and genetic algorithm were used. The result indicated that applying meta-heuristic methods was much better than other methods to estimate copula parameters. Numerous studies related to copula have been investigated including Song and Singh (2010); Kao and Govindaraju (2010), on Korea; Kwak et al. 2014; Kwon et al. 2016; Azam et al. 2018, on India; Ge et al. 2016; Adarsh et al. 2018; Reddy and Ganguli 2012, on Iran; Dodangeh et al. 2017; Amirataee et al. 2018 and Nabaei et al. 2019.

When focused on Turkey Region, a few studies have been performed in the literature. For example, Tosunoglu and Can (2016) was modeled using copula the joint probability distributions of the meteorological drought of Turkey. 173 meteorological stations were used from 1966 to 2006. SPI was applied to detect drought events and to test homogeneity, the principal component analysis was performed. The selection of a more appropriate marginal distribution of drought characteristics was employed in various bivariate distribution functions. Weibull, Gamma and Pareto distributions indicated well fit among marginal distributions. Clayton, Frank, Ali-Mikhail-Haq and Gumbel -Hougaard has conducted the best-fit copula for each region. The other study

over Turkey was assessed by Hesami Afshar et al. (2016) to determine the conditional return period both spatial and temporal scale over Ankara during 1960-2013. They concluded that normal copula showed better than other copulas and found a stronger relationship between drought characteristics. Vazifehkhah et al. (2019) investigated bivariate risk analysis of drought applying the nonparametric multivariate standardized drought index and copula over Konya closed Basin using 10 meteorological stations. First, they determined the best fit marginal distribution for drought event and found as log-logistic (severity) and lognormal (duration), respectively. They modeled bivariate distribution function using four different copula families as well as considering upper tail dependence. Results showed that high risk for the southwestern and southeastern region for the 3-month NMSDI series (Figure 2.4).

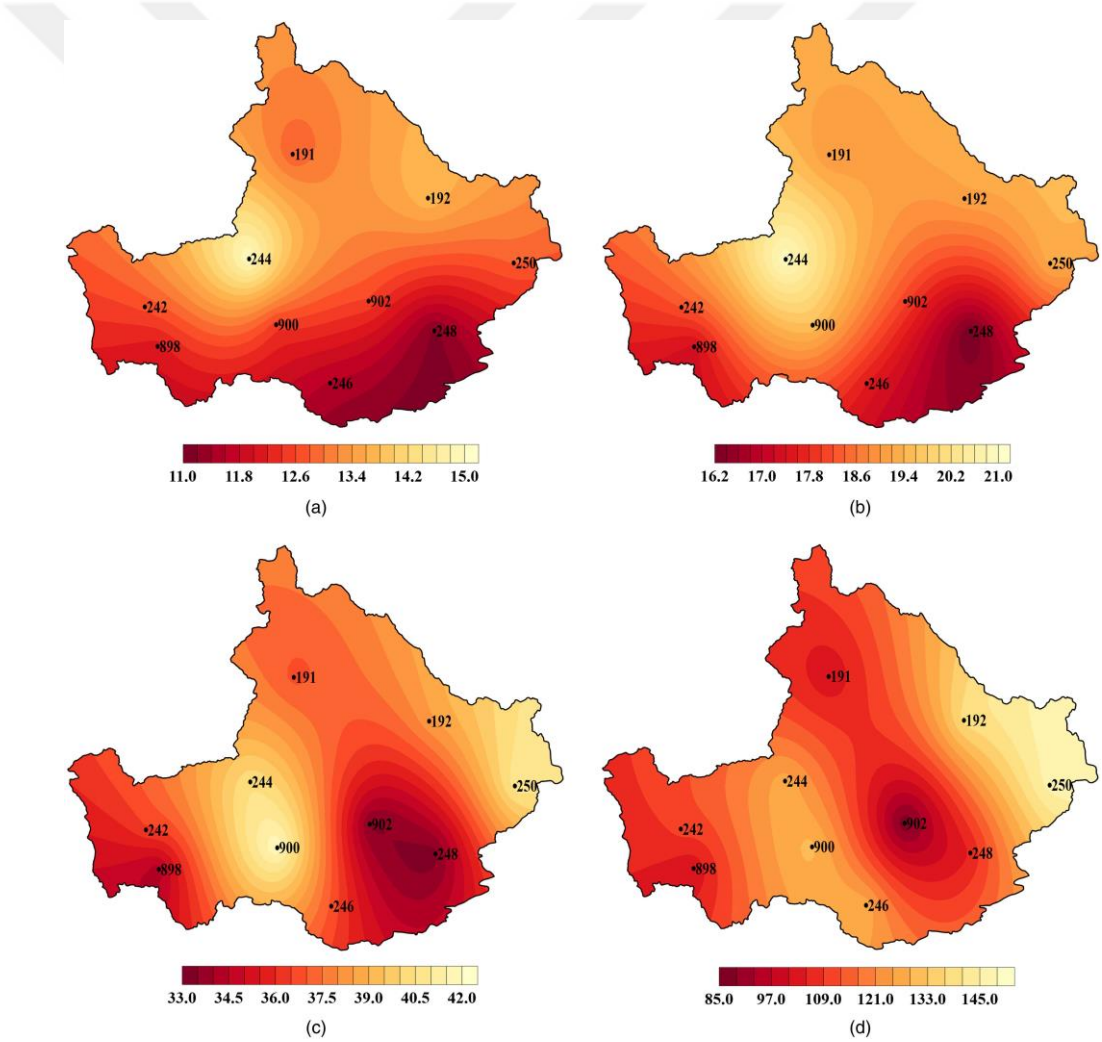

Figure 2.4 The bivariate distribution of Konya closed Basin on 3-month NMSDI, (a-d); (light, moderate, severe and extreme) (Vazifehkhah et al., 2019)

CHAPTER THREE

METHODOLOGY

3.1 Overview

Climate change is inevitable on a wide perspective, according to observations. The melting of land and sea glaciers, as well as rising sea levels, are all regarded primary markers of climate change (about 17 cm). These values are expected to rise in the coming century, according to forecasts. In addition, the majority of these projections agree that precipitation will be a significant decrease in the Mediterranean Basin. According to the outcomes of the Global Circulation Model (GCM), which simulated in the fourth assessment report of the Intergovernmental Panel on Climate Change (IPCC, 2007) for different emission scenarios, significant decreases will occur in the Mediterranean Basin where Turkey is located. With the rise of temperatures towards the end of the twenty-first century, it is stated that this region will be one of the most vulnerable regions against global climate change. Giorgi, (2006) also defines the Mediterranean region as one of the hot spots in terms of climate change based on the twenty-first-century climate change projections. The simulations performed with different GCMs largely match each other concerning rainfall reduction across the Mediterranean Basin. Some research suggests that the orbits followed by the North Atlantic storms eastward will shift northward with the strengthening of the sub-tropic high-pressure system in the Mediterranean region. This change will naturally increase precipitation in upper latitudes while decreasing the precipitation in the Mediterranean Basin.

In recent years, hydro-meteorological disasters occurred with increasing severity, frequency, and duration in different regions. Today, human effects such as industrialization, distorted construction, and the destruction of nature increase the effects of such disasters or allow new ones to occur. In other words, while the

number of occurrences of geological or geophysical disasters did not change significantly, the number of meteorological, hydrological and climatic disasters has increased significantly due to global climate change. Because of climate change, the number of large-scale natural disasters, called "catastrophic", with hydro-meteorological character has been reported to increase continuously and significantly since 1980 (Kadıoğlu, 2012). One of these disasters is drought, a gradual and insidious phenomenon. Assessment of drought with observed historical data analyses future projections and simulation by using developed models, which provide critical information about water use, water resource management, hydraulic structure, social economy, and so on.

In this chapter, some trends that were presented include homogeneity, the magnitude of trends, change point detection, and some specific statistical methods in order to evaluate hydro-climate parameters considering observed historical data (precipitation and temperature) and also extreme events. Determining trends in hydrologic, especially -precipitation, temperature, water level, and other climate variability related to time series, has been an active issue among climatologists, atmospheric researchers, etc., for more than two decades now. The trend detection concept has been considered even greater attention due to the increase in comprehensive studies in the field of climate change.

Second part; numerous drought indices have been developed in recent years. Hence, the well-known drought indices are defined. While some drought indices are used as only precipitation parameters, other indices are performed via various parameters (soil moisture, temperature, evapotranspiration, etc.) as an input. The effective use of drought indices based on different variability such as topographic, aridity classification, precipitation irregularity; differ from one region to another. Hence, every country has developed a more appropriate drought index according to their respective regions.

Finally, to identify the drought return period, both the joint and conditional copula functions are performed. Instead of the use of univariate frequency analysis, multivariate analysis exhibits more accurate to monitor drought. Hence, the copula is a useful tool to assess the dependency and correlation among multiple variables by linking multivariate distribution depending on their univariate marginal distribution.

3.2 Correlation Analysis

It is a statistical approach for determining if two numerical measurements have a linear relationship. In addition to showing the direction and power of this relationship. The p-value must be less than 0.05 in order to interpret a correlation coefficient. There is an inverse relationship between the two variables, that is, "one variable increases while the other decreases," If the correlation coefficient is negative. "one variable increases while the other increases," If the correlation coefficient is positive. The values of these correlation coefficients intervals are -1 and +1 values (Yüce et al., 2018).

The correlation coefficient's interpretation (r);

If r <0.2, there is “no correlation”,

0.2-0.4, “weak correlation”,

0.4-0.6, “moderate correlation”,

0.6-0.8, “high correlation” and

0.8>, “very high correlation”.

Correlation analysis is widely applied to almost every field of hydrology such as rainfall-runoff relations, river flow-sediment discharge, soil moisture-evapotranspiration or temperature- precipitation and so on. It provides great information to solve problems related to hydrology by using appropriate correlation methods. It also allows the creation of mathematical models for a specific phenomenon. For example, Yuce et al., (2015) modeled a relationship between river discharge-hydraulic geometry parameters (width, depth and velocity) using linear regression analysis. Other similar studies have also been performed by sediment discharge- river flow discharge over Ceyhan Basin (Yüce et al., 2018) and related studies can be found in the literature (Lawrence, 2007; Yuce et al., 2019; Yuce and Muratoglu, 20112).

In this study, Kendal rank correlation, Spearman Rho, Pearson correlation, and linear regression analysis were conducted. The Pearson correlation coefficient is often preferred when the data has a normal distribution. Alternatively, the Spearman rank correlation coefficient is usually preferred, if the data is not normally distributed.

3.2.1 Kendall's tau rank correlation

Kendall's tau rank correlation coefficient, which is a non-parametric hypothesis test, is evaluated from a sample of N data pairs (X, Y). Kendall's tau is mathematically expressed as flowed:

$$\tau = \frac{Nc-Nd}{(\frac{1}{2})N(N-1)} \tag{3.1}$$

where n is the sample size, Nc and Nd are the number of concordant and discordant pairs, respectively. The main advantage of Kendall's tau correlation is that the probability distribution has much better statistical properties when compared to other correlation tests (Yüce et al., 2018).

3.2.2 Spearman's Rank Correlation

Spearman's rank correlation coefficient, or Spearman's ρ, is a non-parametric measure of rank correlation firstly introduced by (Spearman, 1961). It is statistically employed to utilize the dependence between the rankings of two variables. Spearman's rho (ρ) coefficient does not make any assumptions about the distribution of multiplicities for the two variables. It evaluates how well the links between two variables are with any monotonic relationships. The following formula is shown to evaluate the Spearman's rank correlation ((Spearman, 1961).

$$p = \frac{6\sum d_i^2}{n(n^2-1)} \tag{3.2}$$

where n is the number of observations, p is the Spearman rank correlation and d_i represents the difference between the ranks of corresponding variables (Zar, 2005).

3.2.3 Pearson r Correlation

The Pearson correlation coefficient, which is the widely employed and the best tool among correlation tests, evaluates how well variables are related. Unlike monotonic relationships, it calculates the linear relationships between data due to the method of covariance. It provides information about the direction of the association, as well as the magnitude of the correlation, or the relation (Benesty et al., 2009). Pearson r correlation formula is given as;

$$r = \frac{n(\sum xy)-(\sum x)(\sum y)}{\sqrt{[n\sum x^2-(\sum x)^2]\,[n\sum y^2-(\sum y)^2]}} \tag{3.3}$$

3.2.4 Linear Regression

Linear regression analysis is based on the variable (s) that can be detected more easily or earlier than the desired variable and to create a model that predicts the desired variable. In general, linear regression models are statistically performed to estimate the relationship between two variables. Simple linear regression is a statistical method showing the relationship between 2 quantitative data. The 1st variable estimator shown on the X-axis is an independent variable. The second variable shown on the Y-axis, which is the dependent variable, is the predicted output (Seber and Lee, 2012). In the presence of multiple independent variables, multiple regressions can be performed. Simple and multiple linear regression equations are expressed as;

$$y = b_0 + b_1 * x \tag{3.4}$$

$$y = b_0 + b_1 * x + \cdots b_n * x_n \tag{3.5}$$

The value shown as "b_0" in the formula is the point where the line intersects the y-axis (y-intercept, y-intersection), which is a constant measure of the error in the analytical method. On the other hand, the value shown as "b_n" is the regression coefficient (slope) of the proportional error in the analytical method.

3.3 Trend Analysis

Trend analysis, especially short and long-term time series of hydro meteorological data, plays an important role to predict future projections. Hence, hydrological structure, atmospheric research, water management, and proper use of water are based on some crucial assumptions. Numerous tests have been developed by researchers to detect and monitor hydrologic parameters considering historical data and simulated pseudo-observation by various models for the last decades. In this study, Wallis-Moore and Wald-Wolfowitz tests are employed for the homogeneity test. The presence of the trend is determined by Mann-Kendall (MK) and Spearman's Rho (SR) tests. Trend's slope is investigated by utilizing Regression and Sen's slope methods. The starting point of the trend is determined by using Buishand Range Test, the Standard Normal Homogeneity Test and the Pettitt Test.

3.3.1 Homogeneity Test

3.3.1.1 Wallis-Moore and Wald-Wolfowitz

Wallis and Moore phase-frequency test, proposed by Wallis and Moore, (1941), is determined to detect deviation as a series for randomness (such as time series) in the sequence of values $X_1, X_2, \ldots, X_n$. This test is based on sign differences (whether – or +) $X_1 - X_0, X_2 - X_1, \ldots, X_n - X_{n-1}$. The first and last phases named sequence of signs are not accounted for. H (the number of phases) is identified. If $n \geq 10$ and continuity correction is applied, a fairly good test may be based on the hypothesis that H is normally disturbed. When $n \geq 25$, the correction is not used (Wallis and Moore, 1941). The z test statistic formula is calculated as:

$$E[H] = \frac{1}{3}(2n - 7) \tag{3.6}$$

$$var[H] = \frac{1}{90}(16n - 29) \tag{3.7}$$

$$z = (H - E[H])/\sqrt{(\frac{1}{90}(16n - 29))} \tag{3.8}$$

The Wald-Wolfowitz test, also known as the Runs test, assesses data randomness and investigates whether one observation effects the next. Time series data is cut from a certain level (this level can be taken as mean, median or mode) to determine if each value in the series is below or above this level. The number of passes from one data to the other above or below a certain level is called the run number. The run number is small if it is under or over long periods. Such series may not have homogeneity (Wald and Wolfowitz, 1943). The result of the test is z, the number of data N, the number of run r, the number of values under the medium level Na, and finally the number of values over the medium level Nu;

$$E[r] = \frac{2Na*Nu}{(Na+Nu)} + 1 \tag{3.9}$$

$$V[r] = \frac{2Na*Nu(2Na*Nu-N)}{(N-1)N^2} \tag{3.10}$$

$$z = \frac{r-1-E[r]}{\sqrt{V[r]}} \tag{3.11}$$

3.3.2 Trend Detection

3.3.2.1 Mann-Kendall Test

The MK test is a non-parametric test to determine the trend in the hydrometeorological variable in a time series and is based on ranks (Helsel and Hirsch, 2002; Kendall, 1975; Mann, 1945). It is the most preferred statistical method for the time series since it is not fitted to any distribution. The application of MK test statistic Z is expressed by the following formula as;

$$S = \sum_{k=1}^{n-1} \sum_{j=k+1}^{n} sgn(x_j - x_k) \tag{3.12}$$

where n is the number of the data, x_j and x_k are the data point in years j and k (j>k) and t_i is the length of the tied rank group.

$$sgn(x_j - x_k) = \begin{cases} 1 & (x_j - x_k) \rangle 0 \\ 0 & (x_j - x_k) = 0 \\ -1 & (x_j - x_k) \langle 0 \end{cases} \tag{3.13}$$

$$Var(S) = \frac{n(n-1)(2n+5) - \sum_i^r t_i(t_i-1)(2t_i+5)}{18} \tag{3.14}$$

$$Z = \begin{cases} \frac{S-1}{\sqrt{Var(S)}} & S > 0 \\ 0 & S = 0 \\ \frac{S+1}{\sqrt{Var(S)}} & S < 0 \end{cases} \tag{3.15}$$

While a negative number denotes a downward trend, a positive Z number denotes an upward trend. Critical test statistical values for different significance levels are 1.645, 1.97 and 2.57 at 90%, 95% and 99% probability levels, respectively (Yu et al., 1993).

3.3.2.2 Spearman's Rho Trend Test

SR test is generally employed as nonparametric method to investigate the presence of trends (Lehmann and D'Abrera, 1975; Sneyers, 1990). Its statistic r_s and z (standardized test statistic) are computed as:

$$r_s = 1 - \frac{[6 \sum_{i=1}^{n} (Rx_i - i)^2)]}{n(n^2-1)} \tag{3.16}$$

$$z = r_s \sqrt{\frac{n-2}{1-{r_s}^2}} \tag{3.17}$$

R_{xi} (rank statistic) is obtained by sorting the data, where n is the length of the time series. Negative z values show decreasing trends while positive z values show increasing trends. At the 10% significance level, for z >±1.645, the null hypothesis of no trend is rejected.

3.3.3 Trend Slope

3.3.3.1 Sen's Slope Estimator

The SS test proposed by Sen, (1968) is a non-parametric test calculating the slope of the trend in a data set. It is used for equiponderant time series. For each data point, the slope difference is calculated per changing time. The slope of the trend can be estimated by the median of all slopes between data pairs in the same season (Helsel and Hirsch, 2002). All slope pairs are ranked from smallest to largest and if the calculated number of slopes (n) is odd, the median slope gives the slope S. If n is even, then the two median slopes are averaged. Where Q is the data, n is the length of the data and T is the time. The slope of n pair of data is predicted by Sen's estimator;

$$S = \frac{Q_2 - Q_1}{T_2 - T_1} \tag{3.18}$$

$$S = \begin{cases} S_{\frac{n+1}{2}} & n = even \\ S_{\frac{n}{2}} & n = odd \end{cases} \tag{3.19}$$

3.3.3.2 Linear Regression Method

Regression analysis is a statistical method used to predict the relationships between one dependent variable and one or more independent variables. Regression analysis forms the basis of complex estimation methods. It is used to assess the strength of the relationship between variables and to model the relationship between them. The dependent variable is usually represented by Y and the explanatory variables X (Gocic and Trajkovic, 2013). Linear regression formula is given as:

$$Y = a + bX \tag{3.20}$$

where a is the intercept, b is the slope of the line. A positive b value shows that increasing, whereas a negative value shows decreasing trend.

3.3.4 Tests for Change-Point Detection

With respect to the significance of climatic variability in terms of water availability, increasing irrigation demands, like crop yields and other habitats, are important to identify and evaluate the trends in the annual and monthly seasonal historical data series. Break point capture is substantial to evaluate the period in which an important change occurs in a time series. In this study, Buishand's Range Test (BRT), the Standard Normal Homogeneity Test (SNHT) and Pettitt's Test are performed to detect change point in a time series.

3.3.4.1 Standard Normal Homogeneity Test (SNHT)

SNHT was proposed by Alexandersson, (1986). Test statistic (T_k) is performed to compare the average of the first n year with the average of the last (n-k) year with n data points (Jaiswal et al., 2015; Vezzoli et al., 2012). The T_k equation is written as below;

$$T_k = kZ_1^2 + (n-k)Z_2^2 \tag{3.21}$$

Z_1 and Z_2 can be calculated as follows;

$$Z_1 = \frac{1}{k}\sum_{i=1}^{k}\frac{(X_i-\overline{X})}{\sigma X} \tag{3.22}$$

$$Z_2 = \frac{1}{n-k}\sum_{i=k+1}^{k}\frac{(X_i-\overline{X})}{\sigma X} \tag{3.23}$$

Here, $\overline{X}$and σX are mean and standard deviation, respectively. The year in which T_k reaches the maximum value is considered as the point of change. For SNHT, significant critical values are given in Table 3.1.

3.3.4.2 Buishand's Range Test (BRT)

The adjusted partial sum (S_k) is computed as:

$$S_k = \sum_{i=1}^{k}(X_i - \overline{X}) \tag{3.24}$$

When the series is homogeneous, the value of S_k fluctuates around zero. This test captures data showing sensitivity to break in the middle of distorting the homogeneity of the data. If there is a change in K year, it reaches the maximum or minimum value

around the year k = K (Buishand, 1982). Significant change can be computed by evaluating rescales adjusted by range R using the following formula;

$$R = \frac{Max(S_k) - Min(S_k)}{\bar{X}} \tag{3.25}$$

3.3.4.3 Pettitt's Test

This test is a non-parametric method proposed by Pettitt, (1979) to determine shift detection in a series. It is widely performed to calculate the occurrence of unexpected change in climatological records (Smadi and Zghoul, 2006; Sneyers, 1990). The null hypothesis indicates that the series has an independent and random distribution, while the alternative hypothesis indicates a sudden change. U_k test statistic is expressed as;

$$U_k = 2\sum_{i=1}^{k} r_i - k(n+1) \qquad \text{k=1,…n} \tag{3.26}$$

U_k test results are shown graphically. In the case of a break-in k=K year, the test statistic is at maximum or minimum values. Significant critical values are given in Table 3.1.

$$K = max|U_k| \tag{3.27}$$

Table 3.1 Critical values for different change point detection tests statistics

Number of Observation	Buishand Range Test			Pettitt Test		SNHT Test		
n	1%	5%	10%	1%	5%	1%	5%	10%
20	1.6	1.43	1.1	71	57	9.56	6.95	6.07
30	1.7	1.5	1.12	133	107	10.45	7.65	6.6
40	1.74	1.53	1.13	208	167	11.01	8.1	6.92
50	1.78	1.55	1.14	293	235	11.38	8.45	7.15
70	1.81	1.59	1.17	488	393	11.89	8.8	7.47
100	1.86	1.62	1.22	841	677	12.32	9.15	7.77

3.4 Drought Indices

3.4.1 Standard Precipitation Index (SPI)

SPI introduced by McKee et al., (1993), was carried out for identifying drought events (Fig. 3.1). The primary benefit of using SPI is that it has statistical consistency and it also enables us to define both long-term and short-term drought effects at various time scales of rainfall anomalies. In statistics, the SPI value is equivalent to the Z-score. However, due to precipitation observations with a time scale of 12 month or less, the

distribution of observation is generally considered skewed. The more appropriate distribution for precipitation data is found as gamma distribution by (Thom, 1958). The probability density function can be calculated for gamma distribution g (x);

$$g(x) = \frac{1}{\beta\Gamma(\alpha)} x^{\alpha-1} e^{-\frac{x}{\beta}} \tag{3.28}$$

where x is precipitation observation, $\alpha > 0$ and $\beta > 0$ are shape and scale parameter respectively. The gamma function $\Gamma(\alpha)$ is defined as;

$$\Gamma(\alpha) = \int_0^\infty y^{\alpha-1} e^{-y}\, dy \tag{3.29}$$

Edwards and McKee (1997) applied the maximum likelihood method for predicting α, β parameters;

$$\hat{\alpha} = \frac{1}{4}\left(1 + \sqrt{1 + \frac{4A}{3}}\right) \tag{3.30}$$

$$\hat{\beta} = \frac{\bar{x}}{\hat{\alpha}} \tag{3.31}$$

where

$$A = \ln(\bar{x}) - \frac{\sum \ln(x)}{n} \tag{3.32}$$

n is the number of precipitation observations, and $\bar{x}$ is the mean of x. The cumulative distribution may be defined as:

$$H(x) = q + (1-q)G(x) \tag{3.33}$$

where q is the probability of zero and G(x) is the cumulative distribution for a desired month and time scale. Finally, the cumulative distribution H(x) is then converted to the standard normal random variable Z (mean zero and variance one) which represents the value of SPI (Tsakiris and Pangalou, 2009). Fig. 3.1 explains the time series of SPI and the drought process. McKee et al., (1993) categorized droughts as the period length in which the SPI is below -1 and SPI classifications for wet and dry events are listed in Table 3.4. Drought duration (D) is expressed as "the number of consecutive intervals (months) where the SPI value fell below zero". Drought severity (S) is expressed as "a cumulative SPI value during drought duration", stated using the following equation as (McKee et al., 1993);

$$S = -\sum_{i=1}^{D} SPI_i \quad (3.34)$$

where S is drought severity, and D is drought duration. Interval time E(L) is the time between the initiation of drought to the beginning of the next drought (Mishra and Singh, 2010).

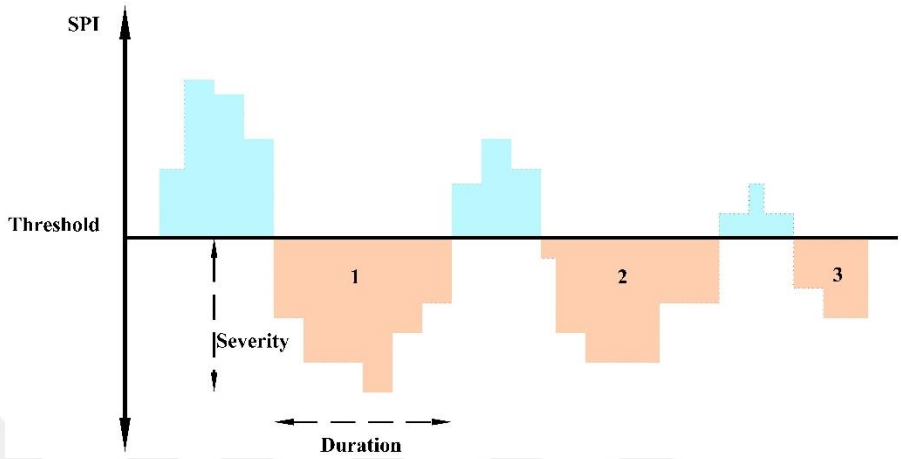

Figure 3.1 The definition of drought characteristics

3.4.2 Standardized Precipitation Evapotranspiration Index (SPEI)

Due to involving potential evaporation, which is evaluated based on the temperature in addition to rainfall, SPEI was proposed by Vicente-Serrano et al., (2009) and it differs from SPI. The computation steps of the SPEI show the same as that of the SPI. SPEI is also calculated at multiple time scales and negative values show dry periods because of precipitation deficit and/or higher potential evaporation as compared to the historical mean (Bayissa et al., 2018). Potential evapotranspiration (PET) was calculated in two ways: The Thornthwaite, which is used in this study, and the Penman-Monteith method. The Thornthwaite method, which needs only air temperature as an input parameter, is mathematically expressed as;

$$PET = 16k\left(\frac{10T}{I}\right)^{m} \quad (3.35)$$

where T is the monthly air temperature (° C), k is a factor evaluated based on the latitude of the gauging station, and I is the annual heat index and m is a coefficient related to I (Tirivarombo et al., 2018; Yu et al., 2014). Using the difference P_i and PET, the climatic water balance D_i of month of *i*, SPEI value is based on normalized D series, which is computed (Vicente-Serrano et al., 2009).

$$D_i = P_i - PET_i \quad (3.36)$$

3.4.3 Self-calibrated Palmer Drought Severity Index (scPDSI)

PDSI has some limitations when it is used in another region due to it being used for agricultural purposes and not for long term hydrological droughts. Palmer was founded to derive the calibration and weighting in the or PDSI. However, due to removing limitations to apply another hydro-climatic region, (Wells et al., 2004) computed a scPDSI that identified the factors using dynamically evaluated values to shift constant parameters in the or PDSI algorithm for various region globally. This provides PDSI values more stationary and homogeneous comparable temporally and spatially than the other indices and performs extreme wet (dry) periods better with frequencies (Jiang et al., 2015). A brief mathematical description can be found in Wells et al., (2004) and Vicente-Serrano et al., (2009).

Table 3.2 Definition of scPDSI classes and corresponding events

Class	scPDSI
Extremely wet	≥ 4
Severely wet	3.0 to 3.99
Moderate wet	2.0 to 2.99
Mild wet	1.00 to 1.99
Incipient wet	0.5 to 0.99
Normal	0.49 to -0.49
Incipient dry	-0.5 to -0.99
Mild dry	-1.00 to -1.99
Moderately dry	-2.0 to -2.99
Severely dry	-3.0 to -3.99
Extremely dry	$\leq$- 4.0

3.4.4 Decile Index (DI) and Percent of Normal Index (PNI)

Decile Index (DI) was firstly introduced by Gibbs et al., (1967), and extensively employed in Australia. Wilhite, (2016) arranges monthly rainfall data into deciles. This approach was developed for avoiding the weakness of the percent of normal index. The first step to construct a cumulative distribution function is to rank the total long-term rainfall data from highest to lowest, and this distribution is divided into ten parts. Each distribution is known as a 'decile'. The first decile is the rainfall value not exceeded by the lowest 10% of all rainfall occurrences in a record. The second decile is the rainfall amount not exceeded by the lowest 20% of occurrence. All deciles proceed until the precipitation value quantified by the tenth decile represented the largest precipitation amount within the long-term record. Particularly, deciles are

commonly classified as five groups, and each group includes two deciles. If rainfall drops into the lowest 20% (called decile 1 and 2), it is categorized as much below normal. A decile of 20 and 40% (decile 3 and 4) show below normal rainfall, 40 and 60% (decile 5 and 6) show near normal rainfall, 60 and 80% (decile 7 and 8) show above normal rainfall and finally, and lastly 80 and 100% (decile 9 and 10) indicate much above normal rainfall (McMahon and Mein, 1986).

PNI is one of the easiest methods to measurements of precipitation for a specific region. It is influential when applied to a single hydro-climatic region and easy. PNI is evaluated by dividing actual rainfall by normal rainfall frequently considered to be 100%. It can be evaluated for a month, season, or year and because of its simplicity, it is easily misunderstood when used in a different region. One of the disadvantages of using PNI is that the average mean precipitation does not show the same as the median precipitation. Hence, the normal distribution shows that the median and mean are considered to be the same (Morid et al., 2006).

3.4.5 China-Z index (CZI), Modified China-Z index (MCZI) and Z index (ZI)

The CZI is relied on Wilson-Hilferty cube-root transformation (Wilson and Hilferty, 1931), from the chi-square variable to Z-score (Kendall and Stuart, 1973) and an assumption that rainfall is well fitted the Pearson Type III distribution. CZI index mathematically expressed as:

$$CZI_j = \frac{6}{C_s}\left(\frac{C_s}{2}\phi_j + 1\right)^{\frac{1}{3}} - \frac{6}{C_s} + \frac{C_s}{6} \tag{3.37}$$

$$C_s = \frac{\sum_{j=1}^{n}\left(x_j - \bar{x}\right)^3}{n \times \sigma^3} \tag{3.38}$$

$$\phi_j = \frac{x_j - \bar{x}}{\sigma} \tag{3.39}$$

where C_s is coefficient of skewness, n is the total number of long-term months, j is the current month, x_j is rainfall of j month, and ϕ_j is standard deviate, also called Z-score. To evaluate MCZI, unlike used mean of rainfall in calculation in CZI, the median of rainfall is used. This empirical method was developed by Wu et al., (2001), to decrease the difference between MCZI and SPI.

3.4.6 Rainfall Anomaly Index (RAI), Reconnaissance Drought Index (RDI) and Aridity Index (AI)

Rainfall Anomaly Index (RAI) was developed by Van Rooy, (1965) and was performed to identify annual rainfall variability. RAI can be analyzed on monthly seasonal and annual time series data. It considers two anomalies: positive and negative anomalies. The first step is to arrange in descending order and the ten highest values are averaged to construct a threshold for positive anomalies. After finding the lowest ten values averaged to construct a threshold, it is considered to be negative anomalies. RAI is evaluated at a given equation 3.38 and 3.39;

$$RAI=+3\left[\frac{RF-M_{RF}}{M_{H10}-M_{RF}}\right] \quad (3.40)$$

$$RAI=-3\left[\frac{RF-M_{RF}}{M_{L10}-M_{RF}}\right] \quad (3.41)$$

where RF shows total precipitation obtained during a year, M_{RF} represents the mean precipitation recorded during a particular period, M_{H10}, M_{L10} constitute the mean values ten highest and ten lowest rainfall data, respectively (Pandey et al., 2014).

Reconnaissance Drought Index (RAI) was developed by Tsakiris and Vangelis, (2005) to cope with the restriction of PDSI and SPI based on an initial value (a_k) for a certain period, which obtained the ratio between cumulative precipitation (P) over the potential evapotranspiration (PET). a_k is formulated as:

$$a_k=\frac{\sum_{j=1}^{j=k} P_{ij}}{\sum_{j=1}^{j=k} PET_{ij}} \quad (3.42)$$

where P_{ij} represents precipitation, PET_{ij} constitutes potential evapotranspiration for j^{th} of the i^{th} year. RDI is computed both as standardized RDI_{st} and normalized RDI_n and can be determined as;

$$RDI_n(k)=\frac{a_k}{\bar{a}_k} \quad (3.43)$$

The computation procedure of RDI_{st} shows similar to the calculation of SPI. The equation can be expressed as;

$$RDI_{st}(k)=\frac{y_k-\bar{y}_k}{\bar{\sigma}_k} \quad (3.44)$$

where y_k is calculated ln ($a_k^{(i)}$), $\bar{y}_k$, $\bar{\sigma}_k$ are its mean and standard deviation, respectively (Rahmat et al., 2015).

Aridity Index (AI) is considered to perform a drought situation and obtain the percentage ratio between water deficit and water need. AI is calculated given the following equation as;

$$AI = \frac{PET\text{-}AET}{PET} \times 100 \quad (3.45)$$

where PET and AET are potential evapotranspiration and actual evapotranspiration, respectively (Middleton and Thomas, 1997). AI identifies the drought occurrence indicator of the degree of dryness of climate in any region as a numerical.

Table 3.3 Aridity classifications

Classification	Aridity Index (AI)
Hyper-arid	AI ≤0.05
Arid	0.05≤AI<0.20
Semi-arid	0.2≤AI<0.50
Dry sub-humid	0.5≤AI<0.65
Sub-humid	0.65≤AI<0.80
Humid	0.80≤AI<1.5
Very humid	1.5≤AI

Table 3.4 Categorizations of wetness and dryness grade based on used drought indices

Class	SPI, SPEI, RDI, CZI, MCZI, Z-Score	DI (%)	PN	RAI
Extremely wet	≥ 2	≥ 90		≥ 3
Very wet	1.5 to 1.99	80 to 90	≥ 110	2.00 to 2.99
Moderately wet	1.00 to 1.49	70 to 80		1.00 to 1.99
Normal	0.99 to -0.99	30 to 70	80 to 110	0.5 to -0.99
Moderately dry	-1.00 to -1.49	20 to 30	55 to 80	-1.00 to -1.99
Very dry	-1.5 to -1.99	10 to 20	40 to 55	-2.00 to -2.99
Extremely dry	≤- 2	≤ 10	≤ 40	≤ -3

3.5 Copula Based Multivariate Distribution

3.5.1 Copula Definition and Sklar's Theorem

The copula is a powerful function that enables us to model a joint distribution function of different univariate random variables (Nelsen, 2006). It is essentially based on the correlation between variables to link different marginal distribution. When compared to traditional multivariate distributions, copula provides great flexibility to select the univariate marginal distributions. The theoretical definition of a copula was first

expressed by Sklar, (1959). According to Sklar's theorem, if two random variables *x* and *y* are considered with following the marginal distribution function $F_X(x)$ and $F_Y(y)$, then there exists a unique copula C where it links these two different marginals to model the joint distribution function. C is defined using the following equation as (Nelsen, 2006);

$$H(x,y) = C[F(x), F(y)], \qquad x, y \in R \tag{3.46}$$

Here, $C: \mathbb{I} \times \mathbb{I} \to \mathbb{I}$, $\mathbb{I} = [0,1]$, a mapping function, called the copula. A probabilistic model for random data (X, Y) is constructed using F(x), F(y), and C.

$$F(x;\delta), \;\; F(y;\varphi), \qquad C(u,v;\theta)$$

where δ and φ represent the parameter vectors of marginal distributions, $u = F(x)$ and $v = F(y)$ are denoted the quantile of the uniformly disturbed variables and θ is the copula parameter of dependency.

The copula is generally called as "dependency function" because of containing all information about between *F(x)* and *F(y)*. For copula function, the theorem is much basic in hydrologic time series modeling. According to the theorem, given any marginal distribution (F(x), F(y), …, F(n)), a copula function C is employed to determine the joint distribution function. The joint probability density function defines as;

$$f_{X,Y}(x, y) = C(F_X(x), F_Y(y)) f_X(x) f_Y(y) \tag{3.47}$$

where $f_X(x)$ and $f_Y(y)$ are the density functions related to $F_X(x)$ and $F_Y(y)$, respectively, and c is the density function of C, defined as

$$c(u, v) = \frac{\partial^2 C(u, v)}{\partial u \, \partial v} \tag{3.48}$$

3.5.2 Copula Classes

The copula is generally classified into four types: Elliptical, Archimedean, extreme value and other miscellaneous classes. It may also be grouped as vector parameter copulas or a single parameter considering dependence structure. In addition, for each copula, more than three copulas may be obtained by employing basic relationships, also noted as associated copulas. Nelsen (2006) and (Joe, 1997) reported properties of a large number of copula classes based on the theoretical background. Salvadori et al.,

(2007) provided a comprehensive application in the field of hydrology as well as geophysics and geosciences. Genest and Favre, (2007) indicate that using the goodness-of-fit tests are evaluated in the copula estimation and inference procedure in detail.

3.5.2.1 Archimedean Copulas

Archimedean copula, compared to other copula families, is a crucial class of copulas that have been extensively used and usually performed in the field of hydrology (Nelsen, 2006). Nelsen (2006) has discussed various reasons why Archimedean copulas are widely used in hydrology. (i) They are described by different copulas, (ii) easy to construct a typical feature of these copulas. The archimedean class has general form is expressed as

$$\emptyset[C(u,v)] = \emptyset(u) + \emptyset(v) \tag{3.49}$$

where, $\emptyset$ is a continuous, strictly decreasing function $\emptyset(t): \mathbb{I} \rightarrow [0,\infty]$, such that $\emptyset(1) = 0$ is referred to as the generating function. The copula probability is mathematically calculated as

$$C(u,v) = \emptyset^{[-1]}\{\emptyset(u) + \emptyset(v)\} \tag{3.50}$$

At this point, $\emptyset^{[-1]}(t): [0,\infty] \rightarrow \mathbb{I}$ is called as the pseudo-inverse of generating function. It is non-increasing and continuous on $[0,\infty]$ and drastically decreasing on $[0,\emptyset(0)]$ and is expressed by

$$\emptyset^{[-1]}(t) = \begin{cases} \emptyset^{[-1]}(t), & 0 \le t \le \emptyset(0) \\ 0, & \emptyset(0) \le t < \infty \end{cases} \tag{3.51}$$

Hence, if $\emptyset(0) = \infty$, then $\emptyset^{[-1]} = \emptyset^{-1}$.

3.5.2.1.1 Frank Copula

Frank copula is one of the Archimedean classes that have been widely applied for various hydrological events. The generating function $\emptyset$ can be obtained as

$$\emptyset(t) = -ln\left(\frac{1-e^{-\theta t}}{1-e^{-\theta}}\right), \qquad \theta \in (-\infty,\infty)\backslash\{0\} \tag{3.52}$$

Finally, the pseudo-inverse of Frank copula generating function is evaluated by

$$\emptyset^{-1}(t) = -\frac{1}{\theta} ln\left[1 - \left(1 - e^{-\theta}\right)e^{-t}\right] \tag{3.53}$$

According to the above generating equation, the cumulative distribution function $C_\theta(u,v)$ for Frank copula is calculated as

$$C_\theta(u,v) = -\frac{1}{\theta} ln\left[1 - \frac{(1-e^{-\theta u})(1-e^{-\theta v})}{1-e^{-\theta}}\right] \quad (3.54)$$

The Frank copula density, due to double differentiating probability, is expressed as

$$c(u,v) = \frac{\partial^2 C_\theta(u,v)}{\partial \mathrm{u}\, \partial \mathrm{v}} = \frac{\theta e^{-\theta(u+v)}}{(1-e^{-\theta})[exp(-\theta C_\theta)]^2} \quad (3.55)$$

For bivariate random variable (X, Y), The joint probability function (pdf) for Archimedean copulas, can be expressed as

$$H(x,y) = C_\theta(u,v) = C[F(x),F(y)] = \theta^{[-1]}\{\theta[F(x)] + \theta[F(y)]\} \quad (3.56)$$

Finally, considering *f (x)* and *f (y)* as marginal densities, pdf for *X* and *Y* variable can be written as

$$h(x,y) = \frac{\partial^2 C_\theta(u,v)}{\partial u\, \partial v}\frac{\partial u\, \partial v}{\partial x\, \partial y} = \frac{\partial^2 C_\theta(u,v)}{\partial u\, \partial v}\frac{\partial F(x)\, \partial F(y)}{\partial x\, \partial y}$$

$$= f(x)g(y)c_\theta(u,v) \quad (3.57)$$

The cumulative distribution function (cdf) for Frank copula, can be written as

$$H(x,y) = -\frac{1}{\theta} ln\left[1 - \frac{\left(1-e^{-\theta F_x(x)}\right)\left(1-e^{-\theta F_y(y)}\right)}{1-e^{-\theta}}\right] \quad (3.58)$$

For Frank copula, its joint pdf, using Eqs. (3.56) and (3.58), can be defined as

$$h(x,y) = f(x)g(y)\frac{\theta e^{-\theta[F(x)+F(y)]}}{(1-e^{-\theta})[exp(-\theta C_\theta)]^2} \quad (3.59)$$

3.5.2.1.2 Clayton Copula

Clayton copula, developed by Clayton, (1978), obtained its generator function as

$$\emptyset_\theta(t) = \frac{t^{-\theta}-1}{\theta} \quad (3.60)$$

The Clayton copula's cdf is

$$c^{Clayton}(u,v;\theta) = \frac{(1+\theta)(u^{-\theta}+v^{-\theta}-1)^{-\frac{1}{\theta}-2}}{(u\,v)^{\theta+1}} \quad (3.61)$$

The pdf is written as

$$C^{Clayton}(u,v;\theta) = \left(u^{-\theta} + v^{-\theta} - 1\right)^{-\frac{1}{\theta}-2} \tag{3.62}$$

In general, the copula parameter range varies between 0 to ∞. When $\theta = 0$, marginals are independent. Otherwise, if the copula parameter goes to infinity, marginals can be more dependent. Clayton copula left dependence is stronger than the right dependence due to asymmetric tail dependency. In addition, this copula type evaluates just for positive dependency (Nelsen, 2006).

3.5.2.1.3 Gumbel Copula

Unlike Clayton copula, Gumbel copula, proposed by Gumbel, (1960), accounts for weak left tail dependence and strong right tail dependence. The feature of the Gumbel copula parameter θ is similar to Clayton copula, evaluates for positive dependence, and its parameter range varies between 1 to ∞. A generator function can be obtained as

$$\emptyset_\theta(t) = (-lnt)^{-1} \tag{3.63}$$

The Gumbel copula's pdf is obtained as

$$C^{Gumbel}(u,v;\theta) = exp\left\{-\left[(-lnu)^\theta + (-lnv)^\theta\right]^{\frac{1}{\theta}}\right\} \tag{3.64}$$

The cdf is written as

$$c^{Gumbel}(u,v;\theta) =$$

$$= \frac{C^{Gumbel}(u,v;\theta)(lnu\ lnv)^{\theta-1}\left\{\left[(-lnu)^\theta + (-lnv)^\theta\right]^{\frac{1}{\theta}}\right\} + \theta - 1}{uv\left[(-lnu)^\theta + (-lnv)^\theta\right]^{2-\frac{1}{\theta}}} \tag{3.65}$$

3.5.2.1.4 Joe Copula

The Joe copula is another one-parameter, commonly referred to as Archimedean family (see Nelsen, 2006), and generator function can be obtained as

$$\emptyset_\theta(t) = -log\left[1 - (1-t)^\theta\right] \tag{3.66}$$

Joe copula is given by

$$C^{Joe}(u,v) = 1 - \left[(1-u)^\theta + (1-v)^\theta - (1-u)^\theta(1-v)^\theta\right]^{\frac{1}{\theta}} \tag{3.67}$$

The Joe copula density is obtained as (with θ >1)

$$c^{Joe}(u,v) = \left[(1-u)^{\theta} + (1-v)^{\theta} - (1-u)^{\theta}(1-v)^{\theta}\right]^{\frac{1}{\theta}-2}(1-u)^{\theta-1}(1-v)^{\theta-1}$$

$$\times \left[\theta - 1 + (1-u)^{\theta} + (1-v)^{\theta} - (1-u)^{\theta}(1-v)^{\theta}\right] \quad (3.68)$$

If $\theta \to 1$, Joe copula shows negative dependence.

3.5.2.1.5 BB1 (Clayton-Gumbel) Copula

BB1 (Clayton-Gumbel Copula), developed by Joe, (1997), is a two-parametric Archimedean copula. It is called BB1 instead of Clayton-Gumbel copula to avoid confusion. Here, BB1 copula does not show any difference between Gumbel and Clayton. If the parameters $\theta \to \infty, \delta \to \infty$, positive dependence will be obtained. BB1 is Gumbel for $\theta \to 0$, and Clayton for $\delta \to 0$.

Its generator is presented as $\emptyset(t) = \left(t^{-\theta} - 1\right)^{\delta}$. BB1 copula pdf is

$$C^{BB1}(u,v) = \left[1 + \left[\left(u^{-\theta} - 1\right)^{\delta} + \left(v^{-\theta} - 1\right)^{\delta}\right]^{\frac{1}{\delta}}\right]^{-\frac{1}{\theta}} \quad (3.69)$$

The following density is given by ($\theta > 0, \delta \geq 1$),

$$c^{BB1}(u,v) = \left\{1 + \left[\left(u^{-\theta} - 1\right)^{\delta} + \left(v^{-\theta} - 1\right)^{\delta}\right]^{\frac{1}{\delta}}\right\}^{-\frac{1}{\theta}-2}$$

$$\times \left[\left(u^{-\theta} - 1\right)^{\delta} + \left(v^{-\theta} - 1\right)^{\delta}\right]^{\frac{2}{\delta}-2}$$

$$\times \left\{\theta\delta + 1 + \theta(\delta - 1)\left[\left(u^{-\theta} - 1\right)^{\delta} + \left(v^{-\theta} - 1\right)^{\delta}\right]^{-\frac{1}{\theta}}\right\}$$

$$\times \quad \left(u^{-\theta} - 1\right)^{\delta-1} u^{-\theta-1}\left(v^{-\theta} - 1\right)^{\delta-1} v^{-\theta-1} \quad (3.70)$$

3.5.2.1.6 BB6 Copula

BB6 copula (Joe, 1997) is another common, two-parametric used Archimedean family. The generation function is $\emptyset(t) = \left[-log\left(1 - (1-t)^{\theta}\right)\right]^{\delta}$,

where ≥ 1, $\delta \geq 1$, and BB6 copula form is written as

$$C^{BB6}(u,v) = 1 - \left(1 - exp\left(-\left(\left(-log\left(1-(1-u)^{\theta}\right)\right)^{\delta} + \left(-log\left(1-(1-v)^{\theta}\right)\right)^{\delta}\right)^{\frac{1}{\delta}}\right)\right)^{\frac{1}{\theta}} \quad (3.71)$$

3.5.2.1.7 BB7 (Joe-Clayton) Copula

Like BB1 copula, BB7 (Joe-Clayton copula) is two-parametric, proposed by Joe (1997). The generator function is defined as $\emptyset(t) = \left[1-(1-t)^{\theta}\right]^{-\delta} - 1$. BB7 copula's pdf is obtained as

$$C^{BB7}(u,v) = 1 - \left[\left[\left(1-(1-u)^{\theta}\right)^{-\delta} + \left(1-(1-v)^{\theta}\right)^{-\delta}\right]^{-\frac{1}{\delta}}\right]^{\frac{1}{\theta}} \quad (3.72)$$

The following density distribution is ($\theta \geq 1, \delta > 0$),

$$c^{BB7}(u,v) = \left(-\frac{1}{\theta}\right)\left(-\frac{1}{\delta}-1\right) \times h^{\frac{1}{\theta}-2} duh \times dvh - \frac{1}{\theta} h^{\frac{1}{\theta}-1} duh \times dvh$$

where

$$h = 1 - \left(\left(1-(1-u)^{\theta}\right)^{-\delta} - \left(1-(1-v)^{\theta}\right)^{-\delta} - 1\right)^{\frac{1}{\delta}}$$

$$duh = -\theta\left(\left(1-(1-u)^{\theta}\right)^{-\delta} - \left(1-(1-v)^{\theta}\right)^{-\delta} - 1\right)^{\frac{1}{\delta}-1} \left(1-(1-u)^{\theta}\right)^{-\delta-1}(1-u)^{\theta-1}$$

$$dvh = -\theta\left(\left(1-(1-u)^{\theta}\right)^{-\delta} - \left(1-(1-v)^{\theta}\right)^{-\delta} - 1\right)^{\frac{1}{\delta}-1} \left(1-(1-v)^{\theta}\right)^{-\delta-1}(1-v)^{\theta-1}$$

$$duvh = \frac{1}{\delta}\left(-\frac{1}{\delta}-1\right)\left(\left(1-(1-u)^{\theta}\right)^{-\delta-1}(1-u)^{\theta-1} - \left(1-(1-v)^{\theta}\right)^{-\delta} - 1\right)^{\frac{1}{\delta}-2} duS \times dvS$$

$$duS = -\theta\delta\left(1-(1-u)^{\theta}\right)^{-\delta-1}(1-u)^{\theta-1}$$

$$dvS = -\theta\delta\left(1-(1-v)^{\theta}\right)^{-\delta-1}(1-v)^{\theta-1} \quad (3.73)$$

3.5.2.1.8 BB8 (Joe-Frank) Copula

BB8 (Joe-Frank) copula is also a two-parametric Archimedean family and its parameters vary for $\theta \geq 0$, and $0 \leq \delta \leq 1$. The independence is obtained as $\delta \to 0$ or $\theta \to 1$. Frank copula is defined for $\delta \to \infty$, while Joe copula is obtained $\delta \to 1$. There is no tail dependence except for $\delta \to 1$ and a single parameter may be evaluated by employing the equation $1-(1-\delta)^{\theta}$. The BB8 copula is defined as (Cheng et al., 2020)

$$C^{BB8}(u,v) = \delta^{-1}\left[1 - \left\{1 - \left[1-(1-\delta)^{\theta}\right]^{-1}\left[1-(1-\delta u)^{\theta}\right]\left[1-(1-\delta v)^{\theta}\right]\right\}^{\left(\frac{1}{\theta}\right)}\right] \quad (3.74)$$

3.5.2.2 Elliptical Copulas

3.5.2.2.1 Gaussian (normal) Copula

With correlation parameter p (1, -1), the bivariate Gaussian copula is written as

$$C^{Gaussian}(u_1, u_2) = \emptyset_p\left((\emptyset^{-1}(u_1), \emptyset^{-1}(u_1)\right) \tag{3.75}$$

The Gaussian copula is one-parameter family for random variables (X_1, X_2) and its cdf is obtained as

$$C^{Gaussian}(u_1, u_2) = \int_{-\infty}^{\emptyset-1}(u_1)\int_{-\infty}^{\emptyset-1}(u_2)\frac{1}{2\pi(1-p^2)^{\frac{1}{2}}}exp\left\{-\frac{x_1^2+x_2^2-2px_1x_2}{2(1-p^2)}\right\}dx_1x_2 \tag{3.76}$$

where, p represents correlation coefficient p = corr (X_1, X_2). While a common method to generate simulation with random variables from selected copula distribution is difficult to detect, the Gaussian copula's generated simulation is demonstrated much easier (Klaus, 2013). If $p \to 1$, Gaussian copula shows positive. However, if $p \to -1$, it exhibits negative dependence.

3.5.2.2.1 Student's t Copula

Student t copula is two-parametric copula (Demarta and McNeil, 2005), and the density of bivariate of Student t copula is obtained with parameters p (1, -1) and $\vartheta > 0$ as;

$$C^{Student\ t}(u_1, u_2) = \int_{-\infty}^{t_\vartheta^{-1}}(u_1)\int_{-\infty}^{t_\vartheta^{-1}}(u_2)\frac{1}{2\pi(1-p^2)^{\frac{1}{2}}}exp\left\{-\frac{x_1^2+x_2^2-2px_1x_2}{\vartheta(1-p^2)}\right\}^{-\frac{(\vartheta+2)}{2}}dx_1x_2 \tag{3.77}$$

Here, ϑ denotes the degree of freedom. If $p \to 1$, Student's t copula shows positive. The opposite ($p \to -1$) exhibits a negative dependence. An example of a simulated sample of Archimedean and Elliptical copula is shown in Figure 3.2.

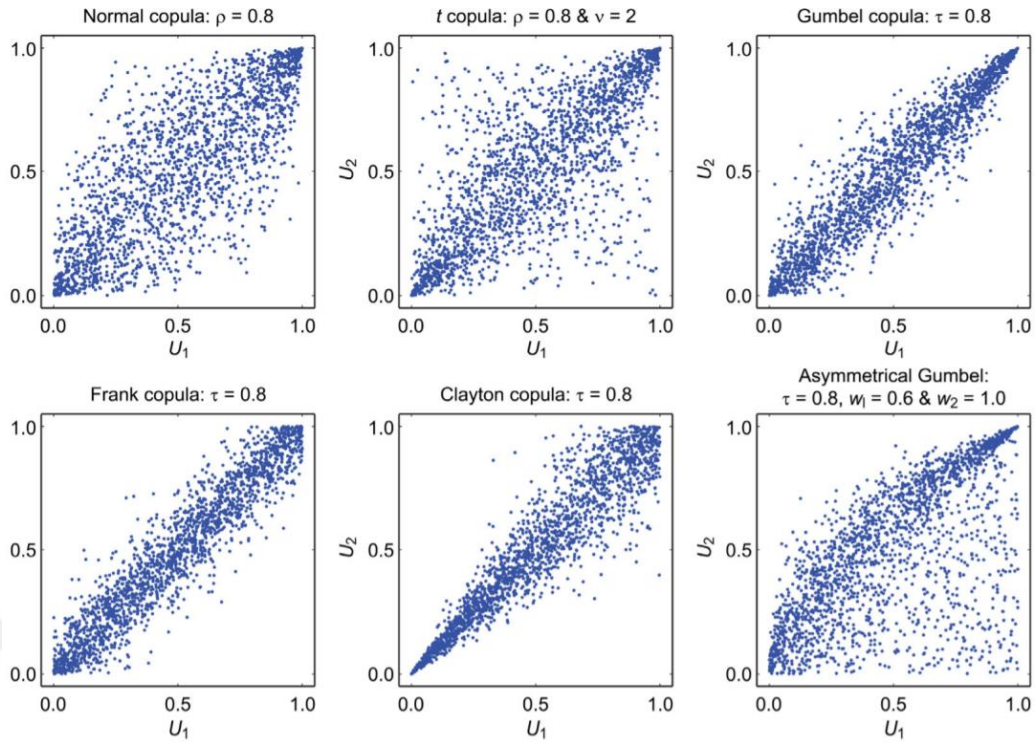

Figure 3.2 This shows an example of simulated data for both the Archimedean and Elliptical copula (Goda and Tesfamariam, 2015)

3.5.3 Tail Dependence Characteristics

The terms of upper and lower tail dependence were introduced by Sibuya, (1960), and are related to dependence between extreme values in the upper and lower tails of bivariate distribution. The lower positive values of the upper tail show that they are poor relations or not strongly dependent (Reddy and Ganguli, 2012). In hydrology, disregarding tail dependencies can cause high uncertainty in extreme quantile prediction. These result in incorrect findings for hydrological design (Xu et al., 2010). On the other hand, frequency analysis of extreme hydrological events (such as droughts and floods) should be considered in terms of tail dependencies (Poulin et al., 2007). The coefficient of upper (lower) tail dependence $\lambda_u(\lambda_L)$ is defined as

$$\lambda_u = \lim_{t \to 1^-} P\{F_X(x) > t | F_Y(y) > t\} \quad (3.78)$$

$$\lambda_L = \lim_{t \to 0^+} P\{F_X(x) < t | F_Y(y) < t\} \quad (3.79)$$

This is where $F_X(x), F_Y(y)$ are CDFs of a random variable of drought duration and severity, respectively, and t is the constant value standard uniform variable. If $\lambda_u(\lambda_L) \in (0,1]$, bivariate distribution function can be said to show upper (lower) tail

dependence. If $\lambda_u(\lambda_L) = 0$, variables are independent. The upper (lower) tail dependence can be expressed in term of a copula function as

$$\lambda_u = \lim_{t\to 1^-} P\left[Y > F_y^{-1}(t) | X > F_x^{-1}(t)\right] = \lim_{t\to 1^-} P\left[t < F_y(t) | t < F_x(t)\right]$$

$$= \lim_{t\to 1^-} P\left[V > t | U > t\right] = \lim_{t\to 1^-} \frac{P[V > t, U > t]}{P[U > t]}$$

$$= \lim_{t\to 1^-} \frac{1 - 2t + C(t,t)}{1-t} = 2 - \lim_{t\to 1^-} \frac{1 - C(t,t)}{1-t}$$

$$\lambda_u = \lim_{t\to 1^-} \frac{1-2t+C(t,t)}{1-t} \tag{3.80}$$

λ_L, the lower tail dependence can be obtained from the following formula:

$$\lambda_L = \lim_{t\to 0^+} P\left[Y \le F_y^{-1}(t) | X \le F_x^{-1}(t)\right] = \lim_{t\to 0^+} P\left[t \ge F_y(t) | t \ge F_x(t)\right]$$

$$= \lim_{t\to 0^+} P\left[V \le t | U \le t\right] = \lim_{t\to 1^-} \frac{P\left[V \le t, U \le t\right]}{P\left[U \le t\right]}$$

$$\lambda_L = \lim_{t\to 0^+} \frac{C(t,t)}{t} \tag{3.81}$$

Tail dependence just applies to choose the appropriate copula family (not on the selection of marginal distribution). Previous studies showed that the best fit copula is Clayton, without using tail dependence. However, with using tail dependence, while non-Gaussian copulas have a quite lower upper (lower) tail dependency, Gaussian copula does not have tail dependence (AghaKouchak et al., 2010). The coefficients of tail dependence for different copula families are presented in Table 3.5. This paper focuses on the upper tail dependence due to analyzing the occurrence of extreme events. That is according to test results and literature. Ali-Mikhail -Haq ($\lambda_u = 0, \lambda_L = 0$), Frank ($\lambda_u = 0, \lambda_L = 0$), Galambos ($\lambda_u \neq 0, \lambda_L = 0$), and Plackett ($\lambda_u = 0, \lambda_L = 0$) copulas did not take consideration (Nelsen, 2006). The nonparametric upper tail dependence (λ_u^{CFG}) is given by the following

$$\lambda_u^{CFG} = 2\text{-}2\exp\left\{\frac{1}{n}\sum_{i=1}^{n} \log\left[\frac{\sqrt{\log\left(\frac{1}{u_1}\right)\log\left(\frac{1}{v_1}\right)}}{\log\left(\frac{1}{\max(u_1, v_1)^2}\right)}\right]\right\} \tag{3.82}$$

Table 3.5 The coefficients of tail dependence for both Archimedean and Elliptical copula families

Copula Family/Copula	Tail Dependence Coefficients	
	λ_L	λ_U
Archimedean		
Frank	0	0
Clayton	$2^{-\frac{1}{\theta}}$	0
Gumbel	0	$2-2^{\frac{1}{\theta}}$
Joe	0	$2-2^{\frac{1}{\theta}}$
BB1	$2^{-\frac{1}{(\theta\delta)}}$	$2-2^{\frac{1}{\delta}}$
BB6	0	$2-2^{\frac{1}{(\theta\delta)}}$
BB7	$2^{-\frac{1}{\delta}}$	$2-2^{\frac{1}{\theta}}$
BB8	0	$2-2^{\frac{1}{\theta}}$, if δ=1, 0 otherwise
Elliptical		
Gaussian	0	0
Student's t	$2t_{v+1}\left(-\sqrt{v+1}\sqrt{\frac{1-p}{1+p}}\right)$	$2t_{v+1}\left(-\sqrt{v+1}\sqrt{\frac{1-p}{1+p}}\right)$

3.5.4 Parameter Estimation Methods

Before constructing bivariate distribution of drought variables (duration and severity), a univariate distribution of drought characteristics must first be described. Some previous studies showed that exponential for drought duration and gamma distribution for drought severity were commonly used in drought analysis (Lee et al., 2013; Shiau, 2006; Shiau and Modarres, 2009). However, Yusof et al., (2013) suggested the two mostly used probability distributions are not appropriate in every case. Therefore, several distributions are used to fit the drought severity and drought duration in this study. These distributions are Lognormal, Logistic, Gamma, Exponential, Weibull and Normal distributions. The performance of used distributions for each drought characteristic is tested by the Anderson-Darling (AD) (Stephens, 1974), Kolmogorov-Smirnov (K-S) (Smirnov, 1948), Cramers-von Mises (CvM), Akaike's Information Criterion (AIC) (Akaike, 1976), Bayesian Information Criterion (BIC) (Stone, 1979), and Maximum likelihood (ML) methods. The performance in selecting the best copula among used copula family is also tested by AIC, BIC, and ML statistical methods.

3.5.4.1 Marginal Distribution Tests for Drought Characteristics

3.5.4.1.1 Lognormal Distribution (LN)

Lognormal statistical distribution is crucial for probabilistic design since sometimes in engineering phenomena and negative values lead to complications. Practical applications of lognormal distribution are constructed in the description of failure rates, fatigue failure, and other conditions including a large range of data (Chang, 2015). Lognormal distribution of random variable X, considering expected value μ_x, standard deviation σ_x , noted as LN (μ_x, μ_x), is written as

$$f_X(x) = \frac{1}{\sqrt{2\pi}\sigma_Y} e^{-\frac{1}{2}\left(\frac{\ln(x)-\mu_Y}{\sigma_Y}\right)^2}, \qquad 0 < x < \infty \tag{3.83}$$

where, $f_X(x)$ is the pdf of the variable *X*, and

$$\sigma_y = \sqrt{ln\left(\left(\frac{\sigma_x}{\mu_x}\right)^2 + 1\right)} \tag{3.84}$$

and

$$\mu_Y = \ln(\mu_X) - \frac{1}{2}{\sigma_y}^2 \tag{3.85}$$

If Y variable shows a normal distribution, then $X = exp(Y)$. In a similar way, if X variable has a normal distribution, $Y = \ln(X)$.

3.5.4.1.2 The Logistic Distribution

The logistic distribution is a continuous probability distribution function in statistics and is described as two parameters. It is generally employed in several areas such as neural networks, logit models, and logistic regression. It has been applied in the finance, sport modeling, physical science, and recently in hydro-climatologic fields (Kissell and Poserina, 2017). Mathematical notation is expressed as $X \sim Logistic\ (\mu, s), s > 0$, here μ ($0 \leq \mu \leq \infty$) and s ($s > 0$) represent location parameter and scale parameter respectively. The probability density function (pdf) of logistic distribution is obtained by

$$f_X(x) = \frac{e^{-\frac{x-\mu}{s}}}{s\left(1+e^{-\frac{x-\mu}{s}}\right)^2}, \qquad -\infty < x < \infty \tag{3.86}$$

The cumulative distribution function (cdf) is written as

$$F_X(x) = \int_{-\infty}^{x} x f_X(x)dx = \frac{1}{1+e^{-\frac{x-\mu}{s}}}, \quad -\infty < x < \infty \tag{3.87}$$

Mean and variance are expressed by

$$E(X) = \int_{-\infty}^{\infty} x f_X(x)dx = \int_{-\infty}^{\infty} \frac{xe^{-\frac{x-\mu}{s}}}{s\left(1+e^{-\frac{x-\mu}{s}}\right)^2} dx = \mu \tag{3.88}$$

$$V(X) = E(X^2) - \big(E(X)\big)^2$$

$$= \int_{-\infty}^{\infty} \frac{x^2 e^{-\frac{x-\mu}{s}}}{s\left(1+e^{-\frac{x-\mu}{s}}\right)^2} dx - \mu^2 = \frac{s^2\pi^2}{3} \tag{3.89}$$

where, $E(X)$ and $V(X)$ are mean and variance.

3.5.4.1.3 Gamma Distribution

The gamma distribution is extensively applied in statistics because it depends on normal and exponential distributions. Like the logistic distribution, it is defined as two-parametric distribution of continuous probability. Chi-squared, Erlang and exponential distributions are called special cases of the gamma distribution (J et al., 2019). The general formula for the pdf of the gamma distribution is expressed as

$$f_{(x)} = \frac{\left(\frac{x-\mu}{\beta}\right)^{\gamma-1} exp\left(-\frac{x-\mu}{\beta}\right)}{\beta\Gamma(\gamma)} \qquad x \geq \mu; \gamma, \beta > 0 \tag{3.90}$$

where, $\gamma, \beta,$ and μ represent shape, location, and scale parameter. Γ is the gamma function which is expressed by

$$\Gamma(a) = \int_0^{\infty} t^{a-1} e^{-t} dt \tag{3.91}$$

If $\beta = 1$ and $\mu = 0$, it is defined as the standard gamma distribution and its equation is written as

$$f_{(x)} = \frac{x^{\gamma-1} e^{-x}}{\Gamma(\gamma)} \qquad x \geq 0; \gamma > 0 \tag{3.92}$$

The cdf of gamma distribution has the formula

$$F(x) = \frac{\Gamma_x(\gamma)}{\Gamma(\gamma)} \quad x \geq 0; \gamma > 0 \tag{3.93}$$

where, Γ is defined above and Γ_x(a) is called as incomplete gamma function. Its formula is

$$\Gamma(a) = \int_0^x t^{a-1} e^{-t} dt \tag{3.94}$$

The hazard function of gamma distribution is

$$h_{(x)} = \frac{x^{\gamma-1} e^{-x}}{\Gamma(\gamma) - \Gamma_x(\gamma)} \qquad x \geq 0; \gamma > 0 \tag{3.95}$$

The cdf of hazard function is obtained as

$$H_{(x)} = -log\left(1 - \frac{\Gamma_x(\gamma)}{\Gamma(\gamma)}\right) \qquad x \geq 0; \gamma > 0 \tag{3.96}$$

Parameter estimation of the two-parametric gamma distribution is performed with a different statistical method. The maximum likelihood method is largely used to estimate parameter as

$$\hat{\beta} = \frac{\bar{x}}{\hat{\gamma}} = 0,$$

$$log\hat{\gamma} - \psi(\hat{\gamma}) - log\left(\frac{\bar{x}}{(\prod_{i=1}^{n} x_i)^{\frac{1}{n}}}\right) = 0 \tag{3.97}$$

Where $\bar{x}$ and s are the sample mean and standard deviation, ψ is called as the digamma function. In order to overcome solving these equations, statistical software is needed (EL-Sagheer, 2018).

3.5.4.1.4 Exponential Distribution

The exponential distribution is generally used for another continuous distribution to observe the time for an event to happen. For instance, in engineering, it is performed to observe the time related to receiving a defective part on an assembly line. For physics, it is usually applied to observe radioactive decay. In Finance it is generally employed to measure the likelihood of the next default for a portfolio of financial assets (Kissell and Poserina, 2017). The pdf of the exponential distribution is

$$f(x) = \frac{1}{\beta} e^{-\frac{(x-\mu)}{\beta}} \qquad x \geq \mu; \beta > 0 \tag{3.98}$$

where β and μ are called as scale parameter and location parameter, respectively and scale parameter is generally denoted as $1/\beta$. If $\beta = 1$ and $\mu = 0$, it is referred to the standard exponential distribution. The formula of standard exponential has form

$$f(x) = e^{-x} \qquad for\ x \geq 0 \tag{3.99}$$

The cdf of exponential distribution is given by

$$F(x) = 1 - e^{-\frac{x}{\beta}} \qquad for\ x \geq 0; \beta > 0 \tag{3.100}$$

The hazard and cdf hazard are obtained for exponential distribution by

$$h(x) = \frac{1}{\beta} \qquad for\ x \geq 0; \beta > 0,$$

$$H(x) = \frac{x}{\beta} \qquad for\ x \geq 0; \beta > 0 \tag{3.101}$$

3.5.4.1.5 Weibull Distribution

The Weibull distribution, proposed by the Swedish physicist Waloddi Weibull, is one of the most frequently applied in different areas. It defines the measured failure of some various classes of phenomena and components (Lai et al., 2006). The pdf of Weibull distribution is

$$f(x) = \frac{\gamma}{\alpha}\left(\frac{x-\mu}{a}\right)^{\gamma-1} exp\left(-\left(\frac{x-\mu}{a}\right)^{\gamma}\right) \qquad x \geq \mu; \gamma, a > 0 \tag{3.102}$$

where α, μ and γ denote scale, location and shape parameter. If $a = 1$ and $\mu = 0$, it is referred to as the standard Weibull distribution and if $\mu = 0$, it is called the two-parametric Weibull distribution. The formulation of standard Weibull distribution is given by

$$f(x) = \gamma x^{(\gamma-1)} exp\left(-(x^{\gamma})\right) \quad x \geq 0; \gamma > 0 \tag{3.103}$$

The cdf of Weibull distribution is

$$F(x) = 1 - e^{-\left(\frac{x^{\gamma}}{a}\right)} \qquad x \geq 0; \gamma > 0 \tag{3.104}$$

The hazard and cdf of hazard function for Weibull distribution is obtained as

$$h(x) = \gamma x^{(\gamma-1)} \quad x \geq 0; \gamma > 0,$$

$$H(x) = x^{\gamma} \quad x \geq 0; \gamma > 0 \tag{3.105}$$

3.5.4.1.6 Normal (Gaussian) Distribution

Normal distribution plays an important role in statistics and is generally applied in the social sciences. In natural sciences, it demonstrates real-valued random variables when their distribution is not clear. Normal distribution, often referred as Gaussian, Laplace-

Gauss and Gauss, is 2-parametric continuous probability distribution (Lyon, 2014). The pdf of normal distribution is expressed as

$$f(x) = \frac{e^{-\frac{(x-\mu)^2}{2\sigma^2}}}{\sigma\sqrt{2\pi}} \tag{3.106}$$

Here, μ represents mean and σ denotes standard deviation. The case where $\mu \to 0$ and $\sigma \to 1$ is referred to the standard normal distribution and its equation is shown by

$$f(x) = \frac{e^{-\frac{x^2}{2}}}{\sqrt{2\pi}} \tag{3.107}$$

The cdf of standard normal distribution is

$$F(x) = \int_{-\infty}^{x} \frac{e^{-\frac{x^2}{2}}}{\sqrt{2\pi}} \tag{3.108}$$

The hazard function is written as

$$h(x) = \frac{\emptyset(x)}{\Phi(-x)} \tag{3.109}$$

where Φ denotes the probability density function and $\emptyset$ represents the cumulative distribution function of the standard normal distribution.

3.5.4.2 Goodness-of-Fit Tests

The goodness of fit tests (GoF) is performed to test if a variable fits a distribution from a certain population. In order words, these tests figure out which distribution is appropriate for random data. There are various methods for evaluating the goodness of fit test. In this study, the most popular include Anderson-Darling (AD) (Stephen, 1974), Kolmogorov-Smirnov (K-S) (Smirnov, 1948), Cramer-von Mises (CvM), Akaike's Information Criterion (AIC) (Akaike, 1976), Bayesian Information Criterion (BIC) (Stone, 1979), and Maximum likelihood (ML) methods.

3.5.4.2.1 Anderson-Darling Test

Anderson -Darlin Test (Stephens, 1974) can be performed to any distribution and also evaluated if a random variable came from a population with a specific distribution. It is derived from the Kolmogorov-Smirnov (K-S) test and provides more weight to the tails than the K-S test (Marsaglia and Marsaglia, 2004). For the lognormal and normal, Weibull and Gumbel distributions, A^2 test statistic can be obtained as

$$A^2 = -n - \left(\frac{1}{n}\right)\sum_{i=1}^{n}(2i-1)[ln(w_i) + ln(1-w_{n-i+1})] \quad (3.110)$$

where w is the standard normal cdf ($\Phi\left[\frac{(x-\mu)}{\sigma}\right]$), and n is the sample size. This equation should be modified for small size for lognormal and normal distribution

$$A_m^2 = A^2\left(1 + \frac{0.75}{n} + \frac{2.25}{n^2}\right) \quad (3.111)$$

For Weibull and Gumbel distribution

$$w_i = F(x) = 1 - \exp\left(-\left(\frac{x_i}{n}\right)^{\beta}\right) \quad (3.112)$$

where n, β denotes the model scale and shapes parameters.

3.5.4.2.2 Kolmogorov-Smirnov (K-S) Test

Kolmogorov-Smirnov Test, developed by Kolmogorov and (Smirnov, 1939), is not strong against differences in the tails of distributions. The directional hypotheses are calculated

$$D^+ = max\{F_{(x)} - G_{(x)}\}$$
$$D^- = min\{F_{(x)} - G_{(x)}\} \quad (3.113)$$

where, $F_{(x)}\ and\ G_{(x)}$ represents the empirical distribution function for the data compared and the combined statistic is given by

$$D = max(|D^+|, |D^-|) \quad (3.114)$$

The *p*-value for this theoretical statistic can be demonstrated by calculating the asymptotic limiting distribution.

$$\lim_{m,n\to\infty} Pr\left\{\sqrt{\frac{mn}{(m+n)}}D_{m,n} \le z\right\} = 1 - 2\sum_{i=1}^{\infty}(-1)^{i-1}exp(-2i^2z^2) \quad (3.115)$$

A corrected *p*-value is obtained as

$$Z = \Phi^{-1}(P_a) + \frac{1.04}{\min(m,n)} + \frac{2.09}{\max(m,n)} - \frac{1.35}{\sqrt{\frac{mn}{(m+n)}}},$$

$$p\text{-value} = \Phi(z) \quad (3.116)$$

where, $\Phi(.)$ is the cumulative distribution function.

3.5.4.2.3 Cramer-von Mises (CvM) Test

Cramer-von Mises test copes with the modeling of a probability distribution of a sample vector $X = (X^1, \dots, X^{nx})$. It investigates to confirm the compatibility between a random data $\{x_1, x_{2,} \dots., x_N\}$ and a candidate probability distribution previously is chosen (Laio, 2004). The Cramer-von Mises distance is

$$D = \int_{-\infty}^{\infty} \big(F(x) - F_0(x)\big)^2 dF_0(x) \tag{3.117}$$

This test is related to the distance between the cumulative distribution function F_0 and candidate distribution called F. For testing the hypothesis, $H_o \rightarrow F = F_0$. The test statistic mathematically is expressed by

$$\widehat{D_N} = \frac{1}{12N} + \sum_{i=1}^{N} \left[\frac{2i-1}{2} - F(x_i)\right]^2 \tag{3.118}$$

where $\widehat{D_N}$ is the probability distribution distance, and is asymptotically known with N denoting the sample size.

If $\widehat{D_N} > d_a$, it rejects the candidate distribution with risk of error a.

If $\widehat{D_N} \leq d_a$, the candidate distribution is not rejected.

3.5.4.2.4 Akaike's Information Criterion (AIC) Test

Akaike's Information Criterion (AIC) (Akaike, 1976), is another way to select the appropriate model between selected models. The selected model shows minimum distance between the truth and the model (Burnham and Anderson, 2002). This test is based on information theory and it is calculated as

$$AIC = -2\big(ln(likelihood)\big) + 2K \tag{3.119}$$

where likelihood represents the probability of a variable given a model, K denotes the number of free parameters in the model. AICc is referred to as the second-order information criterion considering sample size and it is obtained as

$$AICc = -2\big(ln(likelihood)\big) + 2K \times \left(\frac{n}{n-K-1}\right) \tag{3.120}$$

where n is the sample size.

3.5.4.2.5 Bayesian Information Criterion (BIC) Test

Bayesian Information Criterion (BIC) (Stone, 1979), is another way to select suitable models among a finite set of them. In general, BIC is different from AIC especially in the second term which is related to sample size and calculated as

$$BIC = -2logp(L) + plog(n) \tag{3.121}$$

Where p is the number of estimated parameter, and n is the number of the observations. Here, the minimum AIC and BIC are chosen as the best model.

3.5.4.2.6 Maximum likelihood (ML) Method

The maximum likelihood (ML) method, developed by Sir. R. A. Fisher, a well-known statistician and geneticist, finds a suitable approach to parameter prediction problems (Schwarz, 2011). The main advantage of using ML is that it extracts all the useful information from data. Consider a sample $y = [y_1 \ \dots y_i \ \dots \ y_n]$ from the population. Pdf (or the probability density function) of a random variable y_i conditioned on parameters θ is written by $f(y_i, \theta)$. The joint density of *n* identically and individually disturbed observation is expressed as

$$f(y, \theta) = \prod_{i=1}^{N} f(y_i, \theta) = L(\theta|y) \tag{3.122}$$

And first term $f(y_i, \theta)$ can be obtained as

$$f(y_i, \theta) = f(y_i, \mu|\sigma^2 = 1) = \frac{1}{\sqrt{2\pi\sigma^2}} \, e^{\frac{-(y_i-\mu)^2}{2\sigma^2}} \tag{3.123}$$

It is general practice to study with the Log-Likelihood function.

$$L(\theta|y) = \sum_{i=1}^{N} ln\left(\frac{1}{\sqrt{2\pi\sigma^2}} \, e^{\frac{-(y_i-\mu)^2}{2\sigma^2}}\right) \tag{3.124}$$

It is showed how varying the value of μ, permits the determination of the maximum log-likelihood value for the mean of random variables *y*.

3.5.5 Return Period (Joint and Conditional)

A general approach to management of water resources systems, hydrologic, and hydraulic facilities is to the estimation of return periods of drought characteristics (Shiau and Shen, 2001). Particularly, drought return periods give crucial information

under drought conditions. Univariate return of drought duration greater than or equal to a certain value can be calculated as

$$T_D = \frac{E(L)}{1-F_D(d)} \tag{3.125}$$

Where L is expected drought interval time, T_D is the return period defined solely by drought duration. The return period of drought severity, greater than or equal to a certain value, can be obtained using the same formula defined as

$$T_S = \frac{E(L)}{1-F_S(s)} \tag{3.126}$$

Joint drought duration and severity can be estimated in two cases: return period for D ≥ d and S ≥ s and joint return period for D ≥ d or S ≥ s, which is stated by T_{DS} and T'_{DS}, respectively as follows

$$T_{DS} = \frac{E(L)}{P(D \geq d,\ S \geq s)} = \frac{E(L)}{1-F_D(d)-F_S(s)+F_{DS}(d,s)} = \frac{E(L)}{1-F_D(d)-F_S(s)+C(F_D(d),F_S(s))} \tag{3.127}$$

$$T'_{DS} = \frac{E(L)}{P(D \geq d \text{ or } S \geq s)} = \frac{E(L)}{1-F_{DS}(d,s)} = \frac{E(L)}{1-C(F_D(d),F_S(s))} \tag{3.128}$$

Where $F_S(s)$ and $F_D(d)$ are CDFs of univariate of drought severity, duration, and C is any type of copula.

The conditional probability of drought severity with drought duration exceeding various threshold values is showed by d'.The conditional probability of drought duration with drought severity exceeding various threshold values is showed by s'. The conditional probabilities are obtained as follows

$$P(S \leq s \mid D \geq d') = \frac{P(D \geq d', S \leq s)}{P(D \geq d')} = \frac{F(s)+F(d',s)}{1-F(d')} = \frac{F_s(s)-C(F_D(d'),F_S(s))}{1-F_D(d')} \tag{3.129}$$

Similarly

$$P(D \leq d \mid S \geq s') = \frac{P(D \leq d, S \geq s')}{P(S \geq s')} = \frac{F(d)-F(d,s')}{1-F(s')} = \frac{F_D(d)-C(F_D(d),F_S(s'))}{1-F_S(s')} \tag{3.130}$$

The conditional drought duration and severity return period can also be derived as conditional situations for the following two cases: the return period of drought severity given drought duration exceeding a certain threshold, and the return period of drought duration given a drought severity that exceeds a certain threshold. Both conditional return period defined by Shiau, (2006) based on copula theory are indicated below,

$$T_{D|S\geq s}=\frac{T_S}{P(D\geq d,\ S\geq s)}=\frac{E(L)}{[1-F_S(s)][1-F_D(d)-F_S(s)+C(F_D(d),F_S(s))]} \quad (3.131)$$

$$T_{S|S\geq d}=\frac{T_D}{P(D\geq d,\ S\geq s)}=\frac{E(L)}{[1-F_D(d)][1-F_D(d)-F_S(s)+C(F_D(d),F_S(s))]} \quad (3.132)$$

CHAPTER FOUR

STUDY AREA CEYHAN BASIN

4.1 Overview

In Turkey, the mean annual precipitation is 643 mm, which corresponds to an average of 501 billion m³ of water per year. 186 billion m³ of this amount flows to various seas, rivers, and lakes in closed basins. In addition, there are 7 billion m³ of water coming from neighboring countries. Thus, the renewable surface freshwater potential of our country is about 193 billion m^3. Turkey's 77.95 million hectares, which occupies approximately one-third of the surface area of 28.05 million hectares, constitutes as part of the arable land.25.85 million hectares of this land consists of irrigable land. However, as a result of the studies conducted, the amount of economically irrigable land in today's conditions has been determined as 8.5 million hectares (Turan, 2002).

Turkey is divided into 26 hydrological basins. Six of them, Meriç-Ergene, Asi, Çoruh, Aras, Dicle, Fırat Basin, are within the scope of trans boundary waters. The annual average water potentials of these basins are provided with their respective order; 1.33 billion m³, 1.17 billion m³, 6.30 billion m³, 4.63 billion m³, 21.33 billion m³, and 31.61 billion m³. In addition to this, trans boundary waters are of great importance considering the geopolitical situation of the geographical region in which our country is located.

Due to the vast increase in the global population, the studies related to the supply and use of water is compulsory to care for the development and use of new technologies and methods, which can be achieved with the help of experienced and qualified personnel and sufficient financing resources. In Turkey, precipitation-flow relationships, which vary according to the seasons throughout the year, also show great differences between each respective year. As a result, the management of water

is vital to meet the needs that change depending on time and quantity. As a result of this process, during its peak levels in the summer months, natural water supply decreases to a minimum level. In addition, there are periodic droughts that cause significant problems, as the ongoing one right now which is in its 15th year. In order to meet the needs of these periods, storage facilities are being built by developing projects for water reserves for dry periods.

In this chapter, comprehensive information about the study area and data will be given in detail. The Ceyhan Basin, which is critical basin in Turkey for agriculture, is selected for both hydro-climatic parameter trend analysis and drought monitoring.

4.2 Study Area and Used Data

The Ceyhan basin is located between latitudes of 36º30′ and longitudes of 35º20′ in the eastern Mediterranean region of Turkey. It is bordered by the Asi basin in the south the Seyhan Basin in the west and northwest, and the Euphrates in the east and northeast (Fig.4.1) (Tanrıverdi et al., 2010). The Ceyhan basin, covering an area of about 20.670 km^2, includes three main provinces: Adana, Kahramanmaraş, and Osmaniye. An areal description by province is demonstrated in Table 4.1. According to the rainfall regime of the Mediterranean climate type in Ceyhan Basin, the rainiest season is winter (December, January, February), and the least rainfall in summer (June, July, August). The basin is under the influence of different pressure centers. However, the influence of these pressure centers varies during the year. The climate of the Ceyhan basin is of arid environment, where rainfalls are infrequent with short duration in summer. The annual depth of evaporation is low, varying from 0 mm to 325 mm. Evaporation increases especially in summer, especially in June, July and August. On the contrary, evaporation decreases in winter in the months of in December, January, and February. The total length of the Ceyhan River is 425 km, an annual discharge of 82.9 m^3 / sec, and basin yield of 10.7 L / h / km^3. The total annual rainfall in Kozan is at least 842 mm, and the lowest rainfall area of the basin is in Elbistan with 395.7 mm. The average annual temperature is at most in Kozan (19.3 ° C) and the least in Göksun (8.9 ° C) (Uzunkol and Kızılelma, 2016).

The Ceyhan River flowing through narrow and deep valleys has become a very favorable situation for the construction of hydroelectric power plants. Three hydroelectric power plants have been built on the river. Menzelet, the largest of these

power plants, was completed in 1992. The Sır Dam and HEPP Dam, which started production in 1991, is operated by the Çukurova Power Corporation. The oldest hydroelectric power plant in the province of Kahramanmaraş Province is the Ceyhan Hydroelectric Power Plant, which started electricity generation in 1958.

Table 4.1 Areal distribution of Provinces in Ceyhan Basin

Province	Part of the Province Area in the Basin (%)	Distribution of the Basin by Provinces (%)
Kayseri	2.24	1.76
Osmaniye	80.6	14.13
Sivas	1.61	2.14
Adiyaman	0.22	1.71
Gaziantep	0.34	1.89
Malatya	0.88	0.5
Adana	27.67	18.35
Hatay	0.03	0.01
K.Maraş	89.26	59.51

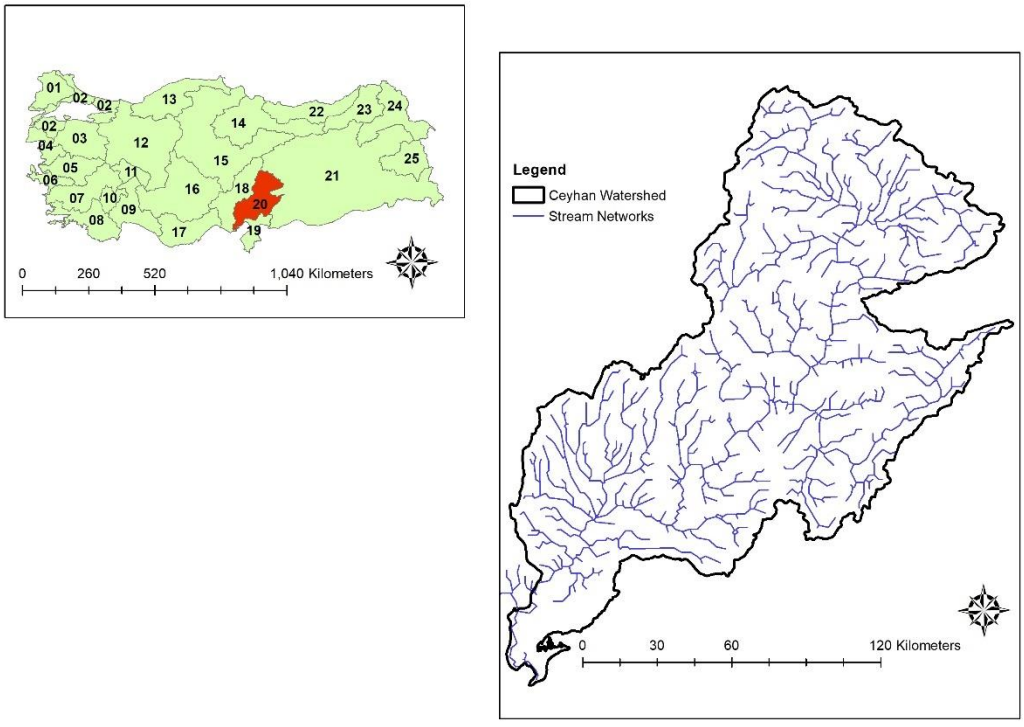

Figure 4.2 The location of Ceyhan Basin on the map

A total of 24 gauging stations, distributed evenly, were selected in the Ceyhan basin and its surrounding areas (Fig. 4.2). The monthly precipitation data were obtained from the National General Directorate of Meteorology and State Hydraulic Works (DSI). The DSI, funded by the Central Government Budget, "is responsible for the planning,

management, development, and operation of all water resources in Turkey." The Environmental impact assessment studies for energy, irrigation, and drainage projects are within the scope of the environmental sector governed by the DSI General Directorate. With the assistance of the Ministry of Environment and other organizations, the following projects are ongoing: preparation of pollution research projects water pollution atlases on basins, preparation of data and reports, and monitoring the surface and groundwater resources throughout the country.

The location of the observed corresponding 24 stations is displayed in Figure 4.3. The statistical parameters for the 24 rain gauge stations are also presented in Table 4.2. Gauging stations are selected at different branches throughout the Ceyhan Basin to get more accurate information about basin characteristics.

Table 4.2 The statistical parameters of observed rainfall stations; S.D., standard deviation; Cv, coefficient of variance; Cs, skewness; r1, kurtosis

Station	Earliest record year	Latest record year	Latitude	Longitude	Mean (mm)	St. Dev.	Cv	Cs	r1
7767	1998	2012	37.3575	36.0907	65.64	55.53	0.85	1.06	0.26
8275	1964	1995	37.0901	36.3094	85.75	83.87	0.98	1.28	0.39
17255	1963	2016	37.5760	36.9150	60.39	65.57	1.09	1.27	0.50
17355	1986	2016	37.1021	36.2539	69.10	63.75	0.92	1.12	0.33
17866	1963	2011	38.0240	36.4823	51.19	46.29	0.90	1.07	0.39
17868	1970	2011	38.2405	36.9190	35.31	31.16	0.88	0.99	0.34
17870	1963	2011	38.2038	37.1982	33.30	28.87	0.87	0.97	0.33
17871	1993	2011	37.7867	37.6532	60.15	66.40	1.10	1.55	0.46
17908	1963	2011	37.4337	35.8188	70.24	58.79	0.84	1.11	0.23
17960	1964	2011	37.0153	35.7955	59.00	58.64	0.99	1.43	0.33
17979	1964	2011	36.7687	35.7903	67.54	70.99	1.05	1.55	0.33
D20M001	1963	2009	38.3000	37.5833	29.13	26.70	0.92	1.12	0.31
D20M002	1980	2005	37.5458	36.7747	58.40	66.96	1.15	1.51	0.42
D20M004	1970	1988	37.3833	37.1666	41.15	41.77	1.02	0.96	0.42
D20M006	1963	1974	37.1666	35.7000	53.98	60.21	1.12	1.85	0.30
D20M009	1963	2009	37.8833	36.8500	78.89	81.62	1.03	1.28	0.44
D20M011	1963	1996	38.6166	36.9333	32.32	29.73	0.92	1.28	0.27
D20M013	1968	2015	37.4666	37.2500	50.28	54.04	1.07	1.36	0.41
D20M014	1973	2015	37.3352	36.0056	90.27	78.25	0.87	1.15	0.25
D20M015	1976	2015	37.0500	36.0666	76.15	66.45	0.87	1.12	0.28
D20M016	1977	2015	37.5000	35.8333	78.27	69.64	0.89	1.25	0.25
D20M017	1980	2003	38.1520	36.4654	65.48	65.48	1.00	1.43	0.33
D20M018	1982	2002	38.2918	36.7604	25.09	28.13	1.12	2.29	0.19
D20M020	1990	2015	37.1500	36.4500	64.72	59.47	0.92	1.06	0.27

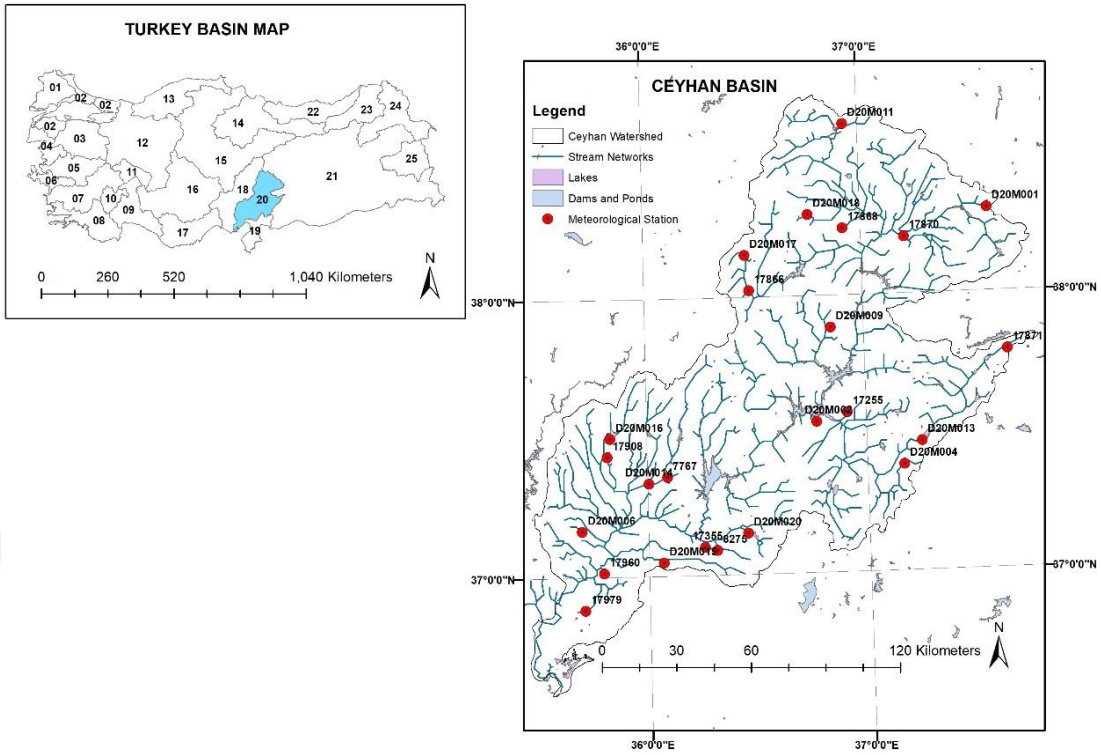

Figure 4.3 The location of the meteorological stations in the Ceyhan Basin

Besides being a significant parameter of the hydrological cycle, temperature is important with regards to climate change. It is also a crucial factor in world energy balance, sweating, evaporation, and droughts, etc. Hence, temperature data, obtained from the National General Directorate of Meteorology, are also analyzed in terms of monthly min, max, and average value. The statistical properties of seven meteorological stations for temperature data are presented in Table 4.3 and their positions are presented in Figure 4.4.

Table 4.3 The statistical parameters of observed temperature data; S.D., standard deviation; Cv, coefficient of variance; Cs, skewness; r1, kurtosis

Stations	Earliest record year	Latest record year	Statistical Parameters	Tmin	Tmax	Tavg
17255	1963	2018	Mean	6.57	28.92	16.77
			St. Dev.	8.33	9.46	8.58
			Cv	1.27	0.33	0.51
			Cs	0.13	-0.21	-0.03
			r1	0.81	0.83	0.85
17355	1986	2018	Mean	7.32	30.95	18.56
			St. Dev.	8.07	7.28	7.12

			Cv	1.10	0.24	0.38
			Cs	0.10	-0.34	-0.02
			r1	0.81	0.78	0.84
			Mean	-5.11	22.29	8.97
			St. Dev.	10.31	9.38	8.73
17866	1963	2018	Cv	-2.02	0.42	0.97
			Cs	-0.78	-0.29	-0.20
			r1	0.75	0.82	0.83
			Mean	-2.87	23.33	10.58
			St. Dev.	9.48	9.86	9.34
17868	1971	2018	Cv	-3.30	0.42	0.88
			Cs	-0.48	-0.29	-0.14
			r1	0.77	0.82	0.84
			Mean	-3.60	24.36	10.79
			St. Dev.	9.76	9.68	9.12
17870	1963	2018	Cv	-2.71	0.40	0.85
			Cs	-0.57	-0.28	-0.15
			r1	0.77	0.82	0.83
			Mean	9.45	31.85	19.45
			St. Dev.	6.91	7.72	7.01
17908	1963	2018	Cv	0.73	0.24	0.36
			Cs	0.05	-0.31	-0.06
			r1	0.80	0.80	0.84
			Mean	7.03	30.98	18.13
			St. Dev.	7.81	7.37	7.17
17960	1966	2018	Cv	1.11	0.24	0.40
			Cs	0.14	-0.37	-0.04
			r1	0.81	0.79	0.85
			Mean	10.17	29.07	19.07
			St. Dev.	7.19	6.40	6.25
17979	1964	2018	Cv	0.71	0.22	0.33
			Cs	0.04	-0.29	-0.05
			r1	0.81	0.75	0.84

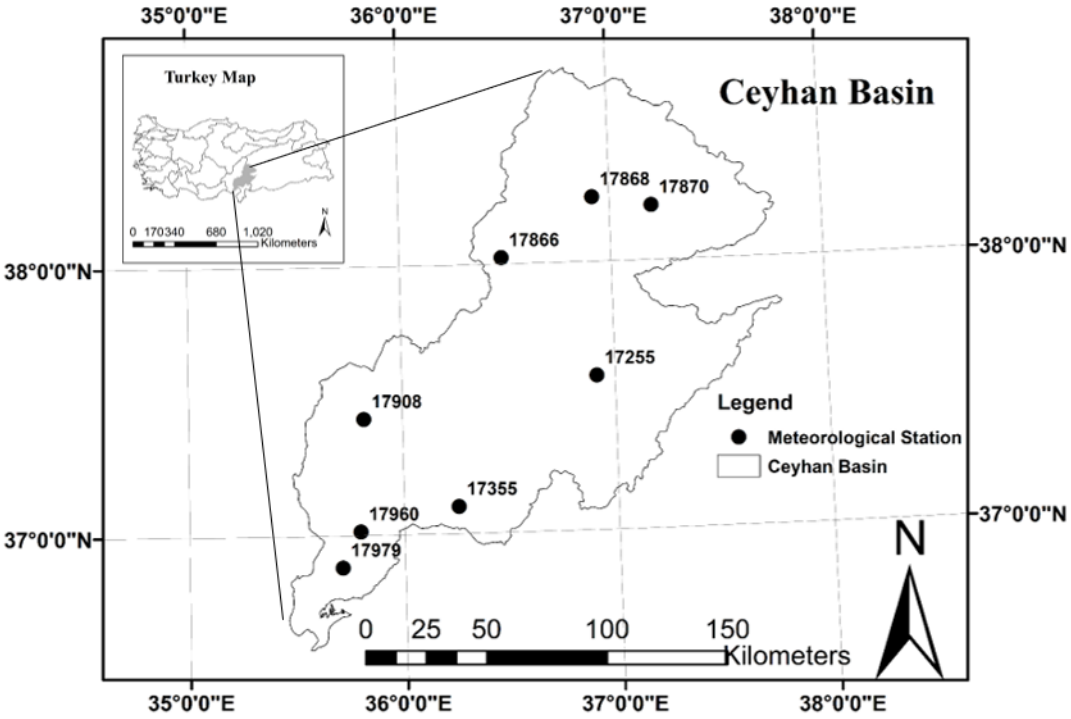

Figure 4.4 The location of the temperature data stations in the Ceyhan Basin

CHAPTER FIVE

INVESTIGATION OF DROUGHT INDICES ON CEYHAN BASIN

5.1 Overview

Drought may result in severe impact on the society and on the environments such as Dust bowls, carrying capacity of livestock, decreased crop growth, or yield production. These impacts provide discovering and detecting drought extremely crucial. Investigating of drought plays an important role in both science and art. Researcher analyses at both drought indicators and indices to provide a wide view of precipitation, rainfall, temperature, soil moisture deficiency over a location. All of these variables are combined to obtain the full drought picture.

Numerous drought indices have been proposed by scientists in the last century. Each drought indices are developed considering the hydrological, topological and climate situations of the location. Due to the region's hydro-climate complexity, while some drought indices perform with good results over a specific region, these indices do not apply for a different region. For example, the most appropriate index among popular indices is PDSI for the USA, whereas CZI and MCZI are shown more appropriately with applying to China. But SPI are accepted as a popular index among researchers because of its applicable, simplicity and data availability with using single parameter including precipitation variable. Hence, the other indices results are generally correlated and calibrated with the results of SPI.

In this thesis part, ten drought indices will be discussed on the Ceyhan Basin. These indices include Standard Precipitation Evaporation Index (SPEI), Standard Precipitation Index (SPI), Self-Calibrated Palmer Drought Severity Index (scPDSI), China Z-Index (CZI), modified (CZI), Reconnaissance Drought Index (RDI), Rainfall Anomaly Index (RAI)**,** Percent of Normal Index (PNI), Decile Index (DI) and Z-score Index (ZI), and calculate their performance corresponding with

historic drought events. According to statistical test results such as correlation tests including Mann-Kendall, Spearman Rho and Pearson, the most appropriate indices will be investigated. After getting indices, it will be compared in terms of drought categories considering normal, moderate, severity, extreme and wet. Finally, the Ceyhan Basin risk map will be spatially presented.

5.2 Time Series of the Drought Indices

The historical time series of the drought indices are obtained for all stations. Only the result obtained at 17255 station is given in Figure 5.1. Because of temperature data availability, scPDSI, SPEI and RDI are performed for eight stations including 17255, 17355, 17866, 17868, 17870, 17908, 17960 and 17979. Hence, the performance of drought indices is illustrated at monthly time series for RD, PN, CZI, MCZI, RAI, ZSI and scPDSI. Different time scales (3-, 6-, 9- and 12 month) are indicated to derive for SPEI, SPI and RDI indices.

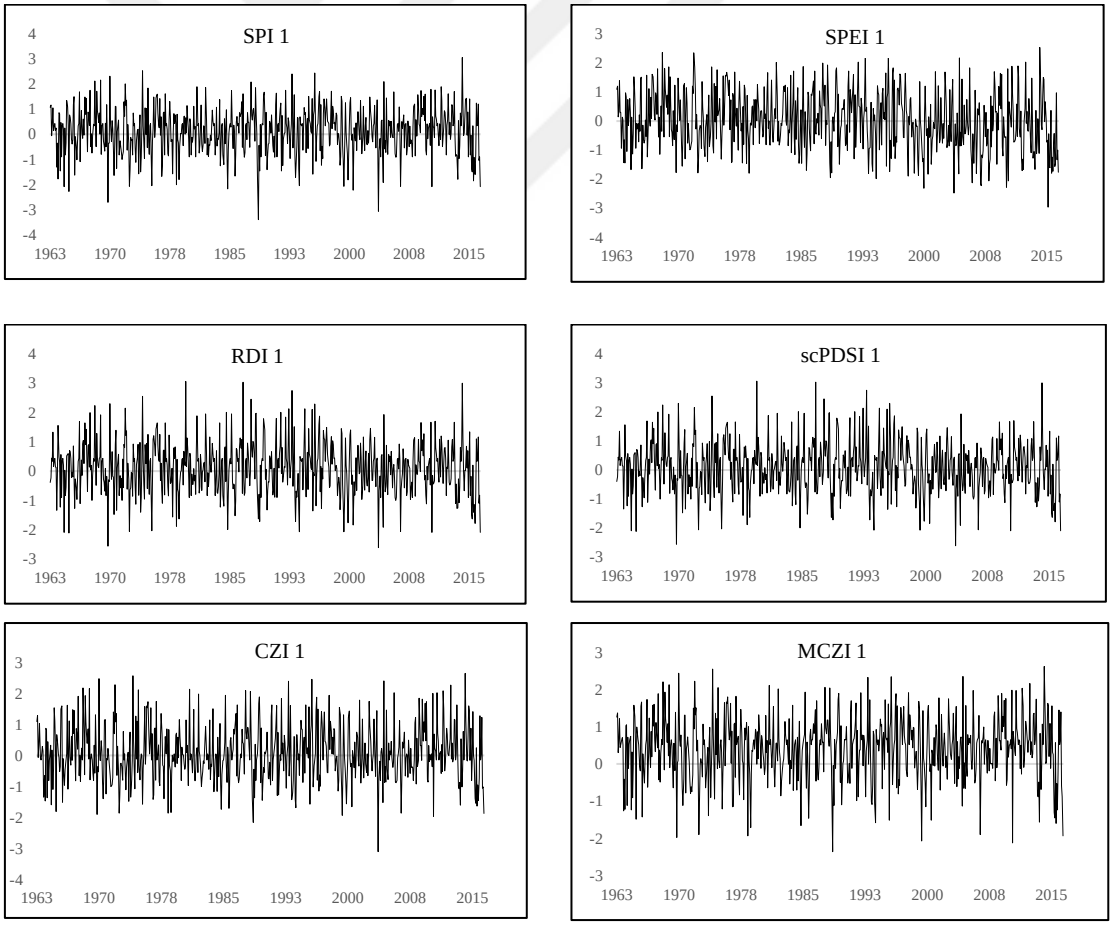

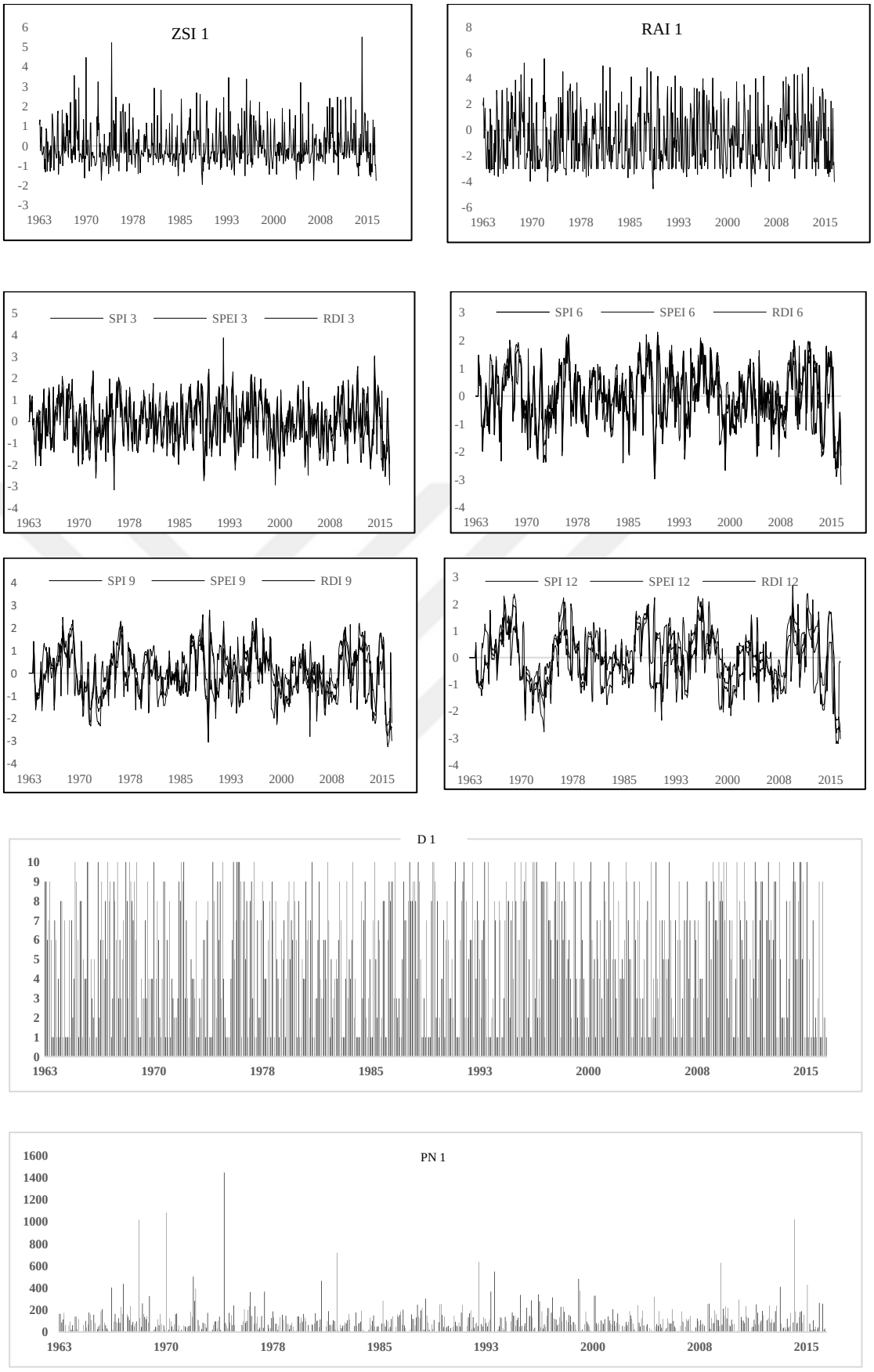

Figure 5.1 Time series plot of drought indices for 17255 station

5.3 Comparison of drought indices with the SPI

The SPI versus other used indices were calculated using three correlation tests (Mann-Kendall tau, Spearman rho and Pearson). Figure 5.2 indicates the linear regression the values of SPI versus the other indices for station 17255. According to results, three indices including MCZI, CZI and ZSI for 1-month time scale, have a perfect relationship, particularly during the dry and wet season. While the R^2 value of SPEI, RAI, RDI versus the SPI vary from 0.5 to 0.8 which is good relationships, the R^2 between scPDSI and SPI indicates poor relations for all stations.

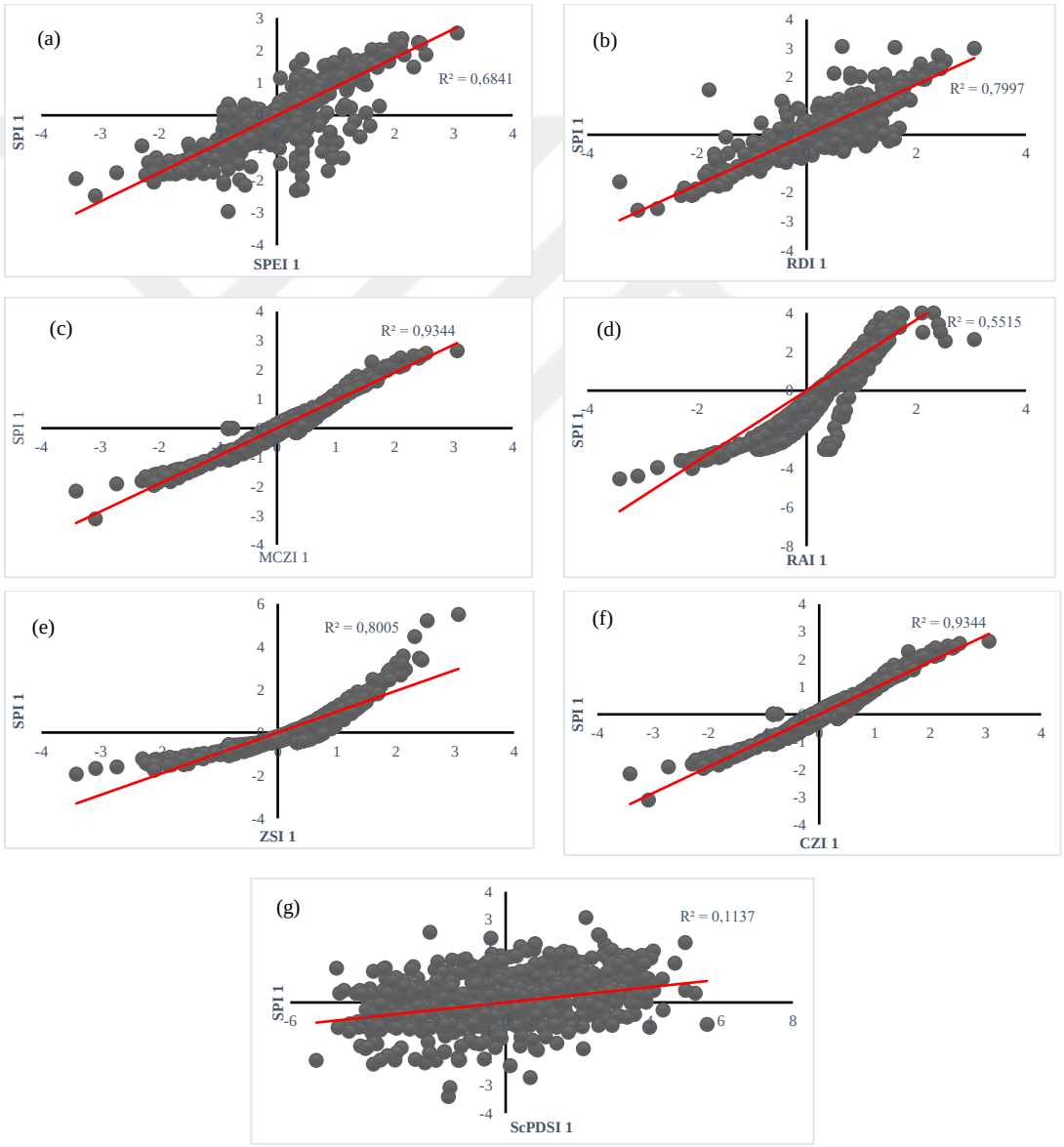

Figure 5.2 Scatter plots for selected drought deciles versus SPI for 17255 station from 1963-2016 (1-month)

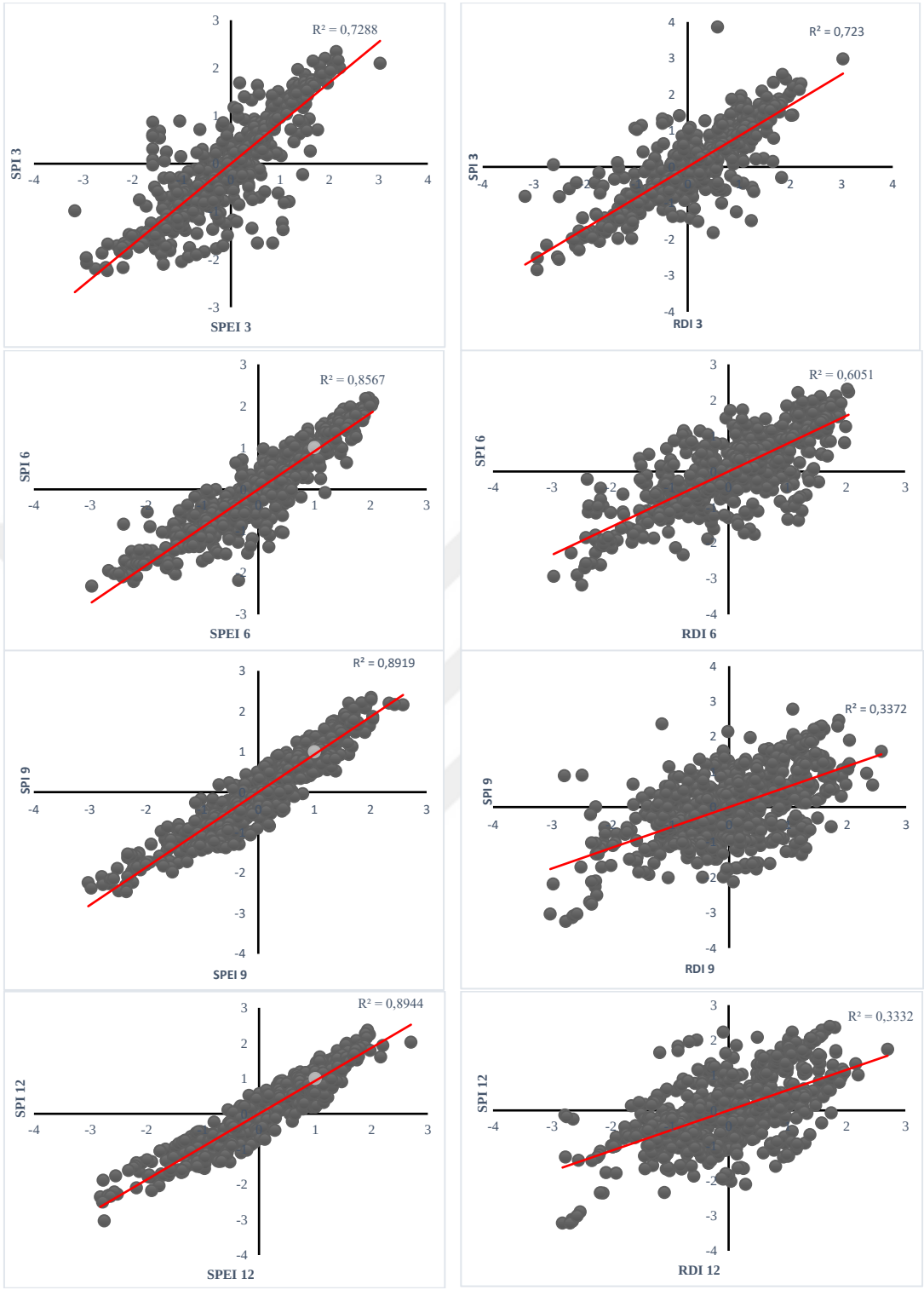

Figure 5.3 Scatter plots for selected SPEI and RDI versus SPI for 17255 station from 1963-2016 (3-, 6-, 9-, 12-month)

When different time series are evaluated for selected drought indices, SPI and SPEI indicates a good relationship in terms of R^2 value for 3-,6-,9- and 12- month. However, RDI shows poor relation versus SPI especially 9- and 12-month time series. When considered SPEI versus SPI at different time scales, two indices relation is below 0.67 at 1-month time scale, whereas these relations reveal over 0.75 at the 3-, 6-, 9- and 12-month time scale. Unlike SPEI, while RDI shows a good relation to versus SPI at 1-month, another time scales have lower R^2 value.

5.4 Correlation Analysis of Drought Indices

Correlation tests including Mann-Kendall, Spearman and Pearson, are applied to different time scale. While 24 gauging station are considered at 1-month time scale due to data availability, the multi-time scales are performed to three indices: SPI, SPEI and RDI. The correlation matrix considering three tests for the 17255 station as an example is presented in Table 5.1.

Table 5.1 The correlation matrix for 1-month scale drought indices for 17255

Kendall										
	RD	PN	CZI	MCZI	RAI	ZSI	SPI	SPEI	RDI	ScPDSI
RD	1.00	0.68	0.85	0.78	0.91	0.84	0.80	0.75	0.69	0.32
PN	0.68	1.00	0.71	0.63	0.84	0.84	0.66	0.58	0.61	0.24
CZI	0.85	0.71	1.00	0.96	0.90	0.95	0.97	0.85	0.84	0.38
MCZI	0.78	0.63	0.96	1.00	0.80	0.90	0.96	0.82	0.83	0.36
RAI	0.91	0.84	0.90	0.80	1.00	0.96	0.83	0.79	0.73	0.35
ZSI	0.84	0.84	0.95	0.90	0.96	1.00	0.90	0.82	0.79	0.37
SPI	0.80	0.66	0.97	0.96	0.83	0.90	1.00	0.83	0.87	0.36
SPEI	0.75	0.58	0.85	0.82	0.79	0.82	0.83	1.00	0.75	0.40
RDI	0.69	0.61	0.84	0.83	0.73	0.79	0.87	0.75	1.00	0.32
ScPDSI	0.32	0.24	0.38	0.36	0.35	0.37	0.36	0.40	0.32	1.00
Pearson										
	RD	PN	CZI	MCZI	RAI	ZSI	SPI	SPEI	RDI	ScPDSI
RD	1.00	0.84	0.74	0.68	0.87	0.77	0.72	0.64	0.56	0.23
PN	0.84	1.00	0.64	0.55	0.89	0.71	0.62	0.57	0.47	0.22
CZI	0.74	0.64	1.00	0.89	0.72	0.90	0.88	0.70	0.68	0.25
MCZI	0.68	0.55	0.89	1.00	0.62	0.81	0.88	0.68	0.70	0.25
RAI	0.87	0.89	0.72	0.62	1.00	0.80	0.69	0.63	0.52	0.23
ZSI	0.77	0.71	0.90	0.81	0.80	1.00	0.84	0.70	0.65	0.25
SPI	0.72	0.62	0.88	0.88	0.69	0.84	1.00	0.69	0.76	0.25
SPEI	0.64	0.57	0.70	0.68	0.63	0.70	0.69	1.00	0.58	0.27
RDI	0.56	0.47	0.68	0.70	0.52	0.65	0.76	0.58	1.00	0.21
ScPDSI	0.23	0.22	0.25	0.25	0.23	0.25	0.25	0.27	0.21	1.00
Spearman										
	RD	PN	CZI	MCZI	RAI	ZSI	SPI	SPEI	RDI	ScPDSI
RD	1.00	0.94	0.85	0.78	0.96	0.89	0.80	0.74	0.67	0.32
PN	0.94	1.00	0.77	0.68	0.98	0.85	0.72	0.68	0.60	0.31
CZI	0.85	0.77	1.00	0.97	0.84	0.97	0.96	0.84	0.84	0.37
MCZI	0.78	0.68	0.97	1.00	0.75	0.93	0.97	0.82	0.85	0.36
RAI	0.96	0.98	0.84	0.75	1.00	0.91	0.79	0.76	0.66	0.34
ZSI	0.89	0.85	0.97	0.93	0.91	1.00	0.95	0.85	0.81	0.37
SPI	0.80	0.72	0.96	0.97	0.79	0.95	1.00	0.83	0.89	0.36
SPEI	0.74	0.68	0.84	0.82	0.76	0.85	0.83	1.00	0.74	0.40
RDI	0.67	0.60	0.84	0.85	0.66	0.81	0.89	0.74	1.00	0.31
ScPDSI	0.32	0.31	0.37	0.36	0.34	0.37	0.36	0.40	0.31	1.00

It is important to report that the values of all used correlation coefficients with each other indicate much higher at 1-month time scale except with scPDSI. However, when the correlation tests are compared to each other, The Spearman coefficients values reveals much higher than the Mann-Kendall and Pearson coefficient. For example, SPI-1 with RDI-1 has Spearman coefficient (r) value 0.89 computed higher than Kendall and Pearson have 0.87 and 0.76, respectively. However, scPDSI correlation coefficient values considering three tests with other indices indicate much lower than 0.5 due to input parameters complexity. While SPEI and RDI indicated a good correlation mostly greater than 0.6, also consider the temperature data with precipitation data as input parameters, scPDSI does not perform a good relationship with other indices. It can be clearly seen ten drought indices in terms of Spearman coefficient values in Figure 5.4.

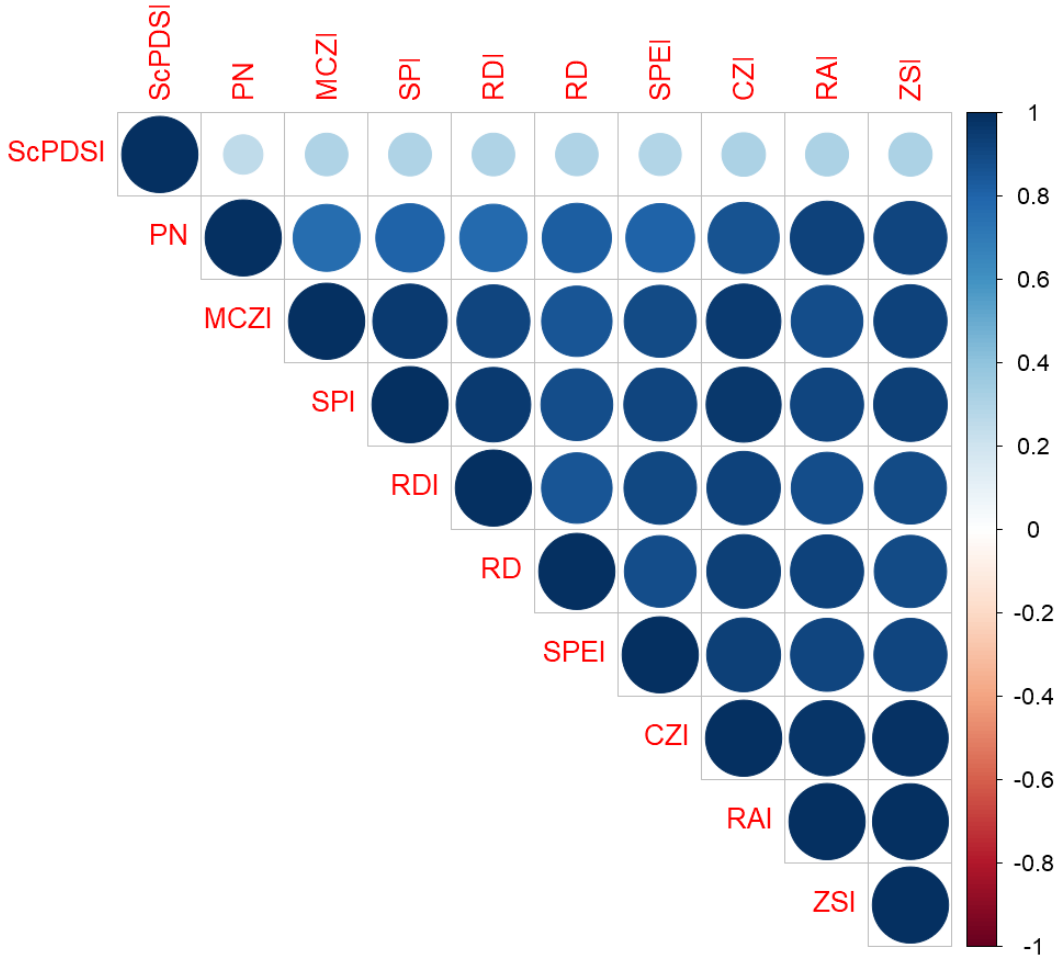

Figure 5.4 The correlation circle for 1-month scale considering Spearman coefficient for station 17255

Multi-time scales are performed only SPI, SPEI and RDI drought indices for eight gauging station. Hence, drought severity value using three indices for 3-, 6-, 9- and 12-month time steps are evaluated and also the correlation between three indices of different time steps is calculated. A reference station (17255) as an example is chosen to identify the correlation of different time step (Figure 5.5). The results show that SPI and SPEI for different time steps are mostly higher correlated and correlations coefficients range between 0.85 to 0.95. Unlike SPI and SPEI, RDI-3 has much higher correlation coefficient (0.85) as compared to the RDI-6 (0.78), 9 (0.58)- and 12 (0.58). It is suggested that the correlation of SPI and SPEI is very strong (r >0.85) at all different time steps. Generally, the findings indicate that an increase in the correlation as the time scale increase for the SPI and SPEI. For instance, correlation of SPI-3 with SPEI-3 is equal to 0.85. Likewise, values of correlation coefficient of SPI-6&SPEI-6, SPI-9&SPEI-9 and SPI-9&SPEI-9 are 0.93, 0.94 and 0.95, respectively. it can be concluded that higher time steps show stronger correlation between two indices.

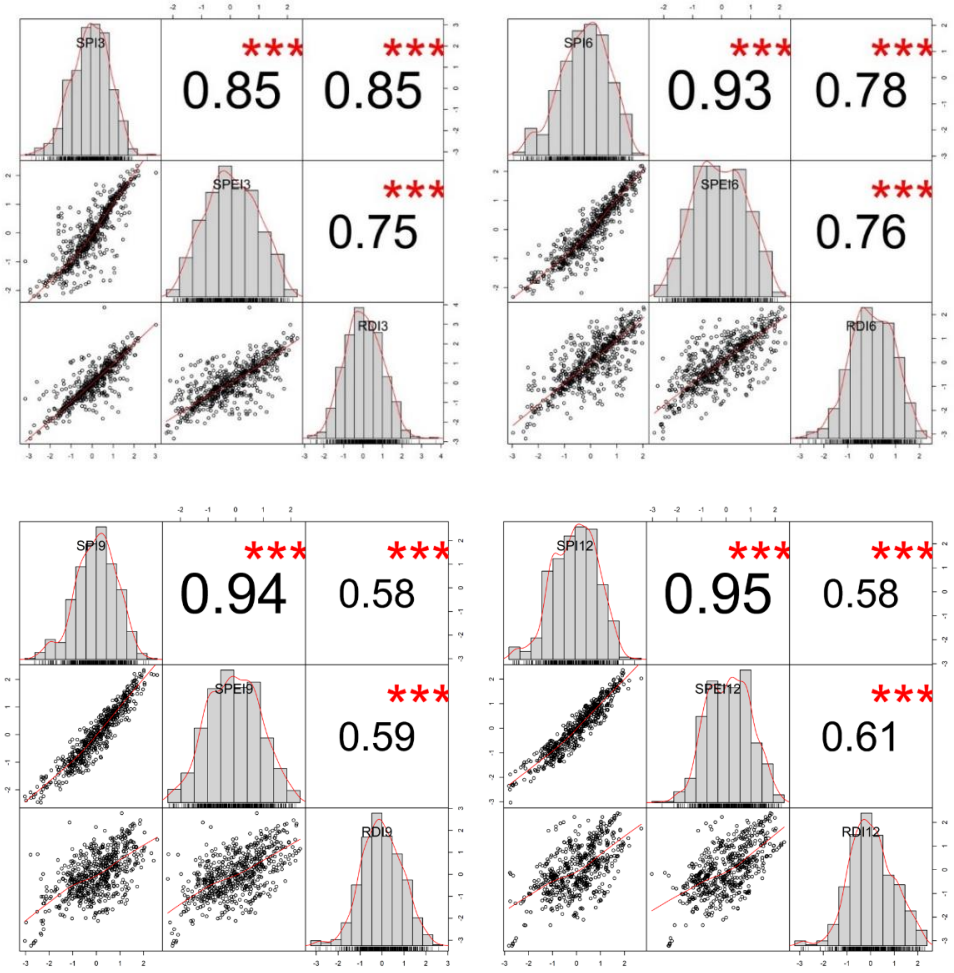

Figure 5.5 The correlation coefficients for multi-time time series for station 17255

Spider chart that enables to plot one or more time series, are used to identify and each data has its own axis then, all axes are combined in the middle of chart. These charts are conducted for the ten drought indices for all stations at 1-month time scale (Figure 5.6). The relationships between each drought deciles at 1-month time scale indicate highly correlated except scPDSI where it shows low correlation coefficient at all selected station. According to severity categories, SPI, SPEI and RDI correlate well as compared the other indices. Therefore, three indices are performed at various time steps (3-, 6-, 9- and 12-month).

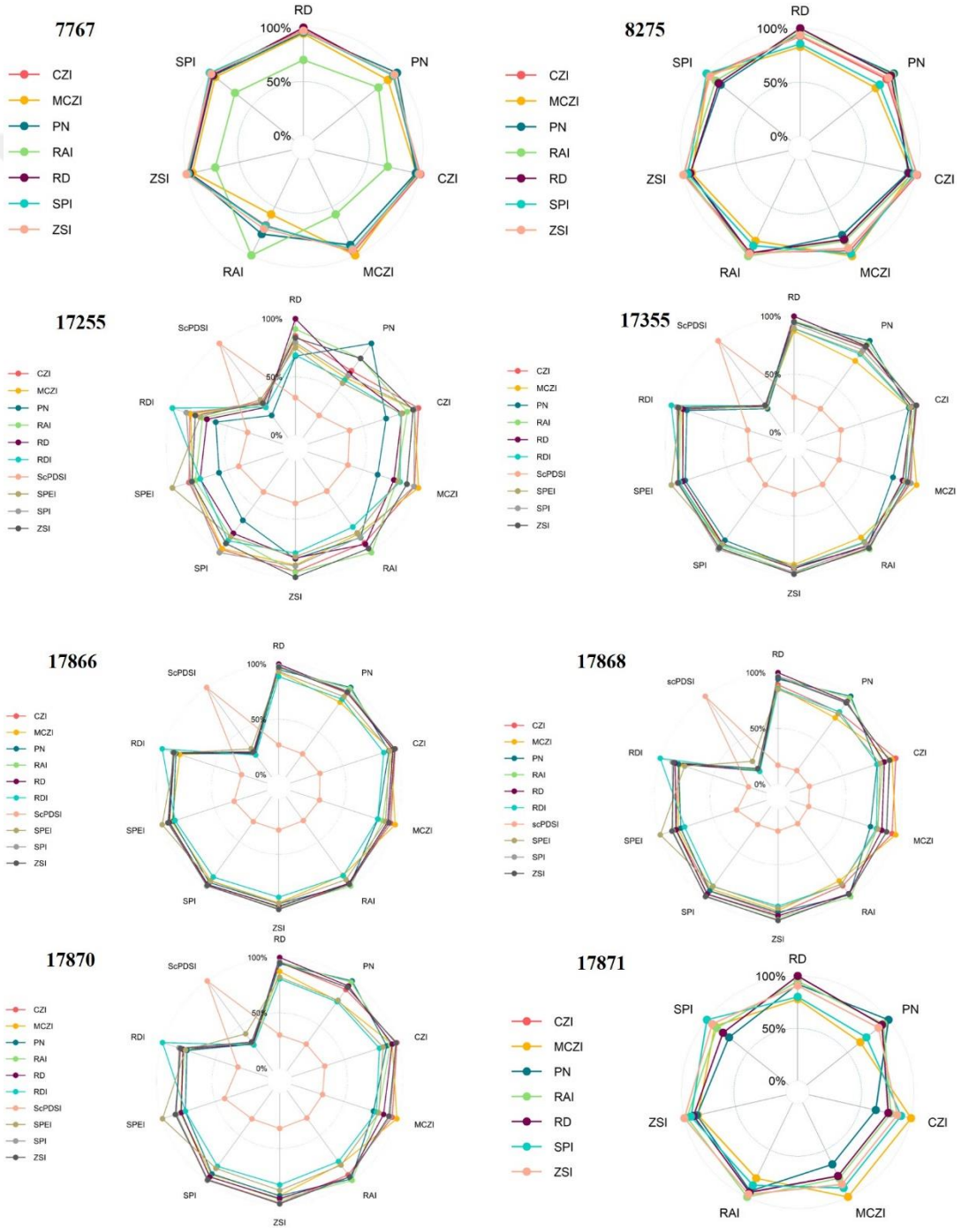

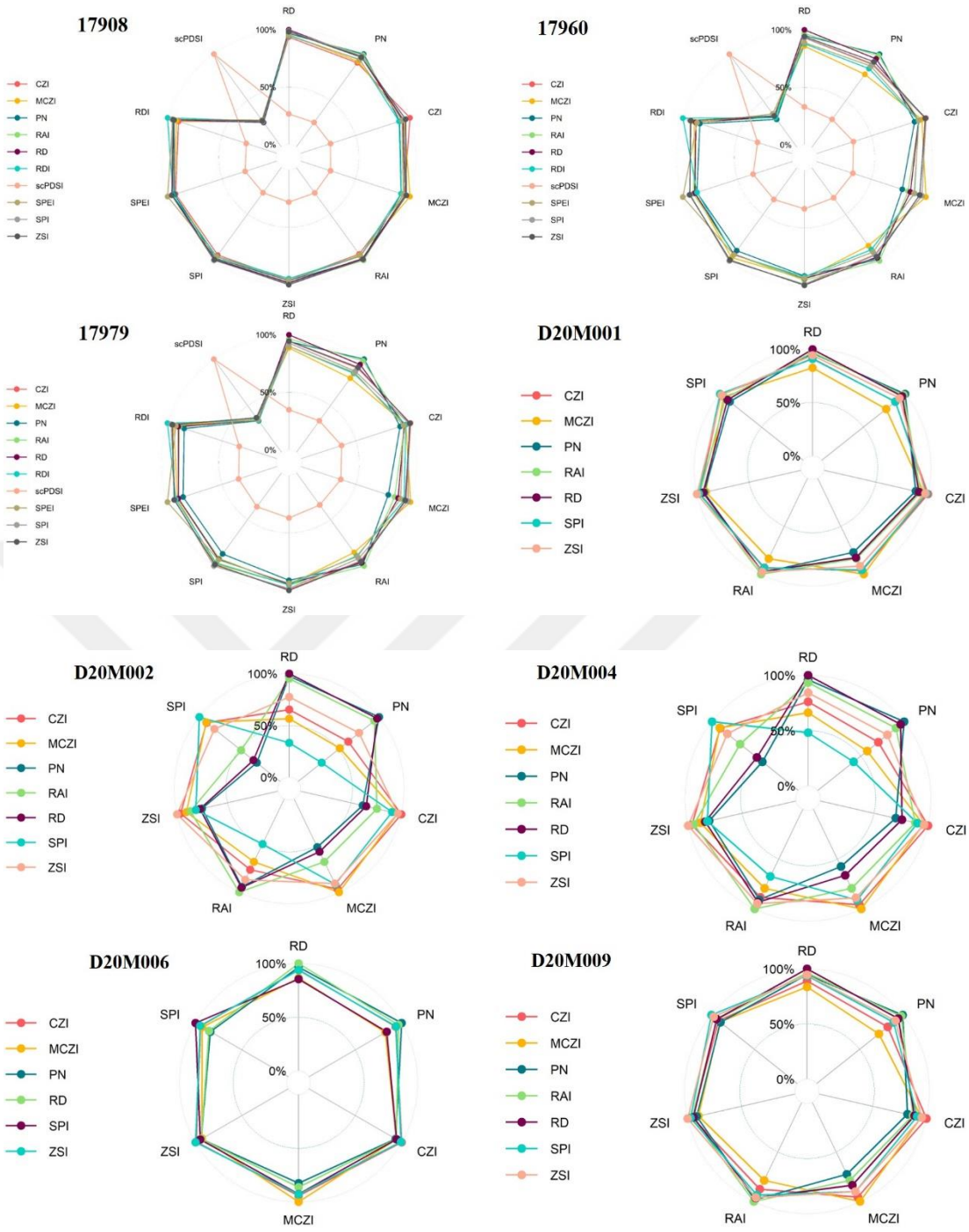
17908
17960
17979
D20M001
D20M002
D20M004
D20M006
D20M009
CZI
MCZI
PN
RAI
RD
RDI
scPDSI
SPEI
SPI
ZSI
100%
50%
0%

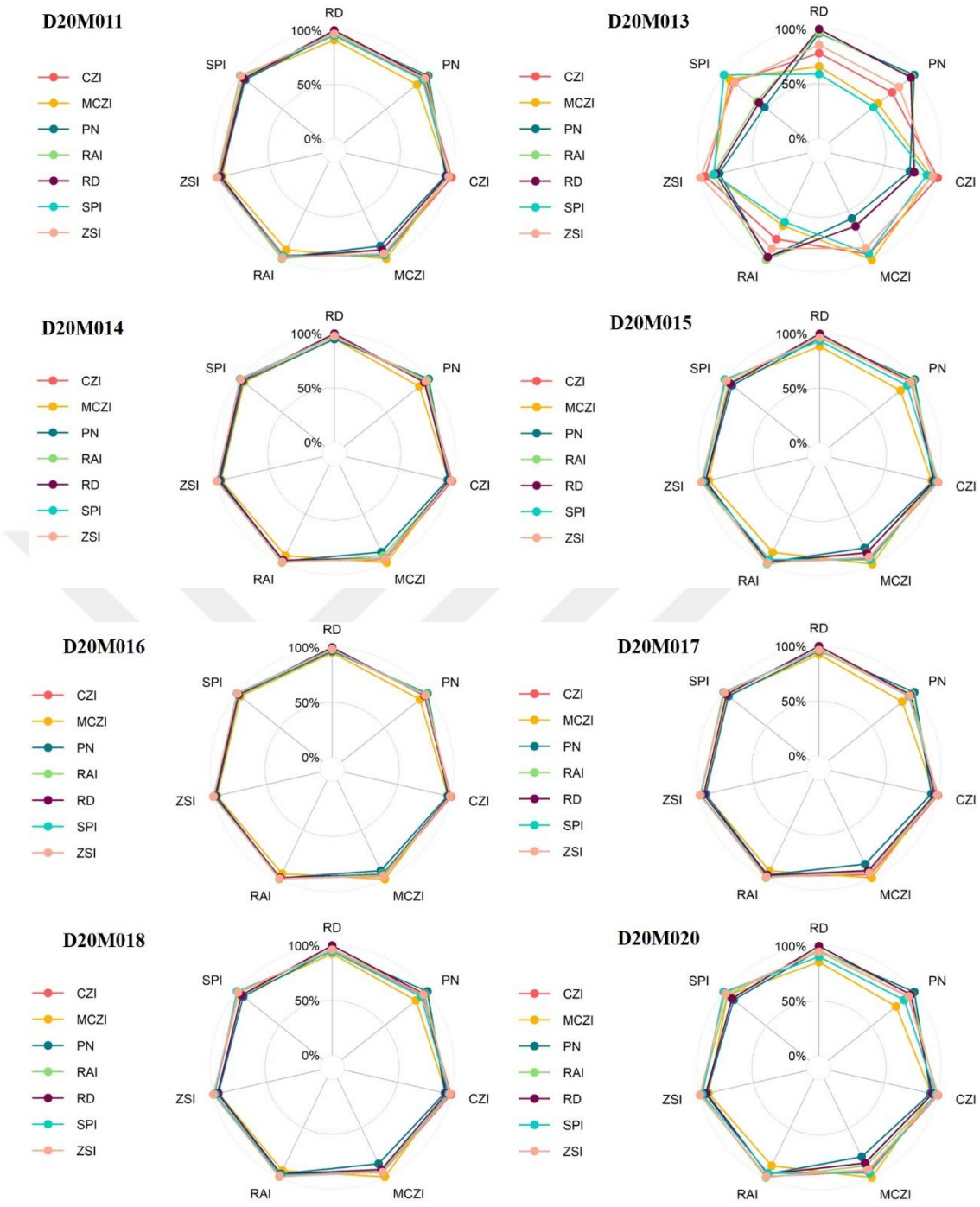

Figure 5.6 Comparison of ten drought deciles at 1-month time series based on percentage of drought severity for selected meteorological stations

When considered 1-month times scale, due to temperature data availability, eight stations are assessed using ten drought indices, whereas seven drought indices are applied to 16 gauging stations. D20M002, D20M004 and D20M013 stations show inconsistent than the other stations. However, SPI, SPEI and RDI indicate a good correlation to each other for these indices as well as the other indices.

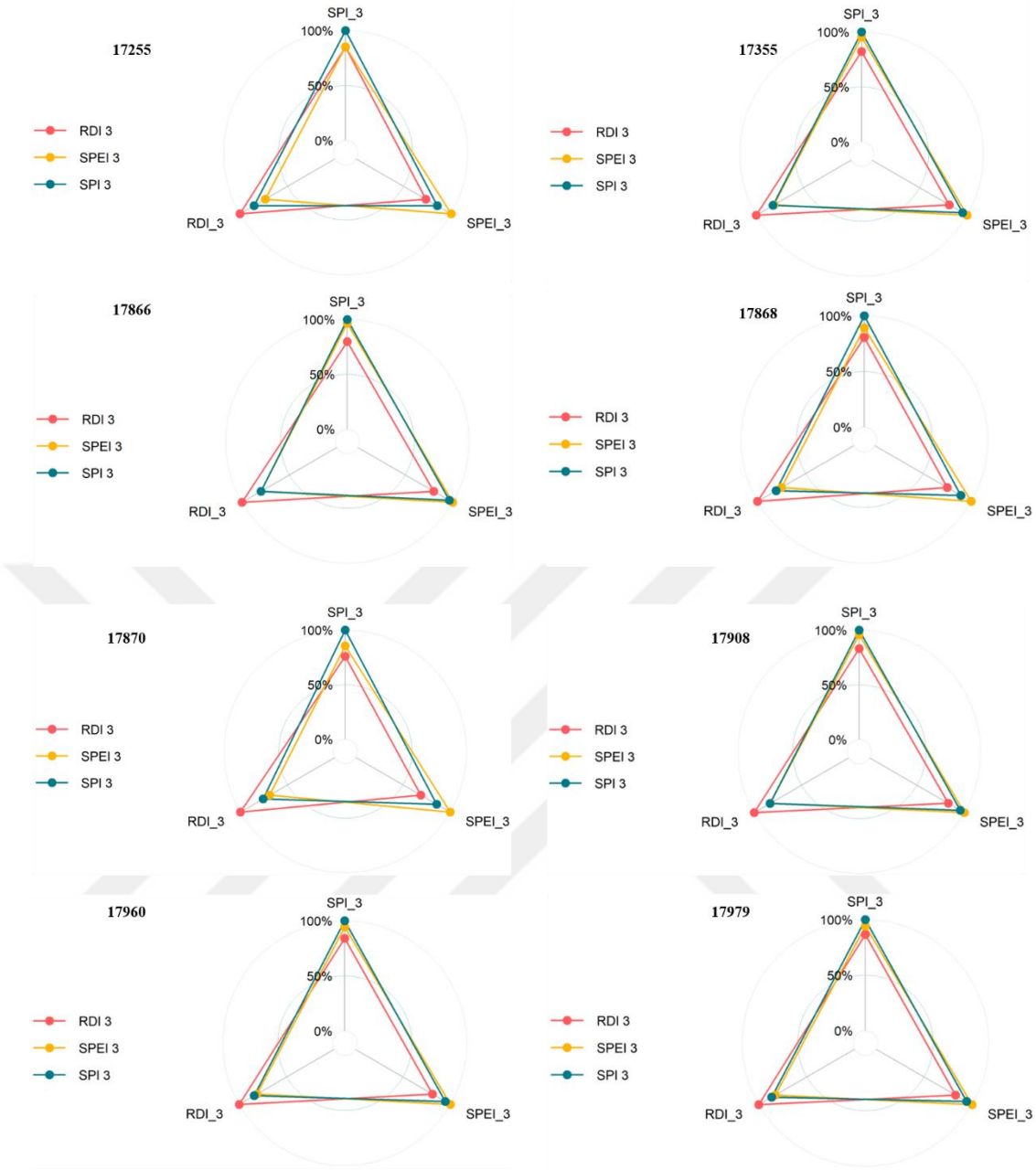

Figure 5.7 Comparison of SPI, SPEI and RDI drought deciles at 3-month time series based on percentage of drought severity for eight meteorological stations

Unlike SPI, in order to determine SPEI and RDI, the calculation of PET is essential. But, the temperature data is not available, especially some stations where obtained only precipitation data from State Hydraulic Works (DSI). Therefore, multi-time scale is applied to eight stations. All stations are much higher correlation performance to one another for 3-month time scale. The value of the Spearman coefficient varies from 0.75 to 0.96. The lowest value of coefficient is found for 0.75 for 17870 and the highest for station 17866.

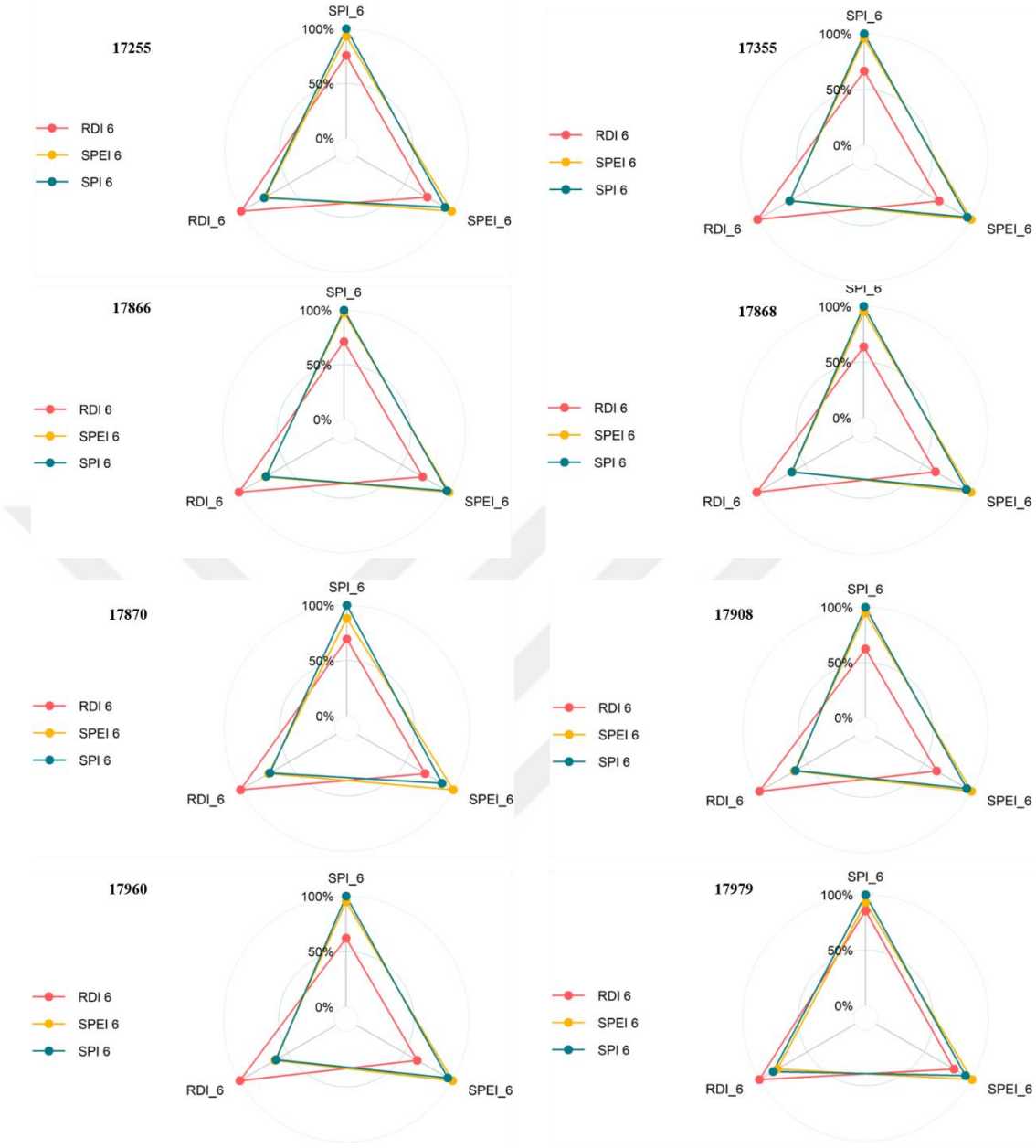

Figure 5.8 Comparison of SPI, SPEI and RDI drought deciles at 6-month time series based on percentage of drought severity for eight meteorological stations

More insights into the performance of different time scales may be expressed from identifying how these indices reflect changing on percentage of drought severity. 6-month time scale reveals more inconsistent than 1- and 3-month time scale, especially comparing RDI 6 with SPI 6 and SPEI 6 except station 17979 that is high correlated. But general view, while SPI 6 and SPEI 6 indicate a strong correlation to each other, RDI 6 shows quite poor relationship with these indices, but its correlation is also over 50%.

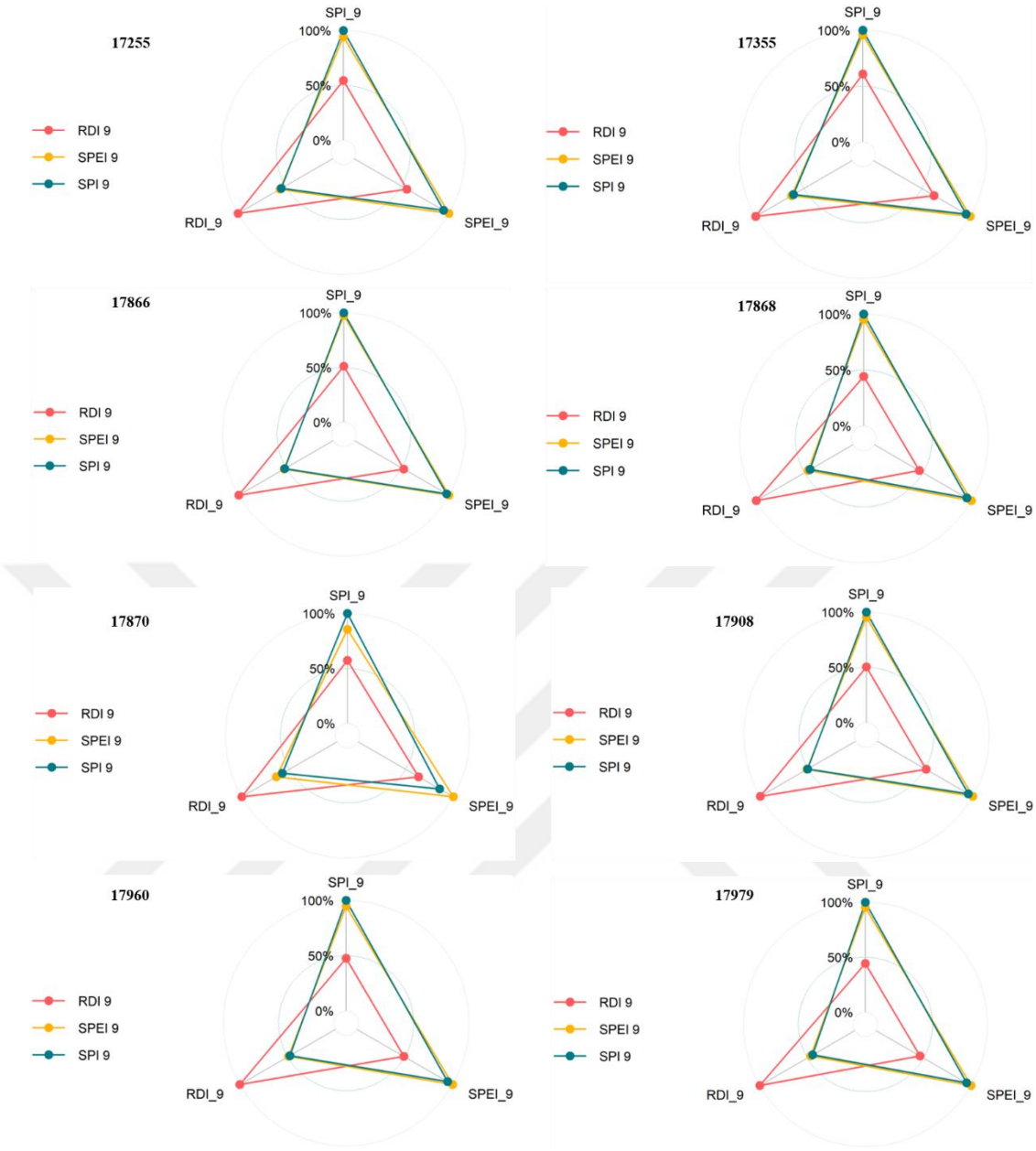

Figure 5.9 Comparison of SPI, SPEI and RDI drought deciles at 9-month time series based on percentage of drought severity for eight meteorological stations

For the 9-month time scale, similar to the 6-month time scale, SPI 9 and SPEI 9 are obtained much high correlation from all stations, whereas the skill correlation performance of RDI 9 doesn't reveal good relationships in addition to station 17979. Stations 17979 and 17868 for RDI 6, the value of Spearman coefficient is below 50% compared to both the other indices.

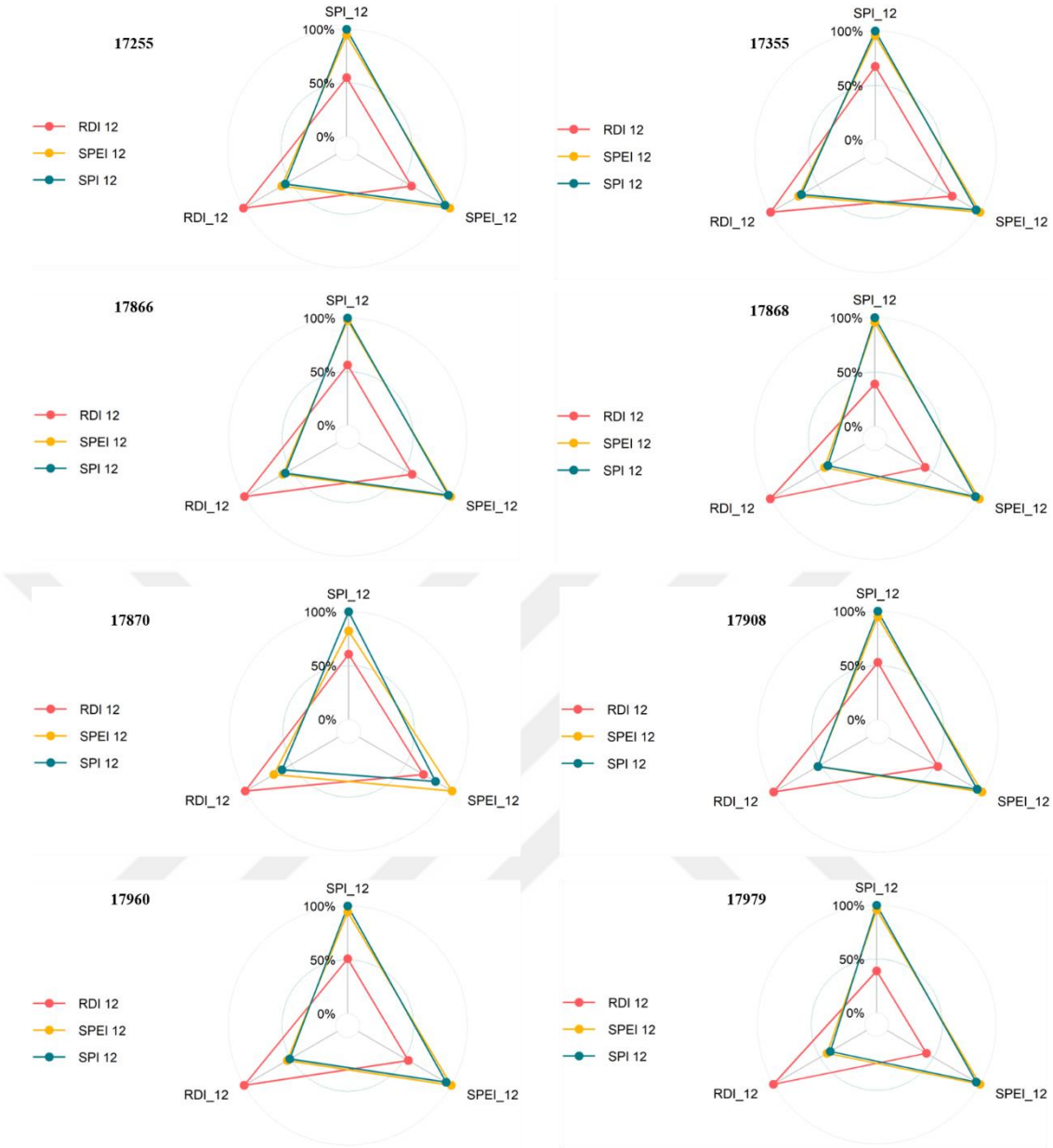

Figure 5.10 Comparison of SPI, SPEI and RDI drought deciles at 12-month time series based on percentage of drought severity for eight meteorological stations

For 12-month time scale, the correlation coefficients of RDI 12 indicate an inconsistent with SPI 12 and SPEI 12 indices. Similar to evaluation the previous different time scale, SPI and SPEI shows much higher the correlation performance at 12-month time scale. However, the value of all stations Spearman coefficients is above 90% except station 17870 that revealed also high correlated over 75% between SPI 12 and SPEI 12.

5.5 Comparison of Drought Indices at Different Drought Classes

It is seen from Figure 5.11 that all stations are classified into drought category. Eight stations including 17255, 17355, 17866, 17868, 17870, 17908, 17960 and 17979 are evaluated in terms of ten drought indices due to temperature data availability that used for SPEI, RDI and scPDSI indices. The CZI, MCZI, RAI, ZSI, SPI, RD and PNI indices need precipitation data as an input parameter.

According to Figure 5.11, For the whole study area, SPI, SPEI and RDI at 1-month time scale illustrate highly similar frequency of all drought severity categories, especially extreme period. MCZI, CZI and ZI show slightly a small difference with that of SPI, SPEI and RDI for all selected stations, while scPDSI, RD and PNI reveals inconsistent compared to other indices. For instance, at 17355 station, scPDSI shows similarity at extreme wet categories and (1.34 % and 47.58 %) as compared to RDI (1.34 % and 54.03 %), SPI (2.15 % and 54.57 %) and SPEI (0.81 % and 49.73%). In contrast, at station 17908, three indices reveal a low frequency of both extreme and wet categories. In general, while the ‘wet class’ of MZSI is much higher than that of the used indices, the ‘normal class’ of ZSI illustrate is much higher. In the light of above information, it can be concluded that ZSI is more sensitivity and consistency than MZSI at ‘wet class’.

Although there are similarities among SPI, SPEI and RDI, there are also small differences. When focused on station 17355, while the relative frequency calculates 54% for SPI, 49.73% and 54.03% are evaluated for SPEI and RDI, respectively. On the other hand, the relative frequency at “wet” class is much higher for SPI compared to SPEI and RDI indices. For “normal” class, SPI and SPEI shows similarity at all stations, whereas RDI indicate much higher.

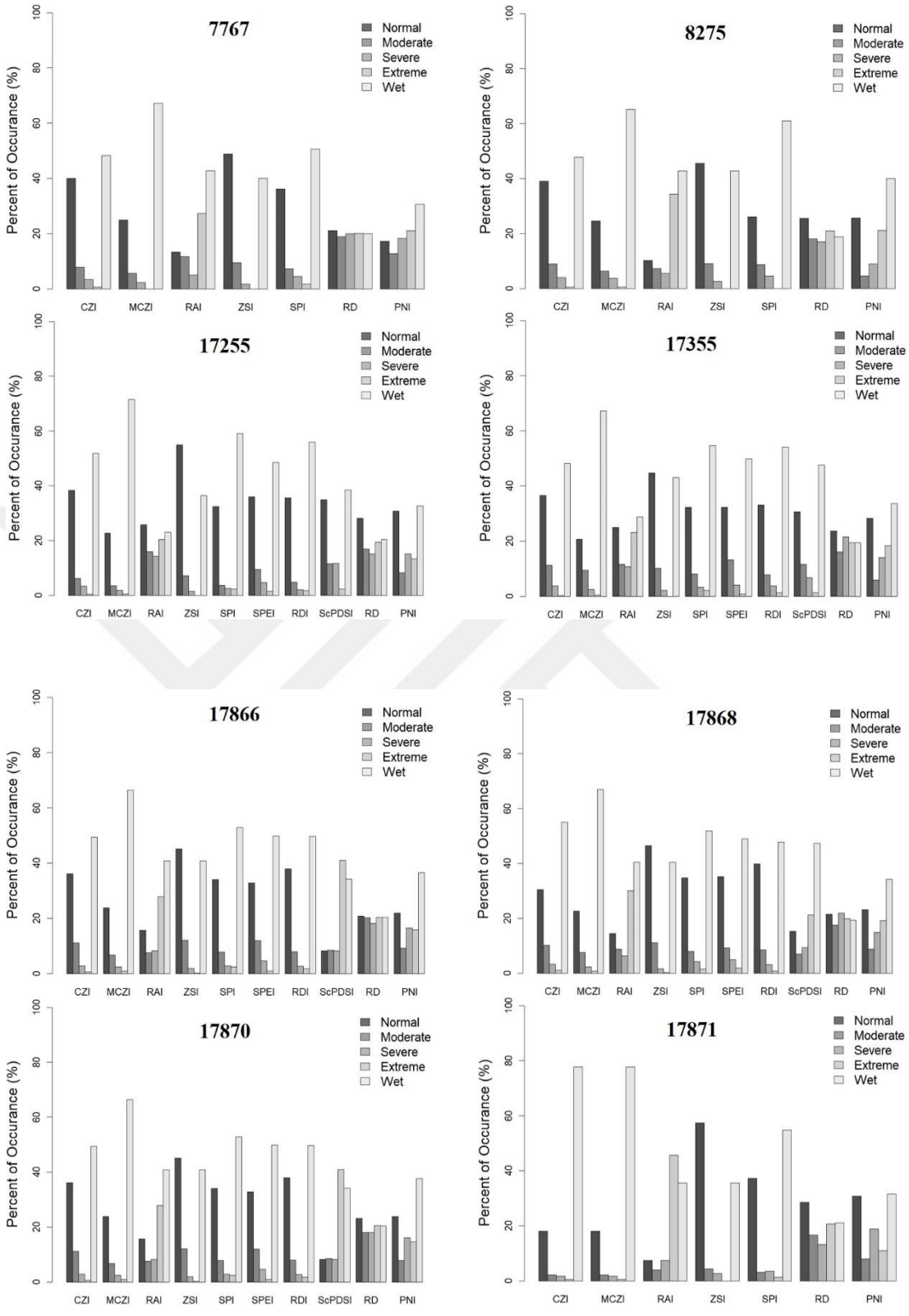
7767
8275
17255
17355
17866
17868
17870
17871
Normal
Moderate
Severe
Extreme
Wet
Percent of Occurance (%)
CZI
MCZI
RAI
ZSI
SPI
SPEI
RDI
ScPDSI
RD
PNI

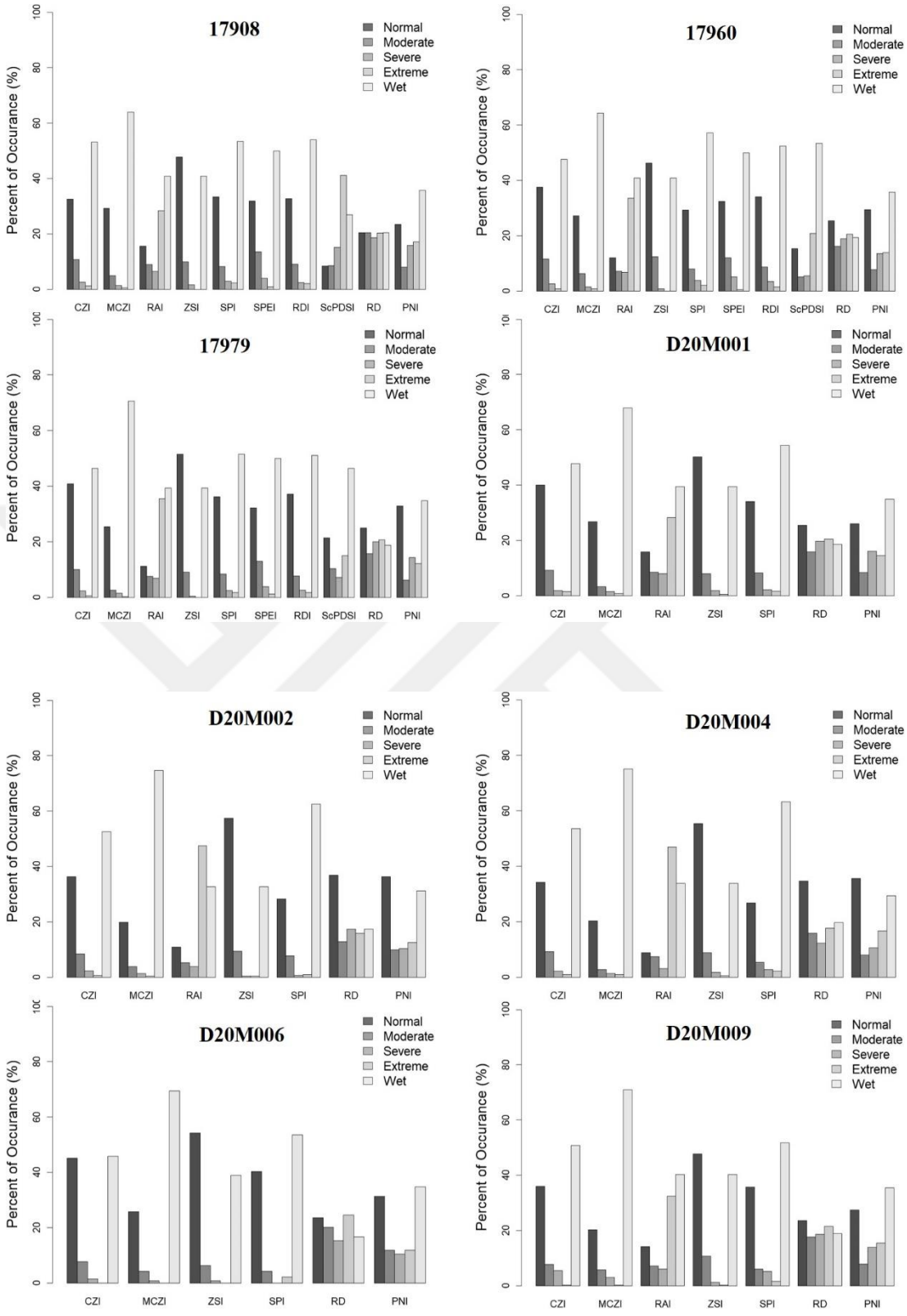
17908
17960
17979
D20M001
D20M002
D20M004
D20M006
D20M009
Normal
Moderate
Severe
Extreme
Wet
Percent of Occurance (%)
CZI
MCZI
RAI
ZSI
SPI
SPEI
RDI
ScPDSI
RD
PNI

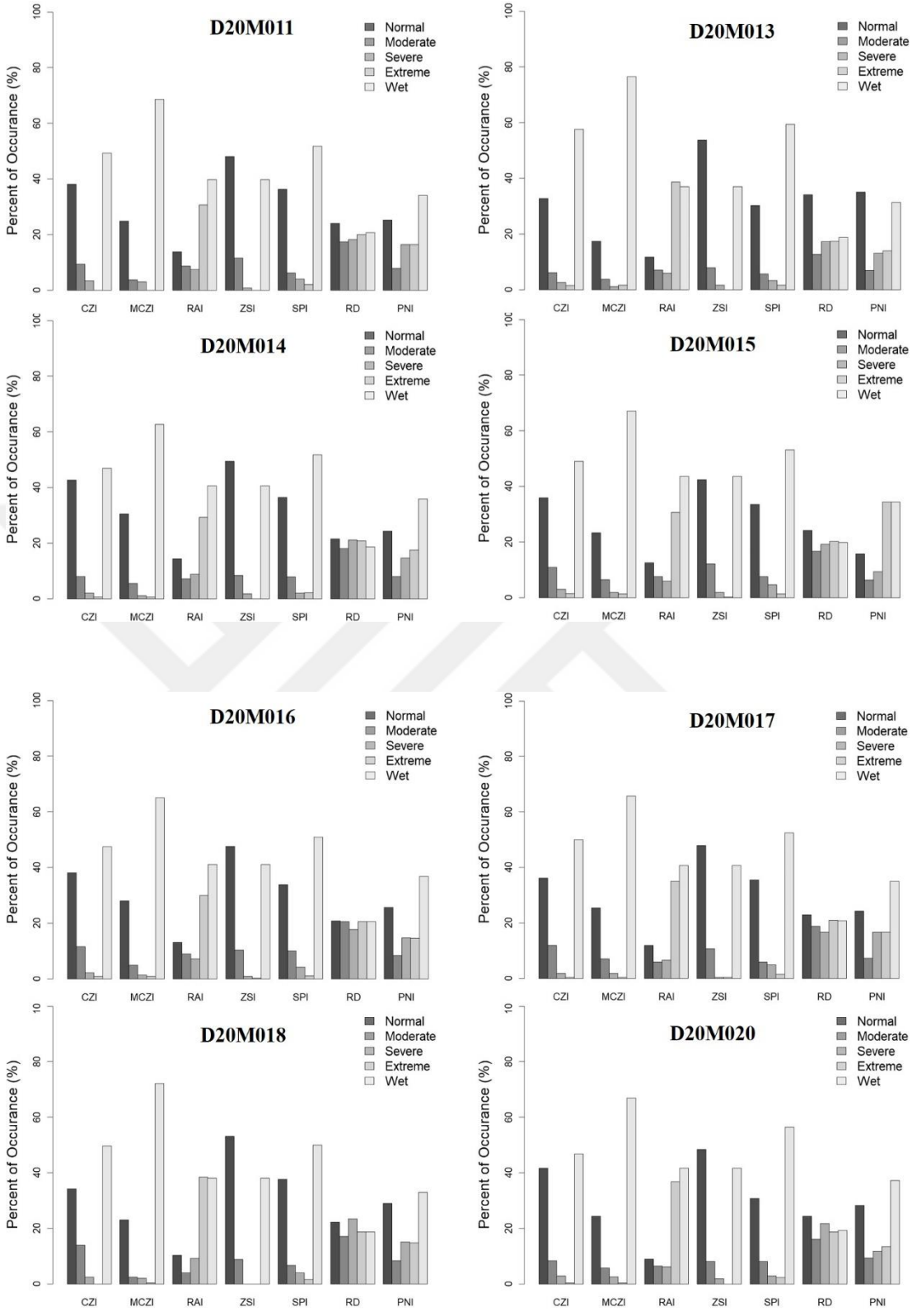

Figure 5.11 Bar plot of the drought severity occurrence with its categories (as percentage) for 1-month time scale

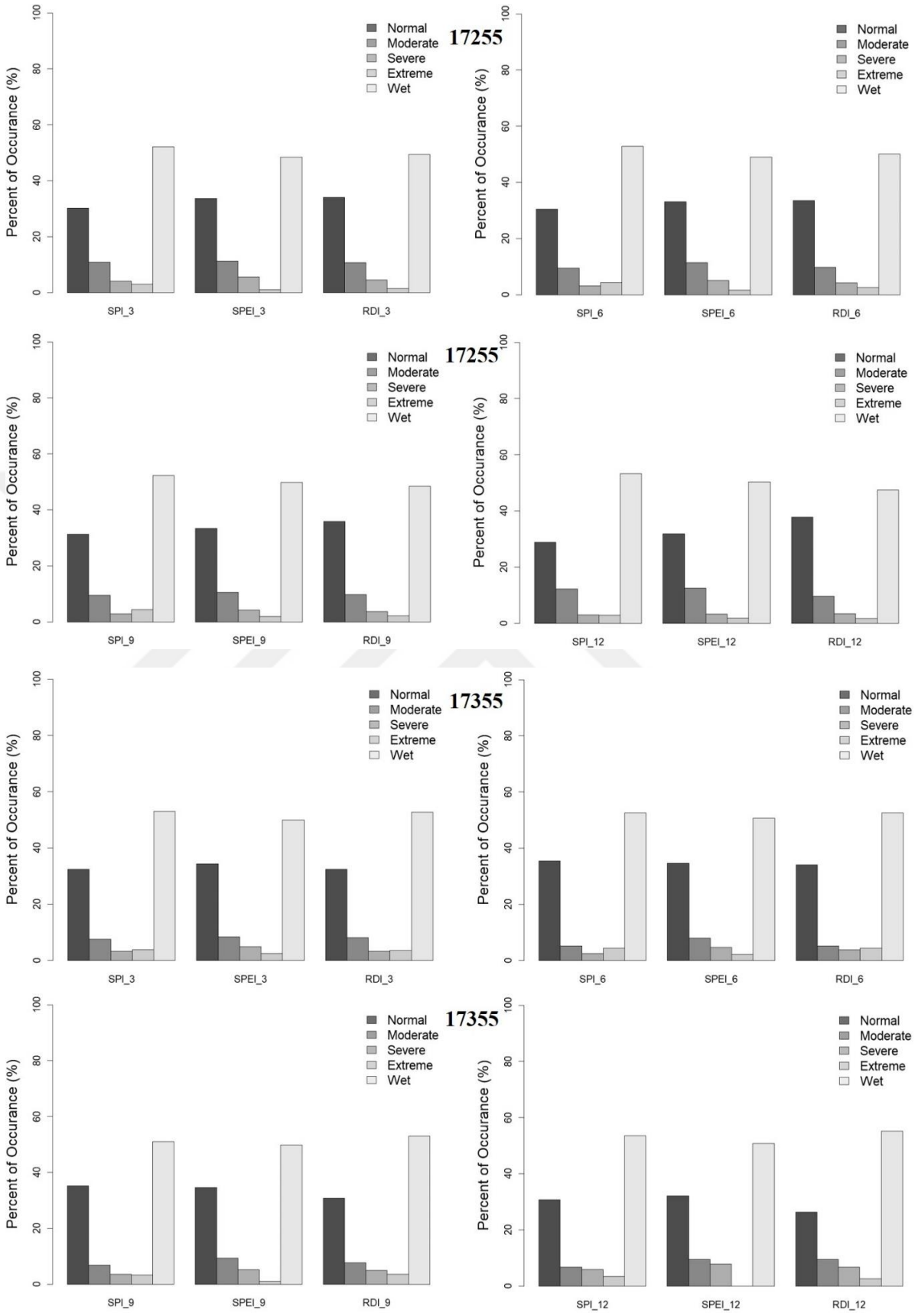
17255
Normal
Moderate
Severe
Extreme
Wet
Percent of Occurance (%)
0
20
40
60
80
100
SPI_3
SPEI_3
RDI_3
SPI_6
SPEI_6
RDI_6
17255
SPI_9
SPEI_9
RDI_9
SPI_12
SPEI_12
RDI_12
17355
17355

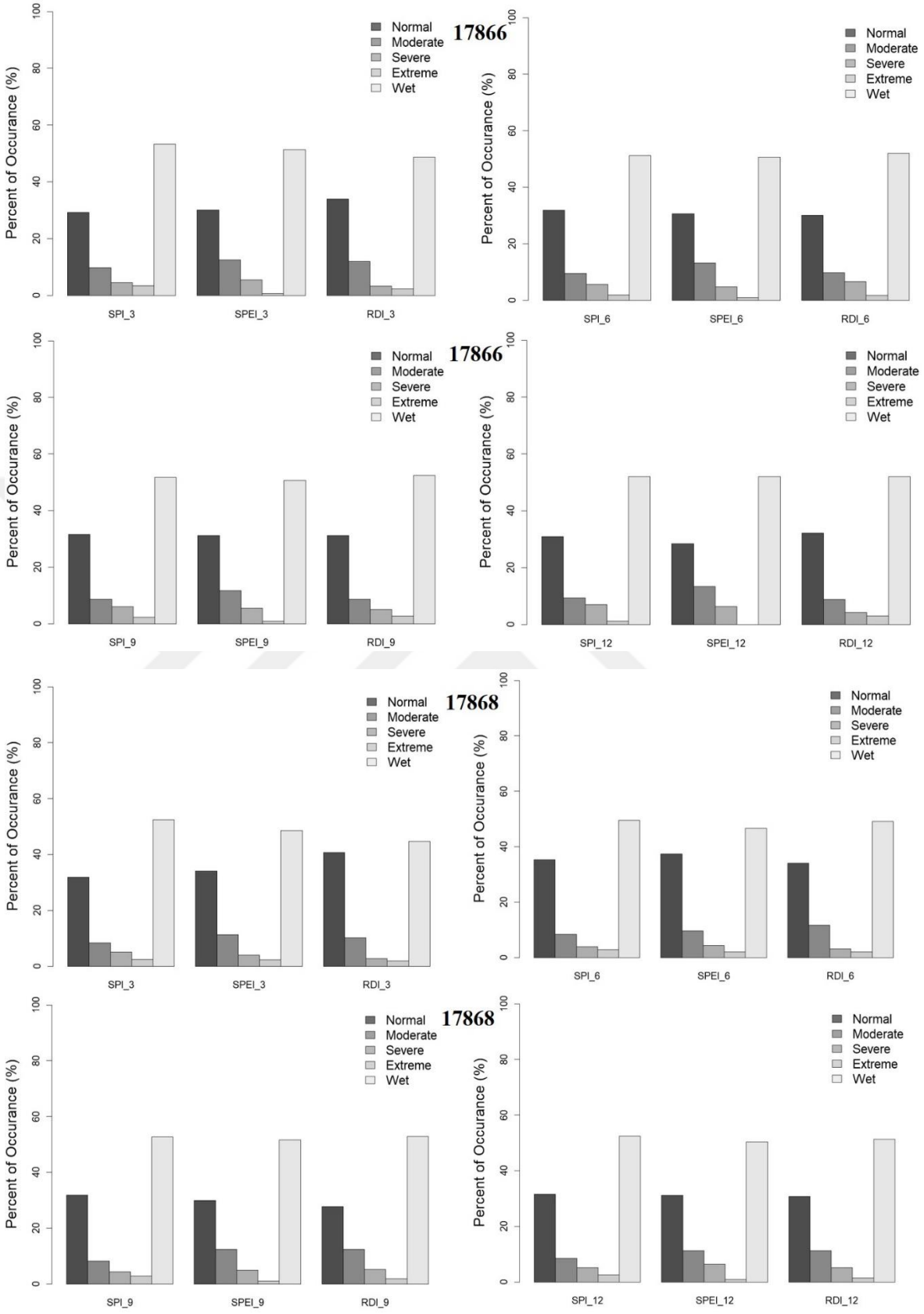
17866
Normal
Moderate
Severe
Extreme
Wet
Percent of Occurance (%)
SPI_3
SPEI_3
RDI_3
SPI_6
SPEI_6
RDI_6
17866
SPI_9
SPEI_9
RDI_9
SPI_12
SPEI_12
RDI_12
17868
SPI_3
SPEI_3
RDI_3
SPI_6
SPEI_6
RDI_6
17868
SPI_9
SPEI_9
RDI_9
SPI_12
SPEI_12
RDI_12

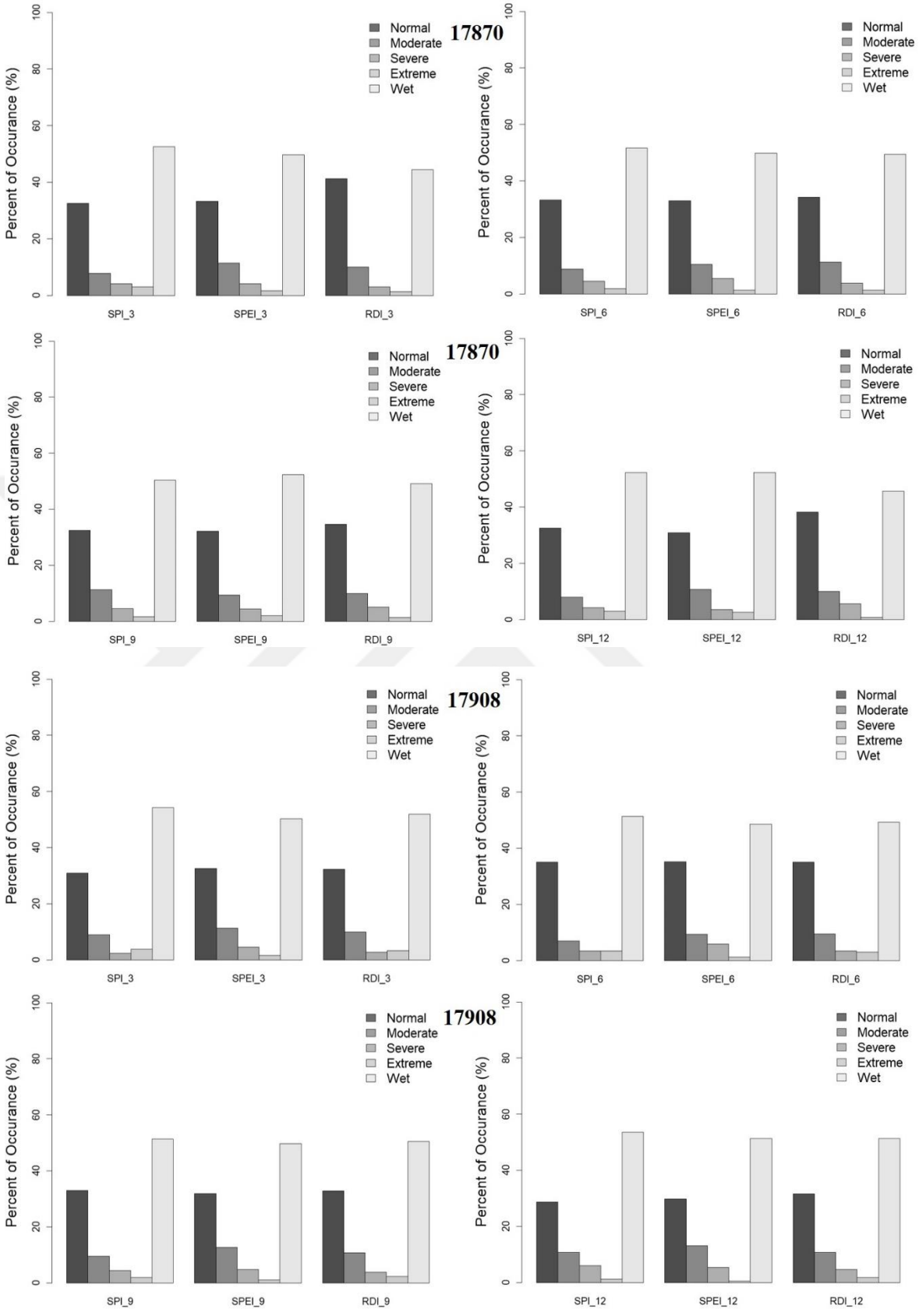
17870
Normal
Moderate
Severe
Extreme
Wet
Percent of Occurance (%)
SPI_3
SPEI_3
RDI_3
SPI_6
SPEI_6
RDI_6
17870
SPI_9
SPEI_9
RDI_9
SPI_12
SPEI_12
RDI_12
17908
SPI_3
SPEI_3
RDI_3
SPI_6
SPEI_6
RDI_6
17908
SPI_9
SPEI_9
RDI_9
SPI_12
SPEI_12
RDI_12

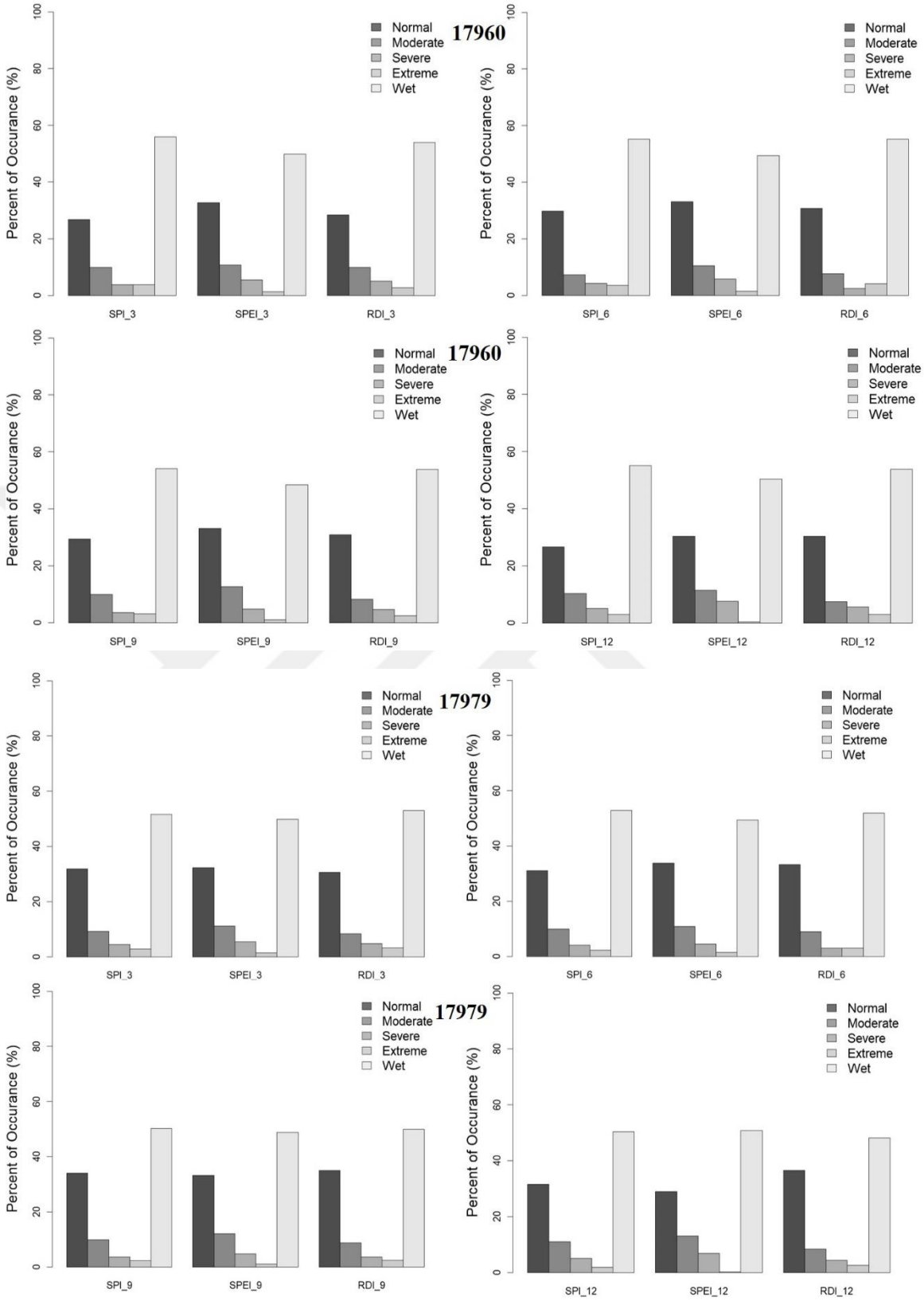

Figure 5.12 Bar plot of the drought severity occurrence with its categories (as percentage) for eight meteorological stations at multi-time scales

According to Figure 5.12, three indices reveal same result in terms of all drought classes. For 3-month time scale, normal classes percentage is found higher at RDI index except 17960 station compared to other indices, while wet classes percentage indicates higher at SPI index except 17979 station showed higher percentage at RDI. Moderate, severe and extreme classes don't show a big difference among indices. On the other hand, small differences have been generally observed in wet and normal classes. At all stations, normal classes percentage are above 50%, whereas extreme classes are generally observed below 5% considering three indices at multi-time scale.

5.6 Performance of SPI, SPEI and RDI Indices at Different Time Scales with Respect to Historical Droughts

The 2007-2009 droughts, which effects seriously on social life, were the most widespread droughts in Turkey. In addition, all stations suffered from these drought periods. The time series of SPI, SPEI and RDI at different time scale for 2007-2009 years are shown in Figure 5.13. Previous section indicates that the performance of SPEI and RDI, based on statistical analysis, are much strength as compared to use evapotranspiration and precipitation data and also these two indices enable to show more realistic picture of drought conditions. It can be seen from Figure 5.12 that SPEI shows much higher negative value followed by RDI and SPI, respectively. Three indices have a good correlation at 3- and 6-month time scale, whereas their performance tendency at 9- and 12 falls downward. For instance, the normal and wet categories at 3-month time scale for SPI (54% and 30%) and RDI (62% and 25%) shows similarity, while SPEI has small discrepancies at 3-month (45% and 12%). On the other hand, cumulative distribution of dry classes for SPI 3, SPEI 3 and RDI 3 are found 70%, 87% and 75%, respectively for the station 17255. In general, SPI and RDI at different time scale indicate much appropriate to detect historical drought at dry classes. Like the 3-month time scale, While SPI and RDI are found same value as 83%, SPEI indicates 100% at 6-month time scale. A closer look on the wet periods, even though SPI 6 and RDI 6 reveal 16%, SPE 6 has not found to monitor clearly. A similar result also found at the 9- and 12-month time scale where SPI and RDI more comparable, in dry and wet classes.

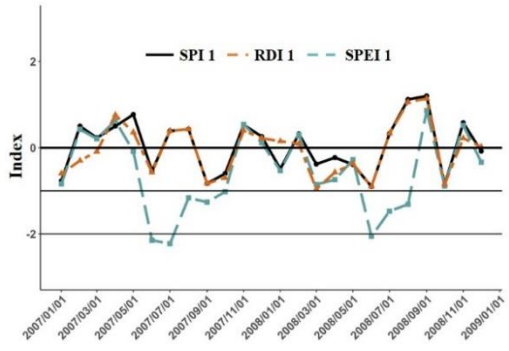
17255
SPI 1
RDI 1
SPEI 1
Index

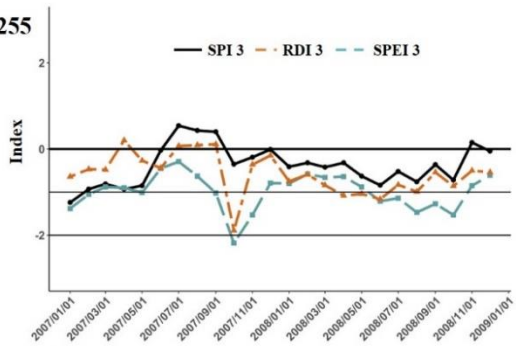
SPI 3
RDI 3
SPEI 3
Index

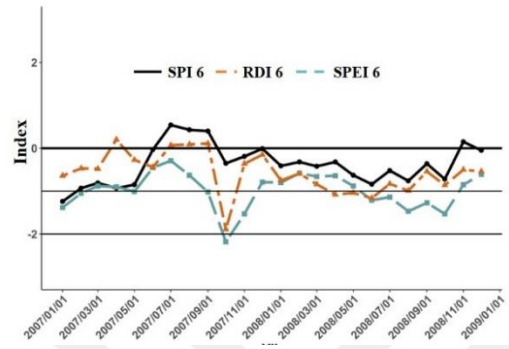
17255
SPI 6
RDI 6
SPEI 6
Index

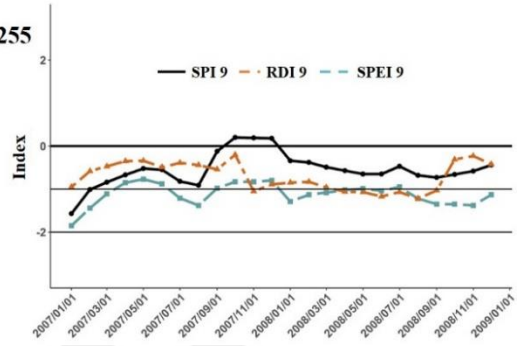
SPI 9
RDI 9
SPEI 9
Index

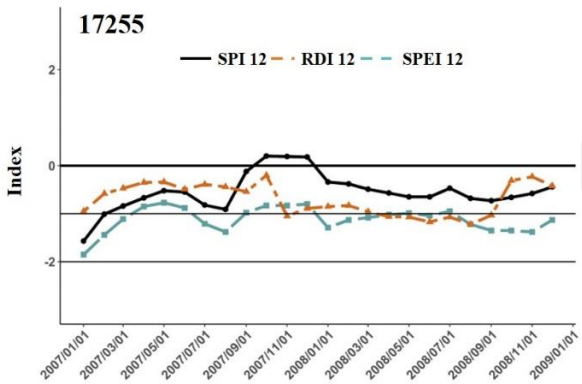
17255
SPI 12
RDI 12
SPEI 12
Index

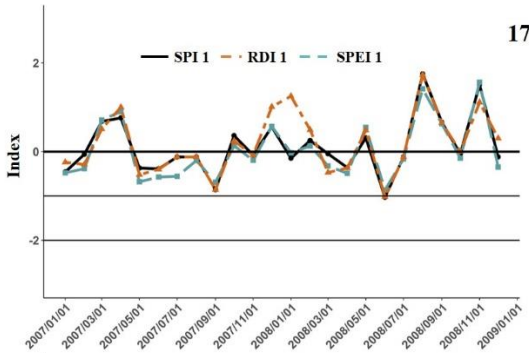
17355
SPI 1
RDI 1
SPEI 1
Index

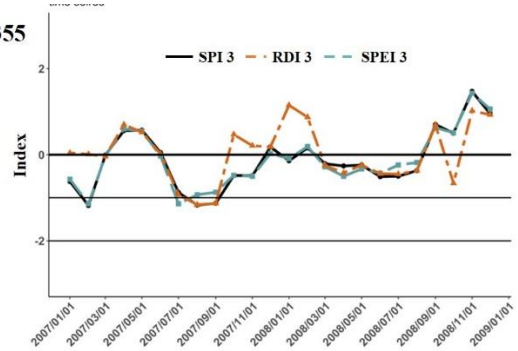
SPI 3
RDI 3
SPEI 3
Index

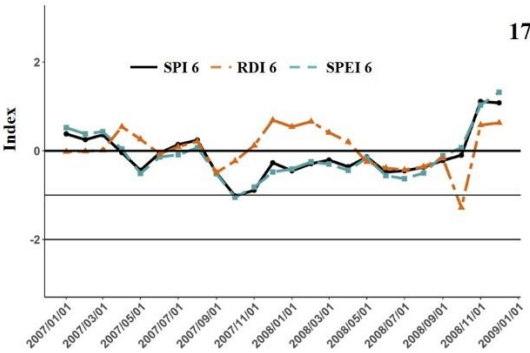
17355
SPI 6
RDI 6
SPEI 6
Index

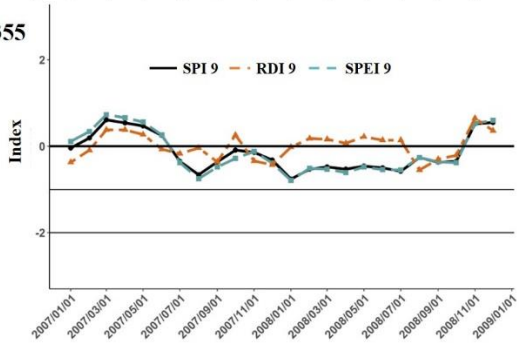
SPI 9
RDI 9
SPEI 9
Index

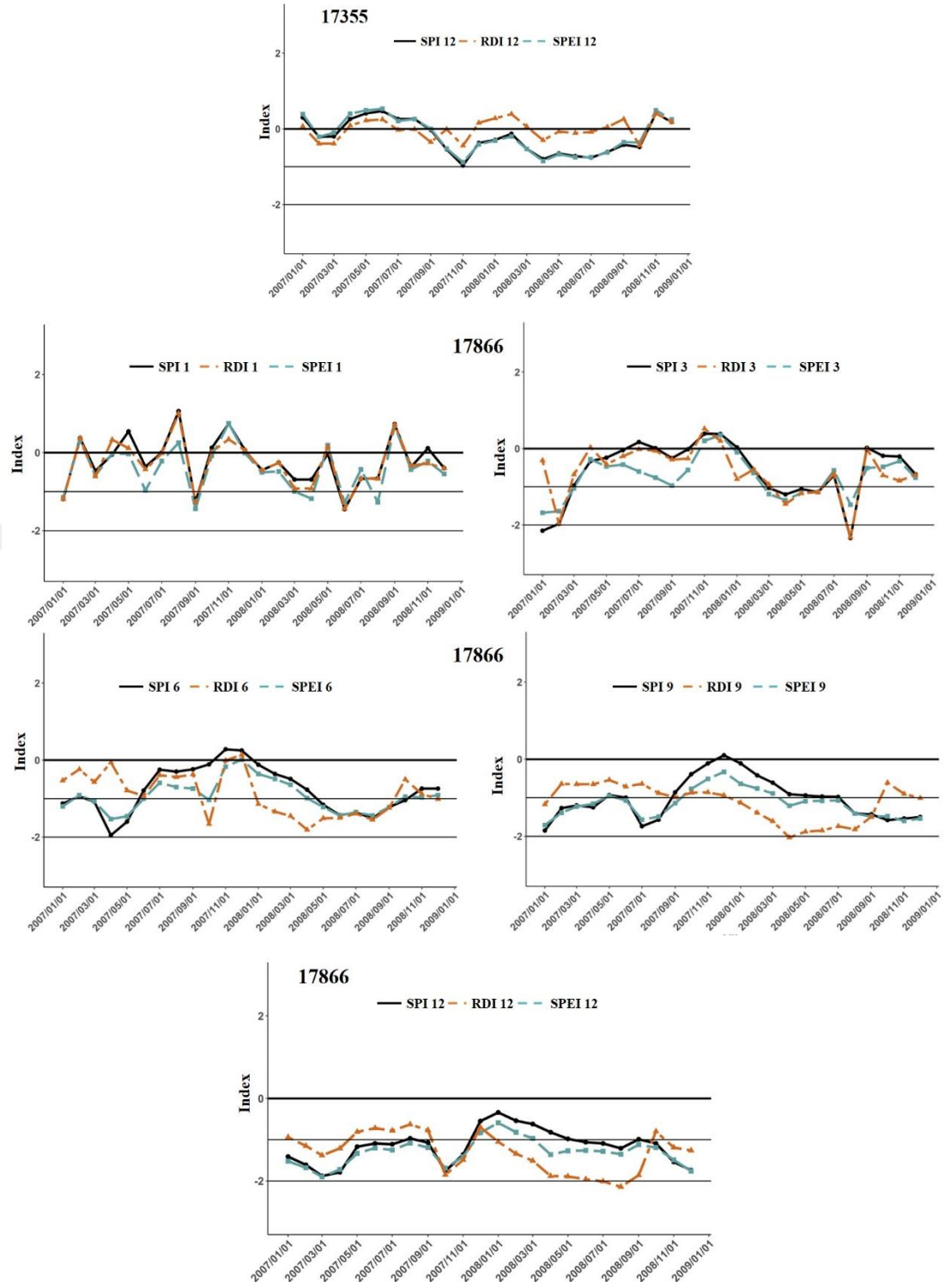
17355
SPI 12
RDI 12
SPEI 12
Index
17866
SPI 1
RDI 1
SPEI 1
17866
SPI 3
RDI 3
SPEI 3
17866
SPI 6
RDI 6
SPEI 6
17866
SPI 9
RDI 9
SPEI 9
17866
SPI 12
RDI 12
SPEI 12

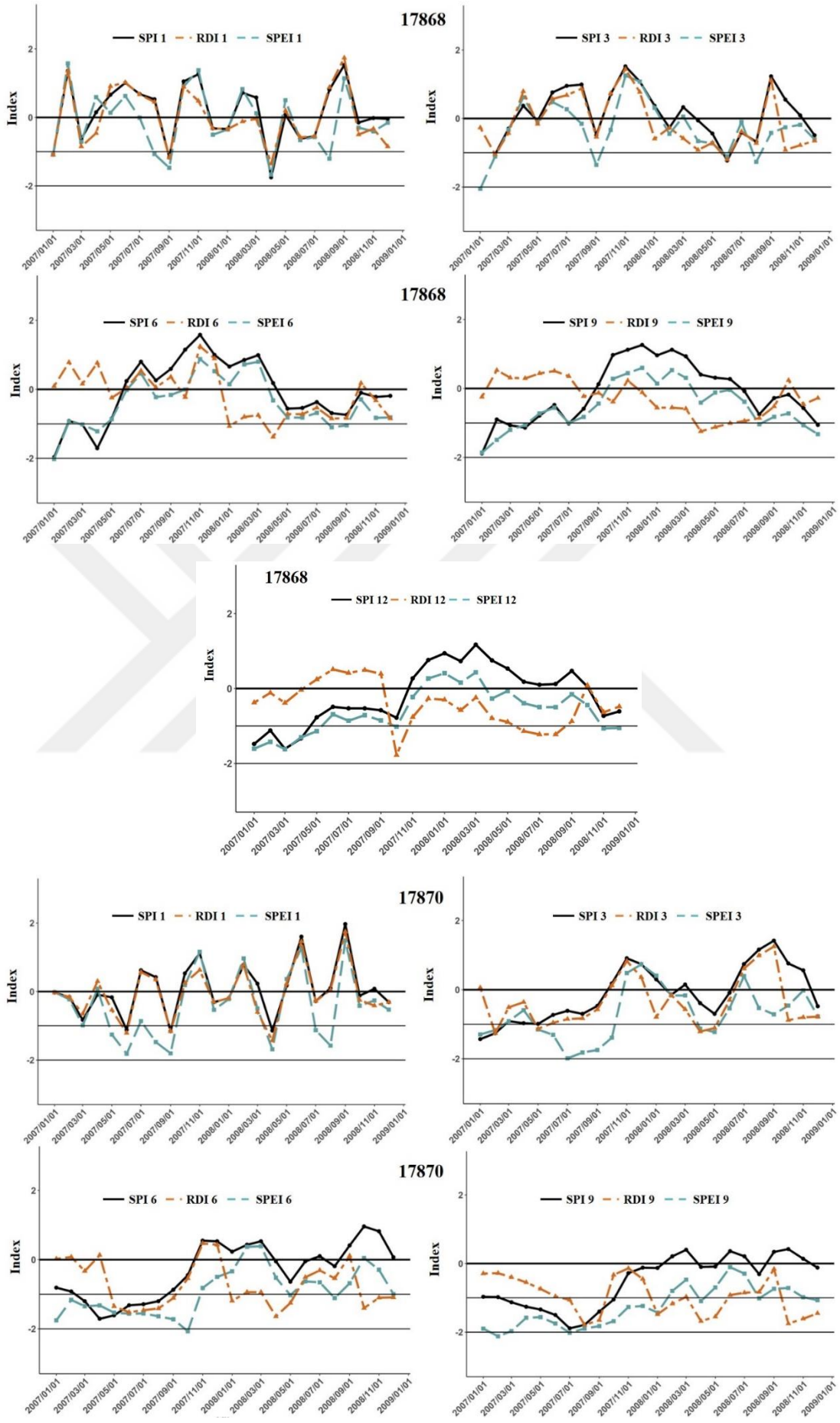
17868
SPI 1
RDI 1
SPEI 1
SPI 3
RDI 3
SPEI 3
SPI 6
RDI 6
SPEI 6
SPI 9
RDI 9
SPEI 9
SPI 12
RDI 12
SPEI 12
17870
Index

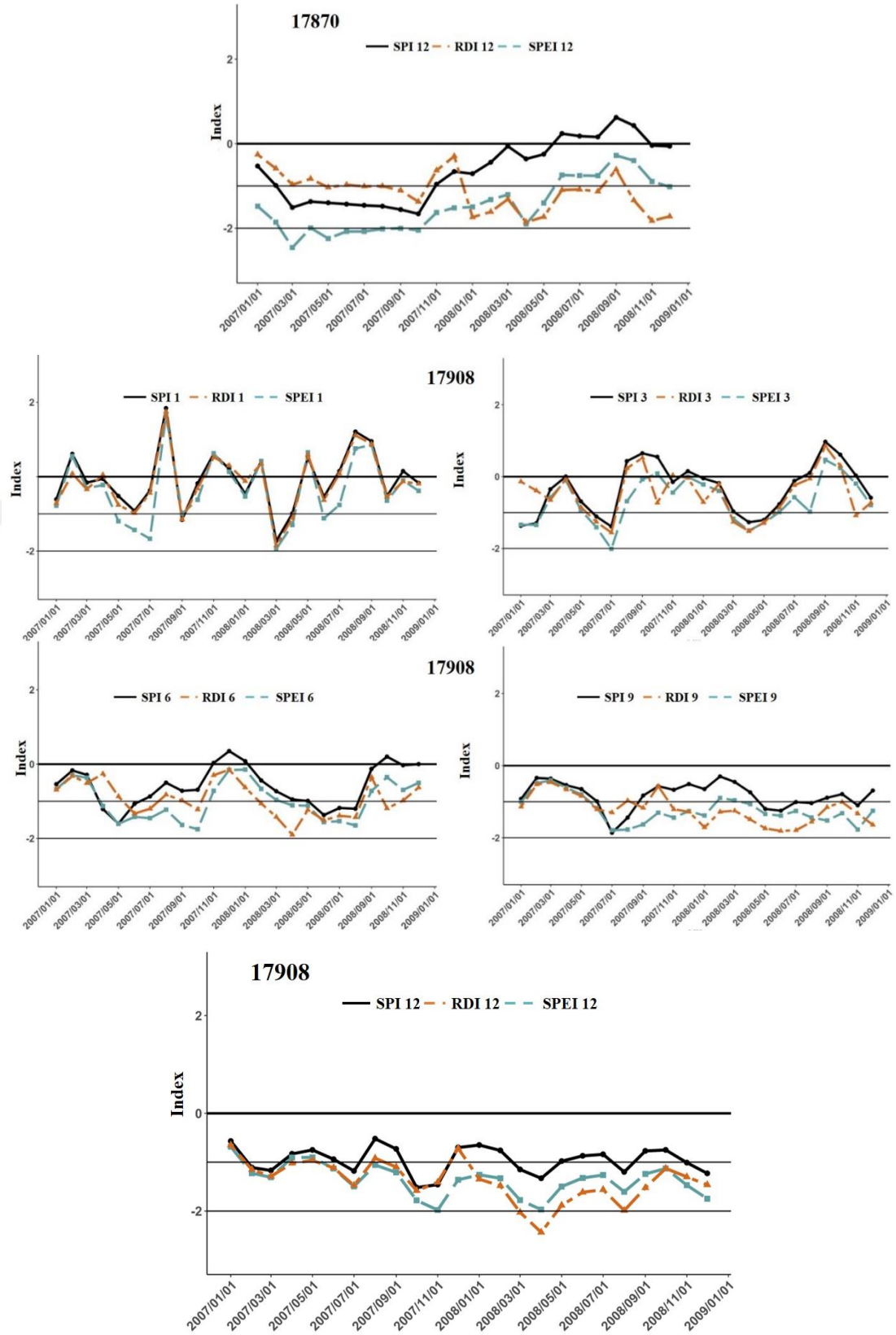
17870
SPI 12
RDI 12
SPEI 12
Index
17908
SPI 1
RDI 1
SPEI 1
SPI 3
RDI 3
SPEI 3
SPI 6
RDI 6
SPEI 6
SPI 9
RDI 9
SPEI 9
SPI 12
RDI 12
SPEI 12

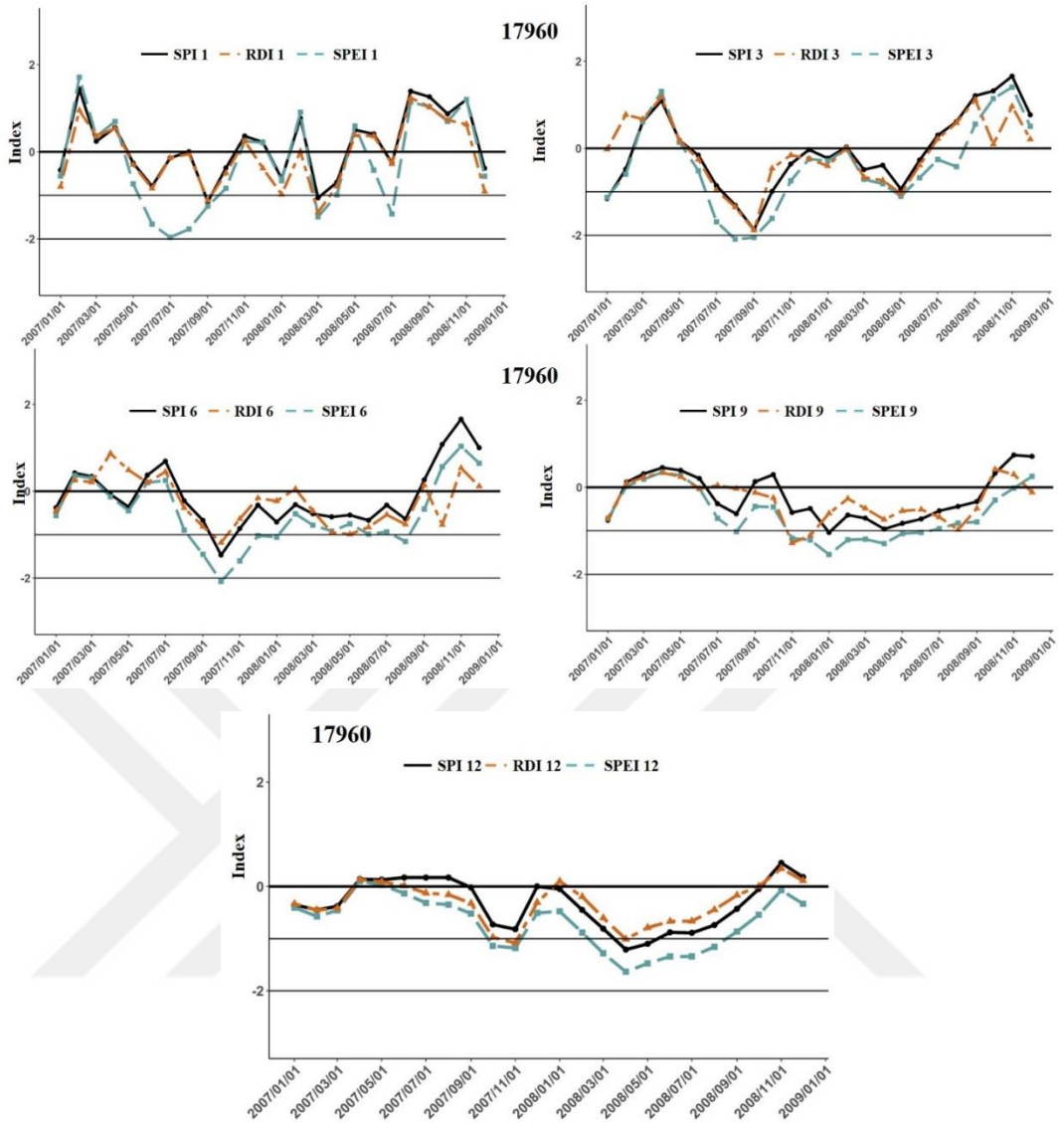
17960
SPI 1
RDI 1
SPEI 1
SPI 3
RDI 3
SPEI 3
SPI 6
RDI 6
SPEI 6
SPI 9
RDI 9
SPEI 9
SPI 12
RDI 12
SPEI 12
Index

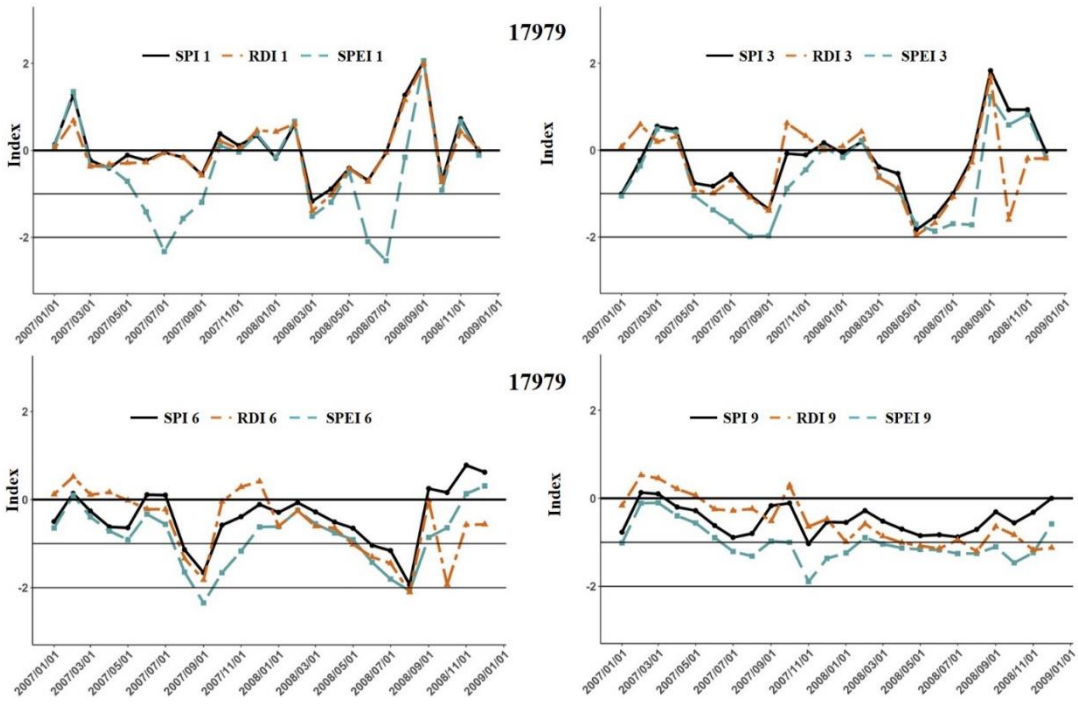
17979
SPI 1
RDI 1
SPEI 1
SPI 3
RDI 3
SPEI 3
SPI 6
RDI 6
SPEI 6
SPI 9
RDI 9
SPEI 9
Index

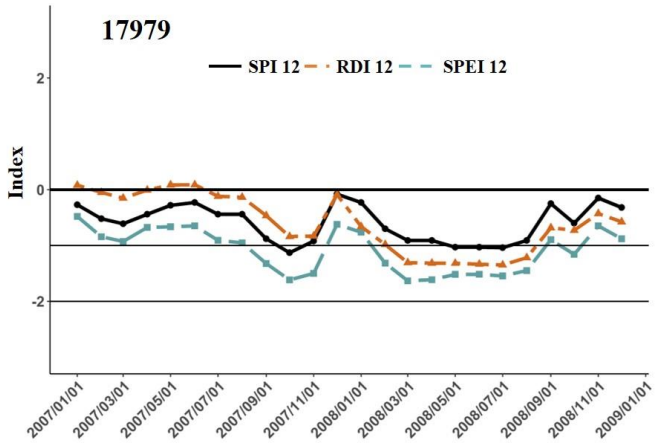

Figure 5.13 The comparison of SPI, SPEI and RDI at different time scale with respect to historical drought

5.6.1 The Spatial Distribution of Drought Classification of SPI and SPEI

It is investigated according to the normal and severe drought class between the period of 1986-1995, 1996-2005 and 2006-2011 to understand the effects and differences of SPI and SPEI indices on the basin. In Figure 5.14 (a-d) and Figure 5.15 (a-d), the performance of SPI and SPEI according to the normal and severe drought category at the 1- and 3-month time scales are evaluated, respectively.

Considering the normal drought category, it is observed that the drought curve at all stations increase in the SPI 1-month time series from the period of 1986 to 2011 except 17866 and 17960 stations decreased when the period of 1986-1995 are compared to 1996-2005. When the same time interval is examined for SPEI 1-month time series, drought time is positive increase in 17866, 17868, 17870, 17355, 17979, 17255 stations, while the drought months decrease in 17908 and 17960 stations.

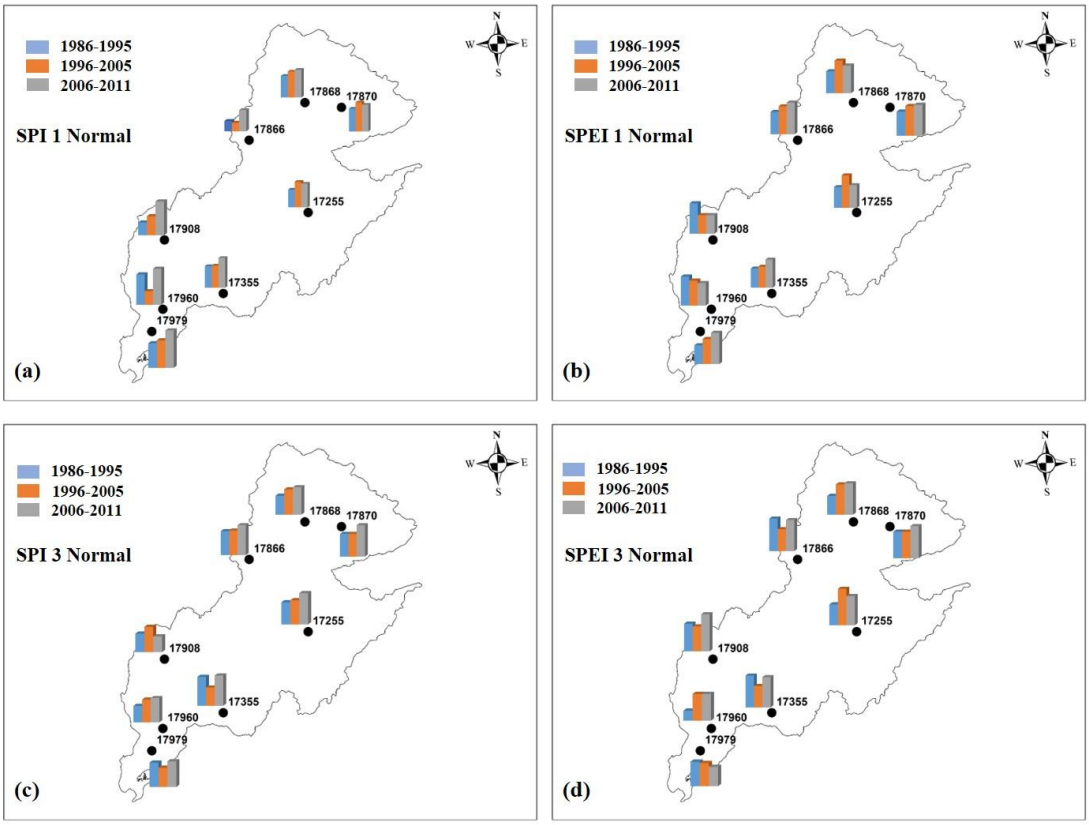

Figure 5.14 The spatial distribution of SPI and SPEI over Ceyhan Basin according to normal drought category (1- and 3-month)

When the 3-month time series are analyzed for both drought indices, it is analyzed that the longest drought period is between the period of 2006 and 2011, except for 17908 stations that the longest drought period is seen in the years of 1996-2005, in the SPI 3-month. In the SPEI 3-month time series, normal drought increases positively except 17979 station. However, as in the SPEI 1-month time series, the longest drought period in 17255 station is observed in 1996-2005. For station 17979, unlike the SPEI 1-month time series, drought trend is negative and the longest drought occurred between the period of 1986-1995.

According to the severe drought category (Figure 5. 15), considering the SPI 1-month time series, drought severe category is observed that it decreases in the following years except 17960 and 17870 stations. The longest severe drought is between 1986-2005 in terms of three periods. The longest severe drought in 17960 and 17970 stations is 2006-2011 and 1996-2005, respectively. According to the SPI 1-time scale, there is no severe drought in 17255 stations between the years of 2006-2011.

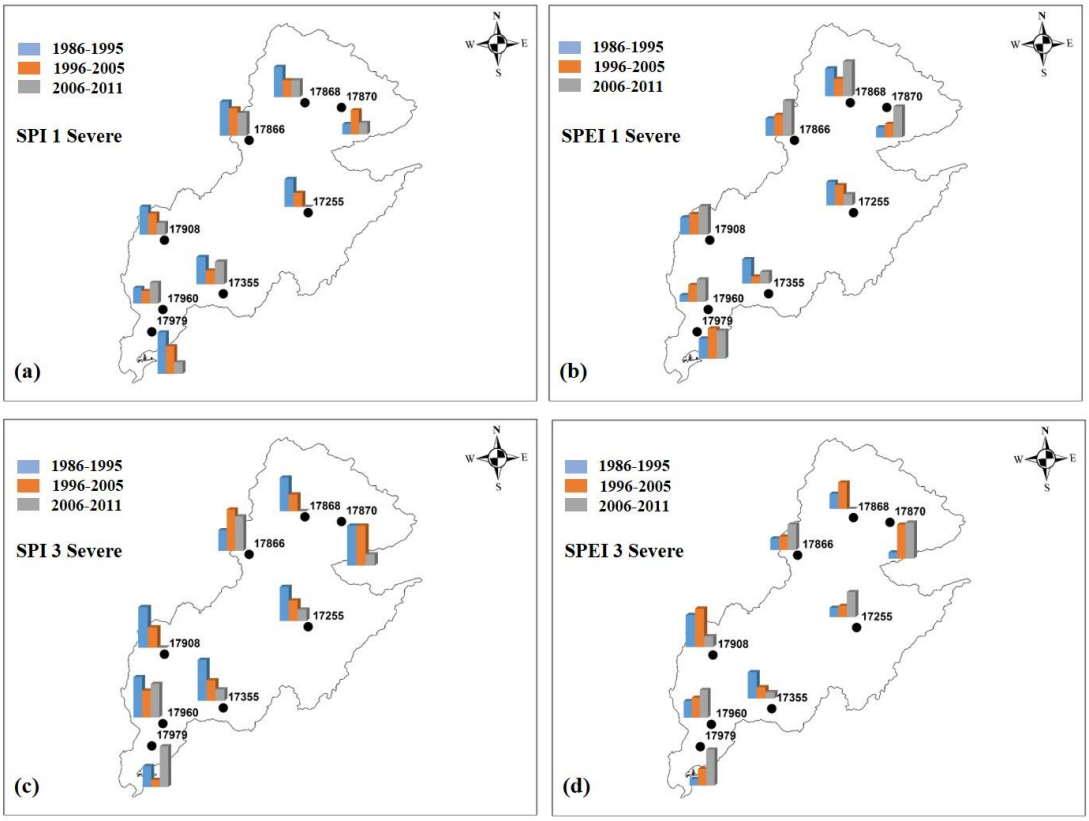

Figure 5.15 The spatial distribution of SPI and SPEI over Ceyhan Basin according to severe drought category (1- and 3-month)

SPEI 1-month time series severe drought periods are obtained differently from the SPI 1-month time series. In general, it is observed that severe drought increases in the following periods except 17255 and 17355 stations. However, these increases have very small values compared to other drought categories. For example, while the longest drought severe period has 15.27% at the 17870 station between 2006-2011, drought severe period has been calculated as 2.77% at the 17255 station and they have less percentile compared to other drought categories.

SPI 3-month time series results are in line with 1-month time series results. there is no severe drought at 17908 station between the period of 2006-2011, according to the results of both drought indices. As a general view for the SPEI 3-month time series, the trend is negative at 17355, 17908 and 17868 stations, whereas severe drought periods are observed to increase positively at other stations. The spatial distribution of SPI and SPEI over Ceyhan Basin according to moderate and extreme classes are presented in Figure 5.16 and 5.17, respectively.

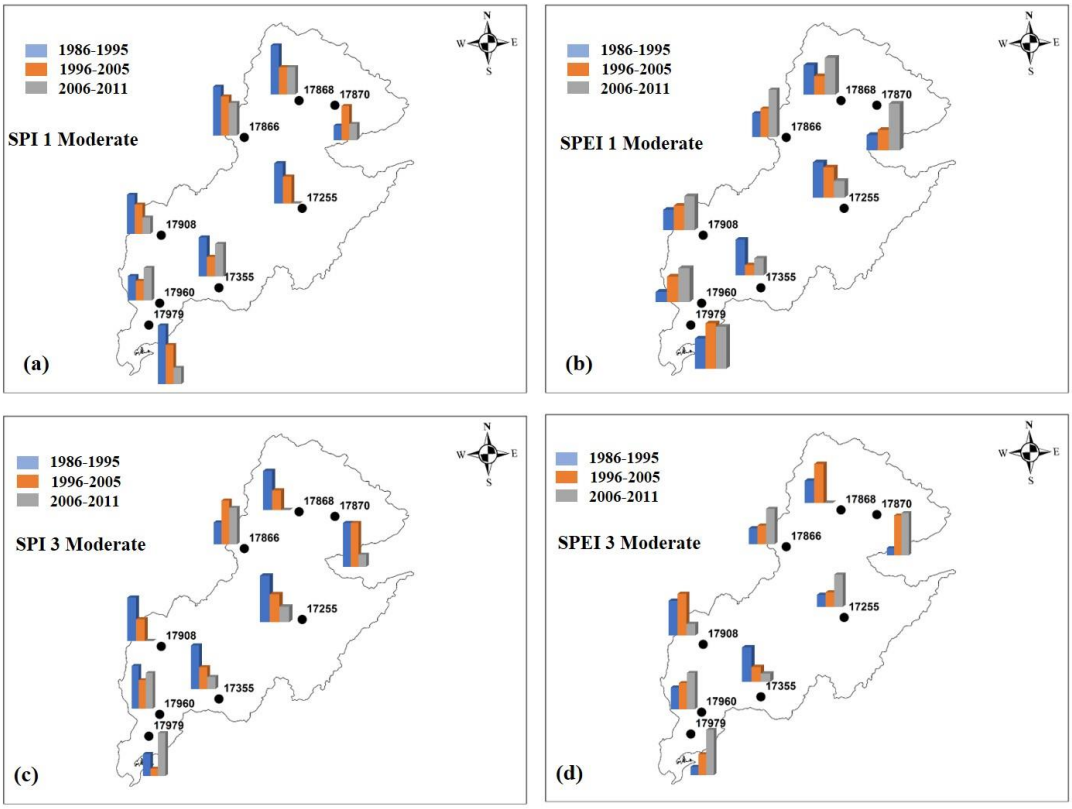

Figure 5.16 The spatial distribution of SPI and SPEI over Ceyhan Basin according to moderate drought cateogy (1- and 3-month)

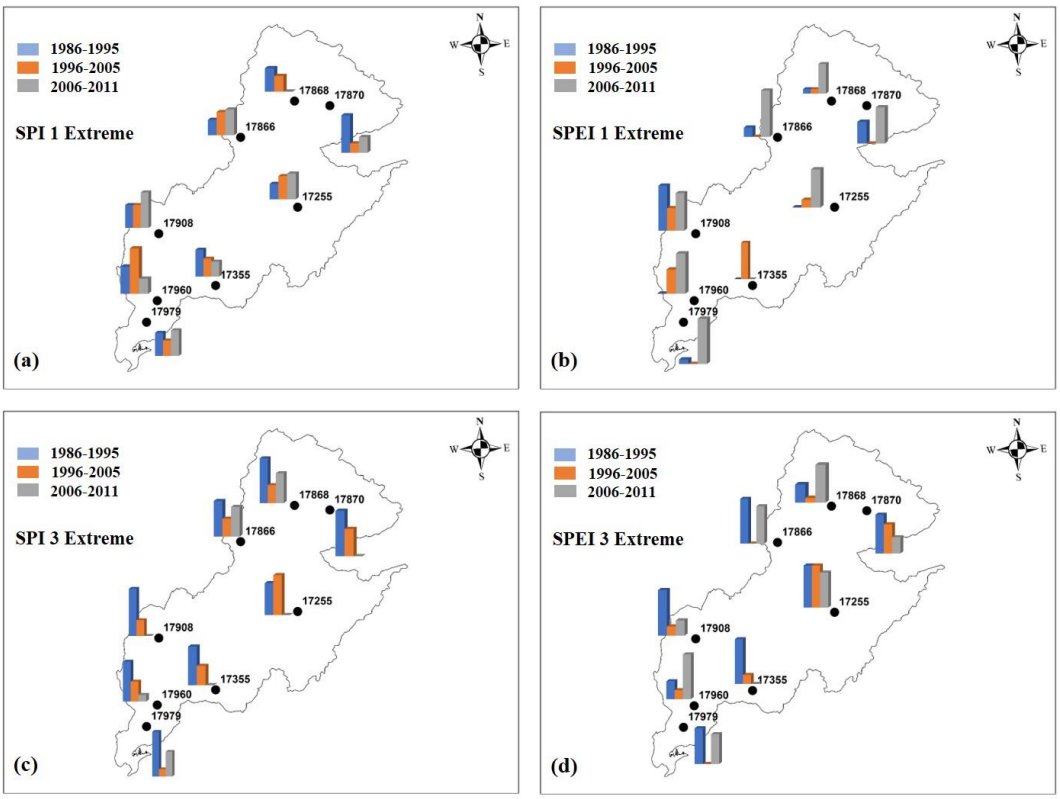

Figure 5.17 The spatial distribution of SPI and SPEI over Ceyhan Basin according to extreme drought cateogy (1- and 3-month)

Among the drought classes, moderate, severe and extreme classes are lower percentage compared to wet and normal classes. According to this small percentage for moderate class, the higher occurrence percentage are evaluated at first decade (1986-1995) among three periods for SPI 1-month scale except 17870 stations found at the second decade (1996-2005). For SPEI 1-month scale, the higher occurrence percentage are found between the year of 2006-2011 except 172255 and 17355 station showed the higher percentage at first decade. Like SPI 1-month time scale, the higher occurrence percentage are demonstrated at first decade except 17866 and 17979 stations for SPI 3-month time scale (Figure 5.16). At the SPEI 3-time series, Moderate class is no observed at 17868 station between the period of 2006-2011, while the highest moderate class are observed at the same time for 17979 station.

At the SPEI 1-month time scale, the highest extreme occurrence percentage are obtained between 2006-2011 except 17355 station (Figure 5.17). Extreme drought doesn't find at 17868 station for SPI 1-month scale. But the highest relative frequency is obtained at first decade with regard to SPI 3-month time scale. Interestingly, SPI 3 and SPEI 3 have indicated the same results at the extreme class.

Spatially, SPI 1-and 3-month time scale normal and severe drought relative frequencies of spatial distribution on Ceyhan Basin are presented in Figure 5.18.

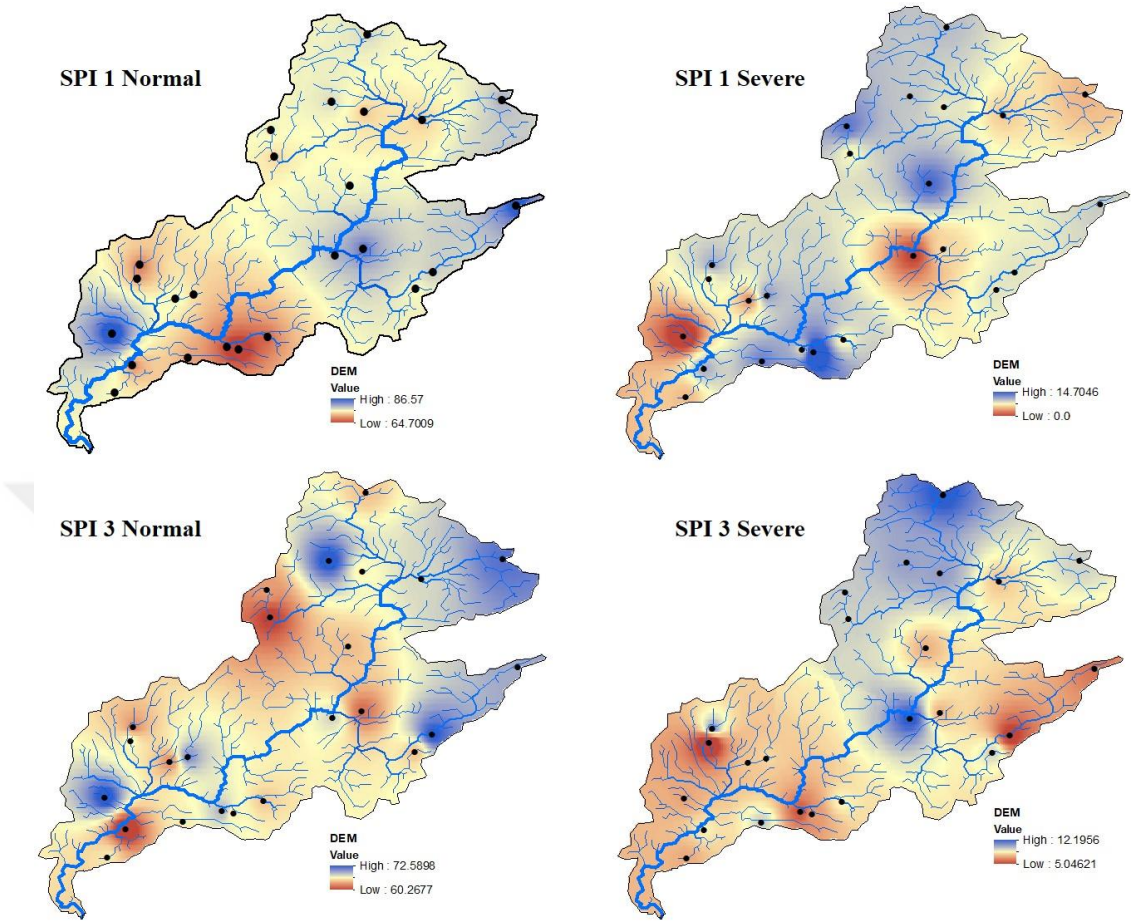

Figure 5.18 The spatial distribution of SPI normal and severe drought categories on the Ceyhan Basin (1-and 3-month scale)

CHAPTER SIX

TREND ANALYSIS OF EXTREME DROUGHT EVENTS IN CEYHAN BASIN

6.1 Overview

Drought is a complicated natural hazard that may be primarily described by its duration and severity. These parameters are generally obtained from hydro-meteorological data including stream flow, groundwater and rainfall, using numerous model approaches. If the basic data of interest is precipitation among these parameters, it can be described as a meteorological drought. The drought severity and duration characteristics of the meteorological drought are the primary interest of hydrologists, meteorologists, agriculturists for management, planning, and design of hydraulic structure related to water. These can also be mainly of great importance for hydraulic design, reservoir policies.

Annual total precipitation trend analyses, on various temporal and spatial scales, are of great interest during the last century due to concern given to climate change globally from the researcher community. In this chapter, firstly, annual total precipitation, and temperature will be investigated in terms of statistical tests. Our main concern is to evaluate any changes using the historical data in the Ceyhan Basin. Hence, if the presence of a trend is detected, the magnitude of trend, change-point detection will be discussed in detail. Secondly, the trends of extreme drought events such as annual maximum drought severity (AMS), defined as the largest cumulative severity value for each year, and drought duration (AMD), are described as the length of maximum drought duration for each year, will be investigated. It should be noted that two-parameter is independent of one another. Here, the length of the AMS may not be the same as the length of the AMD in a year. Hence, AMS and AMD will be evaluated as a different part concerning statistical analysis tests. Two extreme events are calculated using the SPI program for different time steps (1-, 3-,

6-, 9- and 12-month). Finally, it will be extensively evaluated how climate change effects on the Ceyhan Basin by applying trend tests, the magnitude of trend, and change-point detection tests.

6.2 Time Series of Annual Total Precipitation

Before the investigation of extreme drought events, firstly, annual total precipitation time series are drawn graphically for each station in Ceyhan Basin. These graphs don't give any idea about the presence of trend statistically significant but provide a view at least about varying the data with time. Hence, annual total precipitation time series are presented in Figure 6.1 for used all stations.

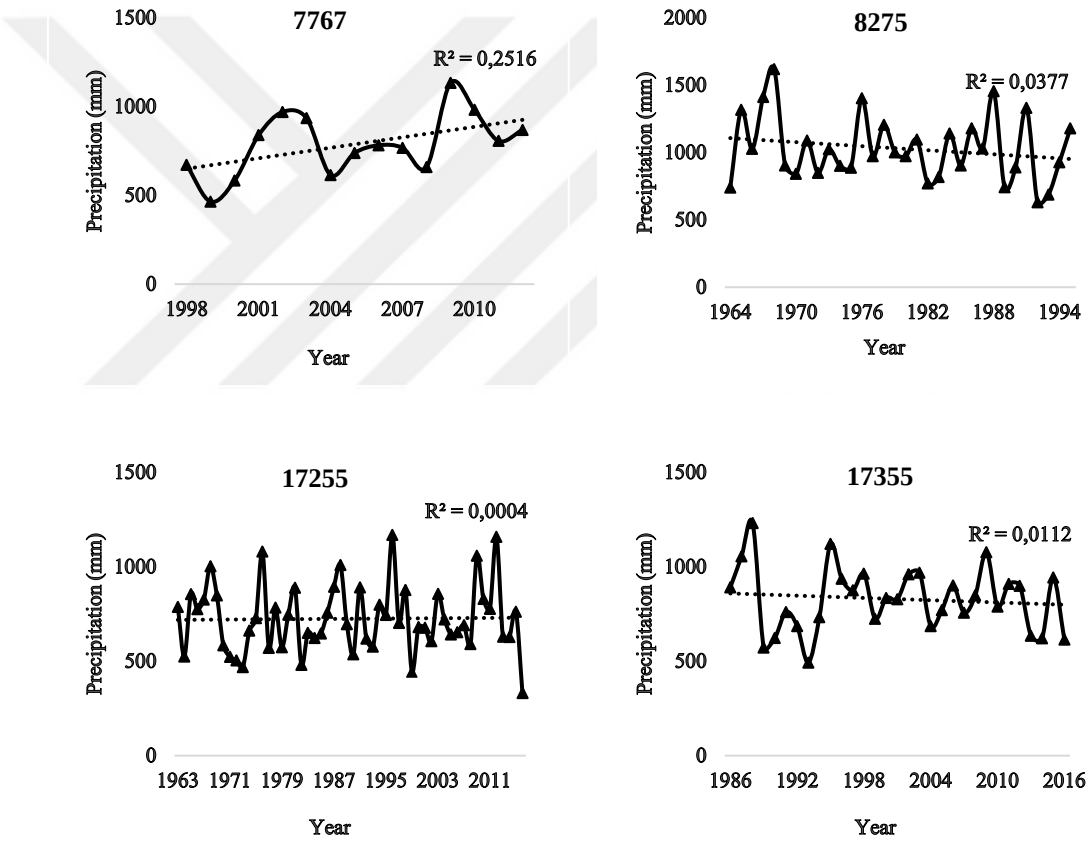

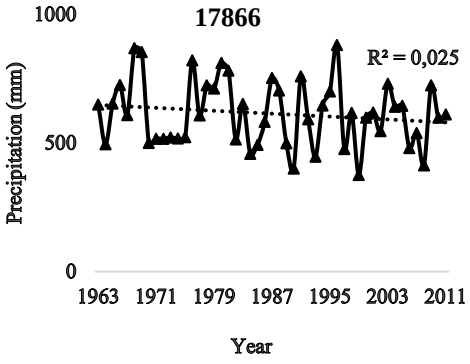
17866
R² = 0,025
Precipitation (mm)
1000
500
0
1963 1971 1979 1987 1995 2003 2011
Year

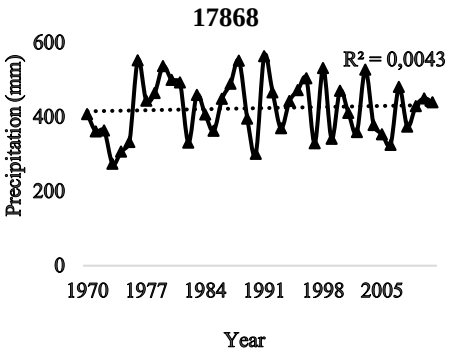
17868
R² = 0,0043
Precipitation (mm)
600
400
200
0
1970 1977 1984 1991 1998 2005
Year

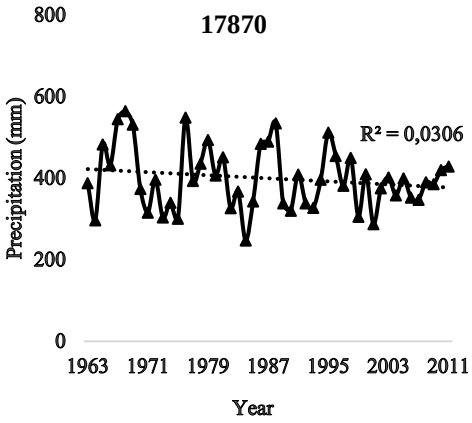
17870
R² = 0,0306
Precipitation (mm)
800
600
400
200
0
1963 1971 1979 1987 1995 2003 2011
Year

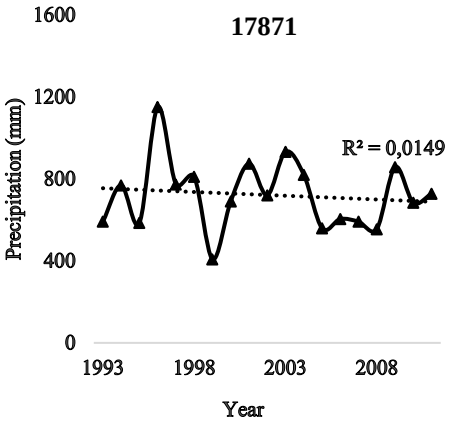
17871
R² = 0,0149
Precipitation (mm)
1600
1200
800
400
0
1993 1998 2003 2008
Year

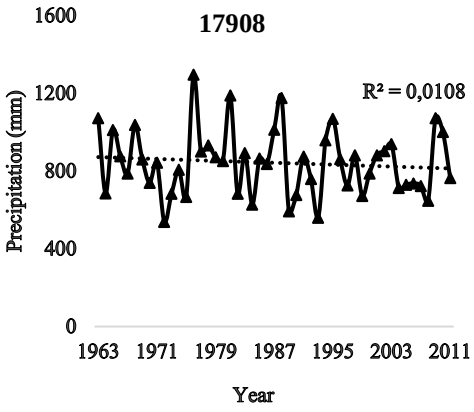
17908
R² = 0,0108
Precipitation (mm)
1600
1200
800
400
0
1963 1971 1979 1987 1995 2003 2011
Year

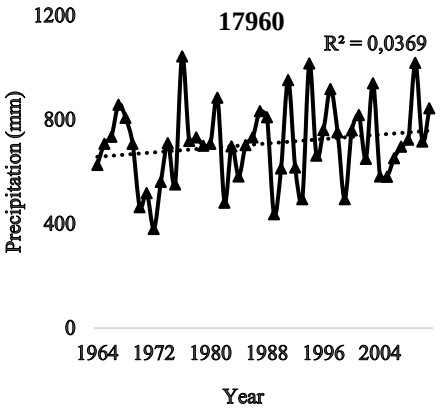
17960
R² = 0,0369
Precipitation (mm)
1200
800
400
0
1964 1972 1980 1988 1996 2004
Year

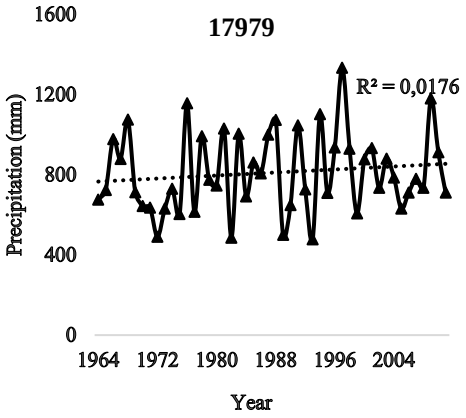
17979
R² = 0,0176
Precipitation (mm)
1600
1200
800
400
0
1964 1972 1980 1988 1996 2004
Year

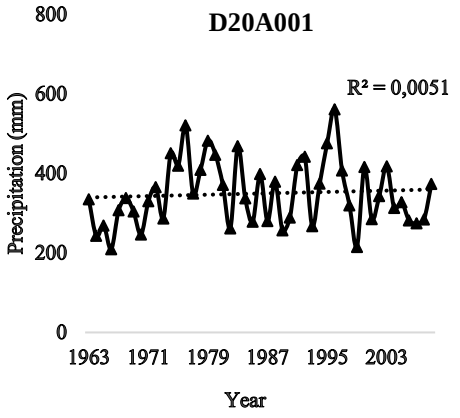
D20A001
R² = 0,0051
Precipitation (mm)
800
600
400
200
0
1963 1971 1979 1987 1995 2003
Year

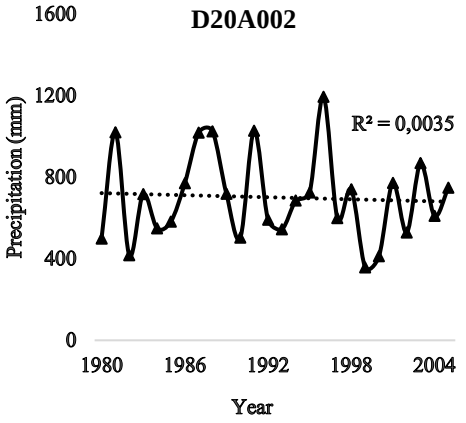
D20A002
R² = 0,0035
Precipitation (mm)
1600
1200
800
400
0
1980 1986 1992 1998 2004
Year

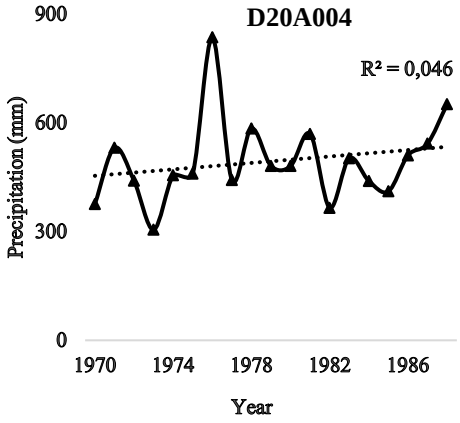
D20A004
R² = 0,046
Precipitation (mm)
900
600
300
0
1970 1974 1978 1982 1986
Year

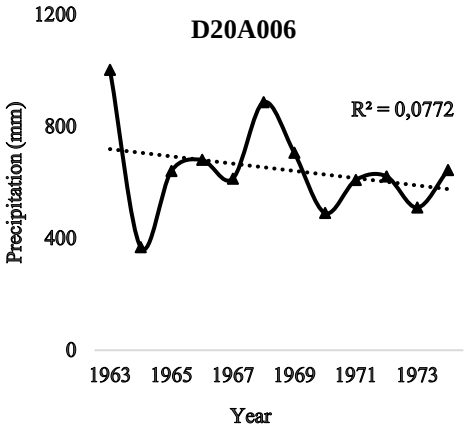
D20A006
R² = 0,0772
Precipitation (mm)
1200
800
400
0
1963 1965 1967 1969 1971 1973
Year

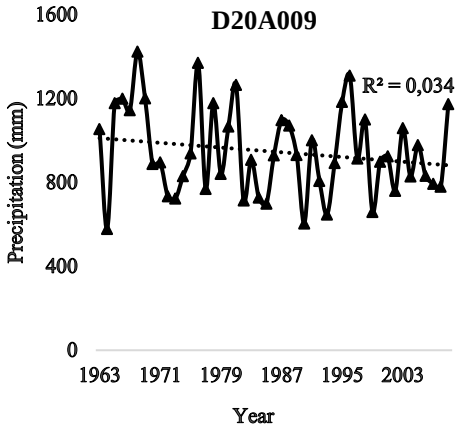
D20A009
R² = 0,034
Precipitation (mm)
1600
1200
800
400
0
1963 1971 1979 1987 1995 2003
Year

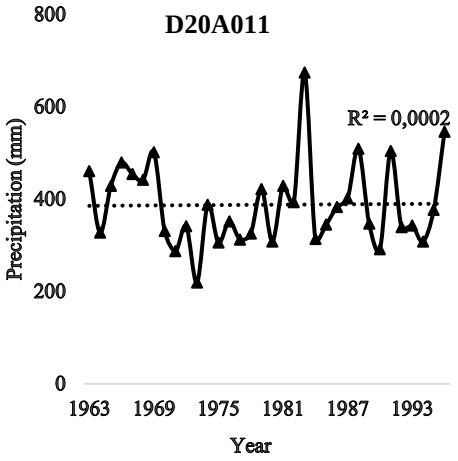
D20A011
R² = 0,0002
Precipitation (mm)
800
600
400
200
0
1963 1969 1975 1981 1987 1993
Year

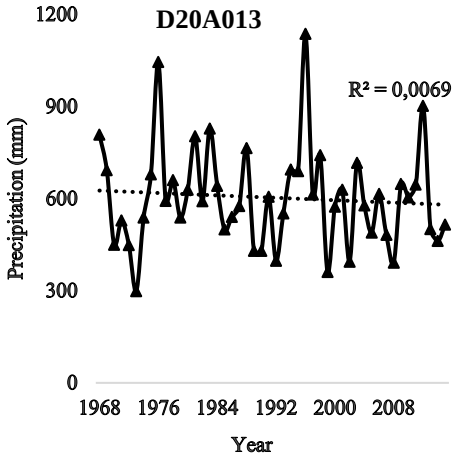
D20A013
R² = 0,0069
Precipitation (mm)
1200
900
600
300
0
1968 1976 1984 1992 2000 2008
Year

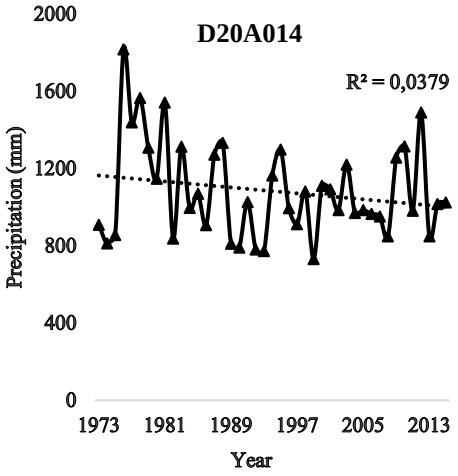
D20A014
R² = 0,0379
Precipitation (mm)
2000
1600
1200
800
400
0
1973 1981 1989 1997 2005 2013
Year

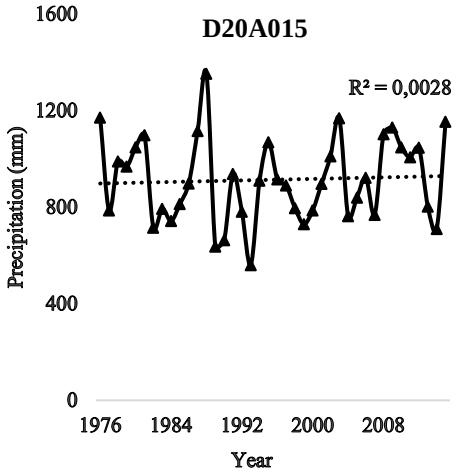
D20A015
R² = 0,0028
Precipitation (mm)
1600
1200
800
400
0
1976 1984 1992 2000 2008
Year

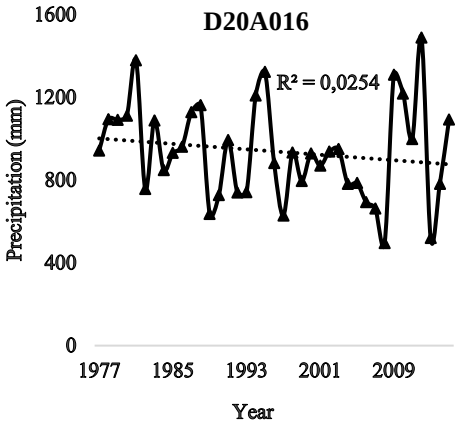
D20A016
R² = 0,0254
Precipitation (mm)
1600
1200
800
400
0
1977 1985 1993 2001 2009
Year

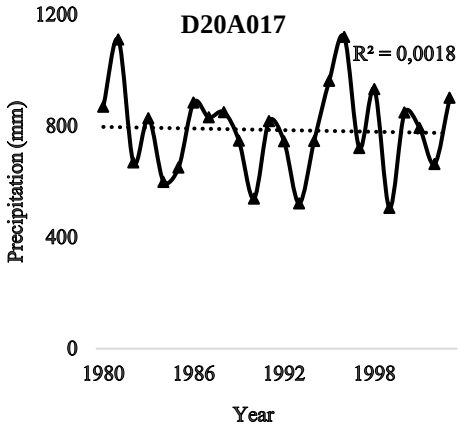
D20A017
R² = 0,0018
Precipitation (mm)
1200
800
400
0
1980 1986 1992 1998
Year

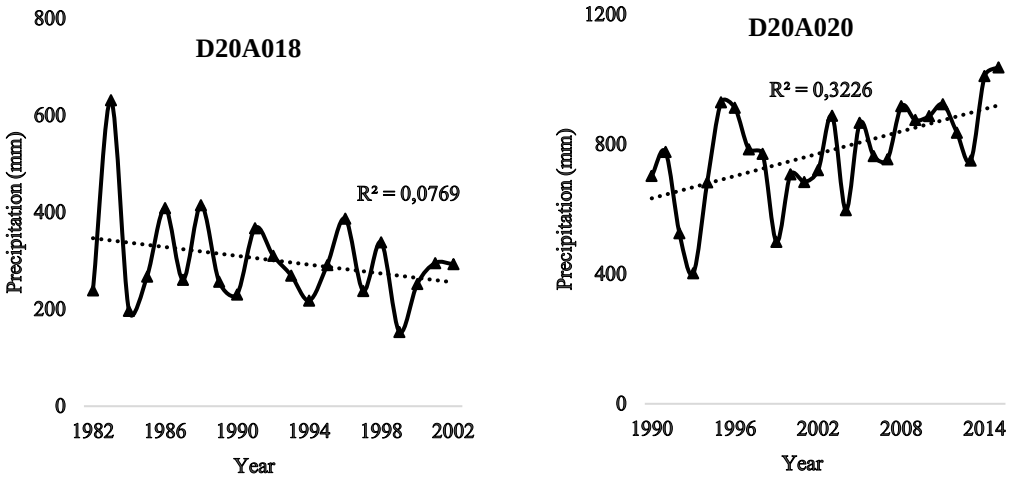

Figure 6.1 The total annual precipitation time series for all stations

6.2.1 Spatial Distribution of Precipitation Data

Although there are differences between the regions in terms of the distribution of precipitation throughout the seasons, a significant part of Turkey is under the effect of the Mediterranean precipitation regime. Summers are arid in places affected by this precipitation regime, while most of the annual precipitation falls in winter. This precipitation regime is observed in the Marmara Region, which is located in southwest Anatolia. According to Figure 6.2, the highest distribution annual depth of precipitation is seen in the lower basin as 381 mm while the lowest distribution depth of precipitation occurs in the upper basin as 894 mm.

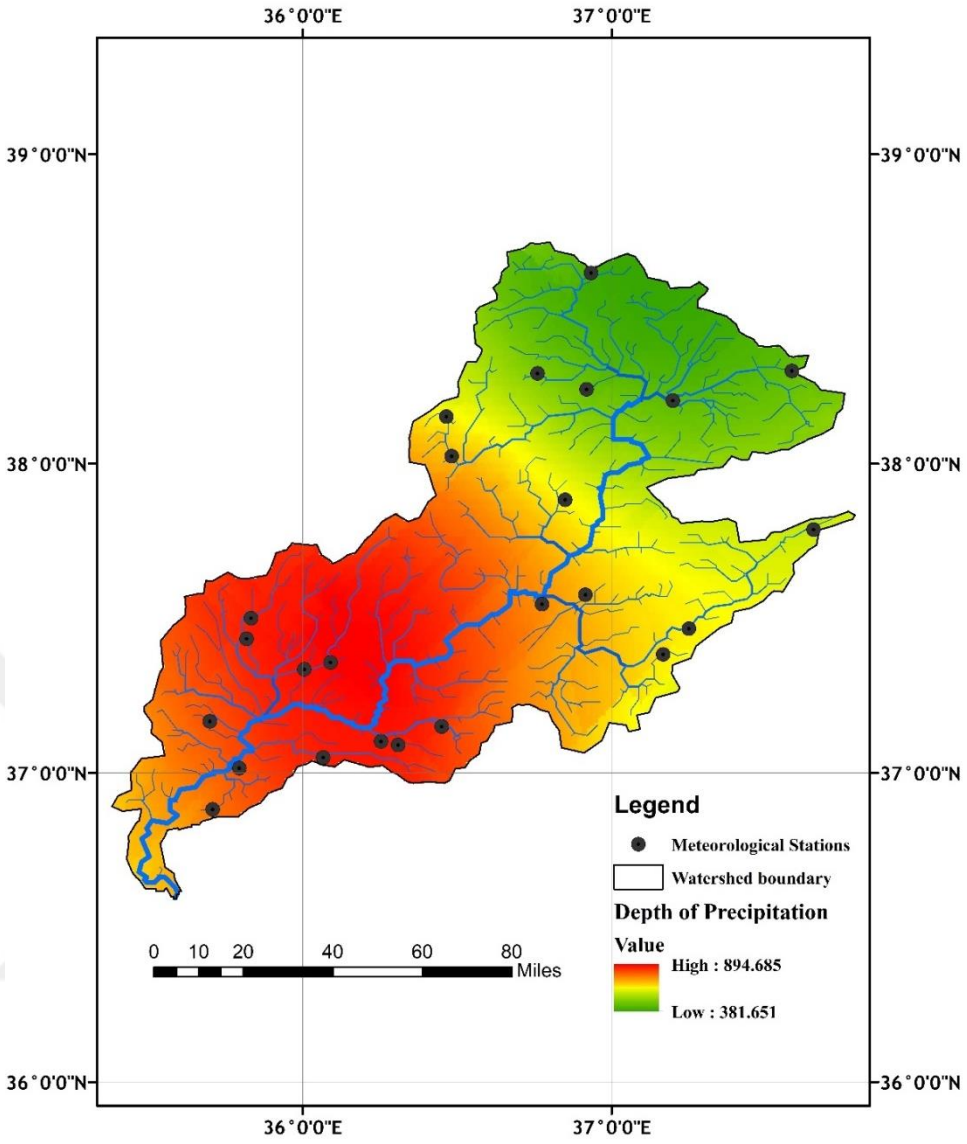

Figure 6.2 Annual depth of precipitation distribution in Ceyhan basin

6.2.2 Homogeneity of Annual Total Precipitation

The Wallis and Moore Phase-Frequency (WM) and Wald-Wolfowitz test (WW) are applied to the annual total precipitation data. The z statistics evaluated both WM and WW tests for all stations are given in Table 6.1. According to z statistic, the null hypothesis cannot be rejected between -1.96 > z > 1.96 and -164 > z > 1.64 at 95% and 90% significance level, respectively. it is seen from the results; all stations indicate homogeneous (H) at both two-significance levels in terms of WM tests. The same results show for the WW test except for stations 17870, D20A018, and D20M020. Hence, the null hypothesis cannot be rejected at 90% significance level for three stations, while it cannot be rejected at 95% significance level for station 17870 and D20A020.

Table 6.1 Homogeneity results of annual total precipitation for all stations

Station	WW			WM		
	z	**90%(±1.64)**	**95% (±1.96)**	**z**	**90%(±1.64)**	**95% (±1.96)**
7767	1.587	H	H	0.762	H	H
8275	-0.304	H	H	0.863	H	H
17255	0.160	H	H	0.219	H	H
17355	0.952	H	H	0.146	H	H
17866	0.911	H	H	1.266	H	H
17868	0.192	H	H	0.998	H	H
17870	2.026	**N-H**	**N-H**	0.575	H	H
17871	-0.065	H	H	1.240	H	H
17908	-0.317	H	H	0.230	H	H
17960	-0.020	H	H	0.931	H	H
17979	-0.593	H	H	0.116	H	H
D20A001	1.440	H	H	0.233	H	H
D20A002	-0.476	H	H	-0.241	H	H
D20A004	-0.592	H	H	0.477	H	H
D20A006	-0.815	H	H	-0.124	H	H
D20A009	0.930	H	H	0.353	H	H
D20A011	0.429	H	H	0.697	H	H
D20A013	0.918	H	H	0.116	H	H
D20A014	1.158	H	H	0.616	H	H
D20A015	1.364	H	H	1.663	H	H
D20A016	0.678	H	H	0.259	H	H
D20A017	-0.008	H	H	0.420	H	H
D20A018	-1.646	**N-H**	H	-0.090	H	H
D20A020	2.057	**N-H**	**N-H**	0.723	H	H

H: Homogeneous, **N-H**: Non-Homogeneous

6.2.3 Trend Detection of Annual Total Precipitation

As for the identification of trend detection, the most popular Mann-Kendall and Spearman's rho trend tests are applied to all stations. Table 6.2 presents the results of trend detections. As mention earlier 6.1.1 section, z statistics are the same for both MK and SR tests. Negative value shows and decreasing trend and vice versa. The trend analysis for annual total precipitation at each station shows that most stations have no trend in the Ceyhan Basin, but a few stations have statistically significant increasing trends at the 90% level both station 7767 and D20A020, at 95% level only for D20A020. Considering the trend results, Mann-Kendall and Spearman's rho trend tests indicate similar performance for trend detection.

Table 6.2 Trend detection results of annual total precipitation for all station

Station	Mann-Kendall			Spearman's Rho		
	z	90%(±1.64)	95% (±1.96)	z	90%(±1.64)	95% (±1.96)
7767	1.782	**I**	N	1.844	I	N
8275	-0.665	N	N	-0.739	N	N
17255	0.090	N	N	0.120	N	N
17355	-0.340	N	N	-0.360	N	N
17866	-0.974	N	N	-0.988	N	N
17868	0.238	N	N	0.314	N	N
17870	-0.655	N	N	-0.720	N	N
17871	-0.280	N	N	-0.402	N	N
17908	-0.552	N	N	-0.563	N	N
17960	1.191	N	N	1.141	N	N
17979	0.809	N	N	1.010	N	N
D20A001	0.062	N	N	0.049	N	N
D20A002	0.441	N	N	0.186	N	N
D20A004	1.330	N	N	1.243	N	N
D20A006	-0.617	N	N	-0.789	N	N
D20A009	-1.082	N	N	-1.109	N	N
D20A011	-0.148	N	N	-0.171	N	N
D20A013	-0.631	N	N	-0.647	N	N
D20A014	-0.921	N	N	-0.683	N	N
D20A015	0.454	N	N	0.405	N	N
D20A016	-1.113	N	N	-1.126	N	N
D20A017	-0.273	N	N	-0.075	N	N
D20A018	-0.393	N	N	-0.337	N	N
D20A020	2.645	**I**	**I**	2.617	**I**	**I**

N; No-Trend, **I**: Increasing

6.2.4 Magnitude of Trend of Annual Total Precipitation

Linear Regression and Sen's slope are performed to predict the magnitude of the trend. Table 6.3 shows the results obtained from the two tests. The signs of the slopes are much appropriate with the results Mann-Kendall and Spearman's rho trend test. The highest magnitude is obtained from the existence of trends that occurred at station 7767 (19.668 and 20.196 separately) and D20A020 which are 11.550 and 11.470 for linear Regression and Sen's slope, respectively.

Table 6.3 The slope of trends of annual total precipitation for all station

Station	Sen's Slope	Linear Regression
	z	z
7767	19.668	20.196
8275	-3.836	-5.003
17255	0.186	0.214
17355	-1.804	-1.999
17866	-1.196	-1.411
17868	0.333	0.413
17870	-0.707	-0.941
17871	-2.354	-3.662
17908	-0.849	-1.220
17960	1.906	2.133
17979	1.532	1.885
D20A001	0.141	0.160
D20A002	1.318	1.432
D20A004	5.475	4.438
D20A006	-11.037	-12.991
D20A009	-2.836	-2.817
D20A011	-0.400	-0.563
D20A013	-1.128	-0.981
D20A014	-3.200	-3.855
D20A015	1.180	0.792
D20A016	-4.000	-3.296
D20A017	-1.652	-0.970
D20A018	-1.755	-4.550
D20A020	11.550	11.470

6.2.5 Change-Point Detection of Annual Total Precipitation

The findings of shift-point detection reveal that most of the stations are homogeneous (as illustrated in Table 6.1), but some of the series shows change-point due to climate variability occurred in the basin. Considering the uncertainty of variation in the series, more than two methods are utilized for comparison. These tests are the Pettitt's Test (PT), the Standard Normal Homogeneity Test (SNHT) and Buishand Range Test (BRT), after obtained trend tests that indicate positive or negative. The results of the three tests are compared to determine a more precise breaking point. Therefore, if two outcomes of the three tests are the same, a break point is selected for that station. However, if the results of all used tests differ from each other, the choice of the break point will be suspect (S). When we consider station 7767 for, SNHT and BRT capture

at the year 2000 whereas PT captures in the year of 2008 (Table 6.4). Figures 6.3 and 6.4 indicate the annual total precipitation data break point is graphically presented for station 7767 and D20A020, respectively.

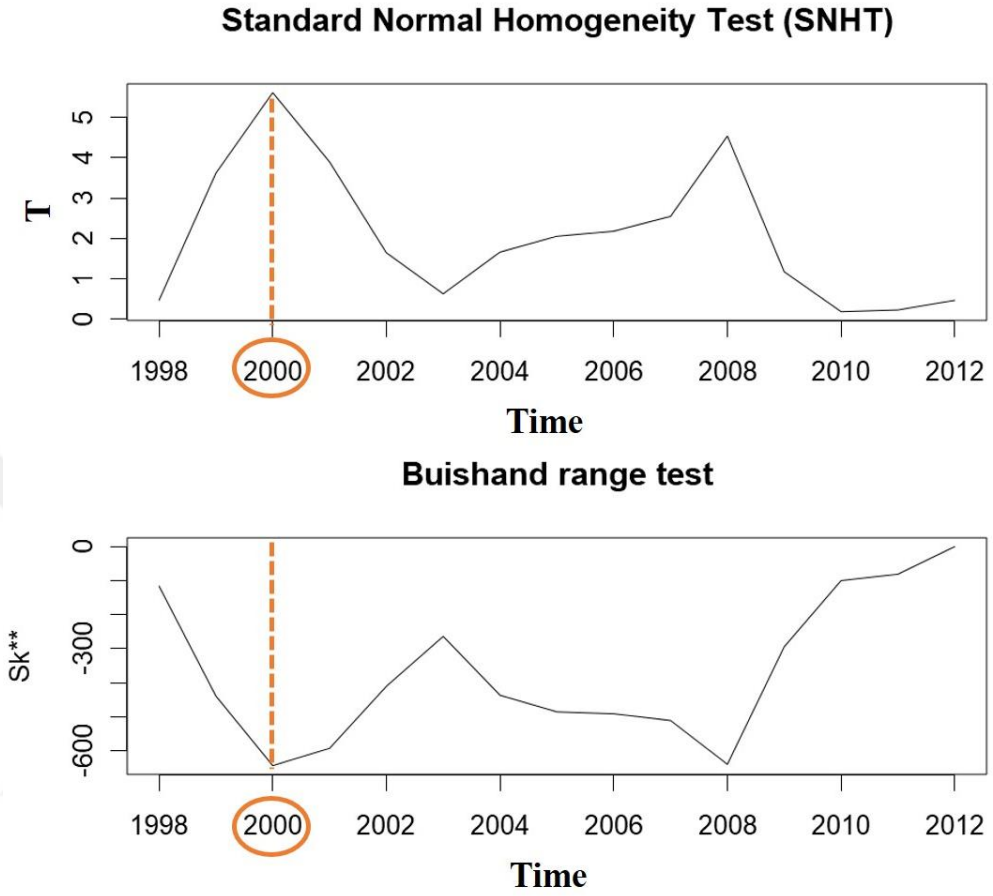

Figure 6.3 The annual total precipitation series change point for 7767 station

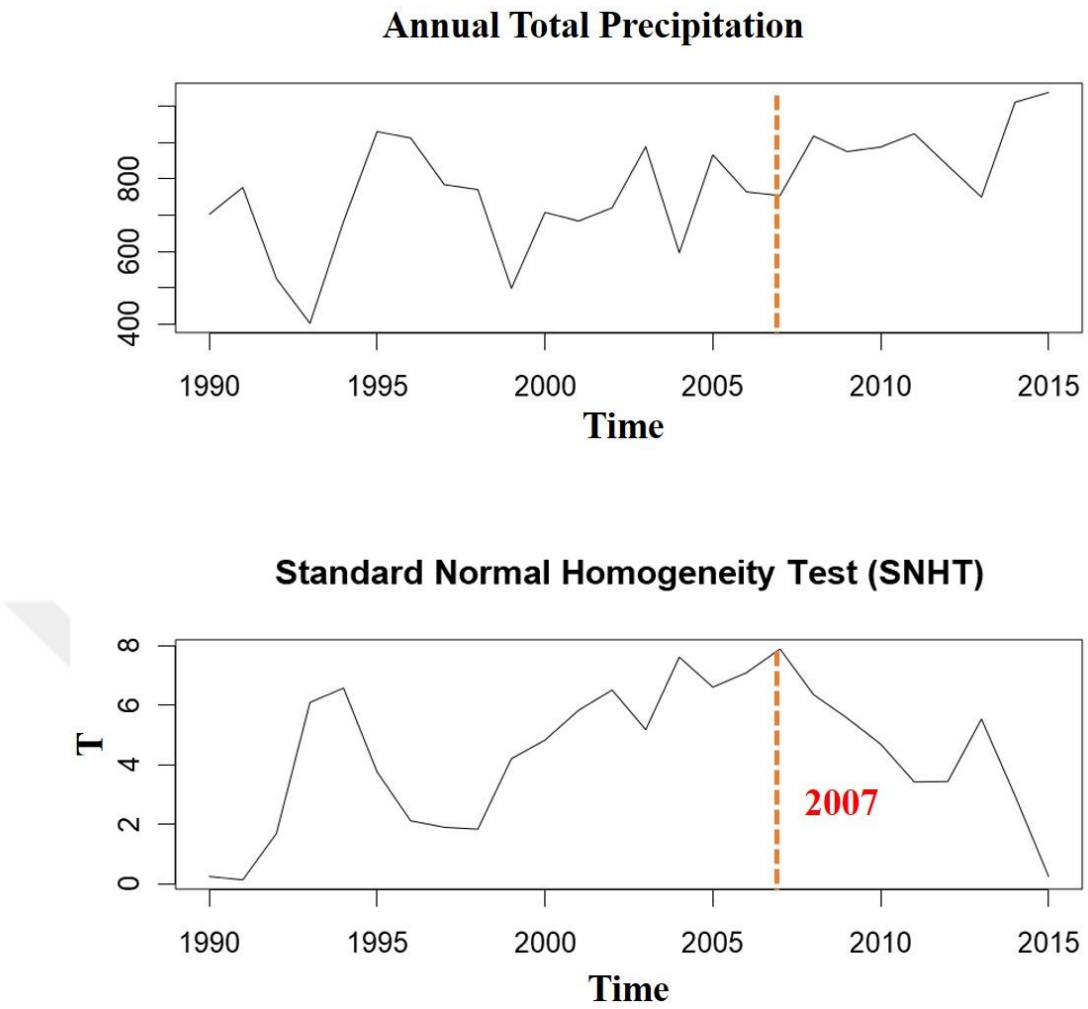

Figure 6.4 The annual total precipitation series change point for station D20A020

Table 6.4 The change point detection for the annual total precipitation

	SNHT		PT		BRT		
Station	**T**	**CP**	**U**	**CP**	**R / sqrt(n)**	**CP**	**Result**
7767	5.614	2000	34	2008	0.947	2000	**2000**
D20A020	7.88	2007	102	2007	1.3629	2004	**2007**

CP; Change-Point

6.3 Time Series of Temperature Data

In recent years, rising temperatures, floods, and droughts in Turkey, especially in the Mediterranean basin, have been brought to light due to global climate change. Temperature appears to be an important parameter of climate change. Hence, comprehensive studies about temperature data are performed to monitor any changes over the Ceyhan Basin.

Temperature parameters are examined in two stages: monthly and annual. For the annual studies, their annual maximum, mean, and minimum values are considered.

Their trends are tested by Spearman Rho and Mann-Kendall tests. Trend's slope is investigated by utilizing Regression and Sen's slope methods. The starting point of the trend is determined by using the Buishand Range Test, Standard Normal Homogeneity Test, and the Pettitt Test. Monthly (a) maximum, (b) minimum, and (c) mean temperature for all stations, from 1963-2018, are presented in Figures 6.5-6.12. The boundary of the box nearest to zero and farthest to zero show the 25th and 75th percentile, respectively. The line within the box indicates the median and error bars below and above the box show the 10th and 90th percentiles. The highest maximum temperature generally occurs at its peak in August and its lowest value in January for three cases. While the highest monthly maximum temperature is about 40° C, the lowest temperature is not below 10° C. The highest minimum temperature is seen below 20° C in summer whereas the lowest minimum falls below 0° C in January, February, and December. When focused on the monthly mean temperature, both the highest and lowest temperature degrees are analyzed above 0° C for station 17255 in Figure 6.5.

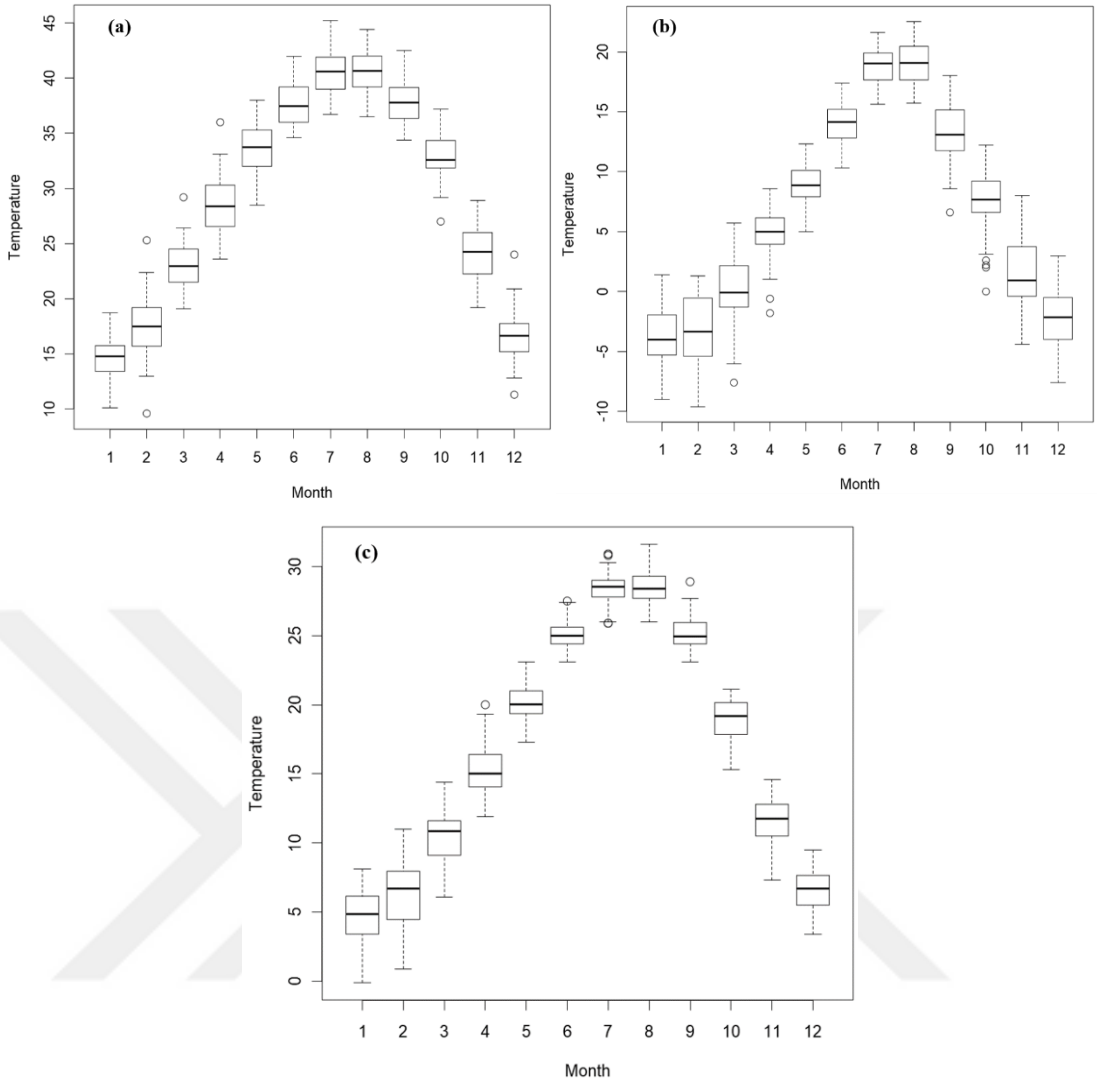

Figure 6.5 Monthly (a) maximum, (b) minimum and (c) mean temperature for station 17255 between the years of 1963-2018

The highest maximum temperature takes place at its peak in August and its lowest value in January for three cases. While the highest monthly maximum temperature is about 38° C (August), the smallest temperature is around 10° C (January). The highest minimum temperature is seen below 20° C in summer whereas the smallest minimum falls below 0° C (between 0 and -5° C) in January, February, and December. When focused on the monthly mean temperature, both the highest and lowest temperature degrees are analyzed above 0° C for station 17355 in Figure 6.6.

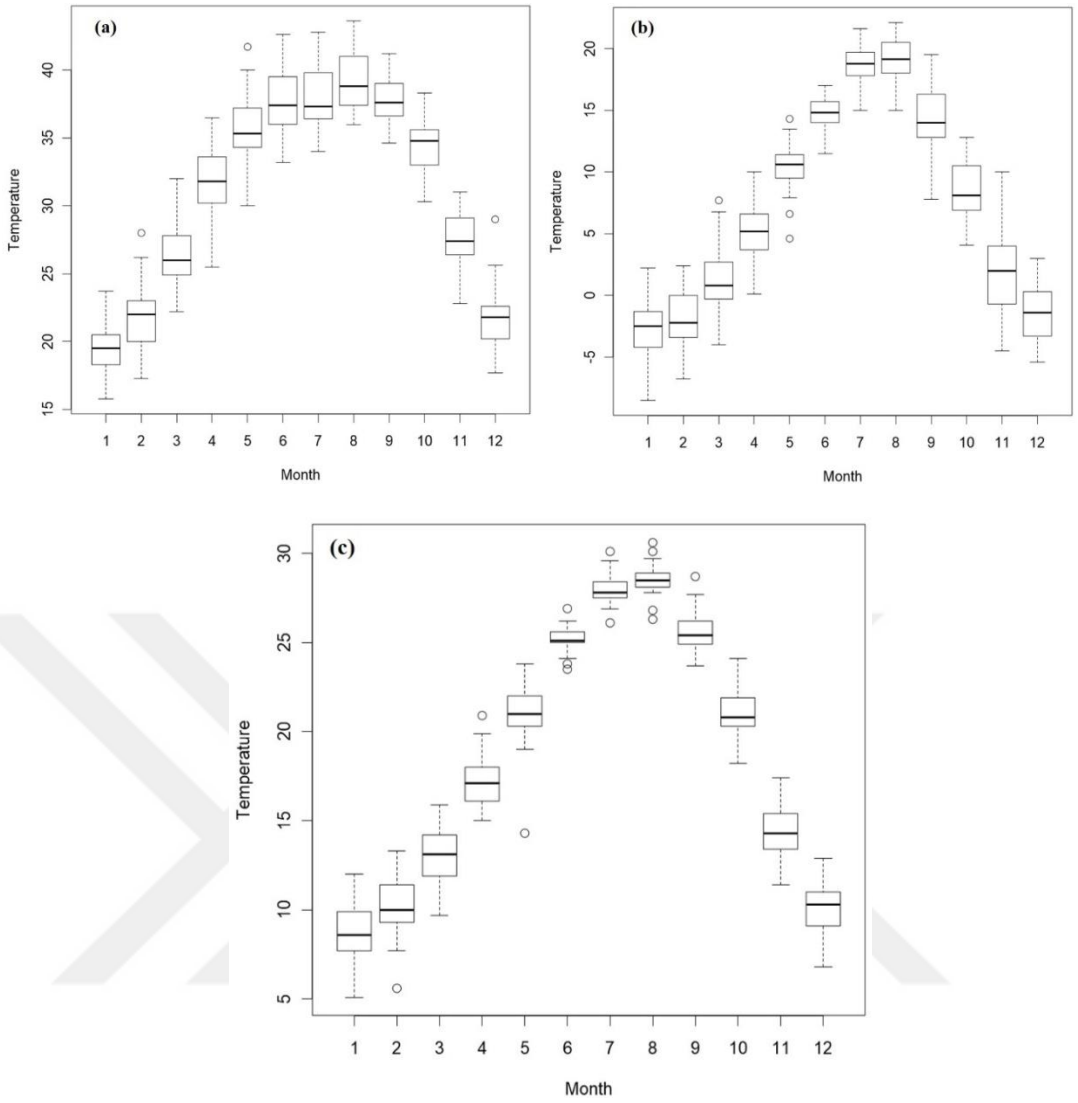

Figure 6.6 Monthly (a) maximum, (b) minimum and (c) mean temperature for station 17355 between the years of 1963-2018

The highest maximum temperature, for station 17866, takes place at its peak in August and its lowest value in January for three cases. While the highest monthly maximum temperature is about 35° C (August), the lowest temperature is between 5° C and - 10° C (January). The highest minimum temperature is seen below 10° C in summer whereas the lowest minimum falls below -20° C in January, February, and December. While the highest mean temperature occurs in July about 21° C, the lowest temperature degrees are analyzed below 0° C for January, February and December in Figure 6.7.

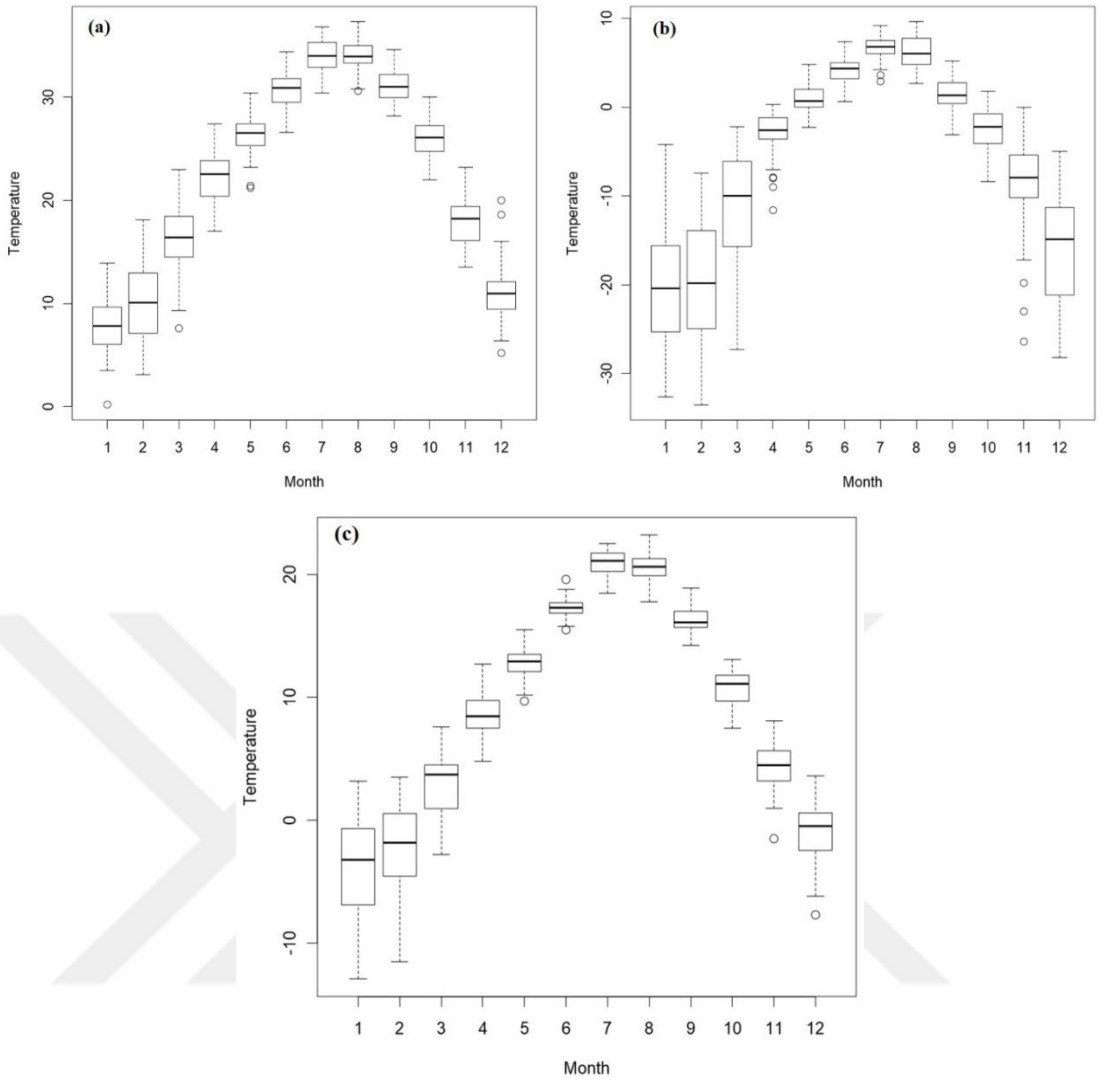

Figure 6.7 Monthly (a) maximum, (b) minimum and (c) mean temperature for station 17866 between the years of 1963-2018

The highest maximum temperature, for station 17868, takes place at its peak in July and August and its lowest value in January for three cases. While the highest monthly maximum temperature is about 35° C (July and August), the lowest temperature is between 5° C and - 10° C (January). The highest minimum temperature is seen below 10° C in summer whereas the lowest minimum temperature is between -10° C and -20° C in January, February and December. While the highest mean temperature occurs in July and August about 25° C, the lowest temperature degrees are analyzed below 0° C for January, February and December in Figure 6.8.

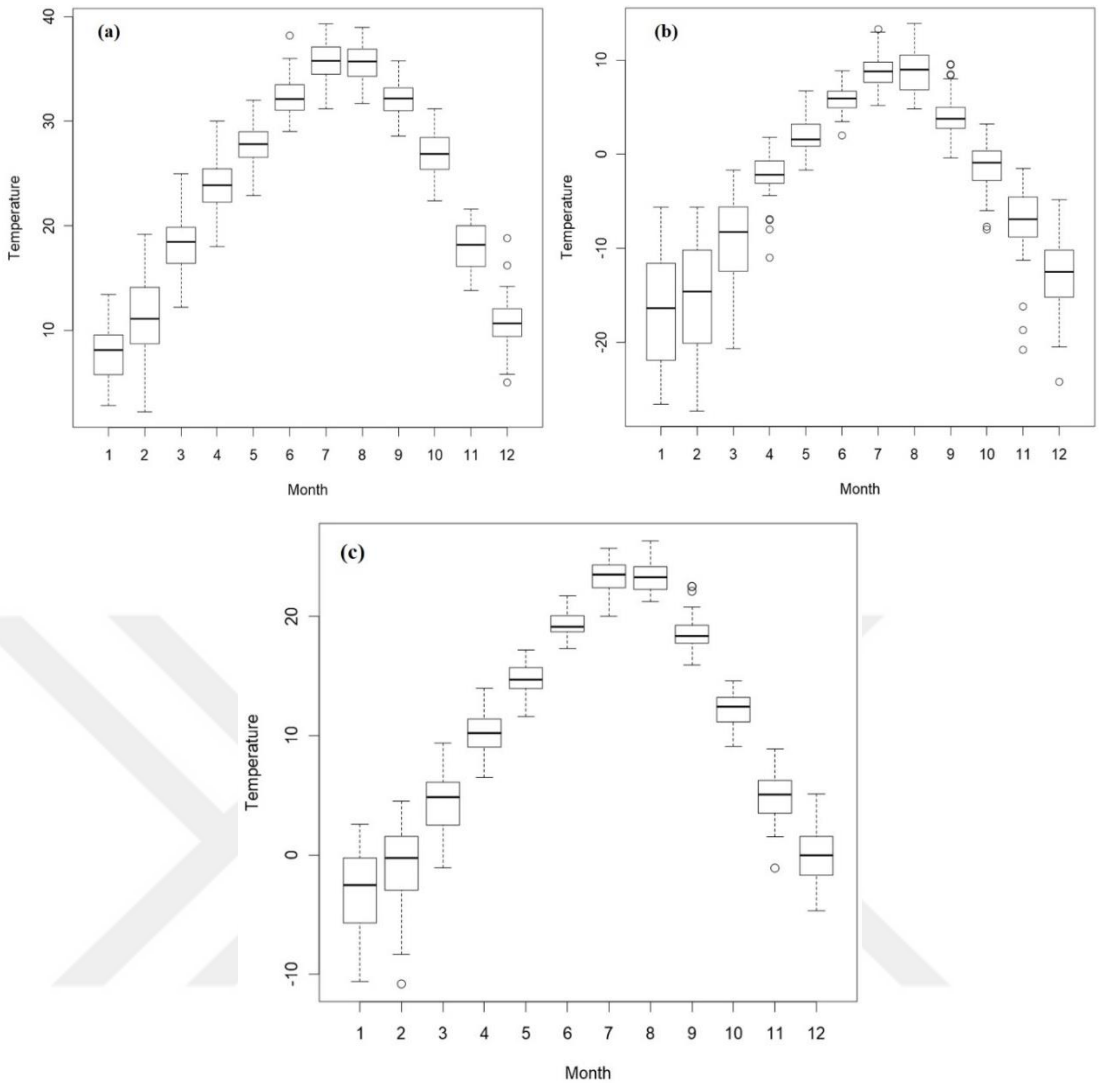

Figure 6.8 Monthly (a) maximum, (b) minimum and (c) mean temperature for station 17868 between the years of 1963-2018

The highest maximum temperature, for station 17870, occurs at its peak in July and August and its lowest value in January for three cases. While the highest monthly maximum temperature is about 35° C (July and August), the lowest temperature is between near 10° C (January). The highest minimum temperature is seen below 10° C in summer whereas the lowest minimum temperature is between -10° C and -20° C in January, February and December. While the highest mean temperature occurs in July and August about 25° C, the lowest temperature degrees are analyzed below 0° C for January, February and December in Figure 6.9.

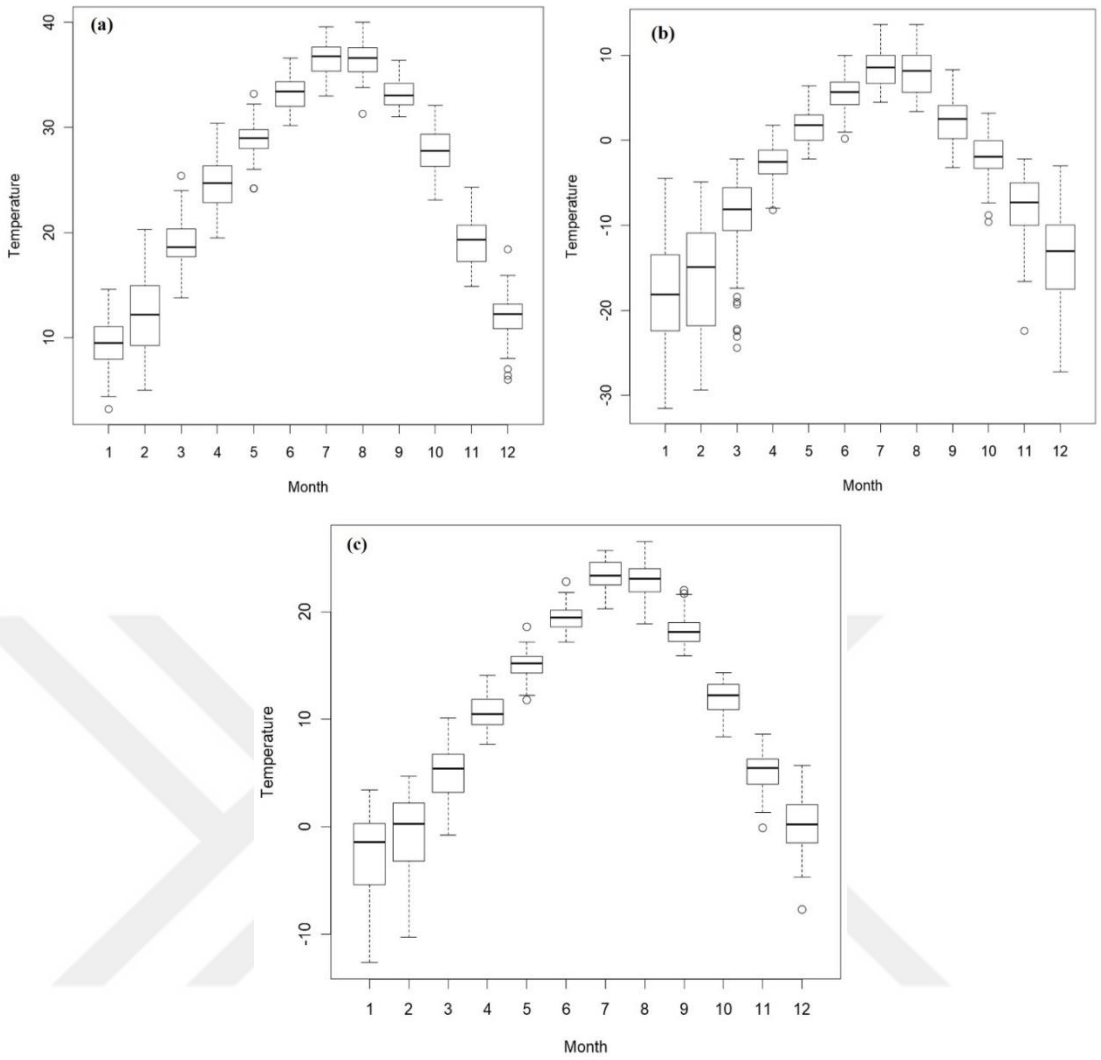

Figure 6.9 Monthly (a) maximum, (b) minimum and (c) mean temperature for station 17870 between the years of 1963-2018

The highest maximum temperature, for station 17908, occurs at its peak in July and August and its lowest value in January for three cases. While the highest monthly maximum temperature is about 40° C (July and August), the smallest temperature is between near 20° C (January). The highest minimum temperature is seen below 20° C in summer whereas the smallest minimum temperature is between 0° C and 3° C in January, February and December. While the highest mean temperature occurs in July and August about 30° C, the lowest temperature degrees are analyzed between 10° C and 13° C for January, February and December in Figure 6.10.

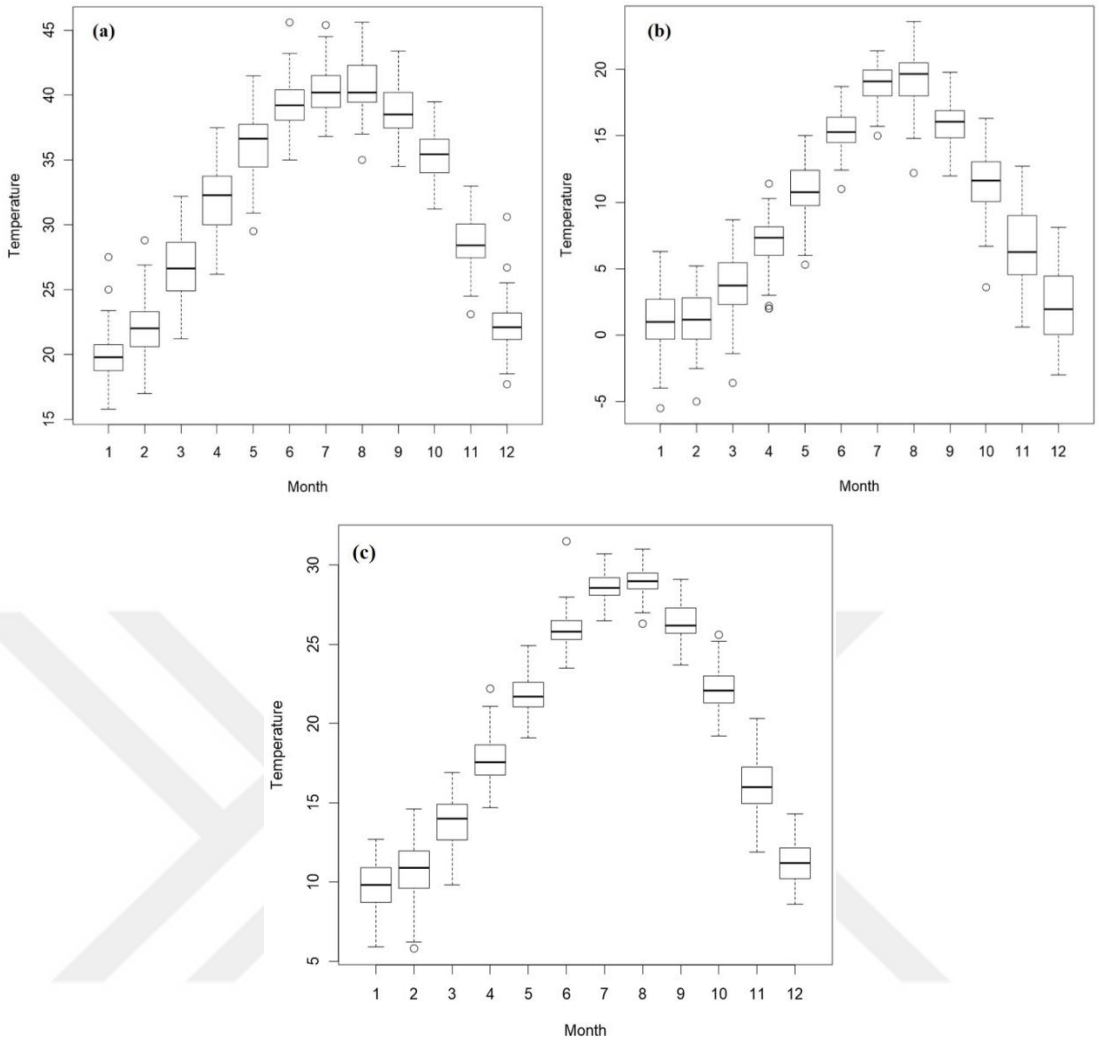

Figure 6.10 Monthly (a) maximum, (b) minimum and (c) mean temperature for station 17908 between the years of 1963-2018

The highest maximum temperature, for station 17960, occurs at its peak in June, July, August and September its lowest value in January for three cases. While the highest monthly maximum temperature is between 35° C and 40° C, the lowest temperature is between near 18° C (January). The highest minimum temperature is seen below 20° C in summer whereas the lowest minimum temperature is between 0° C and -5° C in January, February and December. While the highest mean temperature occurs in July and August about 28° C, the lowest temperature degrees are analyzed between 8° C and 10° C for January, February and December in Figure 6.11.

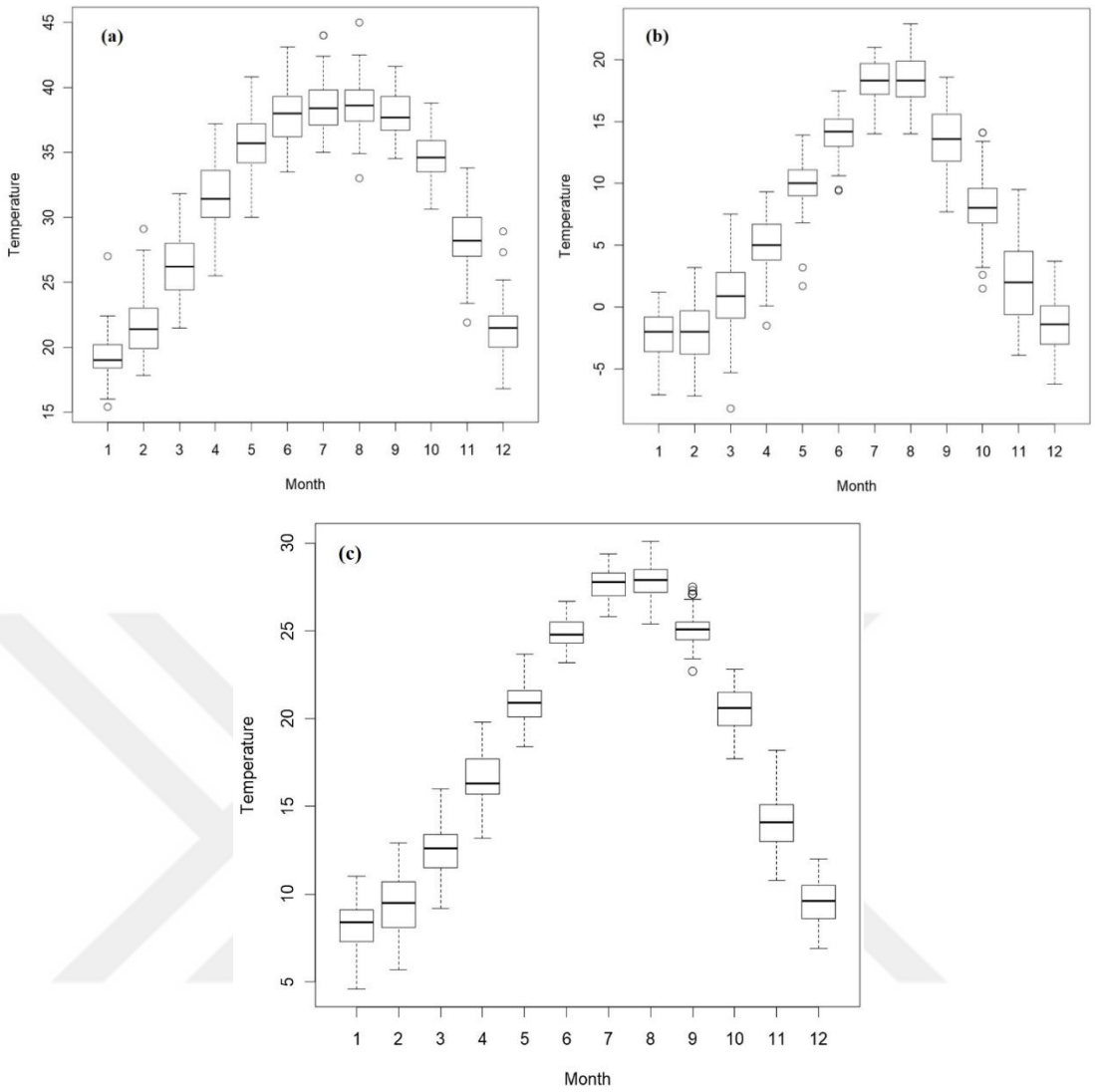

Figure 6.11 Monthly (a) maximum, (b) minimum and (c) mean temperature for station 17960 between the years of 1963-2018

The highest maximum temperature, for station 17979, occurs at its peak in August and September its lowest value in January for three cases. While the highest monthly maximum temperature is between 35° C, the lowest temperature is between near 18° C (January). The highest minimum temperature is seen about 20° C in summer whereas the lowest minimum temperature is between 0° C and 5° C in January, February and December. While the highest mean temperature occurs in July and August about 28° C, the lowest temperature degrees are analyzed between 10° C and 13° C for January, February and December in Figure 6.12.

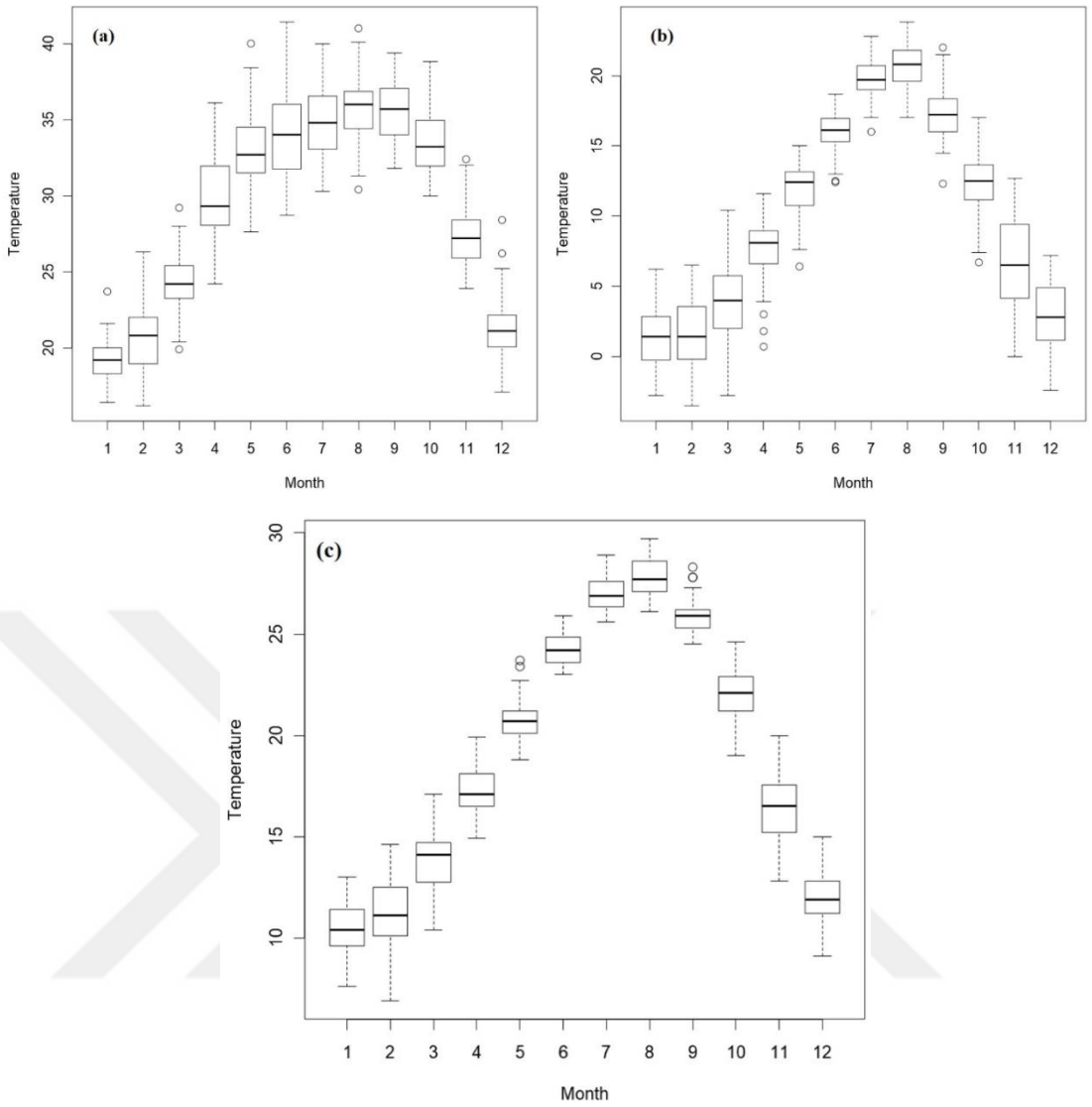

Figure 6.12 Monthly (a) maximum, (b) minimum and (c) mean temperature for station 17979 between the years of 1963-2018

In order to understand temperature data variability, 1-, 3-, 5- and 10-year moving average are employed. The moving average is an important indicator that is often used in technical analysis. Moving average refers to the average of the changes of the relevant data in a certain time interval and shows the general direction of the trend. Moving average for the monthly maximums, minimum and mean temperatures are presented in Figures 6.13-6.36.

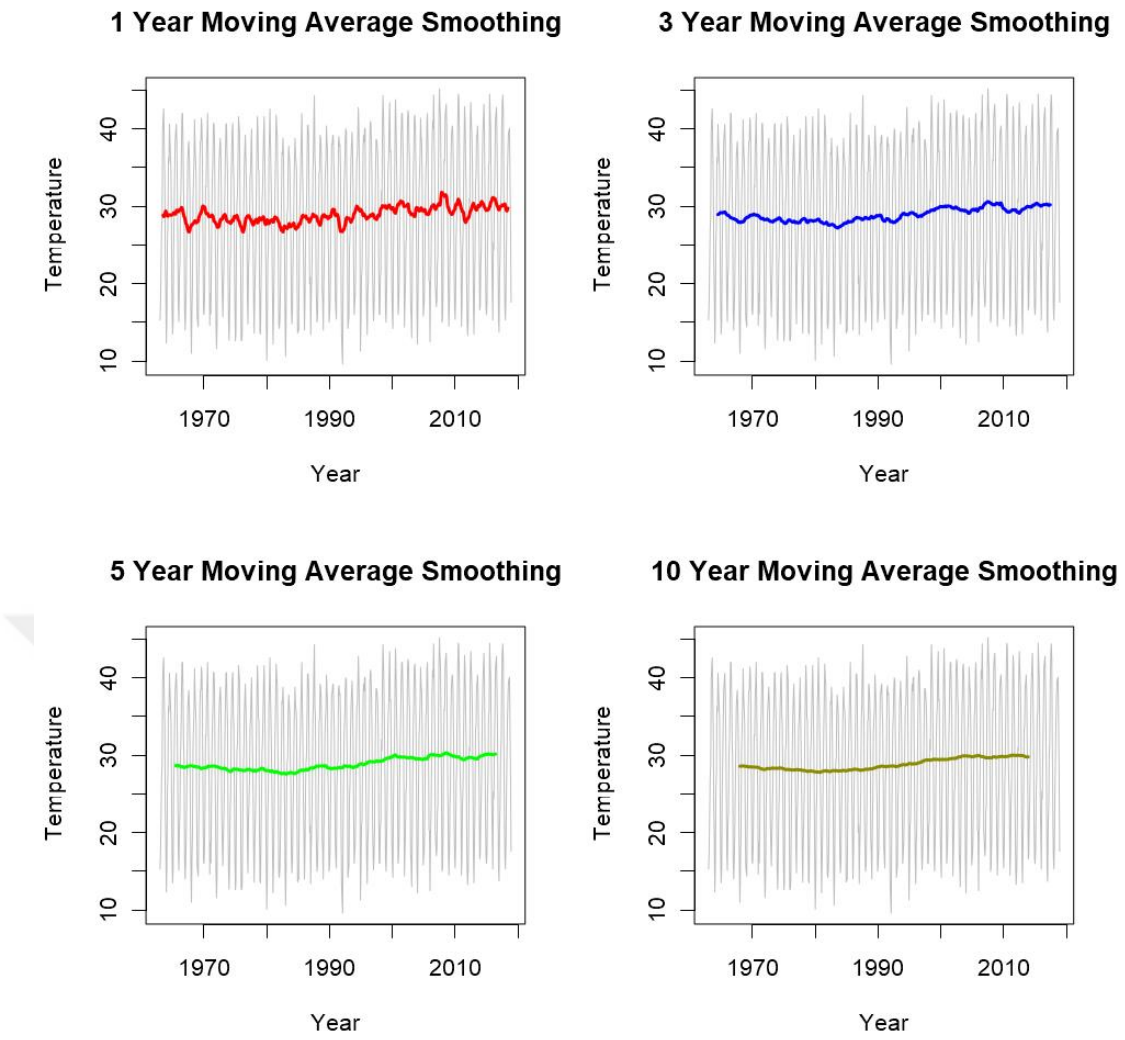

Figure 6.13 The monthly maximum temperature data at different moving average time for station 17255

Now consider 1963-2018 the monthly maximum temperature data are shown in the diagram above. The solid lines represent the 1-, 3-, 5-, and 10-yr moving average, and the thin lines show the individual years. As an example, the smoothed value for 1970 is evaluated as the sum of the temperatures 1969-1971(for 3-yr moving average smoothing), divided by the length of the smoothing interval. The purpose of the smoothing data should be apparent from this illustration. The variance of the original data is reduced by smoothing; the longer the smoothing interval, the greater the reduction. The most significant problem of smoothing or filtering is the shift, relative to the original results, of peaks and troughs in the smoothed curve. If the original dataset shows asymmetric peaks, the smoothing may shift the peak positions seriously and persistently; the actual error increases with the length of the smoothing period adopted in all such cases. According to moving average smoothing results, it is noted

that the temperature data for three cases, slightly increase as well as the length of the smoothing increase. However, it doesn't give precise information about the presence of the trend within a certain confidence interval.

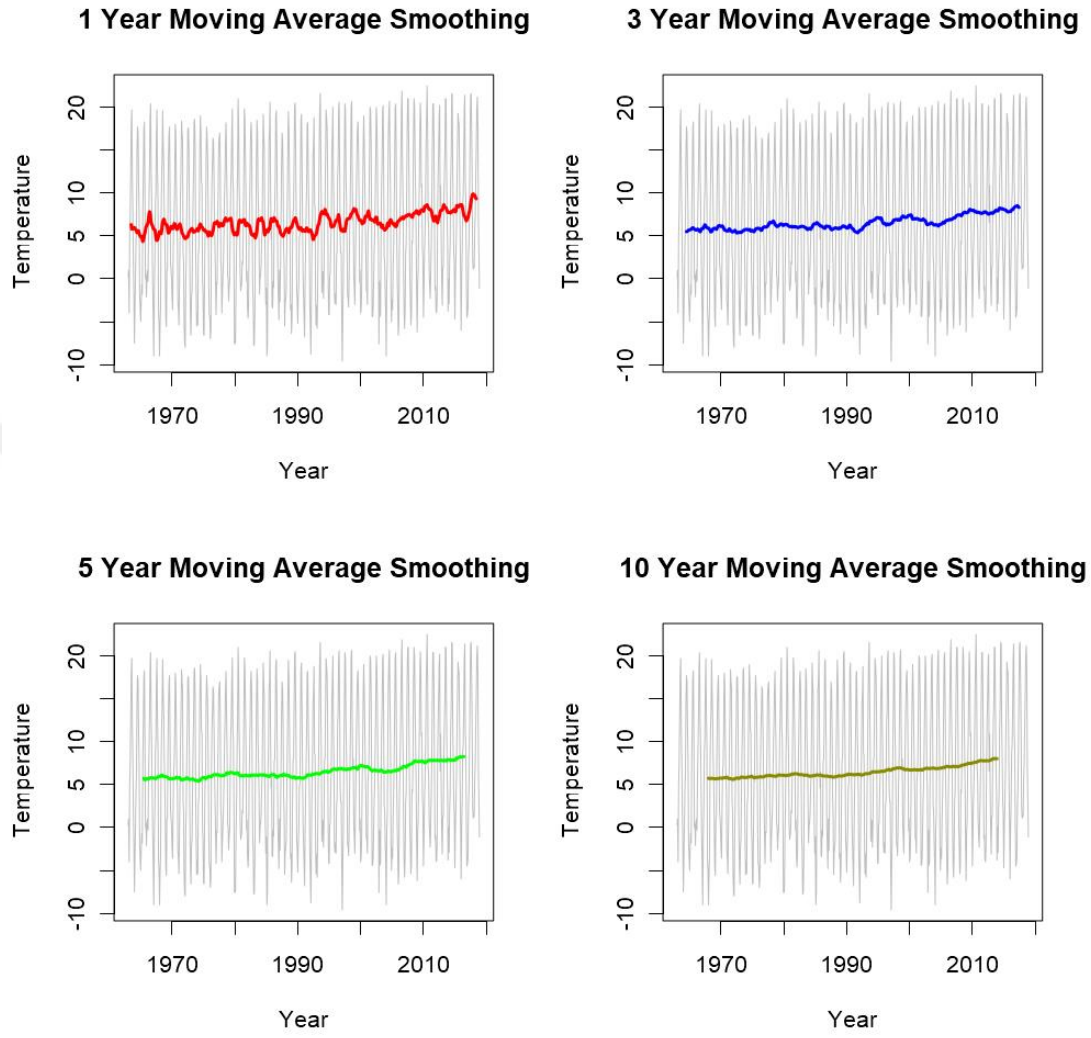

Figure 6.14 The monthly minimum temperature data at different moving average time for station 17255

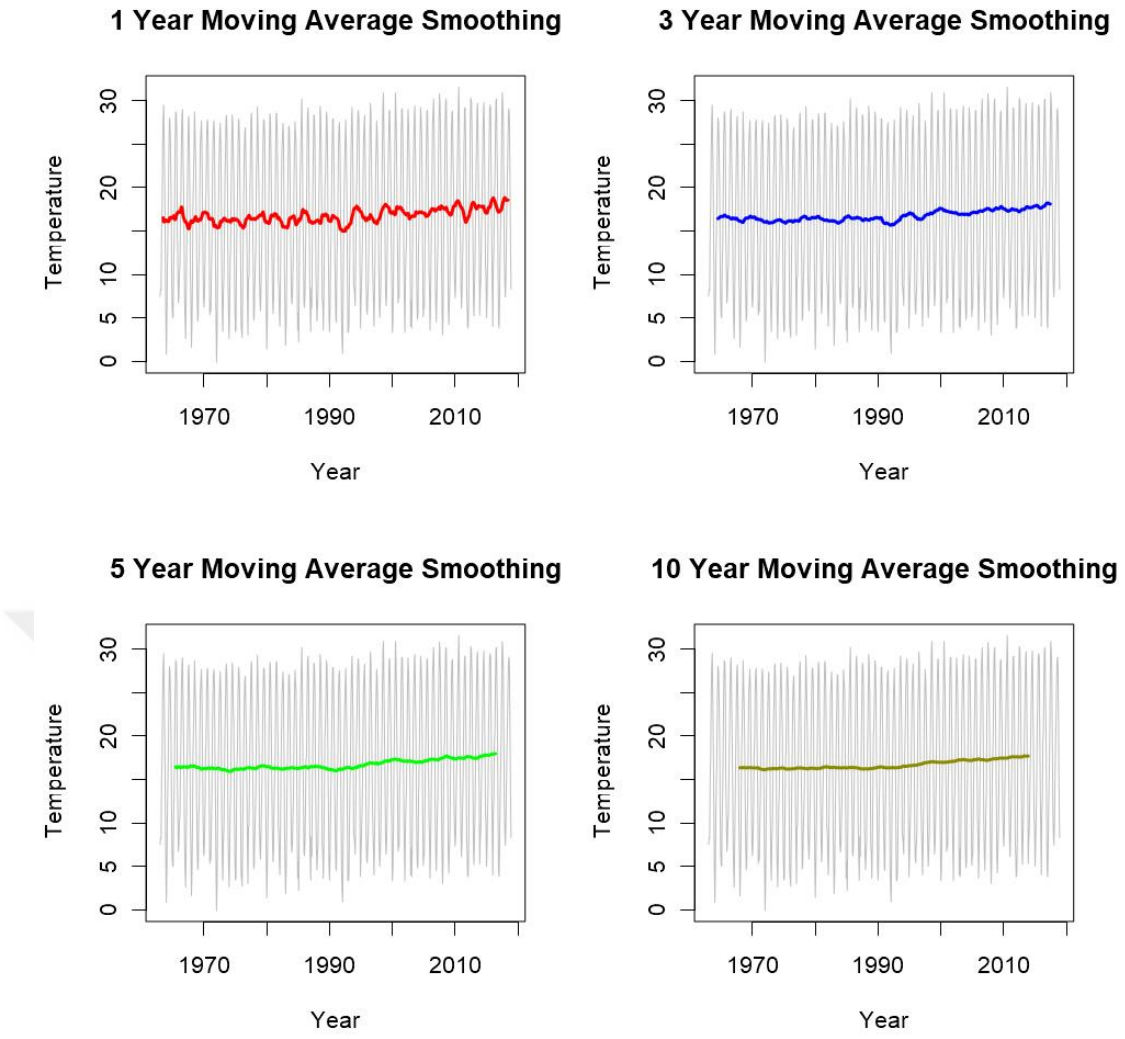

Figure 6.15 The monthly mean temperature data at different moving average time for station 17255

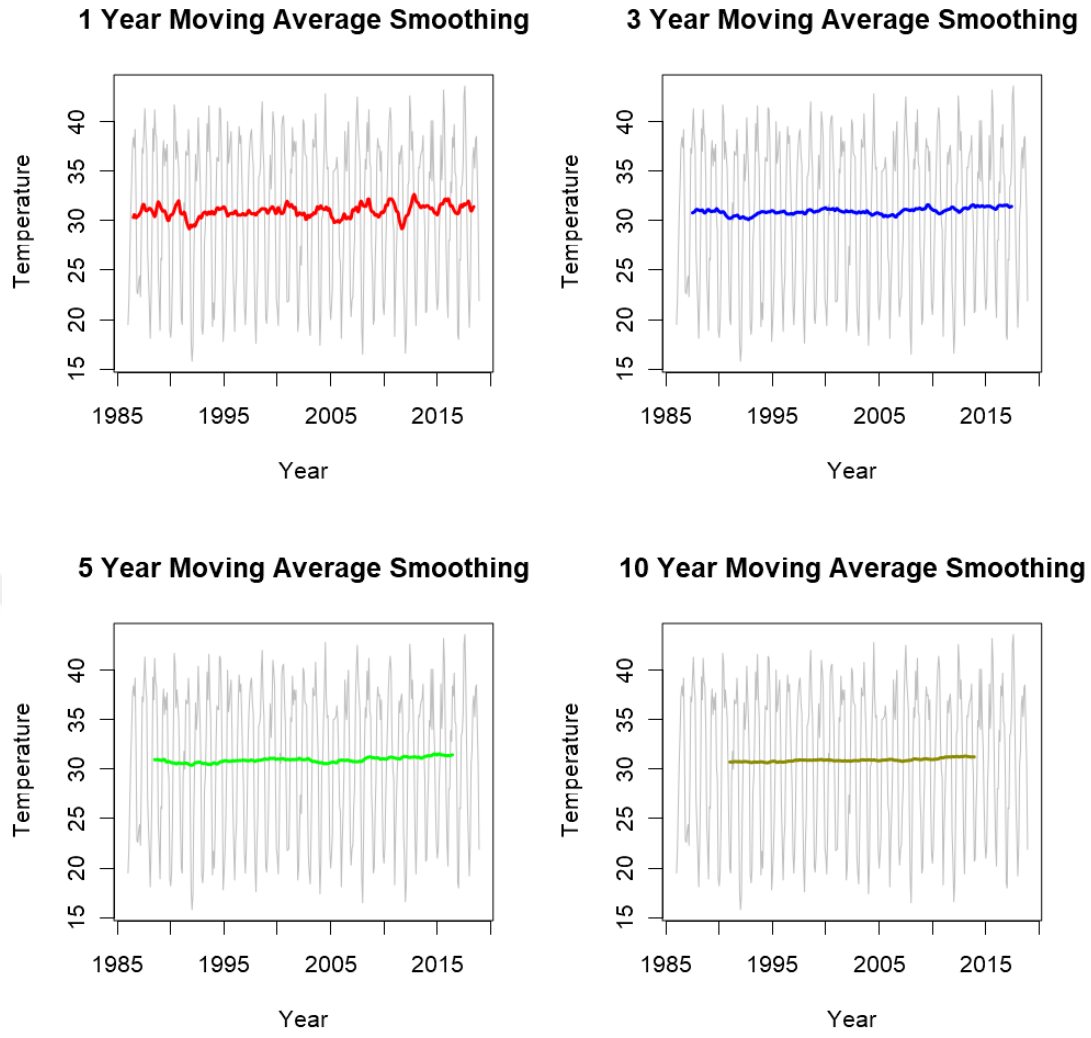

Figure 6.16 The monthly maximum temperature data at different moving average time for station 17355

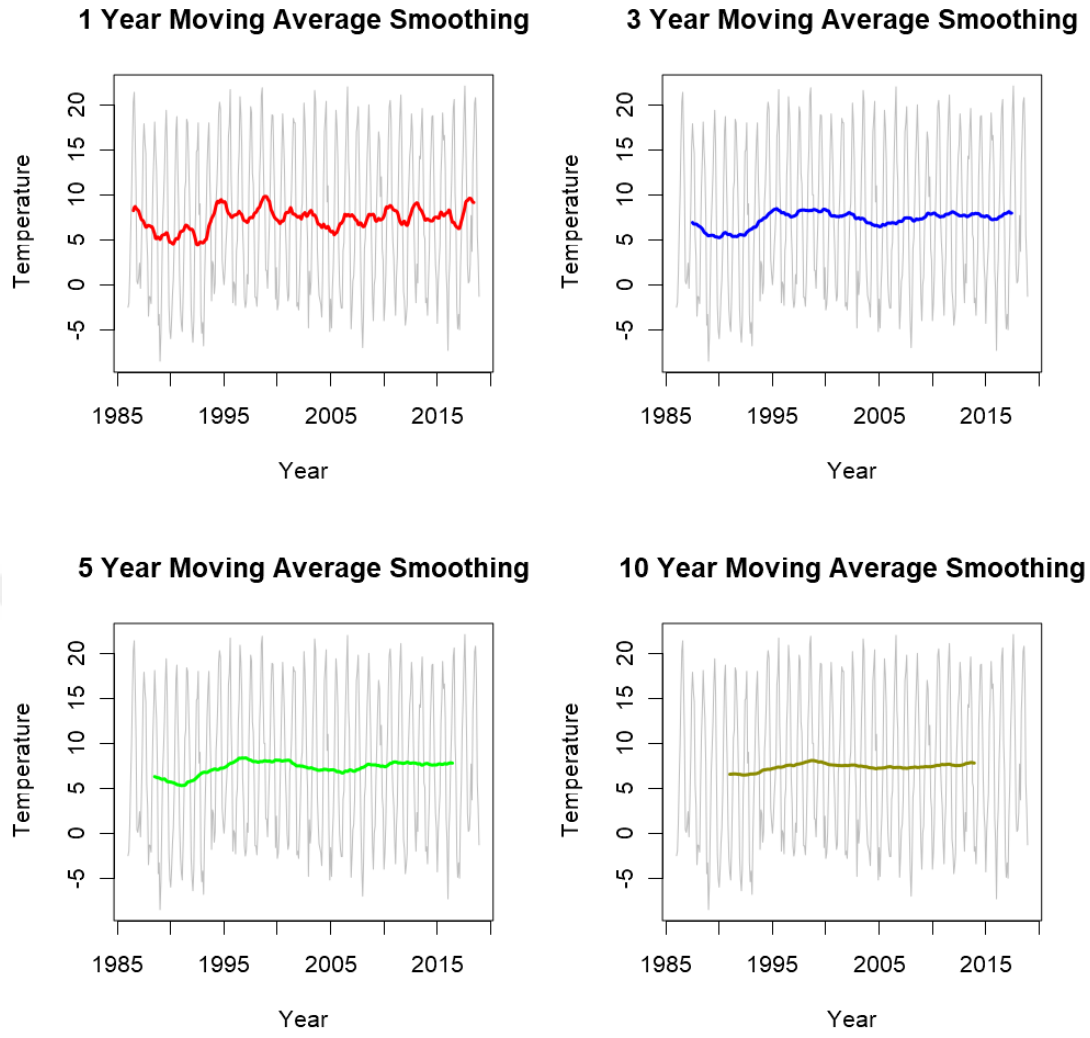

Figure 6.17 The monthly minimum temperature data at different moving average time for station 17355

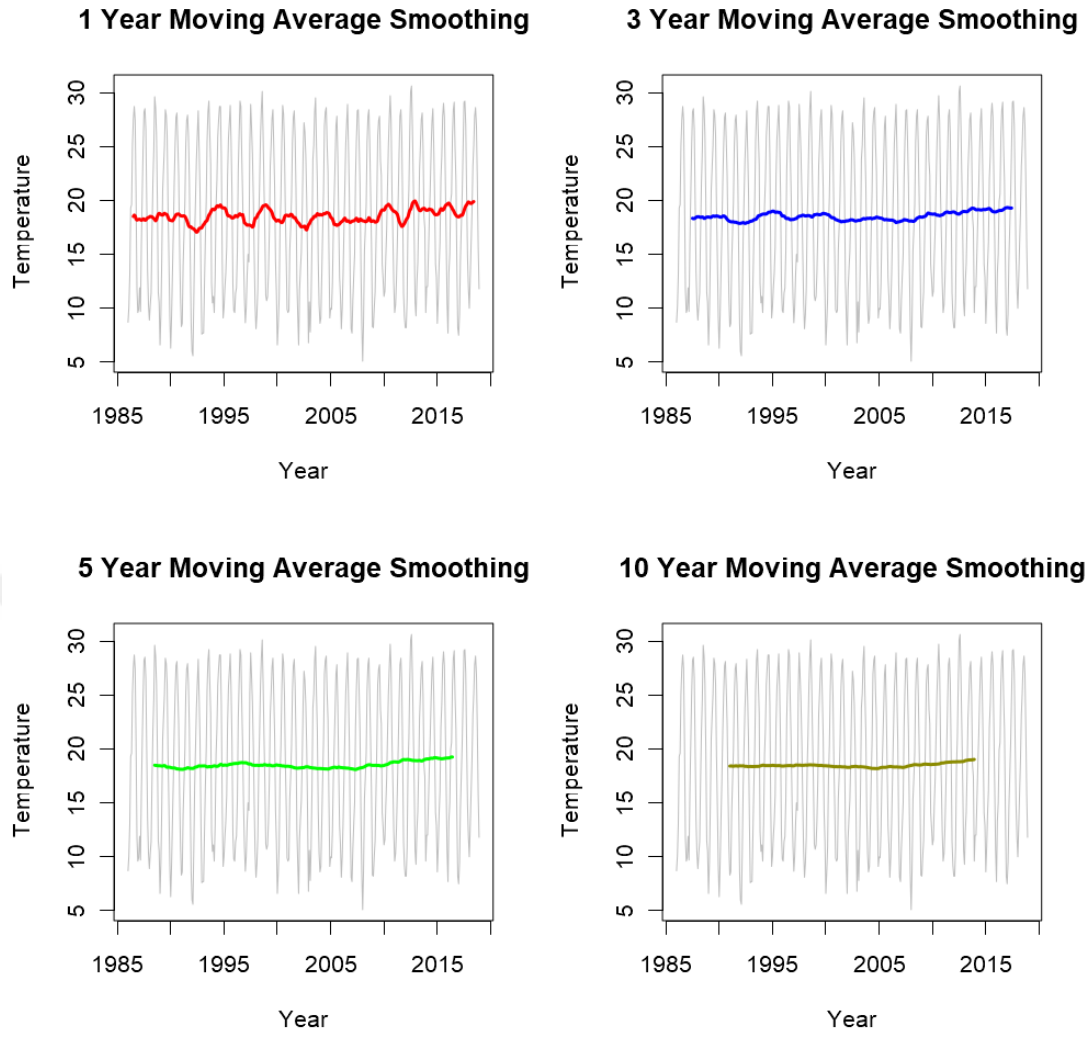

Figure 6.18 The monthly mean temperature data at different moving average time for station 17355

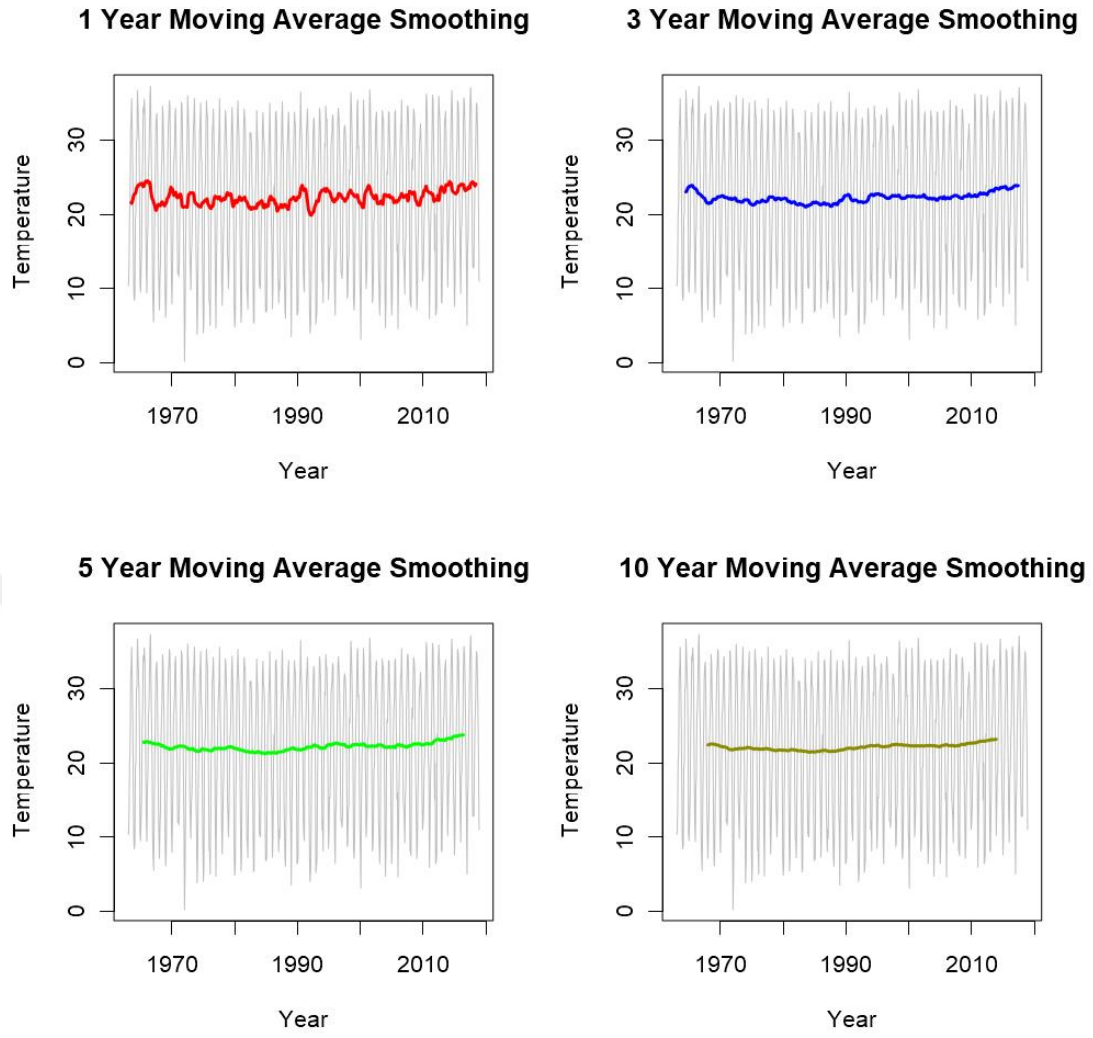

Figure 6.19 The monthly maximum temperature data at different moving average time for station 17866

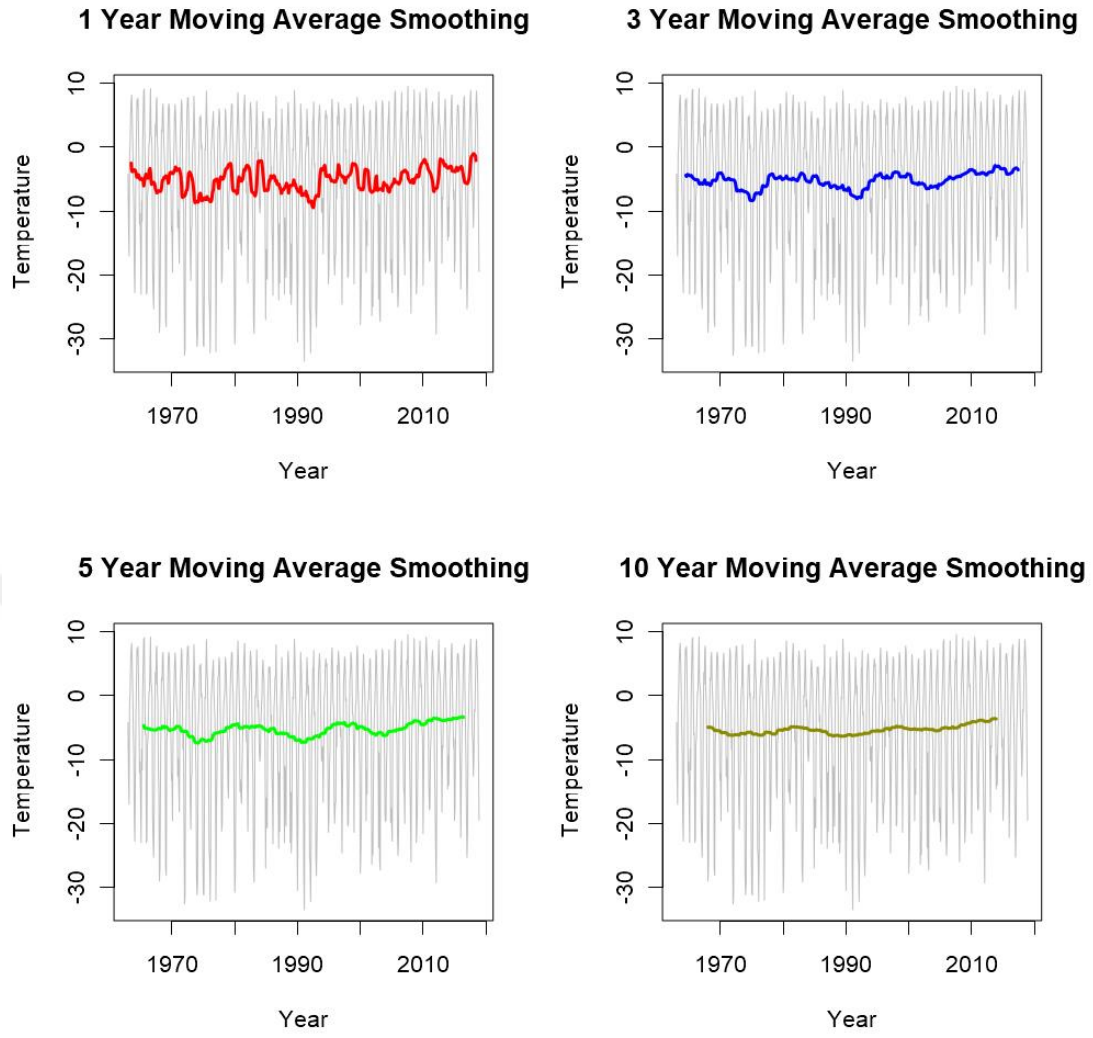

Figure 6.20 The monthly minimum temperature data at different moving average time for station 17866

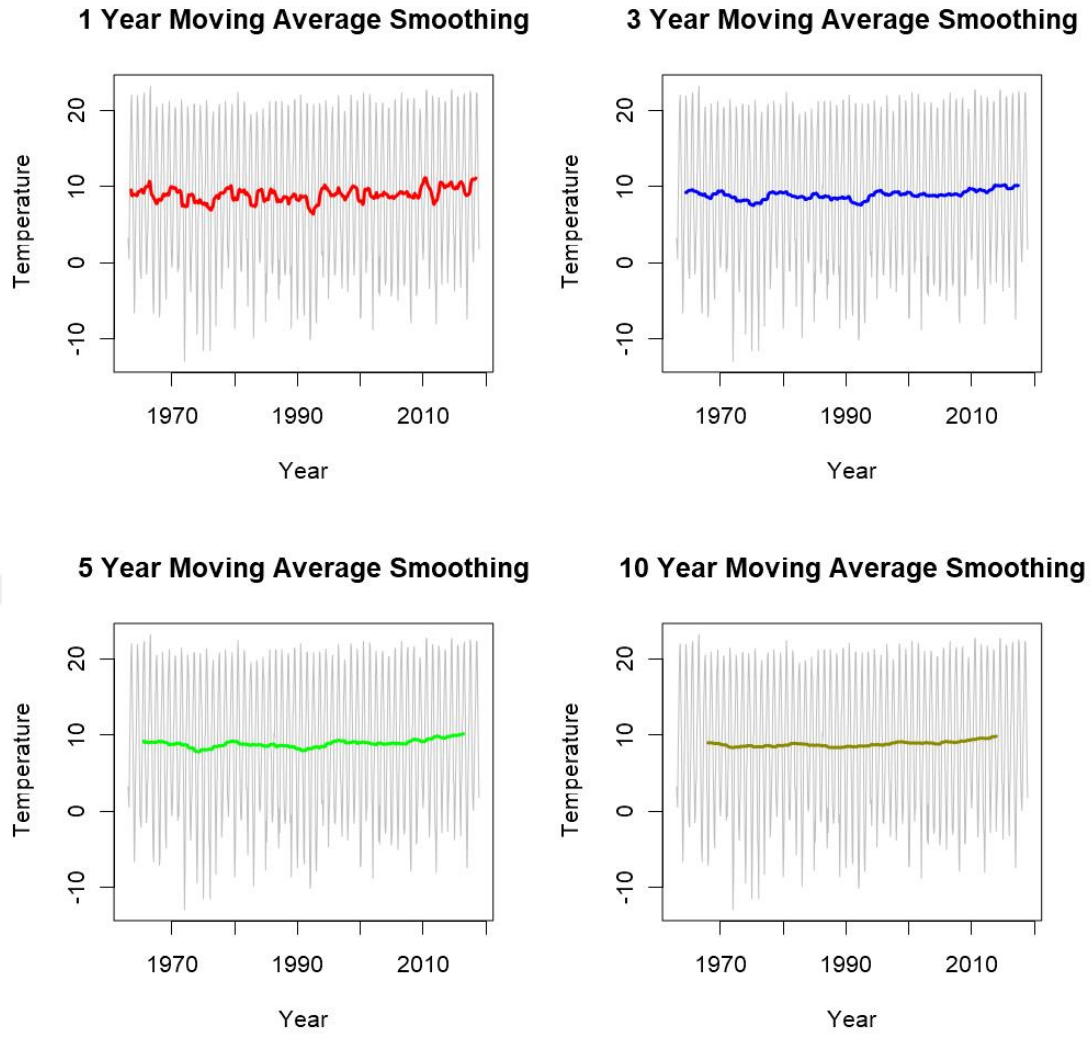

Figure 6.21 The monthly mean temperature data at different moving average time for station 17866

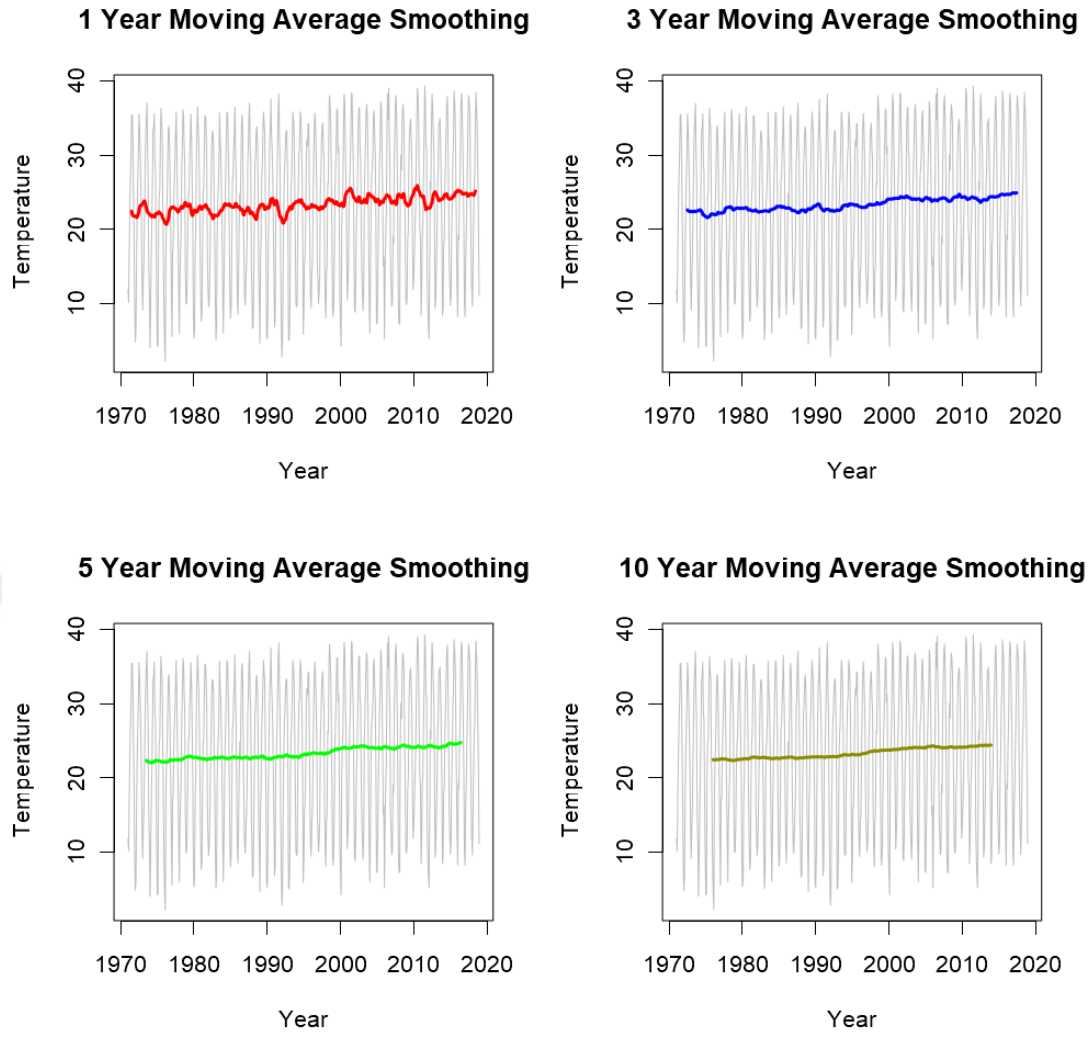

Figure 6.22 The monthly maximum temperature data at different moving average time for station 17868

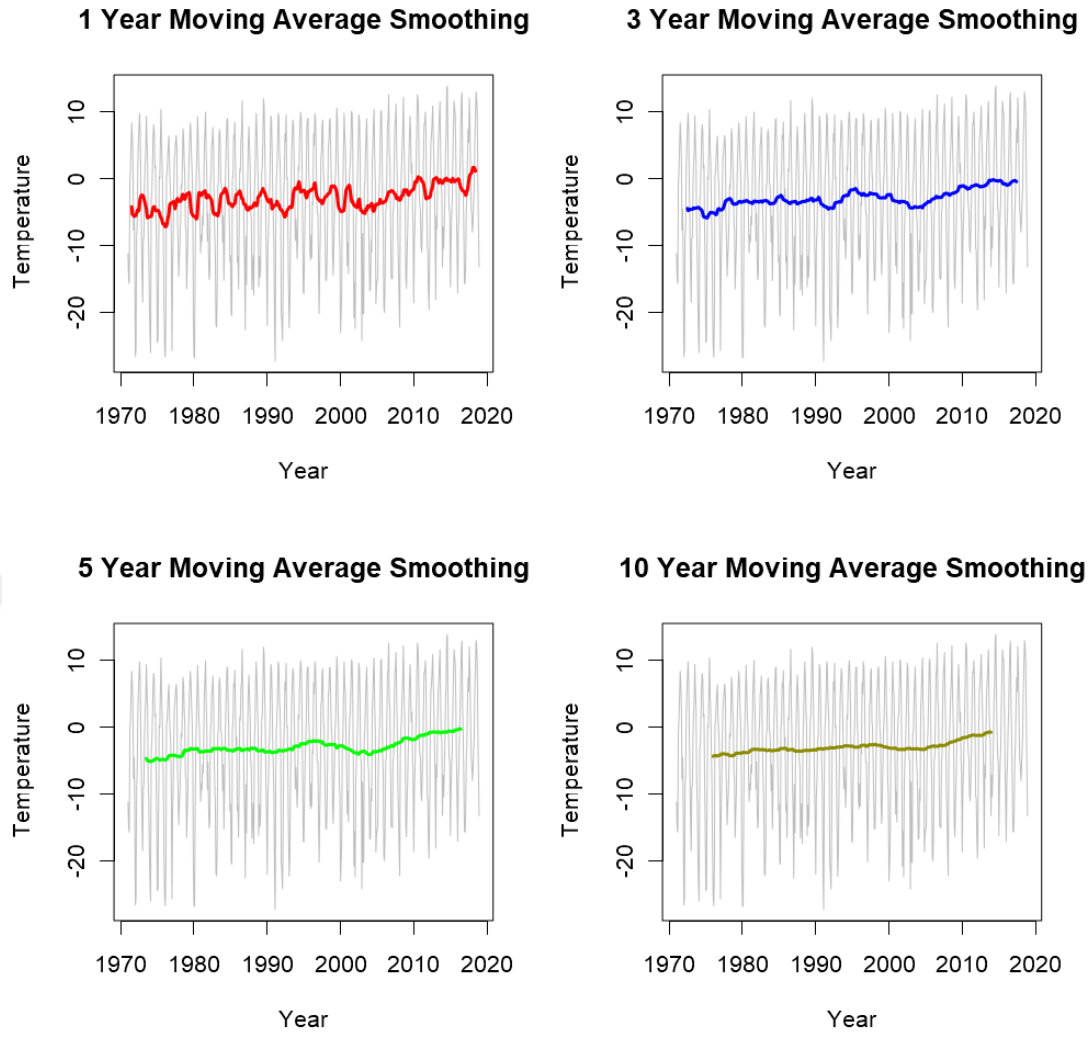

Figure 6.23 The monthly minimum temperature data at different moving average time for station 17868

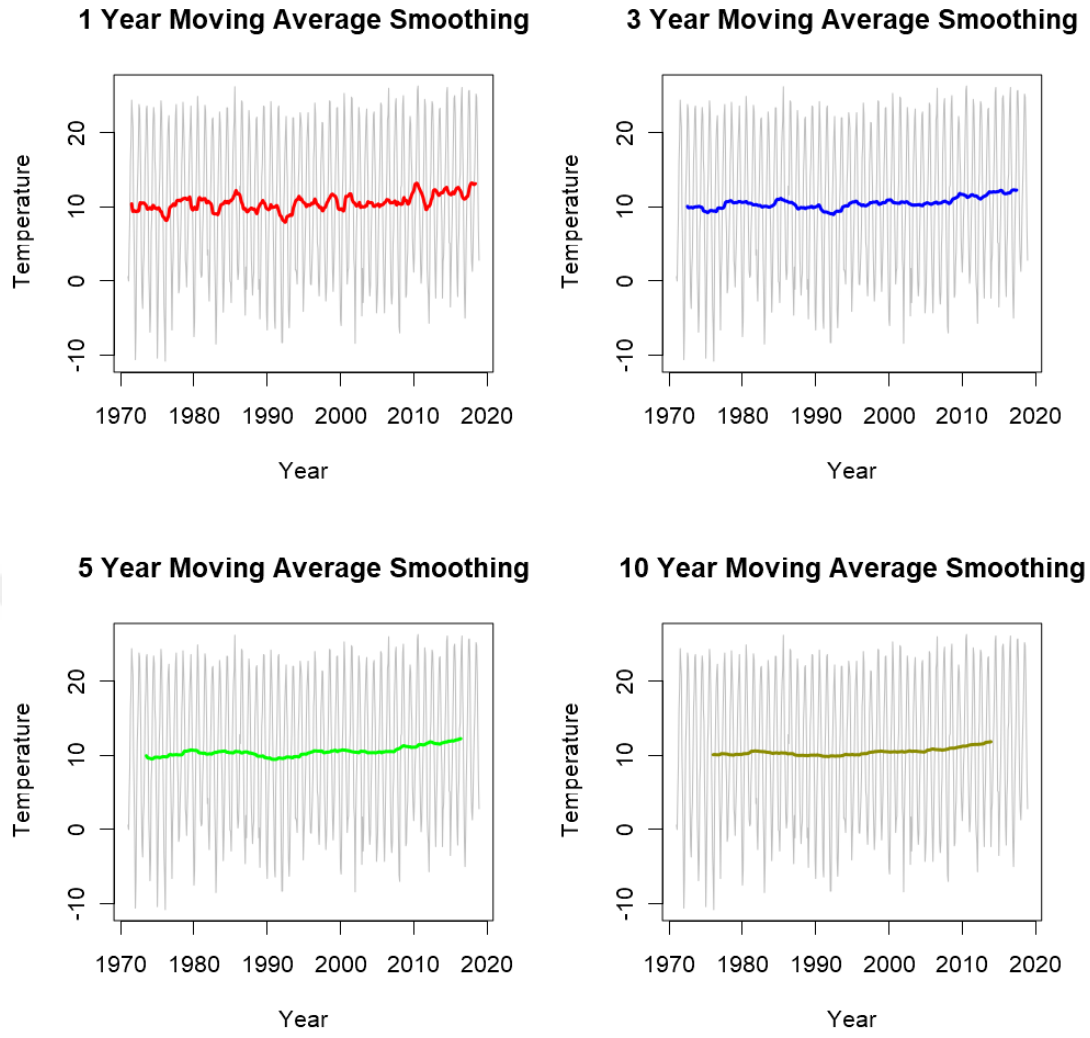

Figure 6.24 The monthly mean temperature data at different moving average time for station 17868

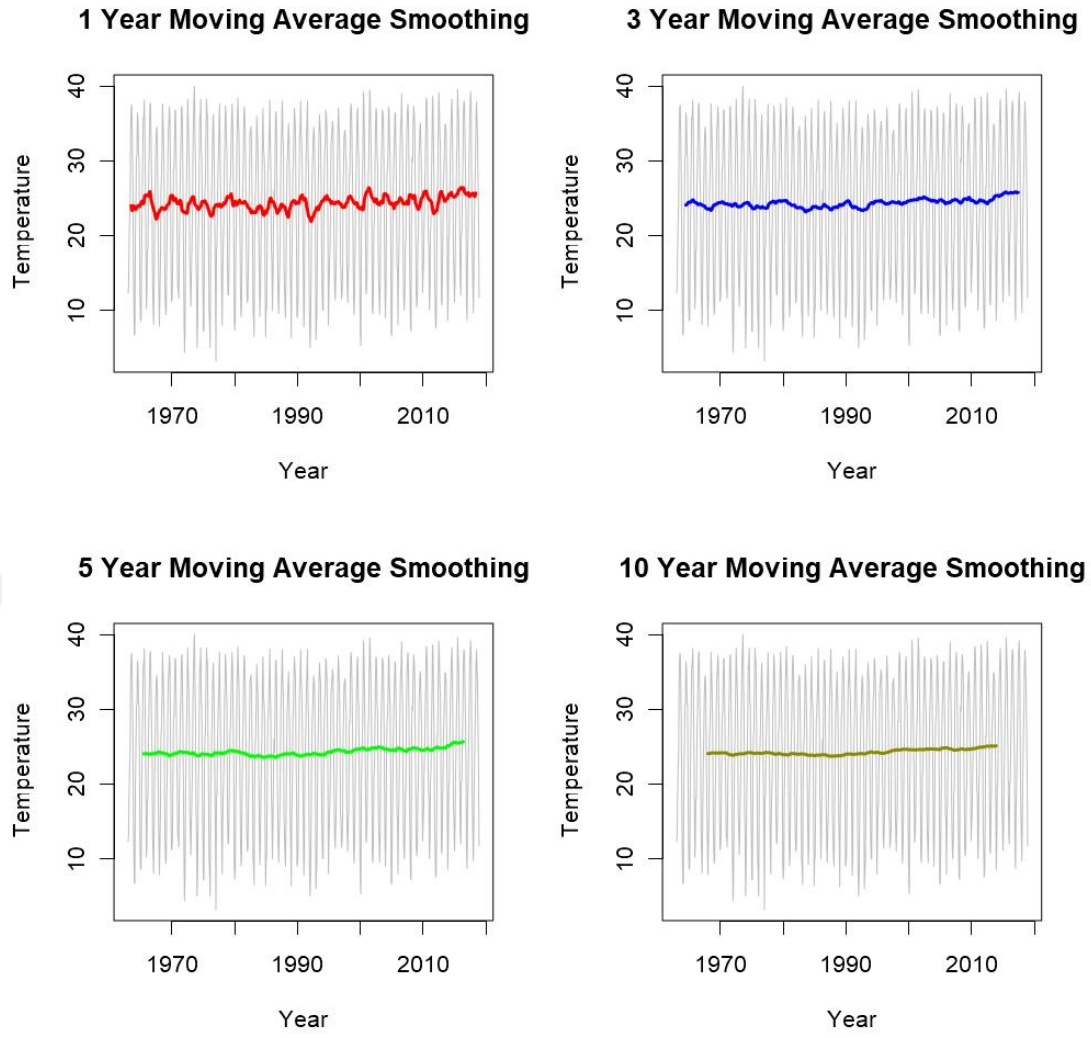

Figure 6.25 The monthly maximum temperature data at different moving average time for station 17870

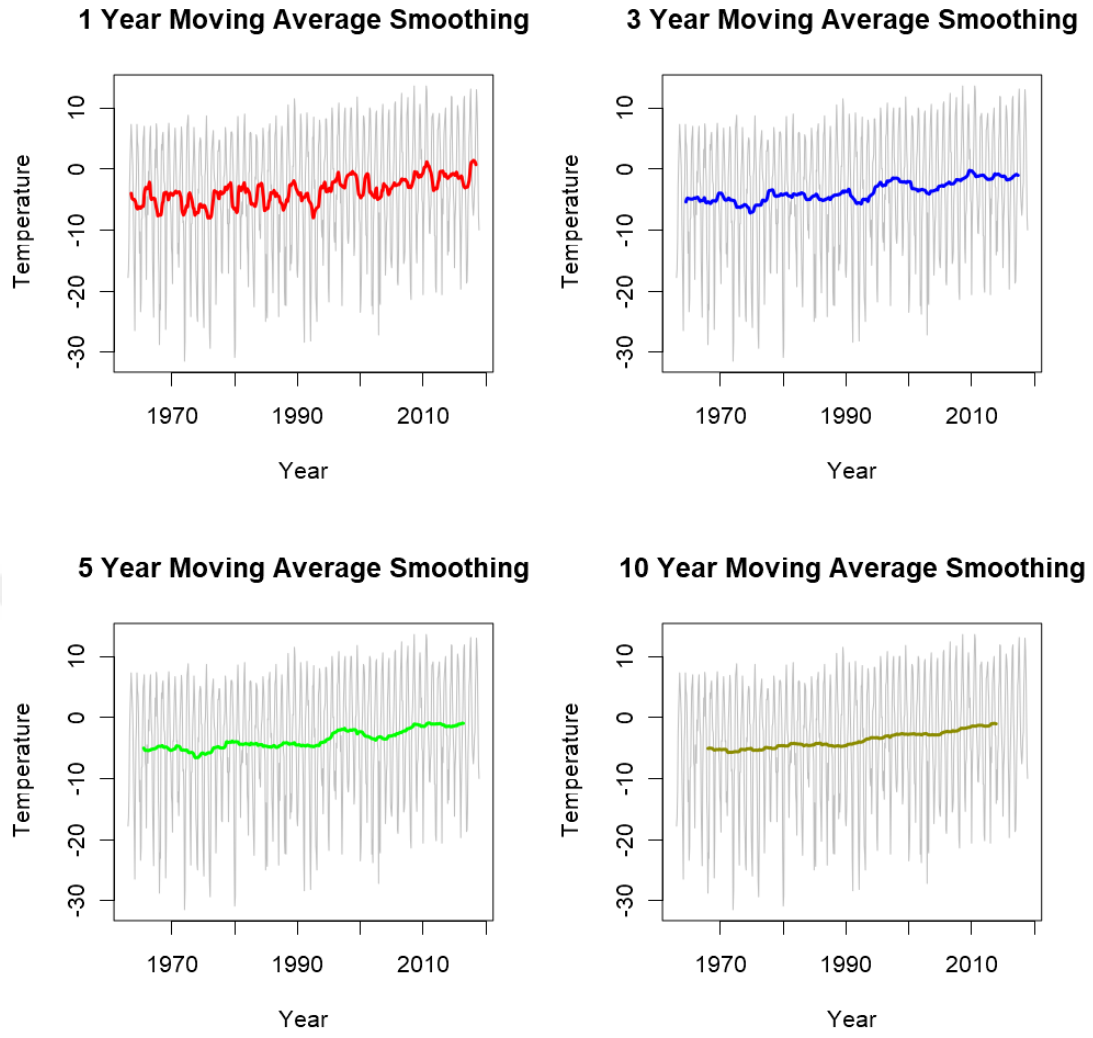

Figure 6.26 The monthly minimum temperature data at different moving average time for station 17870

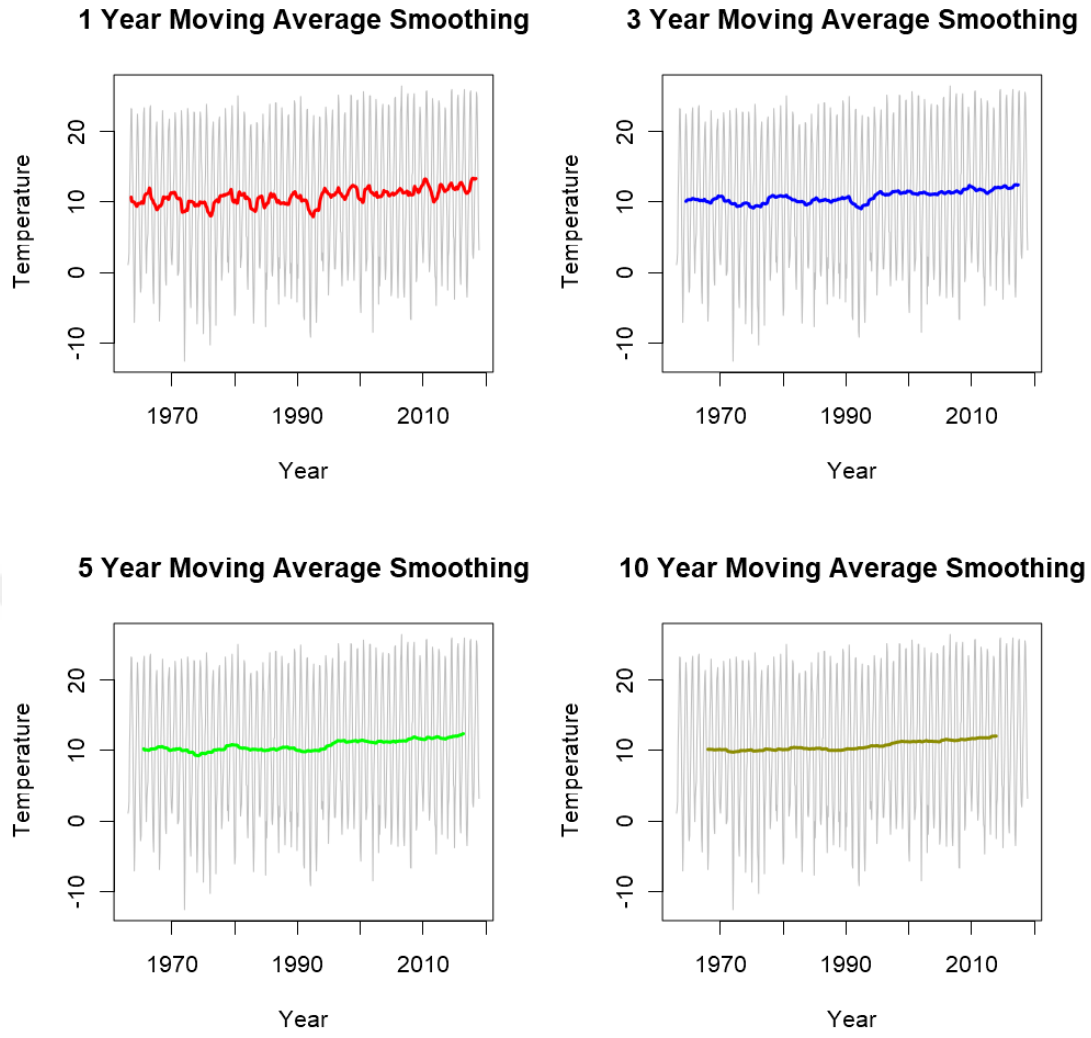

Figure 6.27 The monthly mean temperature data at different moving average time for station 17870

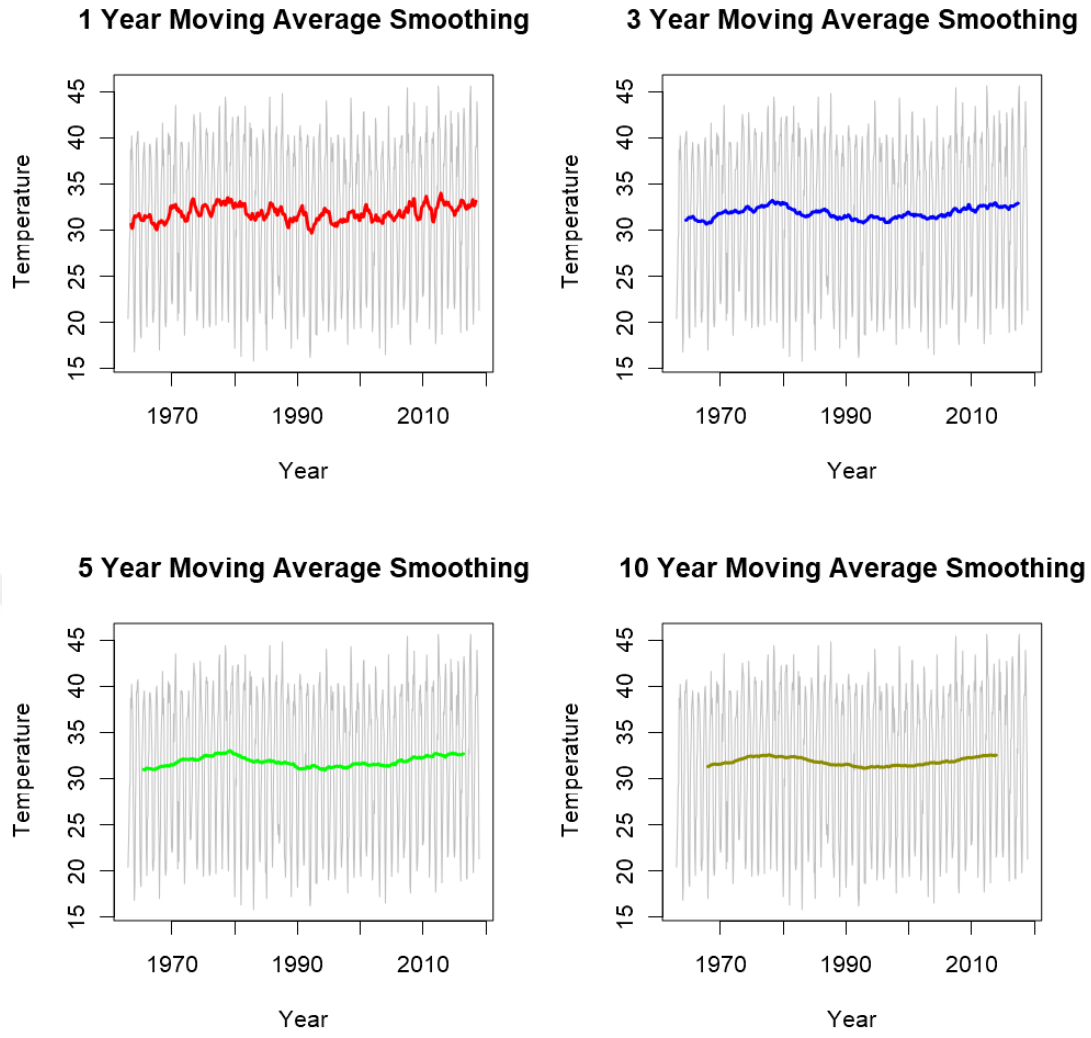

Figure 6.28 The monthly maximum temperature data at different moving average time for station 17908

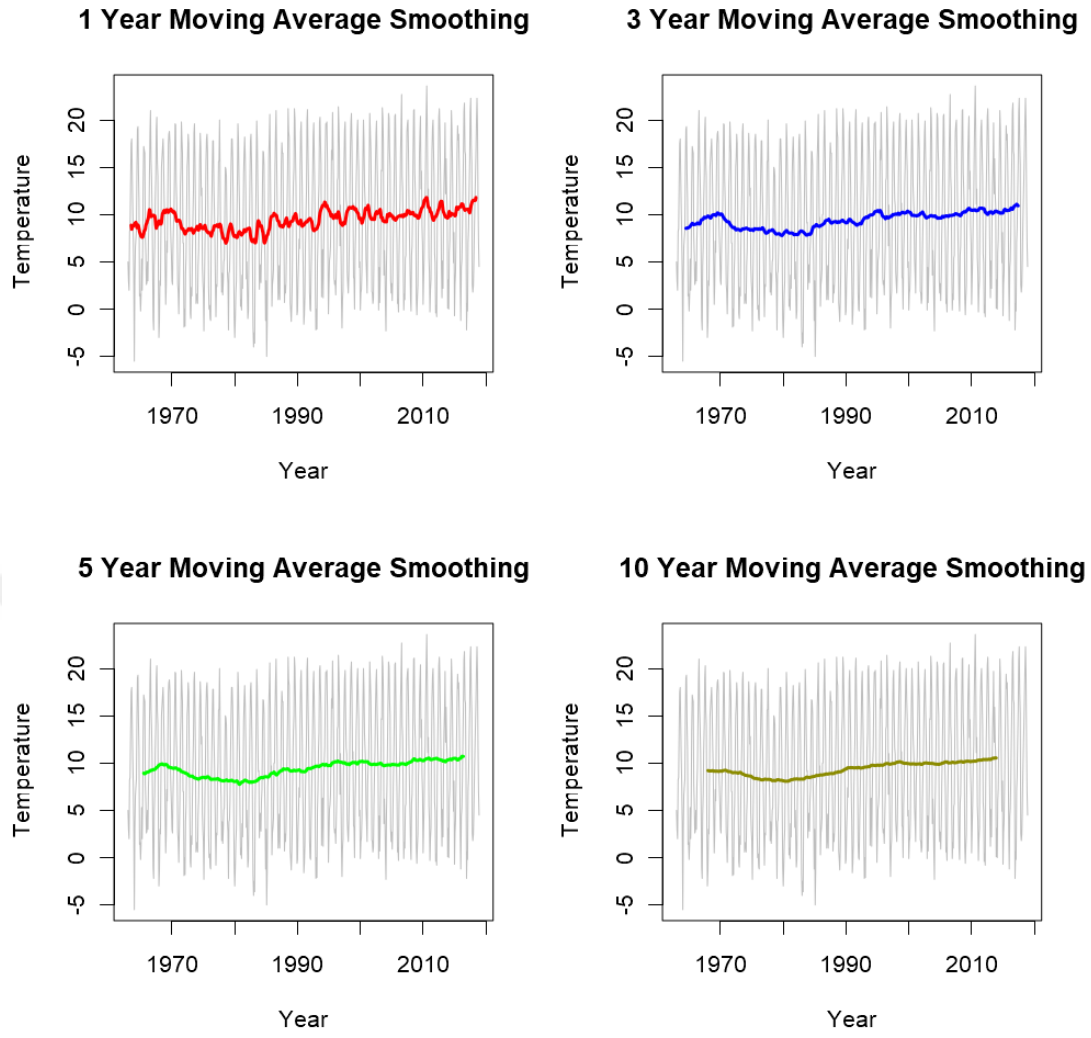

Figure 6.29 The monthly minimum temperature data at different moving average time for station 17908

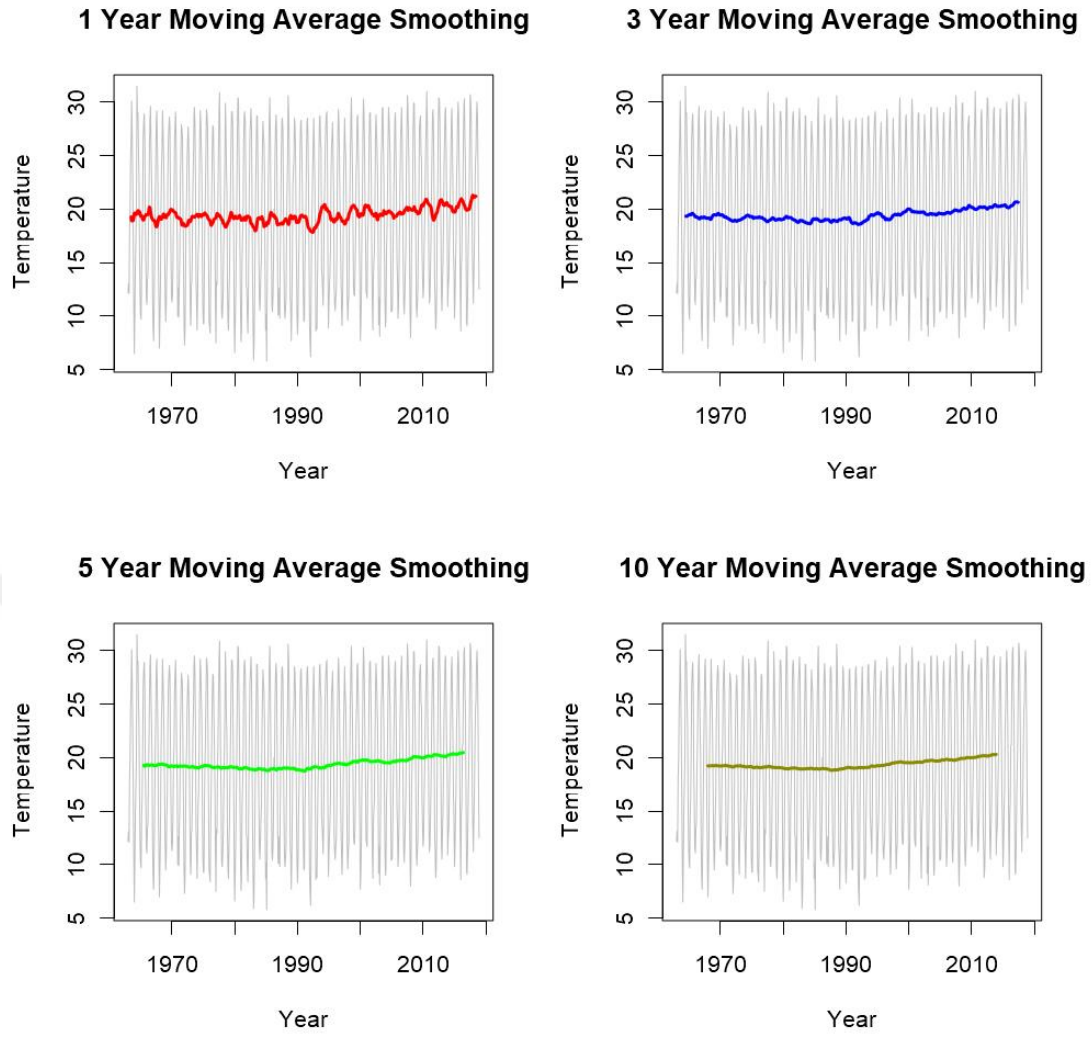

Figure 6.30 The monthly mean temperature data at different moving average time for station 17908

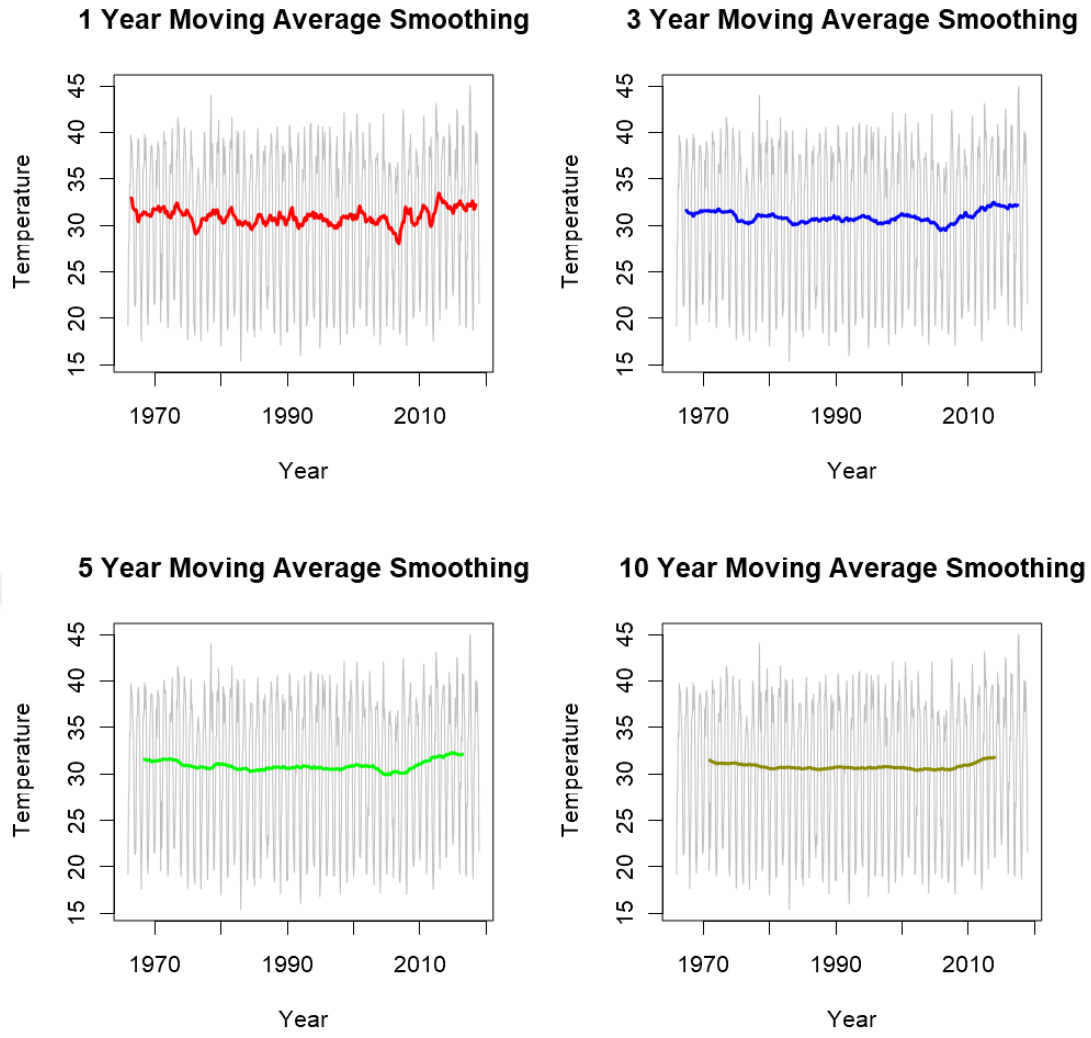

Figure 6.31 The monthly maximum temperature data at different moving average time for station 17960

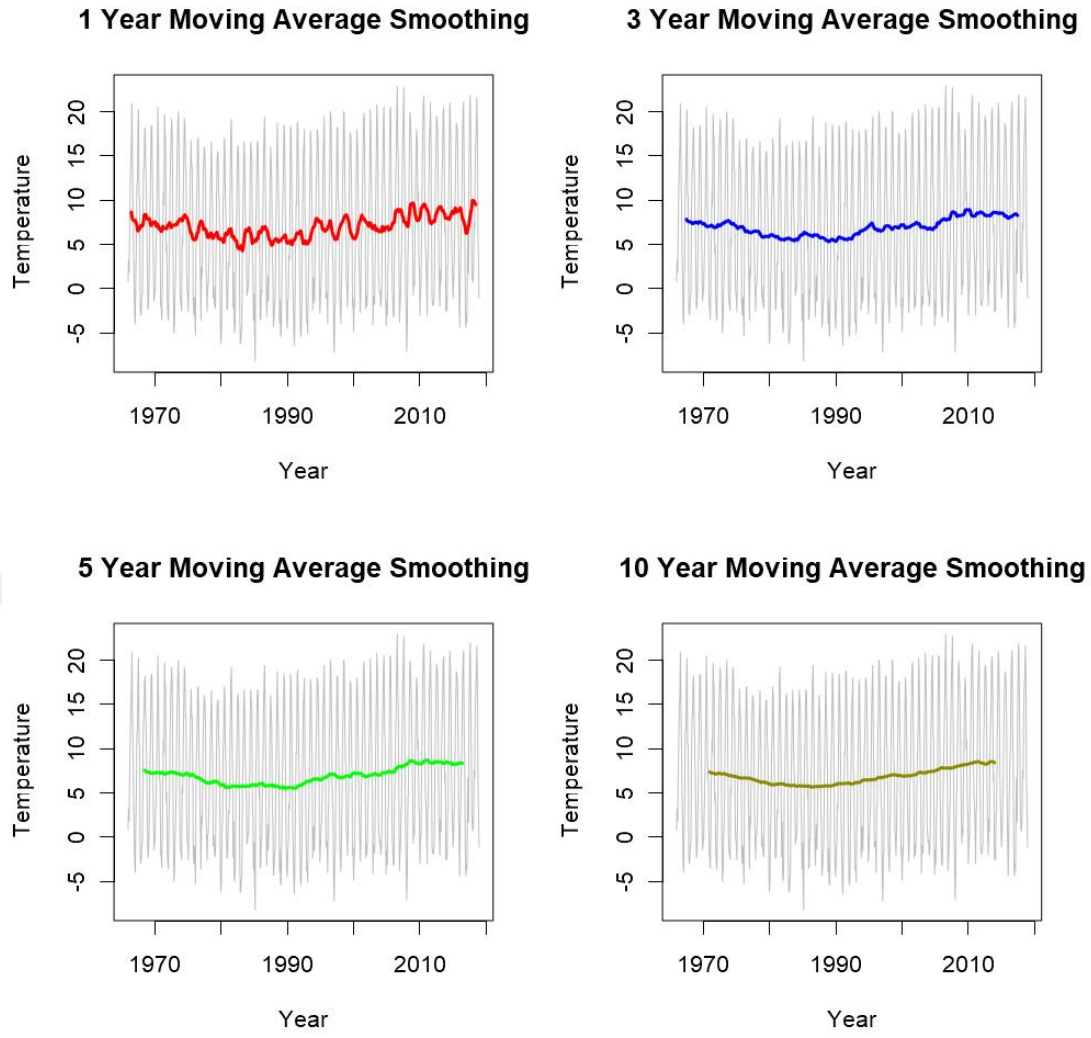

Figure 6.32 The monthly minimum temperature data at different moving average time for station 17960

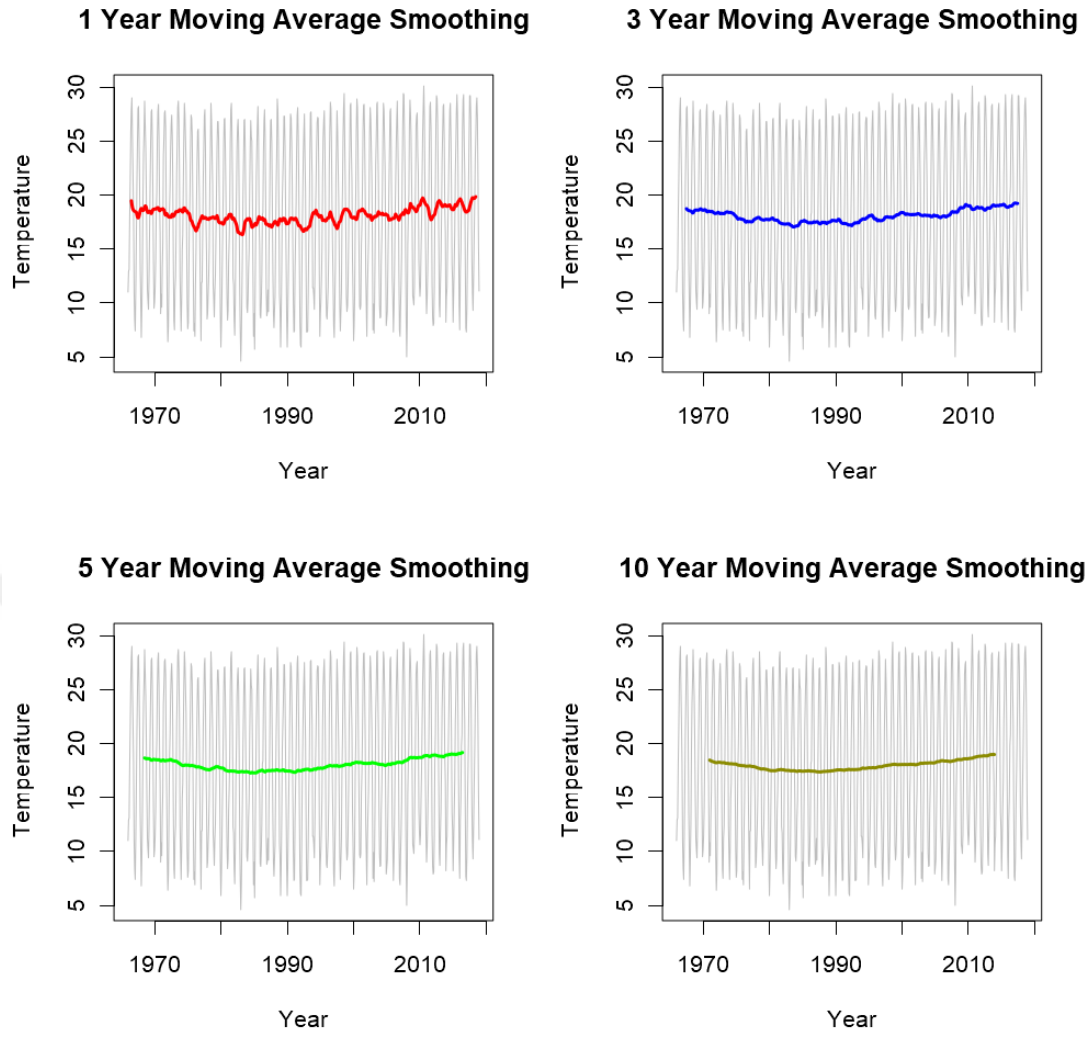

Figure 6.33 The monthly mean temperature data at different moving average time for station 17960

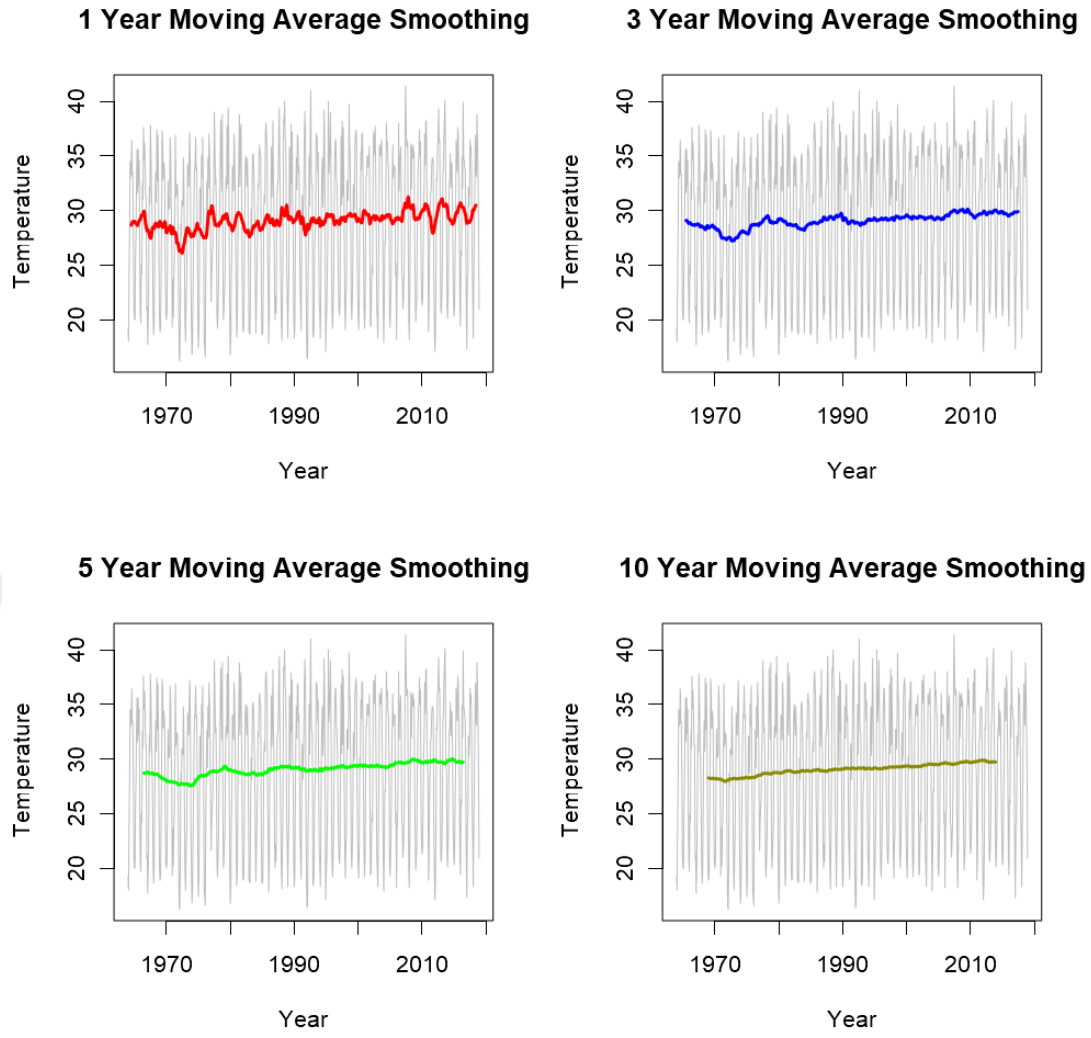

Figure 6.34 The monthly maximum temperature data at different moving average time for station 17979

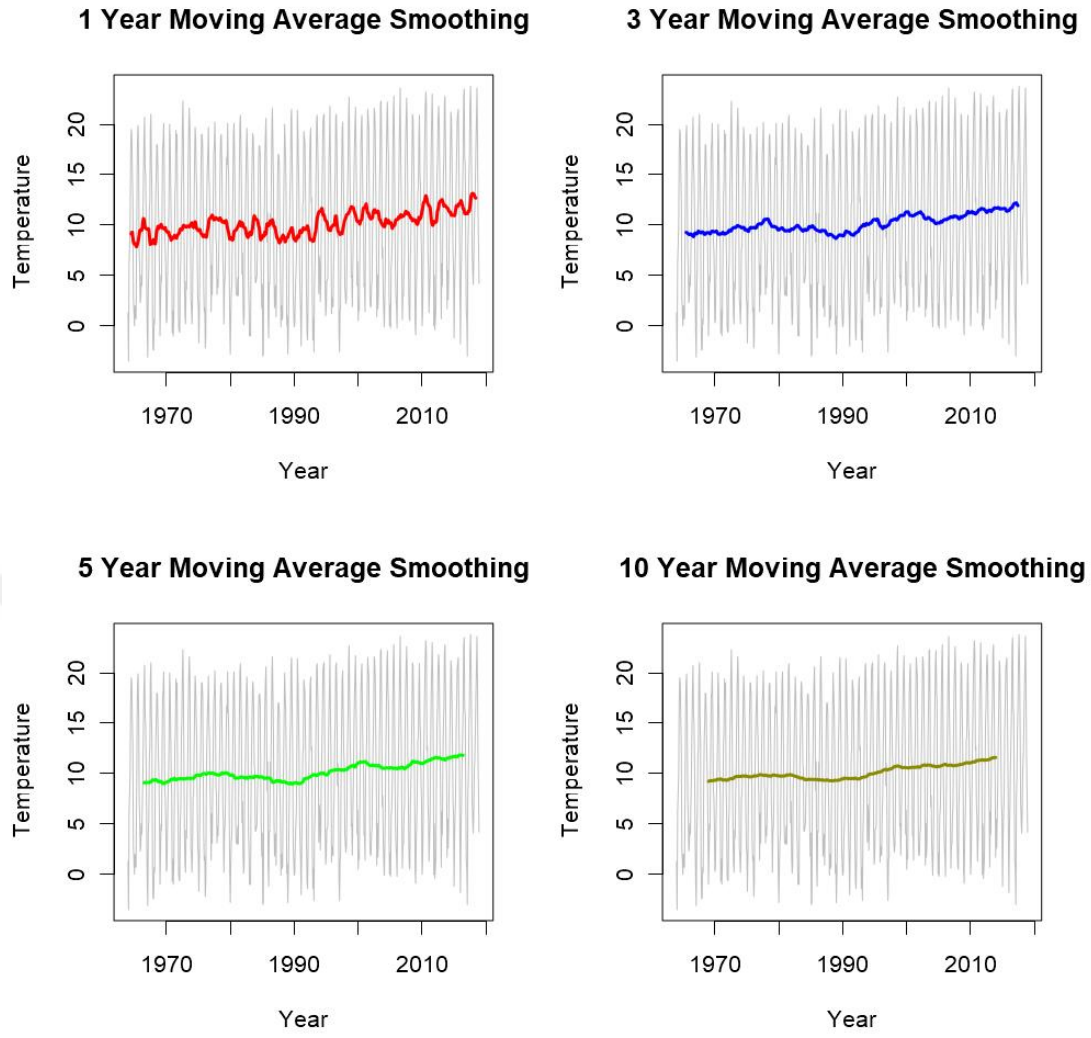

Figure 6.35 The monthly minimum temperature data at different moving average time for station 17979

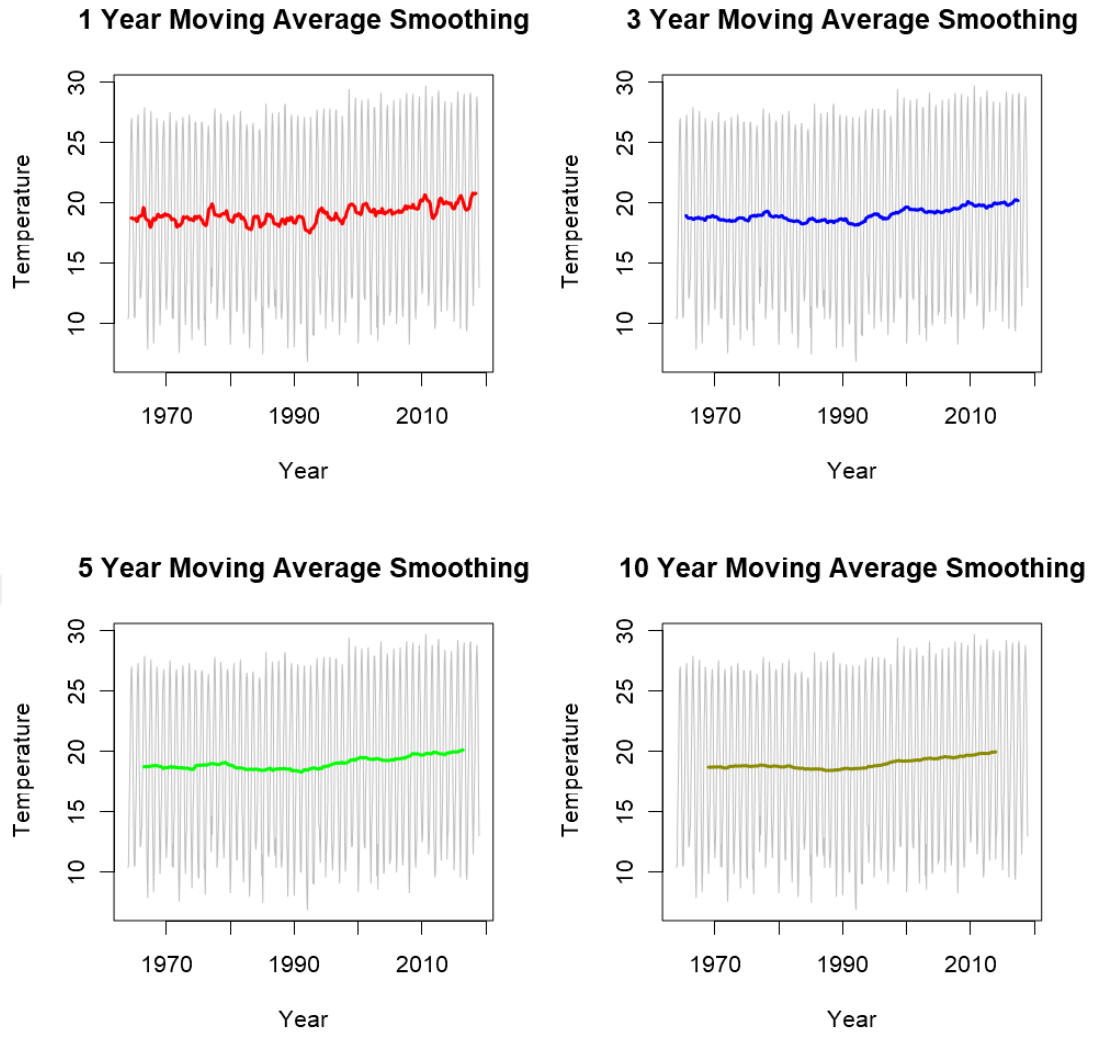

Figure 6.36 The monthly mean temperature data at different moving average time for station 17979

When focused on average annual temperature variability, the annual average maximum, minimum and mean temperature data are considered the same as the monthly temperature data. For three cases, time series are demonstrated for all stations in Figures 37-44. The maximum temperature data falls between the 1963-1980 period, and it increases both minimum and mean temperatures during the 1963-2018 period. Notably, it has been increasing rapidly for three cases after 1990 for station 17255 (Figure 6.37).

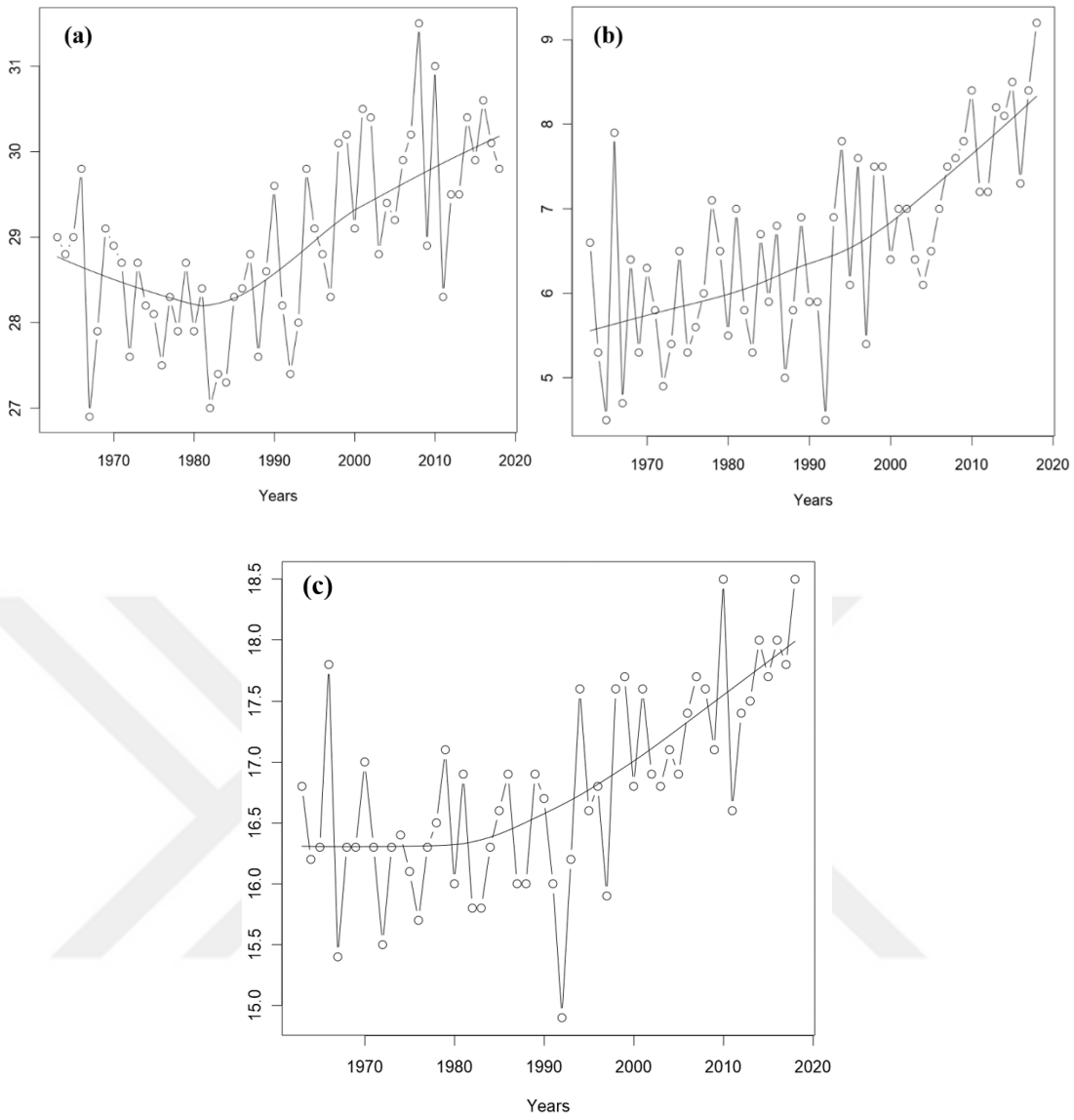

Figure 6.37 The average annual (a) maximum, (b) minimum and (c) mean temperature data time series for station 17255

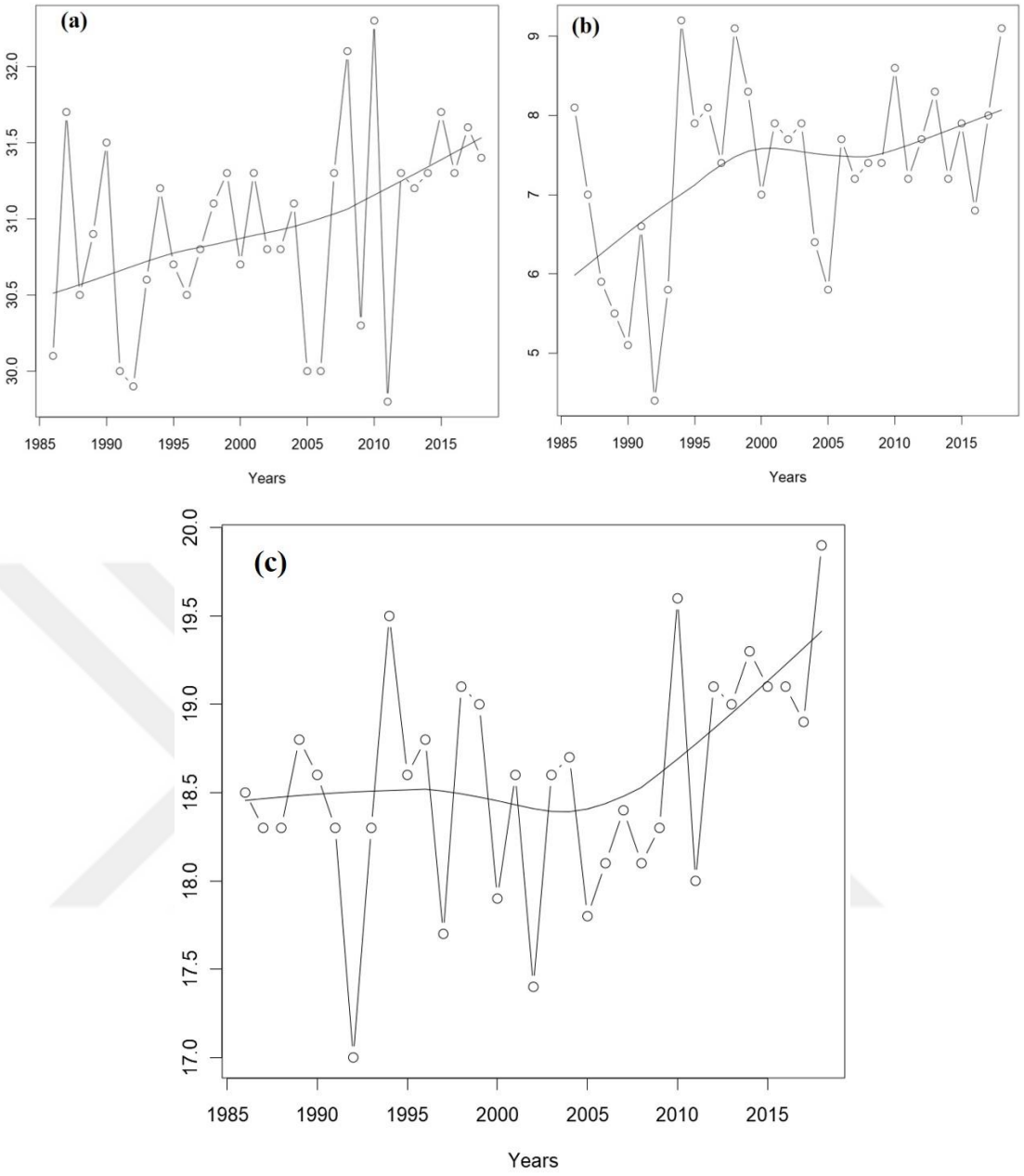

Figure 6.38 The average annual (a) maximum, (b) minimum and (c) mean temperature data time series for station 17355

The average annual minimum, maximum and mean temperatures increase steadily between the 1963-2018 period. The highest average annual minimum, maximum and mean temperature is 9.2, 32.3 and 19.9 ° C, respectively. Besides, the lowest average annual minimum, maximum and mean temperature is 4.4, 29.8 and 17° C, respectively. The highest increase in mean temperature has been observed since 2005 for station 17355 (Figure 6.38).

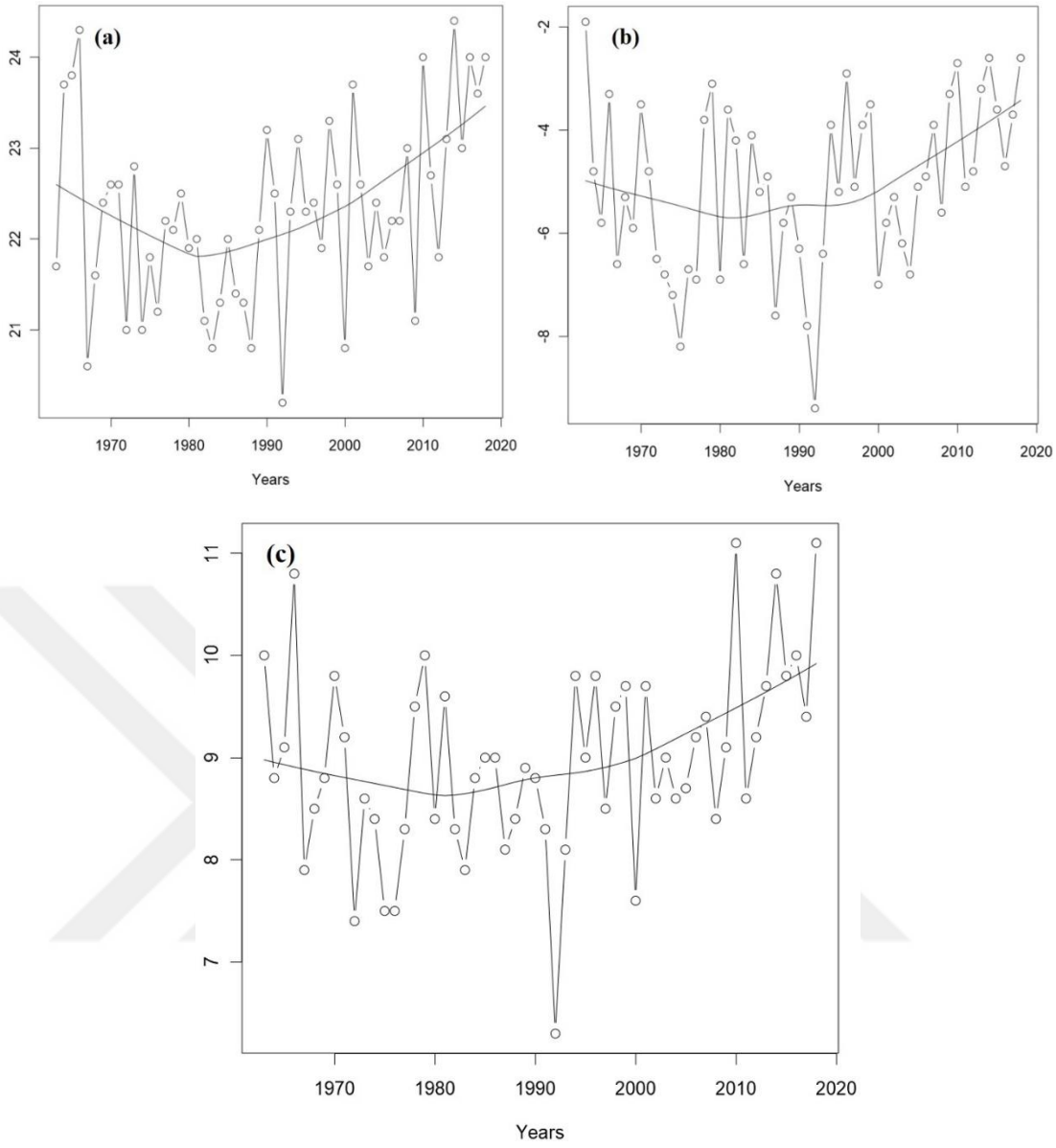

Figure 6.39 The average annual (a) maximum, (b) minimum and (c) mean temperature data time series for station 17866

The average annual minimum, maximum and mean temperatures increase steadily between the 1981-2018 period. The highest average annual minimum, maximum and mean temperature is -1.9, 24.4 and 11.1 ° C, respectively. Besides, the lowest average annual minimum, maximum and mean temperature is -9.4, 20.2 and 6.3° C, respectively for station 17866 (Figure 6.39).

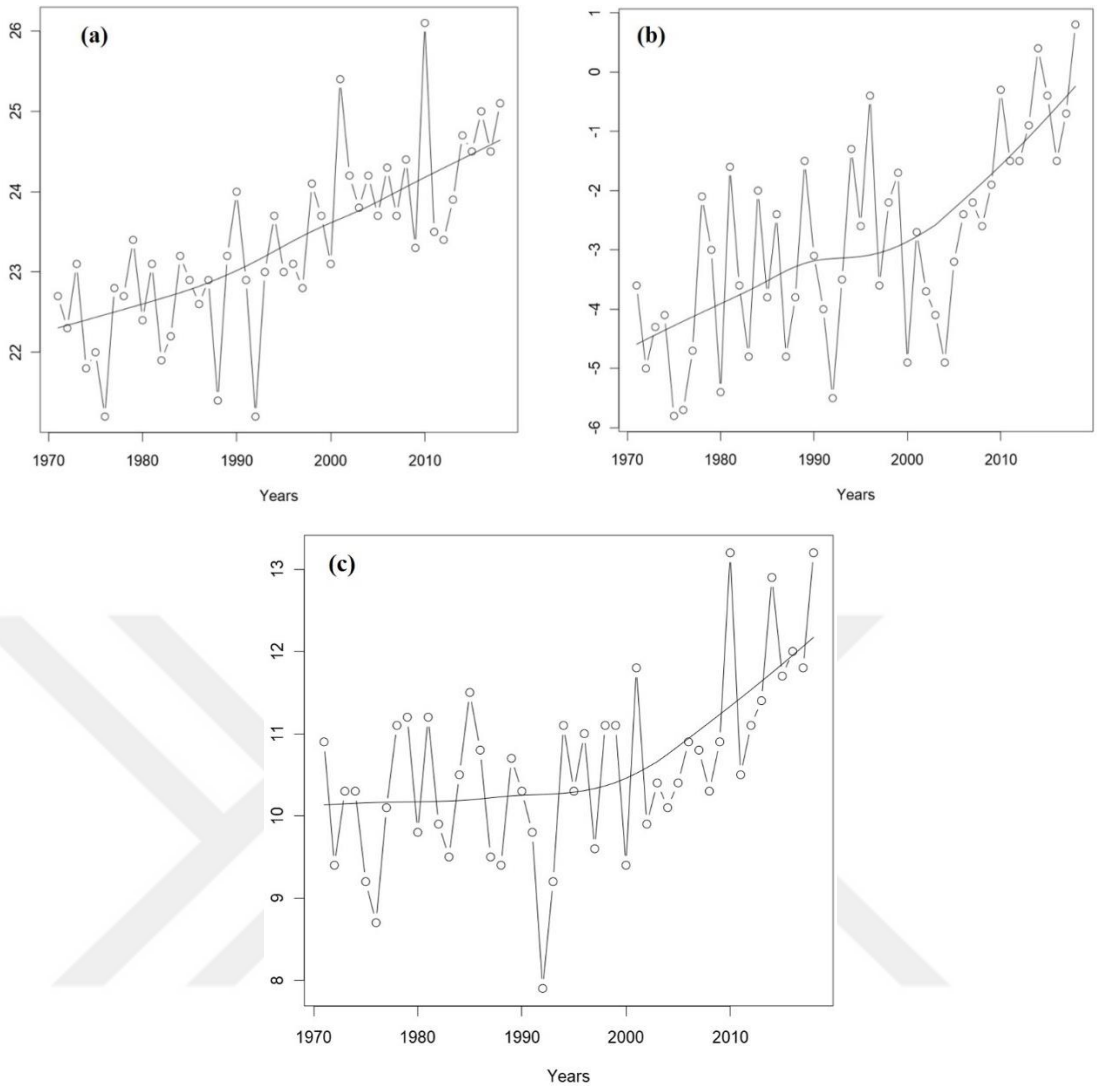

Figure 6.40 The average annual (a) maximum, (b) minimum and (c) mean temperature data time series for station 17868

The average annual minimum, maximum and mean temperatures increase steadily between the 1971-2018 period. The highest average annual minimum, maximum and mean temperature is 0.8, 26.1 and 13.2 ° C, respectively. Besides, the lowest average annual minimum, maximum and mean temperature is -5.8, 21.2 and 7.9° C, respectively for station 17868 (Figure 6.40).

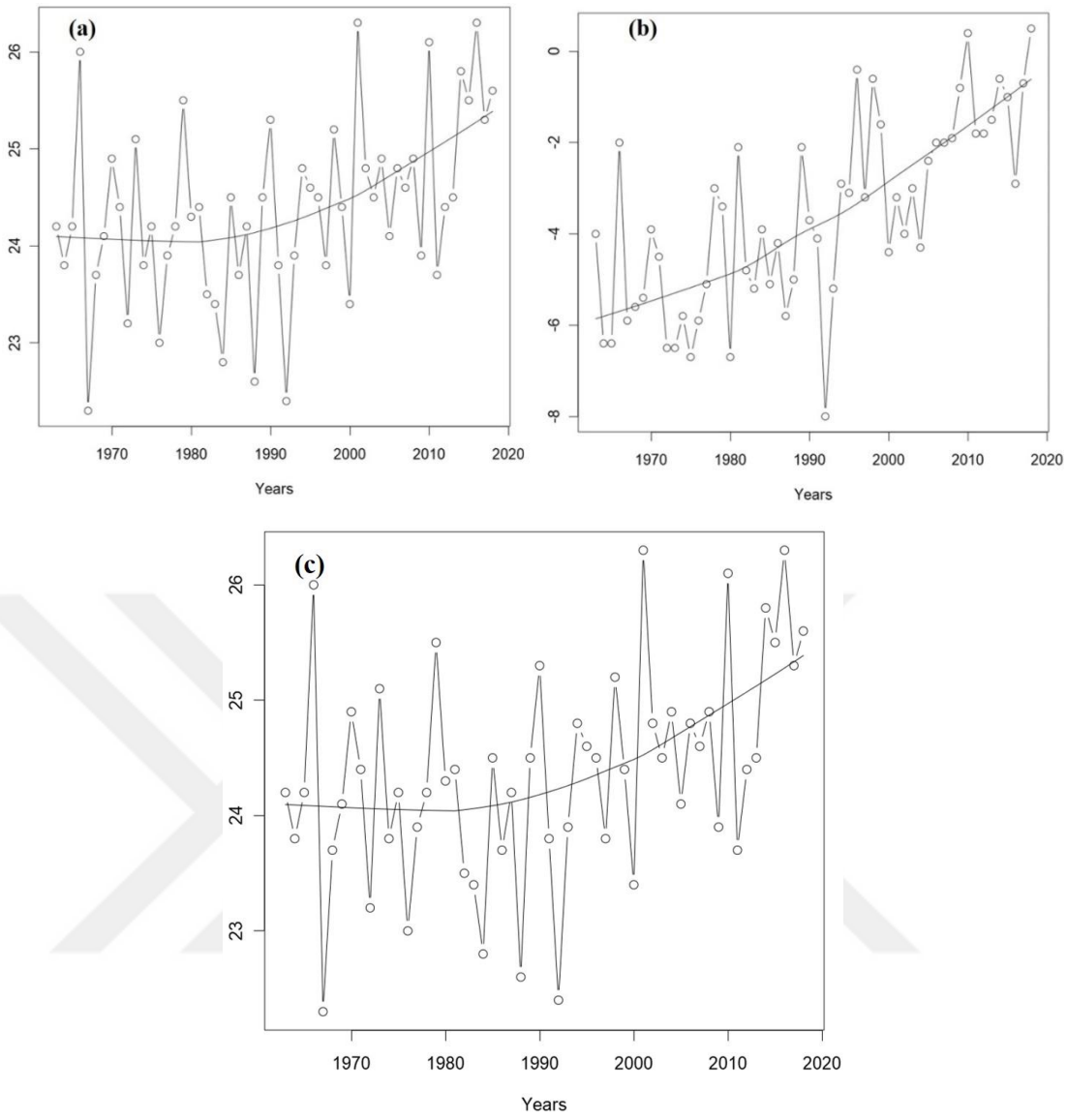

Figure 6.41 The annual (a) maximum, (b) minimum and (c) mean temperature data time series for station 17870

The average annual minimum, maximum and mean temperatures increase steadily between the 1963-2018 period. The highest average annual minimum, maximum and mean temperature is 0.5, 26.3 and 13.5 ° C, respectively. Besides, the lowest average annual minimum, maximum and mean temperature is -8.0, 22.3, and 7.9° C, respectively for station 17870 (Figure 6.41).

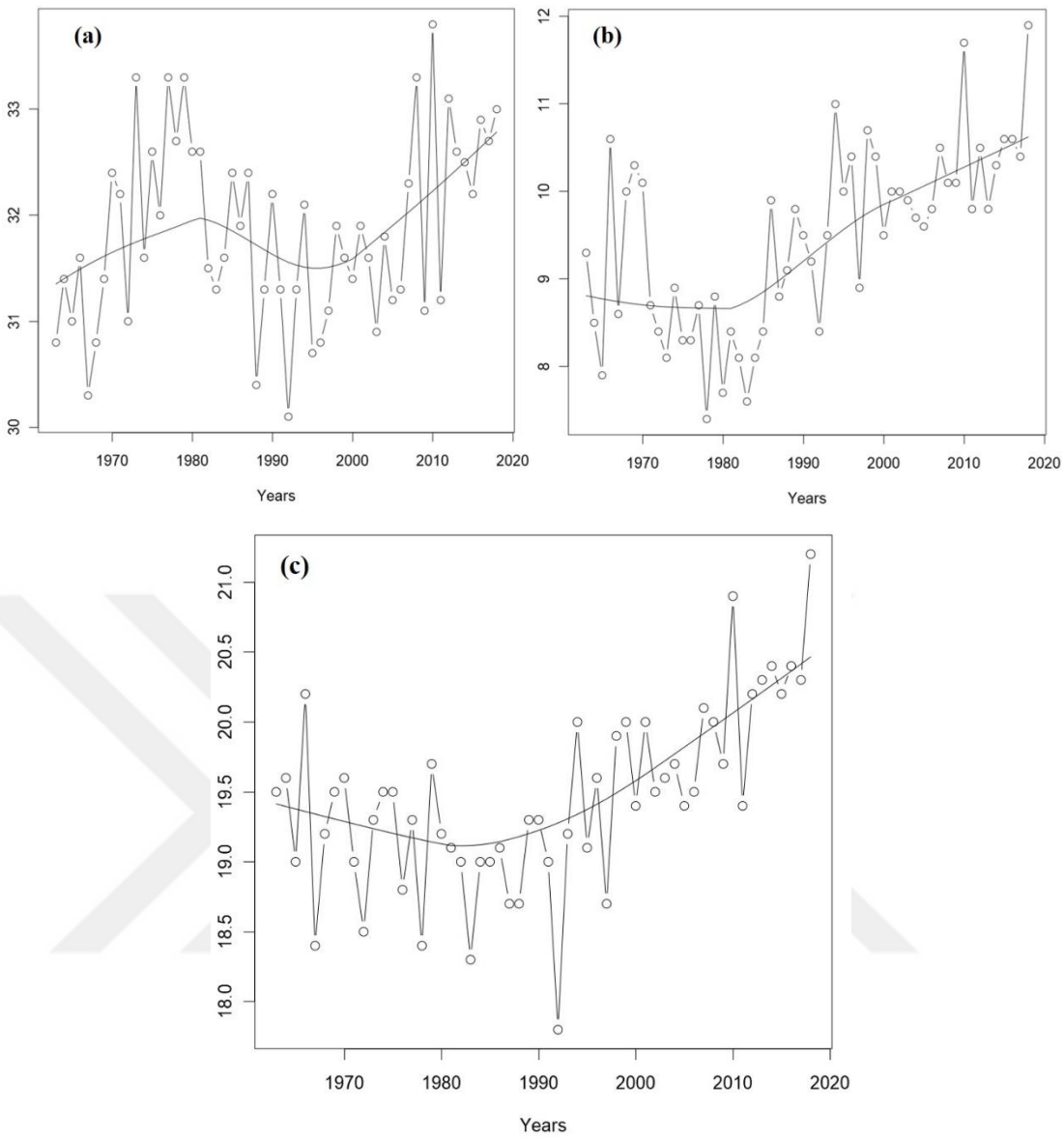

Figure 6.42 The annual (a) maximum, (b) minimum and (c) mean temperature data time series for station 17908

The average annual minimum, maximum and mean temperatures increase steadily between the 1984-2018 periods. The highest average annual minimum, maximum and mean temperature is 11.9, 33.8 and 13.5° C, respectively. Besides, the lowest average annual minimum, maximum and mean temperature is 7.4, 30.1 and 17.8° C, respectively for station 17908 (Figure 6.42).

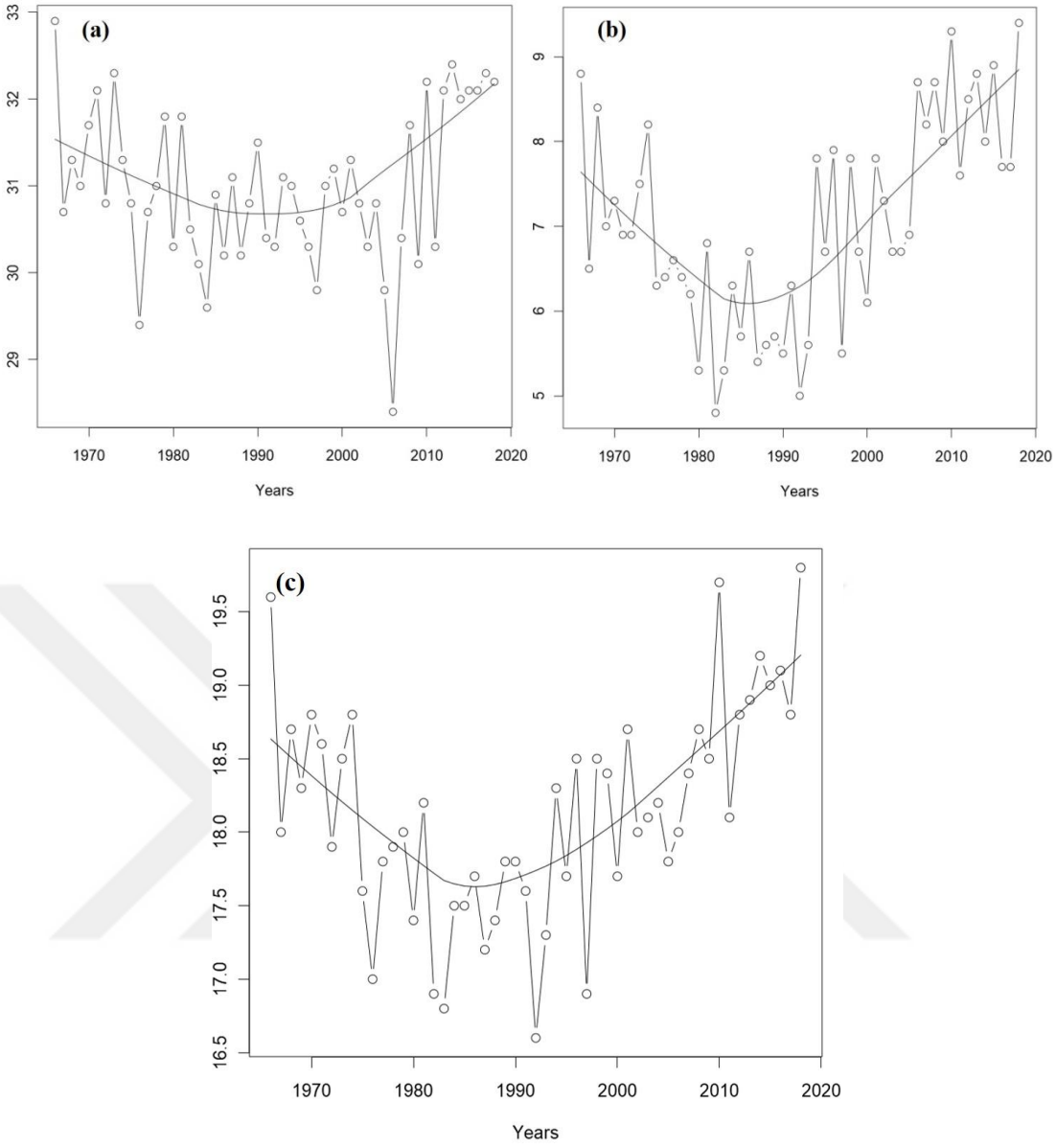

Figure 6.43 The annual (a) maximum, (b) minimum and (c) mean temperature data time series for station 17960

While The average annual maximum temperature increase after 2000, the average minimum and mean temperatures increase steadily between the 1984-2018 period. The highest average annual maximum, minimum and mean temperature is 32.9, 9.4 and 19.8° C, respectively. Besides, the lowest average annual maximum, minimum and mean temperature is 28.4, 4.8 and 16.6° C, respectively for station 17960 (Figure 6.43).

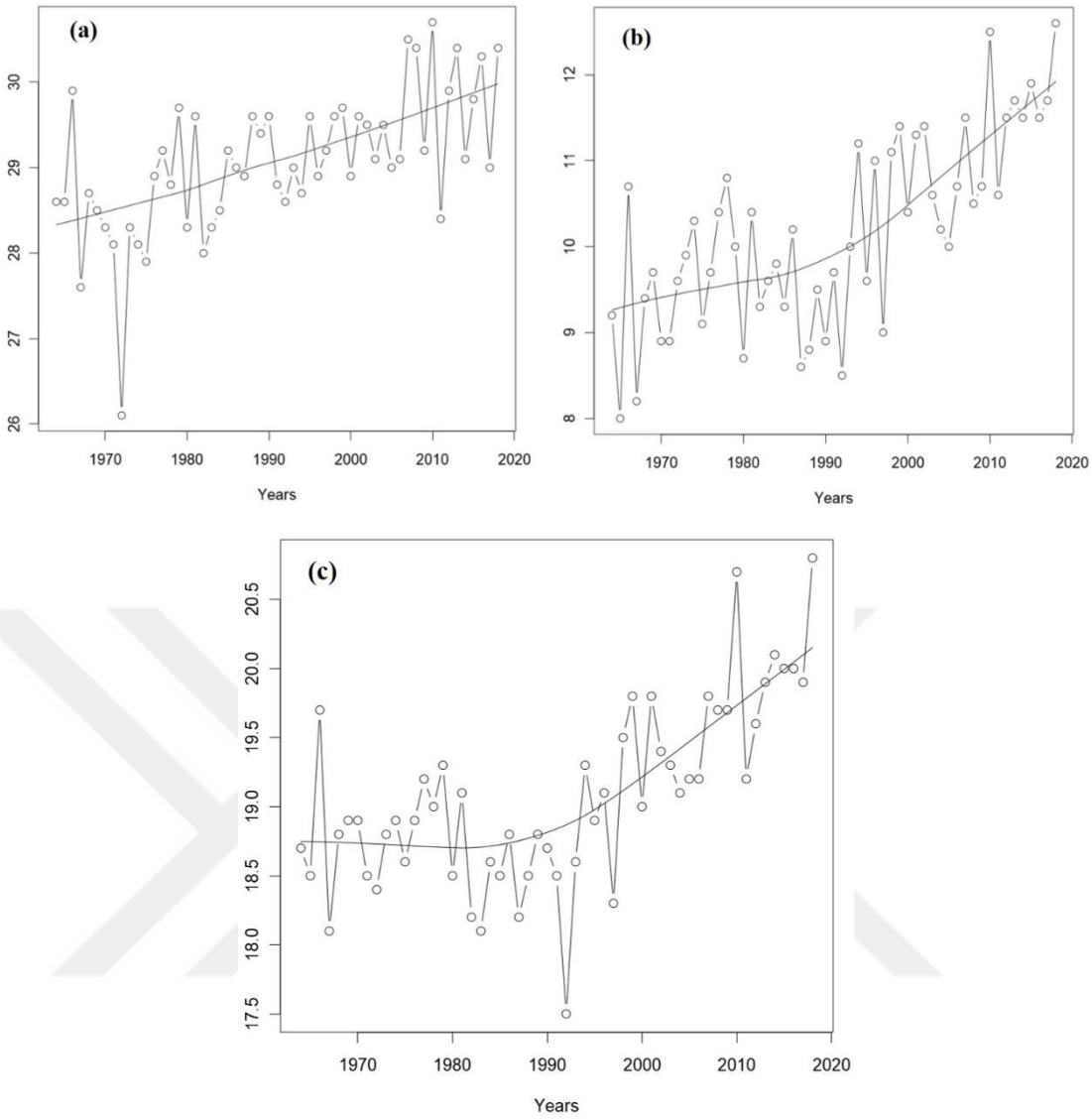

Figure 6.44 The annual (a) maximum, (b) minimum and (c) mean temperature data time series for station 17979

While The average annual maximum and minimum temperatures increase between 1964-2018, the average mean temperature increase steadily after the 1984 period. The highest average annual maximum, minimum and mean temperature is 30.7, 12.6 and 20.8° C, respectively. Besides, the lowest average annual maximum, minimum and mean temperature is 26.1, 8.0 and 17.5° C, respectively for station 17979 (Figure 6.44).

6.3.1 Trend Detection of Annual Temperature Data

According to trend test results**,** an increasing trend in temperature sequences has been detected at all stations (Table 6.5). Notably, according to Mann-Kendall and Spearman Rho test results, 17255, 17870 and 17979 stations indicate a more increasing trend at the annual minimum temperature, while the annual maximum temperature shows higher significance at 17255, 17868 and 17979. When focused on the annual mean temperature, stations 17255, 17908 and 17979 a relatively higher increased trend than the other stations. The lower values of z in used trend tests indicate that the annual maximum temperature and minimum temperature have no significant trend for 17960 (0.522) and 17355 (1.5385) stations at 95% significant level (±1.96), respectively. However, for the annual mean temperature, all stations have an increasing trend.

Table 6.5 The trend test results of the annual temperature data

	Minimum		Maximum		Mean	
Station	**Mann-Kendall**	**Spearman Rho**	**Mann-Kendall**	**Spearman Rho**	**Mann-Kendall**	**Spearman Rho**
17255	5.49	4.86	4.29	4.28	4.97	4.55
17355	1.54	1.76	2.26	2.12	2.02	2.12
17866	2.16	2.12	2.38	2.24	2.36	2.25
17868	4.64	4.35	5.89	5.46	3.58	3.45
17870	5.88	5.38	3.24	3.16	3.24	3.16
17908	4.82	4.47	1.50	1.62	4.37	4.18
17960	2.80	2.94	0.52	0.61	2.64	2.47
17979	5.66	5.23	4.77	4.56	5.22	4.91

6.3.2 Magnitude of Trend of Annual Temperature Data

The trend slope for three cases using Regression and Sen's Slope test are shown for all station in Table 6.6. In evaluation trend detection, MK and SR show the similar results. However, SR trend detection results reveal higher sensitive as compared to Mann-Kendall due to higher numerical value. Their sensitive about trend direction is completely same for all stations.

Table 6.6 The trend slope results for annual temperature data

	Minimum		Maximum		Mean	
Station	**Sen's Slope**	**Regression**	**Sen's Slope**	**Regression**	**Sen's Slope**	**Regression**
17255	0.048	0.045	0.038	0.038	0.031	0.030
17355	0.039	0.046	0.028	0.023	0.023	0.024
17866	0.028	0.026	0.024	0.018	0.018	0.017
17868	0.082	0.078	0.052	0.056	0.039	0.041
17870	0.098	0.090	0.023	0.023	0.023	0.023
17908	0.042	0.039	0.013	0.012	0.023	0.022
17960	0.034	0.033	0.004	0.004	0.020	0.016
17979	0.050	0.049	0.031	0.032	0.027	0.027

After detecting the presence of trend and trend's slope, the Buishand Range Test (BRT), Standard Normal Homogeneity Test (SNHT) and the Pettitt Test (PT) are used to determine the change of point in long-term time series. SNHT and BRT can be shown as graphically where the break occurs. The annual maximum temperature data break point is presented for station 17355 in Figure 6.45.

The break point of long-term time series using SNHT and BRT tests is displayed graphically at the same point for the station 17355, although different mathematical functions are applied. The results of the three tests are compared to determine a more precise breaking point. Therefore, if two outcomes of the three tests are the same, a break point is selected for that station. However, if the results of all used tests differ from each other, the choice of the break point will be suspect (S). Change point detection results are presented considering the annual maximum, minimum, and mean temperature data in Table 6.7-6.9. According to the annual maximum temperature, no change point detection is observed at 17908 and 17960 stations due to the presence of the trend. Except for a few stations, BRT and PT are good convenient tests to detect critic break points rather than SNHT because of the sensitivity to middle break points. For example, when we consider 17255 station for all cases, BRT and PT captures at the year of 1993 year whereas SNHT capture at the year of 1997 for maximum temperature data. For minimum temperature, while BRT and PT result indicates at the year of 1992, the year of 2006 is captured by the SNHT test. However, the break point is the same as the year of 1997 for mean temperature data.

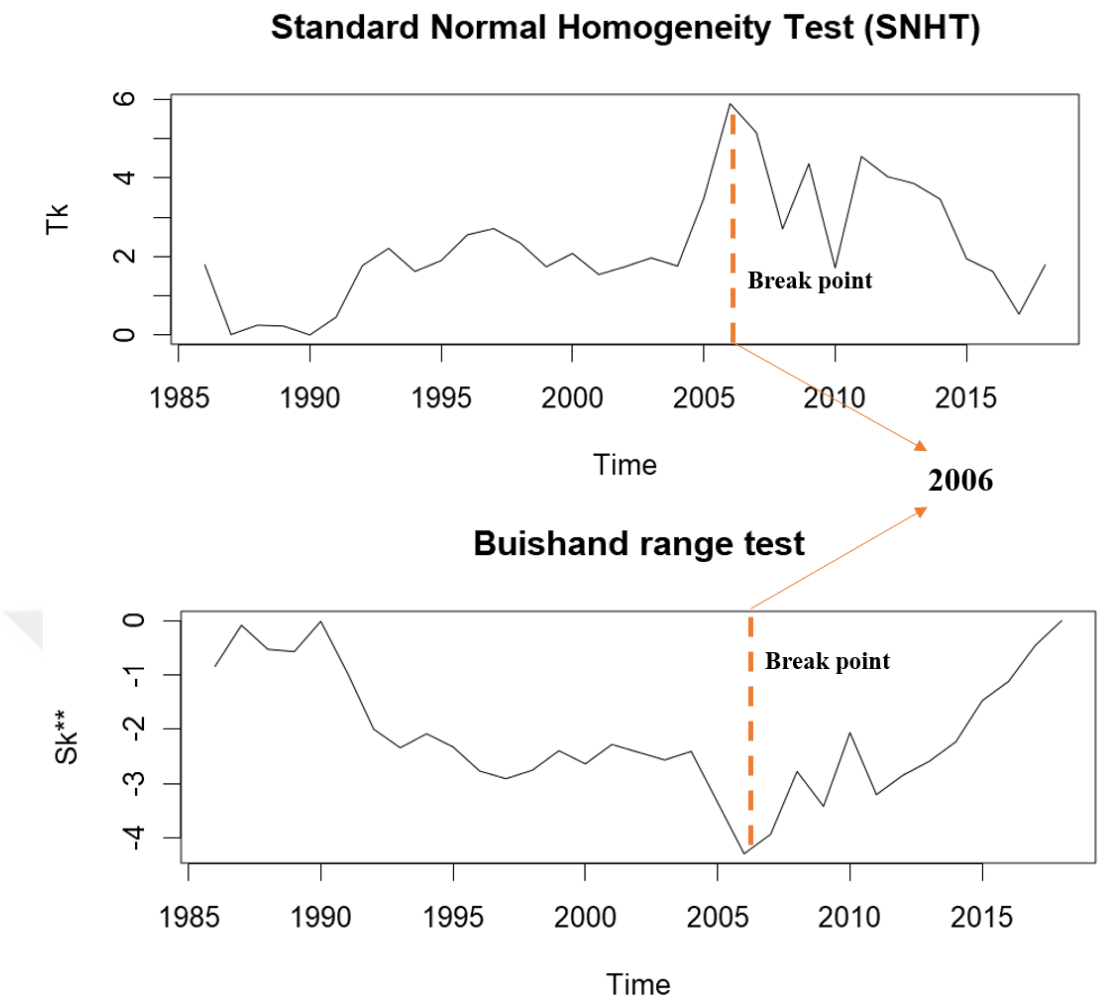

Figure 6.45 The annual maximum temperature data break point for station 17355

Table 6.7 The change point detection for the annual maximum temperature data; CP; change point, S; Suspect, NC; no change

	SNHT		BRT		PT		
Station	**Tmax**	**CP**	**R / sqrt(n)max**	**CP**	**Umax**	**CP**	**Result**
17255	27.598	1997	2.7045	1993	648	1993	1993
17355	5.8894	2006	1.1674	2006	138	2006	2006
17866	12.689	2009	1.928	1992	338	1992	1992
17868	25.69	1997	2.5144	1997	526	1997	1997
17870	12.473	2000	1.7756	1993	424	1993	1993
17908	10.29	NC	1.5872	NC	301	NC	NC
17960	14.05	NC	2.1447	NC	296	NC	NC
17979	17.44	1984	2.0447	1987	502	1987	1987

Table 6.8 The change point detection for the annual minimum temperature data; CP; change point, S; Suspect, NC; no change

	SNHT		BRT	PT			
Station	**Tmin**	**CP**	**R / sqrt(n)min**	**CP**	**Umin**	**CP**	**Result**
17255	23.96	2006	2.4087	1992	599	1992	1992
17355	12.942	NC	1.6597	NC	149	NC	NC
17866	10.215	2008	1.7456	1993	341	2004	S
17868	20.235	2008	1.9498	2005	374	2005	2005
17870	28.776	1993	2.6667	1993	663	1993	1993
17908	26.404	1993	2.56	1992	626	1993	1993
17960	23.357	2005	2.5888	2000	471	2000	2000
17979	29.077	1997	2.6269	1993	631	1997	1997

Table 6.9. The change point detection for the annual mean temperature data; CP; change point, S; Suspect, NC; no change

	SNHT		BRT	PT			
Station	**Tmean**	**CP**	**R / sqrt(n)mean**	**CP**	**Umean**	**CP**	**Result**
17255	27.163	1997	2.5274	1997	621	1997	1997
17355	9.204	2009	1.3511	2009	156	2009	2009
17866	12.149	2009	1.8375	1993	366	1993	1993
17868	18.465	2009	1.794	2005	318	2005	2005
17870	12.473	2000	1.7756	1993	424	1993	1993
17908	24.347	1997	2.4913	1997	607	1997	1997
17960	17.728	2007	2.5458	1997	420	1997	1997
17979	30.35	1997	2.6765	1997	658	1997	1997

The annual temperature for three cases using Mann-Kendall method are shown spatially on the Ceyhan Basin in Figure 6.46. The annual mean temperature trend increases less when compared to the annual maximum and minimum data. The northern part of the Ceyhan Basin indicated a high temperature increase in the maximum and minimum temperature data. When focused on station 17255, it had a higher statistically significant at 95% for three cases.

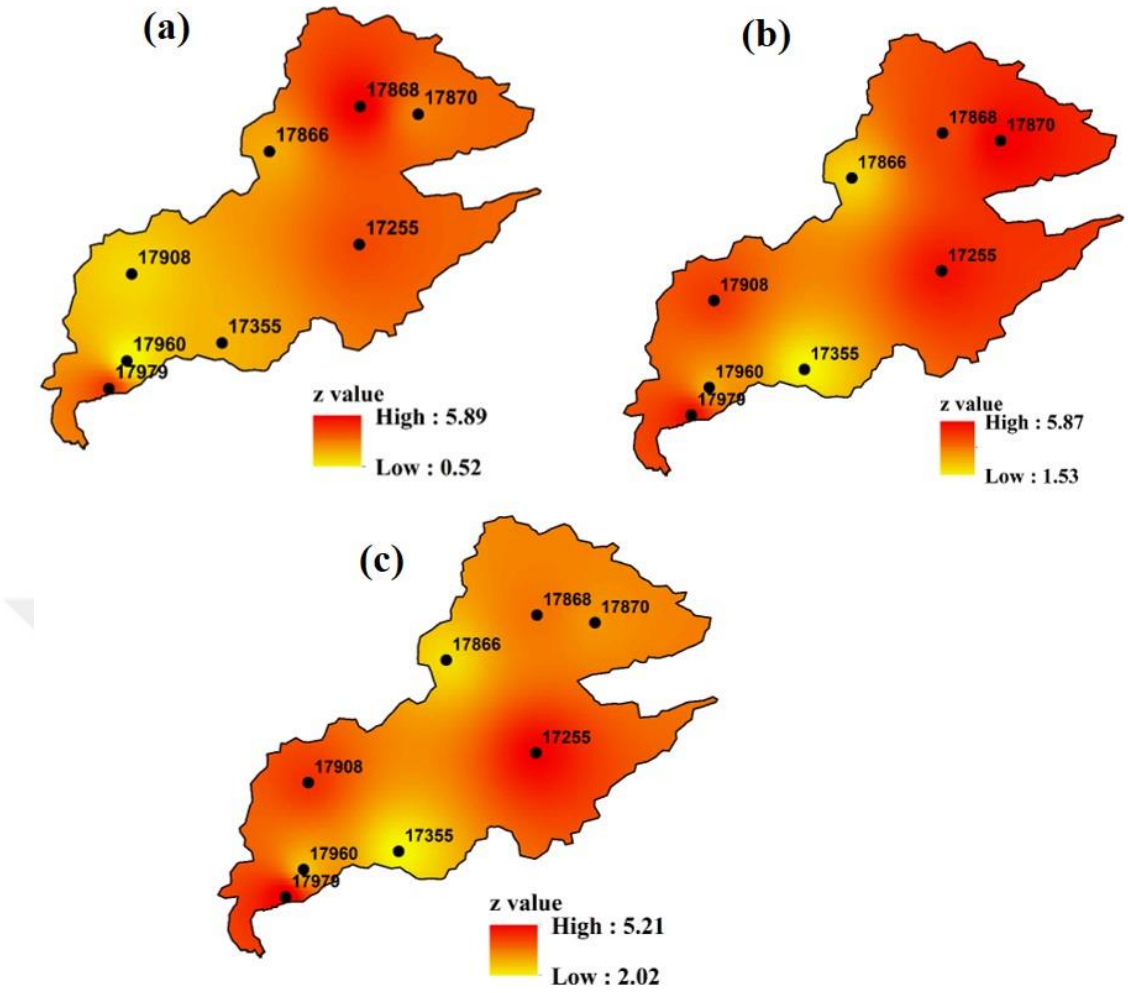

Figure 6.46 Trend of temperature in Ceyhan basin at 95% significant level (a) the annual maximum (b) the annual minimum and (c) the annual mean

6.4 Time Series of Extreme Drought Events

The intensity and frequency of extreme drought events including annual maximum drought severity (AMDS) and annual maximum drought duration (AMDD) have significantly increased in several regions. Hence, we determine extreme drought events over the Ceyhan Basin using multiple time series (SPI 1-, 3-, 6-, 9- and 12). Figure 6.47, 6.48, 6.49, 6.50, and 6.51 present the variability of the multiple time series for AMDD and AMDS parameters.

For annual maximum drought severity (AMDS) time series at SPI-1 month, many stations indicate a slight and insignificant decreasing trend, while others exhibit slightly insignificant decreasing trend. For instance, the highest AMDS and AMDD are found as 5.69 and 5 months for the year 1999 at station 7767, respectively. There

should be noted that the highest AMDS doesn't generally occur at corresponding to the highest AMDD. For station 7767, the highest AMDS and AMDD exhibit as the same year 1999. However, while the highest AMDS are determined as 5.17 in the years 1989, the highest AMDD shows as 5 month at the different years (1966, 1973 and 2004) in the Figure 6.47.

As it can be seen from Figure 6.47, in SPI 1-month time scale, AMDS is more frequent but shorter, and the highest AMDS (over 10) value are calculated for station 17355 (1989), 17866 (1989), 17908 (1989), 17960 (1989), 17979 (1989), D20A001 (2010) and D20A015 (1989). The year 1989 is found as for both two extreme drought events. The corresponding AMDD are evaluated for these stations as 8-, 9-, 5-, 7-, 8-, 7- and 7-month, respectively.

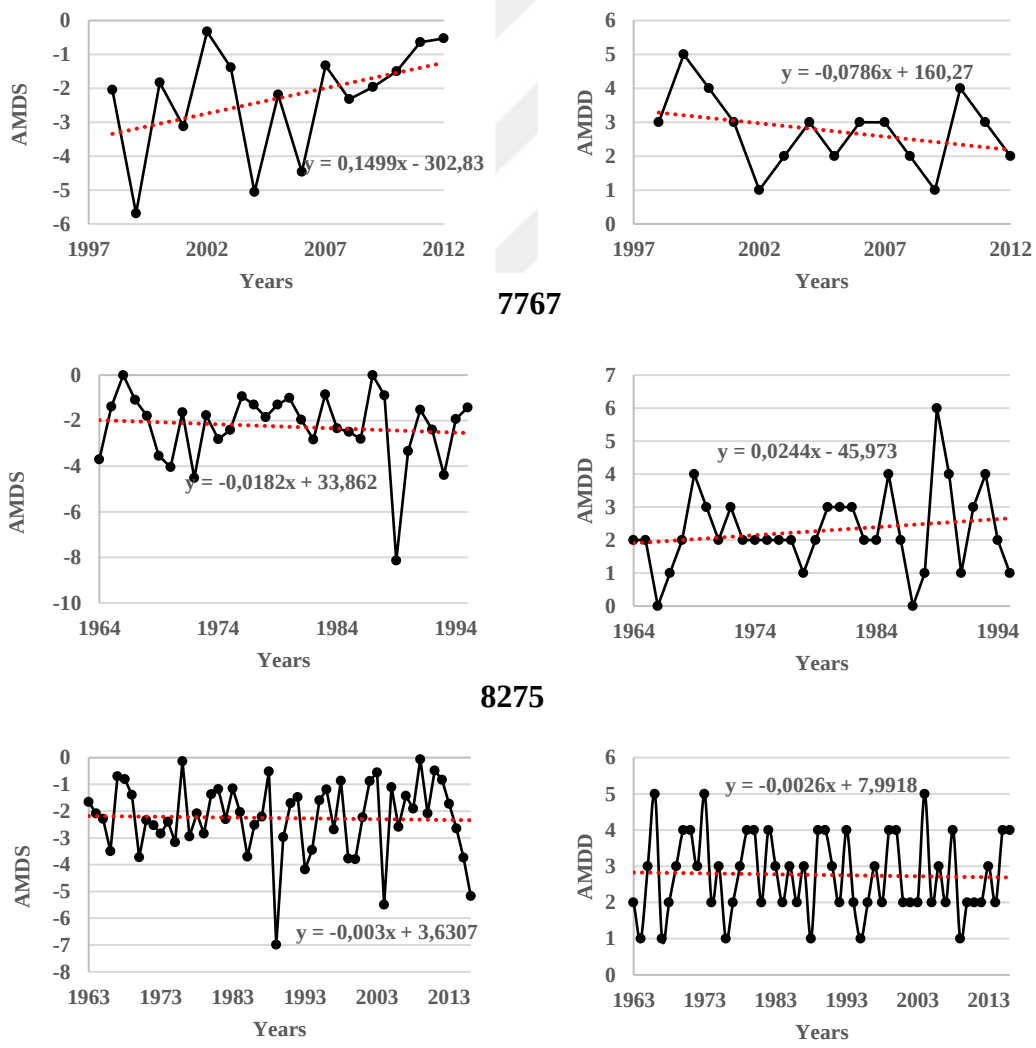

17255

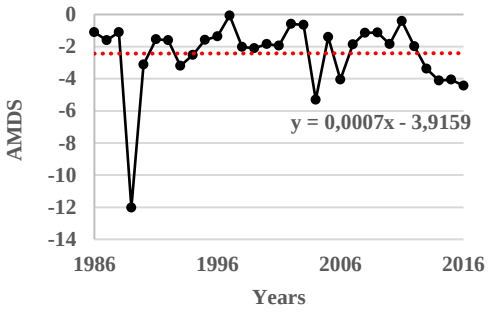

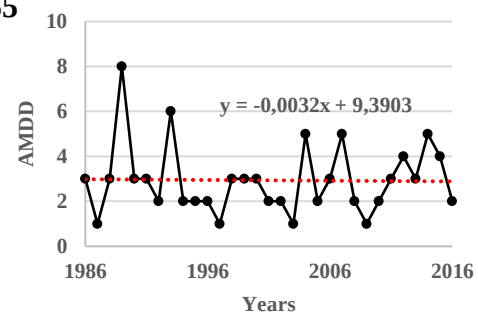

17355

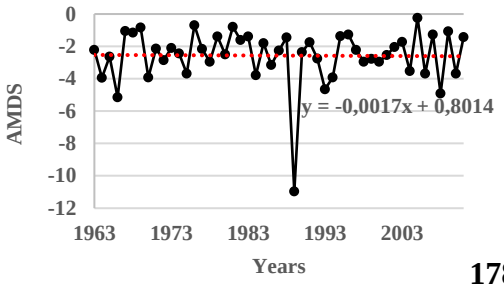

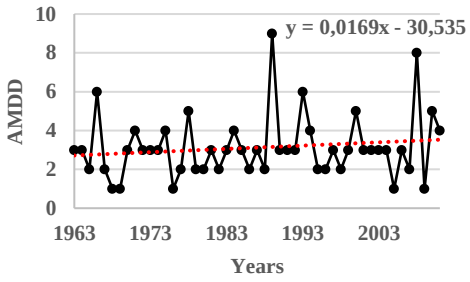

17866

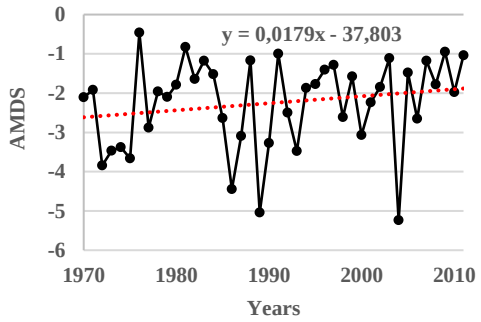

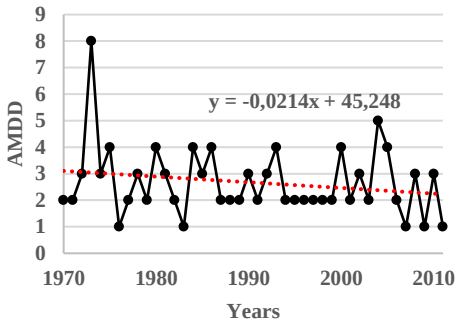

17868

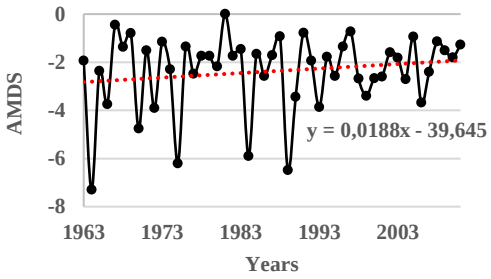

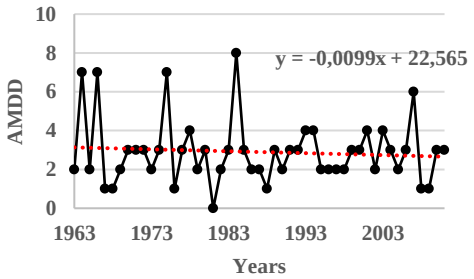

17870

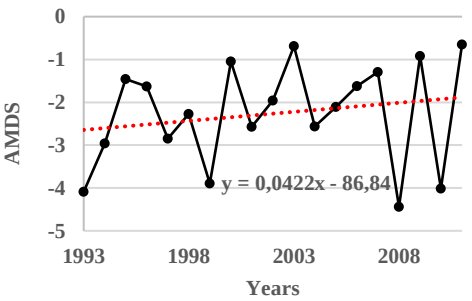

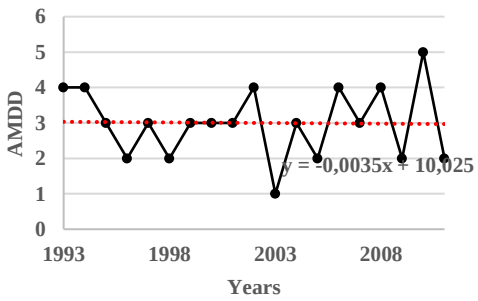

17871

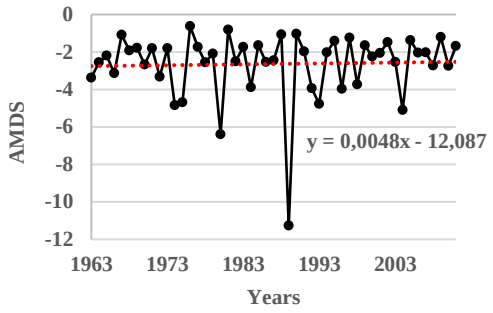

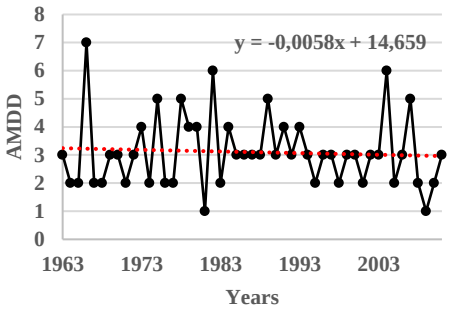

17908

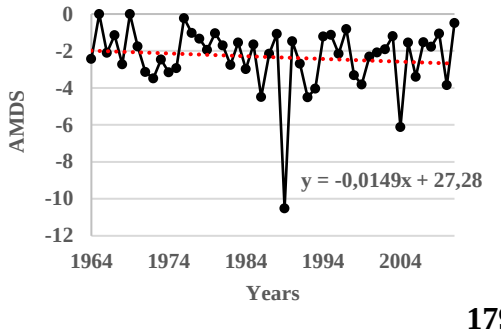

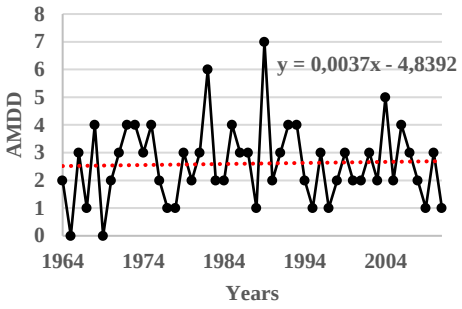

17960

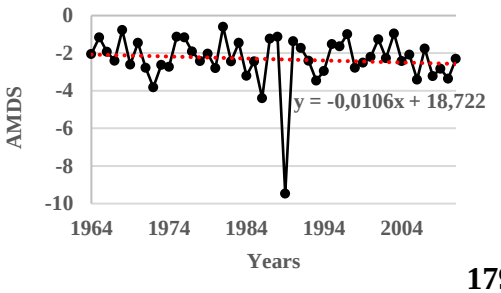

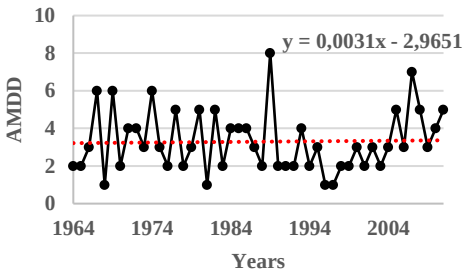

17979

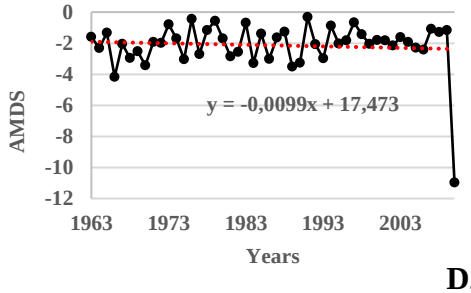

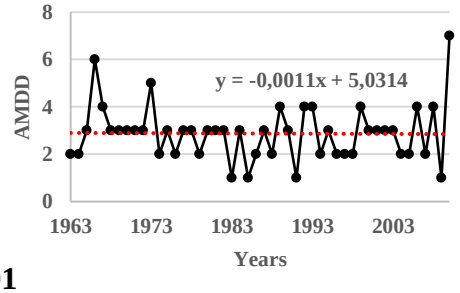

D20A001

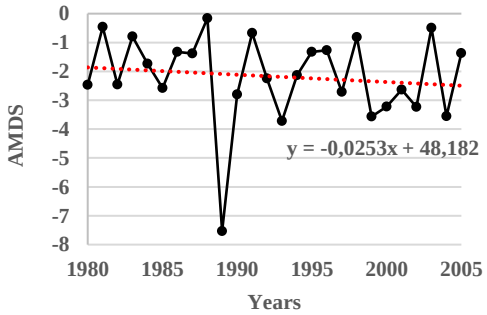

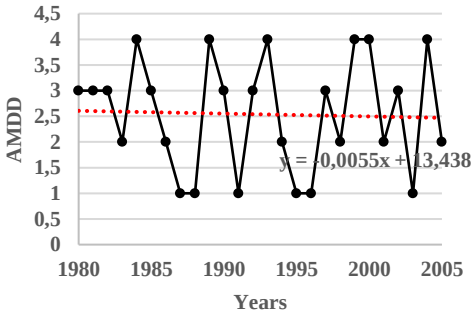

D20A002

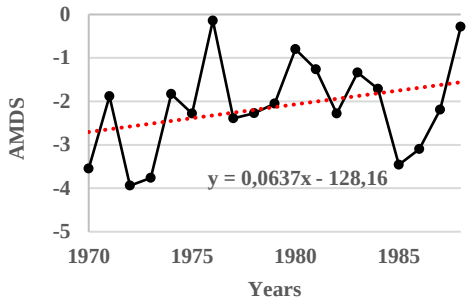

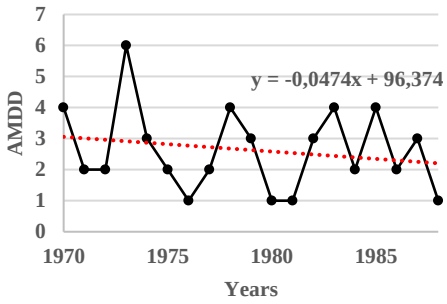

D20A004

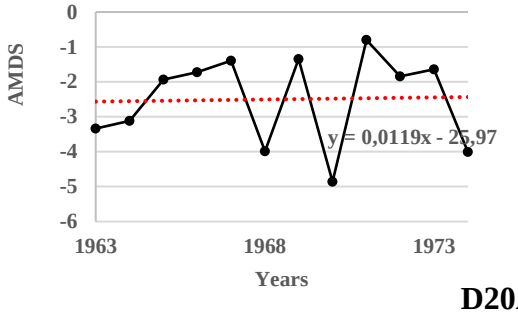

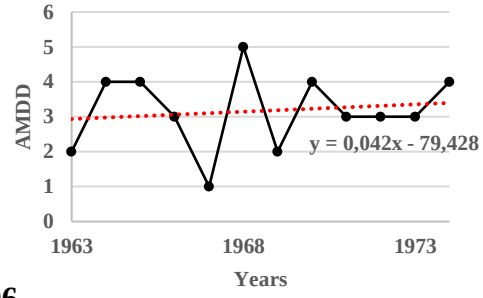

D20A006

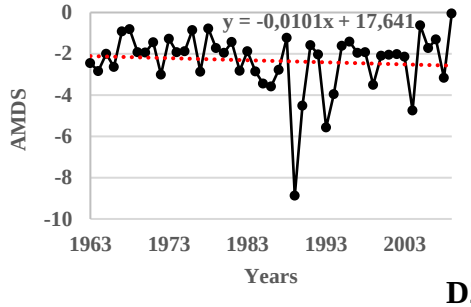

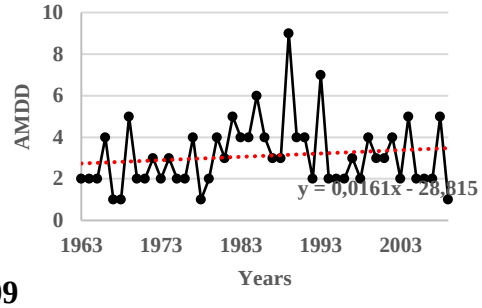

D20A009

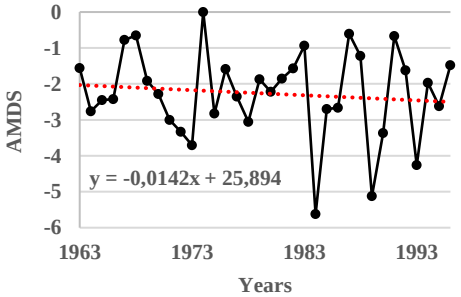

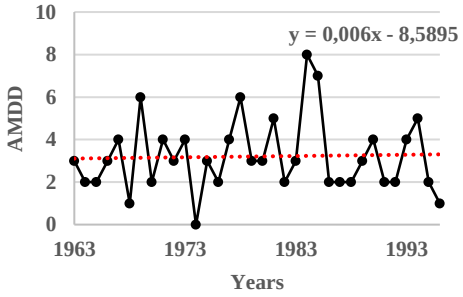

D20A011

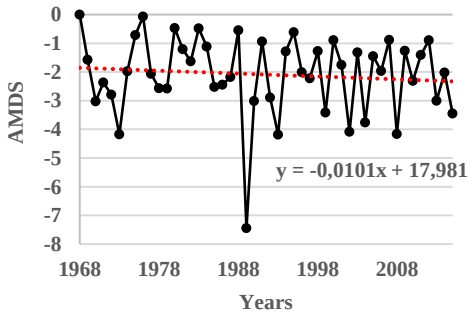

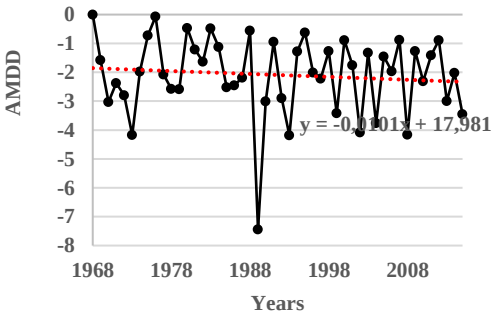

D20A013

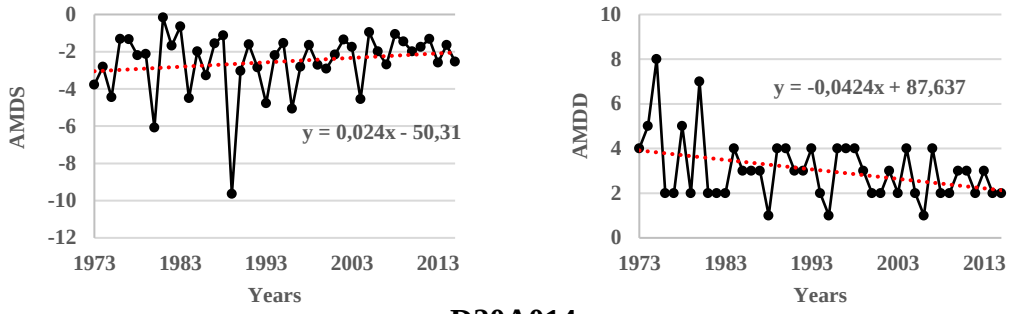

D20A014

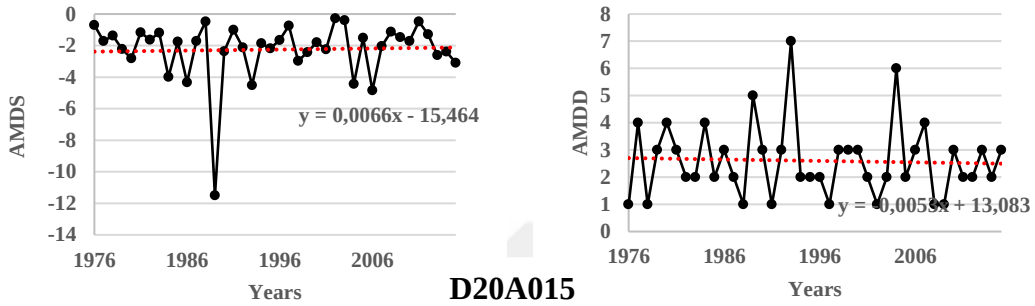

D20A015

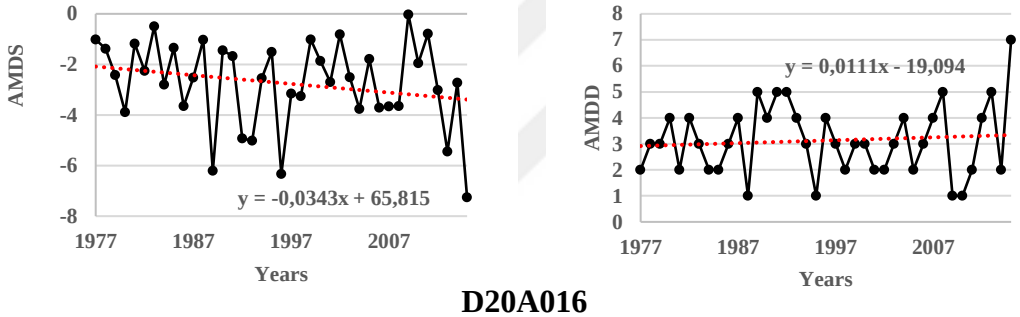

D20A016

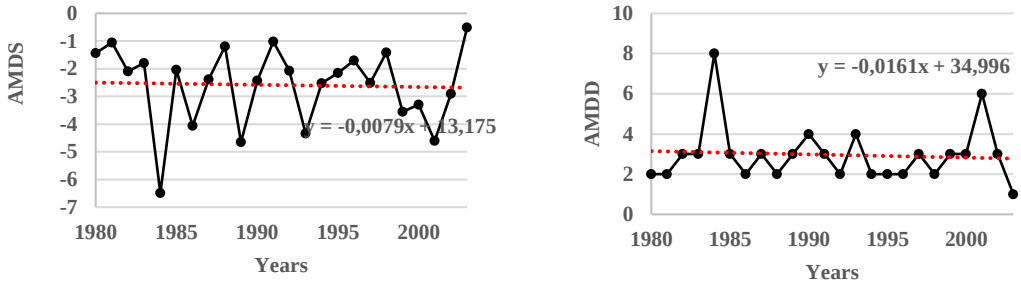

D20A017

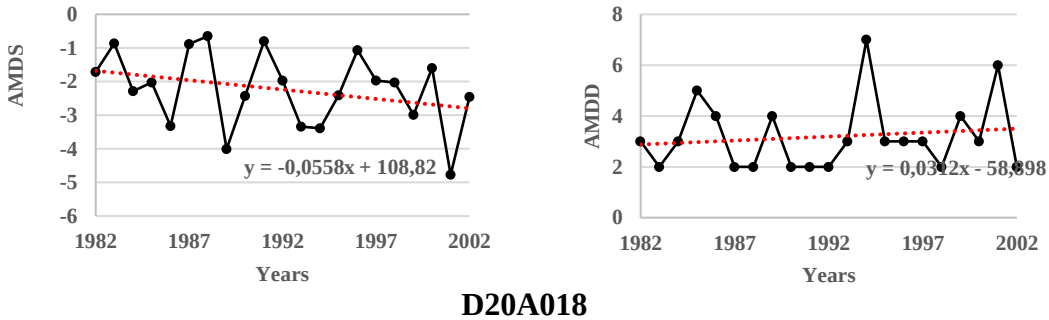

D20A018

Figure 6.47 SPI 1-month extreme drought events time series

For following other time scales (3-, 6-, 9- and 12-month), the AMDS value inceases as well as AMDD increases for six stations, but decreases for 17 stations. These time series plots of the calculated AMDS and AMDD for all station are shown in Figures 6.48, 6.49, 6.50 and 6.51. For SPI 3-month, it is clearly seen that the AMDD are evaluated in 1989 that is highest value for the majority of stations. In general view, many of stations indicate a slight and insignificant decreasing trend (8275, 17255, 17355, 17866, D20A001, D20A002, D20A006, D20A009, D20A0011, D20A0015, D20A0016 and D20A0018), while others (7767, 17868, 17870, 17871, 17908, 17960, 17979, D20A004, D20A013, D20A014 and D20A017) exhibit slightly insignificant increasing trend. Station D20A001 exhibits the highest AMDS and AMDD values as 22.16 and 12 month, respectively. Increase in AMDD and AMDS is a primary indicator of more dangerous circumstances both in the natural environment and human lives. Therefore, their statistically significant about the existence of trends are discussed at the 6.2.2 section.

AMDD and AMDS trend characteristics reveal slightly difference except six stations (17871, 17960, D20A002, D20A009, D20A013 and D20A015). While positive trends are seen in AMDS, negative trends are detected in AMDD with time. For example, it is observed that AMDS increase with time, but AMDD decrease with time for station 7767. The highest AMDD (over 10-month) value are found at stations 8275 (1983), 17866 (2001), 17868 (1990), 17870 (1984, 2001), D20A001 (1999, 2010), D20A004 (1973), D20A009 (1964, 2007), D20A0011 (1973), D20A0013 (1973) and D20A0016 (2007).

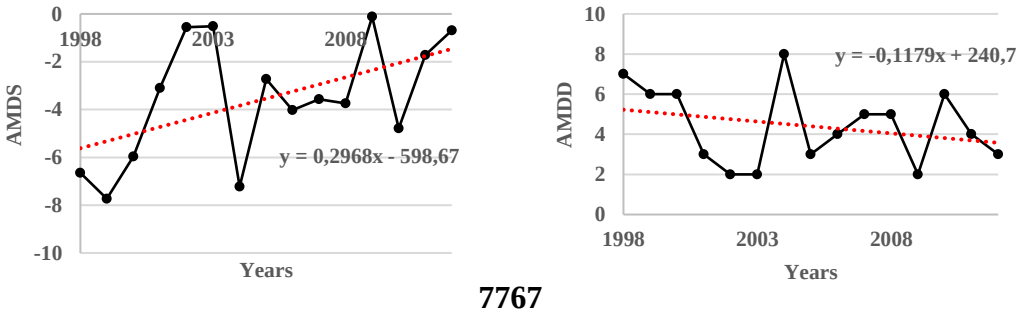

7767

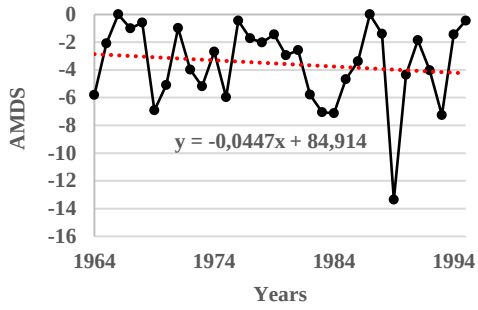

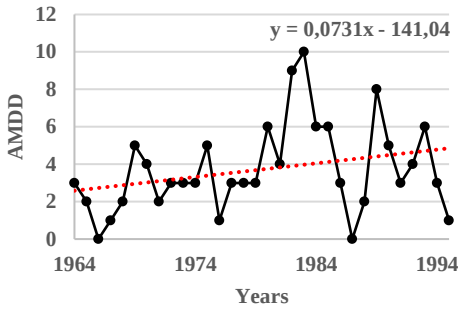

8275

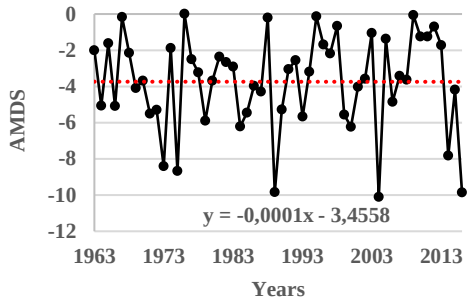

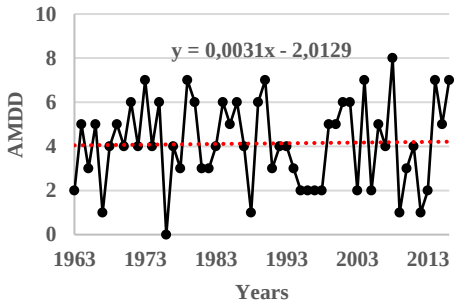

17255

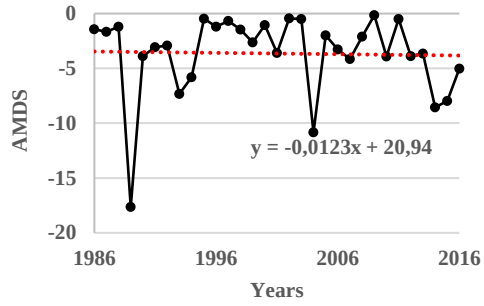

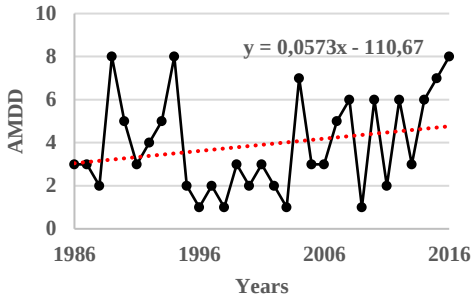

17355

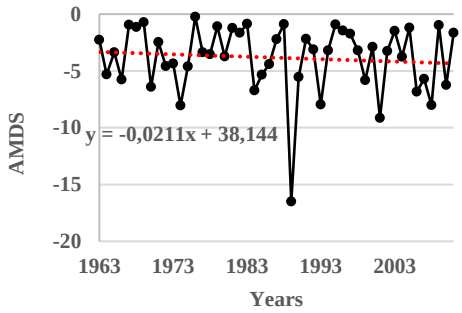

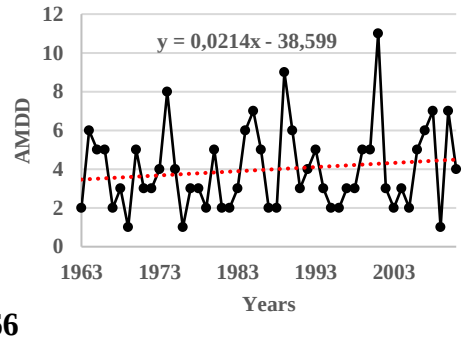

17866

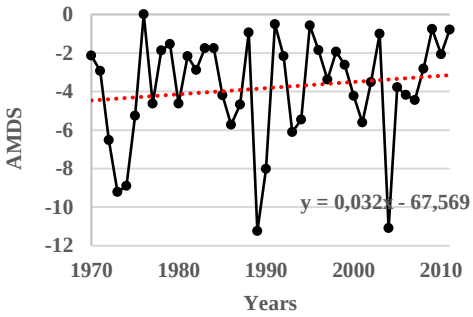

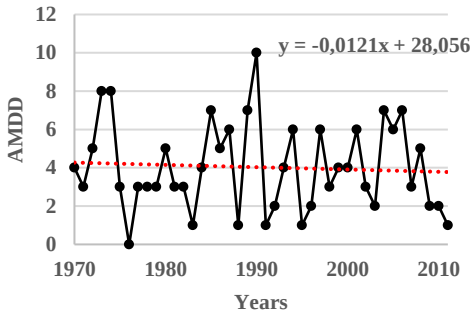

17868

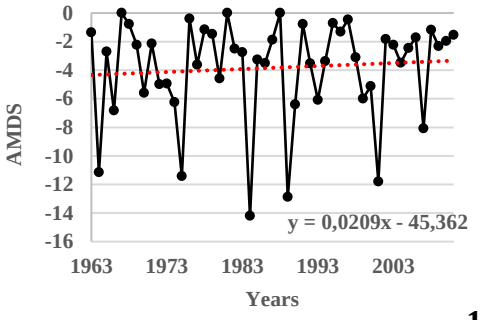

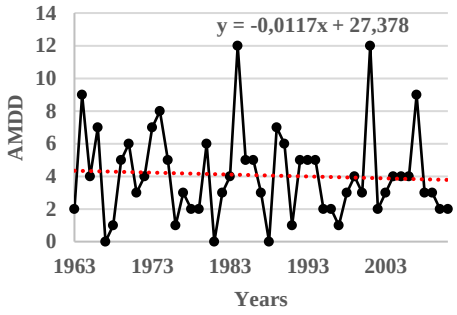

17870

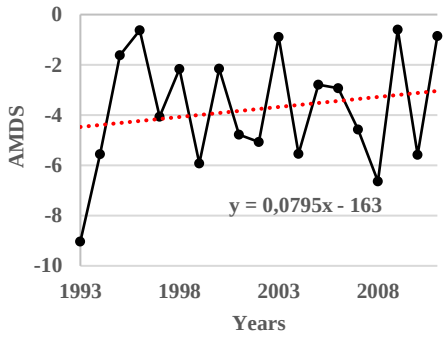

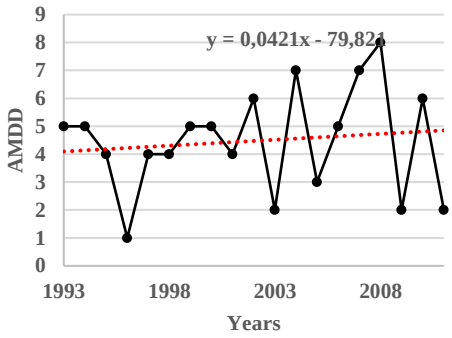

17871

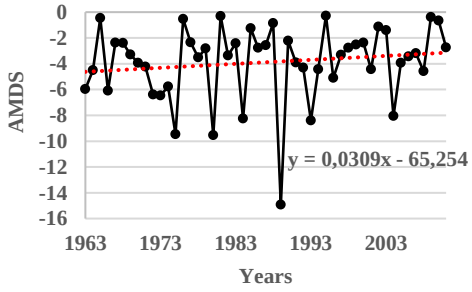

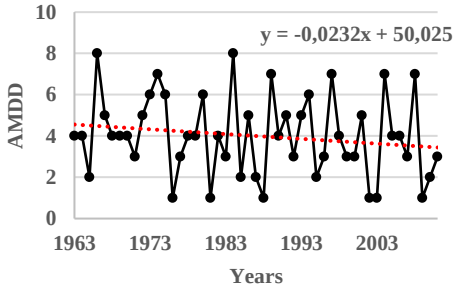

17908

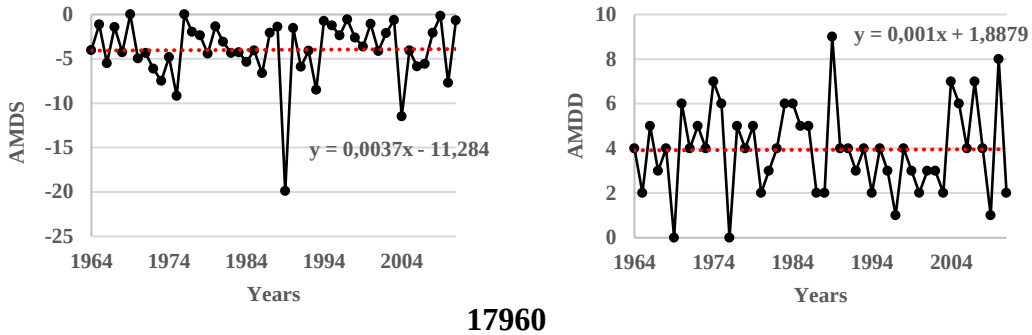

17960

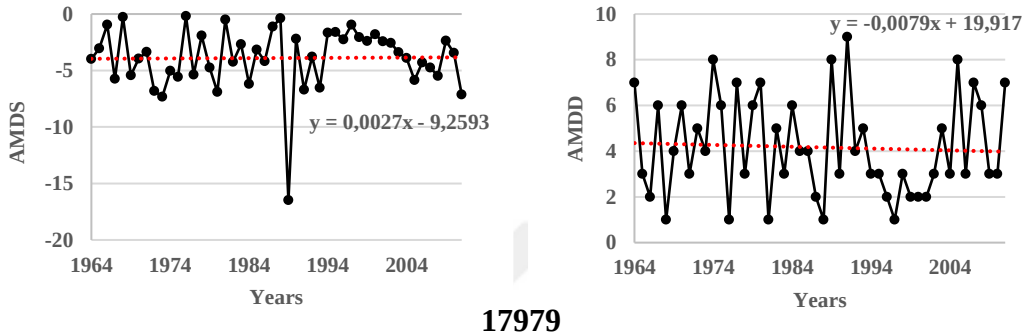

17979

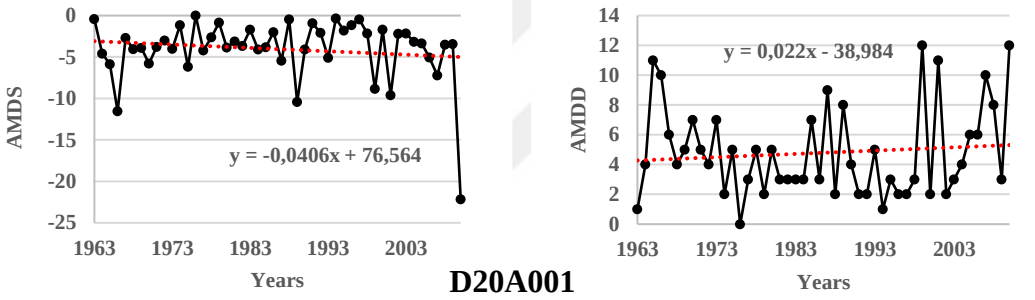

D20A001

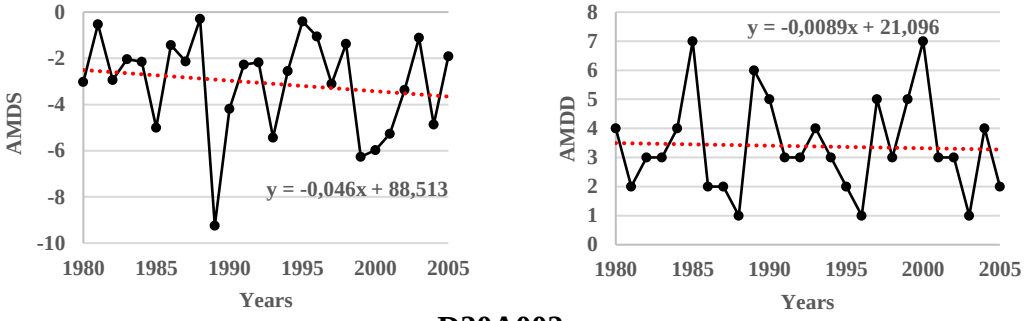

D20A002

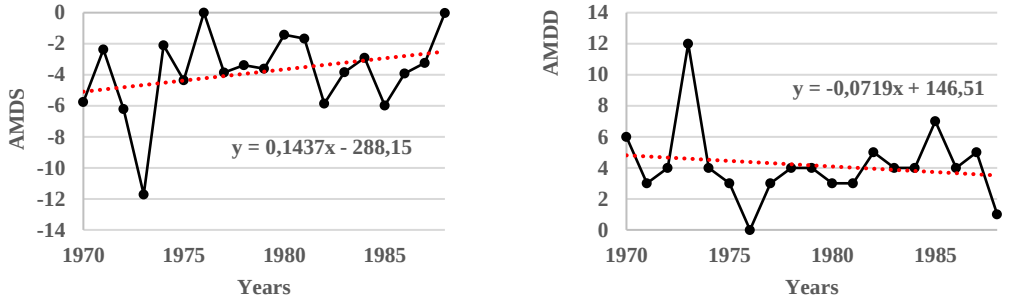

D20A004

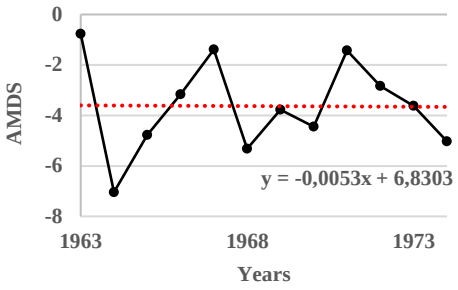

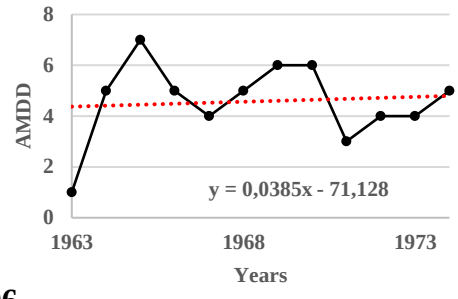

D20A006

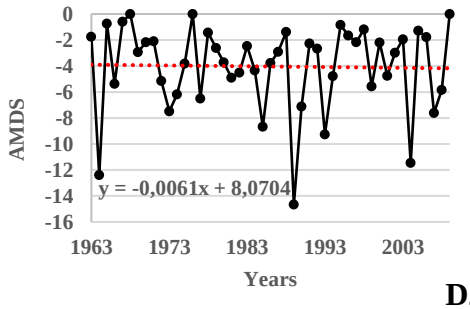

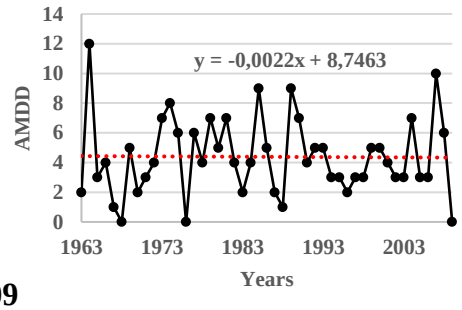

D20A009

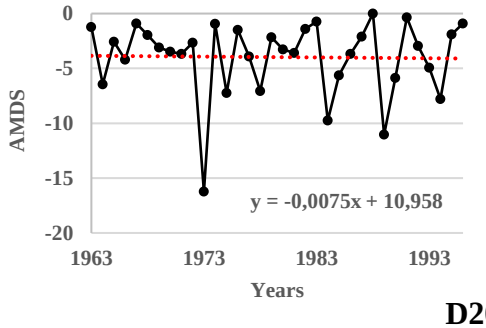

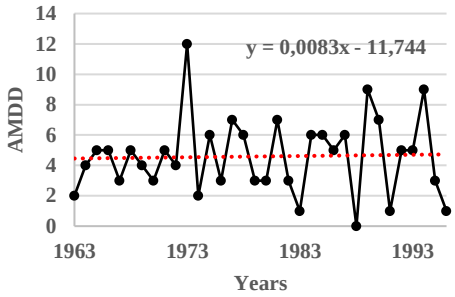

D20A011

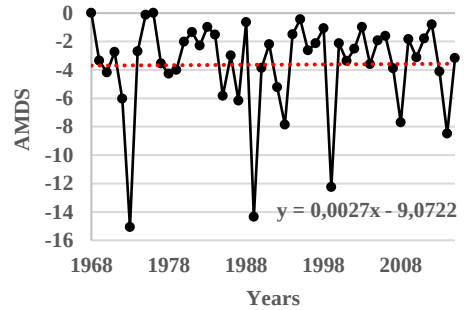

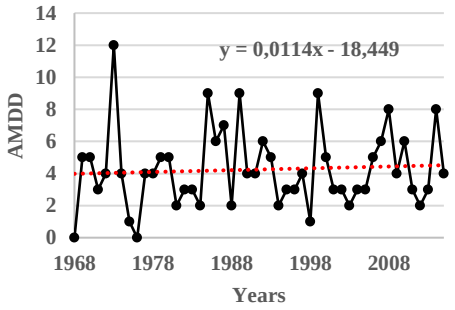

D20A013

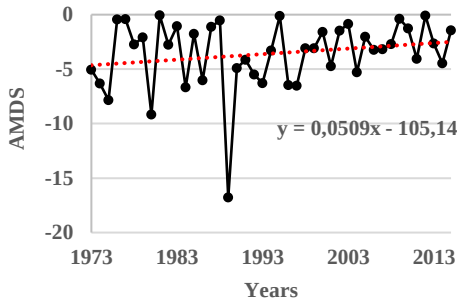

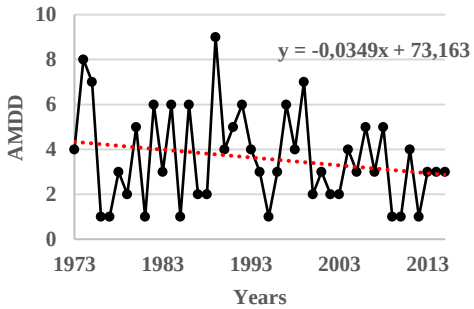

D20A014

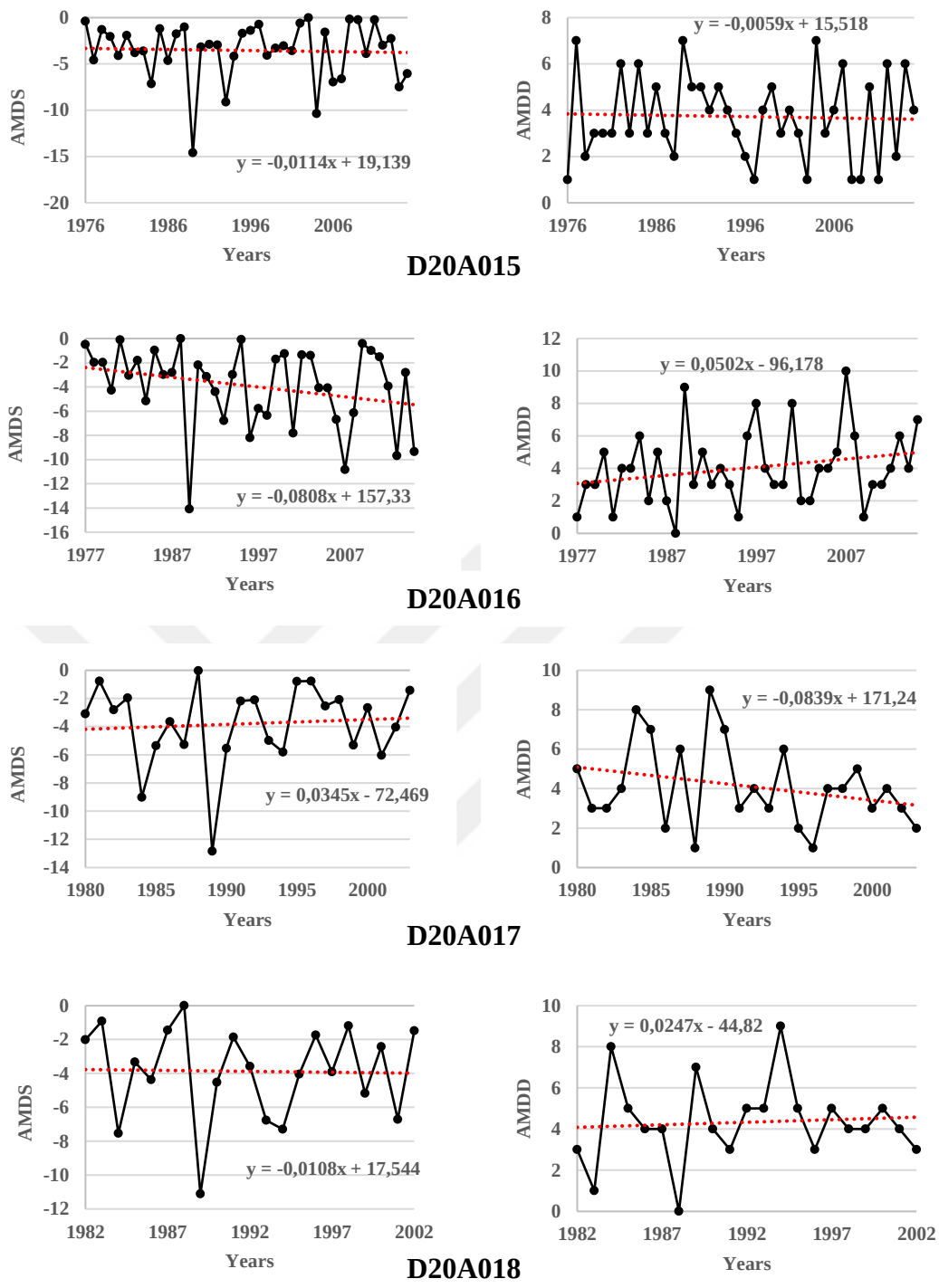

Figure 6.48 SPI 3-month extreme drought events time series

For SPI 6-month, AMDD is calculated in the 1989 year showing the highest value for the majority of stations. In general picture, many of stations demonstrate a slight and insignificant decreasing trend (8275, 17255, 17355, 17866, 17871, D20A001, D20A002, D20A006, D20A009, D20A0011, D20A0015, D20A0016, D20A017 and D20A0018), while others (7767, 17868, 17870, 17908, 17960, 17979, D20A004, D20A013 and D20A014) exhibit slightly insignificant increasing trend. Station

D20A001 exhibits the highest AMDS and AMDD values as 22.63 and 12 months, respectively (Figure 6.49).

AMDD and AMDS trend characteristics reveal a slight difference except for six stations (17870, 17908, D20A013, D20A014, D20A015, and D20A018). Even if the station numbers show the same compared to the SPI 3-month time scale, the station's name is completely different. While positive trends are seen in AMDS, negative trends are detected in AMDD with time. For example, it is observed that AMDS increase with time, but AMDD decreases with time for station 7767. The highest AMDD (over 12-month) value are found at stations 8275 (1993), 17255 (1973 and 2016), 17355 (1993, 1994 and 2016), 17866 (2008), 17868 (1973 and 1974), 17870 (1964, 1973, 1984 and 2001), 17871 (2001), D20A001 (1965, 1966, 1999 and 2010), D20A002 (1999, 2000), D20A009 (1964, 1973), D20A0011 (1973, 1978), D20A0013 (1970, 1973, 1992 and 2007), D20A014 (1986, 1999 and 2008), D20A015 (1993) and D20A0016 (2007, 2008 and 2014).

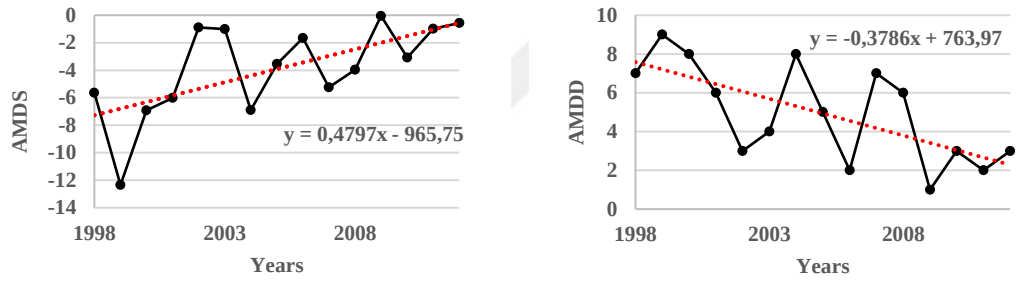

7767

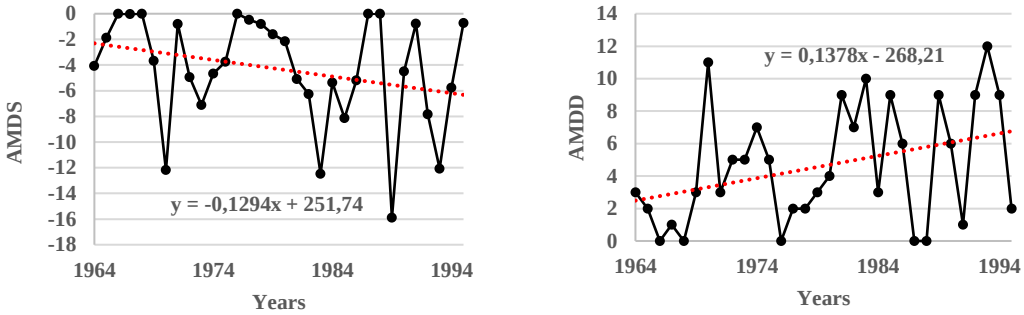

8275

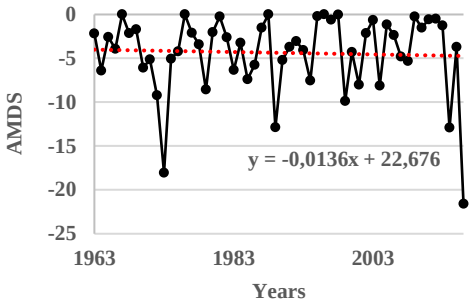

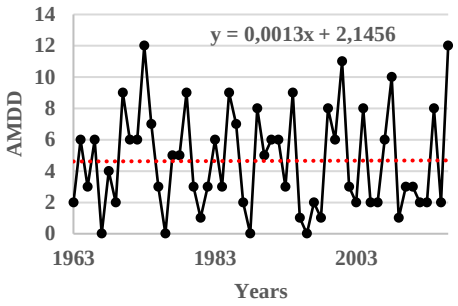

17255

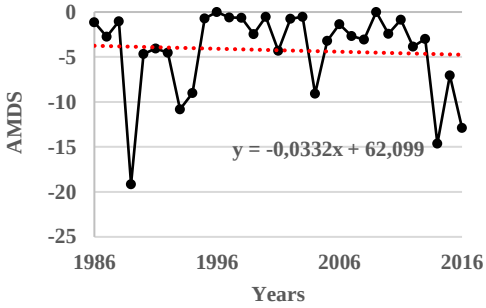

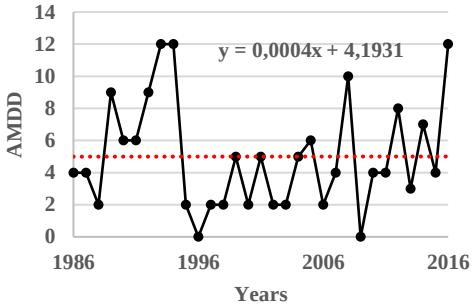

17355

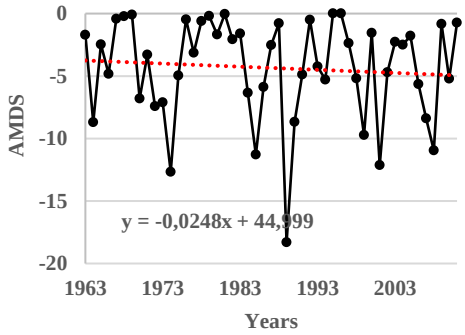

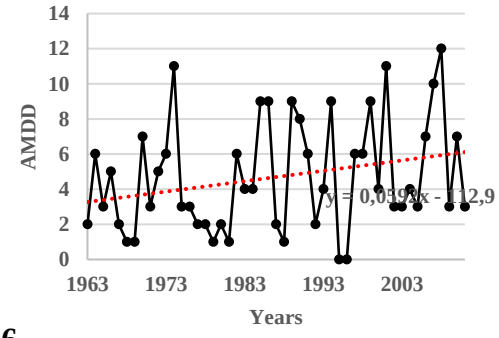

17866

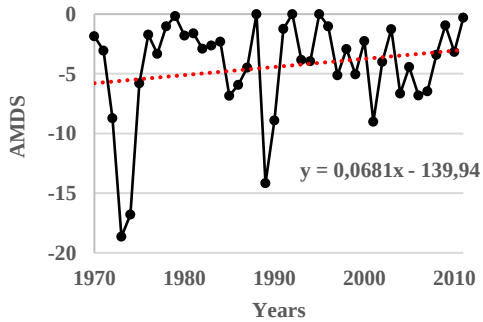

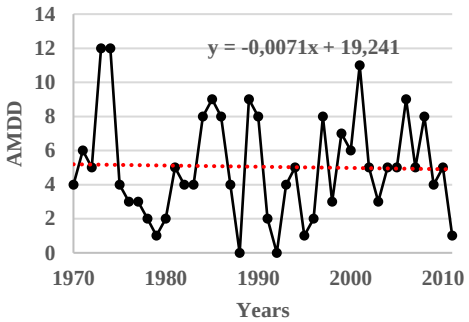

17868

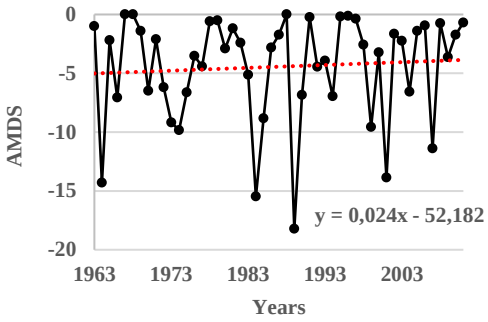

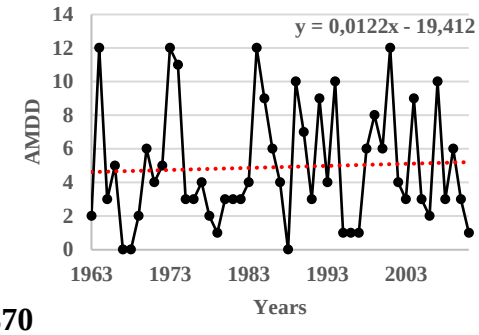

17870

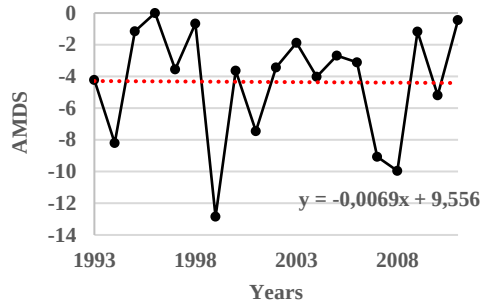

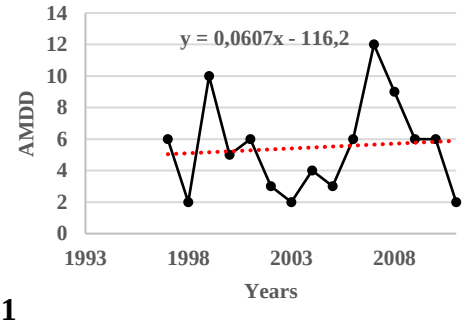

17871

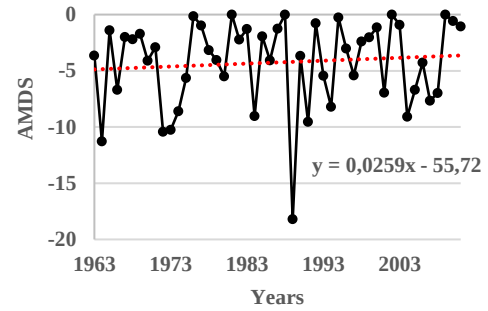

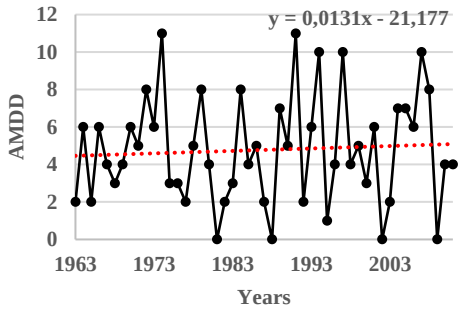

17908

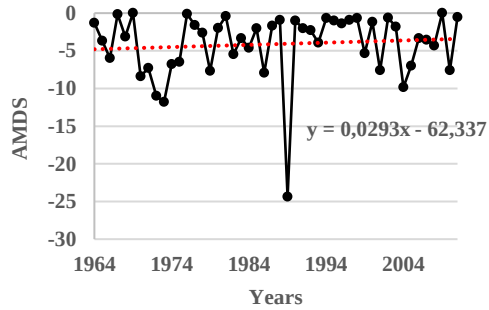

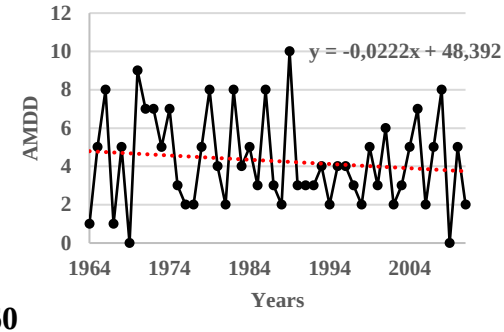

17960

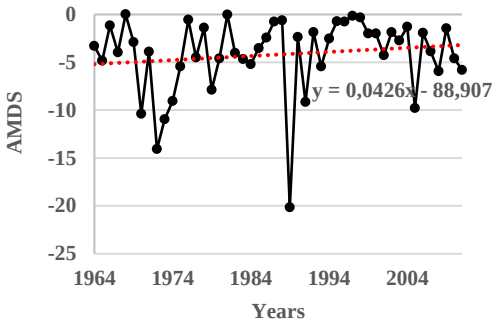

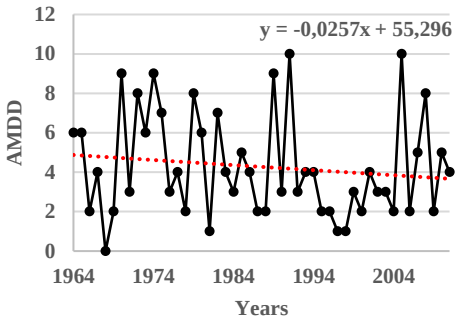

17979

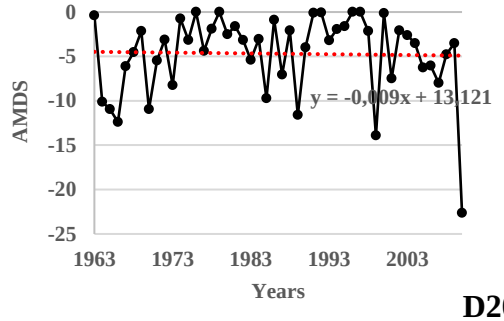

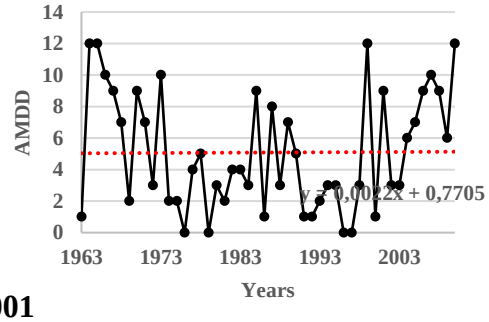

D20A001

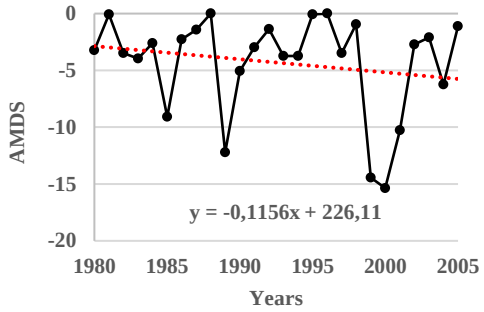

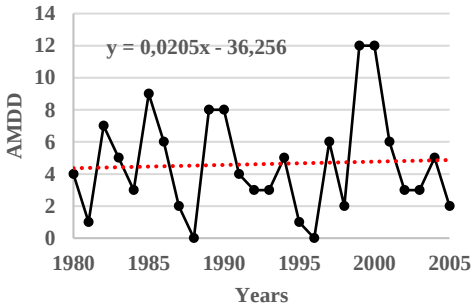

D20A002

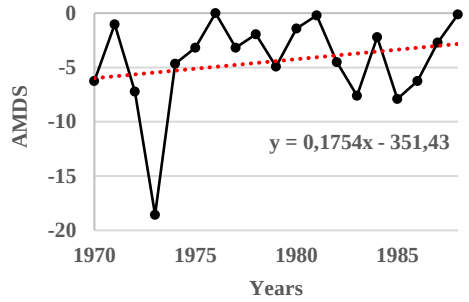

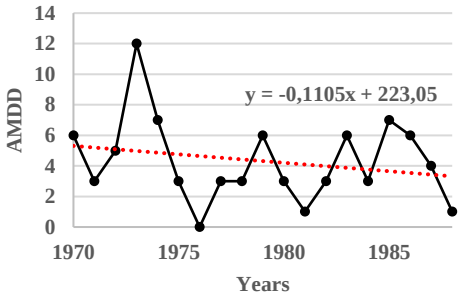

D20A004

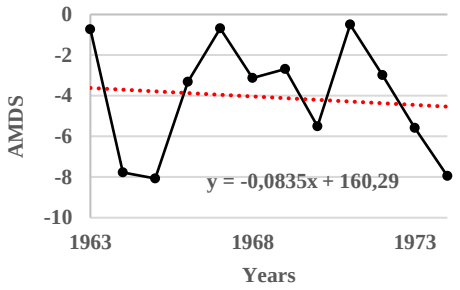

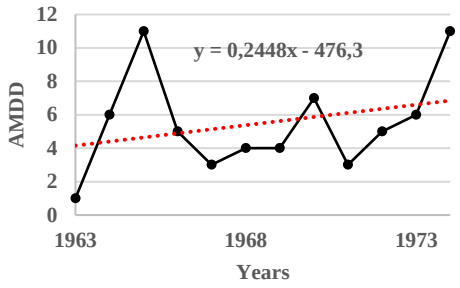

D20A006

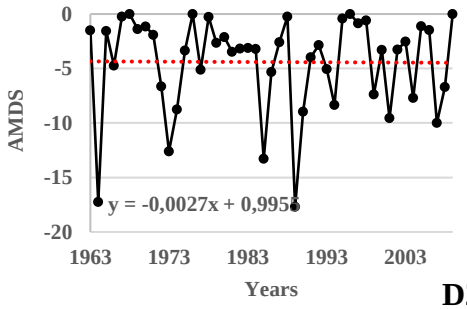

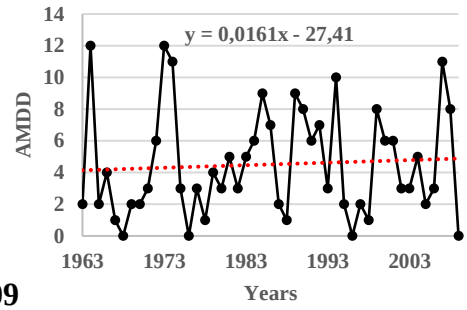

D20A009

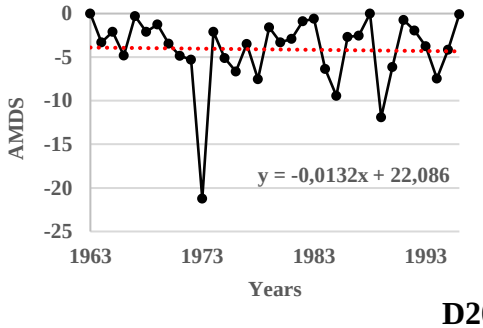

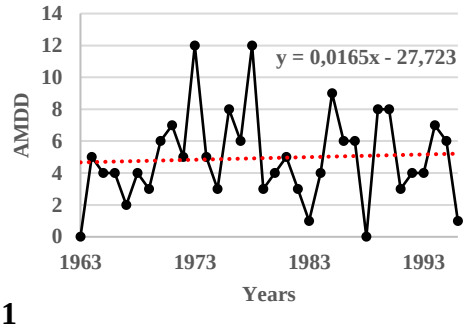

D20A011

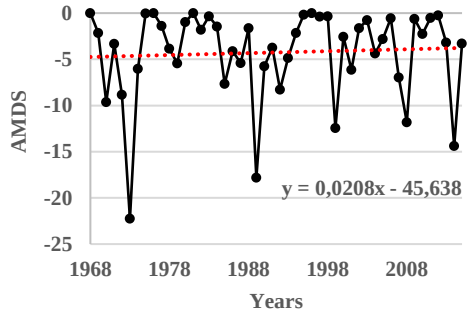

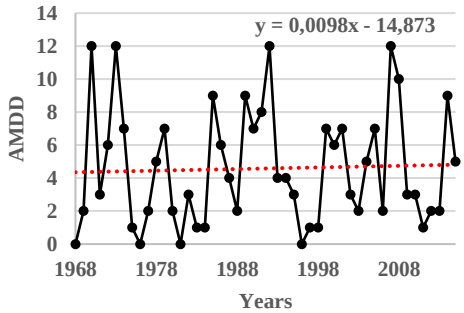

D20A013

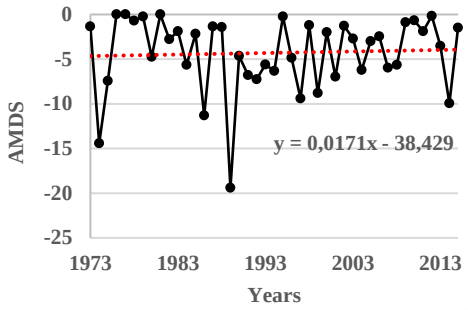

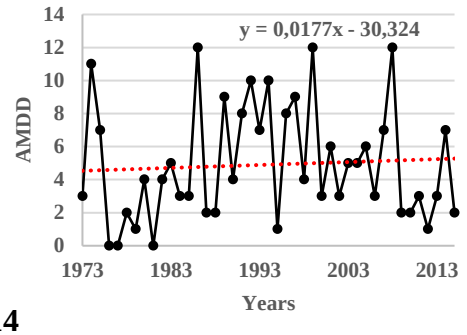

D20A014

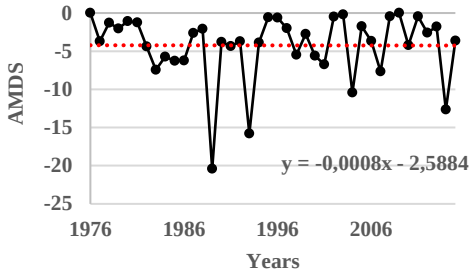

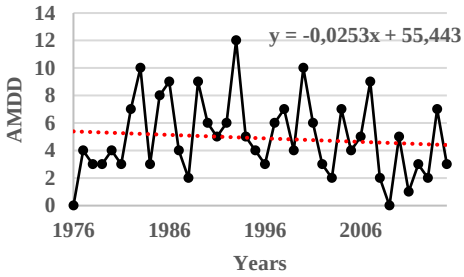

D20A015

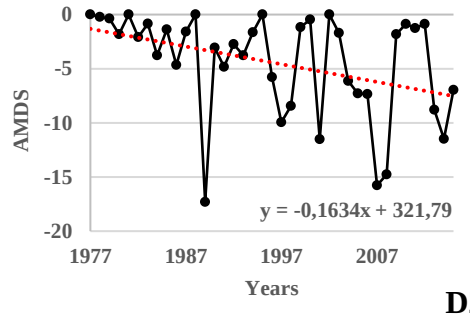

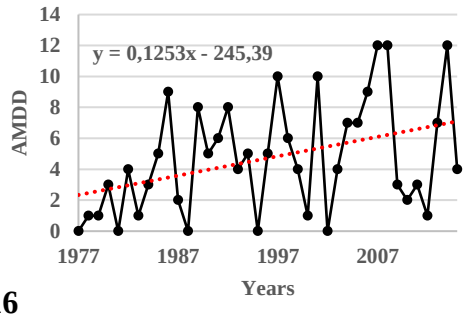

D20A016

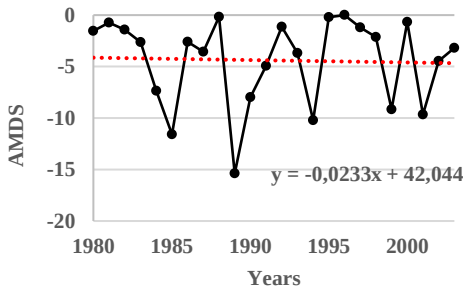

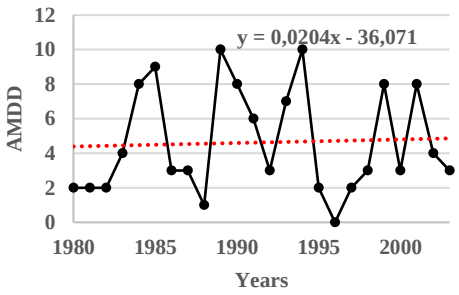

D20A017

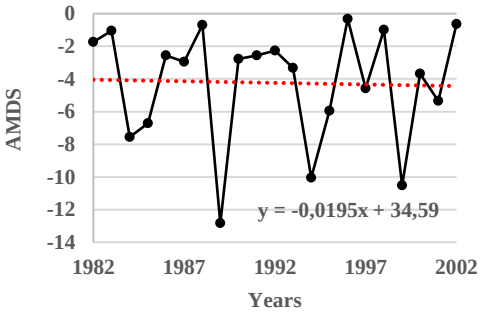

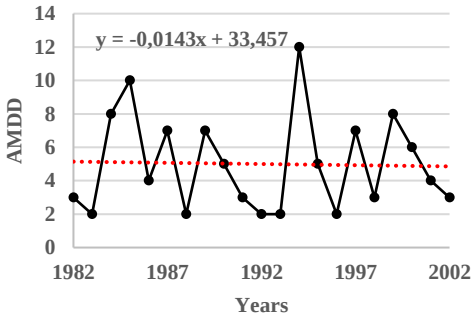

D20A018

Figure 6.49 SPI 6-month extreme drought events time series

For SPI 9-month, like SPI 1-, 3-month, the 1989 year shows the highest value for the majority of stations. Many of stations exhibits a slight and insignificant decreasing trend (8275, 17255, 17355, 17866, 17871, 17908, D20A001, D20A002, D20A006, D20A009, D20A0011, D20A0015, D20A0016, D20A017 and D20A0018), while others (7767, 17868, 17870, 17960, 17979, D20A004, D20A013 and D20A014) show slightly insignificant increasing trend. Station D20A0013 exhibits the highest AMDS and AMDD values as 25.89 and 12 months, respectively (Figure 6.50).

AMDD and AMDS trend characteristics reveal a slight difference except for six stations (17255, 17868, 17870, D20A001, D20A002 and D20A013). Even if the station numbers show the same compared to the SPI 3- and 6-month time scale, the station's name is almost different. While positive trends are shown in AMDS, negative trends are detected in AMDD with time. For example, it is observed that AMDS increase with time, but AMDD decreases with time for station 7767.

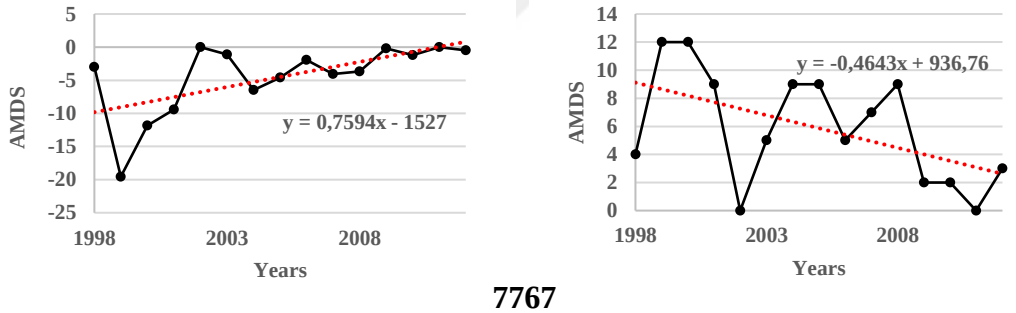

7767

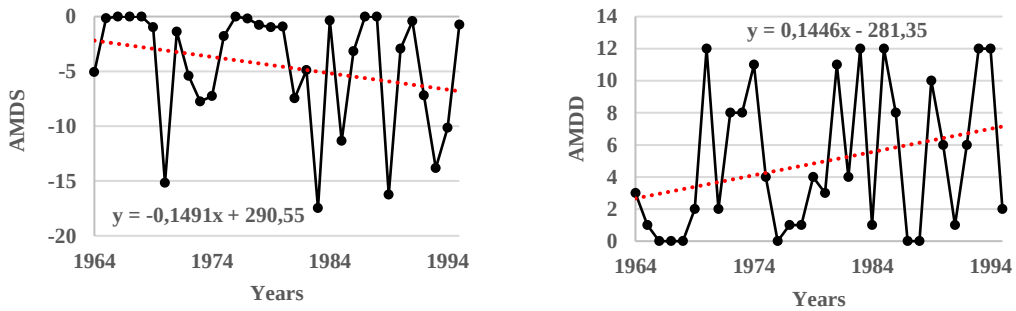

8275

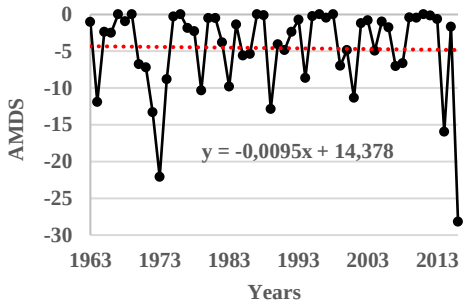

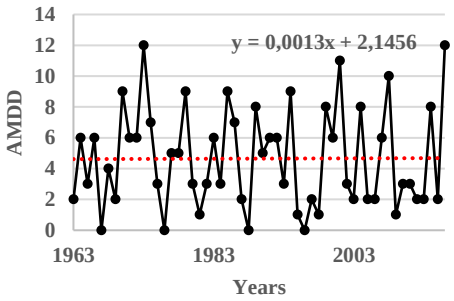

17255

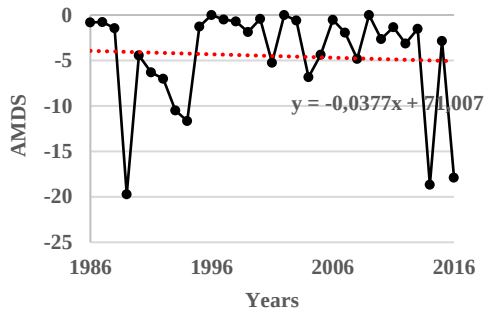

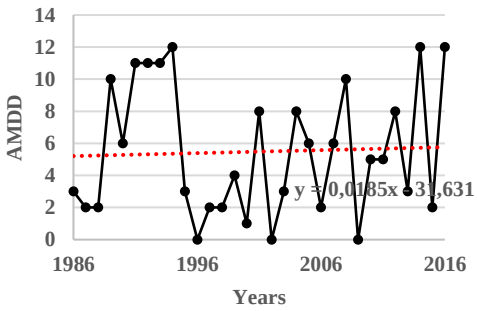

17355

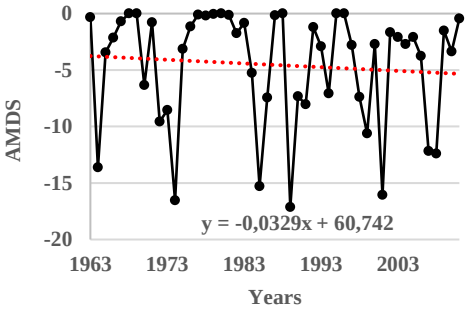

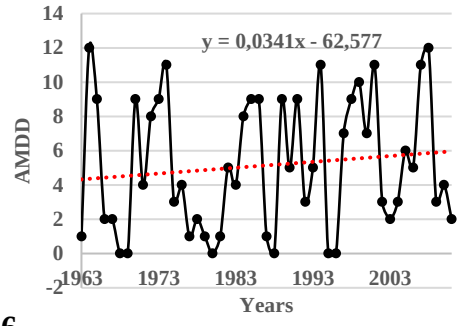

17866

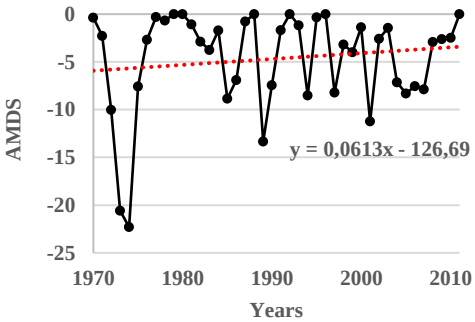

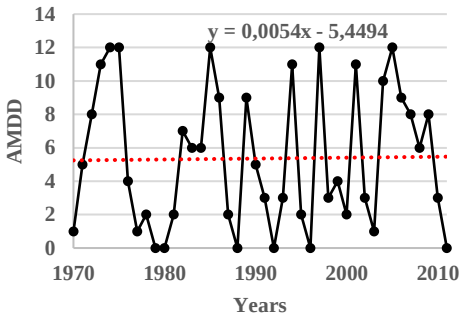

17868

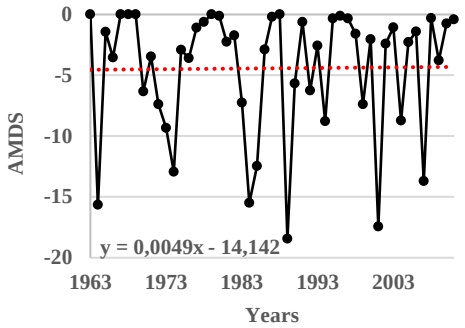

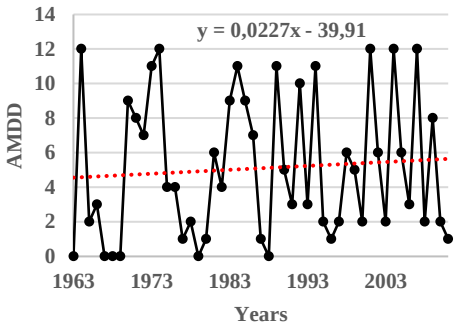

17870

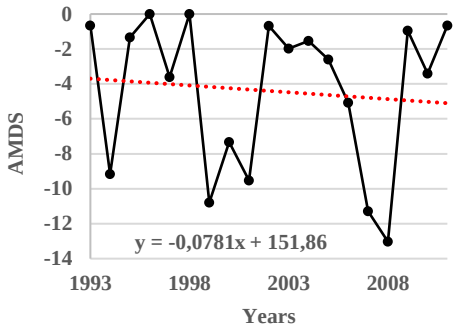

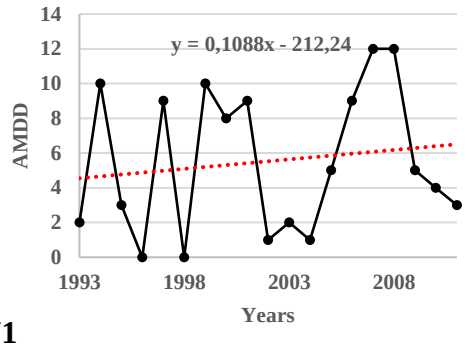

17871

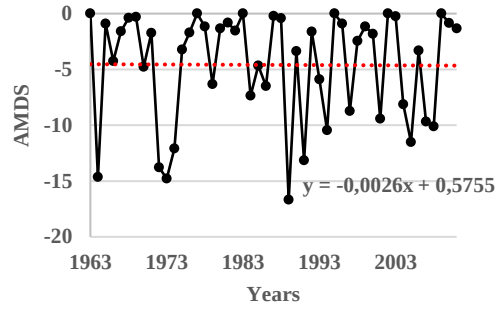

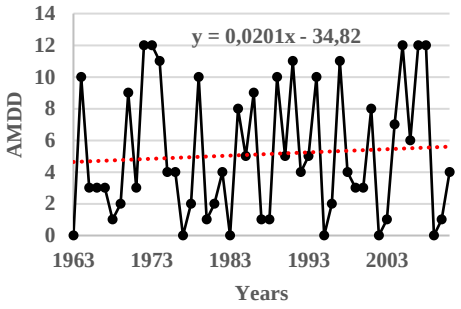

17908

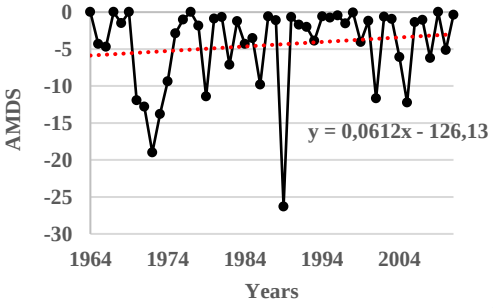

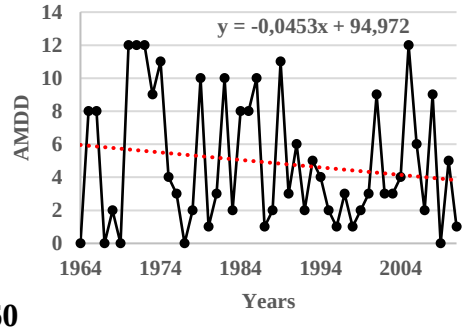

17960

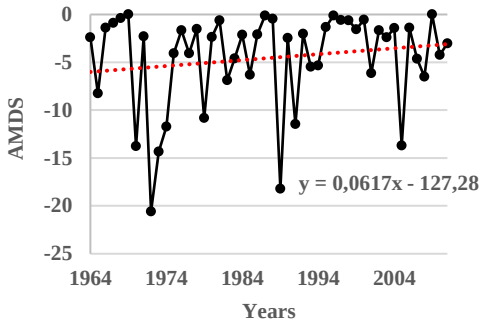

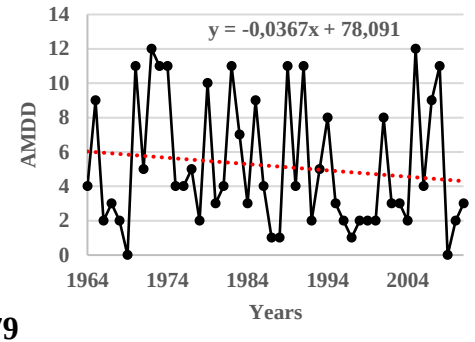

17979

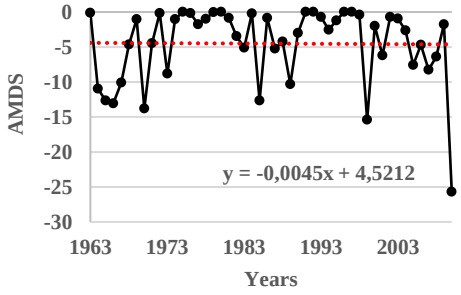

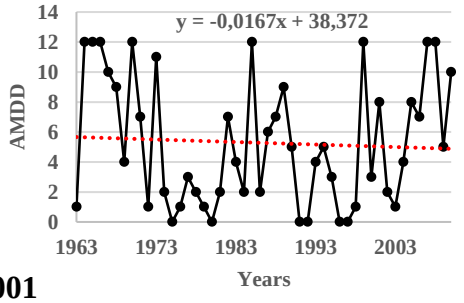

D20A001

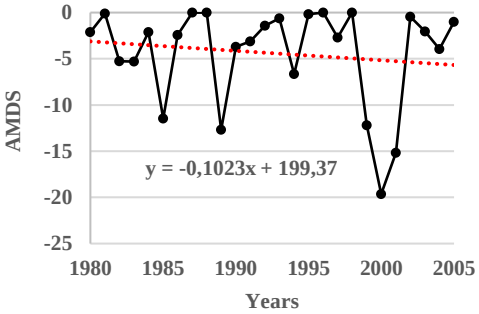

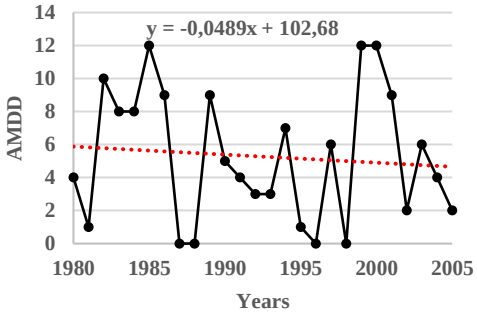

D20A002

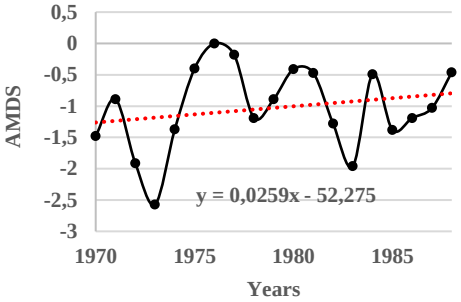

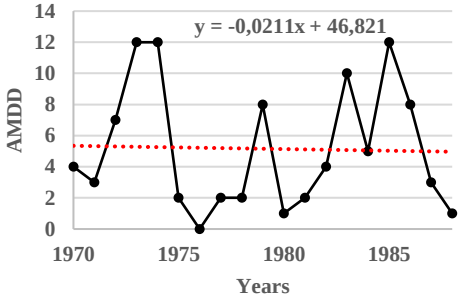

D20A004

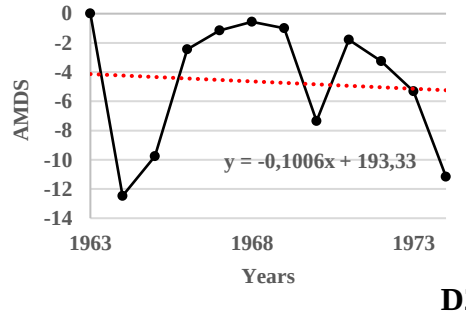

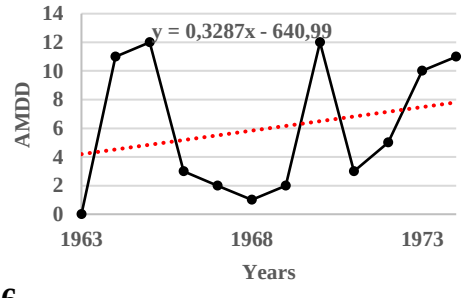

D20A006

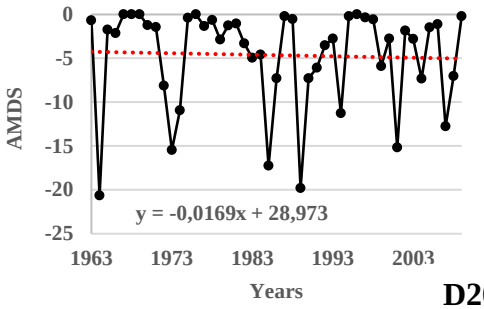

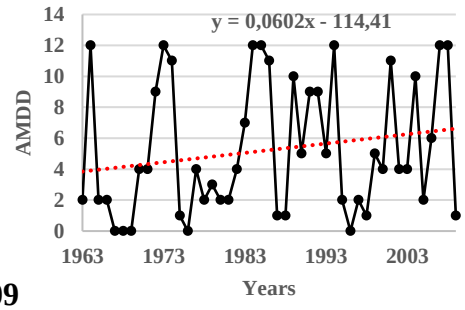

D20A009

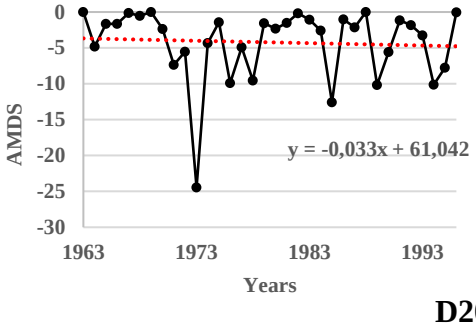

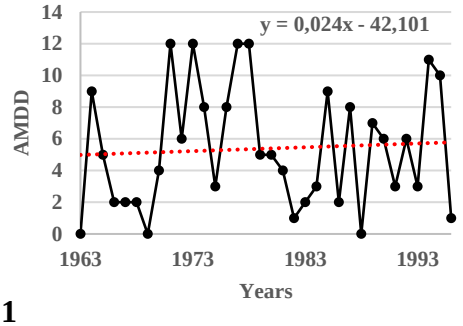

D20A011

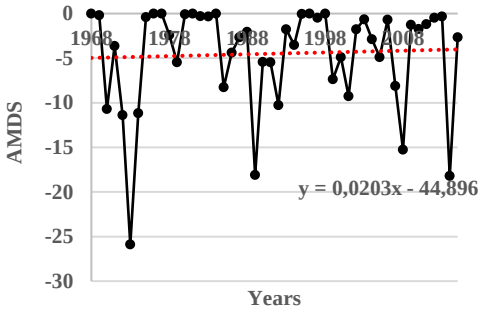

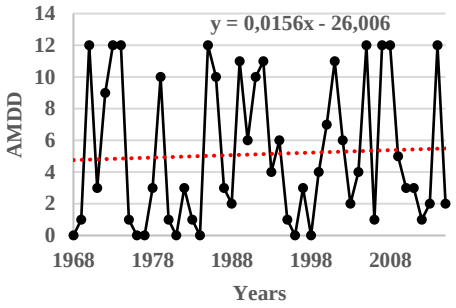

D20A013

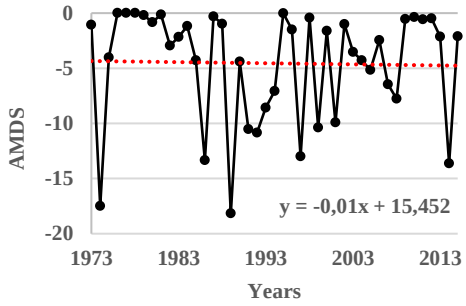

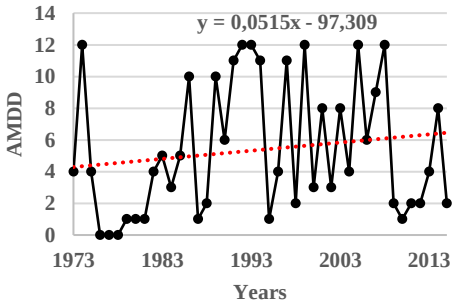

D20A014

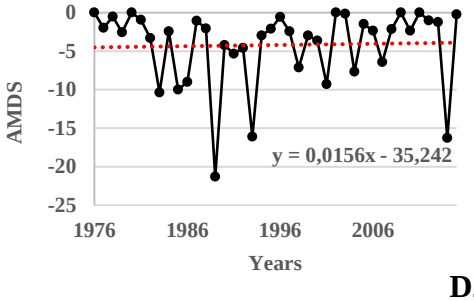

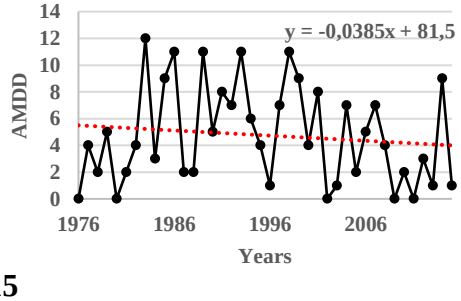

D20A015

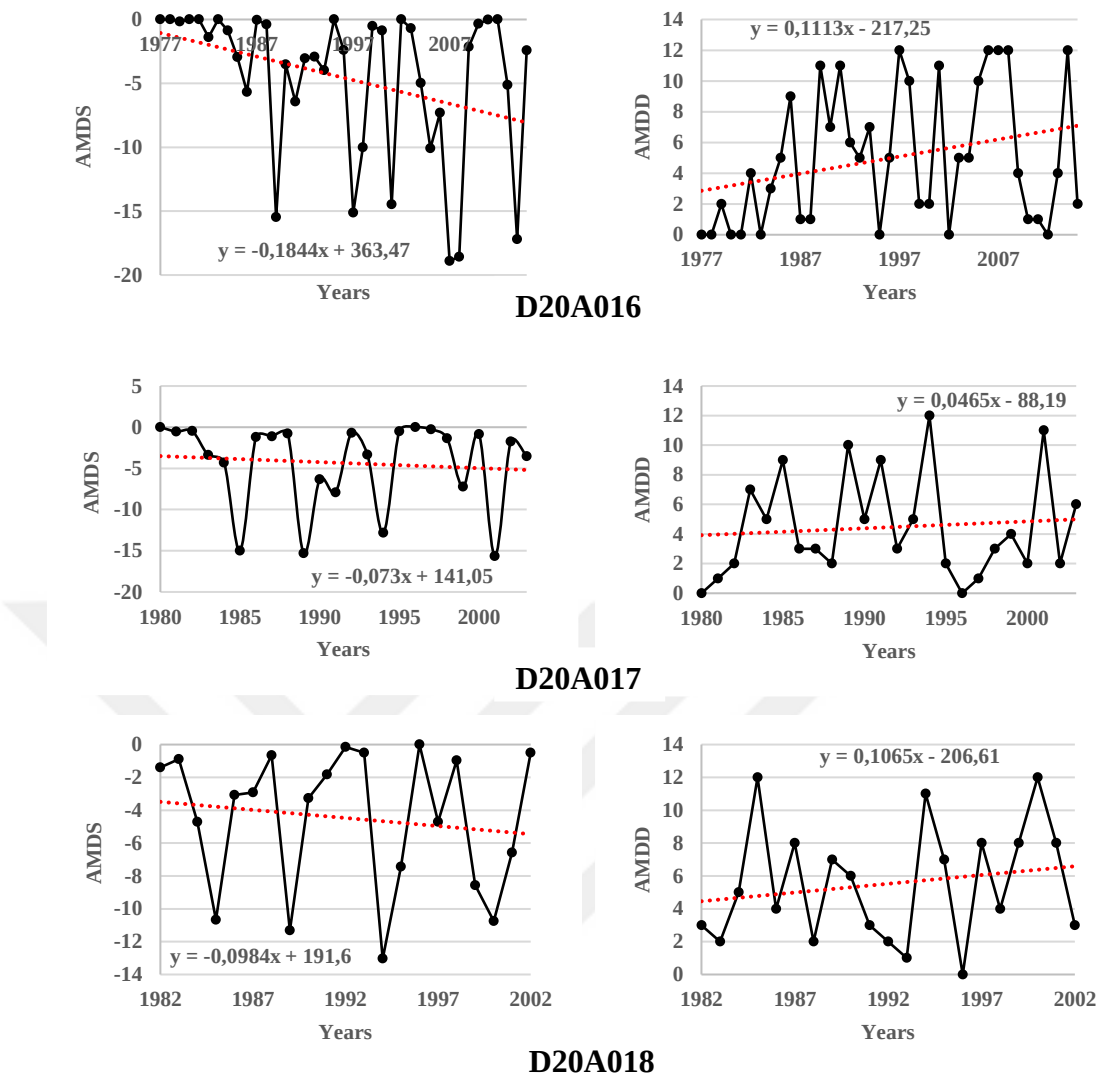

Figure 6.50 SPI 9-month extreme drought events time series

Figure 6.51 illustrates the increasing and decreasing trend appearance of the extreme drought events for 12-month time scale. Unlike previous computed for various time steps (SPI 1-, 3-, 6- and 9-month), SPI 12-month time scale fluctuations are less but high values. AMDS data of the stations indicate high as well as appeared high value in AMDD. Like the previous time scale, Many of stations demonstrate a slight and insignificant decreasing trend (8275, 17355, 17866, 17870, 17871, 17908, D20A001, D20A002, D20A006, D20A009, D20A0011, D20A014, D20A0015, D20A0016, D20A017 and D20A0018), while others (7767, 17255, 17868, 17960, 17979, D20A004 and D20A013) exhibit slightly insignificant increasing trend. Station D20A001 exhibits the highest AMDS and AMDD values as 31.17 and 11 months, respectively (Figure 4.8). As for AMDD parameter, seven stations named 7767,

17255, 17868, 17960, 17979, D20A002 and D20A011, show a decreasing trend, while other stations indicate increasing trends.

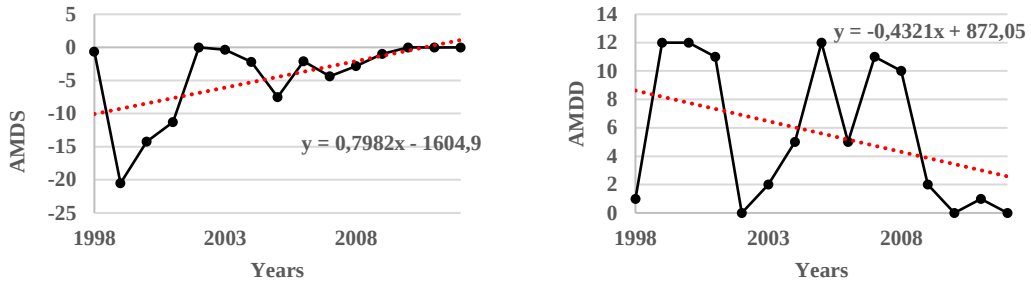

7767

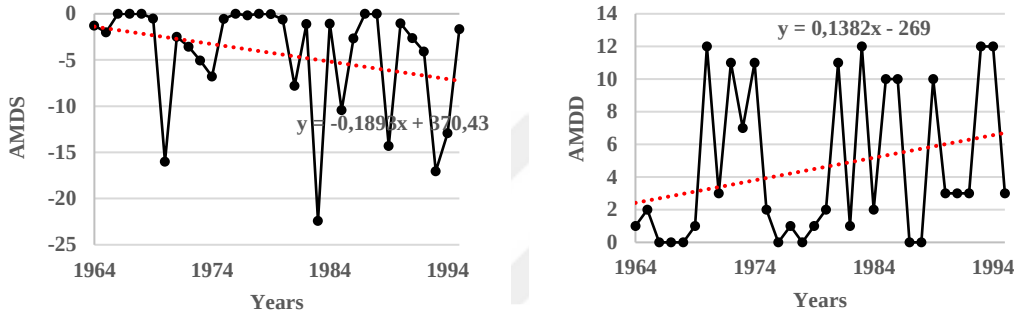

8275

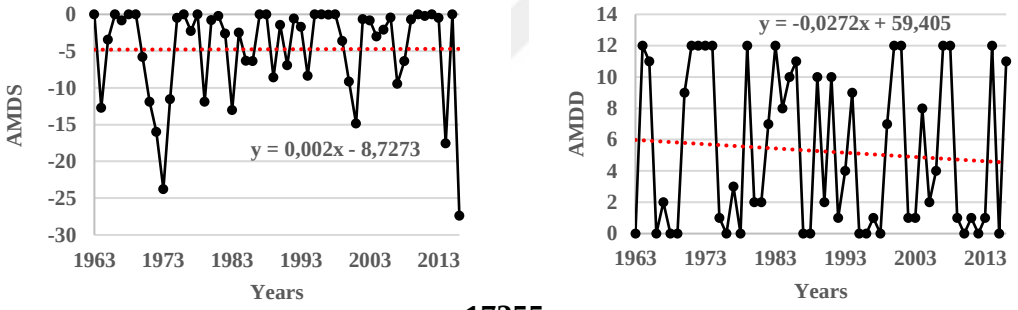

17255

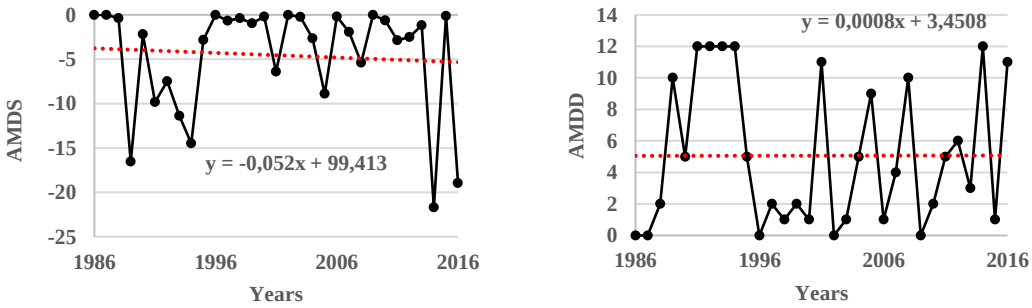

17355

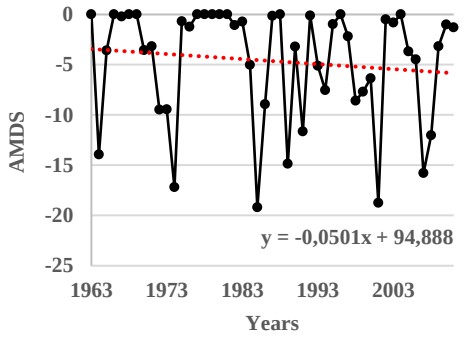

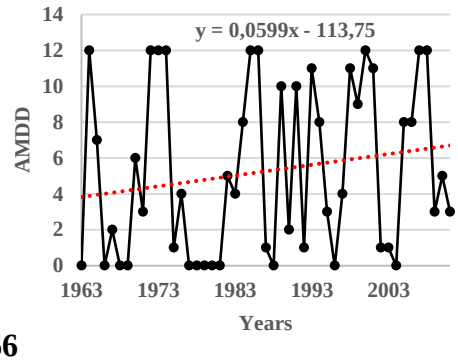

17866

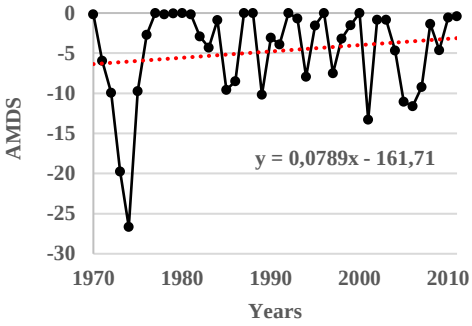

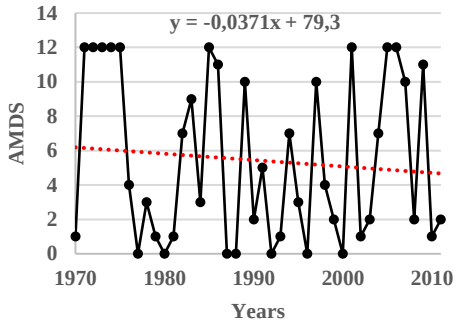

17868

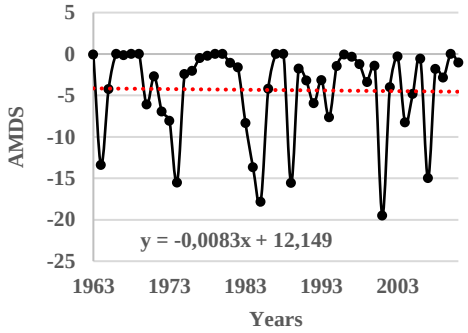

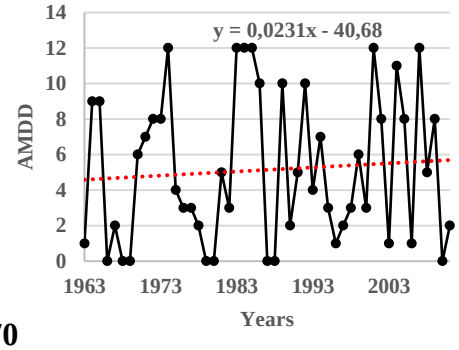

17870

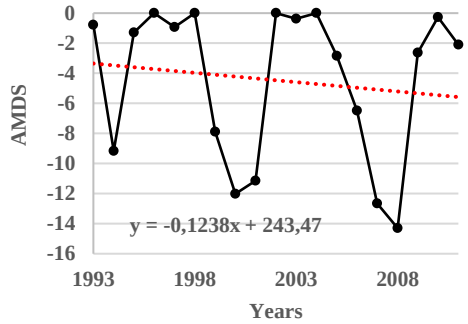

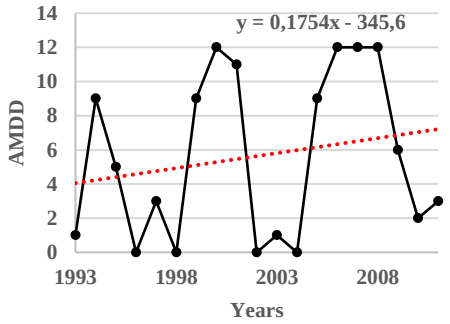

17871

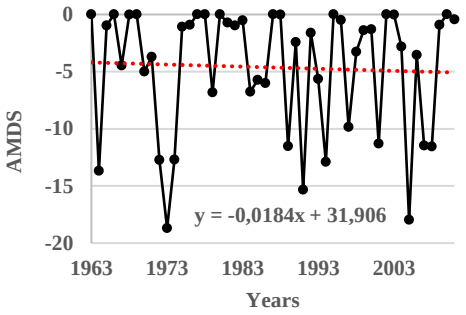

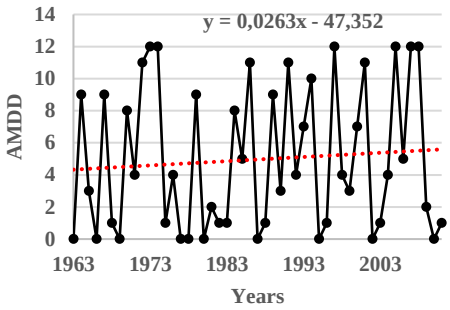

17908

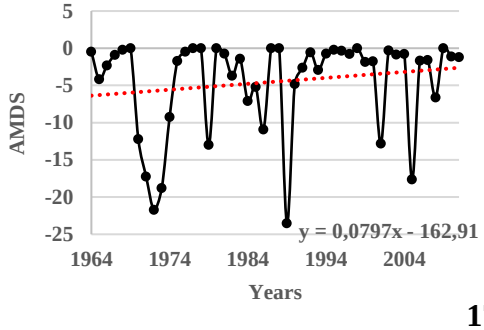

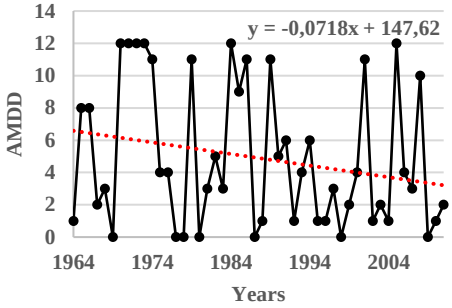

17960

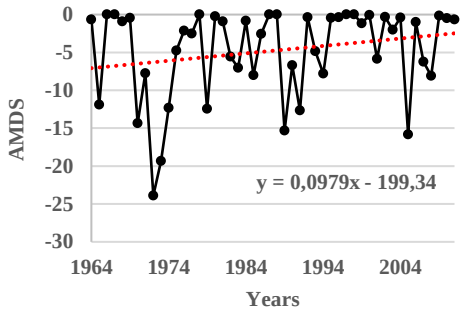

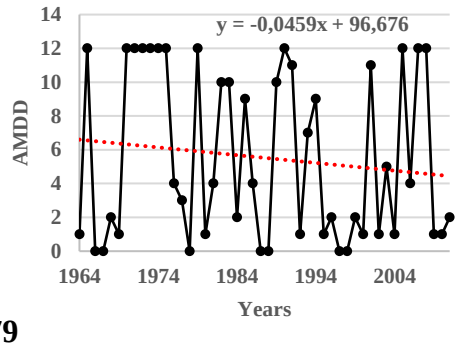

17979

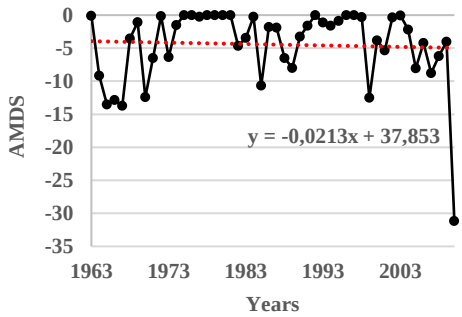

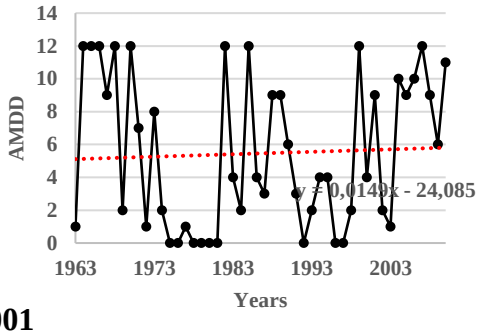

D20A001

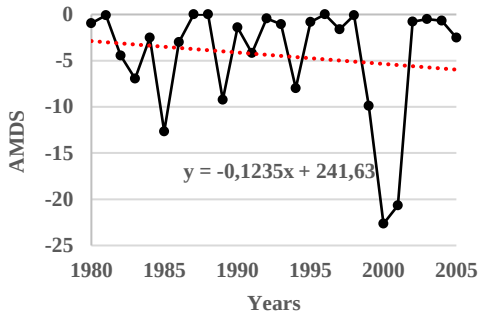

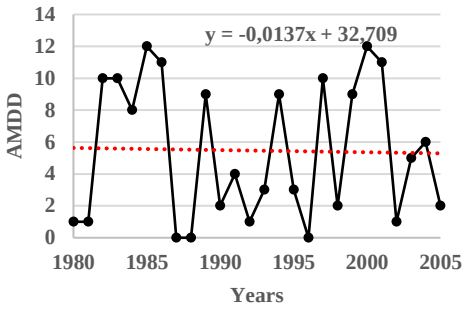

D20A002

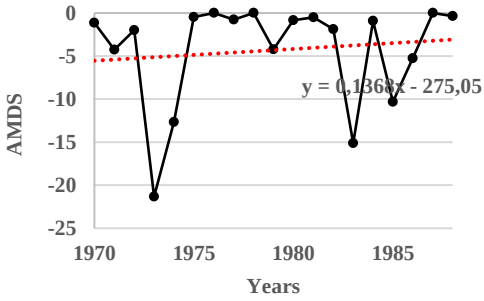

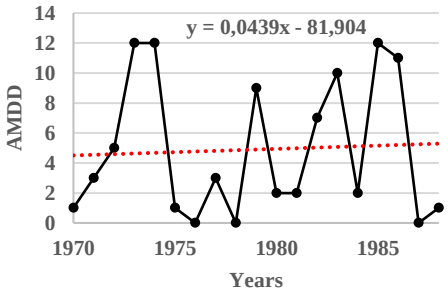

D20A004

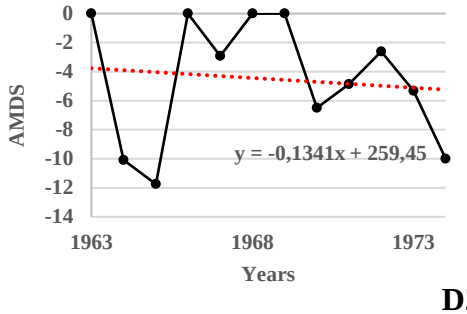

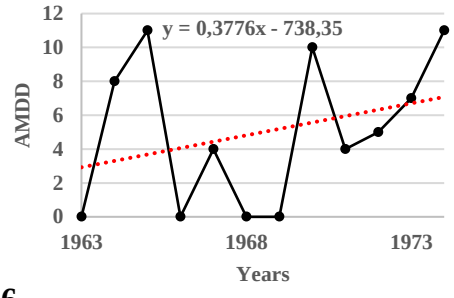

D20A006

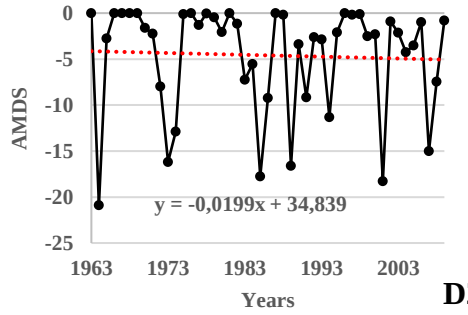

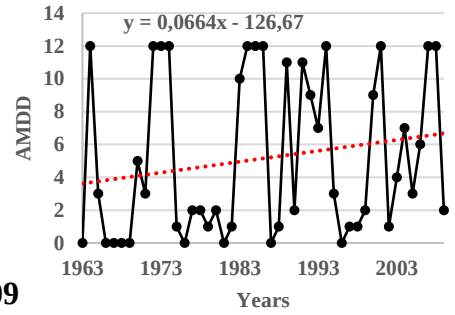

D20A009

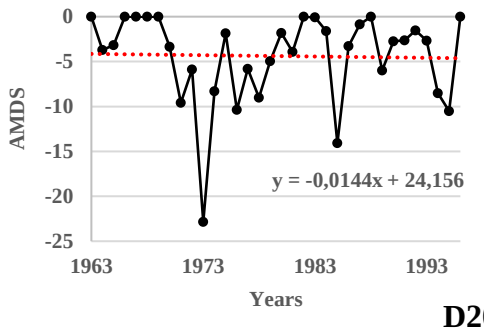

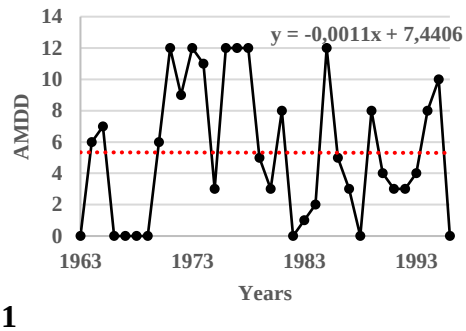

D20A011

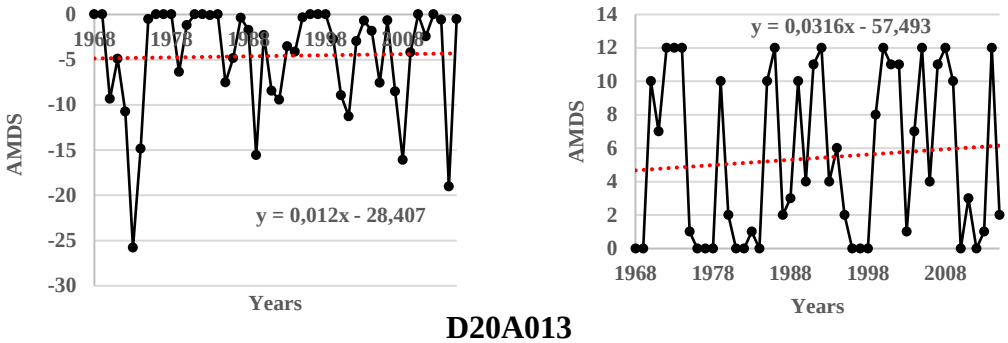

D20A013

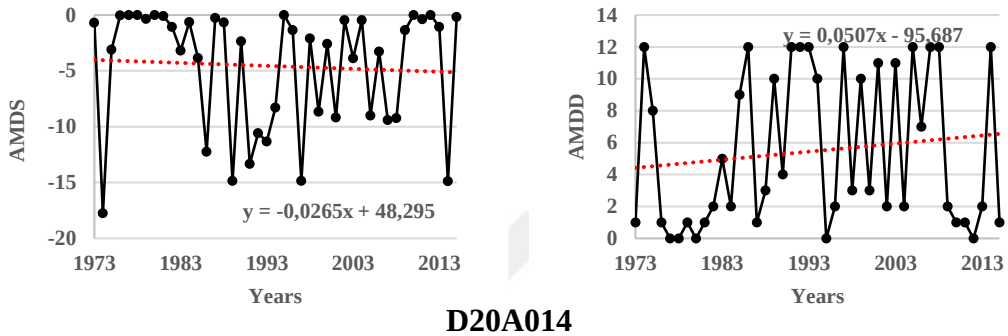

D20A014

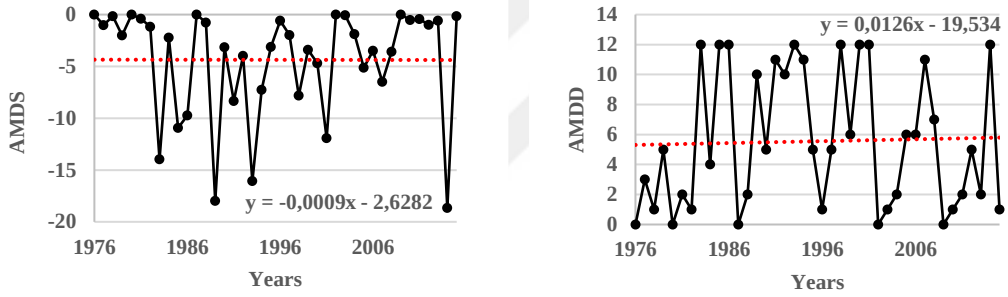

D20A015

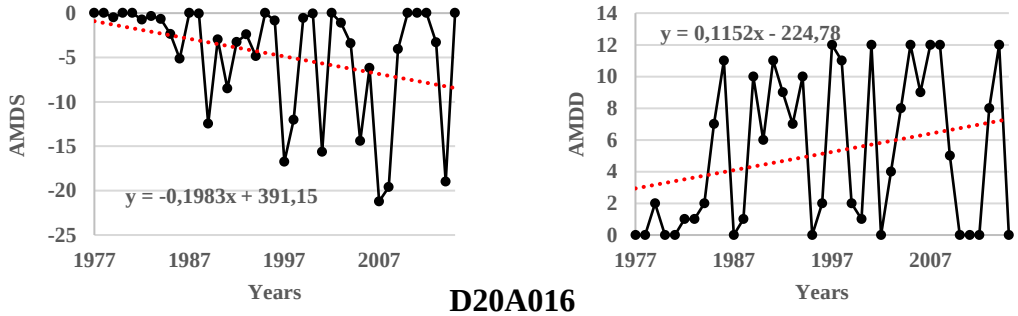

D20A016

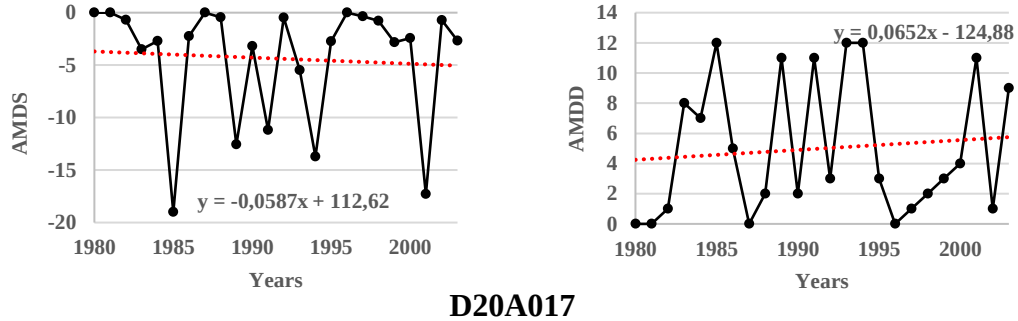

D20A017

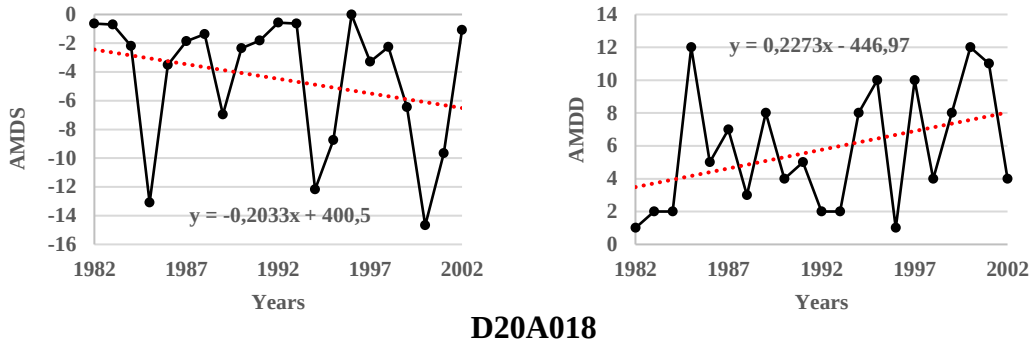

Figure 6.51 SPI 12-month extreme drought events time series

6.4.1 Homogeneity Test Results of Extreme Drought Events

One of the most significant characteristics of hydrologic time series, such as precipitation, rainfall, evapotranspiration and groundwater etc., is homogeneity which the data indicates similar. There are various tests used in the literature. In this research, Wallis and Moore Phase-Frequency Test, Bartel Test and Wald-Wolfowitz Test are employed for analysis of extreme drought events (AMDS and AMDD) in verifying the homogeneity at various time steps (1-, 3-, 6-, 9- and 12-month). The results of the three tests are compared to determine a more accurate about homogeneity and randomness. Therefore, if two outcomes of the three tests are the same, the presence of homogeneity will be accepted. Three tests results are presented in Table 6.10.

The three test findings clearly show that for SPI 1-month time scale, all stations demonstrate homogeneity (H) except stations 17908 and D20A006 at the 90% significance level (±1.96). AMDS and AMDD are not homogeneous for station 17908 and D20A006, respectively. Like SPI 1 month, all stations shows homogeneous except two stations (8275 and D20A006) at SPI 3-month time scale. Interestingly, non-homogeneous (N-H) are seen in the AMDD series for two stations. When we consider to SPI 6-month, except station 8375 and D20A013 which non-homogeneous are evaluated in AMDD series, all used stations shows homogeneous according to 90% significance level. With increase in time scales, non-homogenous stations are also increase. For instance, three stations and five stations are seen as non-homogenous for SPI 9-month and SPI 12-month, respectively. Station 17868 for AMDS and AMDD, station D20A001 for AMDD and station D20A016 for AMDD at SPI 9-month indicate non-homogenous. Station 17868 for AMDS, station D20A009 for AMDD, station D20A011 for AMDS and AMDD, station D20A013 for AMDS and AMDD and,

finally station D20A016 for AMDD are illustrated as non-homogenous at SPI 12-month time scale.

Table 6.10 Homogeneity tests results for extreme drought events at different time scales

Station	Tests	SPI 1		SPI 3		SPI 6		SPI 9		SPI 12	
		AMDS	AMDD	AMDS	AMDD	AMDS	AMDD	AMDS	AMDD	AMDS	AMDD
7767	BT	-0.204	-0.597	1.732	**1.919**	1.175	1.244	1.227	1.238	1.101	1.196
	WM	-0.109	0.762	-0.109	1.415	0.762	0.109	0.109	1.415	0.762	0.762
	WW	-0.023	1.023	0.601	-0.369	1.607	1.513	**2.246**	**1.815**	**2.161**	**1.714**
	Result	H	H	H	H	H	H	H	H	H	H
8275	BT	-0.450	-0.675	-0.750	**-1.688**	-1.160	-1.035	-0.809	-0.814	-1.111	-1.176
	WM	**1.727**	**3.453**	0.863	**3.453**	**2.590**	**1.727**	**1.727**	**1.727**	1.295	0.432
	WW	0.387	1.238	0.671	**2.887**	1.331	**1.710**	0.103	0.837	-0.011	0.608
	Result	H	H	H	**N-H**	H	**N-H**	H	H	H	H
17255	BT	-0.073	0.105	-0.082	0.057	-0.566	-0.014	-0.743	-0.496	-0.455	-0.593
	WM	0.875	0.547	0.438	0.438	0.219	0.438	0.219	0.219	0.875	0.875
	WW	0.875	0.54718	0.438	0.438	0.219	0.438	0.219	0.219	0.875	0.875
	Result	H	H	H	H	H	H	H	H	H	H
17355	BT	-0.609	-0.147	-0.375	-0.324	-1.273	-0.481	-0.778	-0.284	-0.342	-0.818
	WM	0.585	**2.341**	0.732	0.146	0.293	1.024	0.146	1.024	0.293	1.499
	WW	0.455	0.027	0.309	0.438	0.858	1.039	0.080	0.450	-0.476	0.759
	Result	H	H	H	H	H	H	H	H	H	H
17866	BT	-0.062	0.330	0.162	-0.292	-0.782	-0.671	-1.166	-0.965	-1.244	-1.237
	WM	**1.957**	1.151	1.266	**2.187**	0.115	1.496	0.806	0.806	0.460	1.496
	WW	-1.505	-1.232	-0.184	0.665	1.381	1.244	1.283	**1.930**	1.495	1.289
	Result	H	H	H	H	H	H	H	H	H	H
17868	BT	0.031	0.106	-0.318	**-0.447**	-0.809	-0.965	-1.204	-1.061	-1.018	-0.744
	WM	0.499	0.624	1.372	**1.746**	0.624	1.372	**2.120**	**2.120**	**2.120**	**1.746**
	WW	0.099	0.312	1.236	0.977	**3.192**	**1.961**	**3.302**	**2.038**	**3.348**	1.585
	Result	H	H	H	**N-H**	H	H	**N-H**	**N-H**	**N-H**	H
17870	BT	0.476	0.137	0.068	-0.155	-0.300	-0.537	-0.562	-0.497	-0.997	-0.694
	WM	1.266	**2.532**	0.575	**2.877**	0.806	1.496	0.806	0.806	1.841	1.841
	WW	-0.988	-0.854	-0.293	0.048	0.217	0.839	0.348	0.603	0.956	1.540
	Result	H	H	H	H	H	H	H	H	H	H
17871	BT	0.731	0.767	0.602	0.637	0.171	-0.030	-0.026	-0.157	-1.003	-1.345
	WM	0.095	0.095	0.095	0.474	0.667	-0.095	0.667	-0.095	0.477	0.477
	WW	**-2.218**	**-1.781**	-1.531	-1.103	-0.379	0.603	0.910	0.747	**2.095**	**2.133**
	Result	H	H	H	H	H	H	H	H	H	H
17908	BT	0.964	0.570	0.333	0.411	-0.029	-0.041	-0.292	-0.386	-0.461	-0.279
	WM	**2.302**	0.906	0.806	1.496	0.230	0.230	0.460	1.151	0.460	0.230
	WW	**-2.217**	**-1.924**	-1.293	-1.062	-0.166	0.088	0.452	0.511	0.742	0.336
	Result	**N-H**	H	H	H	H	H	H	H	H	H
17960	BT	0.307	0.228	0.378	0.218	0.146	0.548	-0.035	-0.256	-0.582	-0.463
	WM	0.465	0.233	**1.861**	**2.160**	0.116	0.116	0.116	0.582	0.931	0.233
	WW	-1.060	-0.731	-1.440	-0.941	0.116	0.116	1.137	0.989	**2.242**	1.343
	Result	H	H	H	H	H	H	H	H	H	H
17979	BT	0.126	0.345	0.216	0.211	-0.124	0.152	-0.222	-0.444	-0.355	-0.627
	WM	**1.861**	0.233	0.814	**2.155**	0.465	0.465	0.116	0.931	0.465	1.603
	WW	-1.273	-1.320	-1.346	-0.790	0.376	-0.471	0.358	0.229	**1.829**	1.483

	Result	H	H	H	H	H	H	H	H	H	H
D20A001	**BT**	0.452	0.409	0.339	0.028	-0.445	-0.707	-1.044	-1.275	-1.933	-1.427
	WM	1.163	1.629	0.465	0.931	0.233	1.629	1.629	**2.327**	1.629	1.214
	WW	-1.294	-1.493	-1.297	-0.574	-0.276	1.231	0.166	**1.945**	1.098	**2.059**
	Result	H	H	H	H	H	H	H	**N-H**	H	H
D20A002	**BT**	0.613	0.136	0.299	-0.117	-0.153	-0.167	-0.121	-0.410	-0.474	-0.392
	WM	0.723	0.723	0.723	**1.688**	0.723	0.723	0.723	0.723	0.241	**1.741**
	WW	-1.070	-0.054	-0.142	0.224	**1.844**	0.199	**1.867**	1.189	**2.366**	0.952
	Result	H	H	H	H	H	H	H	H	H	H
D20A004	**BT**	-0.298	-0.172	0.180	-0.538	-0.394	-0.889	-0.767	-1.468	-0.983	-0.450
	WM	0.477	0.477	0.095	0.477	0.477	1.621	1.621	1.621	0.095	0.477
	WW	0.299	-0.257	-0.097	0.129	0.970	1.265	1.596	**1.685**	0.927	0.960
	Result	H	H	H	H	H	H	H	H	H	H
D20A006	**BT**	1.107	1.006	0.126	-0.796	-0.693	-0.620	-0.797	-0.624	-0.266	-0.381
	WM	-0.124	**2.849**	0.124	1.610	0.124	1.610	1.610	1.610	0.124	0.124
	WW	-1.027	**-1.976**	-0.951	0.360	0.104	-0.491	0.142	0.053	0.091	-0.351
	Result	H	**N-H**	H	H	H	H	H	H	H	H
D20A009	**BT**	-0.041	0.035	0.268	-0.239	-0.461	-0.778	-1.111	-1.269	-1.155	-1.404
	WM	0.353	0.353	1.059	**1.764**	0.353	1.059	**1.764**	1.282	1.059	**2.470**
	WW	0.707	0.005	-0.629	0.244	0.484	1.610	0.675	**2.166**	0.763	**2.414**
	Result	H	H	H	H	H	H	H	H	H	**N-H**
D20A011	**BT**	0.002	-5.034	0.457	0.566	-0.371	-0.273	-0.607	-0.519	-1.162	-1.291
	WM	**1.812**	0.558	0.975	**2.443**	0.975	0.975	0.139	**1.665**	**1.812**	**2.648**
	WW	-0.190	0.403	-1.091	-1.233	0.382	0.539	0.822	1.163	**1.719**	**2.297**
	Result	H	H	H	H	H	H	H	H	**N-H**	**N-H**
D20A013	**BT**	0.033	0.039	-0.221	-0.383	-1.127	-1.089	-1.342	-0.708	-1.472	-1.575
	WM	0.233	0.931	0.582	**1.978**	0.582	**2.676**	0.582	**1.978**	**1.978**	**1.978**
	WW	-0.688	0.043	-0.491	0.253	1.180	**1.729**	1.738	1.273	**2.021**	**2.414**
	Result	H	H	H	H	H	**N-H**	H	H	**N-H**	**N-H**
D20A014	**BT**	0.293	0.105	0.177	0.185	-0.018	-0.274	-0.724	-1.183	-0.858	-1.125
	WM	0.562	1.601	0.616	0.985	1.355	0.616	0.862	1.601	0.616	0.862
	WW	-0.977	-0.156	-0.549	-0.235	-0.371	0.349	-0.201	1.510	-0.061	1.018
	Result	H	H	H	H	H	H	H	H	H	H
D20A015	**BT**	-0.021	0.438	0.292	0.700	-0.345	-0.296	-0.573	-0.451	-0.710	-0.633
	WM	1.024	1.279	0.640	0.128	0.640	0.128	0.128	0.640	0.640	0.128
	WW	-0.954	-0.985	-0.952	**-1.960**	-0.189	0.732	-0.192	1.006	-0.103	1.576
	Result	H	H	H	H	H	H	H	H	H	H
D20A016	**BT**	-0.020	-0.200	-0.052	0.060	-0.773	-0.797	-1.437	-1.252	-1.056	-0.971
	WM	0.519	**1.815**	1.037	**1.815**	0.648	1.426	1.426	**2.204**	1.426	**2.204**
	WW	-0.636	-0.255	-0.496	-0.544	1.628	**1.699**	**1.753**	**2.184**	1.482	**2.095**
	Result	H	H	H	H	H	H	H	**N-H**	H	**N-H**
D20A017	**BT**	0.011	-0.268	0.103	0.320	-0.060	-0.912	-0.896	-0.629	-0.857	-0.967
	WM	0.420	1.594	0.420	0.084	1.091	**2.602**	0.084	0.084	0.084	1.091
	WW	-0.044	0.614	-0.176	-0.187	0.187	1.160	-0.375	-0.120	-0.358	0.290
	Result	H	H	H	H	H	H	H	H	H	H
D20A018	**BT**	-0.068	-0.004	0.408	-0.011	0.454	0.296	-0.049	0.041	-0.713	-0.211
	WM	0.090	1.173	0.451	1.173	0.451	0.090	1.173	0.090	**1.715**	-0.090
	WW	-0.095	-0.103	-0.592	-0.373	-0.755	-0.362	0.410	0.056	1.151	0.282
	Result	H	H	H	H	H	H	H	H	H	H

H: Homogenous, **N-H**: Non-homogenous

6.4.2 Trend Detection for Extreme Drought Events

As for the identification of homogeneity test and time series, trend detection of extreme drought events in changing climate is crucial to utilize climate changes and suggest useful management strategies. The results of the employed Spearman Rho (SR) and Mann-Kendall (MK) statistical test for SPI 1-, 3-, 6-, 9- and 12-month time scales are summarized in Table 6.11. At the 90% significance level ($-1.64 < z < 1.64$), the null hypothesis cannot be rejected. As shown in the Table, MK and SR show similar performance for analysis of trend detection. For SPI 1-month time scale, there is no significant trend detected by applying both two tests although increasing and decreasing trends exist in the extreme drought events except two stations (17868 and D20A014). While two tests indicate statistically significant increasing trend for AMDS series of station 17868, decreasing trend are detected for AMDD series of D20A014.

In the SPI 3-month time scale, statistically significant increasing trend are evaluated only for AMDS series of station 7767 and for AMDD series of station 8275. For SPI 6-month time scale, four stations are found statistically significant with respect to both two test results. Increasing and decreasing trend are demonstrated for AMDS and AMDD series of station 7767, respectively. Increasing trends for AMDS series of stations 8275, 17866 and D20A016 and decreasing trend for AMDS series of station D20A016 are detected at 90% significance level. Like SPI 3-month, similar results are clearly seen for SPI 9-month time scale for stations 7767, 8275 and D20A016. Five stations indicate statistically significant for SPI 12-month time scale. It can be inferred that increasing trend for AMDS series of stations 7767 and D20A018 and, decreasing trend for AMDS series of stations 8275 and D20A016 are detected. Finally both two tests demonstrate statistically significant increasing for AMDD series of stations 8275 and D20A009.

Table 6.11 Trend detection results for extreme drought events

Station	Tests	SPI 1		SPI 3		SPI 6		SPI 9		SPI 12	
		AMDS	AMDD	AMDS	AMDD	AMDS	AMDD	AMDS	AMDD	AMDS	AMDD
7767	**MK**	**1.683**	-1.093	**1.683**	-0.855	**2.474**	**-2.448**	**2.428**	**-1.910**	**2.138**	**-1.706**
	SR	1.537	-1.131	**1.684**	-0.974	**2.499**	**-2.497**	**2.160**	**-1.935**	**1.918**	-1.628
	Result	N	N	**I**	N	**I**	**D**	**I**	**D**	**I**	N
8275	**MK**	-0.276	0.685	-0.584	**1.755**	**-1.674**	**1.947**	-1.384	**1.704**	**-1.860**	**1.874**
	SR	-0.297	0.697	-0.534	**1.691**	-1.595	**1.787**	-1.409	**1.693**	**-1.762**	**1.957**
	Result	N	N	N	**I**	N	**I**	N	**I**	**D**	**I**

	MK	0.149	-0.265	0.261	0.008	0.351	-0.196	0.441	-0.565	0.211	-0.479
17255	**SR**	0.143	-0.273	0.411	0.079	0.425	-0.259	0.478	-0.506	0.179	-0.419
	Result	N	N	N	N	N	N	N	N	N	N
	MK	-1.105	0.283	-0.952	1.211	-0.391	0.242	-0.255	0.377	-0.307	0.309
17355	**SR**	-1.203	0.369	-1.014	1.123	-0.370	0.066	-0.234	0.345	-0.474	0.251
	Result	N	N	N	N	N	N	N	N	N	N
	MK	-0.060	0.894	-0.681	0.755	-0.534	**1.712**	-1.036	1.050	-1.529	1.432
17866	**SR**	-0.063	0.897	-0.674	0.787	-0.663	**1.901**	-1.151	1.086	-1.616	1.440
	Result	N	N	N	N	N	**I**	N	N	N	N
	MK	**1.767**	-1.019	0.900	-0.373	0.293	0.000	-0.163	0.087	0.043	-0.515
17868	**SR**	**1.667**	-1.012	1.009	-0.512	0.282	0.232	-0.179	0.153	-0.020	-0.547
	Result	**I**	N	N	N	N	N	N	N	N	N
	MK	0.448	0.323	0.509	-0.731	0.552	0.409	-0.276	0.772	0.000	0.529
17870	**SR**	0.459	0.243	0.413	-0.667	0.498	0.426	-0.333	0.837	0.626	-0.984
	Result	N	N	N	N	N	N	N	N	N	N
	MK	1.469	-0.184	0.350	0.606	0.000	0.748	-0.771	0.634	-0.703	0.958
17871	**SR**	1.236	-0.257	0.055	0.582	-0.045	0.816	-0.760	0.823	-0.800	1.065
	Result	N	N	N	N	N	N	N	N	N	N
	MK	0.620	-0.254	1.121	-1.243	0.992	0.452	-0.173	0.564	-0.476	0.923
17908	**SR**	0.620	0.111	1.228	-1.323	0.946	0.469	-0.104	0.531	-0.463	0.836
	Result	N	N	N	N	N	N	N	N	N	N
	MK	-0.453	0.009	0.604	-0.579	0.871	-0.729	0.792	-0.626	0.561	-1.433
17960	**SR**	-0.513	0.045	0.053	-0.493	0.791	-0.741	0.696	-0.567	0.562	-1.403
	Result	N	N	N	N	N	N	N	N	N	N
	MK	-1.129	0.256	-0.044	-0.469	0.836	-1.044	0.818	-1.117	0.873	-0.777
17979	**SR**	-1.137	0.264	0.200	-0.445	0.852	-1.000	0.655	-1.185	0.938	-0.689
	Result	N	N	N	N	N	N	N	N	N	N
	MK	0.756	-0.347	0.053	0.000	0.231	0.072	-0.044	-0.134	-0.250	0.467
D20A001	**SR**	0.831	-0.325	0.159	0.155	0.216	0.126	-0.010	-0.185	-0.221	0.400
	Result	N	N	N	N	N	N	N	N	N	N
	MK	-1.058	-0.206	-1.236	-0.246	-0.243	-0.178	0.133	-0.621	-0.441	0.155
D20A002	**SR**	-1.250	-0.180	-1.280	-0.203	-0.456	-0.107	-0.175	-0.472	-0.024	0.155
	Result	N	N	N	N	N	N	N	N	N	N
	MK	1.295	-0.616	0.910	0.146	0.560	-0.543	0.070	-0.035	0.596	0.035
D20A004	**SR**	1.396	-0.644	0.968	0.035	0.514	-0.622	0.246	-0.180	0.775	-0.120
	Result	N	N	N	N	N	N	N	N	N	N
	MK	0.480	0.287	-0.069	-0.071	-0.206	0.972	-0.754	1.038	-0.630	1.196
D20A006	**SR**	0.255	0.349	-0.162	-0.250	-0.186	0.971	-0.742	0.864	-0.449	1.031
	Result	N	N	N	N	N	N	N	N	N	N
	MK	-0.578	0.973	-0.604	0.046	-0.569	0.805	-0.991	1.519	-1.584	**1.656**
D20A009	**SR**	-0.541	0.978	-0.205	0.123	-0.396	0.702	-0.965	1.502	-1.575	**1.706**
	Result	N	N	N	N	N	N	N	N	N	**I**
	MK	-0.030	-0.076	-0.030	0.406	-0.445	0.569	-0.742	0.313	-0.388	0.165
D20A011	**SR**	-0.180	-0.109	-0.020	0.422	-0.442	0.577	-0.883	0.449	-0.560	0.158
	Result	N	N	N	N	N	N	N	N	N	N
	MK	-0.764	-0.009	-0.098	0.451	-0.018	0.537	-0.463	0.789	-0.602	0.976
D20A013	**SR**	-0.680	-0.083	-0.090	0.446	0.017	0.580	-0.569	0.881	-0.591	0.897
	Result	N	N	N	N	N	N	N	N	N	N
	MK	1.026	**-1.901**	1.256	-1.063	-0.345	0.453	-1.057	1.381	-0.744	1.157
D20A014	**SR**	0.949	**-1.910**	1.181	-1.058	-0.463	0.520	-1.064	1.204	-0.769	1.084
	Result	N	**D**	N	N	N	N	N	N	N	N
D20A015	**MK**	-0.350	-0.303	0.105	-0.142	0.245	-0.647	0.478	-0.844	-0.117	0.459

	SR	-0.304	-0.316	-0.013	-0.099	0.305	-0.684	0.471	-0.787	-0.178	0.407
	Result	N	N	N	N	N	N	N	N	N	N
	MK	-1.476	0.224	**-1.694**	1.583	**-2.762**	**2.421**	**-2.407**	**2.002**	**-1.947**	**1.783**
D20A016	**SR**	-1.424	0.225	-1.599	1.550	**-2.586**	**2.301**	**-2.335**	**1.917**	**-1.696**	1.514
	Result	N	N	N	N	**D**	**I**	**D**	**I**	**D**	N
	MK	-0.819	-0.027	0.050	-1.236	-0.273	0.505	-0.893	0.526	-0.821	**-1.706**
D20A017	**SR**	-0.776	-0.138	0.123	-1.205	-0.225	0.521	-0.913	0.481	-0.844	0.785
	Result	N	N	N	N	N	N	N	N	N	N
	MK	-1.300	0.415	-0.151	0.093	-0.091	-0.092	-0.151	0.731	-0.967	**1.798**
D20A018	**SR**	-1.377	0.418	-0.279	0.340	-0.087	0.029	-0.296	0.921	-1.078	**1.714**
	Result	N	N	N	N	N	N	N	N	N	**I**

N: No Trend, **D**: Decreasing, **I**: Increasing

6.4.3 The Trend Slope Results of Extreme Drought Events

Sen's Slope estimator and Regression are performed to evaluate the slope of the trend. The results calculated from these two popular tests are compared. The signs of the slopes are appropriate with the results Spearman Rho and Mann-Kendall tests. As for the identification trend detection, trend slopes are shown as dark bold in Table 6.12. The highest slope, which ranges 0.6 to 0.8 for both two tests are detected for AMDS series of station 7767 at the SPI 9 month time scale. The slope of the evaluated trends is 0.067 (for AMDD series of station 8275 at SPI 3-month), 0.179 (for AMDD series of station 8275 at SPI 6-month), 0.106 (for AMDD series of station 8275 at SPI 9-month), 0.083 (for AMDS series of station 8275 at SPI 12-month) and 0.138 (for AMDD series of station 8275 at SPI 12-month).

Table 6.12 Trend slope results of extreme drought events

Station	**Tests**	**SPI 1**		**SPI 3**		**SPI 6**		**SPI 9**		**SPI 12**	
		AMDS	**AMDD**	**AMDS**	**AMDD**	**AMDS**	**AMDD**	**AMDS**	**AMDD**	**AMDS**	**AMDD**
7767	**SS**	0.132	0.000	**0.340**	-0.125	**0.495**	**-0.333**	**0.768**	**-0.600**	**0.710**	-0.500
	R	0.150	-0.079	**0.297**	-0.118	**0.480**	**-0.379**	**0.759**	**-0.464**	**0.798**	-0.432
8275	**SS**	-0.007	0.000	-0.032	**0.067**	-0.091	**0.179**	-0.076	**0.106**	**-0.071**	**0.083**
	R	-0.018	0.024	-0.045	**0.073**	-0.129	**0.138**	-0.149	**0.145**	**-0.189**	**0.138**
17255	**SS**	0.002	0.000	0.006	0.000	0.010	0.000	0.005	0.000	0.000	0.000
	R	-0.003	-0.003	0.000	0.003	-0.014	0.001	-0.010	-0.020	0.002	-0.027
17355	**SS**	-0.025	0.000	-0.050	0.050	-0.025	0.000	-0.018	0.000	-0.007	0.000
	R	0.001	-0.003	-0.012	0.057	-0.033	0.000	-0.038	0.019	-0.052	0.001
17866	**SS**	0.000	0.000	-0.013	0.000	-0.016	**0.042**	-0.028	0.032	-0.023	0.036
	R	-0.002	0.017	-0.021	0.021	-0.025	**0.059**	-0.033	0.034	-0.050	0.060
17868	**SS**	0.024	0.000	0.032	0.000	0.016	0.000	-0.002	0.000	0.000	0.000
	R	0.018	-0.021	0.032	-0.012	0.068	-0.007	0.061	0.005	0.079	-0.037
17870	**SS**	0.005	0.000	0.013	0.000	0.018	0.000	-0.005	0.010	-0.009	0.000
	R	0.019	-0.010	0.021	-0.012	0.024	0.012	0.005	0.023	-0.008	0.023
17871	**SS**	0.081	0.000	0.033	0.000	0.017	0.100	-0.081	0.125	-0.073	0.143
	R	0.042	-0.004	0.080	0.042	-0.007	0.096	-0.078	0.109	-0.124	0.175
17908	**SS**	0.006	0.000	0.030	0.000	0.031	0.000	-0.001	0.000	-0.001	0.000

	R	0.005	-0.006	0.031	-0.023	0.026	0.013	-0.003	0.020	-0.018	0.026
17960	**SS**	-0.006	0.000	0.014	0.000	0.028	0.000	0.019	0.000	0.010	-0.048
	R	-0.015	0.004	0.004	0.001	0.029	-0.022	0.061	-0.045	0.080	-0.072
17979	**SS**	-0.010	0.000	-0.001	0.000	0.029	0.000	0.022	-0.028	0.019	0.000
	R	-0.011	0.003	0.003	-0.008	0.043	-0.026	0.062	-0.037	0.098	-0.046
D20A001	**SS**	0.008	0.000	0.001	0.000	0.008	0.000	0.000	0.000	0.000	0.000
	R	-0.010	-0.001	-0.041	0.022	-0.009	0.002	-0.005	-0.017	-0.021	0.149
D20A002	**SS**	-0.038	0.000	-0.011	0.000	-0.023	0.000	-0.003	-0.077	0.000	0.000
	R	-0.025	0.057	-0.029	-0.009	-0.116	0.021	-0.102	-0.049	-0.123	-0.014
D20A004	**SS**	0.062	0.000	0.106	0.000	0.108	0.000	0.016	0.000	0.038	0.000
	R	0.064	-0.047	0.144	-0.072	0.175	-0.111	0.190	-0.021	0.137	0.044
D20A006	**SS**	0.080	0.000	-0.019	0.000	-0.062	0.367	-0.256	0.438	-0.345	0.500
	R	0.012	0.042	-0.005	0.038	-0.083	0.245	-0.101	0.329	-0.134	0.378
D20A009	**SS**	-0.005	0.000	-0.002	0.000	-0.021	0.000	-0.023	0.050	-0.025	**0.037**
	R	-0.010	0.016	-0.006	-0.002	-0.003	0.016	-0.017	0.060	-0.020	**0.066**
D20A011	**SS**	-0.001	0.000	-0.001	0.000	-0.027	0.000	-0.029	0.000	0.000	0.000
	R	-0.014	0.006	-0.008	0.008	-0.013	0.017	-0.033	0.024	-0.097	0.028
D20A013	**SS**	-0.011	0.000	-0.005	0.000	0.000	0.000	-0.006	0.000	0.000	0.000
	R	-0.010	-0.003	0.003	0.011	0.021	0.010	0.020	0.016	0.012	0.032
D20A014	**SS**	0.014	**0.000**	0.042	0.000	-0.009	0.000	-0.024	0.054	-0.012	0.000
	R	0.024	**-0.042**	0.051	-0.035	0.017	0.018	-0.010	0.051	-0.027	0.057
D20A015	**SS**	-0.006	0.000	0.005	0.000	0.007	0.000	0.017	-0.034	0.000	0.000
	R	0.007	-0.005	-0.011	-0.006	-0.001	-0.025	0.016	-0.038	-0.001	0.013
D20A016	**SS**	-0.033	0.000	-0.072	0.043	**-0.156**	**0.133**	**-0.096**	**0.100**	**-0.071**	0.091
	R	-0.034	0.011	-0.081	0.050	**-0.163**	**0.125**	**-0.184**	**0.111**	**-0.198**	0.115
D20A017	**SS**	-0.034	0.000	0.002	-0.080	-0.034	0.000	-0.042	0.024	-0.034	0.079
	R	-0.008	-0.016	0.034	-0.084	-0.023	0.020	-0.073	0.047	-0.059	0.065
D20A018	**SS**	-0.050	0.000	-0.026	0.000	-0.051	0.000	-0.018	0.100	-0.127	**0.286**
	R	-0.056	0.031	-0.011	0.025	-0.019	-0.014	-0.098	0.106	-0.203	**0.227**

6.4.4 Change-Point Detection Results of Extreme Drought Events

In this step, after identifying the presence of trend and trend's slope, Buishand Range Test (BRT), Standard Normal Homogeneity Test (SNHT) and the Pettitt Test (PT) are utilized to determine the change of point in extreme drought events time series. SNHT and BRT can be shown as graphically where the break occurs. The results of the three tests are compared to determine a more precise breaking point. Therefore, if two outcomes of the three tests are the same, a break-point is selected for that station. However, if the results of all used tests differ from each other, the choice of the break-point will be suspect (S). Change-point detection results are presented considering the extreme drought events data in Table 6.13.

Three tests are performed at the 90% confidence interval. According to test results, any abrupt change doesn't found for both SPI 1 AMDS and AMDD, SP 3 AMDD and SPI 12 AMDD series at the station 7767. Abrupt changes in AMDS series, are occurred in 2000 for SPI 1, in 2001 for SPI 6-, 9- and 12-month time scales. Abrupt change in AMDD series are found in 2008 for SPI 6 and SPI 9 at the station of 7767. There is no

chance in both AMDS and AMDD series for the station of D20A014. Abrupt changes are evaluated in 1981 for the station 17866 at the SPI 6 AMDD, in 1982 for the station D20A009 at the SPI 12 AMDD and, in 1988 for the station D20A018 at the SPI 12 AMDD series.

In general, highly change-points are detected for the stations of 7767, 8275 and D20A016 at the confidence interval. Even if there is no found any changes at the SPI 1 and SPI 3-month for the station 8275, 1979, 1969 and 1980 are found critical years at the SPI 6 AMDS , SPI 9 AMDD and SPI 12 AMDS series, respectively. Finally, when we consider to station D20A016, abrupt changes are found in 1988 as a critical year, at the SPI 6 (AMDS and AMDD), SPI 9 (AMDS and AMDD) and SPI 12 (AMDS). Among all test results, D20A014 shows inconvenient test results, which accept as suspicious.

Table 6.13 Change-points results of extreme drought events

Station	Tests	Test criteria	SPI 1		SPI 3		SPI 6		SPI 9		SPI 12	
			AMDS	AMDD	AMDS	AMDD	AMDS	AMDD	AMDS	AMDD	AMDS	AMDD
7767	BRT	R / sqrt(n)min	0.91	1.14	0.99	0.83	1.48	1.09	1.29	1.17	1.34	1.21
		CP	NC	NC	2000	NC	2001	2008	2001	2008	2001	NC
	SNHT	T	3.15	4.97	6.08	3.80	7.08	6.05	7.62	5.68	7.25	4.94
		CP	NC	NC	2000	NC	2001	2008	2001	2008	2001	NC
	PT	U	28	31	32	28	40	38	36	37	34	34
		CP	NC	NC	2000	NC	2001	2004	2001	2008	2008	NC
		Result	**NC**	**NC**	**2000**	**NC**	**2001**	**2008**	**2001**	**2008**	**2001**	**NC**
8275	BRT	R / sqrt(n)min	0.99	0.93	1.07	1.49	1.2	1.22	1.06	1.5	1.05	0.94
		CP	NC	NC	NC	1979	NC	1980	NC	1969	1980	1980
	SNHT	T	3.92	3.1	2.31	5.91	4.4	5.45	3.55	5.46	4.14	5.05
		CP	NC	NC	NC	1979	NC	1969	NC	1969	1982	1969
	PT	U	65	65	63	123	111	105	92	102	113	105
		CP	NC	NC	NC	1979	NC	1979	NC	1969	1980	1969
		Result	**NC**	**NC**	**NC**	**1979**	**NC**	**SC**	**NC**	**1969**	**1980**	**1969**
17866	BRT	R / sqrt(n)min	0.9	0.93	0.84	0.9	0.94	1.12	0.96	0.95	1.04	1.07
		CP	NC	NC	NC	NC	NC	1984	NC	NC	NC	NC
	SNHT	T	1.3	3.11	2.09	2.38	2.17	4.59	2.17	2.22	2.84	3.49
		CP	NC	NC	NC	NC	NC	1981	NC	NC	NC	NC
	PT	U	102	127	122	135	148	225	185	157	228	195
		CP	NC	NC	NC	NC	NC	1981	NC	NC	NC	NC
		Result	**NC**	**NC**	**NC**	**NC**	**NC**	**1981**	**NC**	**NC**	**NC**	**NC**
D20A009	BRT	R / sqrt(n)min	1.45	1.66	0.77	0.82	0.8	0.87	0.82	1.11	0.83	1.14
		CP	NC	NC	NC	NC	NC	NC	NC	NC	NC	1982
	SNHT	T	3.95	5.77	1.76	2.82	2.65	1.89	2.38	3.88	2.01	4.51
		CP	NC	NC	NC	NC	NC	NC	NC	NC	NC	1982
	PT	U	179	225	112	121	115	126	148	186	208	205
		CP	NC	NC	NC	NC	NC	NC	NC	NC	NC	1982
		Result	**NC**	**NC**	**NC**	**NC**	**NC**	**NC**	**NC**	**NC**	**NC**	**1982**
D20A014	BRT	R / sqrt(n)min	0.95	1.14	1.068	0.96	1.05	1.53	1.14	1.87	1.23	1.64
		CP	NC	1980	NC	NC	NC	NC	NC	NC	NC	NC

	SNHT	**T**	2.78	10.882	3.42	5.53	2.17	3.89	2.7	6.18	3.17	5.32
		CP	NC	1975	NC	NC	NC	NC	NC	NC	NC	NC
	PT	**U**	128	159	134	134	136	157	174	202	168	185
		CP	NC	1999	NC	NC	NC	NC	NC	NC	NC	NC
		Result	**NC**	**SC**	**NC**	**NC**	**NC**	**NC**	**NC**	**NC**	**NC**	**NC**
D20A016	**BRT**	**R / sqrt(n)min**	0.82	0.97	1.04	0.88	1.22	1.26	1.3	1.65	1.34	1.57
		CP	NC	NC	NC	NC	1988	1988	1988	1988	1996	NC
	SNHT	**T**	7.19	8.3	5.16	3.48	7.02	7.28	6.49	7.7	6.09	8.21
		CP	NC	NC	NC	NC	1988	1984	1988	1984	1988	NC
	PT	**U**	116	69	144	120	188	181	193	188	166	158
		CP	NC	NC	NC	NC	1988	1988	1988	1988	1988	NC
		Result	**NC**	**NC**	**NC**	**NC**	**1988**	**1988**	**1988**	**1988**	**1988**	**NC**
D20A018	**BRT**	**R / sqrt(n)min**	0.77	0.85	0.94	0.82	0.61	0.67	0.83	0.84	1.01	1.04
		CP	NC	NC	NC	NC	NC	NC	NC	NC	NC	1988
	SNHT	**T**	3.42	1.82	1.68	2.91	1.42	1.64	1.62	1.94	2.99	4.22
		CP	NC	NC	NC	NC	NC	NC	NC	NC	NC	1984
	PT	**U**	45	34	36	31	22	23	28	42	44	50
		CP	NC	NC	NC	NC	NC	NC	NC	NC	NC	1988
		Result	**NC**	**NC**	**NC**	**NC**	**NC**	**NC**	**NC**	**NC**	**NC**	**1988**

NC: No-Change, **SC:** Suspect

CHAPTER SEVEN

BIVARIATE DROUGHT FREQUENCY ANALYSIS

7.1 Overview

The role of multivariate frequency distributions in hydrological design and risk management has become increasingly recognized. The traditional multivariate distributions are severely limited, as all marginal constituents must be from the same family of distribution. The copula model has become a newly emerging technique for multivariate distribution derivation, which overcomes this restriction. A major stochastic component characterizes hydrological variables, and thus most hydrological designs and management strategies are focused on the frequency analysis of related variables. Hydrological risk management and designs strategies have been generally considered univariate analysis, leading to the dominant role of a single variable. Univariate design procedures have been widespread, partly due to computational limitations and difficulties encountered in having multivariate procedures that were easily amenable. There is a growing awareness that hydrological design and risk management procedures may take advantage of the multivariate consideration. Hence, Multivariate analysis offers an overview of the related stochastic processes and allows hydrological design and management strategies more effective.

This section aims to indicate the distribution of bivariate and derive the joint distribution of probability of meteorological drought in Ceyhan Basin, Turkey. To achieving these purposes, (1) monthly rainfall data are obtained from 24 gauging stations located in the Ceyhan basin and Mann-Kendall is used to assess the homogeneous precipitation basin, (2) the Standard Precipitation Index (SPI) method is used to identify drought variable (severity and duration) and to test their stationary and randomness, Spearman Rho and Mann-Kendall Tests are performed, (3) the best-fit marginal distributions of drought severity and duration are determined

respectively, (4) ten types of copulas (i.e., Student t copula (t-copula), Gaussian copula, Gumbel copula, Clayton copula, Joe copula, Frank copula, BB1 copula, BB6 copula, BB7 copula and BB8 copula) are applied to generate two dimensional joint distributions and (5) consideration with upper and lower tail dependence, the best fit copula for each stationary station, significant probabilistic specifications of droughts are derived. After all, results are presented, and discussed.

7.2 Measure of Dependence Drought Variables

In order to employ copula function, stationarity or independence of drought variables should be defined. In this study, Spearman Rho (SR) and Mann-Kendall (MK), which is nonparametric trend tests mostly used measure of dependence, were applied to calculate serial stationarity structure of drought duration (DD) and severity (DS) at different time scales (1-, 3- and 6-month). According to two test results, computed Z values were lower than critical of ±1.96 at 0.05 significance level (Table 7.1). That is, for fitting copula function, drought variables are displayed to be appropriate. Consequently, after proving that stationarity of random variables, bivariate copula function can be applied. However, nonstationary distribution models would be assessed, if the data were not stationary. To provide extra verification to fit the joint distributions between drought variables, The Kendall's nonparametric rank correlation coefficient was also employed to drought variables. Highly correlated between variables are reasonable for applying joint distribution. Results about correlation coefficients will be discussed section in detail. According to Table 7.1, drought variables (DD and DS) were observed to be independent and stationary random variables in terms of M-K and Spearman Rho test as well as considering *p* values which are greater than a significance level of 0.05.

Table 7.1 Mann-Kendall and Spearman Rho trend test results for drought duration (DD) and severity (DS) at 1-,3-,6-month time scales.

Station	Parameter	Mann Kendall		Spearman Rho		Parameter	Mann Kendall		Spearman Rho		Parameter	Mann Kendall		Spearman Rho	
		z	p	z	p		z	p	z	p		z	p	z	p
7767	DD (SPI1)	-0.440	0.660	-0.719	0.475	DD (SPI3)	-0.595	0.552	-0.719	0.475	DD (SPI6)	-0.552	0.581	-0.417	0.691
	DS (SPI1)	-1.705	0.088	-1.015	0.310	DS (SPI3)	-0.844	0.399	-1.015	0.310	DS (SPI6)	-0.495	0.620	-0.342	0.746
8275	DD (SPI1)	-0.429	0.668	0.559	0.581	DD (SPI3)	0.479	0.632	0.559	0.581	DD (SPI6)	-0.777	0.437	-0.759	0.456
	DS (SPI1)	-0.440	0.660	-0.242	0.812	DS (SPI3)	-0.318	0.751	-0.242	0.812	DS (SPI6)	-0.542	0.588	-0.605	0.552
17255	DD (SPI1)	0.251	0.802	-1.180	0.240	DD (SPI3)	-1.255	0.210	-1.180	0.240	DD (SPI6)	-1.264	0.206	-1.413	0.160
	DS (SPI1)	-1.502	0.133	-1.564	0.118	DS (SPI3)	-1.664	0.096	-1.564	0.118	DS (SPI6)	-1.787	0.074	-1.740	0.082
17355	DD (SPI1)	-0.304	0.761	-0.855	0.397	DD (SPI3)	-0.800	0.424	-0.855	0.397	DD (SPI6)	-0.173	0.862	-0.227	0.824
	DS (SPI1)	-0.862	0.389	-0.588	0.562	DS (SPI3)	-0.664	0.507	-0.588	0.562	DS (SPI6)	-0.185	0.854	-0.205	0.841
17866	DD (SPI1)	1.428	0.153	-0.240	0.812	DD (SPI3)	-0.255	0.799	-0.240	0.812	DD (SPI6)	1.101	0.271	1.219	0.226
	DS (SPI1)	0.133	0.894	-0.068	0.947	DS (SPI3)	-0.086	0.931	-0.068	0.947	DS (SPI6)	0.857	0.392	0.946	0.348
17868	DD (SPI1)	-0.252	0.801	-1.333	0.184	DD (SPI3)	-1.286	0.199	-1.333	0.184	DD (SPI6)	0.619	0.536	0.682	0.501
	DS (SPI1)	-0.168	0.867	-1.247	0.215	DS (SPI3)	-1.171	0.242	-1.247	0.215	DS (SPI6)	0.249	0.804	0.244	0.810
17870	DD (SPI1)	-0.067	0.946	-1.672	0.095	DD (SPI3)	-1.728	0.084	-1.672	0.095	DD (SPI6)	-1.175	0.240	-1.241	0.223
	DS (SPI1)	-0.329	0.742	-1.203	0.232	DS (SPI3)	-1.311	0.190	-1.203	0.232	DS (SPI6)	-1.768	0.077	-1.666	0.099
17871	DD (SPI1)	0.411	0.681	-0.422	0.680	DD (SPI3)	-0.327	0.744	-0.422	0.680	DD (SPI6)	0.314	0.754	0.397	0.701
	DS (SPI1)	-0.391	0.696	-1.102	0.277	DS (SPI3)	-0.918	0.359	-1.102	0.277	DS (SPI6)	-0.141	0.888	-0.023	0.982
17908	DD (SPI1)	-0.509	0.611	-1.438	0.152	DD (SPI3)	-1.530	0.126	-1.438	0.152	DD (SPI6)	-1.221	0.222	-1.192	0.237
	DS (SPI1)	-0.746	0.456	-0.987	0.327	DS (SPI3)	-0.964	0.335	-0.987	0.327	DS (SPI6)	-1.570	0.116	-1.572	0.117
17960	DD (SPI1)	0.004	0.997	-0.697	0.490	DD (SPI3)	-0.712	0.477	-0.697	0.490	DD (SPI6)	-1.508	0.132	-1.562	0.119
	DS (SPI1)	-0.352	0.725	-1.155	0.251	DS (SPI3)	-1.110	0.267	-1.155	0.251	DS (SPI6)	-1.118	0.264	-1.033	0.306
17979	DD (SPI1)	-0.422	0.673	-0.414	0.682	DD (SPI3)	-0.463	0.644	-0.414	0.682	DD (SPI6)	-1.449	0.147	-1.463	0.145
	DS (SPI1)	0.019	0.985	-0.352	0.727	DS (SPI3)	-0.350	0.726	-0.352	0.727	DS (SPI6)	-1.409	0.159	-1.340	0.183
D20M001	DD (SPI1)	0.581	0.561	-0.650	0.520	DD (SPI3)	-0.577	0.564	-0.650	0.520	DD (SPI6)	-0.608	0.543	-0.550	0.588
	DS (SPI1)	1.361	0.174	-0.574	0.570	DS (SPI3)	-0.446	0.656	-0.574	0.570	DS (SPI6)	-1.093	0.275	-0.940	0.353
D20M002	DD (SPI1)	0.617	0.537	-0.467	0.645	DD (SPI3)	-0.541	0.589	-0.467	0.645	DD (SPI6)	-0.739	0.460	-0.832	0.416
	DS (SPI1)	1.747	0.081	0.383	0.706	DS (SPI3)	0.313	0.755	0.383	0.706	DS (SPI6)	-0.104	0.917	-0.188	0.855
D20M004	DD (SPI1)	-0.125	0.900	-0.717	0.482	DD (SPI3)	-0.647	0.518	-0.717	0.482	DD (SPI6)	0.000	1.000	0.017	0.987
	DS (SPI1)	-0.792	0.428	-1.661	0.097	DS (SPI3)	-1.703	0.089	-1.661	0.097	DS (SPI6)	-0.343	0.731	-0.318	0.759
D20M006	DD (SPI1)	0.750	0.453	-0.265	0.800	DD (SPI3)	-0.272	0.786	-0.265	0.800	DD (SPI6)	0.150	0.881	0.162	0.878
	DS (SPI1)	-0.017	0.986	-0.081	0.941	DS (SPI3)	0.000	1.000	-0.081	0.941	DS (SPI6)	-0.050	0.961	-0.227	0.830

D20M009	DD (SPI1)	1.720	0.085	-0.164	0.871	DD (SPI3)	-0.166	0.868	-0.164	0.871	DD (SPI6)	0.370	0.711	0.290	0.774
	DS (SPI1)	0.229	0.819	-0.061	0.952	DS (SPI3)	-0.094	0.925	-0.061	0.952	DS (SPI6)	-0.423	0.672	-0.477	0.637
D20M011	DD (SPI1)	0.264	0.792	-0.701	0.489	DD (SPI3)	-0.660	0.509	-0.701	0.489	DD (SPI6)	-0.013	0.990	-0.110	0.915
	DS (SPI1)	0.213	0.832	-0.551	0.587	DS (SPI3)	-0.474	0.635	-0.551	0.587	DS (SPI6)	-0.026	0.979	-0.086	0.933
D20M013	DD (SPI1)	0.533	0.594	-0.819	0.417	DD (SPI3)	-0.851	0.395	-0.819	0.417	DD (SPI6)	-1.272	0.203	-1.294	0.199
	DS (SPI1)	-0.263	0.792	-1.688	0.092	DS (SPI3)	-1.747	0.081	-1.688	0.092	DS (SPI6)	-1.722	0.085	-1.836	0.066
D20M014	DD (SPI1)	-1.606	0.108	-0.956	0.342	DD (SPI3)	-0.936	0.350	-0.956	0.342	DD (SPI6)	0.249	0.804	0.264	0.795
	DS (SPI1)	-0.728	0.467	-0.971	0.335	DS (SPI3)	-1.026	0.305	-0.971	0.335	DS (SPI6)	-0.388	0.698	-0.346	0.734
D20M015	DD (SPI1)	-0.915	0.360	-0.948	0.347	DD (SPI3)	-0.985	0.325	-0.948	0.347	DD (SPI6)	-1.335	0.182	-1.345	0.182
	DS (SPI1)	-1.167	0.243	-1.252	0.213	DS (SPI3)	-1.238	0.216	-1.252	0.213	DS (SPI6)	-1.057	0.291	-1.147	0.256
D20M016	DD (SPI1)	0.776	0.438	1.261	0.210	DD (SPI3)	1.246	0.213	1.261	0.210	DD (SPI6)	1.309	0.190	1.269	0.209
	DS (SPI1)	1.569	0.117	1.536	0.126	DS (SPI3)	1.597	0.110	1.536	0.126	DS (SPI6)	1.144	0.253	1.000	0.324
D20M017	DD (SPI1)	0.921	0.357	0.794	0.435	DD (SPI3)	0.639	0.523	0.794	0.435	DD (SPI6)	0.675	0.500	0.779	0.446
	DS (SPI1)	0.924	0.355	1.962	0.048	DS (SPI3)	1.748	0.081	1.962	0.048	DS (SPI6)	0.214	0.831	0.305	0.765
D20M018	DD (SPI1)	0.615	0.539	0.562	0.582	DD (SPI3)	0.546	0.585	0.562	0.582	DD (SPI6)	-1.258	0.209	-1.271	0.211
	DS (SPI1)	0.662	0.508	0.950	0.350	DS (SPI3)	0.964	0.335	0.950	0.350	DS (SPI6)	-0.902	0.367	-0.856	0.403
D20M020	DD (SPI1)	-1.512	0.131	-1.770	0.076	DD (SPI3)	-1.605	0.109	-1.770	0.076	DD (SPI6)	-1.139	0.255	-1.180	0.244
	DS (SPI1)	-1.775	0.076	-1.800	0.072	DS (SPI3)	-1.695	0.090	-1.800	0.072	DS (SPI6)	-1.162	0.245	-0.944	0.354

7.3 Selection of the Appropriate Marginal Distribution of Drought Variables

Firstly, Drought characteristics are calculated from monthly precipitation data for each station using SPI (1, 3- and 6-time scales). Before determining the best fit copula, the univariate marginal distributions should be determined for each drought variable. The Exponential and Gamma distributions have been extensively employed to model the drought severity and duration series. However, some researchers found that the other distributions families such as generalized logistic, Weibull and Log-normal, etc. can be more appropriate than the most used distribution functions. Hence, all widely known probability distributions as the Weibull, Log-normal, Gamma, Exponential, Normal and Log-logistic are performed to find the most suitable marginal distribution of the drought duration and severity series. Even if numerous family of goodness of fit exist in the literature, The performance of used distributions for each drought characteristic are tested by the Anderson-Darling (AD) , Kolmogorov-Smirnov (K-S) , Cramers-von Mises (CvM), Akaike's Information Criterion (AIC) , Bayesian Information Criterion (BIC) (Stone, 1979) and Maximum likelihood methods (MLM). MLM is also used to predict the parameters of the fitted distributions.

Table 7.2 exhibits the detail of the used distributions and the performance test results for DD and DS series. From Table 7.2, it can be seen that the smallest performance tests statistics, also called goodness-of-fit (GoF), are shown as bold. It means that the smallest test statistics indicate the shortest distance between the empirical and parametric distributions. Besides, Figure 7.1, 7.2, and 7.3 shows the cumulative distribution function (CDF) and Probability density function (PDF) plots of the defined the most suitable probability distributions to DD and DS series for station 17255 at different time scales.

The drought duration and severity are fitted as Log-normal and gamma distribution, respectively for station 17255 SPI 1-month. For SPI 3-month, Weibull and gamma are fitted for DD and DS. For SPI 6-month, Log-normal and gamma are found to be most suitable for DD and DS series. Their parameters are estimated using the method of MLE. Figures 7.1, 7.2 and 7.3 indicate the observed DD and DS series and obtained CDF and PDF for each distribution. For this station, while the observed DS series and fitted distributions for three figures show that the gamma distribution is much

sufficient to define at all-time scales, DD series are found different distributions for each time scale.

Table 7.2 The used distributions and the performance test results for DD and DS series (station 17255)

Duration (SPI 1-month)	**Lognormal**	**Logistic**	**Gamma**	**Exponential**	**Weibull**	**Normal**
Kolmogorov-Smirnov statistic	0.3069786	**0.24711**	0.297218	0.3923151	0.262544	0.263592
Cramer-von Mises statistic	1.7730333	**1.61499**	1.730818	2.9233872	1.616461	1.970896
Anderson-Darling statistic	10.7295153	10.24558	10.38263	15.4570075	**9.47309**	11.22788
Akaike's Information Criterion	**365.0945**	437.9381	383.7333	446.6027	399.657	451.1928
Bayesian Information Criterion	**370.8449**	443.6885	389.4837	449.4779	405.4074	456.9432
Maximum-Looglikelihood	**-180.5472**	-216.969	-189.867	-222.3013	-197.829	-223.596
Severity (SPI 1-month)						
Kolmogorov-Smirnov statistic	0.09726609	0.14968	0.065258	0.0541243	0.06945	0.17595
Cramer-von Mises statistic	0.267063	0.588674	**0.04409**	0.05685561	0.047251	1.033974
Anderson-Darling statistic	1.920591	4.483293	**0.27459**	0.35605246	0.280965	5.878359
Akaike's Information Criterion	389.7568	444.0749	363.8394	**362.2584**	363.7037	454.2646
Bayesian Information Criterion	395.5072	449.8253	369.5898	**365.1336**	369.4541	460.015
Maximum-Looglikelihood	-192.8784	-220.037	**-179.92**	-180.1292	-179.852	-225.132
Duration (SPI 3-month)						
Kolmogorov-Smirnov statistic	0.1770225	0.1714026	0.1604692	0.2450062	**0.147741**	0.183994
Cramer-von Mises statistic	0.3456877	0.4189789	0.309241	0.639977	**0.293378**	0.55093
Anderson-Darling statistic	2.6878539	3.035979	2.2960573	4.2296493	**2.121012**	3.396376
Akaike's Information Criterion	**371.1694**	408.5607	373.553	392.3089	376.0463	408.1369
Bayesian Information Criterion	**376.0781**	413.4694	378.4617	394.7632	380.95	413.045
Maximum-Looglikelihood	**-183.5847**	-202.2804	-184.7765	-195.1545	-186.023	-202.068
Severity (SPI 3-month)						
Kolmogorov-Smirnov statistic	0.1145938	0.1699019	**0.078064**	0.09674688	0.0818377	0.1620204
Cramer-von Mises statistic	0.2886911	0.3599949	**0.063986**	0.14071677	0.0767107	0.5818476
Anderson-Darling statistic	1.7734271	2.8484942	**0.416164**	1.10540349	0.508684	3.7445888
Akaike's Information Criterion	375.3956	428.1498	**359.5771**	359.833	360.1429	434.5221
Bayesian Information Criterion	380.3043	433.0585	364.4858	**362.2874**	365.0516	439.4308
Maximum-Looglikelihood	-185.6978	-212.0749	**-177.789**	-178.9165	-178.0715	-215.2611
Duration (SPI 6 -month)						
Kolmogorov-Smirnov statistic	**0.137996**	0.1802657	0.1592421	0.1732984	0.157382	0.2094663
Cramer-von Mises statistic	**0.1637291**	0.3274164	0.1925553	0.2277076	0.1797767	0.4326838
Anderson-Darling statistic	**1.0532291**	2.192383	1.1237451	1.6332747	1.0788819	2.5465301
Akaike's Information Criterion	**286.6913**	317.7287	289.3729	294.5003	290.9125	320.2862
Bayesian Information Criterion	**290.7059**	321.7434	293.3875	296.5076	294.9272	324.3009
Maximum-Looglikelihood	**-141.3456**	-156.8644	-142.6864	-146.2501	-143.4563	-158.1431
Severity (SPI 6-month)						
Kolmogorov-Smirnov statistic	0.1033073	0.2031817	**0.0913175**	0.1729189	0.0917353	0.1922852
Cramer-von Mises statistic	0.1233153	0.3961843	**0.0461822**	0.2989266	0.0496313	0.5971533
Anderson-Darling statistic	0.8235572	2.7930586	**0.3091617**	2.1281462	0.3358238	3.3614454
Akaike's Information Criterion	276.0967	328.9718	**268.7159**	272.5453	268.9458	335.2404
Bayesian Information Criterion	280.1114	332.9865	**272.7306**	274.5526	272.9604	339.255
Maximum-Looglikelihood	-136.0484	-162.4859	**-132.358**	-135.2726	-132.4729	-165.6202

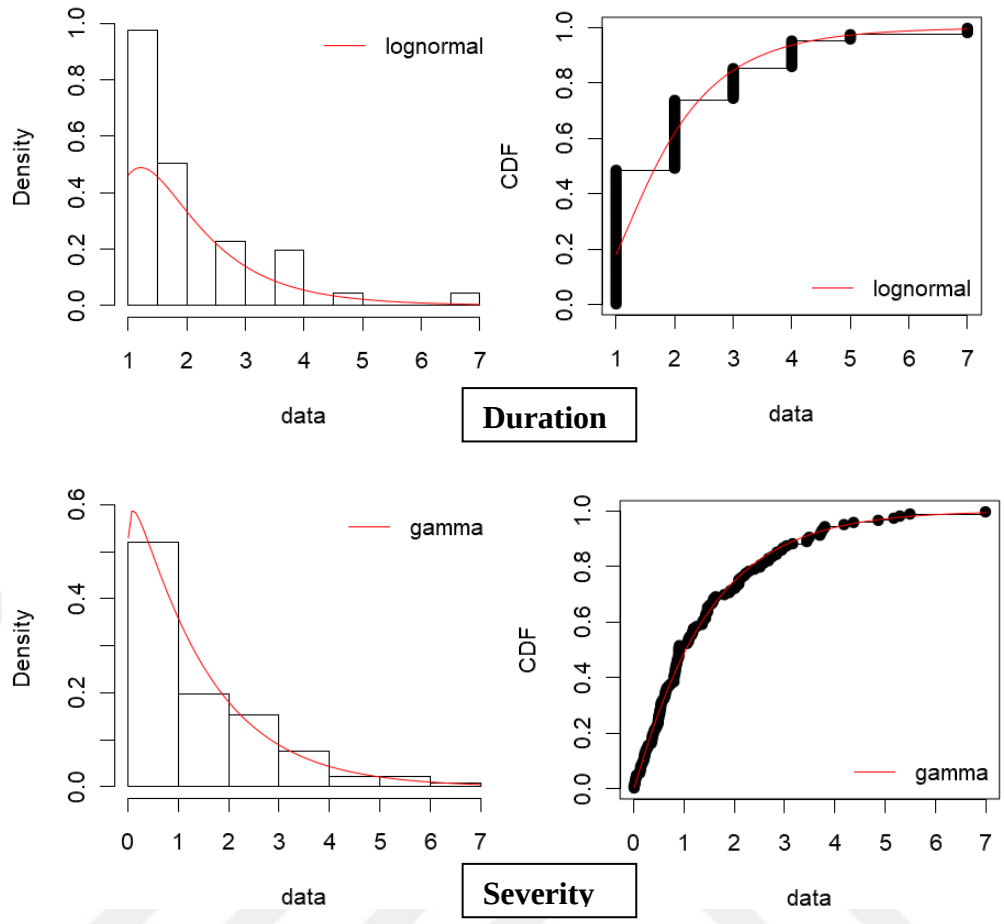

Figure 7.1 Cumulative distribution function (CDF) and Probability density function (PDF) of drought duration and severity (17255 SPI 1-month) for selecting the best fit marginal distribution

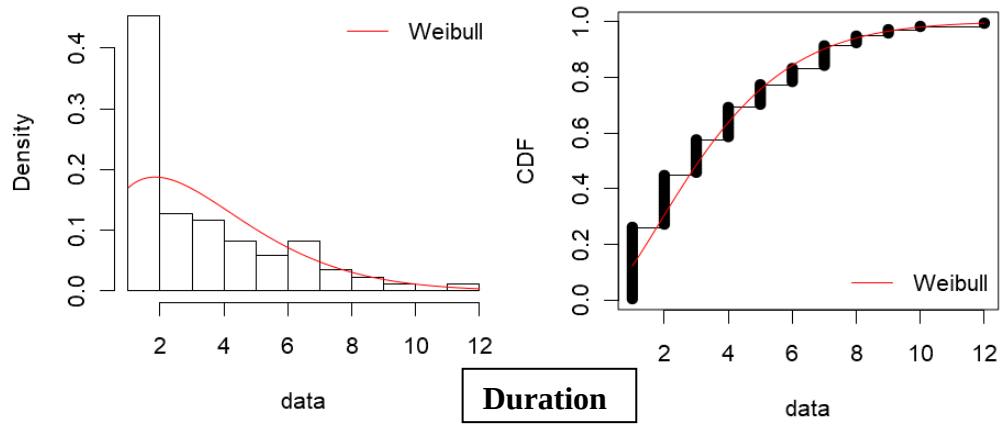

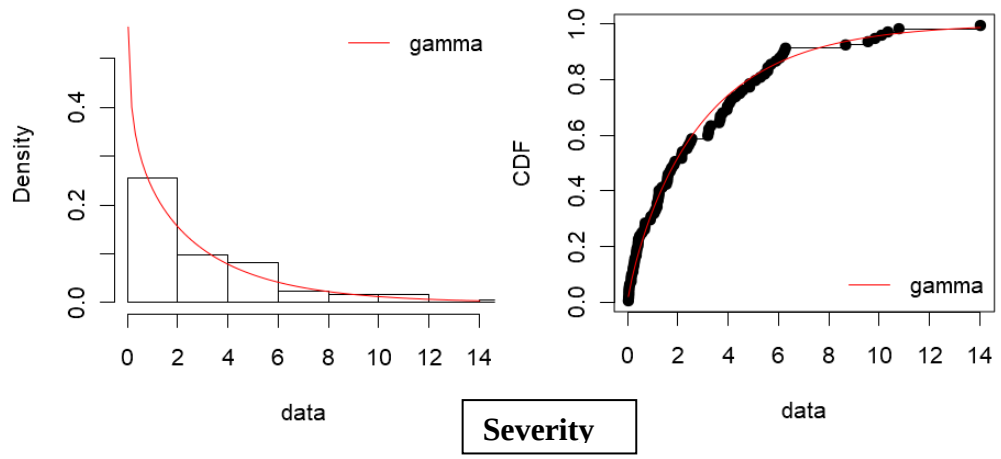

Figure 7.2 Cumulative distribution function (CDF) and Probability density function (PDF) of drought duration and severity (17255 SPI 3-month) for selecting the best fit marginal distribution

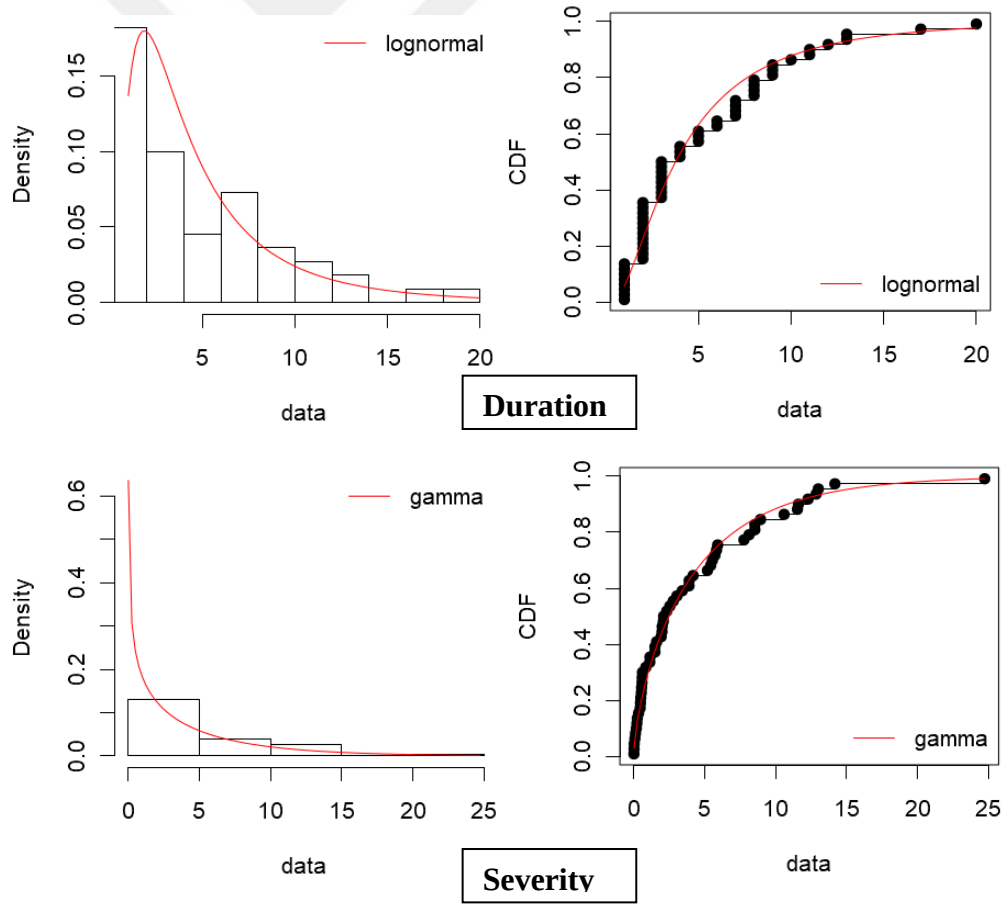

Figure 7.3 Cumulative distribution function (CDF) and Probability density function (PDF) of drought duration and severity (17255 SPI 6-month) for selecting the best fit marginal distribution

Table 7.3, 7.4, and 7.5 lists the fitted univariate distributions as well as the fitted GoF statistics results. According to Table 7.3 results, the Weibull distribution is commonly applied to DD series, while the Gamma distribution is found for DS series. None of the DD and DS series are found suitable for the Exponential distribution among used all stations at 1-month time scale. While the Log-normal distribution is evaluated for six stations DD series, Weibull is more fitted for DS series followed by the Gamma distribution.

For SPI 3-month time scale, the Log-normal distribution is commonly applied to DD series, while the Gamma distribution are commonly evaluated for DS series. The Weibull is the more suitable distribution for both the DD and DS series, followed by Log-normal and Gamma.

For SPI 6-month time scale, the Log-normal are performed better fit compared to other used distributions for DD series, while the Weibull distribution is commonly applied to model DS series. Like SPI 3-month, the other suitable fit distributions are Weibull and Gamma distributions, respectively.

Table 7.3 Determination of the fitted marginal distribution and GoF test results for DD and DS series at 1-month time scale

SPI 1-month									
Station	**Variables**	**Distribution**	**KS**	**CvMS**	**AD**	**AIC**	**BIC**	**MLM**	**Parameters**
7767	DD	Log-normal	0.3024	0.6483	3.9761	121.9786	125.6789	-58.9893	[0.500, 0.514]
	DS	Gamma	0.0874	0.0496	0.3737	127.5373	131.2376	-61.7687	[1.232, 0.892]
8275	DD	Log-normal	0.3355	1.3530	7.7345	193.0617	197.7751	-94.5309	[0.436, 0.525]
	DS	Gamma	0.0644	0.0458	0.2915	220.8951	225.6085	-108.4475	[1.431, 0.934]
17255	DD	Log-normal	0.3070	1.7730	10.7295	365.0945	370.8449	-180.5472	[0.519, 0.571]
	DS	Gamma	0.0653	0.0441	0.2746	363.8394	369.5898	-179.9197	[1.074, 0.738]
17355	DD	Log-normal	0.3078	1.1676	7.0102	234.7788	239.6641	-115.3894	[0.505, 0.567]
	DS	Weibull	0.0690	0.0617	0.5005	230.8200	235.7053	-113.4100	[0.935, 1.355]
17866	DD	Log-normal	0.2781	1.3406	8.4335	380.6875	386.3759	-188.3438	[0.584, 0.594]
	DS	Gamma	0.0388	0.0263	0.2431	385.6150	391.3034	-190.8075	[1.301, 0.771]
17868	DD	Log-normal	0.2948	1.5515	9.5521	322.3165	327.9081	-159.1583	[0.517, 0.537]
	DS	Weibull	0.0731	0.0973	0.5379	325.9929	331.5845	-160.9965	[1.183, 1.503]
17870	DD	Weibull	0.2354	1.5454	9.4622	421.6793	427.4898	-208.8396	[1.583 , 2.295]
	DS	Gamma	0.0423	0.0364	0.2447	378.8344	384.6450	-187.4172	[1.082, 0.732]
17871	DD	Log-normal	0.2627	0.4924	3.2182	138.4252	142.1676	-67.2126	[0.599, 0.539]
	DS	Exponential	0.0824	0.0434	0.3797	128.7024	130.5736	-63.3512	[0.726]
17908	DD	Log-normal	0.3152	1.9684	11.7880	380.8658	386.7203	-188.4329	[0.510, 0.568]
	DS	Weibull	0.0579	0.0610	0.4618	401.1665	407.0210	-198.5833	[1.124, 1.642]
17960	DD	Log-normal	0.3347	2.2137	12.7615	331.7006	337.4510	-163.8503	[0.452, 0.537]
	DS	Gamma	0.0563	0.0409	0.2653	360.3253	366.0757	-178.1626	[1.128 , 0.783]
17979	DD	Weibull	0.2389	1.4588	8.5785	426.0680	431.7564	-211.0340	[1.506, 2.471]
	DS	Weibull	0.0726	0.1149	0.8103	356.9198	362.6082	-176.4599	[1.088, 1.533]
D20M001	DD	Log-normal	0.3006	1.6094	9.9776	358.6781	364.3506	-177.3390	[0.549, 0.570]
	DS	Gamma	0.0762	0.1119	1.1047	325.8150	331.4875	-160.9075	[0.947 , 0.717]
D20M002	DD	Log-normal	0.3294	0.9715	5.8982	161.8422	165.9973	-78.9211	[0.509 ,0.554]

	DS	Gamma	0.0737	0.0448	0.3151	158.9196	163.0747	-77.4598	[0.831, 0.601]
D20M004	DD	Weibull	0.2422	0.4905	2.9286	130.1544	133.5321	-63.0772	[1.565 , 2.336]
	DS	Gamma	0.0681	0.0265	0.1764	120.2859	123.6637	-58.1430	[1.1046, 0.699]
D20M006	DD	Weibull	0.2958	0.4294	2.7155	101.2148	104.0828	-48.6074	[1.753 , 2.446]
	DS	Weibull	0.0976	0.0421	0.2679	89.3864	92.2544	-42.6932	[0.948 , 1.426]
D20M009	DD	Weibull	0.2287	1.3687	8.1051	411.1510	416.8706	-203.5755	[1.603 , 2.376]
	DS	Weibull	0.0918	0.1370	0.7024	351.3746	357.0942	-173.6873	[1.019, 1.425]
D20M011	DD	Log-normal	0.2553	0.8500	5.3597	272.1685	277.1003	-134.0843	[0.612, 0.612]
	DS	Weibull	0.0693	0.0509	0.3246	250.0041	254.9359	-123.0020	[1.145, 1.611]
D20M013	DD	Weibull	0.2745	1.8240	10.1909	365.6472	371.2221	-180.8236	[1.550, 2.175]
	DS	Weibull	0.0735	0.0983	0.6718	297.2119	302.7869	-146.6059	[0.933, 1.211]
D20M014	DD	Log-normal	0.2992	1.5823	9.6968	340.3966	346.0046	-168.1983	[0.527 , 0.566]
	DS	Gamma	0.0588	0.0574	0.3896	347.2000	352.8080	-171.6000	[1.203 , 0.793]
D20M015	DD	Log-normal	0.3396	2.1391	12.2572	303.2088	308.8168	-149.6044	[0.443 , 0.529]
	DS	Gamma	0.0839	0.1707	1.0741	295.0126	300.6206	-145.5063	[0.870, 0.713]
D20M016	DD	Log-normal	0.3225	1.6907	10.2077	312.6846	318.1216	-154.3423	[0.512, 0.575]
	DS	Exponential	0.0670	0.1030	0.6212	319.1850	321.9035	-158.5925	[0.659]
D20M017	DD	Log-normal	0.2709	0.7020	4.4075	188.0935	192.4728	-92.0468	[0.566, 0.553]
	DS	Exponential	0.0764	0.0454	0.2956	191.3973	193.5869	-94.6986	[0.647]
D20M018	DD	Log-normal	0.2757	0.6990	4.3242	173.4045	177.6588	-84.7023	[0.546, 0.549]
	DS	Weibull	0.0916	0.0875	0.5005	168.0044	172.2587	-82.0022	[1.163, 1.47]
D20M020	DD	Log-normal	0.3252	1.2635	7.3836	171.8834	176.5184	-83.9417	[0.435, 0.479]
	DS	Gamma	0.0634	0.0406	0.2598	185.7212	190.3561	-90.8606	[1.298, 1.030]

Table 7.4 Determination of the fitted marginal distribution and GoF test results for DD and DS series at 3-month time scale

SPI 3-month									
Station	**Variables**	**Distribution**	**KS**	**CvMS**	**AD**	**AIC**	**BIC**	**MLM**	**Parameters**
7767	DD	Gamma	0.1542	0.0657	0.4511	100.8122	102.9013	-48.4061	[2.239, 0.522]
	DS	Gamma	0.1533	0.0471	0.2737	94.2916	96.3806	-45.1458	[0.743 , 0.227]
8275	DD	Log-normal	0.1724	0.1850	1.3744	216.1621	219.9861	-106.0810	[0.959 , 0.773]
	DS	Weibull	0.0723	0.0287	0.1941	208.2191	212.0432	-102.1096	[0.824, 2.636]
17255	DD	Weibull	0.1477	0.2934	2.1210	376.0463	380.9550	-186.0232	[1.473, 3.957]
	DS	Gamma	0.0781	0.0640	0.4162	359.5771	364.4858	-177.7886	[0.824,0.279]
17355	DD	Log-normal	0.2223	0.3164	2.2704	219.8280	223.8060	-107.9140	[0.855, 0.758]
	DS	Weibull	0.0922	0.0608	0.4654	203.4746	207.4526	-99.7373	[0.776, 2.112]
17866	DD	Log-normal	0.1456	0.2808	1.9701	326.7158	331.4293	-161.3579	[0.982, 0.716]
	DS	Gamma	0.0585	0.0560	0.3046	329.3022	334.0157	-162.6511	[0.860, 0.288]
17868	DD	Log-normal	0.2187	0.4308	3.1277	306.3870	311.0485	-151.1935	[0.863, 0.745]
	DS	Gamma	0.0682	0.0249	0.1761	302.1615	306.8230	-149.0808	[0.843, 0.319]
17870	DD	Weibull	0.1587	0.3340	2.3998	350.5044	355.2433	-173.2522	[1.309, 3.820]
	DS	Weibull	0.0510	0.0192	0.1316	329.7711	334.5100	-162.8856	[0.862, 2.733]
17871	DD	Gamma	0.1369	0.0876	0.6224	139.0900	141.9580	-67.5450	[2.353, 0.613]
	DS	Exponential	0.1459	0.0977	0.6410	129.9223	131.3563	-63.9612	[0.345]
17908	DD	Log-normal	0.2356	0.5699	4.0678	338.3562	343.1697	-167.1781	[0.897, 0.757]
	DS	Gamma	0.1073	0.1028	0.5415	326.7496	331.5630	-161.3748	[0.690, 0.248]
17960	DD	Weibull	0.1601	0.2147	1.6595	302.8456	307.3426	-149.4228	[1.552, 3.953]
	DS	Exponential	0.0820	0.0965	0.5597	308.4261	310.6746	-153.2130	[0.304]
17979	DD	Weibull	0.1949	0.4801	3.2580	355.8680	360.7056	-175.9340	[1.334, 3.581]
	DS	Gamma	0.0719	0.0596	0.3970	334.2157	339.0534	-165.1079	[0.821, 0.301]
D20M001	DD	Log-normal	0.1525	0.2049	1.5141	303.1241	307.4419	-149.5621	[1.094, 0.838]
	DS	Gamma	0.0854	0.0468	0.2980	276.0013	280.3190	-136.0006	[0.801, 0.255]
D20M002	DD	Log-normal	0.2285	0.3218	2.2104	174.1531	177.8104	-85.0766	[0.767, 0.713]
	DS	Weibull	0.0567	0.0196	0.1357	165.3901	169.0474	-80.6951	[0.791, 1.958]

D20M004	DD	Log-normal	0.1499	0.1144	0.8282	134.1256	137.0571	-65.0628	[0.932, 0.727]
	DS	Weibull	0.0711	0.0189	0.1224	127.5610	130.4924	-61.7805	[0.777, 2.322]
D20M006	DD	Normal	0.2384	0.1589	1.0072	79.7692	81.5500	-37.8846	[4.055, 1.985]
	DS	Normal	0.1595	0.0765	0.5192	85.7126	87.4933	-40.8563	[3.165, 2.341]
D20M009	DD	Weibull	0.1427	0.1958	1.5437	326.3891	330.9144	-161.1945	[1.390, 4.255]
	DS	Weibull	0.0379	0.0118	0.1126	308.4285	312.9539	-152.2143	[0.894, 3.006]
D20M011	DD	Log-normal	0.1985	0.2903	2.1089	228.9782	232.7618	-112.4891	[1.093, 0.805]
	DS	Weibull	0.0550	0.0207	0.1878	218.7043	222.4880	-107.3522	[0.950, 3.219]
D20M013	DD	Gamma	0.1224	0.1979	1.5061	322.4810	327.0064	-159.2405	[1.917, 0.498]
	DS	Log-normal	0.0502	0.0315	0.1833	294.0654	298.5908	-145.0327	[0.459, 1.177]
D20M014	DD	Log-normal	0.2631	0.6987	4.6739	305.5705	310.3345	-150.7852	[0.768, 0.739]
	DS	Gamma	0.0687	0.0534	0.4168	301.6160	306.3801	-148.8080	[0.709, 0.287]
D20M015	DD	Log-normal	0.2318	0.5009	3.5735	277.3136	281.7819	-136.6568	[0.874, 0.731]
	DS	Weibull	0.0593	0.0468	0.3419	271.6867	276.1549	-133.8434	[0.906, 2.460]
D20M016	DD	Weibull	0.1329	0.1445	1.1027	241.6581	245.7088	-118.8291	[1.620, 4.027]
	DS	Exponential	0.0568	0.0248	0.1718	243.0095	245.0349	-120.5048	[0.316]
D20M017	DD	Gamma	0.1264	0.1085	0.8091	165.1002	168.3754	-80.5501	[2.327, 0.645]
	DS	Gamma	0.0813	0.0498	0.3226	163.4208	166.6960	-79.7104	[0.869, 0.288]
D20M018	DD	Gamma	0.1795	0.1832	1.2699	152.9936	156.0463	-74.4968	[2.184, 0.575]
	DS	Gamma	0.0736	0.0335	0.2135	142.9244	145.9771	-69.4622	[0.733, 0.249]
D20M020	DD	Weibull	0.1922	0.2359	1.6720	184.6493	188.2177	-90.3247	[1.363, 3.407]
	DS	Gamma	0.0856	0.0585	0.4002	172.0165	175.5849	-84.0082	[0.765, 0.300]

Table 7.5 Determination of the fitted marginal distribution and GoF test results for DD and DS series at 6-month time scale

SPI 6-month									
Station	**Variables**	**Distribution**	**KS**	**CvMS**	**AD**	**AIC**	**BIC**	**MLM**	**Parameters**
7767	DD	Weibull	0.1662	0.0790	0.4998	99.7718	101.6607	-47.8859	[1.281, 5.196]
	DS	Weibull	0.0810	0.0213	0.1571	88.1544	90.0432	-42.0772	[0.734 , 3.049]
8275	DD	Log-normal	0.2170	0.2095	1.2639	172.2697	175.2627	-84.1348	[1.135, 0.995]
	DS	Weibull	0.1109	0.0676	0.4343	152.8924	155.8854	-74.4462	[0.596, 3.065]
17255	DD	Weibull	0.1574	0.1798	1.0789	290.9125	294.9272	-143.4563	[1.295, 5.719]
	DS	Gamma	0.0913	0.0462	0.3092	268.7159	272.7306	-132.3580	[0.689, 0.160]
17355	DD	Gamma	0.1770	0.1487	1.0471	185.0010	188.1117	-90.5005	[1.283, 0.258]
	DS	Weibull	0.0960	0.0408	0.3193	153.4698	156.5805	-74.7349	[0.626, 2.735]
17866	DD	Log-normal	0.1581	0.2249	1.7110	298.6244	302.7795	-147.3122	[1.178, 0.903]
	DS	Gamma	0.0965	0.0992	0.5978	270.7644	274.9195	-133.3822	[0.584, 0.147]
17868	DD	Gamma	0.1138	0.0946	0.8380	255.4925	259.2349	-125.7462	[1.514, 0.286]
	DS	Weibull	0.0947	0.0760	0.4402	231.7102	235.4526	-113.8551	[0.766, 3.595]
17870	DD	Log-normal	0.1901	0.2120	1.6511	282.4028	286.3807	-139.2014	[1.198, 0.961]
	DS	Weibull	0.1006	0.1036	0.7007	248.7675	252.7455	-122.3837	[0.646, 3.124]
17871	DD	Log-normal	0.1491	0.0547	0.3933	116.3536	118.5357	-56.1768	[1.260, 0.881]
	DS	Weibull	0.1235	0.0758	0.5518	107.1780	109.3601	-51.5890	[0.783, 3.485]
17908	DD	Log-normal	0.1479	0.1429	0.9255	271.1829	275.0854	-133.5914	[1.405, 0.774]
	DS	Gamma	0.0714	0.0387	0.2993	251.7882	255.6907	-123.8941	[0.638, 0.147]
17960	DD	Log-normal	0.1708	0.2508	1.6966	277.6201	281.7409	-136.8100	[1.164, 0.798]
	DS	Gamma	0.0990	0.1061	0.5870	262.8424	266.9633	-129.4212	[0.611, 0.161]
17979	DD	Log-normal	0.1599	0.2391	1.9026	302.8482	307.1970	-149.4240	[1.061, 0.834]
	DS	Weibull	0.0790	0.0658	0.4044	281.4254	285.7742	-138.7127	[0.727, 2.797]
D20M001	DD	Exponential	0.1602	0.1487	1.1633	243.5811	245.3653	-120.7905	[0.174]
	DS	Gamma	0.1336	0.1677	0.9624	205.7104	209.2787	-100.8552	[0.468, 0.098]
D20M002	DD	Log-normal	0.1311	0.0689	0.4673	140.9709	143.5625	-68.4854	[1.289, 0.841]

	DS	Weibull	0.0739	0.0212	0.1765	127.8966	130.4883	-61.9483	[0.657, 3.206]
D20M004	DD	Weibull	0.1825	0.1536	0.9659	114.7821	117.0530	-55.3910	[1.244, 4.609]
	DS	Weibull	0.0771	0.0216	0.1697	107.3575	109.6285	-51.6788	[0.700, 3.118]
D20M006	DD	Gamma	0.1231	0.0369	0.2840	80.4150	81.8311	-38.2075	[1.988, 0.3775]
	DS	Gamma	0.1927	0.0861	0.5137	70.1875	71.6036	-33.0938	[0.617, 0.168]
D20M009	DD	Log-normal	0.2117	0.4032	2.7911	297.8327	302.1505	-146.9163	[0.961, 0.918]
	DS	Weibull	0.1047	0.1225	0.8152	265.5671	269.8849	-130.7836	[0.634, 2.466]
D20M011	DD	Weibull	0.1103	0.0761	0.6076	199.5103	202.7322	-97.7552	[1.379, 6.116]
	DS	Gamma	0.0918	0.0387	0.2390	177.5593	180.7811	-86.7797	[0.603, 0.1417]
D20M013	DD	Log-normal	0.1937	0.2299	1.3759	258.8314	262.6555	-127.4157	[1.212, 0.9203]
	DS	Weibull	0.1064	0.0853	0.5099	236.5995	240.4236	-116.2998	[0.669, 3.3127]
D20M014	DD	Log-normal	0.1385	0.1607	1.1947	248.1518	251.8091	-122.0759	[1.310, 0.927]
	DS	Gamma	0.0911	0.0518	0.3295	223.5484	227.2057	-109.7742	[0.617, 0.140]
D20M015	DD	Weibull	0.1187	0.0887	0.7436	233.0679	236.6812	-114.5340	[1.312, 5.402]
	DS	Weibull	0.0806	0.0438	0.3584	211.6283	215.2416	-103.8142	[0.758, 3.354]
D20M016	DD	Log-normal	0.1846	0.1890	1.3287	200.3593	203.6345	-98.1797	[1.144, 1.023]
	DS	Weibull	0.1216	0.0787	0.4742	177.2437	180.5189	-86.6219	[0.627, 3.101]
D20M017	DD	Log-normal	0.1740	0.1694	1.1665	146.8506	149.6530	-71.4253	[1.049, 0.916]
	DS	Weibull	0.1383	0.0807	0.5860	132.9798	135.7822	-64.4899	[0.644, 2.759]
D20M018	DD	Log-normal	0.1238	0.0526	0.3548	119.3983	121.5804	-57.6992	[1.366, 0.849]
	DS	Weibull	0.1224	0.0555	0.3648	109.5979	111.7800	-52.7990	0.742, 3.657]
D20M020	DD	Log-normal	0.1857	0.1202	0.9728	160.3751	163.3681	-78.1875	[1.062, 0.893]
	DS	Weibull	0.0924	0.0475	0.3221	142.6709	145.6639	-69.3354	[0.695, 2.662]

7.4 Selection of the Appropriate Copula

After getting drought characteristics with fitted marginal distributions, 10 copula functions including Gaussian, Student t, Clayton, Gumbel, Frank, Joe, BB1, BB6, BB7 and BB8 copula were tested to determine the best fit copula for modeling the dependence between drought duration and severity. Their performance for each SPI time scale (1-, 3- and 6-month) were tested by Akaike's Information Criterion (AIC), Bayesian Information Criterion (BIC), Maximum likelihood methods (MLM) Anderson-Darling (AD), Integrated Anderson-Darling (IAD) and Cramér-von Mises (CvM) tests. In addition, as visual tests also were generated and simulated 10,000 random pair (u_1, v_1) for selected best copula. The copula parameters were measured using the Maximum Likelihood Estimation (MLE) method. Once the copula function parameters were predicted, the next step was to identify a copula that best represents the dependence of drought variables using GoF measures / model selection criteria. While there are a variety of metrics available for model selection, it is a nontrivial task to identify proper family of copulas for a specific hydrological application. For evaluating the efficiency of the fitted copula models, one or more model selection methods, graphical tests, and analytical procedures including tail dependency tests should be performed.

It is necessary to analyze structure of dependency between the drought duration and severity before fitting the bivariate copulas. In this section, Kendall's Tau (τ) correlation coefficients were performed, and presented in Table 7.6 and 7.7 for station 17255 as an example and for all stations, respectively. According to correlation results, it was clearly found that there was a statistically significant positive dependence between the DD and DS for all stations at different time scales.

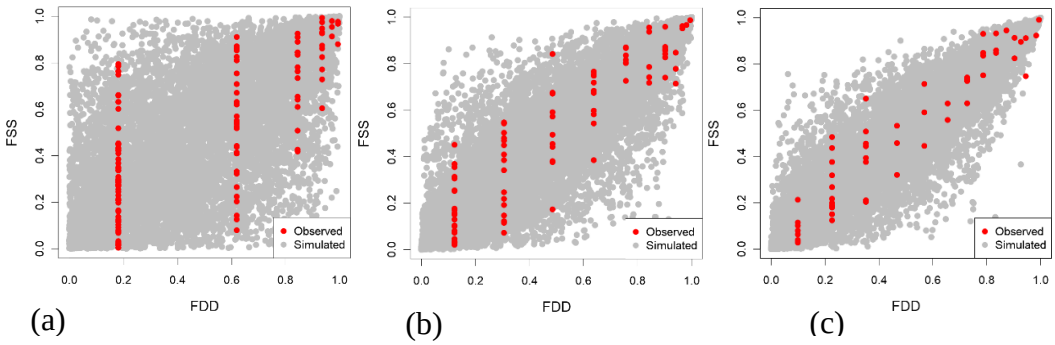

Figure 7.4 Comparision of simulated random data (grey data) and observed data (red data) using (a) fitted Gumbel copula for SPI1, (b) fitted BB1 copula for SPI3 and (c) fitted Gumbel copula for SPI6 (station 17255)

The other main focus for selecting the best fit copula is to evaluate tail dependence. Descritive informations are stated in chapter 4. The comparision of simulated copula functions versus observed DD and DS are demonstrated in Figure 7.4, show that higher dependence is not the lower tail between u_1 and v_1. That is, higher dependencies indicate the upper tail. While test performances results demonstrate Ali-Mikhail -Haq $(\lambda_u = 0, \lambda_L = 0)$, Frank $(\lambda_u = 0, \lambda_L = 0)$, Galambos $(\lambda_u \neq 0, \lambda_L = 0)$ and Plackett $(\lambda_u = 0, \lambda_L = 0)$ copula functions that is more appropriate, according to tail dependence and kendal tau results, these functions are not convenient for bivariate distribution function. Table 7.6 illustrates that Gaussian copula seems to be appropriate for selected stations due to lowest AIC, BIC and highest Log-likelihood value, without considering tail dependence and kendall coefficient. BB1 and Gumbel copula is performing better than Gaussian and Clayton copula due to the absence of tail dependence. BB1 and Gumbel copulas show small diffential in terms of tail dependence and CFG estimator computed 0.728 for selected station. Since Log-likelihood and AIC values are a bit higer than Gumbel copula, BB1 copula is suitable for bivariate drought analysis.

Table 7.6 The performance of test results based on copula family for 17255 station (SPI3 timescale)

					Tail Dependence		Non-parametric T.D (λ_u^{CFG})	Kendal Tau
Number	Family	Log-Lik	AIC	BIC	Lower Tail (λ_u)	Upper Tail (λ_L)		
1	Gaussian copula	63.97	-125.93	-123.48				
2	Student t copula (t-copula)	63.43	-122.86	-117.95	0.17	0.17		
3	Clayton copula	41.17	-80.34	-77.89	0.725			
4	Gumbel copula	62.75	-123.5	-121.05		0.738	0.728	0.749
5	Frank copula	61.68	-121.36	-118.9				
6	Joe copula	56.57	-111.14	-108.69		0.797		
7	**BB1 copula**	**62.9**	**-123.79**	**-116.88**	**0.124**	**0.724**		
8	BB6 copula	62.75	-121.5	-116.59		0.738		
9	BB7 copula	59.71	-115.43	-110.52	0.553	0.768		
10	BB8 copula	62.33	-120.67	-115.76				

The best-fitted copula were defined in two ways for this analysis. For the first approach, the empirical copulas were evaluated and compared by using performance test results. The second approach was based on the comparison of non-parametric and parametric values of the upper tail dependence. As shown in Table 7.7, 7.8 and 7.9, the AIC, BIC, and MLM, AD, IAD and CvM for the considered the appropriate copula family were presented. Tables displays the most appropriate copula family with corresponding parameters and test statistics for 1-, 3-and 6-month time scales. When we consider to SPI 1-month time scale, the results showed that in 18 out of 24 stations, Gumbel copula family was found as better for joint modeling of the drought variables. In addition, while BB1 copula performed as the best-fitted copula types for the stations 17871, 17979 and D20M013 (Table 7.7), BB6 was selected the most appropriate copula family for the stations 17866, 17870 and D20M011.

For SPI 3-month time scale, 13 out of 24 stations demonstrated that Gumbel copula types performed as the best-fitted copula for joint modeling duration and severity series (Table 7.8). In addition, for other selected copula types; BB1 was found the most appropriate copula family for stations 17255, D20M011, D20M014 and D20M015; BB6 was evaluated for stations 17960, D20M001 and D20M004; BB7 was calculated for stations 7767 and D20M018; finally, Joe copula was performed well for the stations D20M009.

Unlike SPI 1- and 3-month time scales, The Gumbel copula family was observed less (11 out of 24 stations) for SPI 6-month time scale, but it was still found higher station numbers compared to other copula types. Joe copula was evaluated as the best-fitted copula types for stations 7767, 17960 and D20M002, while BB1 copula was observed the most appropriate copula family for the stations 17355, 17868, D20M014 and D20M015. In addition, BB7 copula performed well as the best-fitted copula type for the stations 17866, 17868, 17870, 17979, D20M006, D20M016 and D20M017 (Table 7.9).

As discussed above, evaluation of upper tail dependence structure could help to identify the best-fitted copula type. Here, the selected copula family was changed due to considering parametric and non-parametric upper tail dependence. To get more precision about selected the best-fitted copula family, we also simulated 10.000 pairs of DD and DS series using the most appropriate copulas and compared them with historical data for visual interpretation of the tail dependence structure. It can be clearly seen in Figure 7.5, 7.6 and 7.7 for all used stations that the chosen copula types revealed well as the simulated data, which sufficiently overlapped with the observed data, especially for upper tail dependence.

According to results for different time scales, Gumbel, BB1, BB6, BB7 and Joe copula types was evaluated more appropriate for further analysis.

Table 7.7 Best-fit copula type with corresponding parameters and associated goodness-of-fit test statistics at 1-month time scale

		Goodnes of fit tests						Parametric Tail Dependence		Non-parametric Tail Dependence	Correlation	
Station	**Family**	**MLM**	**AIC**	**BIC**	**AD**	**IAD**	**CvM**	**Lower Tail**	**Upper Tail**	**(λ_{CFG})**	**Kendal's Tau**	**Parameters**
7767	Gumbel	15.2	-28.4	-26.55	0.887	4.785	0.825		0.534	0.535	0.555	[1.81]
8275	Gumbel	34.1	-66.2	-63.84	0.932	9.304	1.598		0.597	0.597	0.582	[2.05]
17255	Gumbel	48.21	-94.42	-91.55	0.848	13.565	2.256		0.568	0.569	0.573	[1.93]
17355	Gumbel	26.3	-50.59	-48.15	0.675	6.500	0.911		0.516	0.767	0.494	[1.75]
17866	BB6	54.23	-104.47	-98.78	0.759	9.804	1.531		0.616	0.617	0.599	[1.04, 2.04]
17868	Gumbel	35.58	-69.16	-66.36	0.863	9.219	1.531		0.525	0.515	0.551	[1.78]
17870	BB6	44.38	-84.77	-78.96	0.854	13.060	2.204		0.563	0.572	0.600	[1, 1.91]
17871	BB1	17.71	-31.43	-27.68	0.697	3.190	0.550	0.051	0.575	0.580	0.574	[0.12, 1.96]
17908	Gumbel	44.48	-86.95	-84.02	0.819	13.797	2.150		0.547	0.537	0.590	[1.86]
17960	Gumbel	56.8	-111.6	-108.72	0.945	15.894	2.746		0.605	0.604	0.627	[2.08]
17979	BB1	35.91	-67.82	-62.13	0.805	9.644	1.540		0.506	0.508	0.775	[0.03, 1.73]
D20M001	Gumbel	46.35	-90.7	-87.86	0.888	12.073	2.032		0.575	0.557	0.597	[1.96]
D20M002	Gumbel	26.63	-51.25	-49.17	0.855	6.506	1.093		0.618	0.624	0.624	[2.14]
D20M004	Gumbel	17.93	-33.86	-32.18	0.727	3.738	0.572		0.636	0.649	0.674	[2.23]
D20M006	Gumbel	19.39	-36.79	-35.35	0.872	4.132	0.601		0.708	0.700	0.766	[2.7]
D20M009	Gumbel	37.8	-73.59	-70.73	0.825	8.384	1.242		0.525	0.532	0.526	[1.78]
D20M011	BB6	21.56	-39.11	-38.65	0.646	6.216	0.935		0.482	0.488	0.475	[1, 1.66]
D20M013	BB1	54.61	-105.21	-99.64	0.966	18.414	3.372	0.530	0.631	0.643	0.643	[0.6, 1.82]
D20M014	Gumbel	43.97	-85.93	-83.13	0.814	10.780	1.747		0.569	0.567	0.609	[1.93]
D20M015	Gumbel	37.22	-72.44	-69.63	0.816	9.987	1.543		0.521	0.522	0.555	[1.77]
D20M016	Gumbel	48.47	-94.93	-92.21	0.966	13.510	2.255		0.618	0.613	0.621	[2.14]
D20M017	Gumbel	28.93	-55.86	-53.67	0.705	4.928	0.817		0.614	0.599	0.643	[2.13]
D20M018	Gumbel	21.93	-41.87	-39.74	0.749	5.523	0.916		0.559	0.541	0.579	[1.9]
D20M020	Gumbel	19.22	-36.44	-34.13	0.941	9.920	1.850		0.481	0.468	0.490	[1.66]

Table 7.8 Best-fit copula type with corresponding parameters and associated goodness-of-fit test statistics at 3-month time scale

		Goodnes of fit tests						Parametric Tail Dependence		Non-parametric Tail Dependence	Correlation	
Station	**Family**	**MLM**	**AIC**	**BIC**	**AD**	**IAD**	**CvM**	**Lower Tail**	**Upper Tail**	**(λ_{CFG})**	**Kendal's Tau**	**Parameters**
7767	BB7	23.23	-42.47	-40.38	0.381	0.605	0.068	0.742	0.851	0.828	0.830	[5, 2.32]
8275	Gumbel	36.36	-70.72	-68.81	0.526	1.968	0.263		0.738	0.738	0.754	[2.98]
17255	BB1	62.9	-121.79	-116.88	0.494	2.756	0.311	0.124	0.724	0.728	0.749	[0.12, 2.84]
17355	Gumbel	35.25	-68.5	-66.51	0.635	3.129	0.413		0.713	0.718	0.727	[2.75]
17866	Gumbel	65.91	-129.82	-127.46	0.454	2.495	0.374		0.773	0.770	0.774	[3.39]
17868	Gumbel	53.46	-104.92	-102.59	0.623	3.473	0.473		0.727	0.721	0.743	[2.87]
17870	Gumbel	57.78	-113.56	-111.19	0.534	3.621	0.451		0.751	0.749	0.795	[3.12]
17871	Gumbel	20.18	-38.37	-36.93	0.401	0.782	0.060		0.718	0.752	0.713	[2.79]
17908	BB1	57.73	-111.46	-106.64	0.622	4.362	0.577	0.348	0.727	0.707	0.743	[0.25, 2.6]
17960	BB6	39.85	-77.7	-75.45	0.535	2.279	0.270		0.676	0.664	0.732	[1, 2.47]
17979	Gumbel	55.25	-108.5	-106.08	0.652	4.100	0.517		0.73	0.736	0.795	[2.9]
D20M001	BB6	59.77	-115.54	-115.38	0.453	1.522	0.164		0.794	0.796	0.813	[1, 3.69]
D20M002	Gumbel	35.13	-68.27	-66.44	0.652	3.367	0.522		0.745	0.735	0.777	[3.05]
D20M004	BB6	29.5	-55.01	-52.07	0.531	1.141	0.167		0.798	0.798	0.813	[1, 3.76]
D20M006	Gumbel	7.2	-12.39	-11.5	0.327	0.666	0.112		0.616	0.616	0.610	[2.13]
D20M009	Joe	37.97	-73.94	-71.68	0.507	1.324	0.136		0.759	0.752	0.739	[3.21]
D20M011	BB1	42.88	-81.76	-77.98	0.598	2.212	0.301	0.704	0.771	0.772	0.785	[0.77, 2.55]
D20M013	Gumbel	45.5	-88.99	-86.73	0.448	1.556	0.172		0.714	0.708	0.740	[2.76]
D20M014	BB1	59.51	-115.03	-110.26	0.714	4.610	0.601	0.631	0.733	0.732	0.743	[0.65, 2.32]
D20M015	BB1	49.85	-95.7	-91.23	0.627	3.872	0.509	0.653	0.729	0.729	0.744	[0.72, 2.25]
D20M016	Gumbel	38.65	-75.3	-73.27	0.403	1.355	0.156		0.728	0.725	0.734	[2.88]
D20M017	Gumbel	25.09	-48.18	-46.54	0.416	0.824	0.125		0.715	0.707	0.718	[2.76]
D20M018	BB7	19.93	-35.87	-32.81	0.512	1.016	0.134	0.604	0.68	0.695	0.715	[2.5, 1.38]
D20M020	Gumbel	41.88	-81.76	-79.98	0.435	2.031	0.239		0.811	0.813	0.801	[4]

Table 7.9 Best-fit copula type with corresponding parameters and associated goodness-of-fit test statistics at 6-month time scale

		Goodnes of fit tests						Parametric Tail Dependence		Non-parametric Tail Dependence	Correlation	
Station	**Family**	**MLM**	**AIC**	**BIC**	**AD**	**IAD**	**CvM**	**Lower Tail**	**Upper Tail**	**(λ_{CFG})**	**Kendal's Tau**	**Parameters**
7767	Joe	17.89	-33.77	-32.83	0.205	0.228	0.020		0.864	0.823	0.784	[5.45]
8275	Gumbel	37.24	-72.47	-70.97	0.513	1.610	0.216		0.838	0.841	0.846	[4.61]
17255	Gumbel	51.52	-101.04	-99.03	0.349	0.795	0.088		0.803	0.804	0.825	[3.86]
17355	BB1	25.81	-47.61	-44.5	0.482	0.923	0.108	0.684	0.628	0.607	0.791	[0.83, 2.19]
17866	BB7	58.7	-113.39	-109.24	0.506	2.760	0.342	0.793	0.807	0.819	0.803	[3.92, 2.98]
17868	BB1	41.14	-78.29	-74.54	0.425	0.814	0.083	0.720	0.76	0.759	0.778	[0.9, 2.34]
17870	BB7	60.55	-117.1	-113.12	0.553	2.931	0.354	0.831	0.833	0.831	0.835	[4.61, 3.74]
17871	Gumbel	22.02	-42.04	-40.95	0.422	1.082	0.144		0.811	0.814	0.742	[4]
17908	Gumbel	45.36	-88.73	-86.78	0.291	0.738	0.091		0.785	0.786	0.802	[3.56]
17960	Joe	32.96	-63.92	-61.86	0.357	1.234	0.144		0.77	0.766	0.775	[3.35]
17979	BB7	60.79	-117.59	-113.24	0.508	2.438	0.276	0.748	0.804	0.807	0.838	[3.87, 2.39]
D20M001	Gumbel	45.6	-89.21	-87.42	0.452	1.420	0.137		0.823	0.825	0.847	[4.26]
D20M002	Joe	28.16	-54.32	-53.03	0.317	0.356	0.054	0.830	0.782	0.760	0.833	[6.26]
D20M004	Gumbel	22.84	-43.67	-42.54	0.521	1.100	0.180		0.823	0.827	0.862	[4.26]
D20M006	BB7	13.55	-23.1	-21.69	0.388	0.373	0.038	0.730	0.789	0.798	0.851	[3.62, 2.21]
D20M009	Gumbel	68.18	-134.36	-132.2	0.692	4.611	0.640		0.825	0.815	0.804	[4.3]
D20M011	Gumbel	40.67	-79.34	-77.72	0.387	0.812	0.096		0.841	0.760	0.841	[4.71]
D20M013	Gumbel	44.4	-86.79	-84.88	0.427	1.631	0.222		0.782	0.774	0.756	[3.52]
D20M014	BB1	43.7	-83.4	-79.74	0.453	1.155	0.131	0.730	0.783	0.779	0.788	[0.83, 2.64]
D20M015	BB1	44.01	-84.03	-80.41	0.404	1.161	0.110	0.841	0.75	0.782	0.803	[2.09, 1.92]
D20M016	BB7	41.19	-79.96	-75.1	0.530	1.553	0.181	0.829	0.835	0.828	0.827	[4.54, 3.7]
D20M017	BB7	36.13	-68.25	-65.45	0.535	1.756	0.215	0.866	0.851	0.843	0.800	[4.98, 4.83]
D20M018	Gumbel	20.7	-39.4	-38.31	0.375	0.512	0.065		0.799	0.798	0.809	[3.79]
D20M020	Gumbel	26.18	-50.36	-48.86	0.371	0.905	0.091		0.75	0.743	0.734	[3.11]

7767

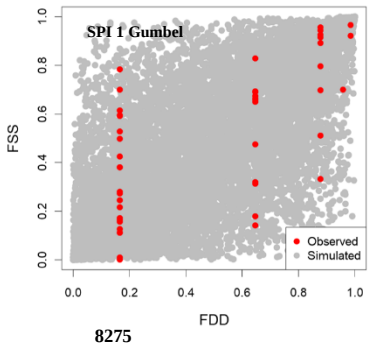

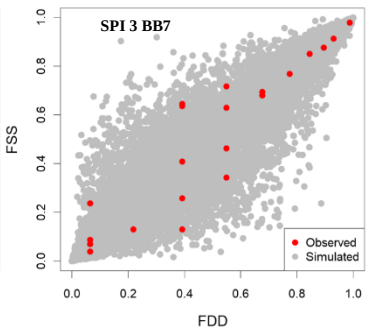

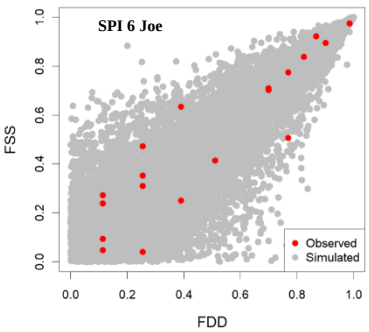

8275

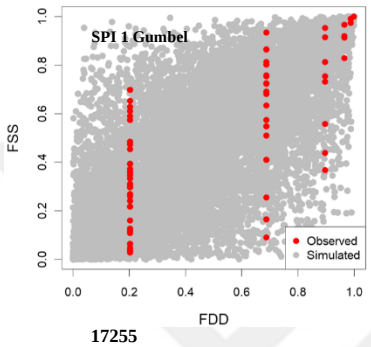

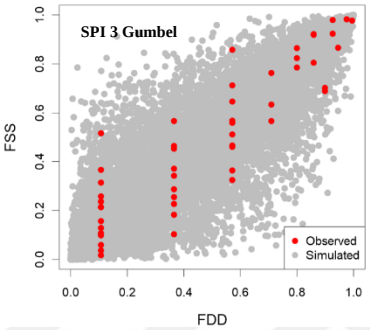

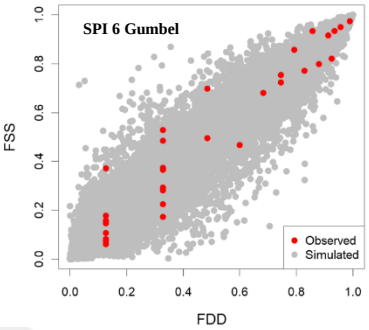

17255

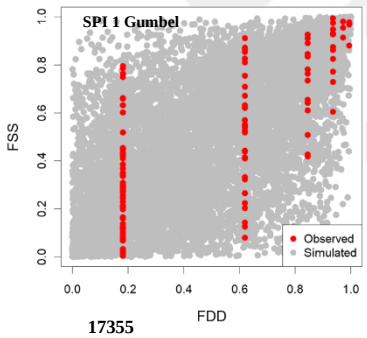

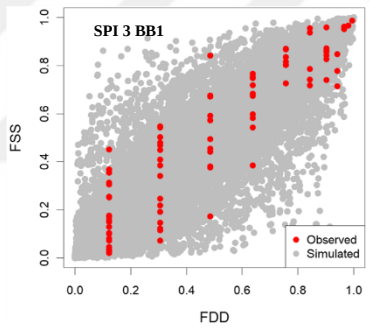

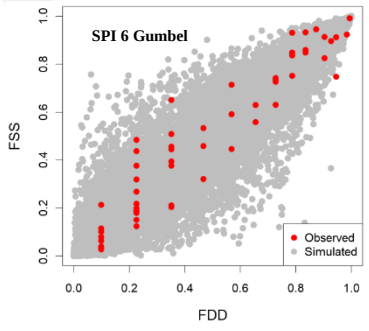

17355

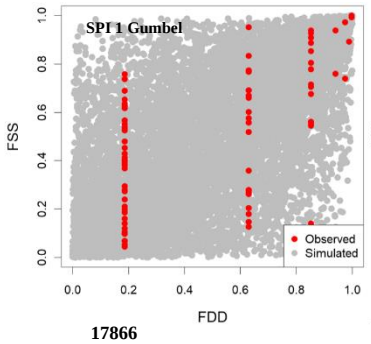

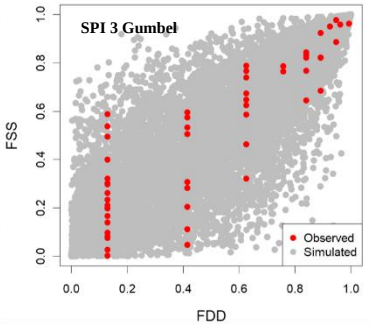

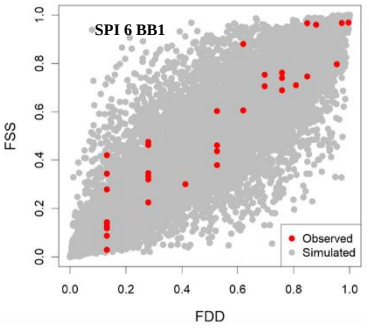

17866

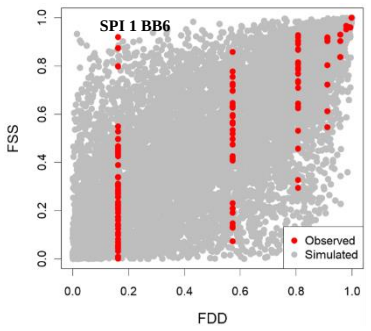

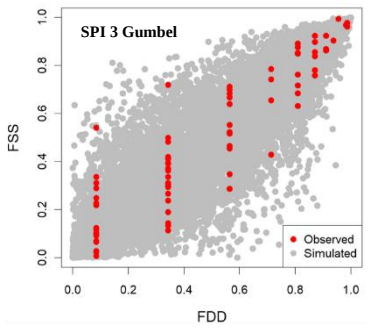

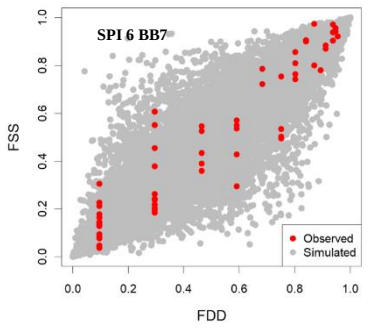

17868

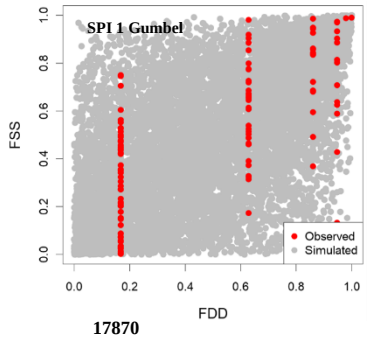

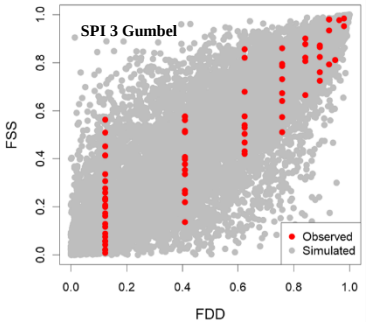

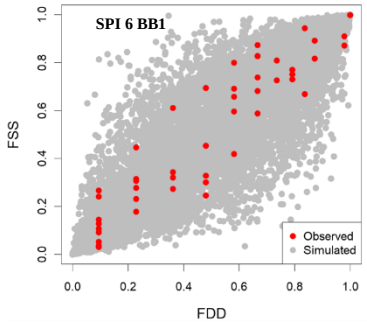

17870

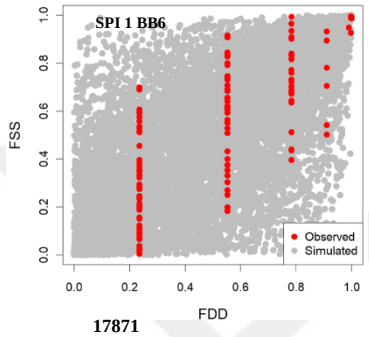

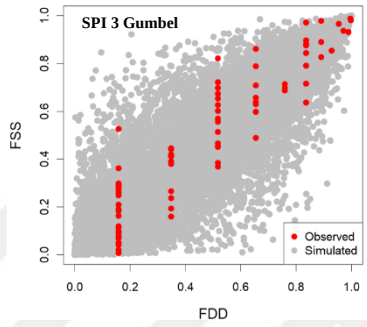

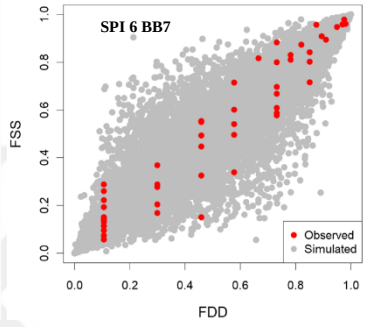

17871

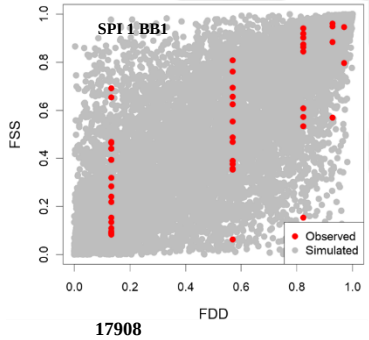

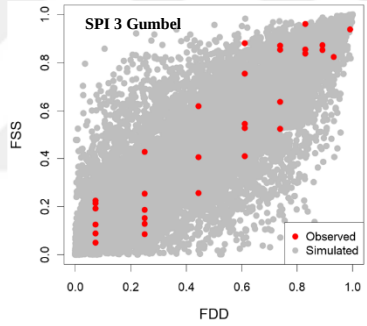

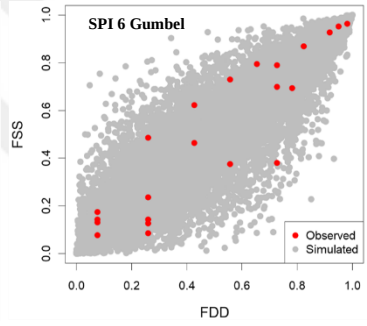

17908

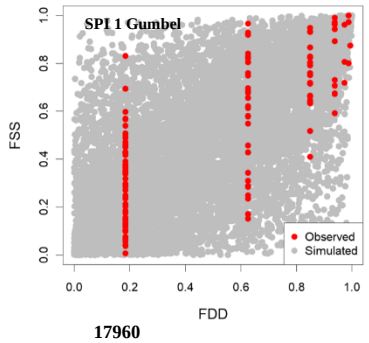

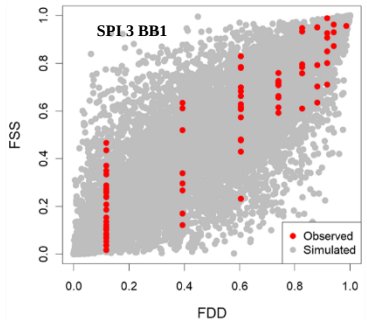

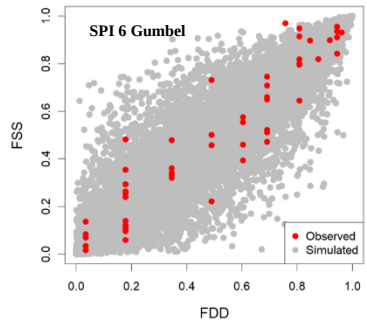

17960

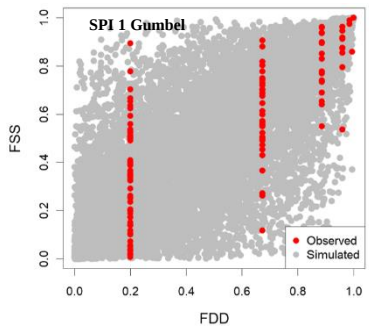

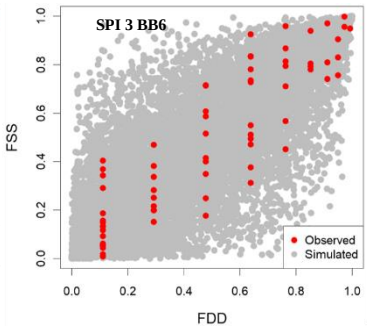

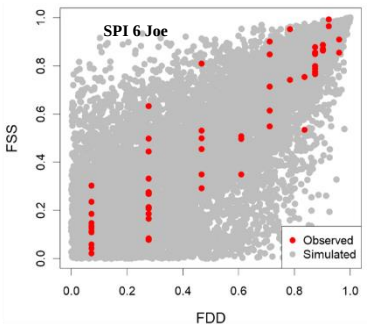

17979

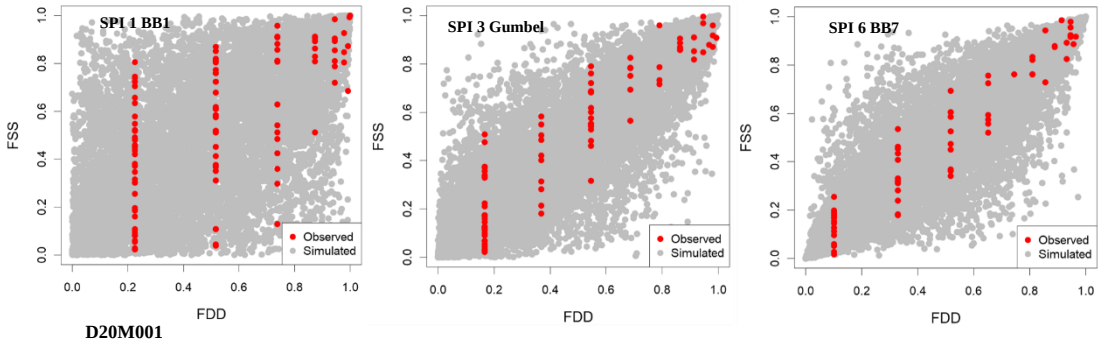

D20M001

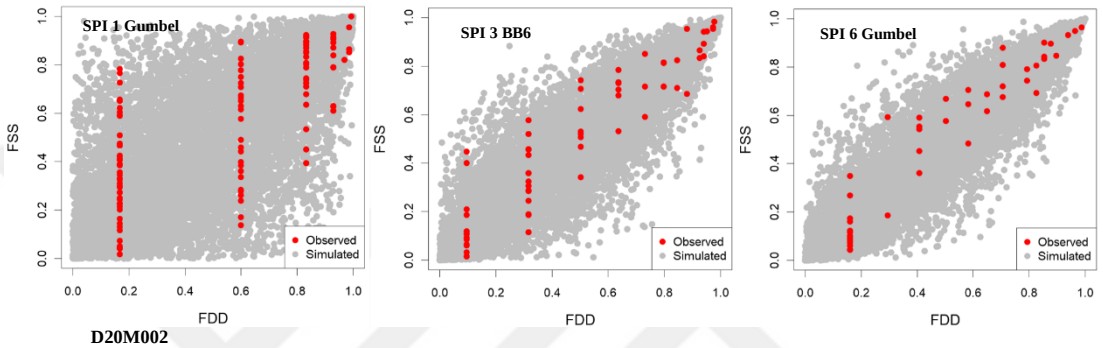

D20M002

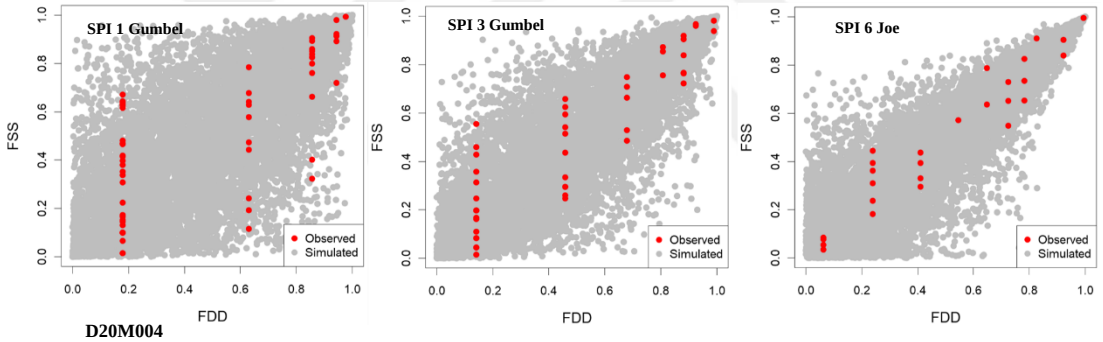

D20M004

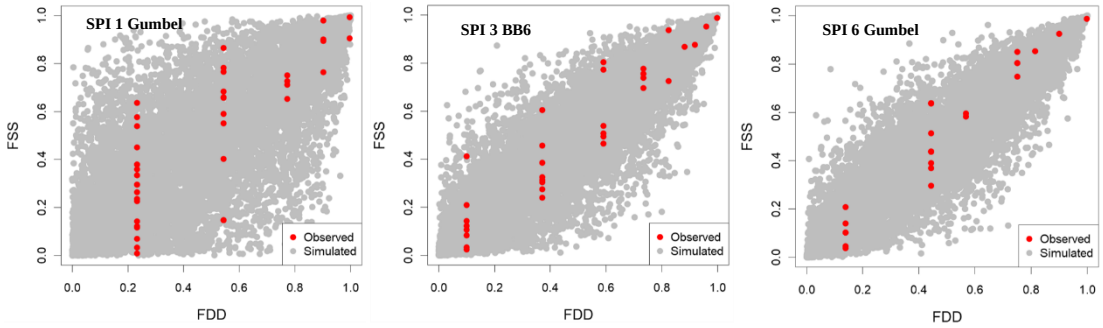

D20M006

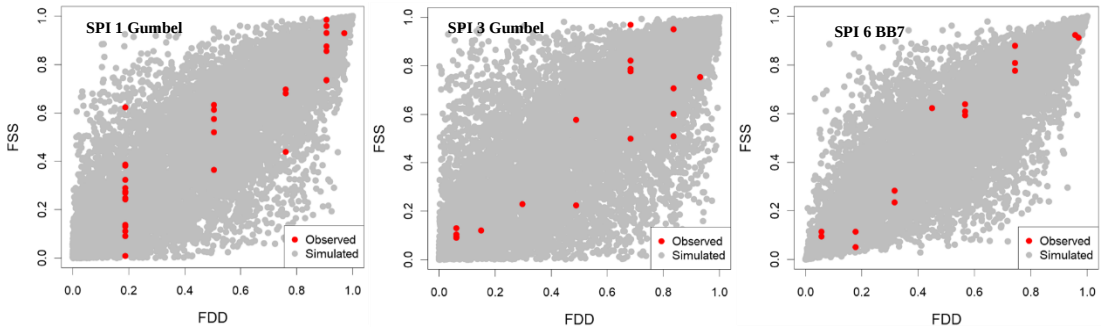

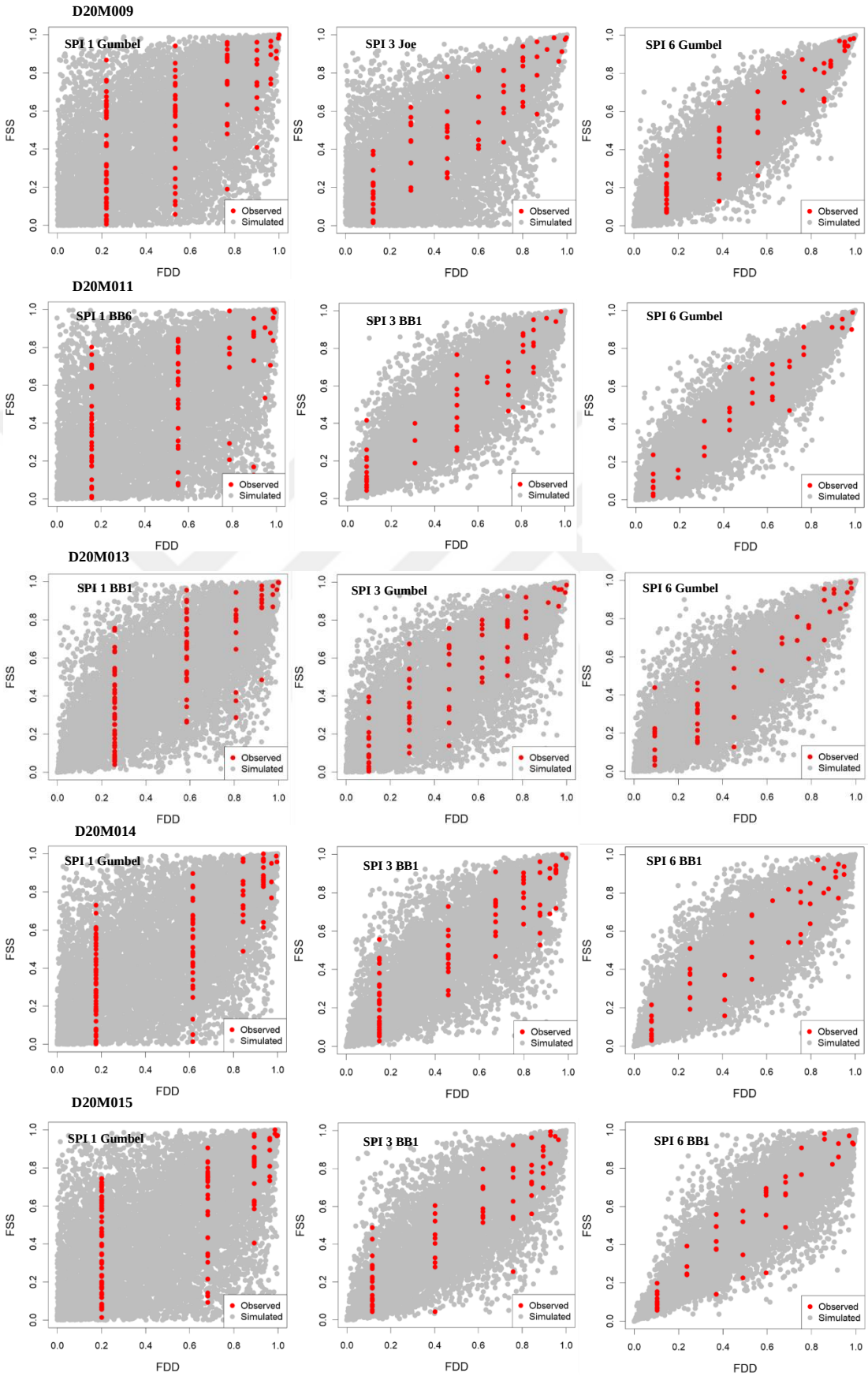
D20M009
SPI 1 Gumbel
SPI 3 Joe
SPI 6 Gumbel
D20M011
SPI 1 BB6
SPI 3 BB1
SPI 6 Gumbel
D20M013
SPI 1 BB1
SPI 3 Gumbel
SPI 6 Gumbel
D20M014
SPI 1 Gumbel
SPI 3 BB1
SPI 6 BB1
D20M015
SPI 1 Gumbel
SPI 3 BB1
SPI 6 BB1
FSS
FDD
Observed
Simulated

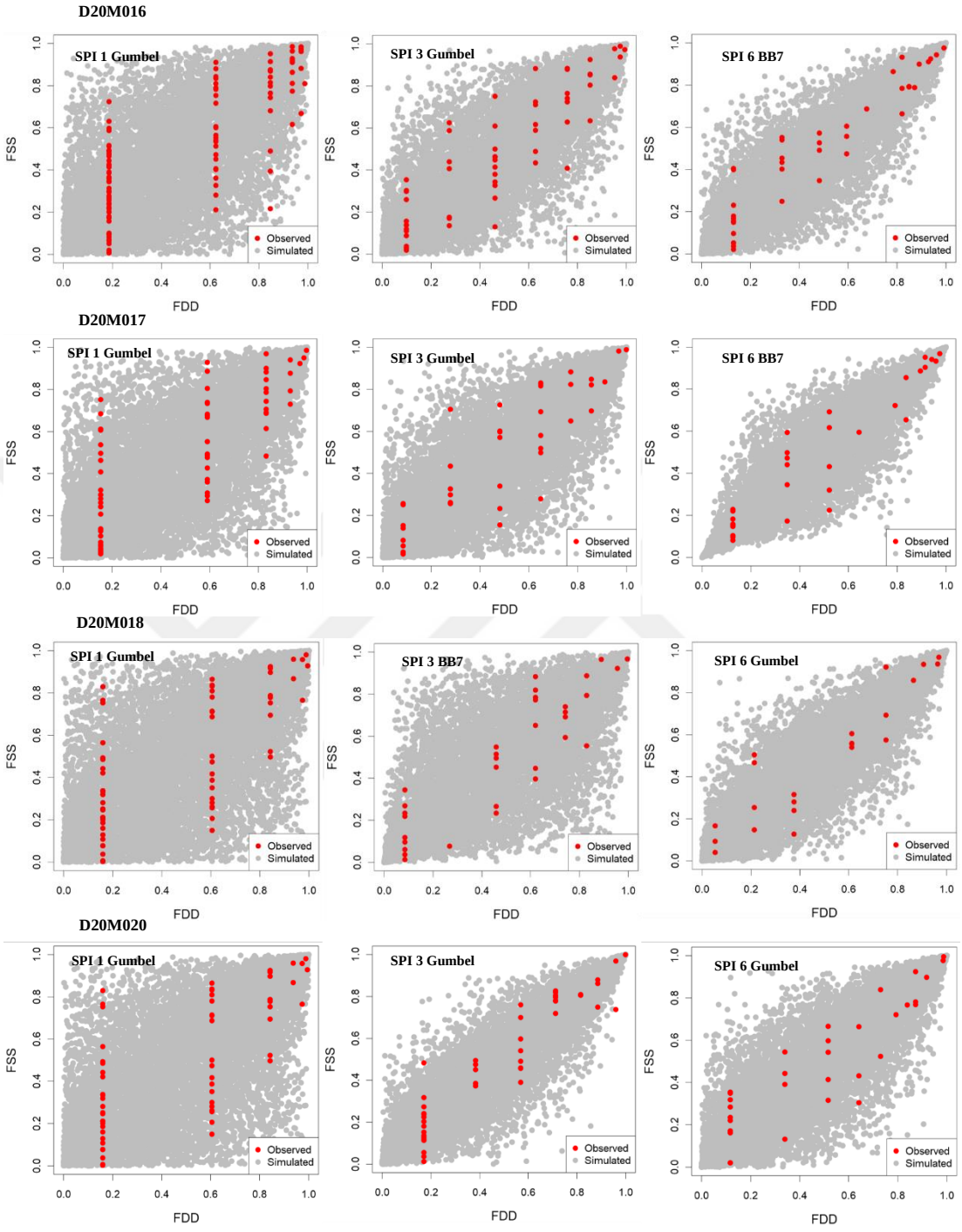

Figure 7.5 Comparison of simulated random data (grey data) and observed data (red data) for all stations at different time scales

7.5 Conditional Probabilities of Drought Characteristics

Conditional probabilities of droughts characteristics are crucial for drought managements. The probability that both the DD and DS simultaneously exceed certain thresholds is of great importance knowledge for government agencies and environmental etc., to enhance water systems management under dry conditions. This probability may not be derived using DD and DS separately. In drought frequency analysis, the main goal is not just to identify whether DD and DS simultaneously exceed certain threshold value. The more significant analysis is to determine probability of DD (or DS) given DS (or DD) a certain threshold value (d' or s'). Hence, the related probability may be easily obtained in terms of copulas.

In this section of the study, the conditional DD and DS distributions were obtained from the copula-based bivariate drought distribution. It was evaluated the conditional DS distribution given that DD exceeds a certain threshold d' (Eq. 3.125) or the DD distribution given that DS exceeds a certain threshold s' (Eq. 3.126).

Figure 7.6 indicates the conditional probabilities of DD distribution given that the DS exceeds various thresholds for all stations at different time scales. The figures are useful to identify the probability of DD for given DS. The figures indicated that the conditional probability of drought occurrence increased when the value of drought duration and severity increased. Referring to station 17255 in Fig. 7.6, the conditional probabilities for DD less than 3 and 5 months given a specific severity exceeding 3 calculated as 0.32 and 0.796 at SPI 1-month time scale. For SPI 3- and 6-month time scales, the conditional probabilities for the same DD as months and given a specific exceeding 3, was observed 0.06 and 0.37 (for SPI 3-month), 0.02 and 0.153 (for SPI 6-month), respectively. These results showed that a 32% and 79% change of drought occurrence under that specific condition at SPI 1-month time scale. This information is much useful when somebody want to estimate the conditional probabilities of drought duration given a specific drought severity exceeding a certain value for any water supply system projects and hydrologic structure etc.,. the probabilities for drought duration less than 4 month given a specific severity exceeding 4 for each station was shown in Table 7.10.

The probabilities of stations 17979 and D20A006 were evaluated much less compared to other stations for SPI 1-month time scale. The conditional probabilities are equal to

0.271 (17979) and 0.182 (D20A006) respectively. The higher probabilities of drought episodes with severity exceeding 4 and duration less than 4 month was observed for stations 8275 (0.513), D20A015 (0.511) and D20A020 (0.561) for SPI 1-month time scale.

For SPI 3-month time scale, As for station 7767 in Table 7.10, given an severity ≥ 4, the conditional probability of drought episode with duration ≤ 4 month was observed much less as 0.007 . In general view, the condition probabitities ranges from 0.01 to 0.3. The higher conditional probabilities under that specific condition, was found stations D20A006 (0.230), D20A014 (0.277) and D20A015 (0.222).

For SPI 6-month time scale, the result for station 7767 in Table 7.10, showed a conditional probability of 0.018 for drought duration less than 4 month, when the given severity exceeds 4. Station 7767 revealed much less the conditional probability compared to other stations. The conditional probabilities under that specific condition, ranges from 0.01 to 0.15. the results of station 17960 presented as the higher conditional probability calculated as 0.152.

Table 7.10 The conditional probability of DD ≤ 4 month for given DS ≥ 4

Station	SPI 1	SPI 3	SPI 6
7767	0.450	0.007	0.018
8275	0.513	0.152	0.044
17255	0.391	0.102	0.032
17355	0.365	0.135	0.083
17866	0.322	0.149	0.105
17868	0.393	0.199	0.054
17870	0.374	0.095	0.054
17871	0.325	0.089	0.048
17908	0.449	0.017	0.047
17960	0.475	0.178	0.152
17979	0.271	0.121	0.053
D20A001	0.313	0.072	0.045
D20A002	0.412	0.183	0.022
D20A004	0.254	0.100	0.035
D20A006	0.182	0.230	0.044
D20A009	0.304	0.048	0.066
D20A011	0.349	0.178	0.086
D20A013	0.305	0.083	0.072
D20A014	0.393	0.277	0.077
D20A015	0.511	0.222	0.039
D20A016	0.398	0.118	0.071
D20A017	0.391	0.129	0.067

D20A018	0.309	0.119	0.041
D20A020	0.561	0.063	0.098

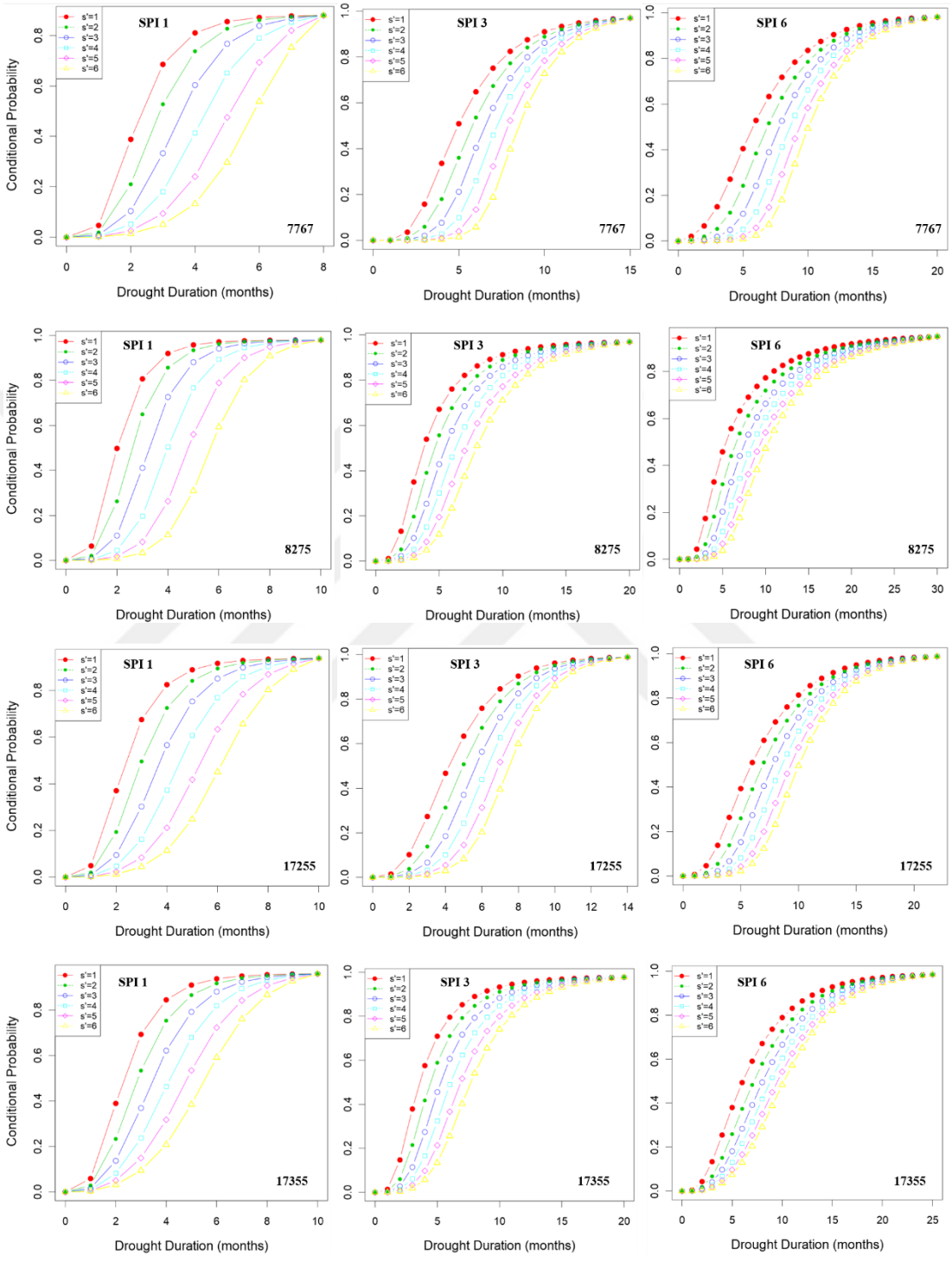

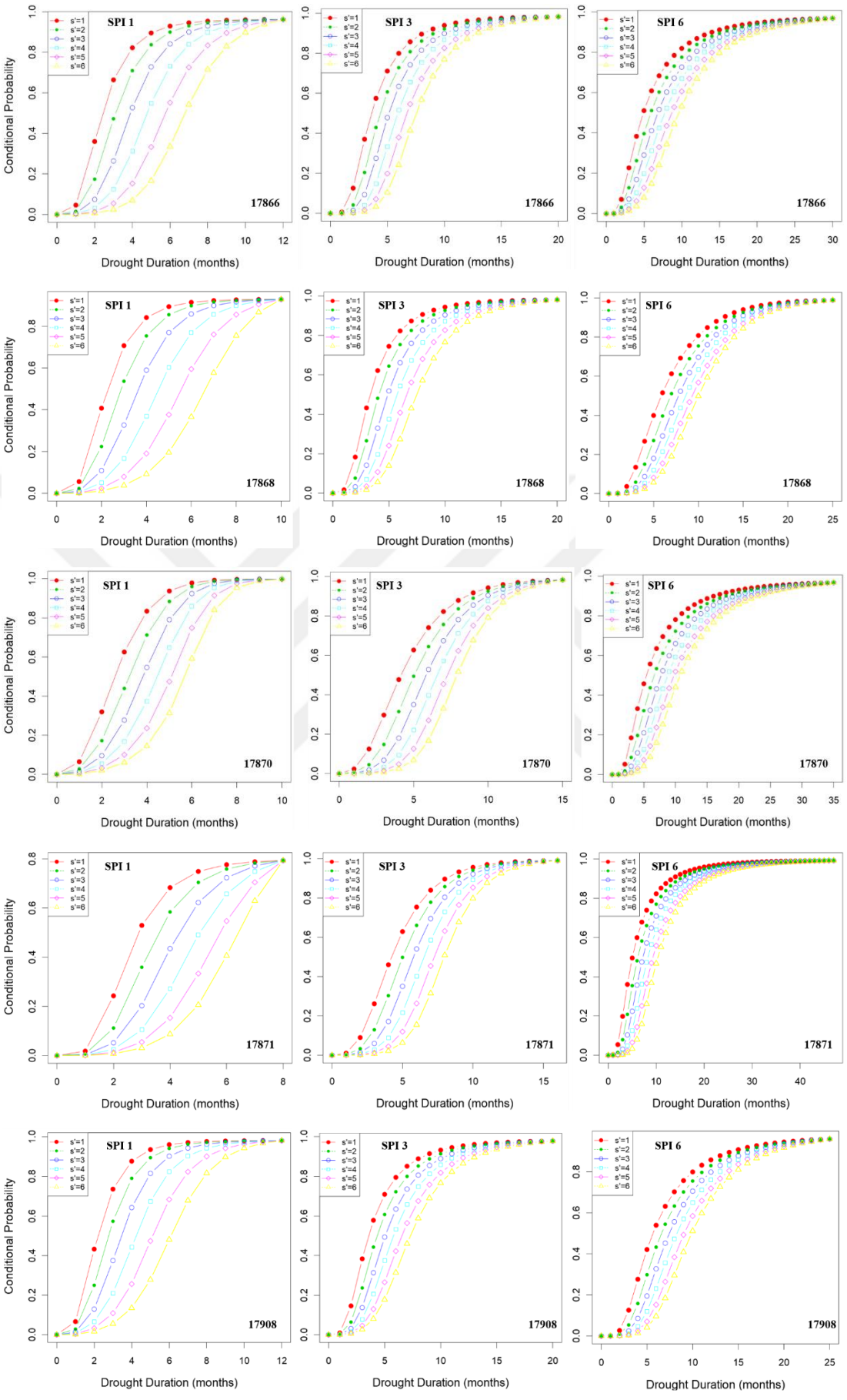
SPI 1
SPI 3
SPI 6
s'=1
s'=2
s'=3
s'=4
s'=5
s'=6
Conditional Probability
Drought Duration (months)
17866
17868
17870
17871
17908

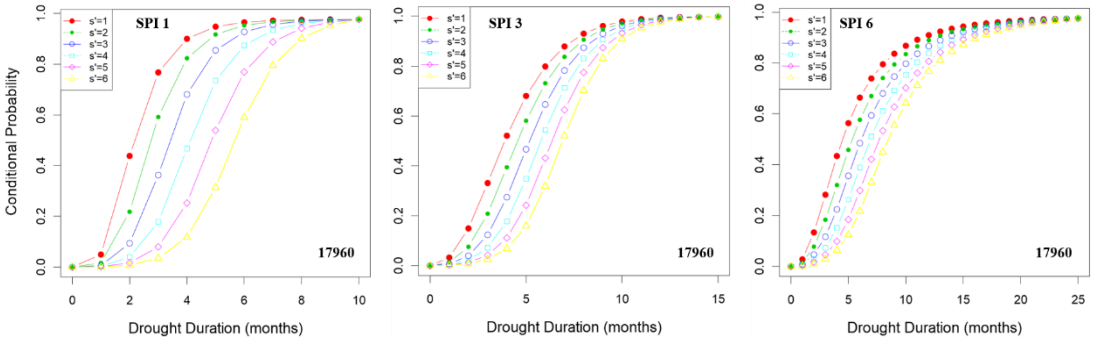
SPI 1
SPI 3
SPI 6
s'=1
s'=2
s'=3
s'=4
s'=5
s'=6
Conditional Probability
Drought Duration (months)
17960

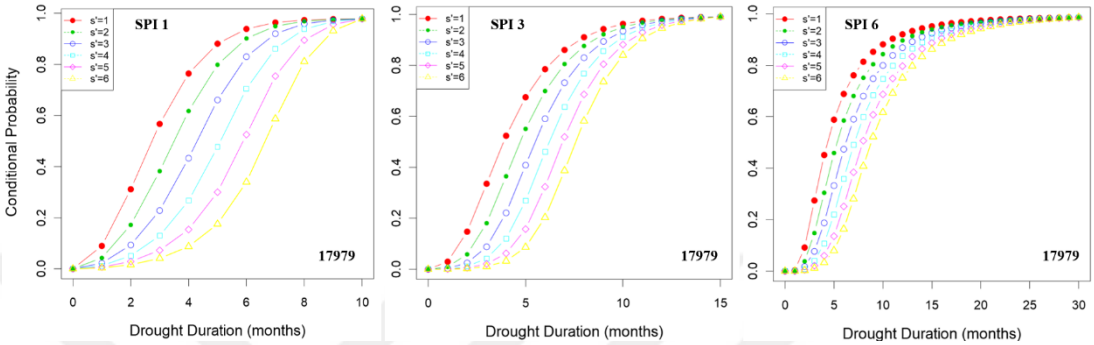
SPI 1
SPI 3
SPI 6
s'=1
s'=2
s'=3
s'=4
s'=5
s'=6
Conditional Probability
Drought Duration (months)
17979

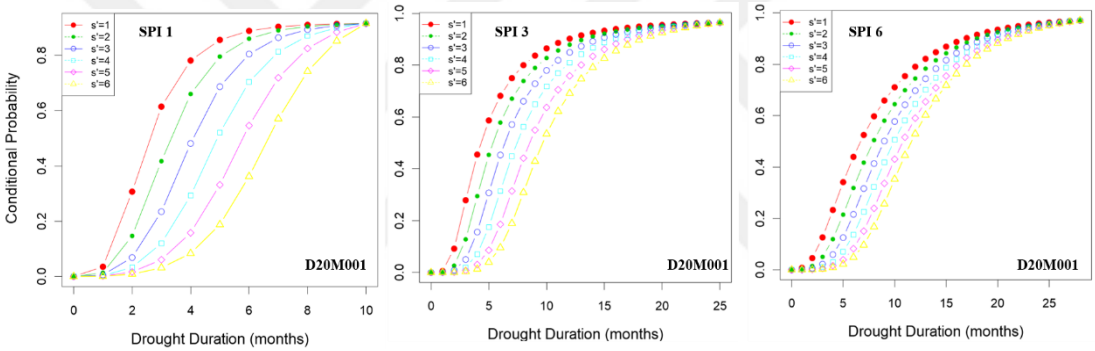
SPI 1
SPI 3
SPI 6
s'=1
s'=2
s'=3
s'=4
s'=5
s'=6
Conditional Probability
Drought Duration (months)
D20M001

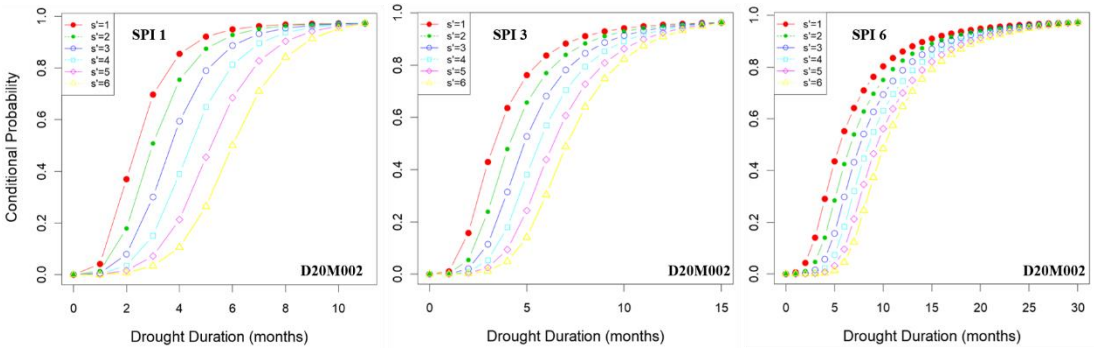
SPI 1
SPI 3
SPI 6
s'=1
s'=2
s'=3
s'=4
s'=5
s'=6
Conditional Probability
Drought Duration (months)
D20M002

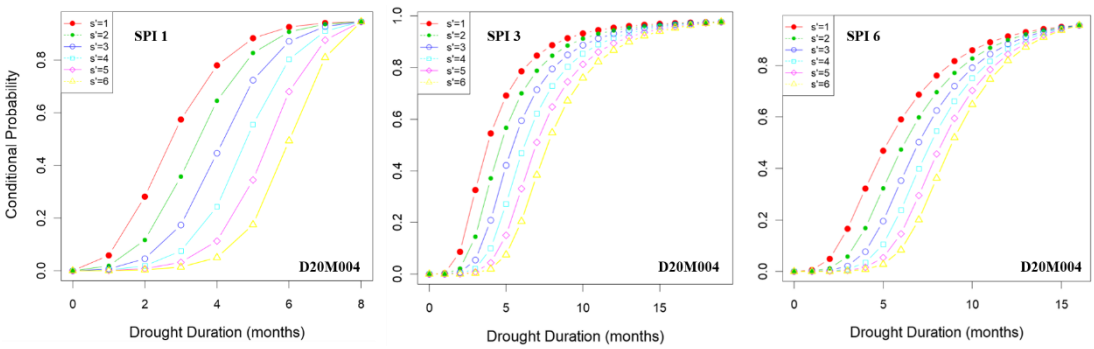
SPI 1
SPI 3
SPI 6
s'=1
s'=2
s'=3
s'=4
s'=5
s'=6
Conditional Probability
Drought Duration (months)
D20M004

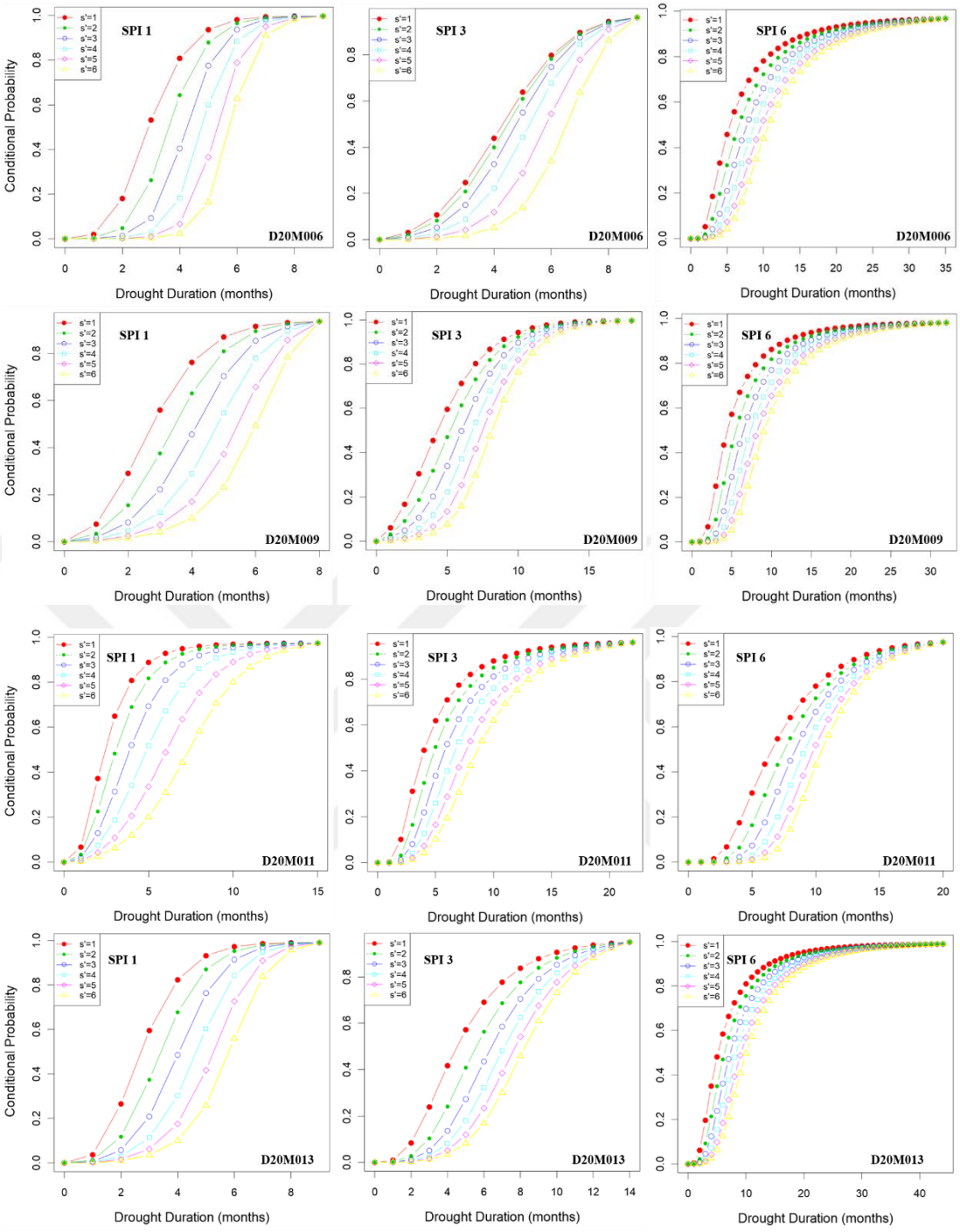
SPI 1
SPI 3
SPI 6
D20M006
D20M009
D20M011
D20M013
s'=1
s'=2
s'=3
s'=4
s'=5
s'=6
Conditional Probability
Drought Duration (months)

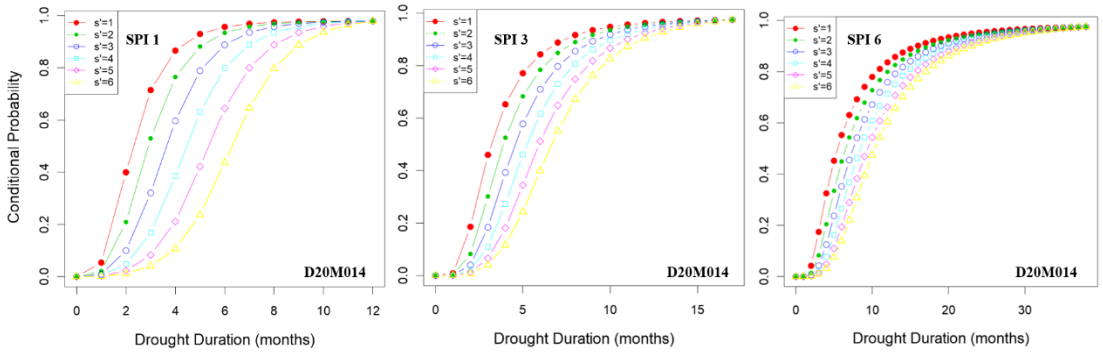
SPI 1
SPI 3
SPI 6
D20M014
Conditional Probability
Drought Duration (months)

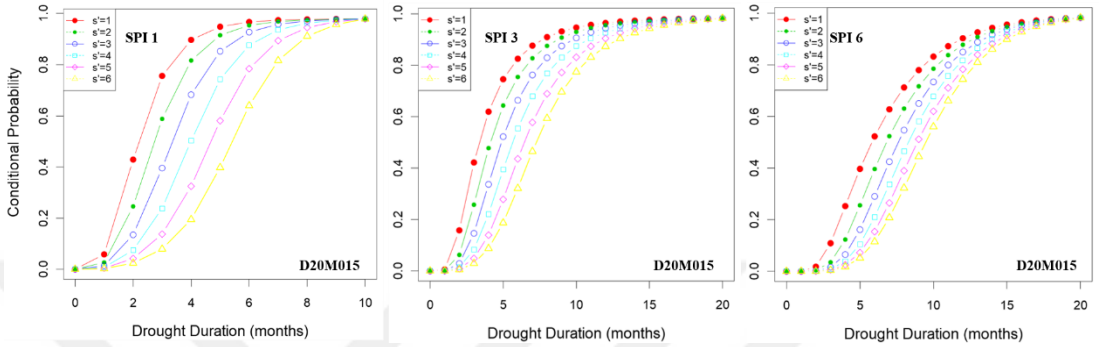
SPI 1
SPI 3
SPI 6
D20M015
Conditional Probability
Drought Duration (months)

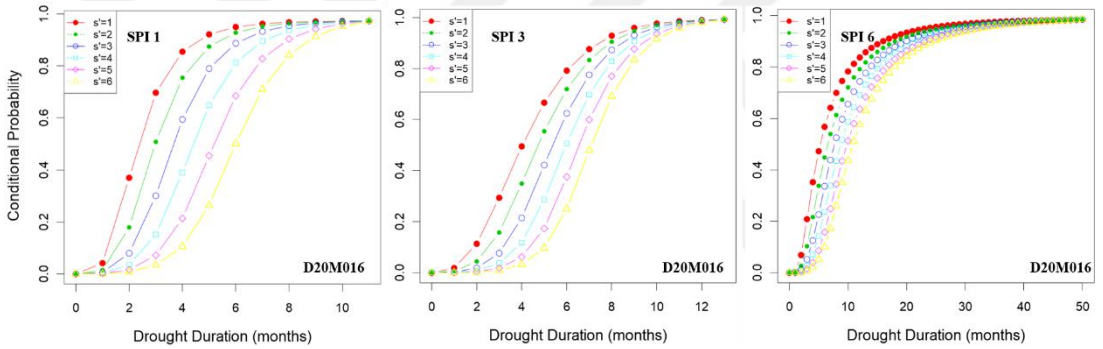
SPI 1
SPI 3
SPI 6
D20M016
Conditional Probability
Drought Duration (months)

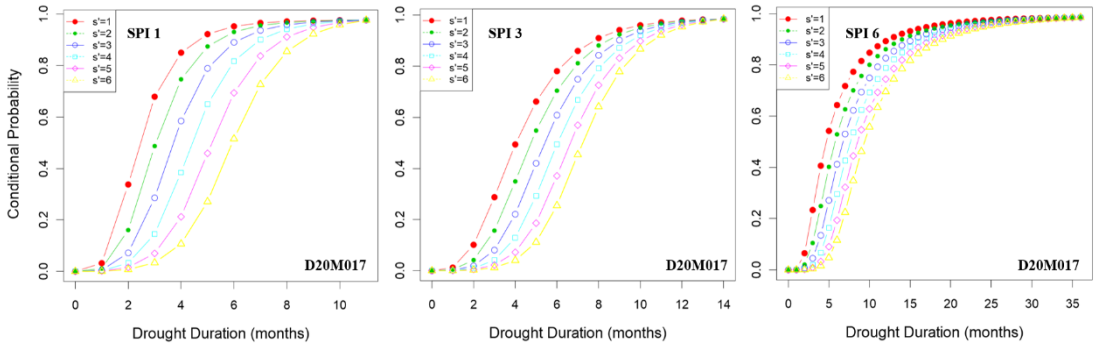
SPI 1
SPI 3
SPI 6
D20M017
Conditional Probability
Drought Duration (months)

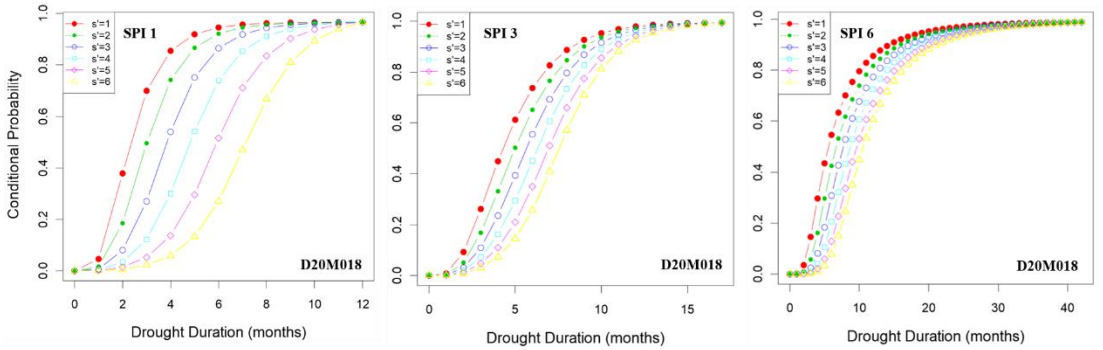
SPI 1
SPI 3
SPI 6
D20M018
Conditional Probability
Drought Duration (months)

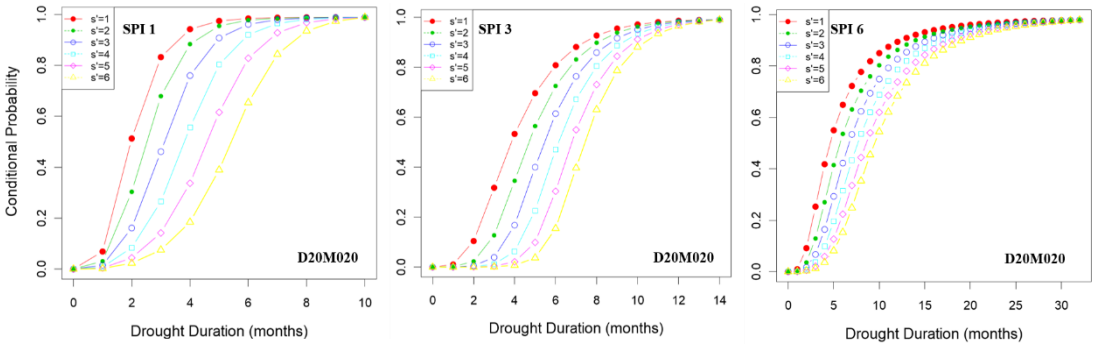

Figure 7.6 The conditional distribution of drought duration given drought severity exceeding a certain value, s′

Figure 7.7 shows the conditional probabilities of DS distribution given that the DD exceeds various thresholds for all stations at different time scales. Referring to station 17255 in Fig. 7.7, the conditional probabilities for DS less than 3 and 5, given a specific duration exceeding 3 month calculated as 0.459 and 0.82 at SPI 1-month time scale. For SPI 3- and 6-month time scales, the conditional probabilities for the same DS, given a specific drought exceeding 3 month, was observed 0.367 and 0.639 (for SPI 3-month), 0.325 and 0.542 (for SPI 6-month), respectively. This results showed that a 45.9% and 82% change of drought occurrence under that specific conditions at SPI 1-month time scale. The probabilities for drought severity less than 4, given a specific drought exceeding 4 month for each station was shown in Table 7.11.

The probabilities of stations 8275 and 17960 were evaluated much less compared to other stations for SPI 1-month time scale. The conditional probabilities are equal to 0.280 (8275) and 0.295 (17960), respectively. The higher probabilities of drought episodes with duration exceeding 4 month and severity less than 4 month was observed for stations 17979 (0.644), D20A009 (0.602) and D20A011 (0.630) for SPI 1-month time scale. The conditional probabilities ranges from 0.2 to 0.68.

For SPI 3-month time scale, As for station 17866 in Table 7.11, given an duration ≥ 4, the conditional probability of drought episode with severity ≤ 4 was observed much less as 0.227. In general view, the condition probabitities ranges from 0.2 to 0.5. The higher conditional probabilities under that specific condition, was found stations 17355 (0.472), 17871 (0.412) and D20A013 (0.477).

For SPI 6-month time scale, the results for stations 7767 and D20A006 in Table 7.11, showed a conditional probabilities of 0.4 and 0.459 respectively, for drought severity less than 4, when the given drought exceeds 4 month. Stations 7767 and D20A006

revealed much higher the conditional probabilities compared to other stations. The conditional probabilities under that specific condition, ranges from 0.2 to 04. The result of station 17355 presented as the less conditional probability calculated as 0.222.

Table 7.11 The conditional probability of DS ≤ 4 month for given DD ≥ 4

Station	SPI 1	SPI 3	SPI 6
7767	0.440	0.380	0.400
8275	0.280	0.288	0.261
17255	0.434	0.365	0.339
17355	0.563	0.472	0.222
17866	0.408	0.227	0.282
17868	0.526	0.264	0.385
17870	0.523	0.347	0.311
17871	0.488	0.412	0.295
17908	0.414	0.279	0.330
17960	0.295	0.329	0.310
17979	0.664	0.350	0.300
D20A001	0.507	0.299	0.314
D20A002	0.321	0.272	0.323
D20A004	0.441	0.265	0.321
D20A006	0.390	0.230	0.459
D20A009	0.602	0.345	0.255
D20A011	0.630	0.329	0.396
D20A013	0.569	0.477	0.298
D20A014	0.430	0.268	0.289
D20A015	0.419	0.321	0.399
D20A016	0.344	0.341	0.292
D20A017	0.342	0.346	0.266
D20A018	0.548	0.245	0.329
D20A020	0.457	0.310	0.333

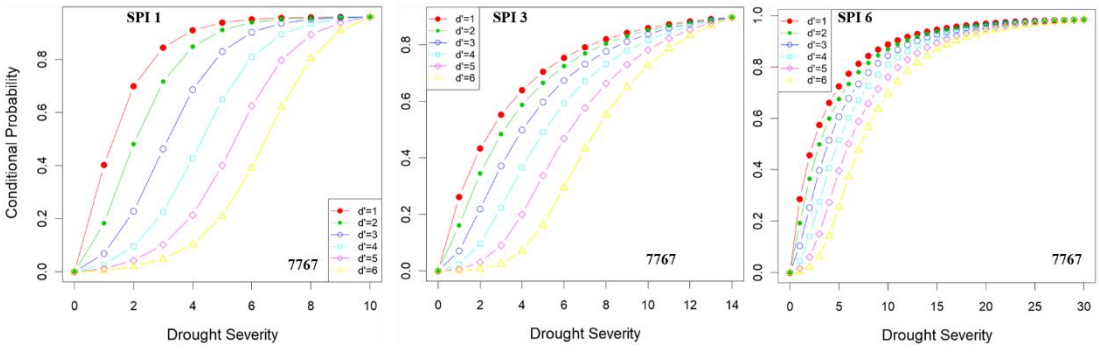

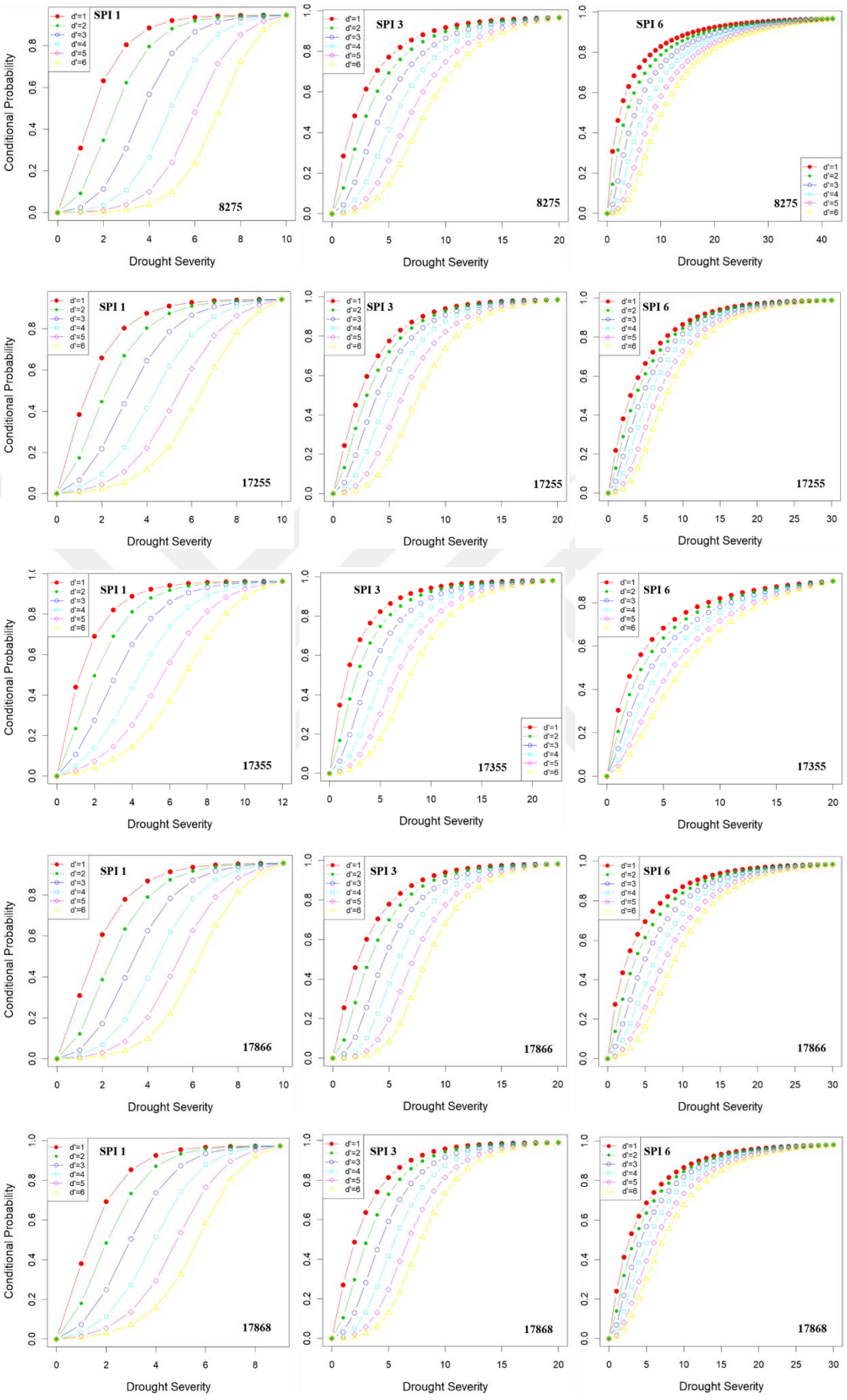
SPI 1
SPI 3
SPI 6
d'=1
d'=2
d'=3
d'=4
d'=5
d'=6
Conditional Probability
Drought Severity
8275
17255
17355
17866
17868

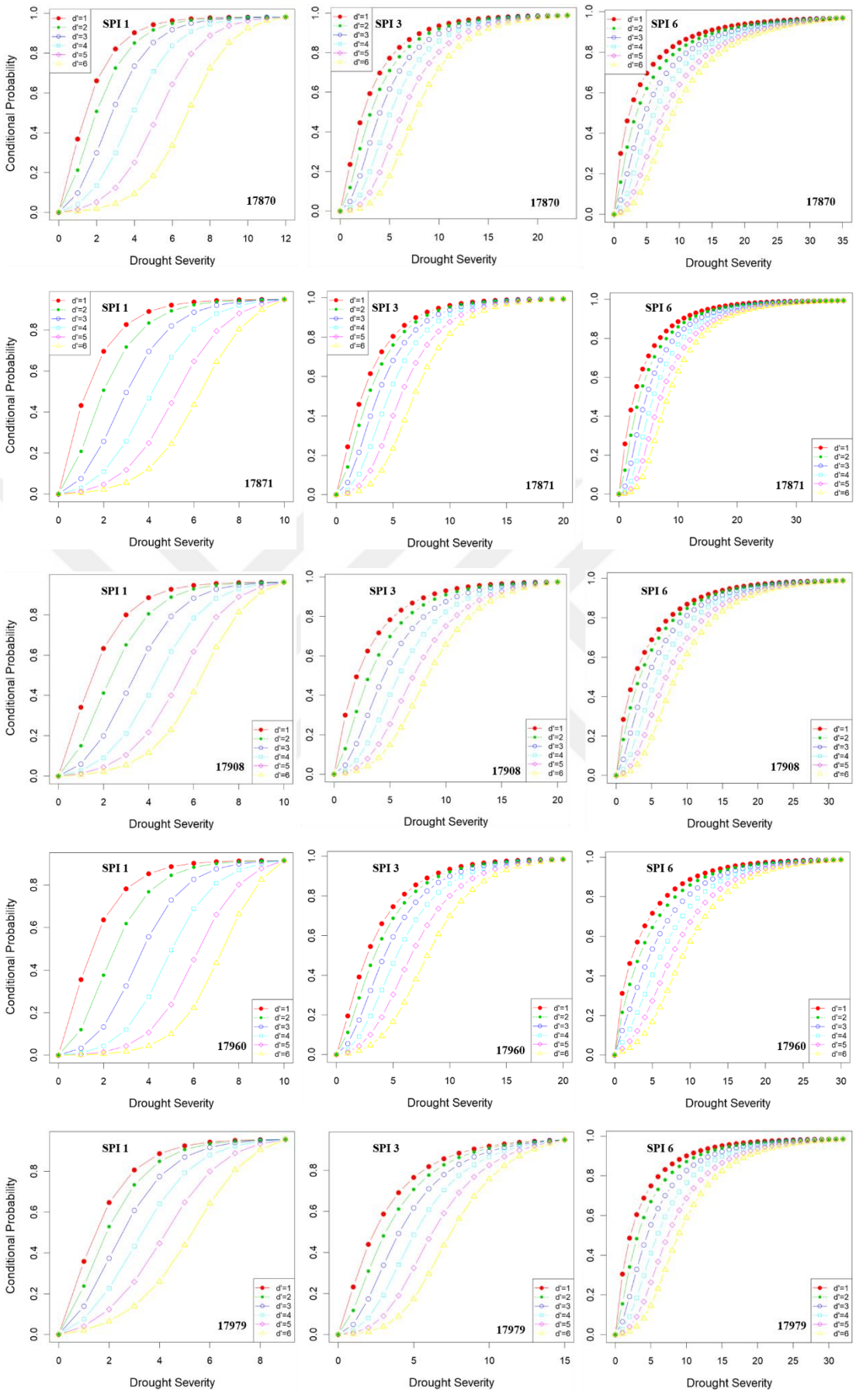
SPI 1
SPI 3
SPI 6
17870
17871
17908
17960
17979
Conditional Probability
Drought Severity
d'=1
d'=2
d'=3
d'=4
d'=5
d'=6

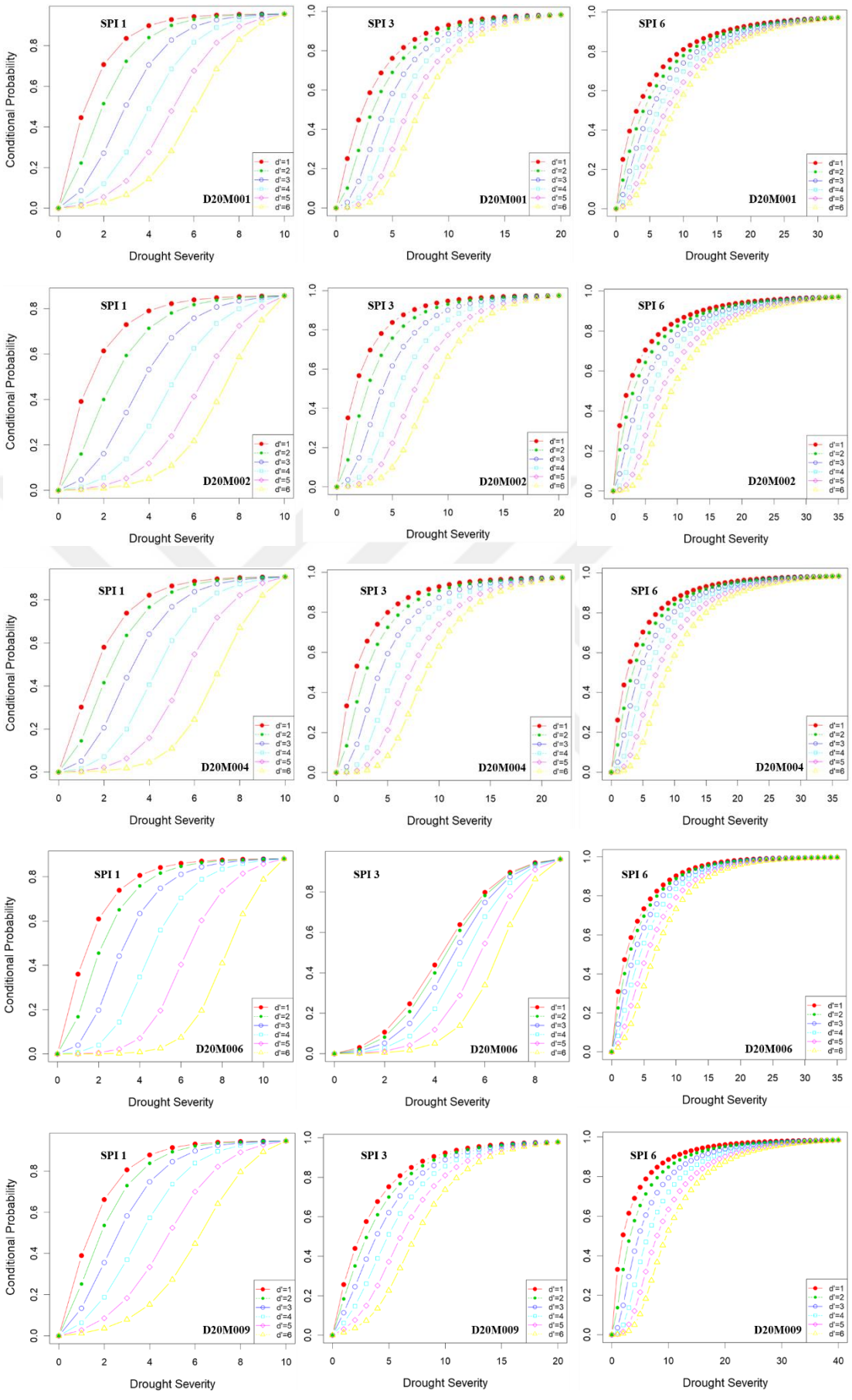
SPI 1
SPI 3
SPI 6
D20M001
D20M002
D20M004
D20M006
D20M009
Conditional Probability
Drought Severity
d'=1
d'=2
d'=3
d'=4
d'=5
d'=6

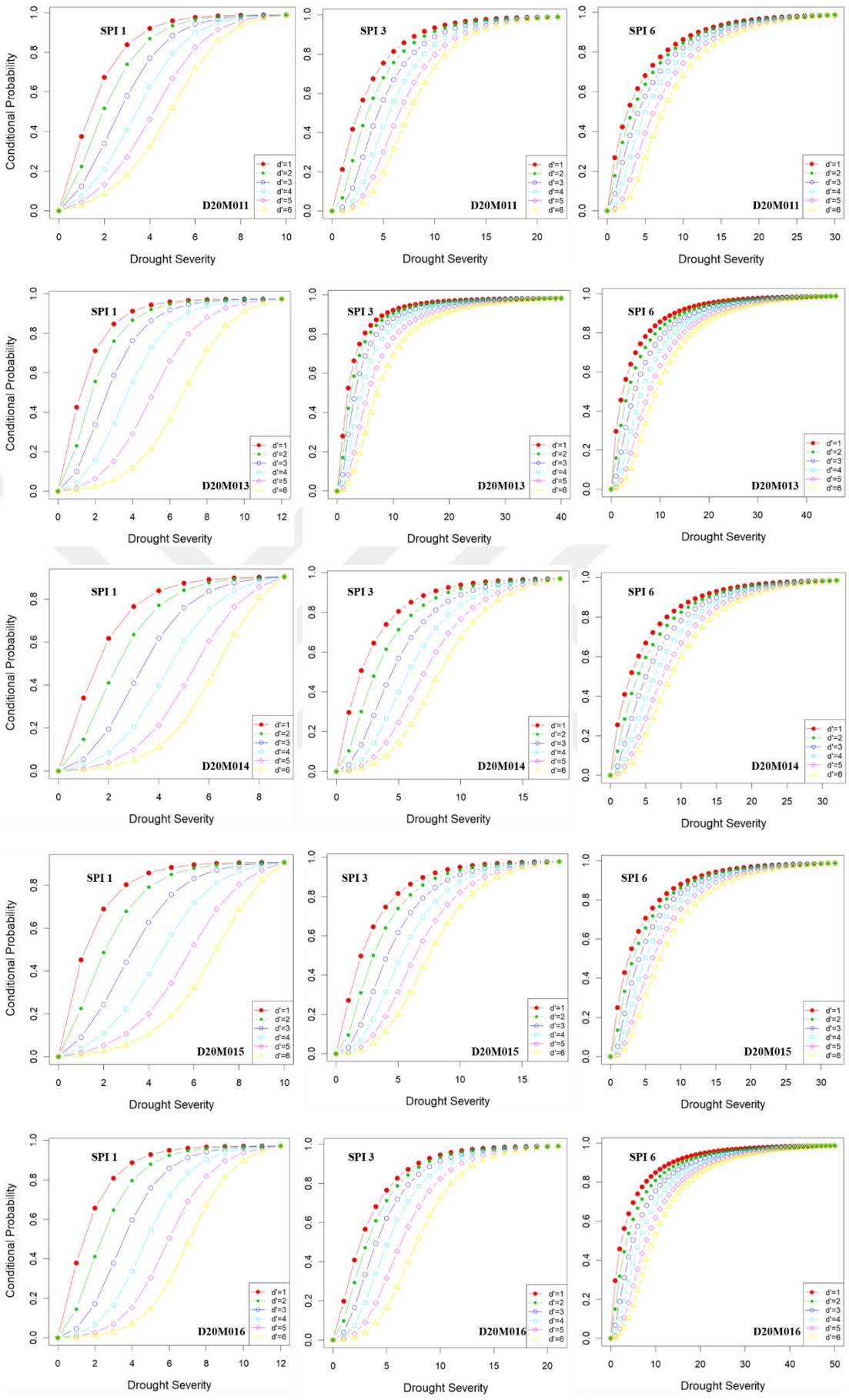
SPI 1
SPI 3
SPI 6
D20M011
D20M013
D20M014
D20M015
D20M016
Conditional Probability
Drought Severity
d'=1
d'=2
d'=3
d'=4
d'=5
d'=6

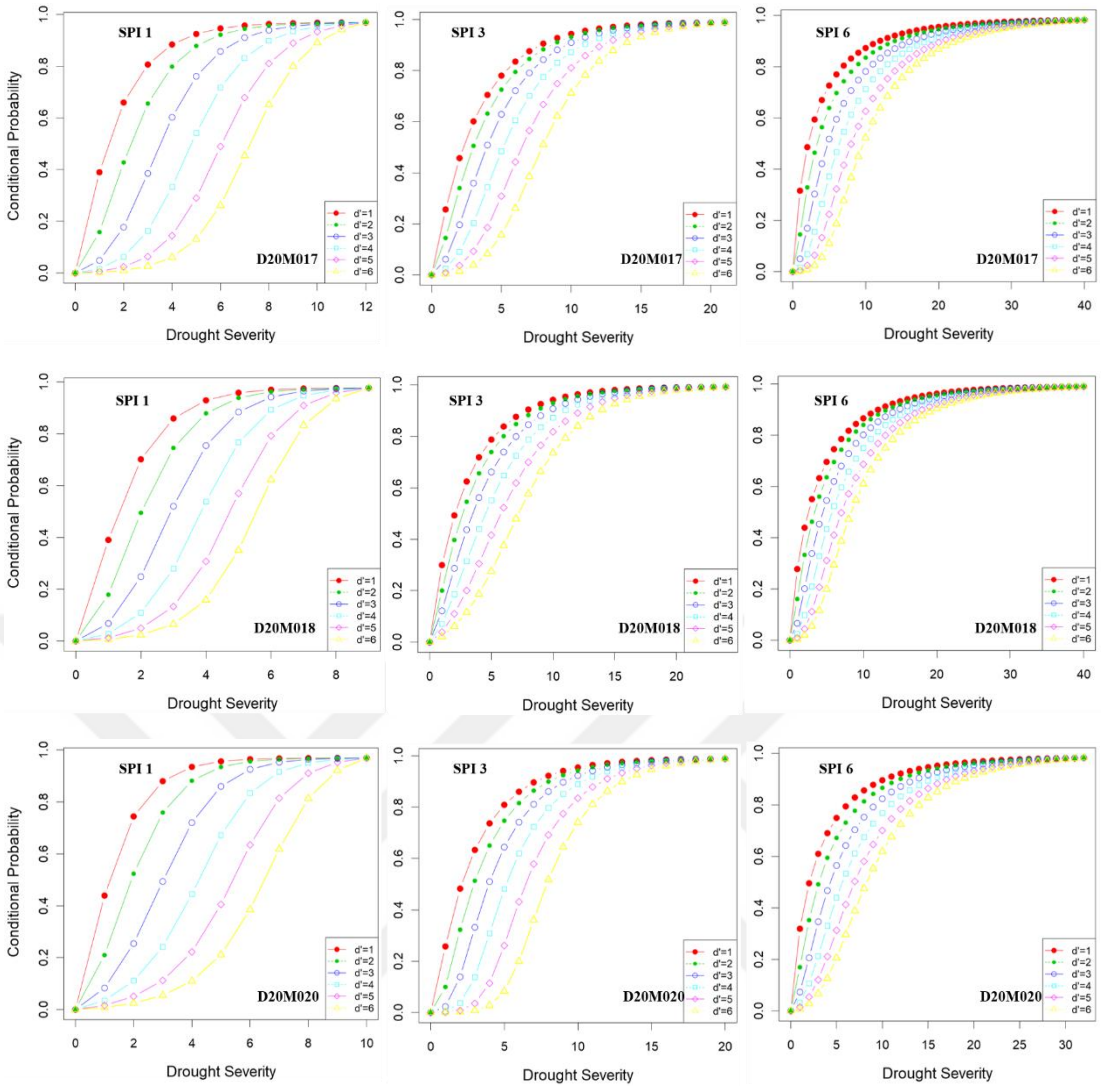

Figure 7.7 The conditional distribution of drought severity given drought duration exceeding a certain value, d′

7.6 Univariate and Bivariate Return Periods of Drought Characteristics

After obtaining the best-fitted copula families for the drought characteristics (DD and DS), the following step is to evaluate univariate (T_D, T_S) and bivariate (T_{DS}, T'_{DS}) return periods explained their procedure in Chapter 3. The estimation of return periods of drought characteristic under drought conditions, is of great importance in the management and planning of water systems. Univariate (T_D, T_S) return periods of drought characteristics can be obtained using equation 3.125 and 3.126. Station 17255 SPI 3-month time scale for the calculation procedure is given an example in detail below. BB1 copula type is selected the best-fitted copula among copula families as follows;

$$F_{D,S}(d,s) = C(F_D(d), F_S(s))$$

$$= \left[1 + [(F_D(d)^{-0.12} - 1)^{2.84} + (F_S(s)^{-0.12} - 1)^{2.84}]^{\frac{1}{2.84}}\right]^{-\frac{1}{0.12}} \quad (7.1)$$

where $F_D(d)$ and $F_S(s)$ represents the cumulative drought duration and severity distribution functions, respectively. The Weibull and Gamma distributions are found as the best marginal distributions for drought duration and severity, respectively,

$$F_D(d) = 1 - e^{-\left(\frac{d}{1.476}\right)^{3.957}} \quad (7.2)$$

$$F_S(s) = \int_0^s \frac{t^{0.176}}{0.279^{0.825}\Gamma(0.825)} e^{-\frac{t}{0.279}} dt \quad (7.3)$$

Univariate return periods of drought duration (T_D) and severity (T_S) are evaluated based on Eq. 3.125 and 3.126, separately. The average drought interarrival time E(L), is estimated from the observed data is 7.41 month for station 17255 at SPI 3-month. Return periods of 10, 20, 50, 100, 200 and 500 years determined by seperate drought duration and severity, according to Eq., are calculated, and summarized in Table 7.12, 7.13 and 7.14 for all stations at different time scales. Copula-based bivariate (T_{DS}, T'_{DS}) return periods, are also defined in Tables 7.12, 7.13 and 7.14 for SPI 1-, 3- and 6-month time scales using the Eq. 3.127 and 3.128.

Like to the joint probability, the joint return period for different drought duration and severity combinations may be illustrated using contour lines. Figure 7.8 shows the contours of the joint drought duration and severity return period for both two cases; (i) T_{DS} (D≥d and S≥s), (ii) T'_{DS} (D≥d or S≥s) at all stations. There are various combinations of duration and severity when adapting the results from the contour plots for a given return period. For example, looking at station 17255 for SPI 1-month in Table 7.12, it is observed that the joint return period of T_{DS} for D≥7.60 month **and** S≥7.68 is estimated as 175.68 years. However, the return period of these values are calculated as 100 years. The joint return period of T'_{DS} for D≥7.60 month **or** S≥7.68 is 69.89 years. When we consider to SPI 3-month, the joint return period T_{DS}, is estimated as 137.95 years for D≥11.90 month **and** S≥16.63. T'_{DS} is 78. 43 years for duration and severity exceeding 11.90 month **or** 16.63, respectively. the return period of these values is calculated as 100 years. For SPI 6-month, the joint return period of T_{DS} (

D≥18.76 month **and** S≥24.35) and T'_{DS} (D≥18.76 month **or** S≥24.35) are estimated as 124.29 years and 83.65 years, respectively. However, the return period is calculated for these values as 100 years. Hence, drought events should be evaluated based on derived copula. Hydrologic facilities in term of water resources system, the significant drought characteristics can be considered as the possible maximum duration likely to happen over the social and economic life.

Univariate return period of station 17979 are calculated as 10 years (T_{DS} = 19.21 years, T'_{DS} = 6.76 years) for D = 5.45 and S = 4.48 at SPI 1-month time scale (Eq. 3.122 and 3.123). the drought duration is observed the highest value among used stations. The highest duration for 20, 50, 100, 200 and 500 return period are found at station D20M011 for SPI 1-month. However, the highest severities are observed as 5.15, 6.22, 7.64 and 8.71 at station D20M017 for 10, 20, 50 and 100 years return period, respectively. 200 and 500 years return period are obtained the highest severities as 9.89 and 11.42 for station D20M016, respectively.

For SPI 3-month time scale, the highest drought durations are observed 10.17, 13.50, 18,68, 23.24, 28.43 and 36.35 month for 10, 20, 50, 100, 200 and 500 return periods at station D20M001, respectively. While the highest severity are detected at station 7767 as 9.55 for 10 years return period, D20M013 are found the highest severities as 13.81, 21.65, 29.34, 38.84 and 54.68 for 20, 50, 100, 200 and 500 year return periods, respectively. When focused on joint return period for station D20M013, the joint return period of T_{DS} (D≥13.95 month **and** S≥29.34) and T'_{DS} (D≥13.95 month **or** S≥29.34) are estimated as 139.78 years and 77.85 years, respectively. However, the return period is calculated for these values as 100 years.

For SPI 6-month time scale, the highest drought duration is evaluated as 14.67, 19.35 and 26.65 month at station D20M018 for 10, 20 and 50 years return period, respectively. However, D20M016 is found the highest duration as 35.69, 44.58 and 57.41 month for 100, 200 and 500 return period, respectively. While the highest drought severity is observed at station D20M018 as 14.70 for 10 years return period, 8275 is found the highest drought severities as 19.79, 30.51, 40.03, 50.56 and 65.96 values for 20, 50, 100, 200 and 500 return periods. The joint return period of T_{DS} (D≥31.87 month **and** S≥40.03) and T'_{DS} (D≥31.87 month **or** S≥40.03) are estimated as

119.22 years and 86.12 years, respectively. However, the return period is calculated for these values as 100 years.

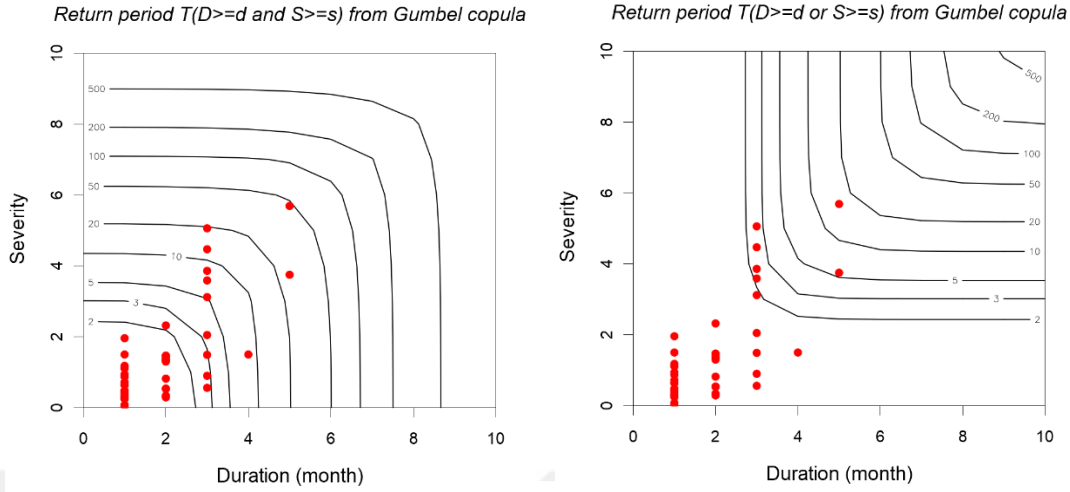

7767 SPI 1-month

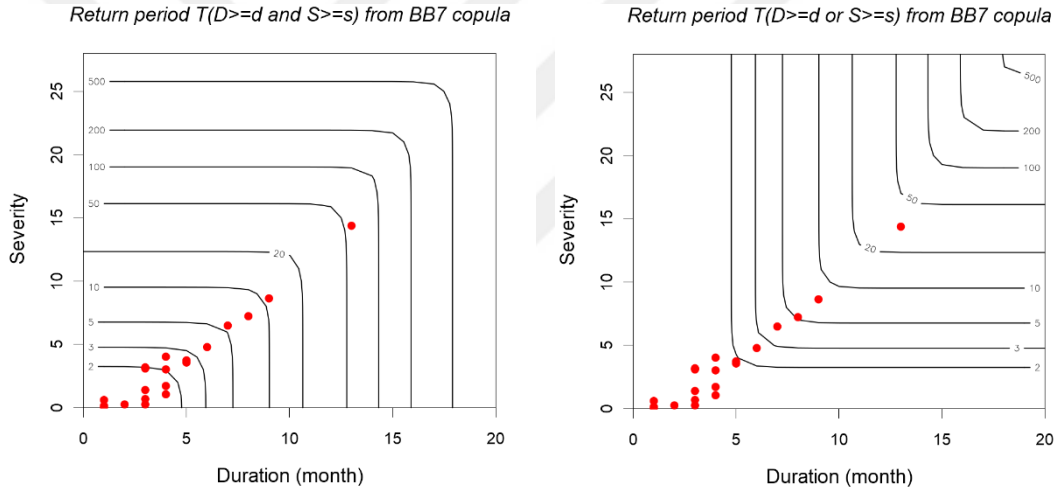

7767 SPI 3-month

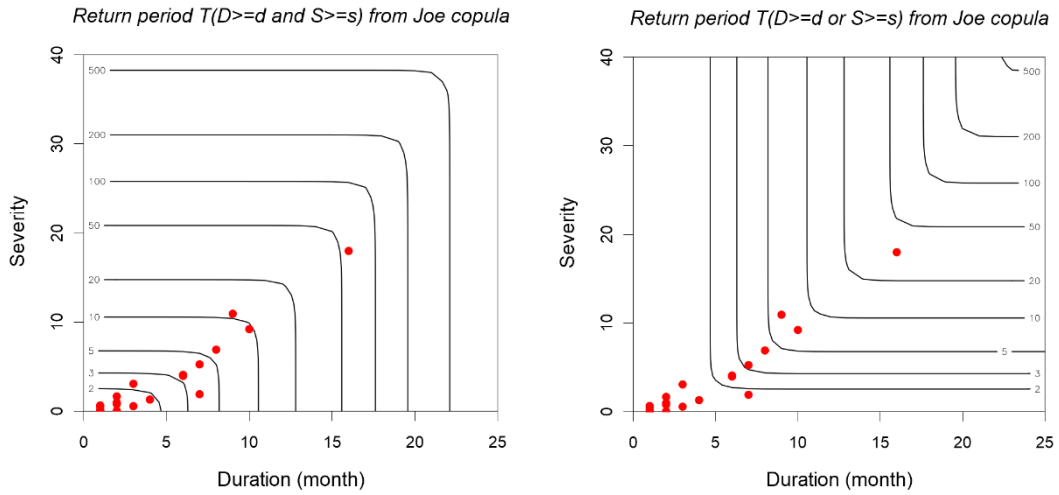

7767 SPI 6-month

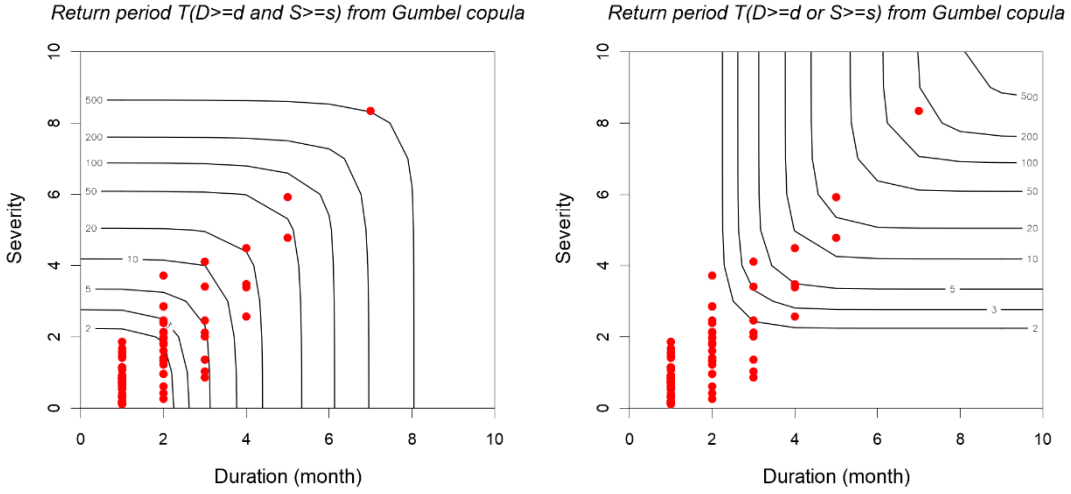

8275 SPI 1-month

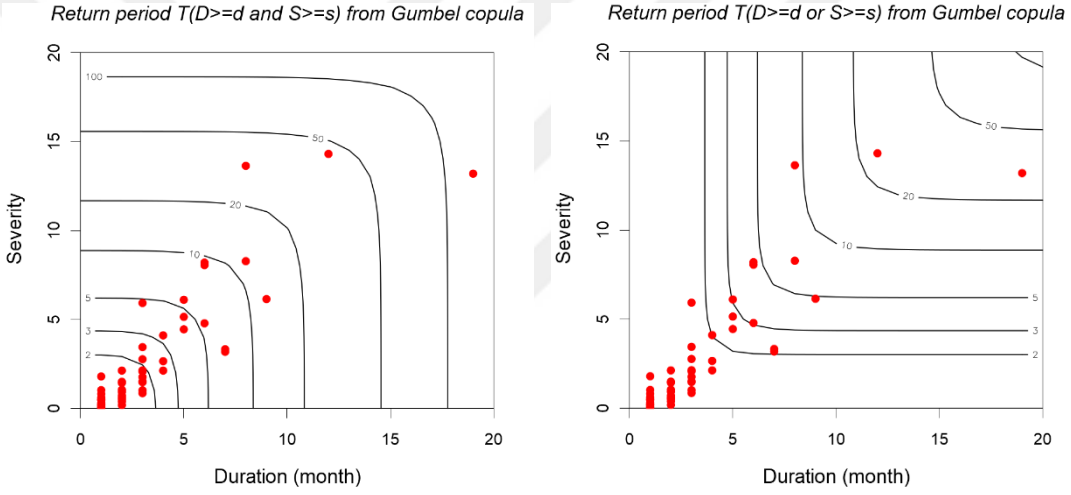

8375 SPI 3-month

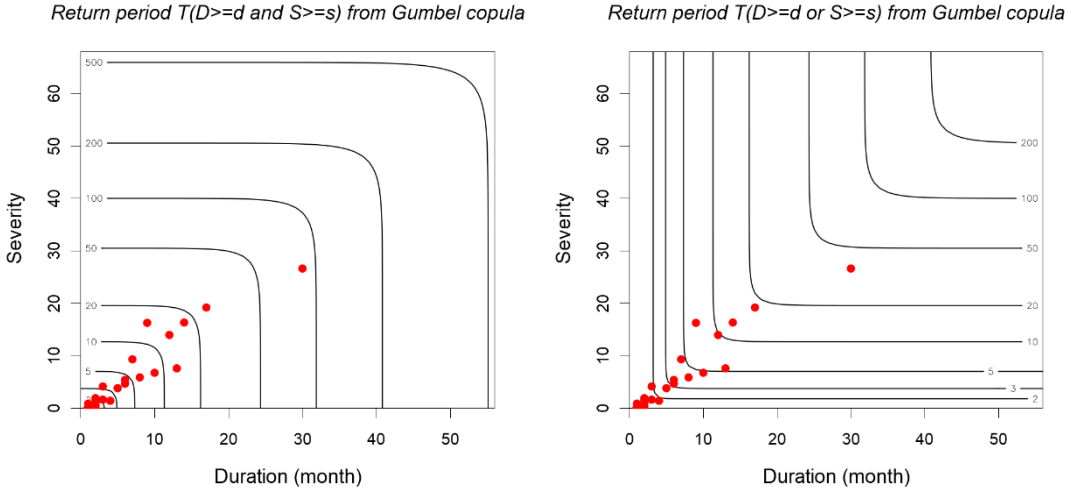

8275 SPI 6-month

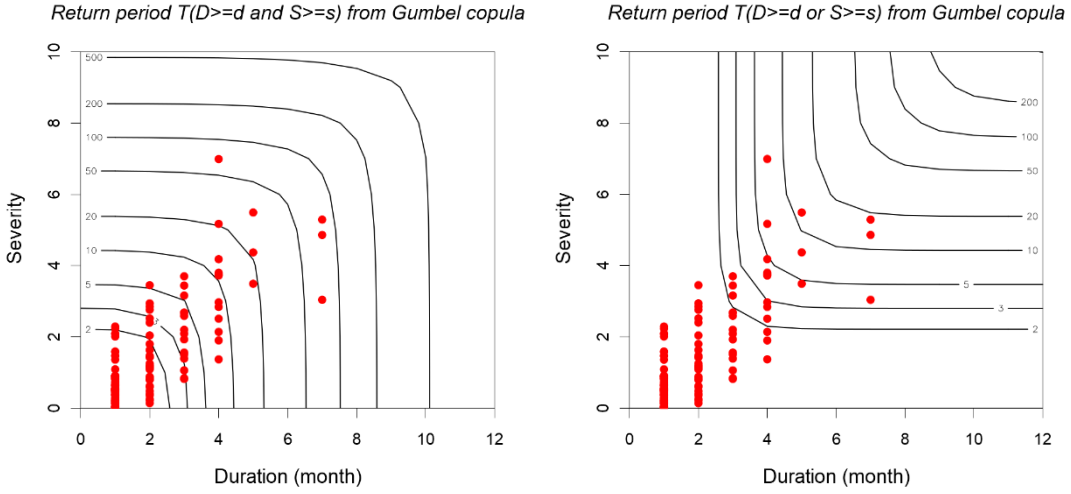

17255 SPI 1-month

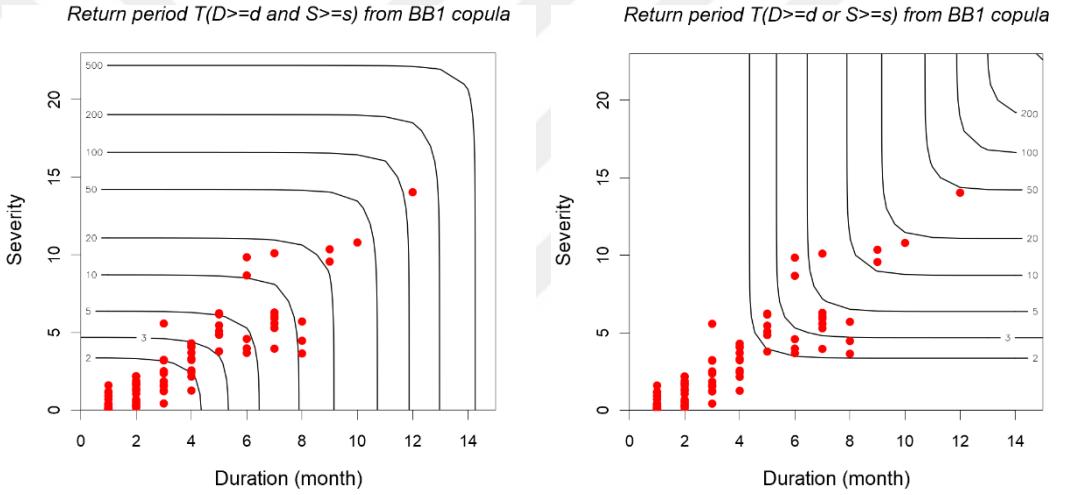

17255 SPI 3-month

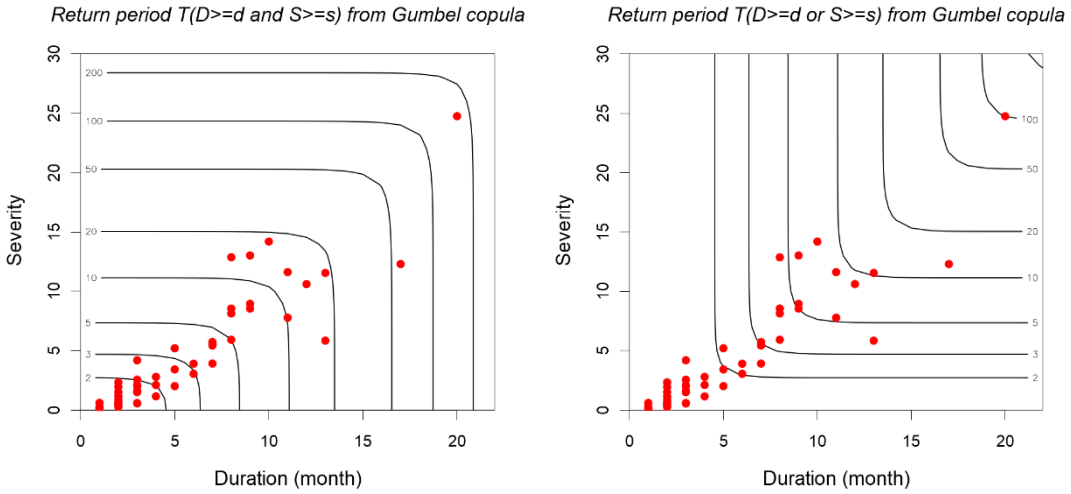

17255 SPI 6-month

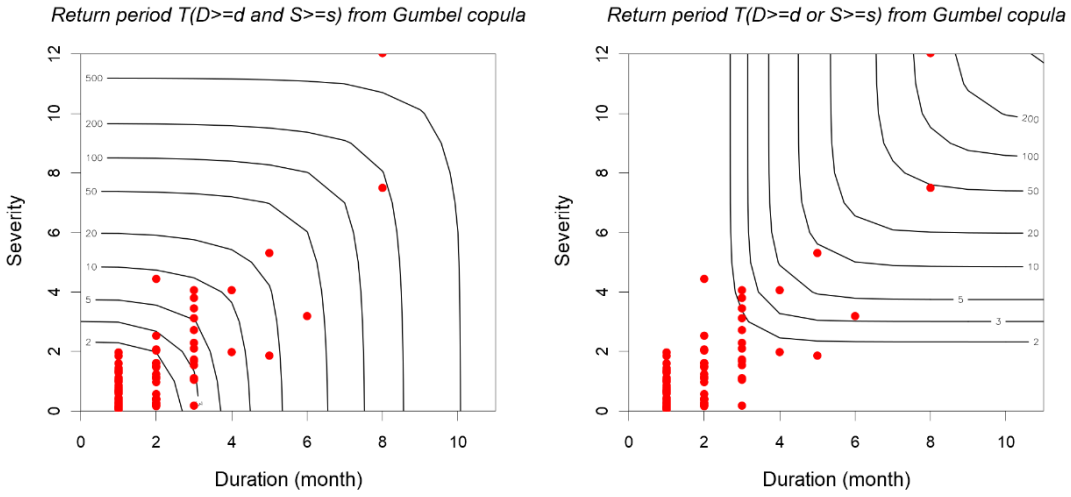

17355 SPI 1-month

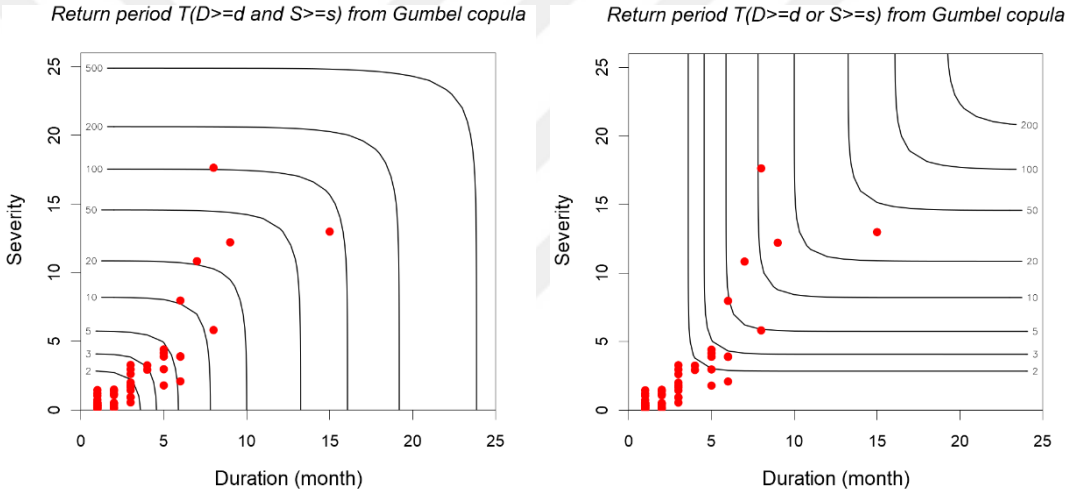

17355 SPI 3-month

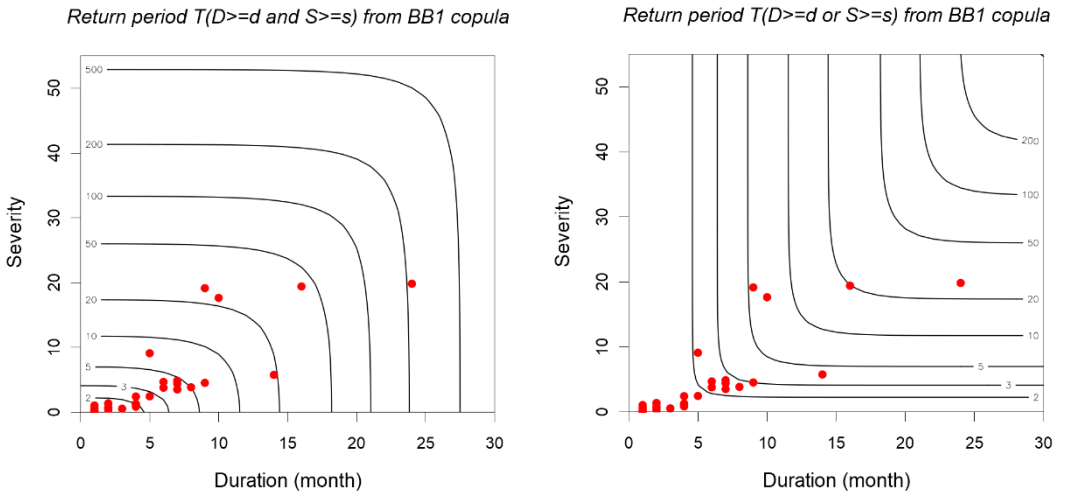

17355 SPI 6-month

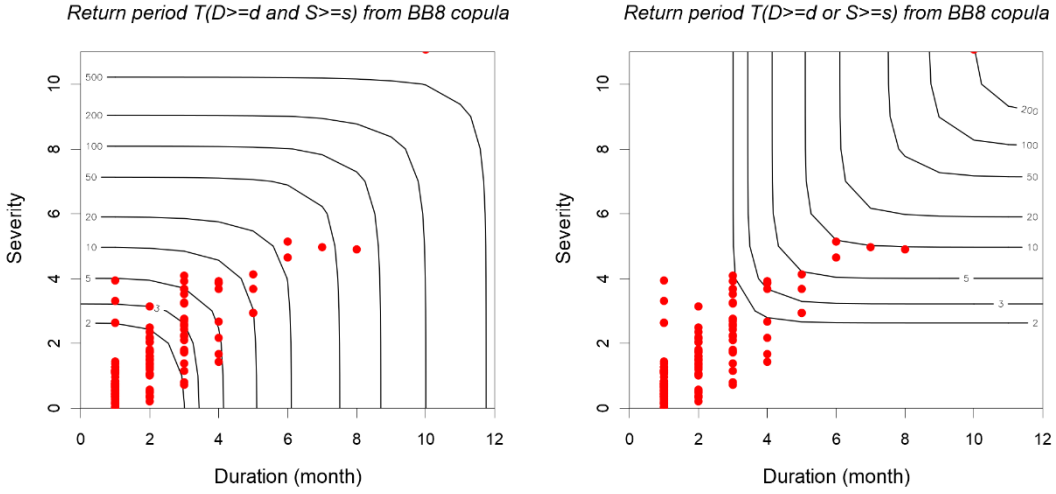

17866 SPI 1-month

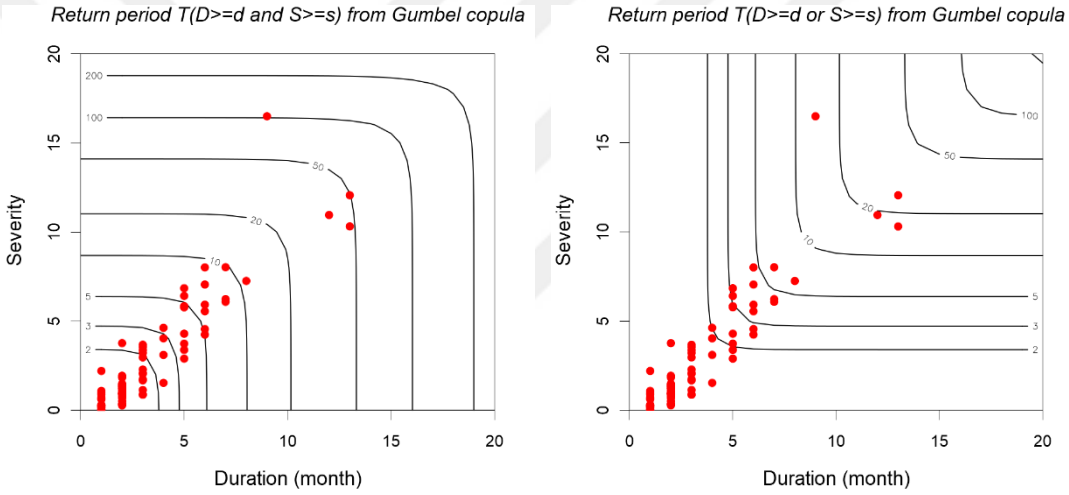

17866 SPI 3-month

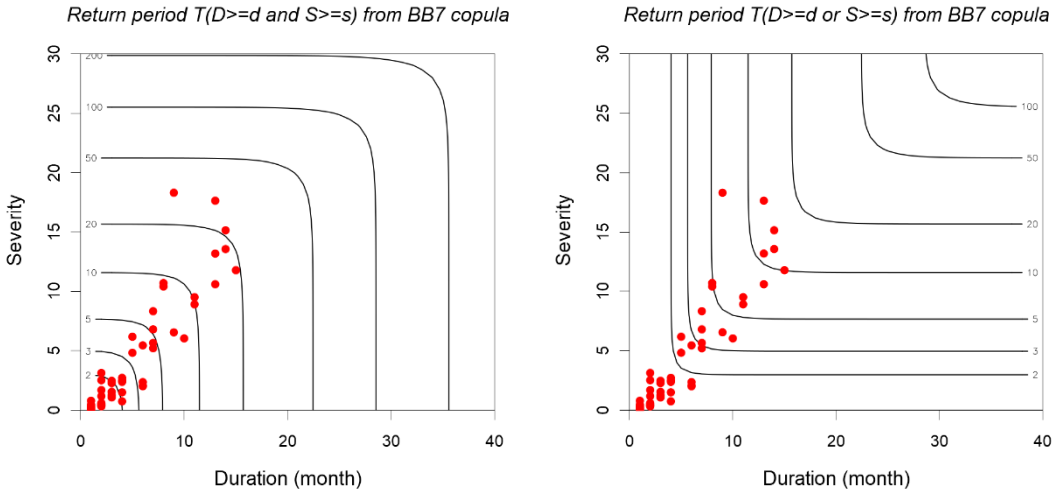

17866 SPI 6-month

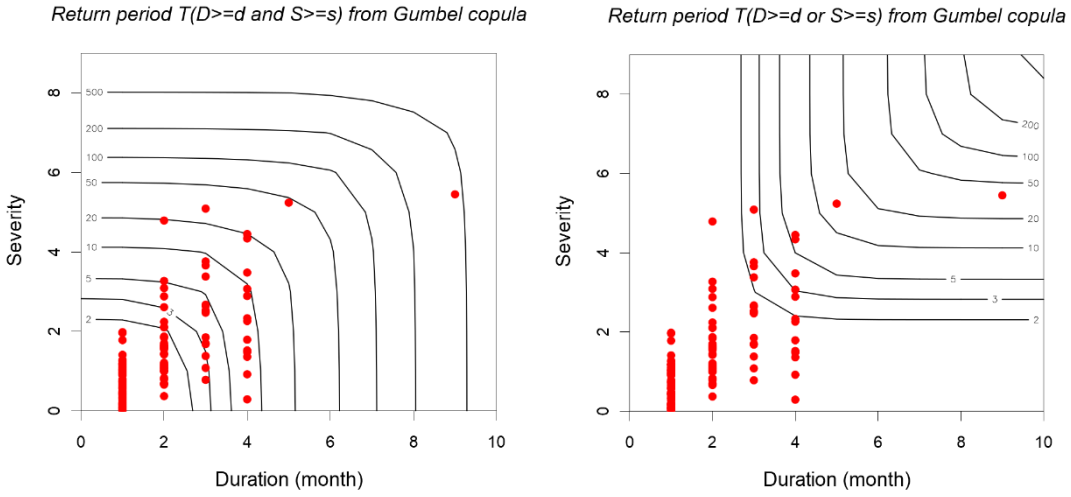

17868 SPI 1-month

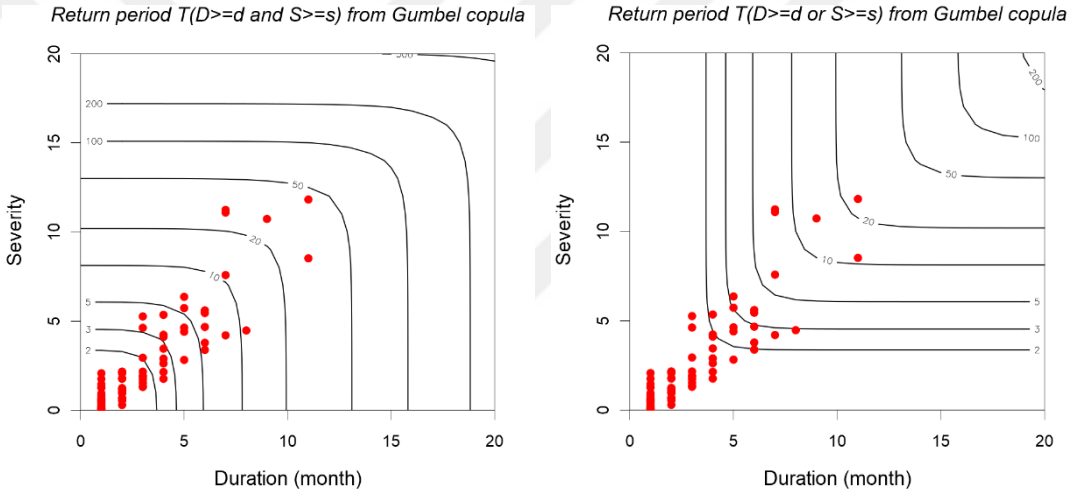

17868 SPI 3-month

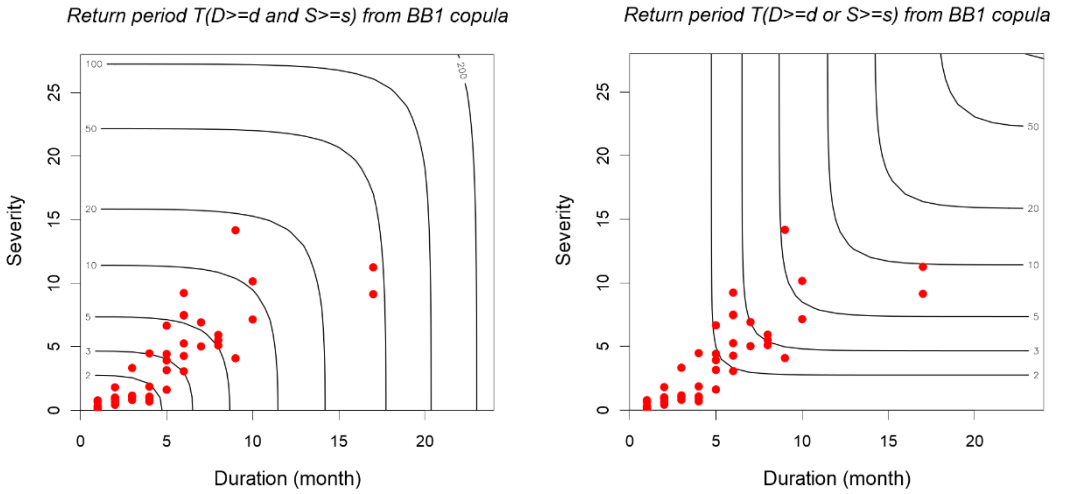

17868 SPI 6-month

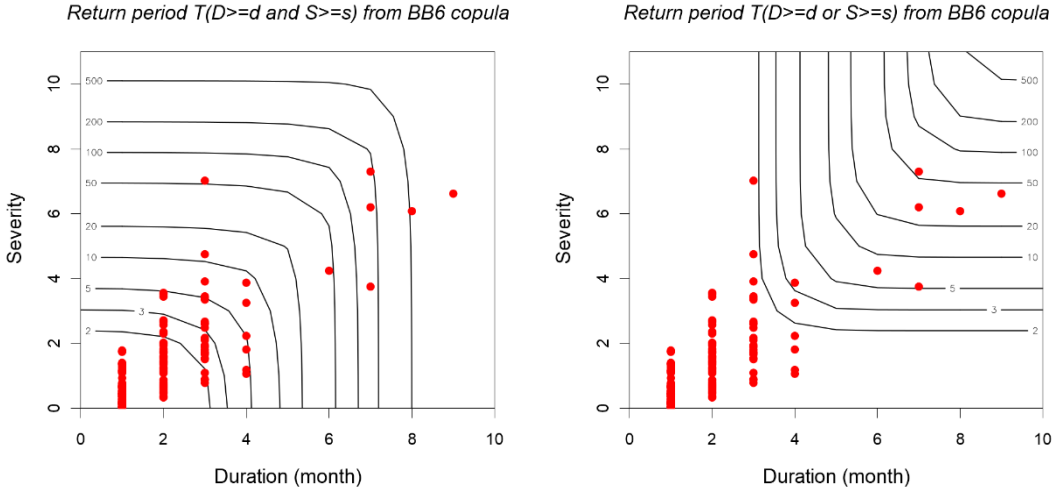

17870 SPI 1-month

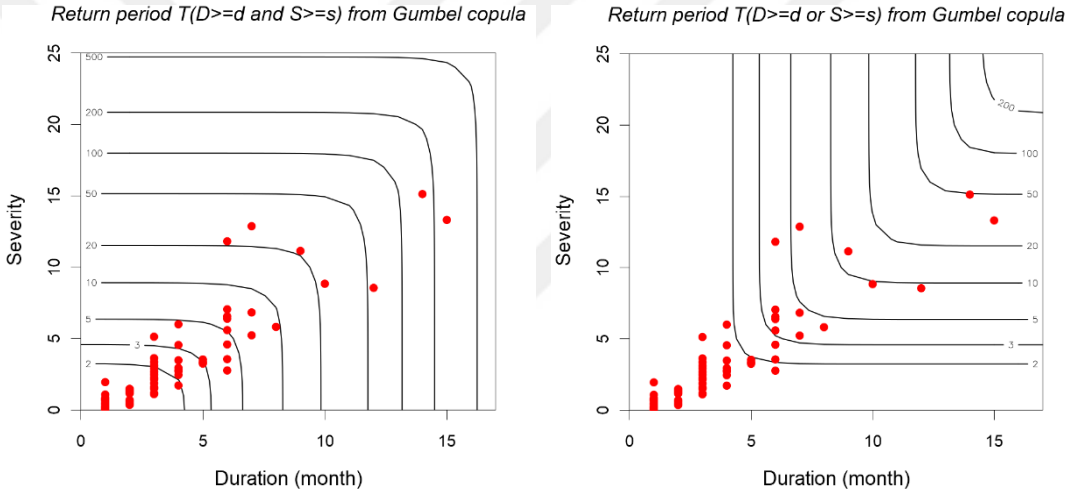

17870 SPI 3-month

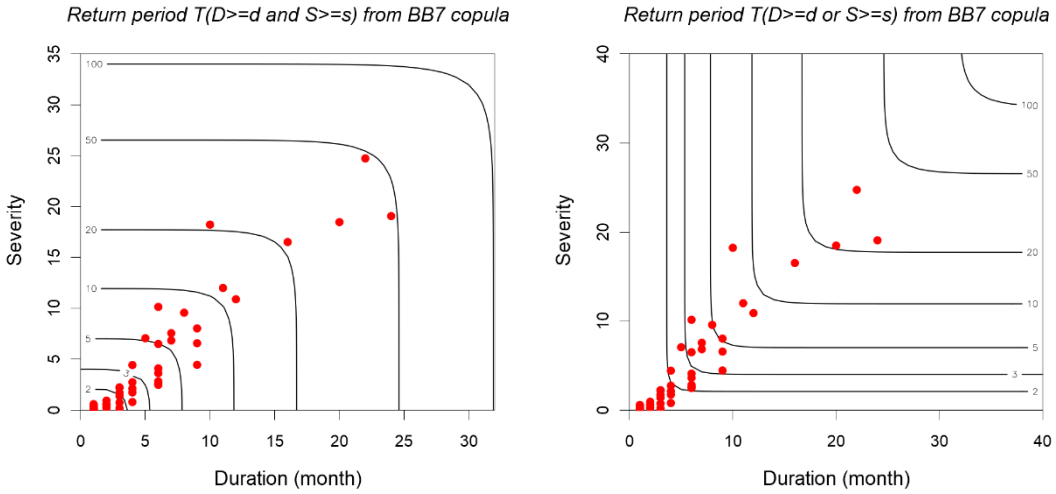

17870 SPI 6-month

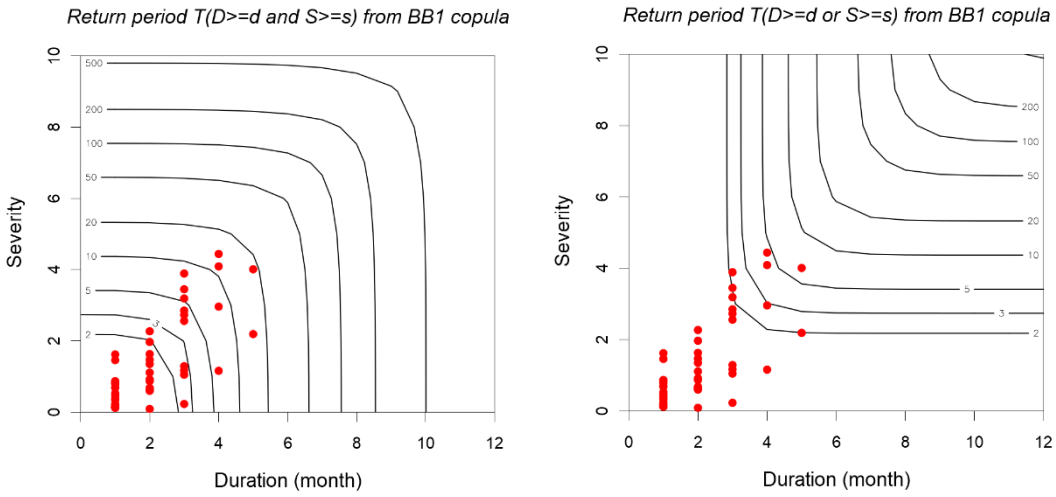

17871 SPI 1-month

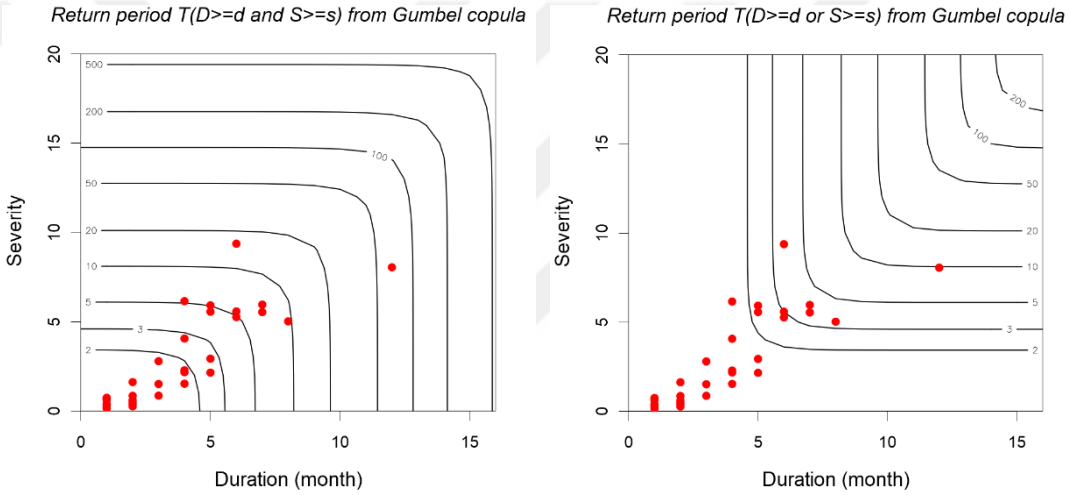

17871 SPI 3-month

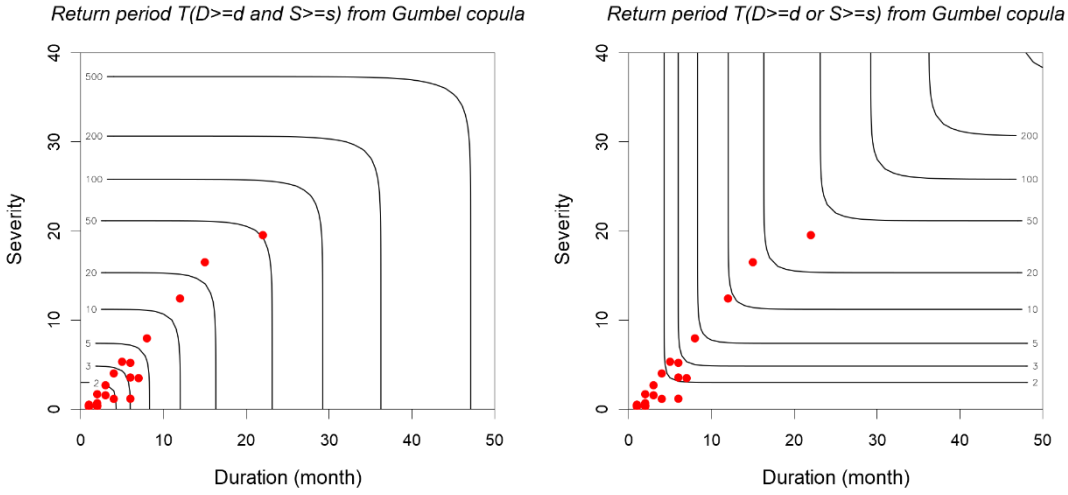

17871 SPI 6-month

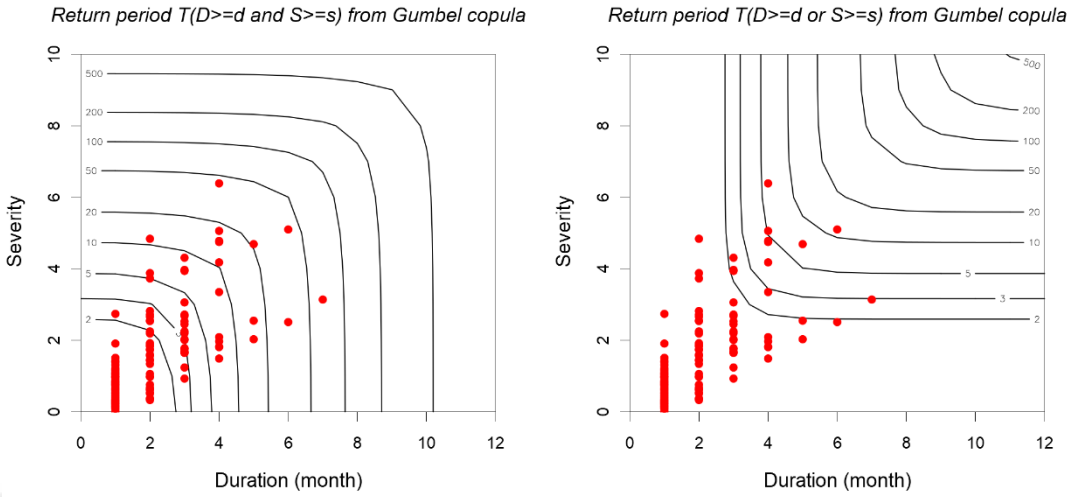

17908 SPI 1-month

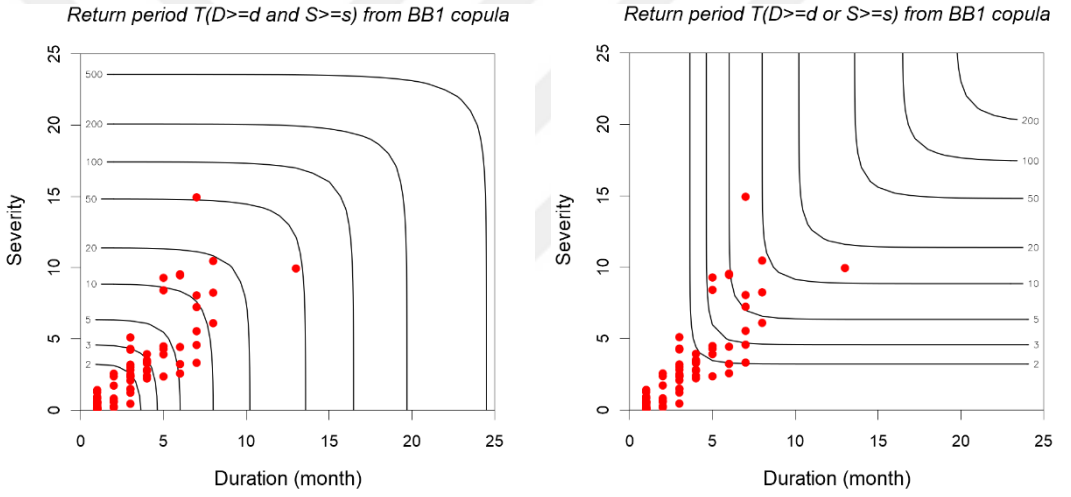

17908 SPI 3-month

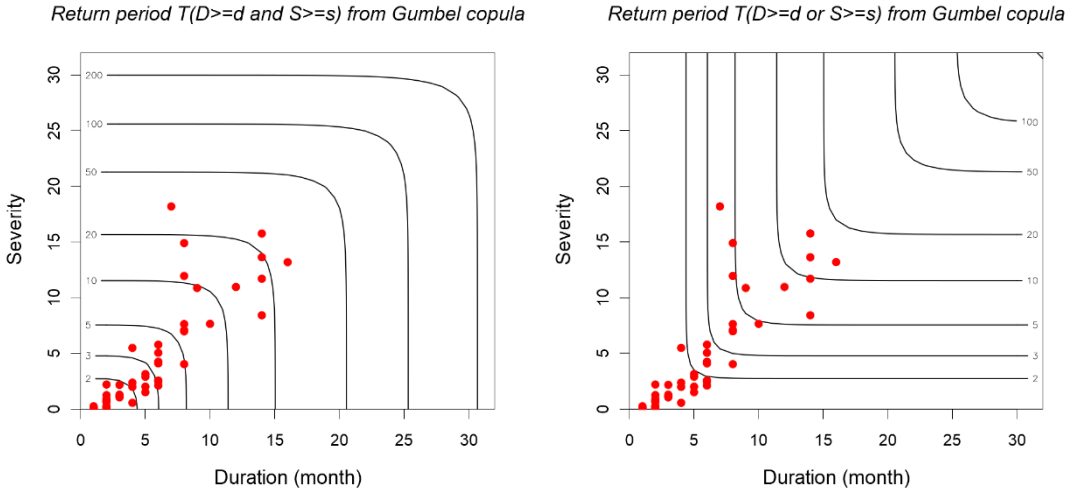

17908 SPI 6-month

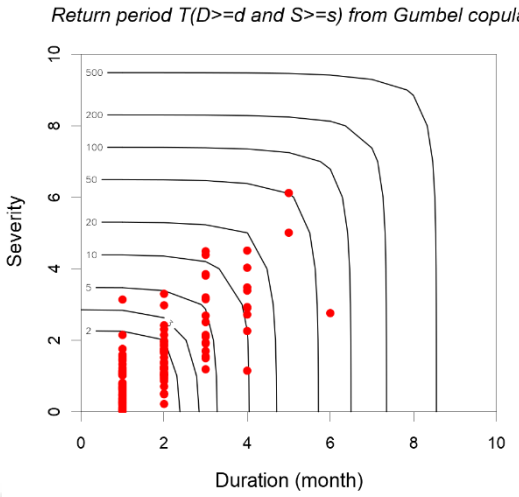

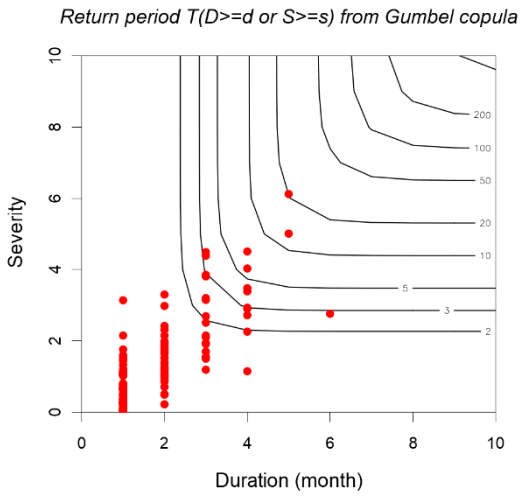

17960 SPI 1-month

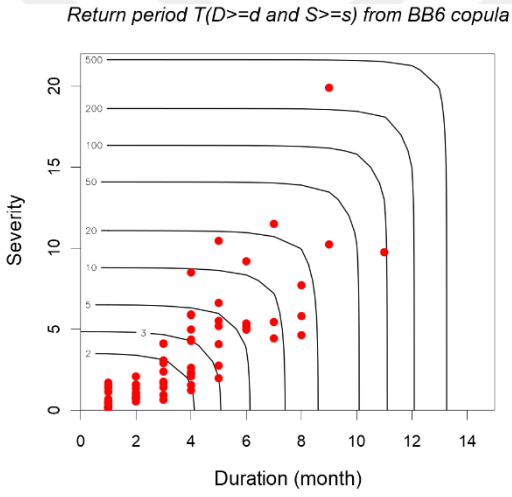

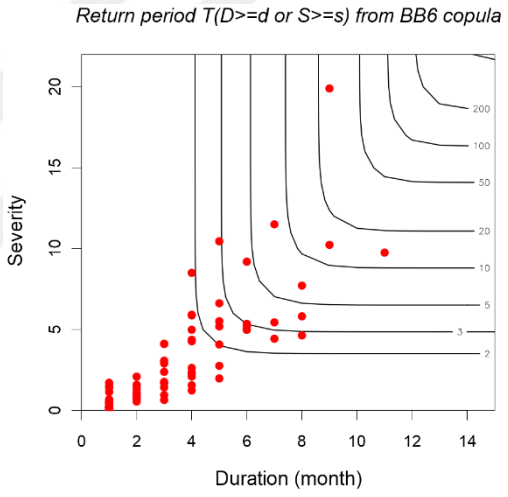

17960 SPI 3-month

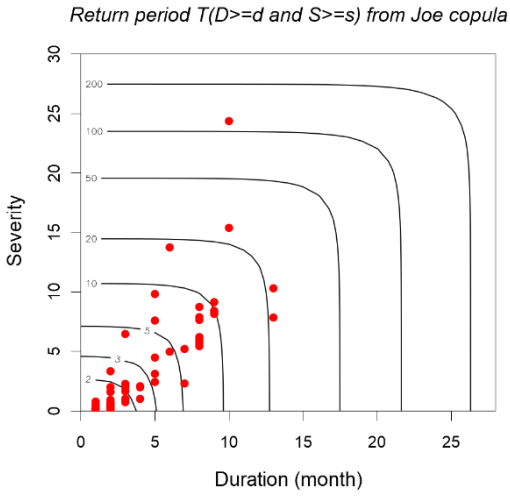

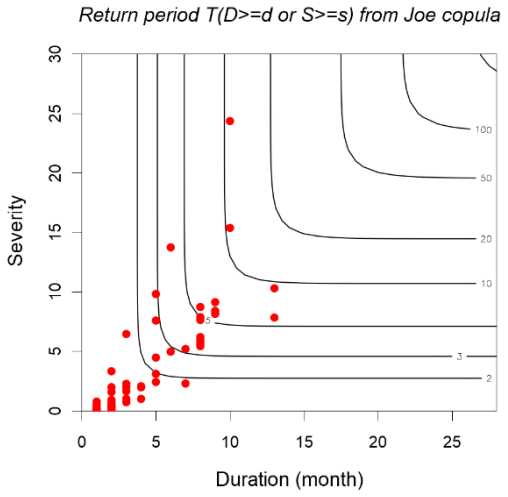

17960 SPI 6-month

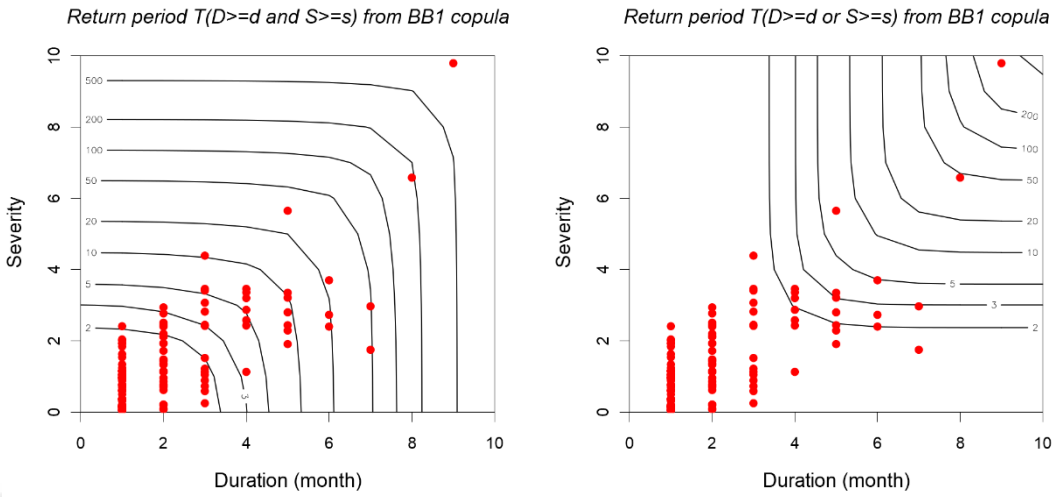

17979 SPI 1-month

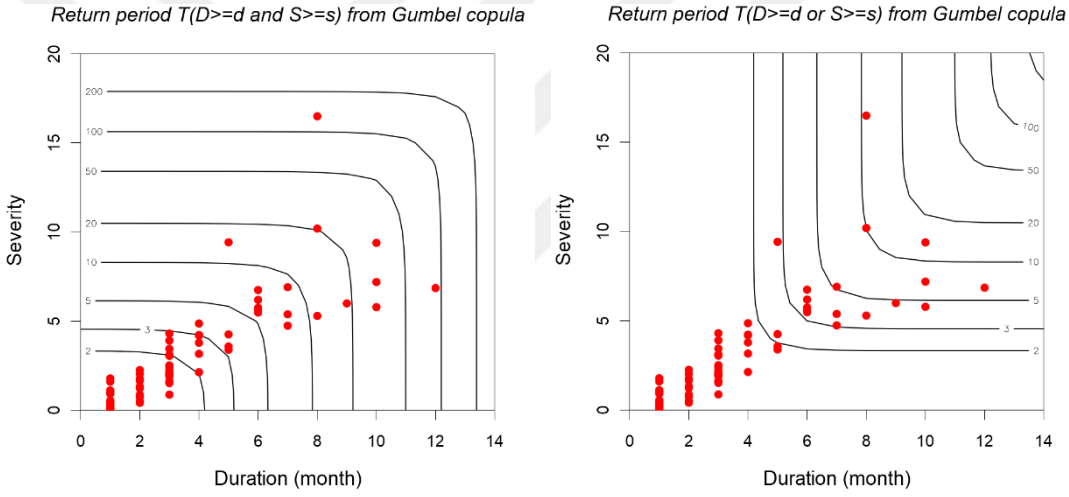

17979 SPI 3-month

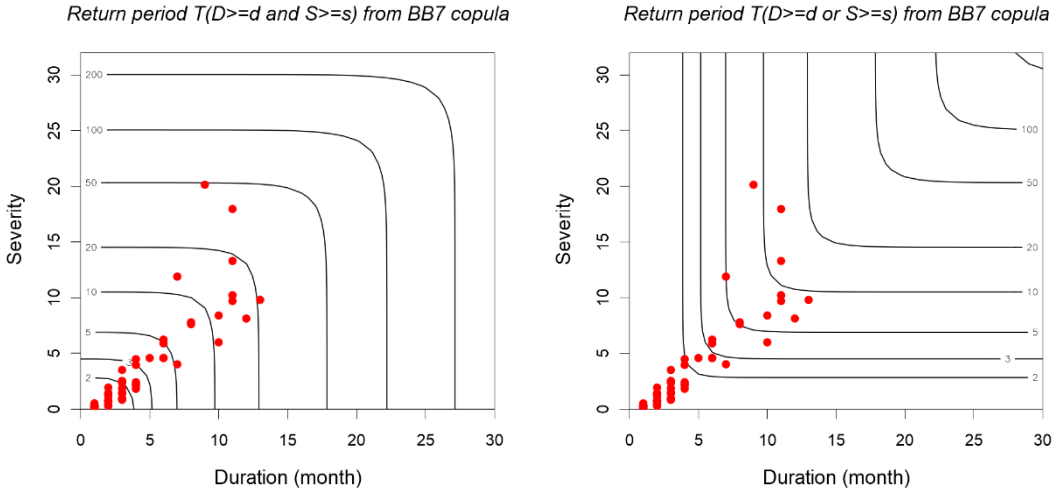

17979 SPI 6-month

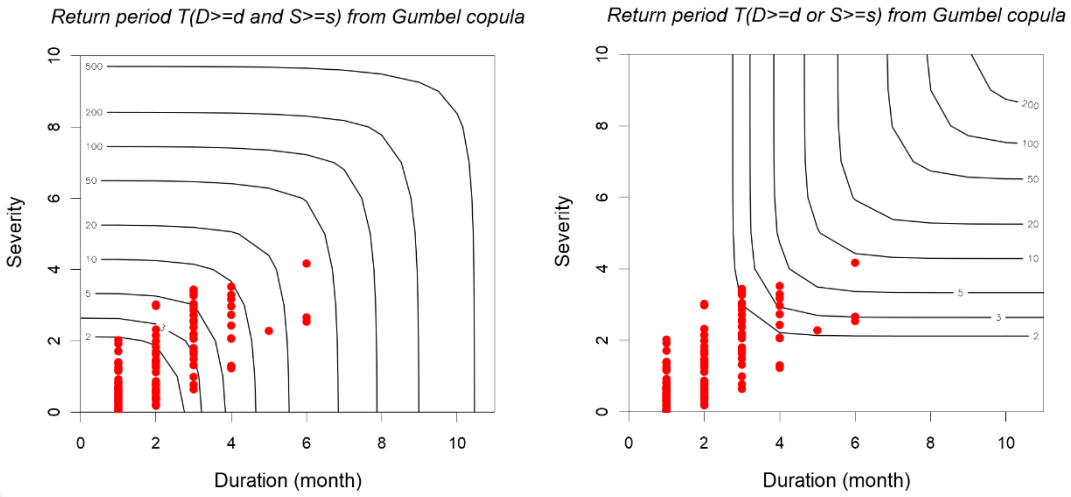

D20M001 SPI 1-month

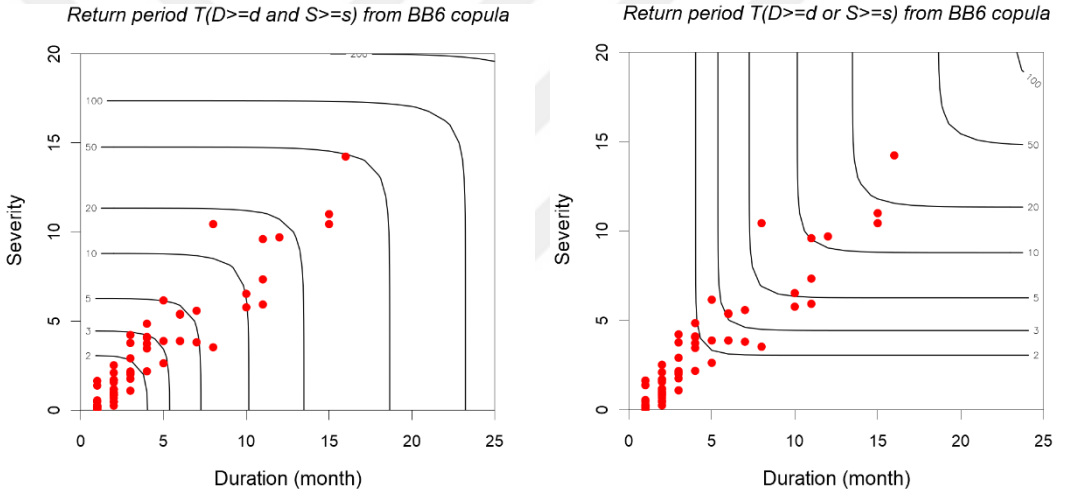

D20M001 SPI 3-month

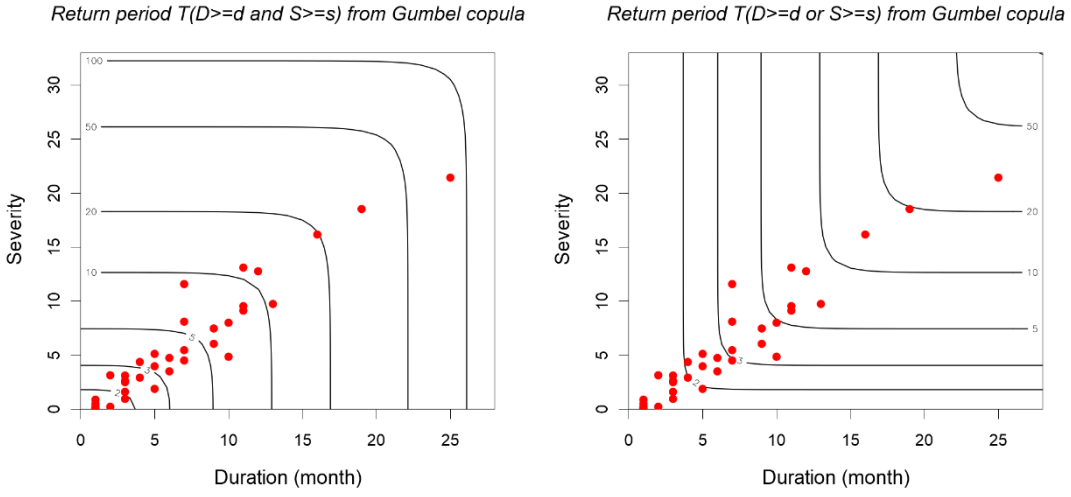

D20M001 SPI 6-month

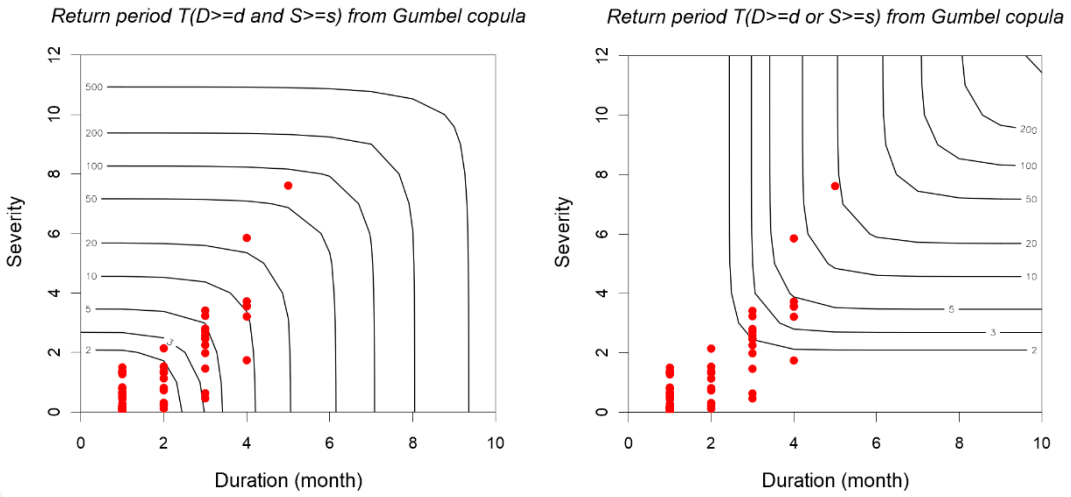

D20M002 SPI 1-month

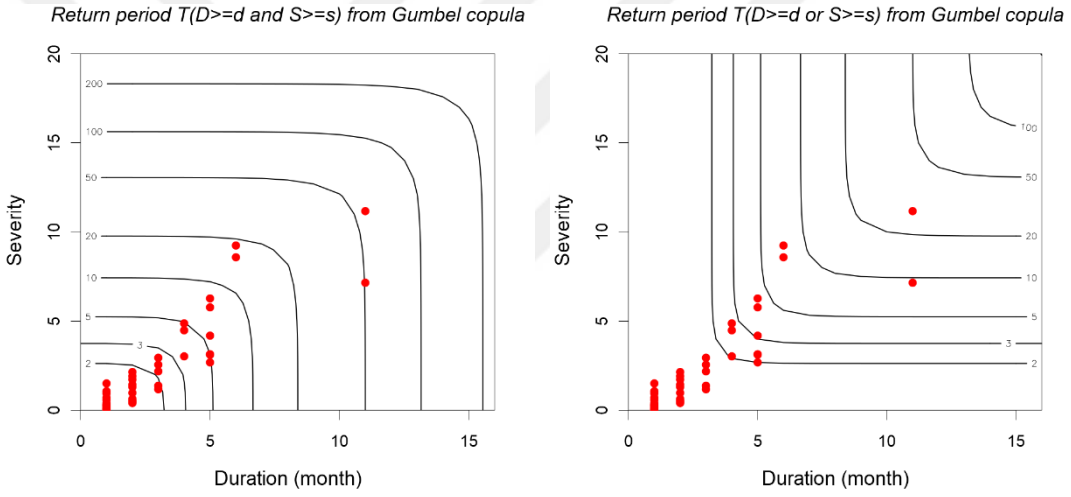

D20M002 SPI 3-month

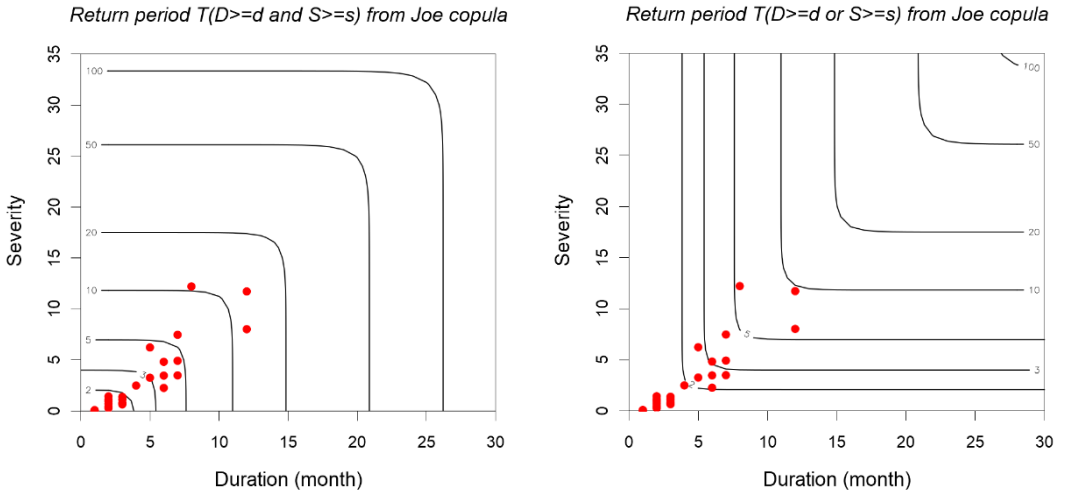

D20M002 SPI 6-month

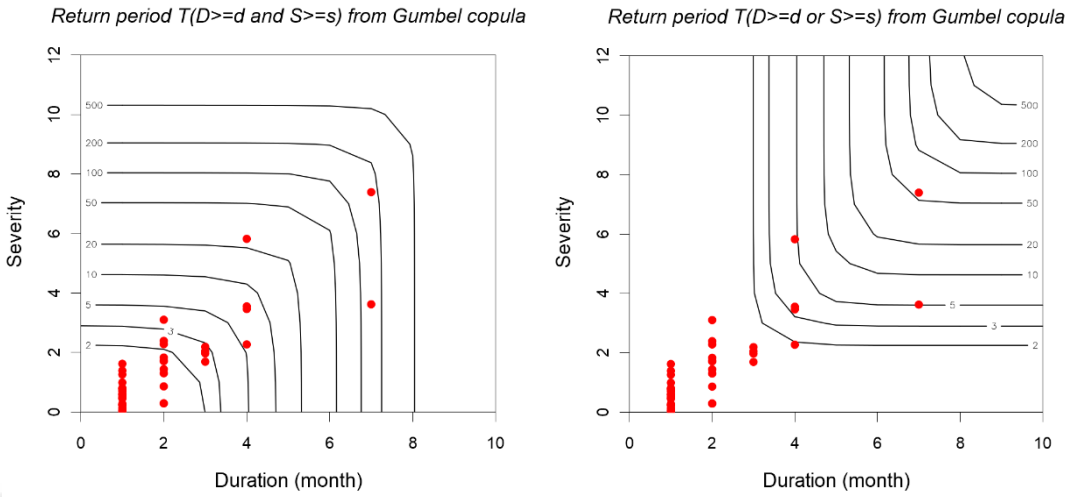

D20M004 SPI 1-month

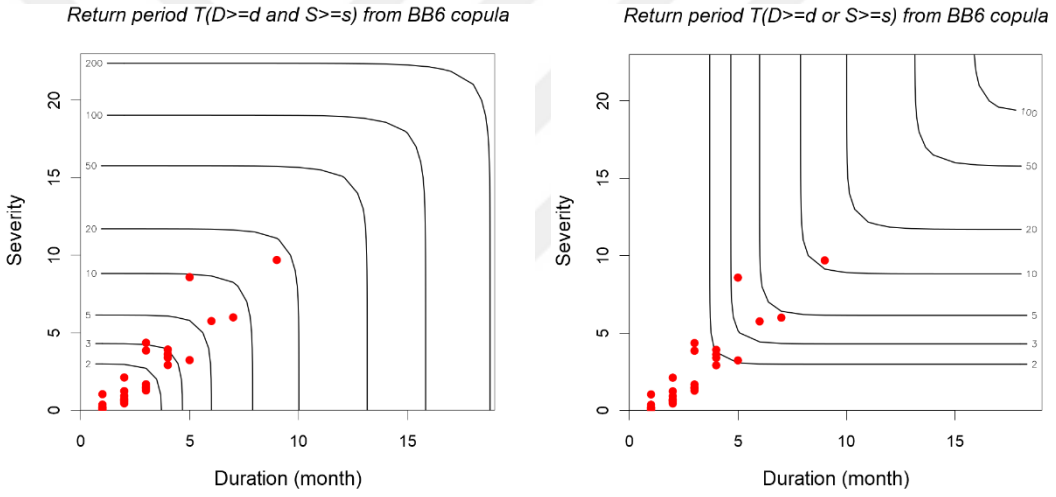

D20M004 SPI 3-month

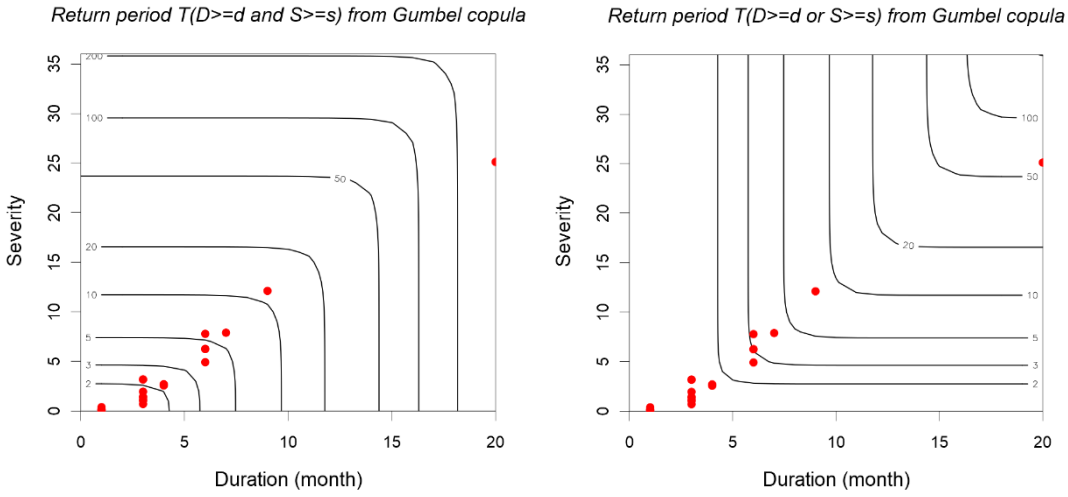

D20M004 SPI 6-month

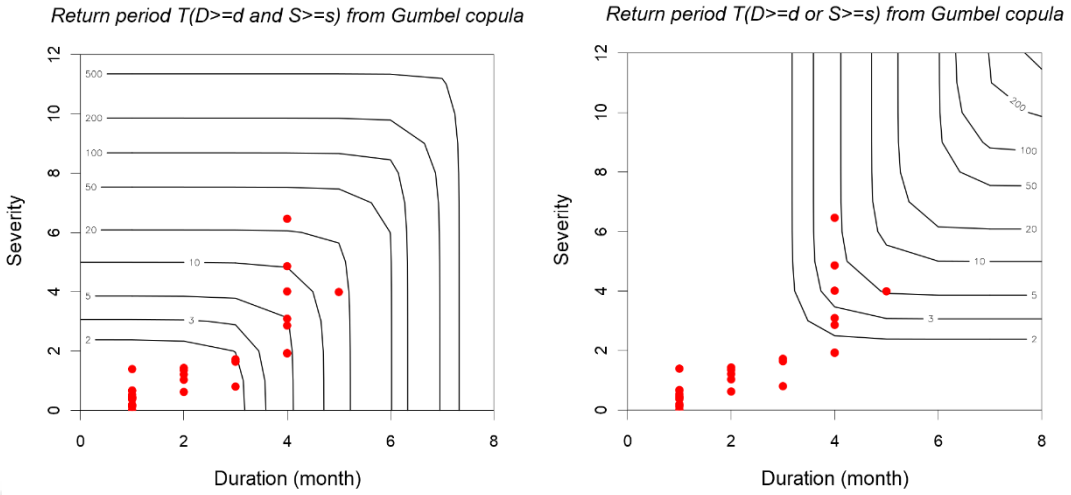

D20M006 SPI 1-month

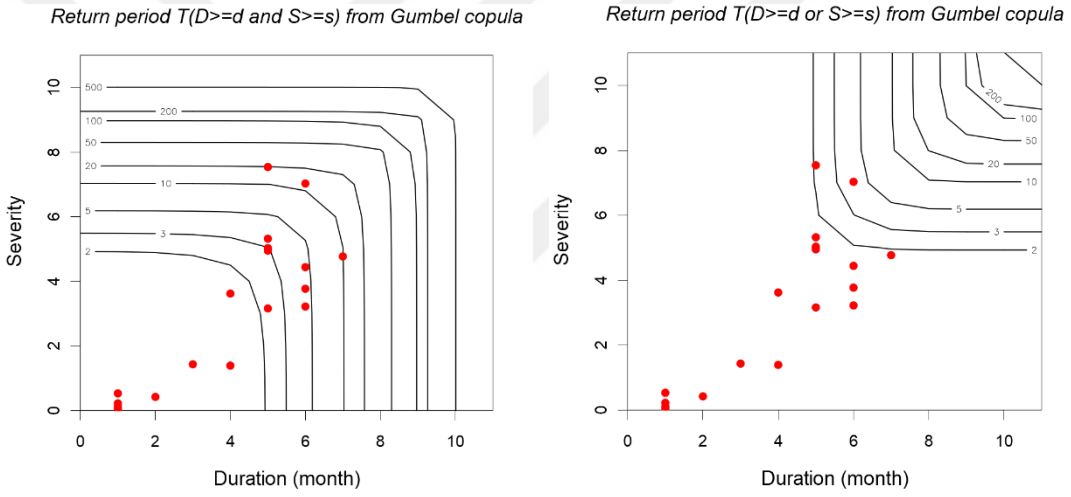

D20M006 SPI 3-month

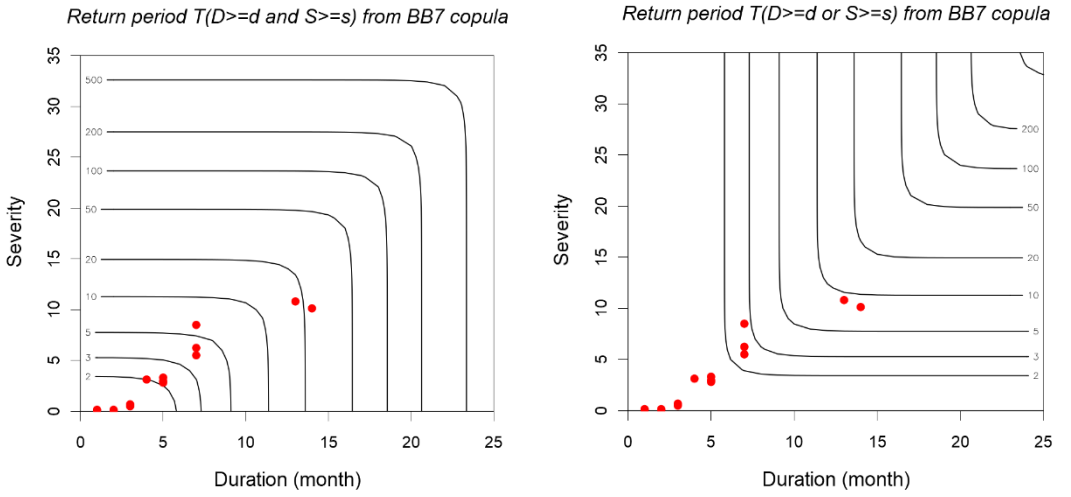

D20M006 SPI 6-month

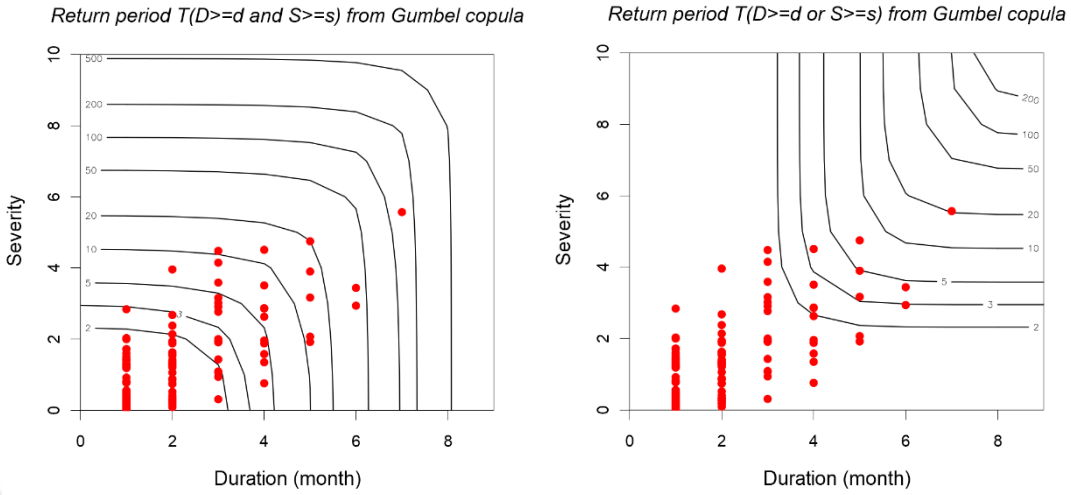

D20M009 SPI 1-month

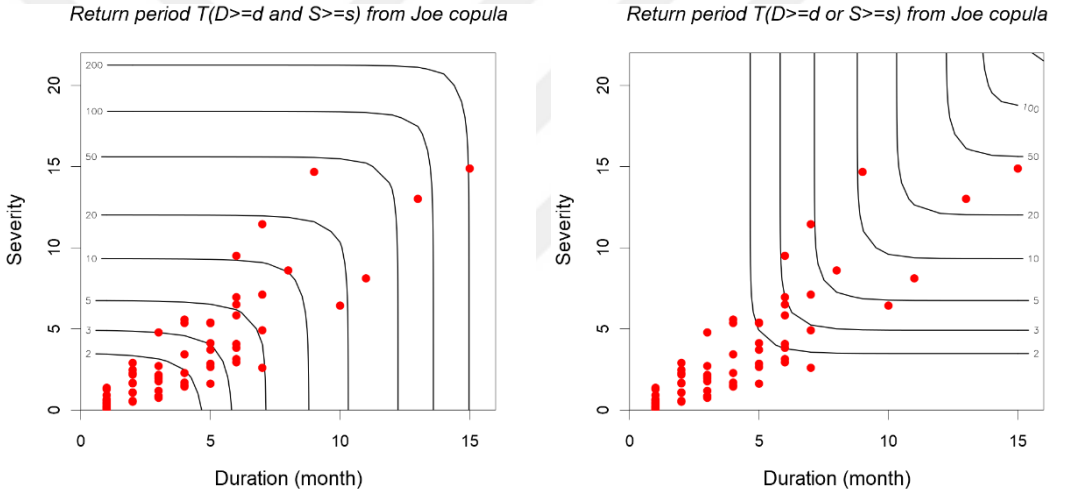

D20M009 SPI 3-month

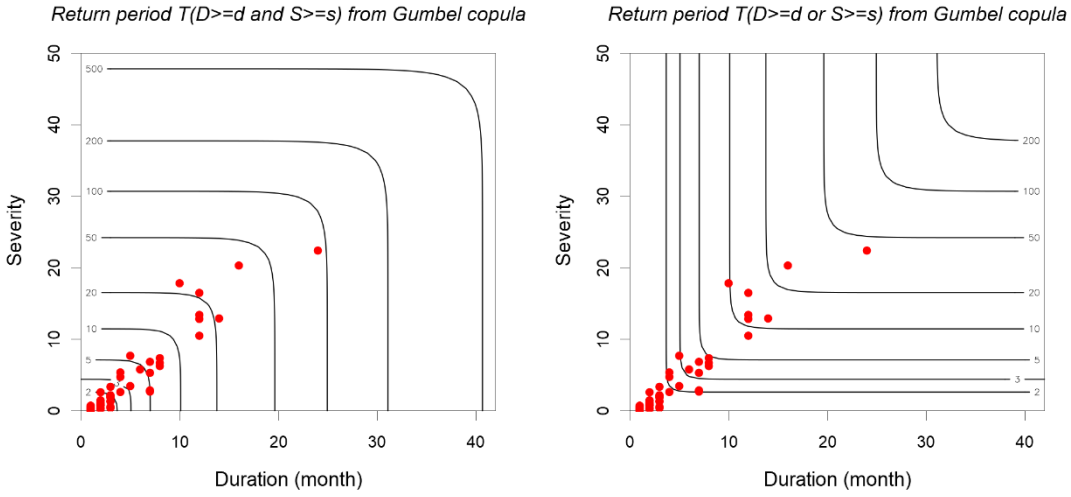

D20M009 SPI 6-month

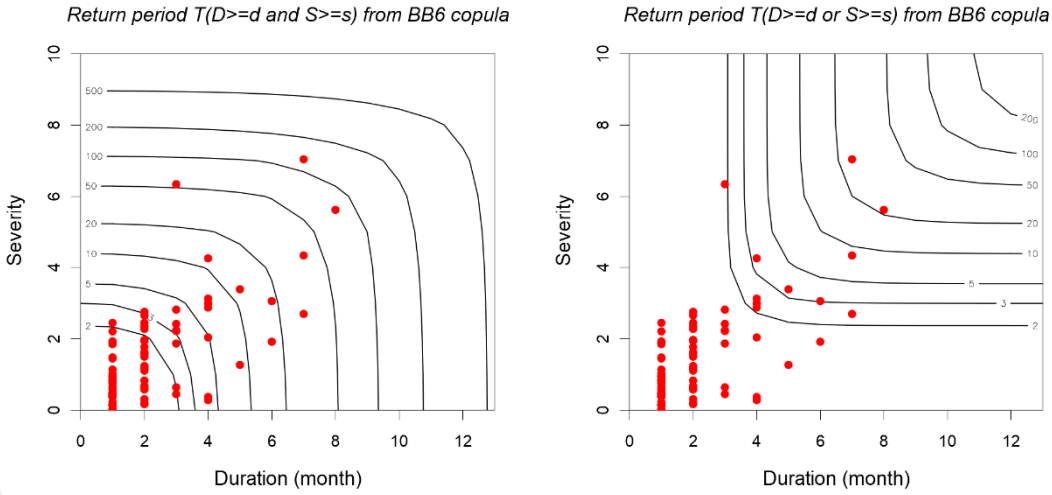

D20M011 SPI 1-month

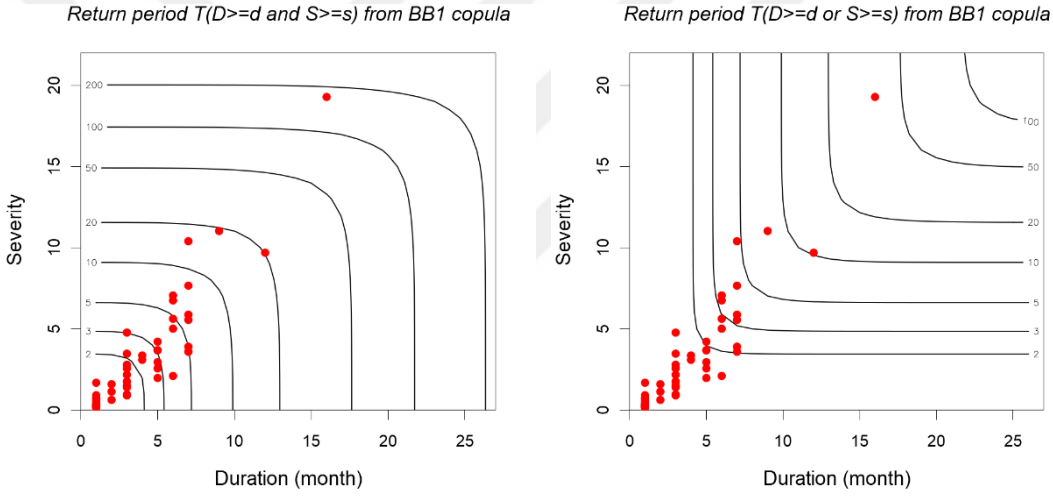

D20M011 SPI 3-month

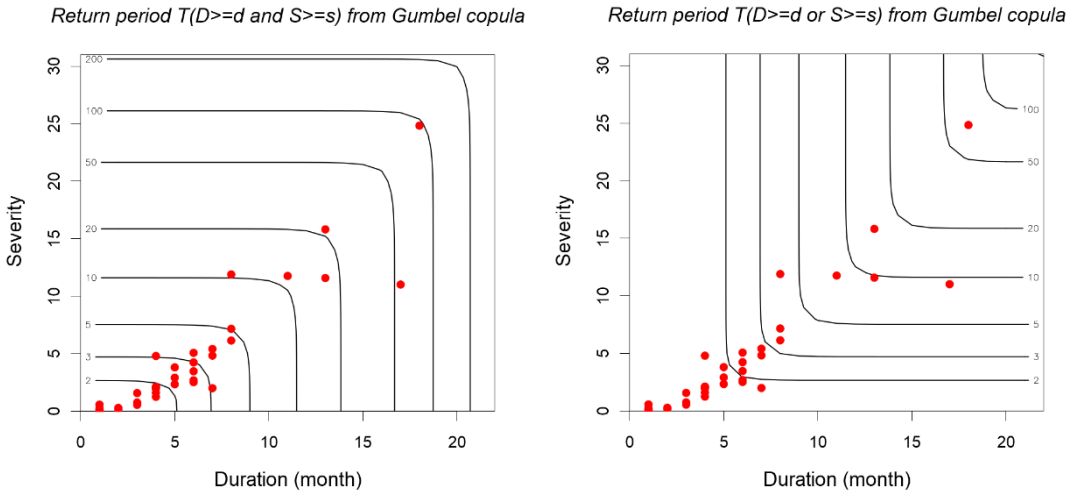

D20M011 SPI 6-month

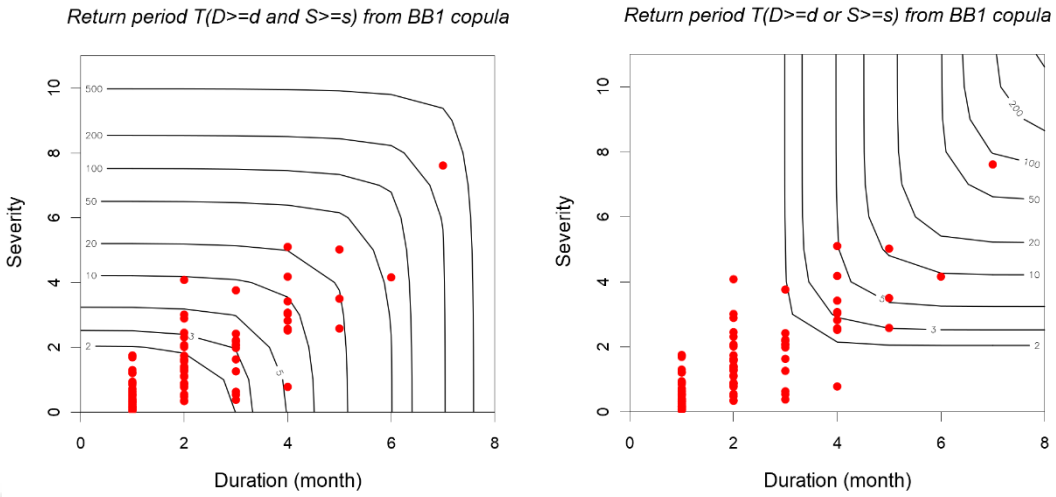

D20M013 SPI 1-month

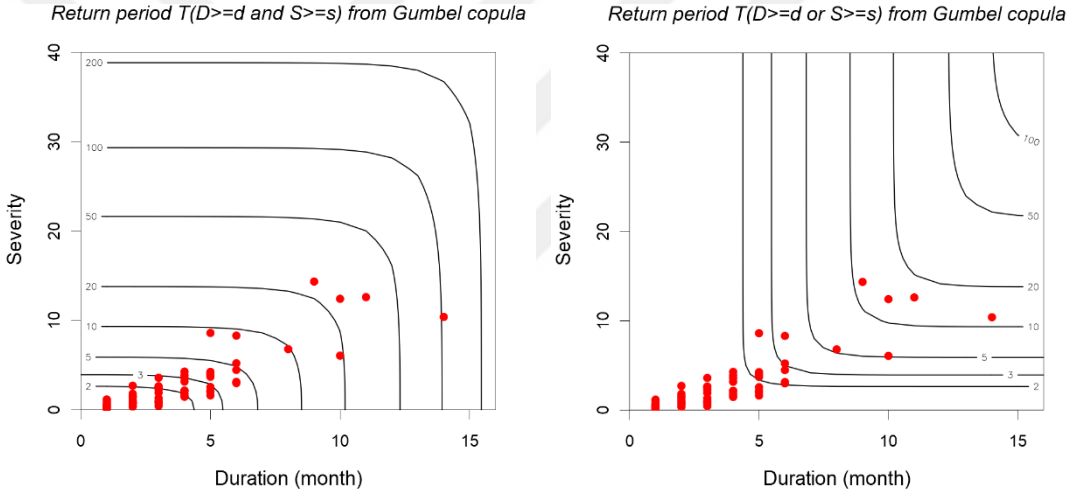

D20M013 SPI 3-month

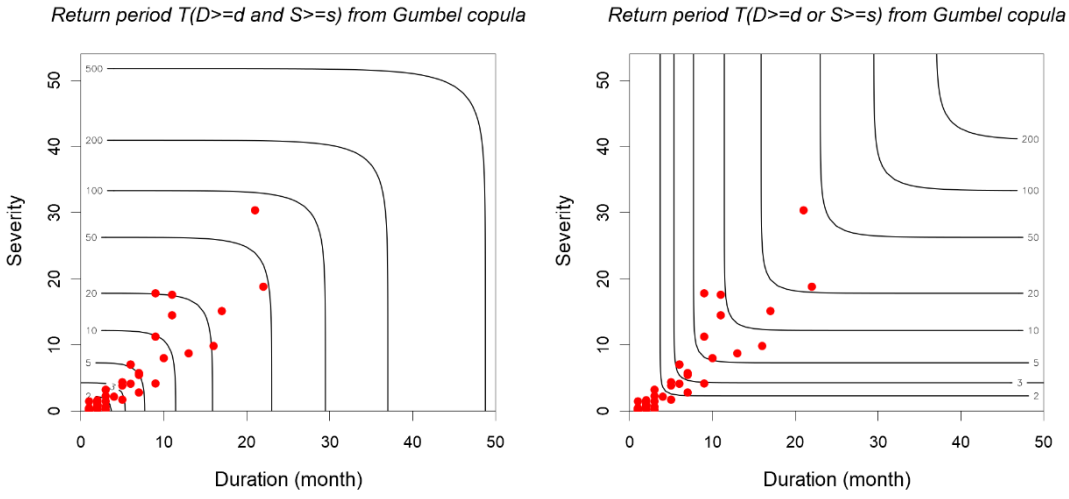

D20M013 SPI 6-month

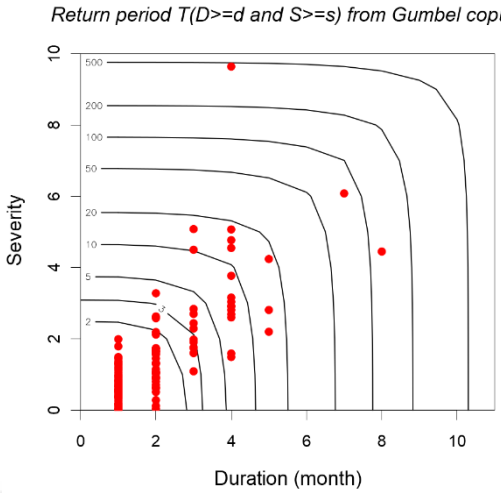

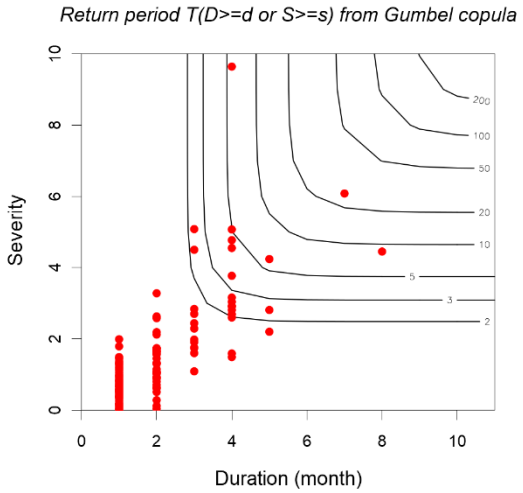

D20M014 SPI 1-month

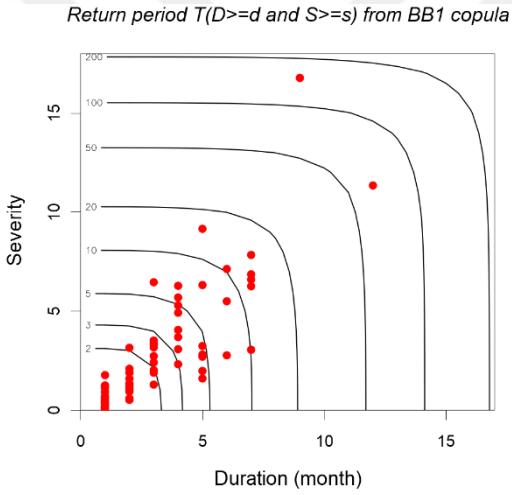

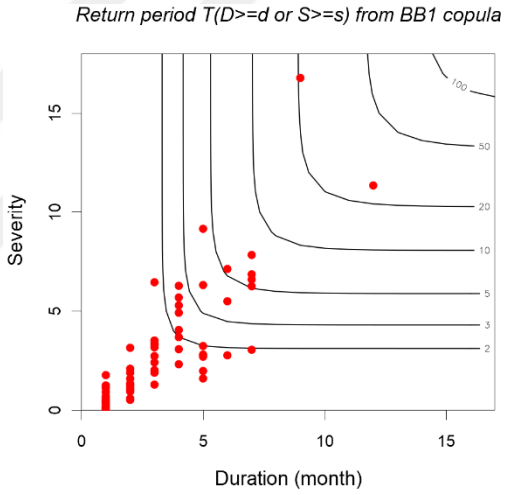

D20M014 SPI 3-month

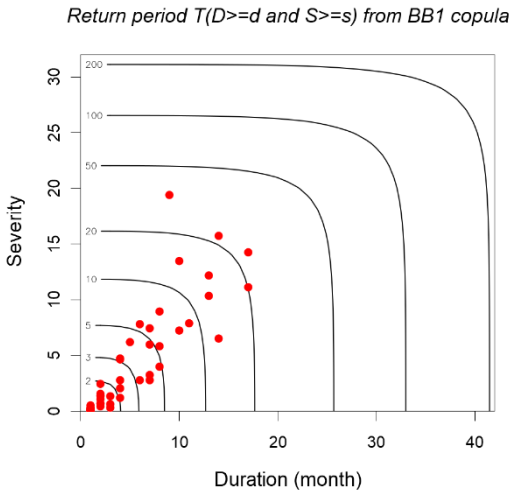

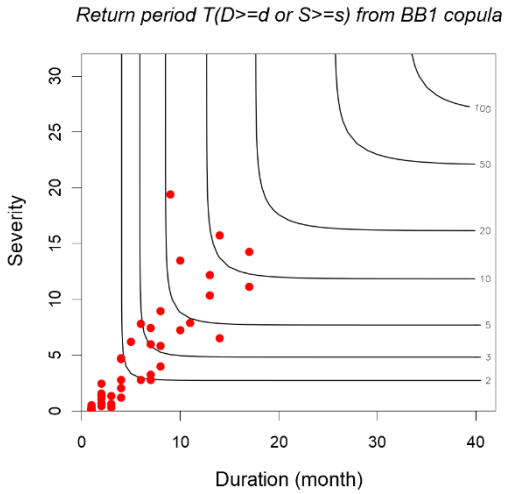

D20M014 SPI 6-month

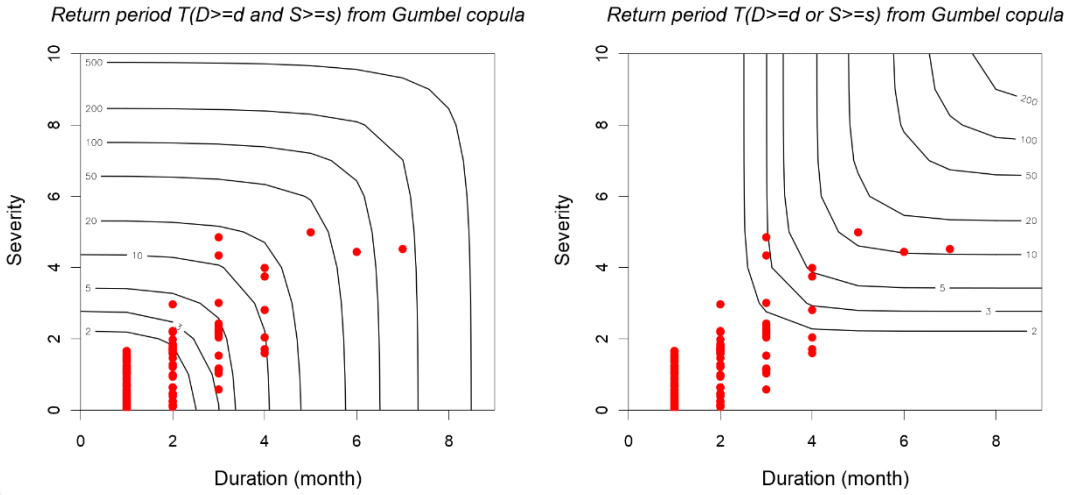

D20M015 SPI 1-month

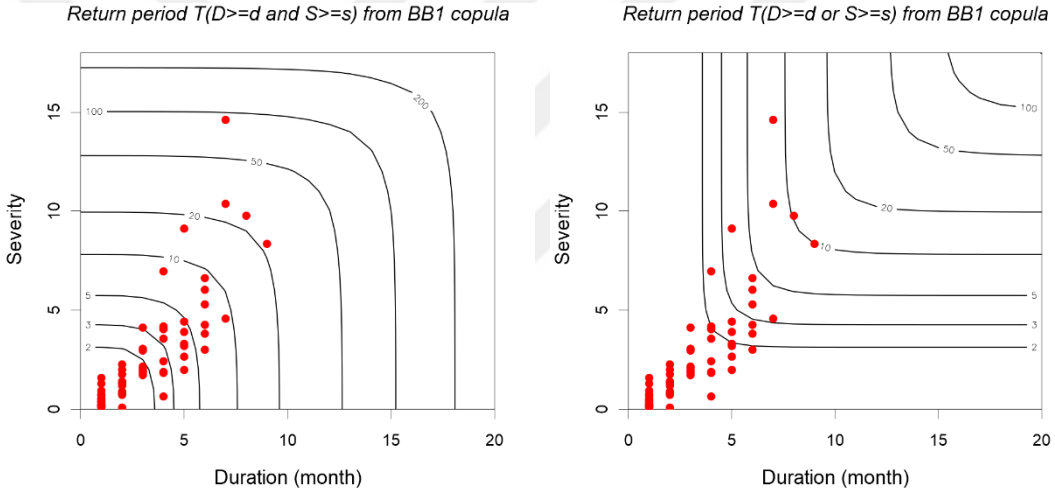

D20M015 SPI 3-month

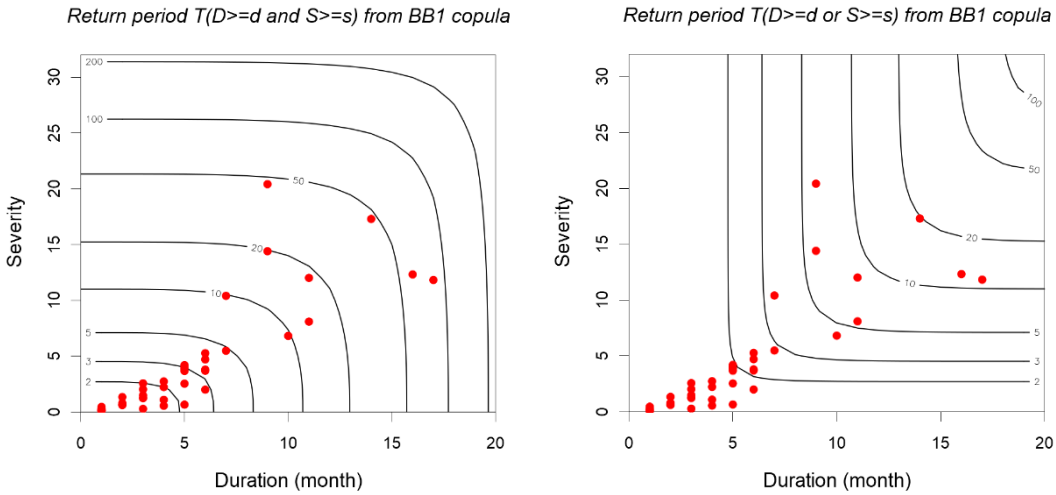

D20M015 SPI 6-month

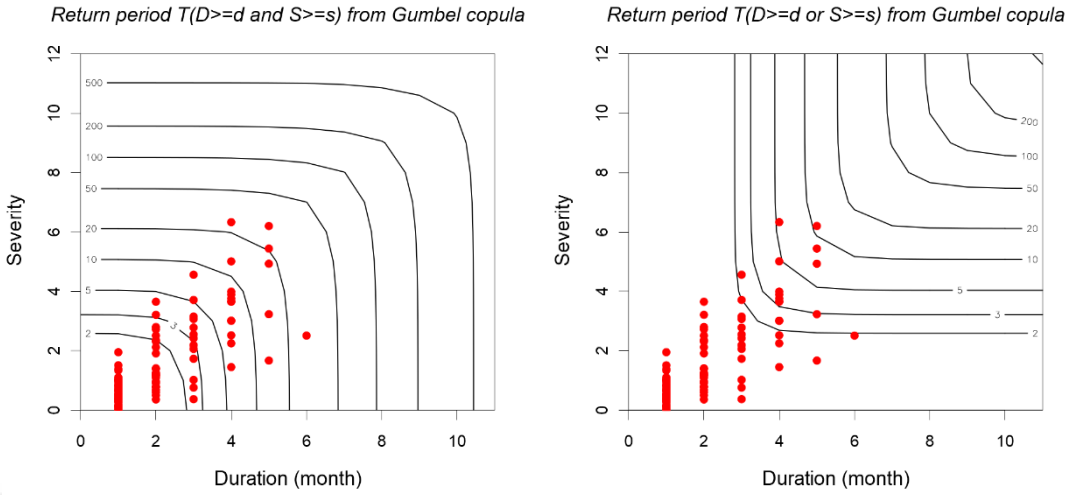

D20M016 SPI 1-month

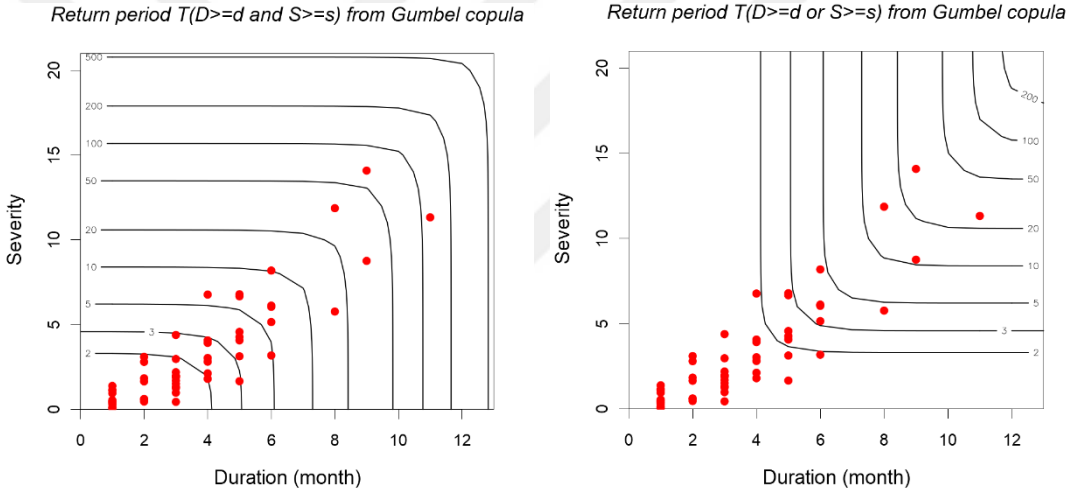

D20M016 SPI 3-month

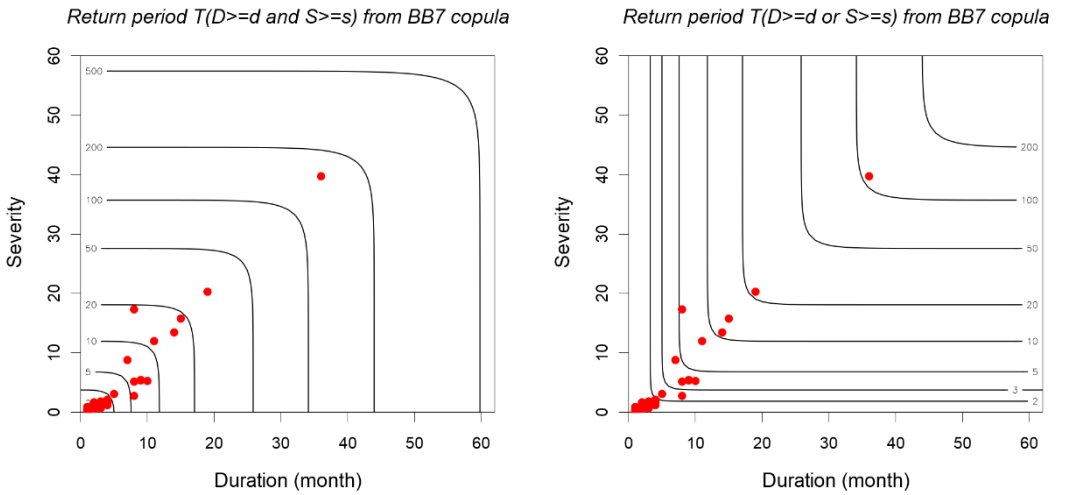

D20M016 SPI 6-month

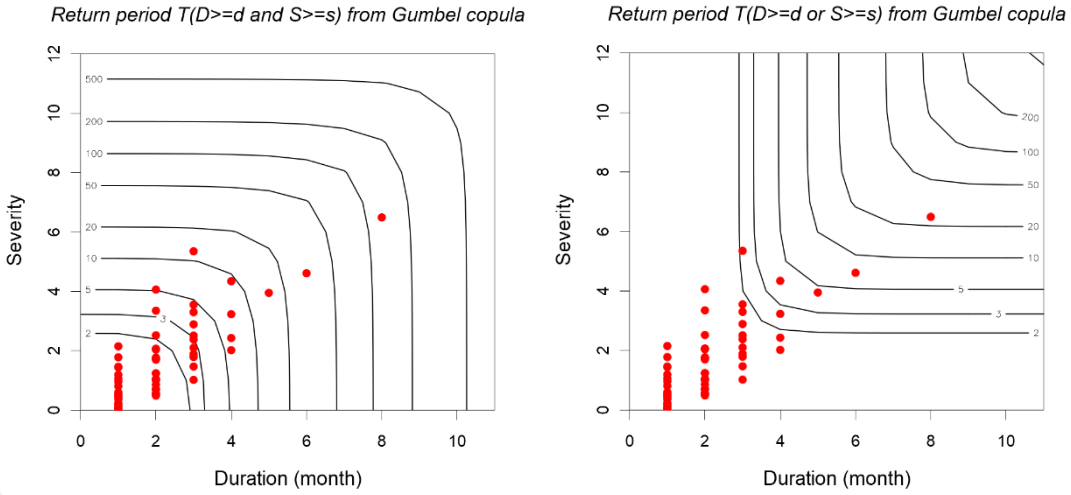

D20M017 SPI 1-month

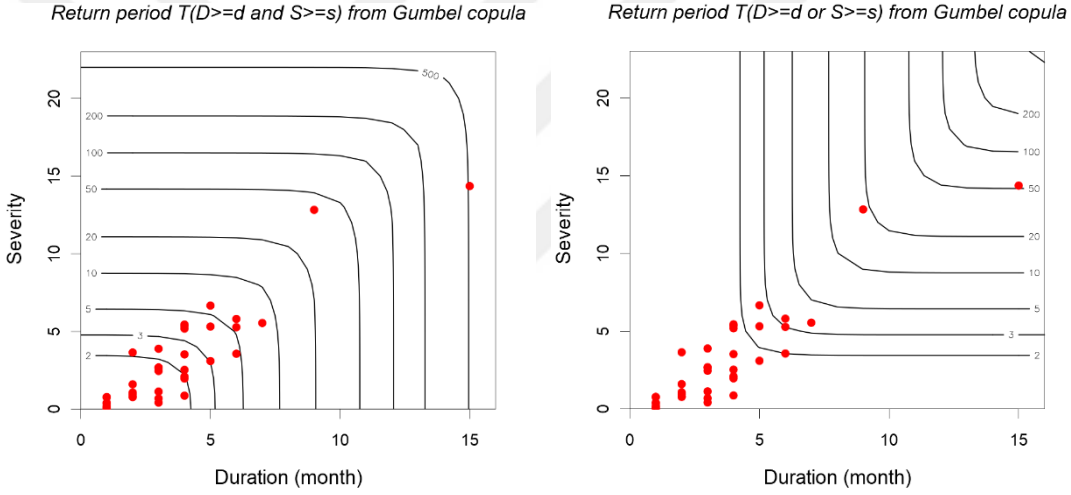

D20M017 SPI 3-month

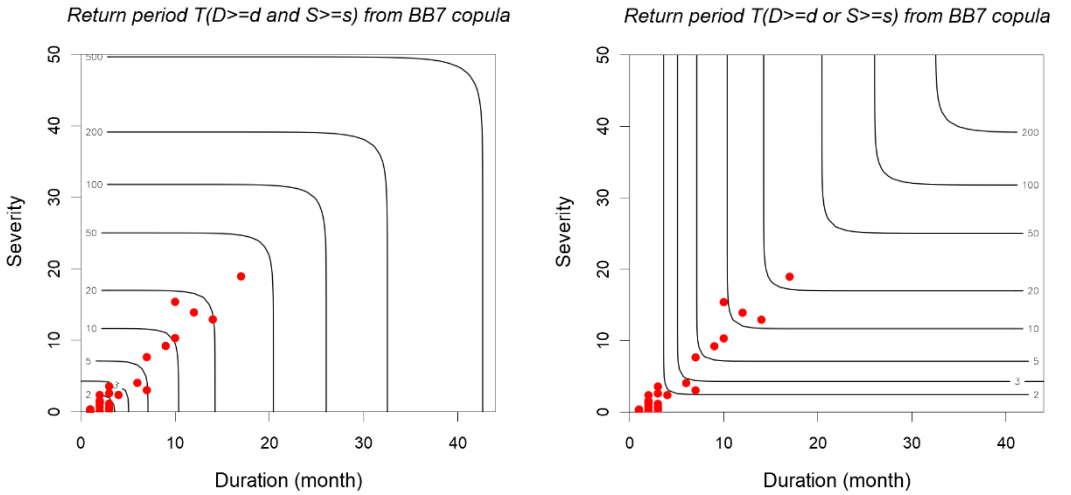

D20M017 SPI 6-month

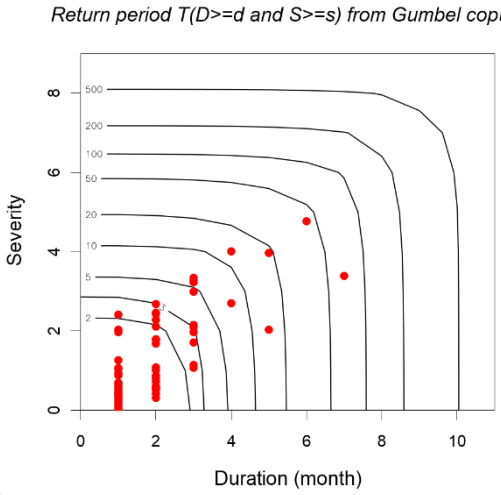

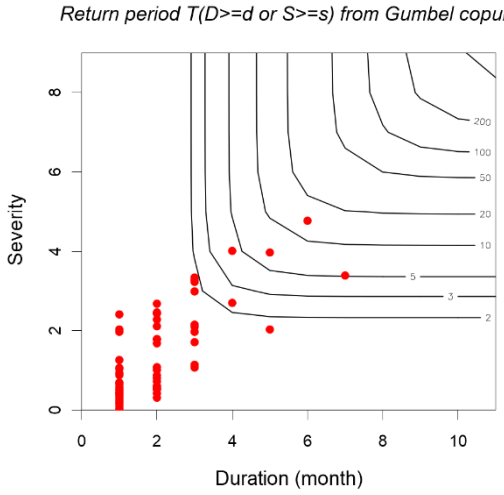

D20M018 SPI 1-month

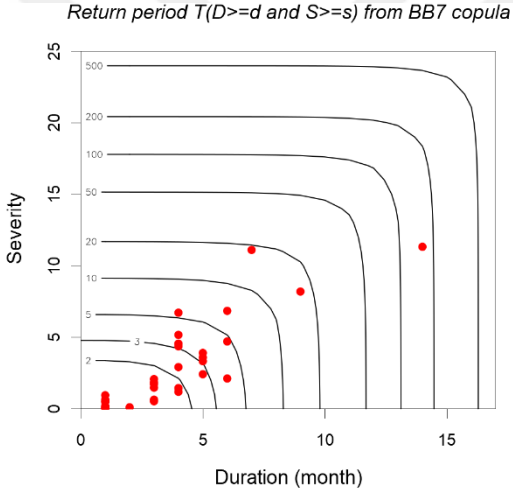

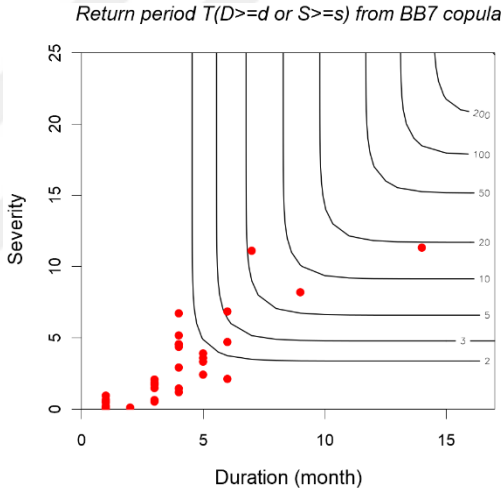

D20M018 SPI 3-month

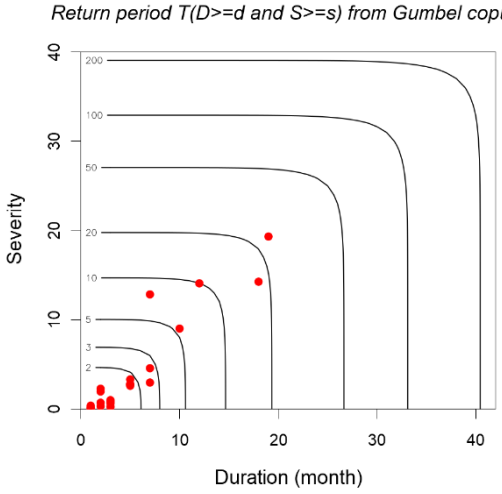

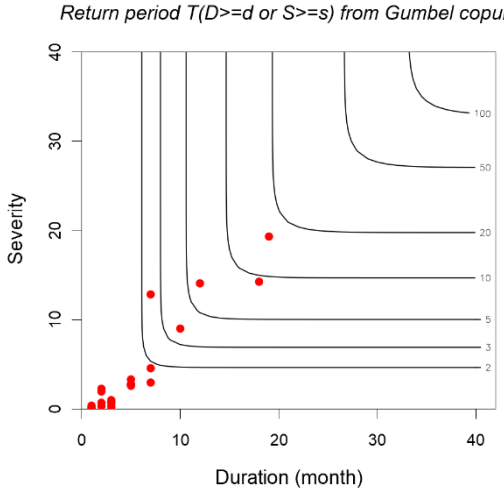

D20M018 SPI 6-month

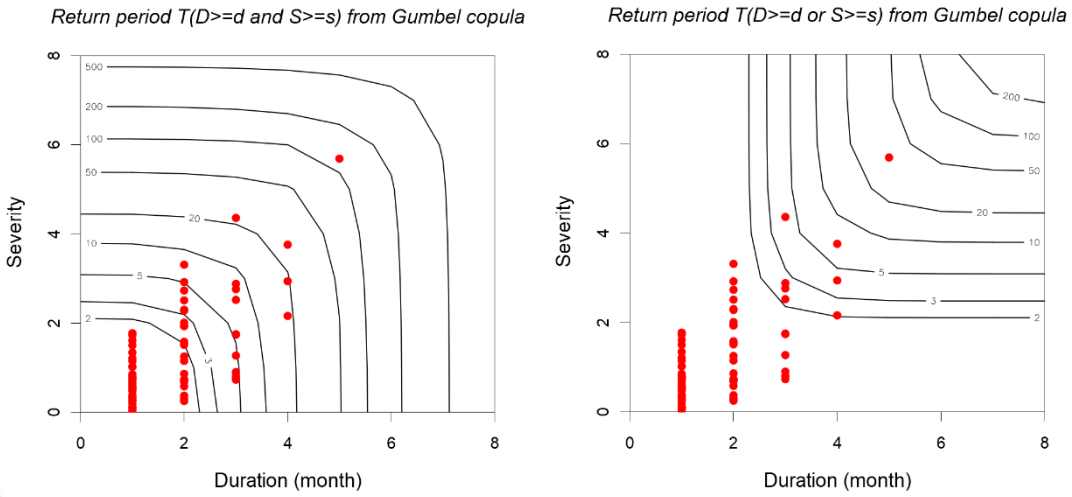

D20M020 SPI 1-month

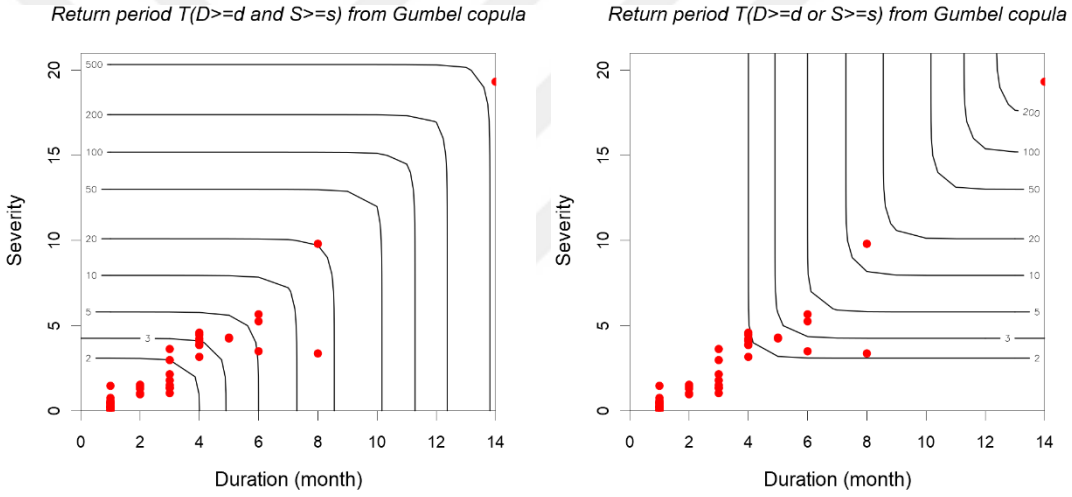

D20M020 SPI 3-month

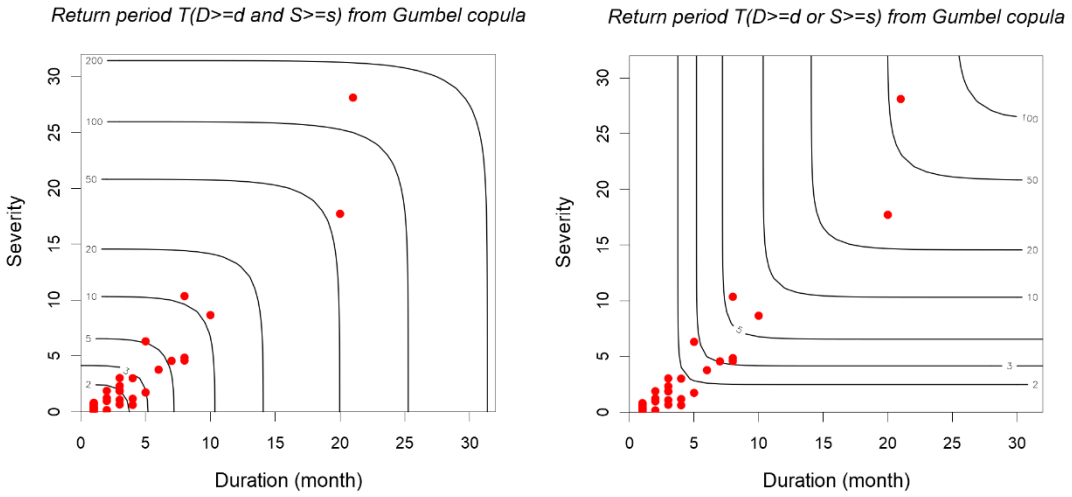

D20M020 SPI 6-month

Figure 7.8 Bivariate drought duration and severity return period, T_{DS} and T'_{DS} for all stations at SPI 1-, 3- and 6-month time scales

Table 7.12 Univariate and bivariate return periods of drought duration and severity for SPI 1-month time scale

Station	Year	D	S	T_{DS}	T'_{DS}
7767	10	4.35	4.45	18.37	6.87
	20	5.04	5.27	37.09	13.69
	50	6.01	6.34	93.25	34.16
	100	6.79	7.14	186.86	68.27
	200	7.60	7.94	374.07	136.49
	500	8.74	9.00	935.72	341.15
8275	10	3.86	4.29	16.78	7.34
	20	4.53	5.10	33.88	14.62
	50	5.47	6.15	85.18	36.46
	100	6.21	6.94	170.69	72.86
	200	7.00	7.73	341.72	145.65
	500	8.10	8.76	854.78	364.05
17255	10	4.53	4.52	17.22	7.05
	20	5.39	5.47	34.82	14.03
	50	6.61	6.73	87.64	34.98
	100	7.60	7.68	175.67	69.89
	200	8.65	8.63	351.74	139.72
	500	10.14	9.88	879.94	349.22
17355	10	4.59	4.88	18.91	6.80
	20	5.43	5.98	38.31	13.53
	50	6.63	7.46	96.49	33.74
	100	7.60	8.58	193.47	67.42
	200	8.63	9.72	387.44	134.79
	500	10.09	11.24	969.33	336.89
17866	10	5.14	4.98	16.01	7.27
	20	6.14	5.93	32.26	14.49
	50	7.58	7.18	80.99	36.16
	100	8.75	8.12	162.21	72.28
	200	10.00	9.06	324.65	144.51
	500	11.79	10.29	811.93	361.22
17868	10	4.45	4.19	18.62	6.84
	20	5.22	4.91	37.67	13.61
	50	6.30	5.83	94.82	33.95
	100	7.16	6.51	190.07	67.85
	200	8.07	7.17	380.59	135.64
	500	9.36	8.04	952.12	339.02
17870	10	4.88	4.73	17.39	7.02
	20	5.51	5.69	35.14	13.98
	50	6.27	6.96	88.39	34.86
	100	6.82	7.92	177.14	69.66
	200	7.34	8.88	354.64	139.27
	500	8.00	10.14	887.15	348.09
17871	10	4.70	4.46	17.00	7.08
	20	5.53	5.41	34.40	14.10
	50	6.70	6.67	86.59	35.15
	100	7.63	7.63	173.58	70.23
	200	8.62	8.58	347.56	140.39
	500	10.01	9.84	869.49	350.89
17908	10	4.66	4.80	17.89	6.94
	20	5.52	5.68	36.16	13.82
	50	6.73	6.81	90.97	34.47

	100	7.71	7.65	182.33	68.89
	200	8.76	8.48	365.05	137.73
	500	10.24	9.57	913.21	344.24
17960	10	4.07	4.48	16.24	7.22
	20	4.79	5.39	32.76	14.39
	50	5.79	6.59	82.34	35.90
	100	6.59	7.49	164.97	71.74
	200	7.44	8.39	330.23	143.44
	500	8.63	9.58	826.00	358.51
17979	10	5.45	4.58	19.21	6.76
	20	6.18	5.45	38.95	13.45
	50	7.10	6.60	98.20	33.54
	100	7.75	7.45	196.96	67.01
	200	8.37	8.29	394.47	133.96
	500	9.16	9.40	987.01	334.80
D20M001	10	4.73	4.37	17.04	7.08
	20	5.62	5.32	34.42	14.09
	50	6.88	6.59	86.59	35.15
	100	7.90	7.54	173.54	70.24
	200	8.99	8.50	347.45	140.41
	500	10.53	9.77	869.15	350.94
D20M002	10	4.29	4.64	15.88	7.30
	20	5.08	5.74	32.05	14.53
	50	6.21	7.21	80.58	36.24
	100	7.11	8.33	161.47	72.43
	200	8.07	9.45	323.24	144.80
	500	9.42	10.94	808.55	361.90
D20M004	10	4.80	4.70	15.45	7.39
	20	5.46	5.71	31.17	14.72
	50	6.28	7.05	78.35	36.72
	100	6.85	8.06	156.97	73.37
	200	7.40	9.06	314.22	146.68
	500	8.10	10.39	785.98	366.61
D20M006	10	4.82	4.99	13.99	7.78
	20	5.38	6.11	28.12	15.52
	50	6.05	7.60	70.50	38.74
	100	6.53	8.74	141.14	77.43
	200	6.98	9.89	282.42	154.82
	500	7.54	11.42	706.27	386.98
D20M009	10	5.02	4.62	18.58	6.84
	20	5.65	5.56	37.61	13.62
	50	6.42	6.81	94.70	33.97
	100	6.97	7.75	189.87	67.87
	200	7.50	8.68	380.19	135.69
	500	8.16	9.92	951.17	339.14
D20M011	10	5.42	4.50	20.11	6.65
	20	6.53	5.32	40.85	13.24
	50	8.11	6.39	103.10	33.00
	100	9.40	7.18	206.86	65.94
	200	10.80	7.96	414.37	131.81
	500	12.79	8.97	1036.92	329.42
D20M013	10	4.65	4.28	17.98	6.93
	20	5.27	5.27	36.65	13.75
	50	6.03	6.59	92.70	34.23
	100	6.57	7.60	186.13	68.37
	200	7.09	8.62	372.98	136.63
	500	7.75	9.98	933.56	341.43
D20M014	10	4.73	4.73	17.24	7.04

	20	5.59	5.64	34.81	14.03
	50	6.82	6.83	87.53	34.99
	100	7.81	7.74	175.40	69.94
	200	8.87	8.63	351.13	139.82
	500	10.36	9.82	878.32	349.47
D20M015	10	4.16	4.45	18.79	6.81
	20	4.85	5.40	37.98	13.57
	50	5.83	6.65	95.56	33.86
	100	6.61	7.60	191.53	67.66
	200	7.43	8.55	383.46	135.28
	500	8.58	9.81	959.28	338.12
D20M016	10	4.75	5.10	15.96	7.28
	20	5.63	6.15	32.15	14.51
	50	6.88	7.54	80.73	36.22
	100	7.89	8.59	161.70	72.38
	200	8.97	9.64	323.63	144.72
	500	10.50	11.03	809.43	361.72
D20M017	10	4.79	5.15	16.02	7.27
	20	5.64	6.22	32.30	14.49
	50	6.85	7.64	81.12	36.14
	100	7.82	8.71	162.48	72.23
	200	8.85	9.78	325.22	144.40
	500	10.31	11.19	813.42	360.93
D20M018	10	4.73	4.23	17.54	6.99
	20	5.56	4.96	35.42	13.93
	50	6.72	5.90	89.05	34.76
	100	7.66	6.59	178.45	69.46
	200	8.66	7.28	357.23	138.88
	500	10.06	8.16	893.58	347.11
D20M020	10	3.72	3.86	20.24	6.64
	20	4.28	4.57	41.03	13.22
	50	5.05	5.51	103.41	32.97
	100	5.67	6.21	207.40	65.88
	200	6.30	6.91	415.37	131.71
	500	7.19	7.83	1039.29	329.19

Table 7.13 Univariate and bivariate return periods of drought duration and severity for SPI 3-month time scale

Station	Year	D	S	T_{DS}	T'_{DS}
7767	10	9.03	9.55	11.75	8.71
	20	10.69	12.37	23.50	17.41
	50	12.81	16.14	58.74	43.53
	100	14.37	19.03	117.48	87.06
	200	15.91	21.94	234.97	174.12
	500	17.92	25.80	587.03	435.52
8275	10	8.39	8.88	13.35	7.99
	20	10.84	11.69	26.90	15.92
	50	14.57	15.59	67.55	39.69
	100	17.79	18.66	135.30	79.31
	200	21.38	21.83	270.79	158.55
	500	26.77	26.13	677.28	396.27
17255	10	7.92	8.73	13.59	7.91
	20	9.20	11.09	27.40	15.75
	50	10.78	14.24	68.86	39.25
	100	11.90	16.63	137.95	78.43
	200	12.98	19.04	276.13	156.78

	500	14.34	22.23	690.67	391.83
17355	10	7.83	8.23	13.81	7.84
	20	10.00	10.87	27.83	15.61
	50	13.27	14.60	69.88	38.93
	100	16.08	17.57	139.96	77.79
	200	19.20	20.66	280.12	155.52
	500	23.86	24.91	700.60	388.71
17866	10	8.04	8.71	12.79	8.21
	20	10.17	11.02	25.73	16.36
	50	13.34	14.10	64.53	40.81
	100	16.03	16.45	129.21	81.56
	200	18.99	18.80	258.56	163.07
	500	23.36	21.91	646.62	407.58
17868	10	7.83	8.14	13.58	7.91
	20	9.94	10.22	27.34	15.77
	50	13.11	13.00	68.61	39.33
	100	15.82	15.11	137.40	78.60
	200	18.83	17.22	274.99	157.15
	500	23.30	20.03	687.74	392.78
17870	10	8.33	8.92	13.15	8.07
	20	9.87	11.56	26.47	16.07
	50	11.81	15.17	66.42	40.09
	100	13.21	17.98	133.02	80.11
	200	14.56	20.86	266.22	160.16
	500	16.30	24.75	665.80	400.31
17871	10	8.26	8.12	13.71	7.87
	20	9.69	10.13	27.63	15.67
	50	11.51	12.78	69.40	39.08
	100	12.85	14.79	139.01	78.09
	200	14.18	16.80	278.24	156.10
	500	15.90	19.45	695.91	390.16
17908	10	8.00	8.87	14.10	7.75
	20	10.24	11.41	28.51	15.40
	50	13.61	14.83	71.73	38.38
	100	16.50	17.44	143.76	76.66
	200	19.72	20.08	287.83	153.24
	500	24.52	23.59	720.03	382.97
17960	10	7.48	8.82	14.48	7.64
	20	8.68	11.10	29.27	15.19
	50	10.12	14.10	73.65	37.85
	100	11.15	16.38	147.62	75.61
	200	12.12	18.66	295.55	151.14
	500	13.35	21.66	739.35	377.72
17979	10	7.87	8.33	13.51	7.94
	20	9.26	10.52	27.20	15.81
	50	10.99	13.44	68.27	39.44
	100	12.25	15.67	136.73	78.82
	200	13.46	17.90	273.65	157.59
	500	15.01	20.86	684.39	393.88
D20M001	10	10.17	8.81	12.45	8.35
	20	13.50	11.37	25.05	16.64
	50	18.68	14.78	62.84	41.52
	100	23.24	17.39	125.83	82.97
	200	28.43	20.00	251.80	165.88
	500	36.35	23.48	629.72	414.60
D20M002	10	6.70	7.46	13.27	8.02
	20	8.43	9.79	26.70	15.99
	50	11.00	13.06	66.99	39.88

	100	13.17	15.66	134.15	79.71
	200	15.57	18.35	268.46	159.36
	500	19.10	22.03	671.38	398.32
D20M004	10	7.90	8.84	12.42	8.37
	20	10.01	11.72	24.96	16.68
	50	13.16	15.79	62.58	41.63
	100	15.84	19.04	125.27	83.21
	200	18.80	22.41	250.65	166.38
	500	23.18	27.05	626.81	415.87
D20M006	10	7.06	6.71	13.60	6.03
	20	7.72	7.48	28.47	12.57
	50	8.47	8.38	76.03	33.87
	100	8.98	8.98	161.26	72.04
	200	9.46	9.54	345.52	152.99
	500	10.03	10.21	962.89	410.88
D20M009	10	8.83	9.35	13.17	8.06
	20	10.37	12.02	26.35	16.12
	50	12.29	15.63	65.87	40.29
	100	13.66	18.43	131.74	80.59
	200	14.98	21.28	263.48	161.17
	500	16.66	25.10	658.69	402.93
D20M011	10	9.90	9.10	14.05	7.76
	20	12.96	11.59	28.58	15.38
	50	17.65	14.92	72.21	38.24
	100	21.74	17.47	144.95	76.33
	200	26.35	20.03	290.42	152.52
	500	33.32	23.45	726.82	381.08
D20M013	10	8.57	9.33	13.76	7.85
	20	10.23	13.81	27.77	15.63
	50	12.36	21.65	69.77	38.96
	100	13.95	29.34	139.78	77.85
	200	15.51	38.84	279.80	155.62
	500	17.55	54.68	699.86	388.93
D20M014	10	7.04	8.08	14.87	7.53
	20	8.92	10.30	30.21	14.95
	50	11.74	13.29	76.24	37.20
	100	14.14	15.57	152.98	74.28
	200	16.80	17.86	306.46	148.44
	500	20.75	20.91	766.90	370.91
D20M015	10	7.60	7.84	15.09	7.48
	20	9.63	9.96	30.73	14.82
	50	12.66	12.83	77.68	36.86
	100	15.24	15.04	155.94	73.60
	200	18.09	17.28	312.48	147.06
	500	22.31	20.28	782.08	367.46
D20M016	10	7.38	8.43	13.51	7.94
	20	8.51	10.63	27.24	15.80
	50	9.87	13.53	68.44	39.39
	100	10.83	15.72	137.10	78.70
	200	11.74	17.91	274.43	157.33
	500	12.88	20.81	686.41	393.21
D20M017	10	7.73	8.78	13.77	7.85
	20	9.08	11.10	27.76	15.63
	50	10.81	14.19	69.74	38.97
	100	12.08	16.54	139.70	77.87
	200	13.33	18.89	279.63	155.67
	500	14.97	22.01	699.41	389.07
D20M018	10	8.35	9.15	14.70	7.58

	20	9.84	11.72	29.41	15.15
	50	11.74	15.17	73.54	37.87
	100	13.15	17.81	147.09	75.75
	200	14.54	20.46	294.18	151.50
	500	16.34	23.99	735.45	378.75
D20M020	10	7.36	7.96	12.23	8.46
	20	8.63	10.12	24.56	16.87
	50	10.21	13.01	61.56	42.10
	100	11.35	15.22	123.21	84.15
	200	12.45	17.43	246.52	168.25
	500	13.85	20.37	616.45	420.55

Table 7.14 Univariate and bivariate return periods of drought duration and severity for SPI 6-month time scale

Station	Year	D	S	T_{DS}	T'_{DS}
7767	10	10.59	10.58	11.57	8.81
	20	12.83	14.78	23.15	17.62
	50	15.63	20.85	57.87	44.05
	100	17.65	25.80	115.73	88.10
	200	19.62	31.01	231.46	176.19
	500	22.13	38.27	578.65	440.48
8275	10	11.33	12.66	11.80	8.68
	20	16.22	19.59	23.74	17.28
	50	24.32	30.51	59.54	43.09
	100	31.87	40.03	119.22	86.12
	200	40.82	50.56	238.57	172.17
	500	55.10	65.96	596.62	430.31
17255	10	11.09	11.15	12.27	8.44
	20	13.53	15.05	24.72	16.79
	50	16.57	20.31	62.06	41.86
	100	18.76	24.35	124.29	83.65
	200	20.88	28.42	248.75	167.22
	500	23.59	33.85	622.15	417.95
17355	10	11.56	11.74	15.04	7.50
	20	14.44	17.36	30.95	14.80
	50	18.20	25.99	78.78	36.68
	100	21.03	33.34	158.51	73.16
	200	23.83	41.35	318.00	146.11
	500	27.52	52.89	796.43	364.95
17866	10	11.49	11.60	12.40	8.38
	20	15.72	15.68	24.79	16.76
	50	22.46	21.24	61.99	41.90
	100	28.54	25.53	123.97	83.80
	200	35.57	29.87	247.95	167.59
	500	46.50	35.67	619.87	418.98
17868	10	11.50	11.42	19.55	9.02
	20	14.23	15.85	39.89	17.89
	50	17.76	22.17	100.96	44.47
	100	20.39	27.26	202.77	88.77
	200	23.01	32.59	406.41	177.38
	500	26.43	39.94	1017.33	443.19
17870	10	11.85	11.94	11.94	8.60
	20	16.70	17.73	23.87	7.21
	50	24.62	26.53	59.68	43.02
	100	31.90	33.98	119.36	86.04
	200	40.45	42.07	238.72	172.09

	500	53.97	53.65	596.83	430.20
17871	10	12.02	11.22	12.19	8.48
	20	16.33	15.33	24.52	16.89
	50	23.14	21.16	61.52	42.11
	100	29.24	25.81	123.18	84.16
	200	36.26	30.66	246.51	168.25
	500	47.10	37.33	616.49	420.54
17908	10	11.41	11.56	12.54	8.32
	20	15.04	15.69	25.28	16.55
	50	20.56	21.30	63.48	41.24
	100	25.33	25.62	127.16	82.40
	200	30.67	29.99	254.51	164.72
	500	38.69	35.81	636.57	411.68
17960	10	9.65	10.73	12.98	8.13
	20	12.75	14.49	25.96	16.26
	50	17.51	19.59	64.91	40.66
	100	21.65	23.52	129.82	81.32
	200	26.32	27.49	259.64	162.64
	500	33.37	32.80	649.11	406.60
17979	10	9.74	10.54	12.44	8.36
	20	12.92	14.55	24.88	16.72
	50	17.85	20.35	62.20	41.80
	100	22.20	25.07	124.41	83.60
	200	27.13	30.05	248.81	167.20
	500	34.64	36.98	622.03	418.00
D20M001	10	12.92	12.67	11.98	8.58
	20	16.89	18.30	24.13	17.08
	50	22.14	26.14	60.57	42.57
	100	26.11	32.27	121.31	85.06
	200	30.08	38.52	242.77	170.04
	500	35.33	46.92	607.18	424.98
D20M002	10	10.98	11.83	11.33	8.95
	20	14.84	17.51	22.65	17.90
	50	20.87	26.10	56.63	44.76
	100	26.21	33.34	113.25	89.52
	200	32.29	41.16	226.51	179.05
	500	41.59	52.34	566.26	447.62
D20M004	10	9.71	11.72	12.02	8.56
	20	11.80	16.57	24.16	17.06
	50	14.42	23.69	60.59	42.56
	100	16.34	29.56	121.31	85.06
	200	18.20	35.80	242.75	170.05
	500	20.58	44.58	607.05	425.05
D20M006	10	11.42	11.30	12.68	8.26
	20	13.64	14.94	25.35	16.51
	50	16.49	19.88	63.38	41.28
	100	18.60	23.67	126.77	82.57
	200	20.68	27.51	253.53	165.13
	500	23.39	32.62	633.83	412.83
D20M009	10	10.12	11.48	12.01	8.56
	20	13.79	16.55	24.13	17.08
	50	19.65	24.23	60.50	42.61
	100	24.96	30.71	121.10	85.16
	200	31.10	37.75	242.30	170.27
	500	40.68	47.83	605.92	425.60
D20M011	10	11.52	11.62	11.76	8.70
	20	13.85	15.87	23.65	17.33
	50	16.72	21.66	59.30	43.22

	100	18.77	26.12	118.73	86.38
	200	20.74	30.64	237.58	172.69
	500	23.24	36.68	594.12	431.62
D20M013	10	11.45	12.18	12.58	8.30
	20	15.89	17.81	25.36	16.51
	50	23.01	26.26	63.71	41.15
	100	29.49	33.34	127.62	82.21
	200	37.01	40.96	255.43	164.34
	500	48.76	51.78	638.88	410.72
D20M014	10	12.70	11.86	13.66	7.89
	20	17.67	16.17	27.94	15.57
	50	25.69	22.04	70.82	38.64
	100	32.98	26.56	142.31	77.08
	200	41.48	31.14	285.29	153.97
	500	54.79	37.25	714.24	384.63
D20M015	10	10.74	11.00	15.63	7.35
	20	12.97	15.26	33.10	14.33
	50	15.75	21.35	86.05	35.24
	100	17.76	26.26	174.49	70.08
	200	19.69	31.41	351.45	139.77
	500	22.16	38.54	882.42	348.83
D20M016	10	11.80	11.93	11.98	8.58
	20	17.05	18.08	23.95	17.17
	50	25.84	27.57	59.88	42.92
	100	34.09	35.69	119.76	85.84
	200	43.95	44.58	239.52	171.68
	500	59.79	57.41	598.81	429.18
D20M017	10	10.39	11.67	11.76	8.70
	20	14.26	16.98	23.51	17.40
	50	20.44	25.02	58.78	43.50
	100	26.03	31.80	117.56	87.00
	200	32.52	39.14	235.13	174.00
	500	42.64	49.64	587.50	435.18
D20M018	10	14.67	14.70	12.40	8.38
	20	19.35	19.78	24.91	16.71
	50	26.65	27.05	62.44	41.69
	100	33.11	32.92	125.00	83.33
	200	40.45	39.07	250.11	166.62
	500	51.67	47.59	625.45	416.47
D20M020	10	10.36	10.34	13.11	8.08
	20	14.08	14.58	26.44	16.08
	50	19.97	20.82	66.41	40.09
	100	25.26	25.97	133.04	80.11
	200	31.37	31.45	266.29	160.14
	500	40.82	39.16	666.03	400.23

7.7 Conditional Return Periods of Drought Characteristics

The conditional drought duration and severity return period can also derived as conditional situations for the following two cases: the return period of drought severity given drought duration exceeding a certain threshold, and the return period of drought duration given a drought severity that exceeds a certain threshold. Both the conditional return periods of drought characteristics are calculated by using Equations. 3.131 and 3.132. The graphical representations of both two cases are given for all stations at multiple time scales in Figure 7.9. For example, a return period for drought duration exceeding 3 months, given drought severity exceeding 4 by using Eq. 3.131 for station 17255 at SPI 1-month, is 138.265 years. The return period of drought severity exceeds 3 given duration exceeds 4 months, based on Eq. 3.132, is 129.049 years for the same station.

For SPI 3-month, the conditional return period for drought duration exceeds 10 months given drought severity exceeds 4 for station 17255, is 123.96 years. When we consider to the return period of drought severity exceeds 10 given drought duration exceeds 4 months, the conditional return period of this situation is calculated as 40.221 years using the historical data. Additionally, it can be reported from Fig. 7.9 that the conditional return periods graphs yield similar drought trends for all different time scales. But all conditional return period graphs for both cases tend to indicate lower return periods at the higher duration/severity values. For SPI 6-month, the conditional return period for drought duration exceeds 15 month given drought severity 4 for the station 17255, is calculated as 85.046 years. The conditional return period for drought severity exceeds 15 given drought duration exceeds 4 months, is evaluated as 37.22 years. The conditional return periods for both two cases are presented in Fig. 7.9 at different time scales.

Table 7.15 and 7.16 show the conditional return periods for both two cases at SPI 1-, 3- and 6-month for all station. For instance, looking to SPI 1-month, the lower conditional return period of drought duration exceeds 3 month given drought severity exceeds 4 are found stations 17866, D20A004, D20A006, D20A0016 and D20A017 as 73.593, 91.716, 79.039, 79.974 and 74.206 years, respectively in Table 7.15. Additionally, the higher conditional return period for the same condition are noted as the stations 17868(245.873 years), D20A015 (212.619 years), D20A018 (223.963

years) and D20A020 (534.994 years). The higher return periods show that extreme events are less likely occurring at these stations.

For SPI 3-month time scales, the higher conditional return periods for drought duration exceeds 10 months given drought severity 4, are noted at the stations 17960, D20A002, D20A006, D20A016 and D20A020 as 156.232, 206.723, 210.217, 193.816 and 208.068, respectively. The lower conditional return periods for the same station are observed at the stations 7767 (52.515 years), 17908 (53.252 years), D20A001 (35.231 years) and D20A011 (35.579 years).

For the SPI 6-month time scale, the higher conditional return periods for the drought duration exceeds 15 month given drought severity exceeds 4, are found at the stations 7767 (137.342 years), 17979 (101.432), D20A004 (202.094), D20A015 (122.781). Additionally, the lower conditional return periods (lower than 50 years) for the same conditions, are noted at the stations 8275 (54.992 years), 17866 (54.596 years), 17870 (51.436 years), 17871 (49.783 years), D20A001 (48.325 years), D20A013 (54.724 years), D20A014 (39.115 years), D20A016 (50.184 years) and D20A018 (30.711 years).

Table 7.15 The conditional return period of drought severity given that drought duration is greater than a certain value ($T_{D|S\geq s}$), d´

Station	SPI 1 (D = 3, S ≥4)	SPI 3 (D = 10, S ≥4)	SPI 6 (D = 15, S ≥4)
7767	193.749	52.515	137.342
8275	190.894	65.582	54.992
17255	138.265	123.396	85.046
17355	137.986	104.167	82.921
17866	73.593	72.827	54.596
17868	245.873	92.112	72.697
17870	114.384	85.269	51.436
17871	149.656	93.379	49.783
17908	103.679	53.252	55.468
17960	152.708	156.232	99.008
17979	126.010	127.106	101.432
D20A001	171.562	35.231	48.325
D20A002	120.652	206.723	65.239
D20A004	91.716	91.574	202.094
D20A006	79.039	210.217	99.613
D20A009	128.613	61.487	95.670
D20A011	140.119	35.579	82.049

D20A013	194.929	85.663	54.724
D20A014	114.364	142.984	39.115
D20A015	212.619	108.317	122.781
D20A016	79.974	193.816	50.184
D20A017	74.206	123.133	80.455
D20A018	223.963	88.010	30.711
D20A020	534.994	208.068	88.344

Table 7.16 indicates the conditional return periods for drought severity given drought duration exceeding a certain threshold at SPI 1-, 3- and 6-month for all station. For instance, looking to SPI 1-month, the lower conditional return period (lower than 100 years) of drought severity exceeds 3 given drought duration exceeds 4 months are found stations 17866, 17870, 17979, D20A004, D20A006, D20A009, D20A011 and D20A018 as 60.790, 65.453, 42.020, 60.505, 50.939, 59.719, 62.369 and 88.762 years, respectively. Additionally, the higher conditional return period (higher than 200 years) for the same condition are noted as the stations 7767 (214.643 years), 8275 (376.092 years), 17960 (259.106 years), D20A015 (299.385 years) and D20A020 (799.378 years) which is recorded the highest conditional return period for drought severity given drought duration.

For SPI 3-month time scale, the higher conditional return periods (higher than 80 years) for drought severity exceeds 10 given drought duration 4 months, are noted at the stations D20A002, D20A006, D20A014 and D20A015 as 110.405, 180.435, 92.175 and 85.013 years, respectively. The lower conditional return periods (lower than 40 years) for the same station are observed at the stations 7767 (24.812 years), 17870 (38.585 years), 17960 (39.962 years), D20A001 (38.013 years), D20A009 (29.776 years), D20A011 (36.085 years), D20A013 (29.461 years) and D20A018 (34.250 years).

For the SPI 6-month time scale, the higher conditional return periods (higher than 50 years) for the drought severity exceeds 15 given drought duration exceeds 4 months, are found at the stations 17960 (56.266 years), 17979 (52.404 years), D20A009 (50.765 years) and D20A020 (59.600 years). Additionally, the lower conditional return periods (lower than 30 years) for the same conditions, are noted at the stations D20A001 (26.913 years) and D20A018 (21.274 years).

Table 7.16 The conditional return period of drought duration given that drought severity is greater than a certain value ($T_{S|D\geq d}$), s´

Station	SPI 1 (S = 3, D ≥4)	SPI 3 (S = 10, D ≥4)	SPI 6(S = 15, D ≥4)
7767	214.643	24.812	42.370
8275	376.092	45.820	32.003
17255	129.049	40.221	37.222
17355	117.164	66.483	32.097
17866	60.790	51.460	43.623
17868	171.543	77.108	33.876
17870	65.453	38.585	34.553
17871	103.059	49.219	42.750
17908	118.180	53.252	34.979
17960	259.106	39.962	56.266
17979	42.020	54.237	52.404
D20A001	107.907	38.013	26.913
D20A002	161.658	110.405	32.767
D20A004	60.505	49.972	37.234
D20A006	50.939	180.435	36.710
D20A009	59.719	29.776	50.765
D20A011	62.369	36.085	30.335
D20A013	102.213	29.461	33.678
D20A014	107.515	92.175	35.589
D20A015	299.385	85.013	37.780
D20A016	100.533	44.326	35.273
D20A017	88.762	41.129	43.782
D20A018	116.846	34.250	21.274
D20A020	799.378	66.810	59.600

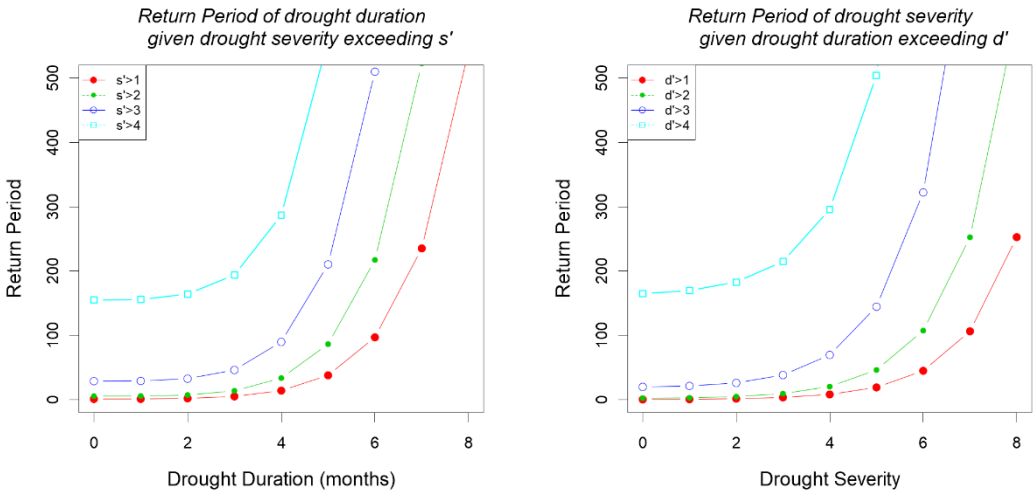

7767 SPI 1-month

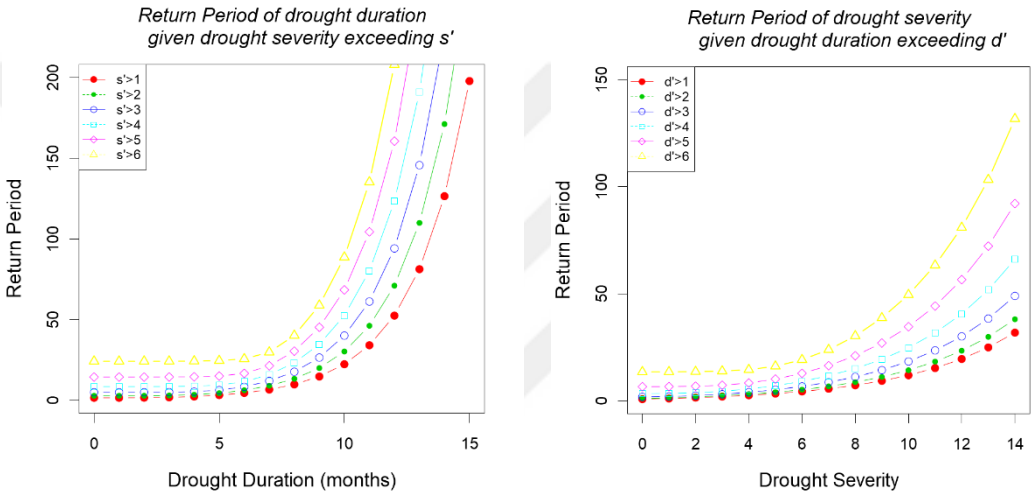

7767 SPI 3-month

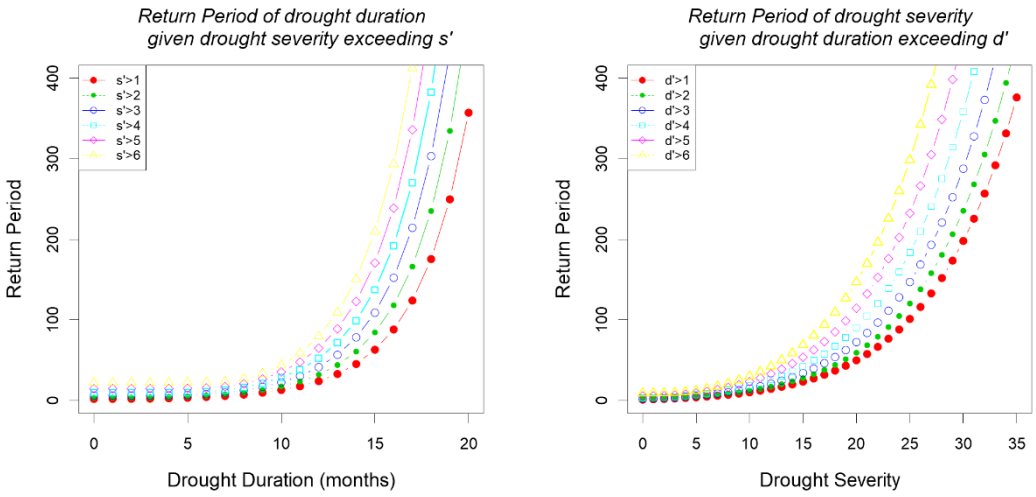

7767 SPI 6-month

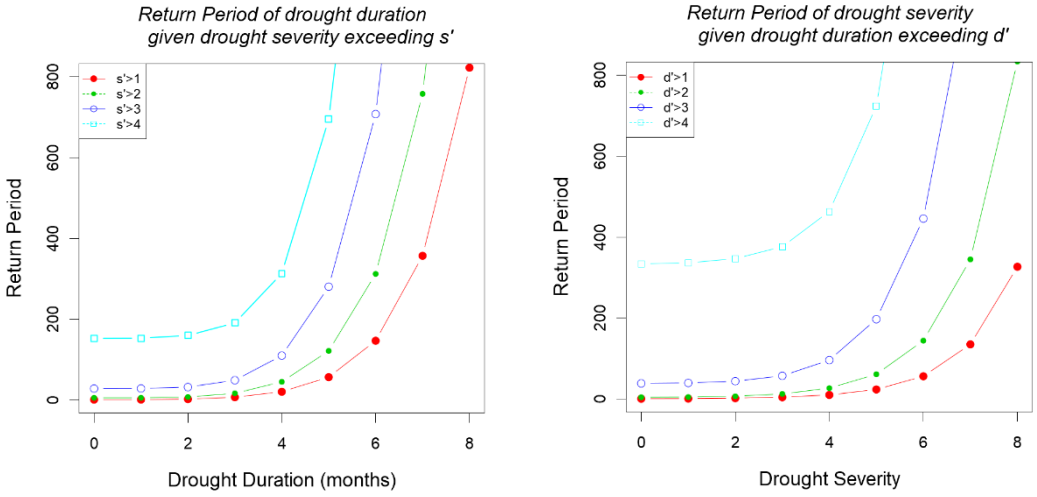

8275 SPI 1-month

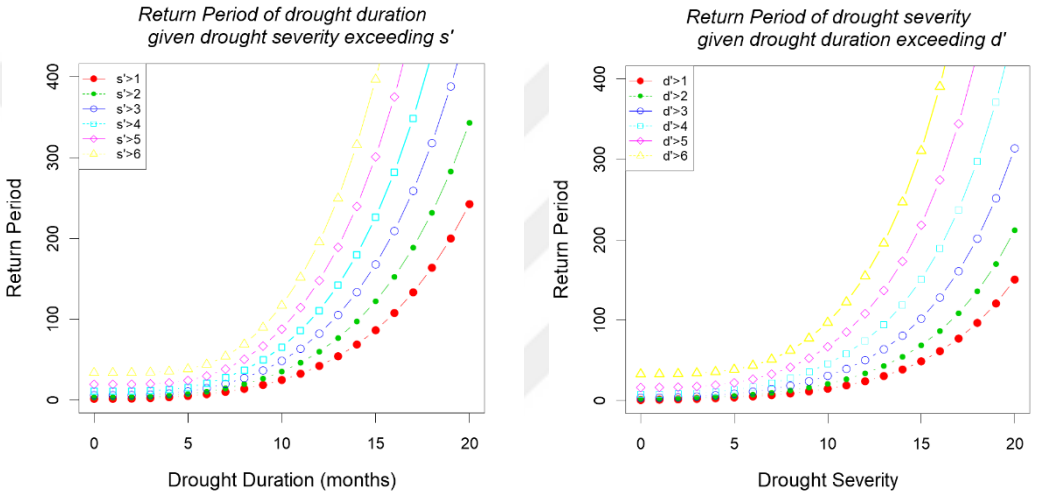

8275 SPI 3-month

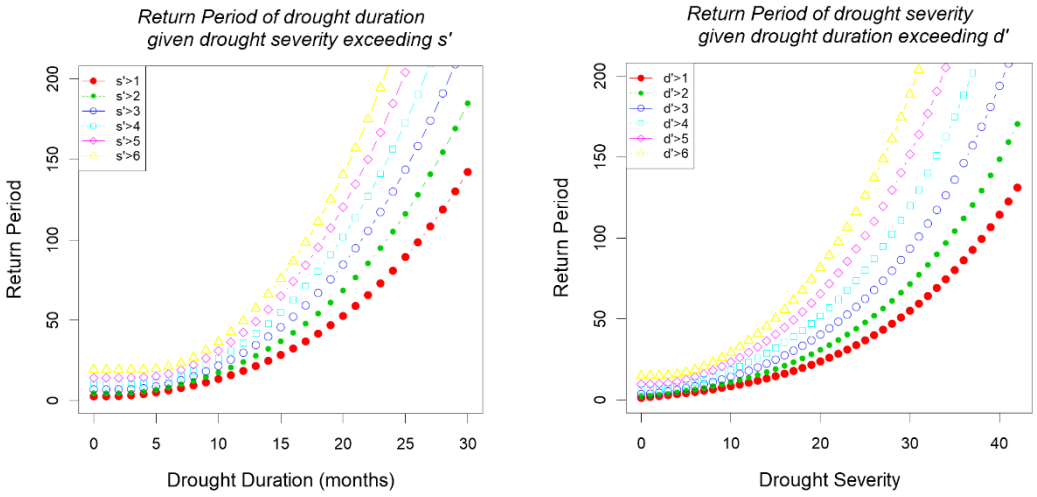

8275 SPI 6-month

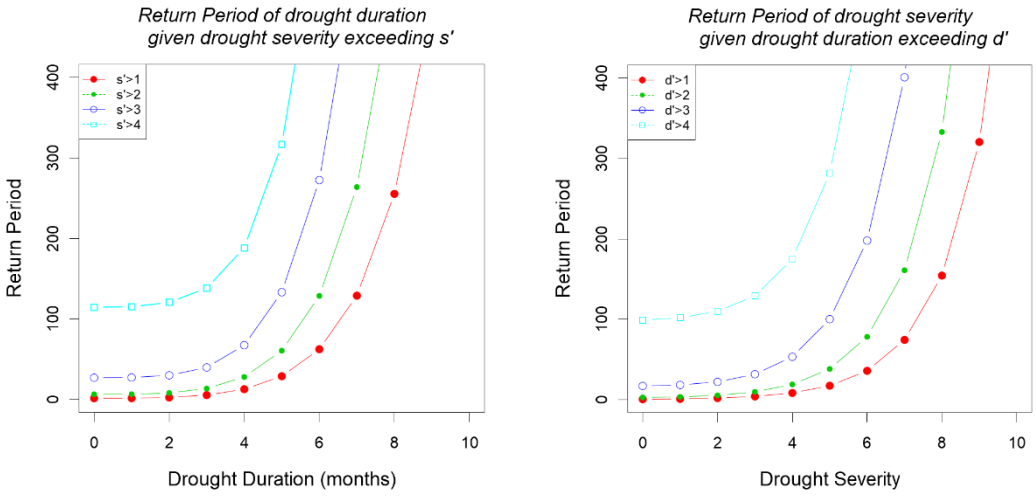

17255 SPI 1-month

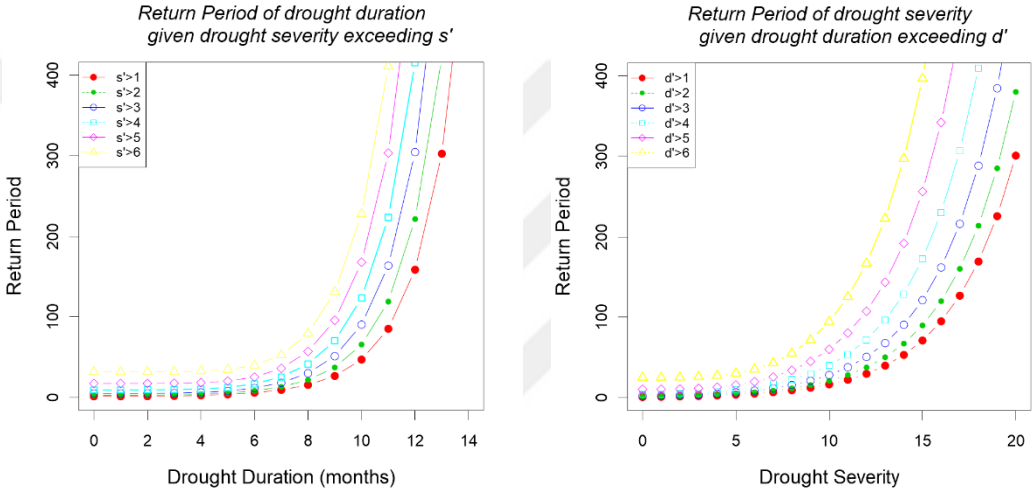

17255 SPI 3-month

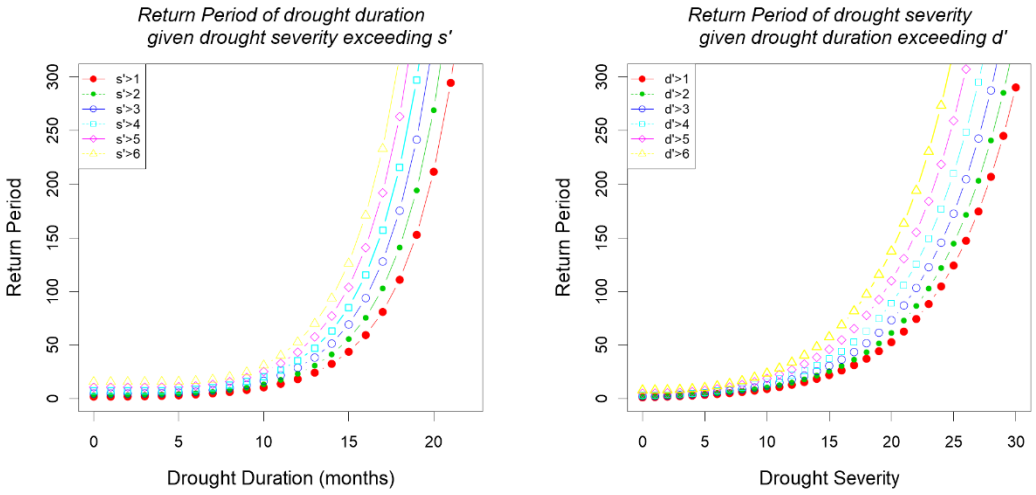

17255 SPI 6-month

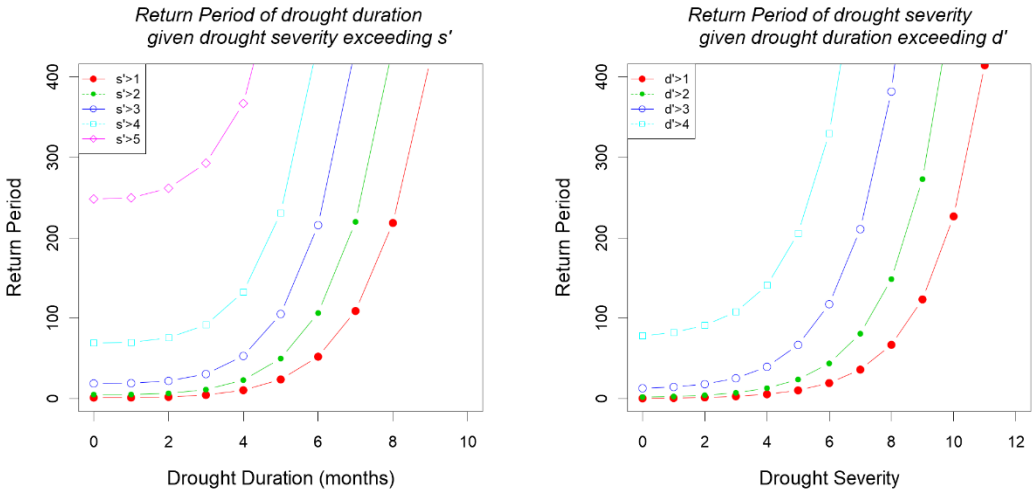

17355 SPI 1-month

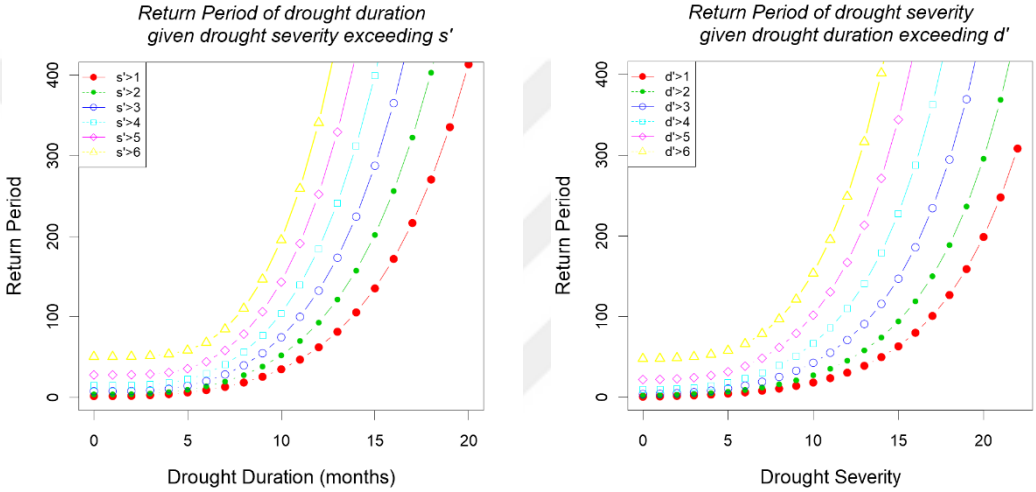

17355 SPI 3-month

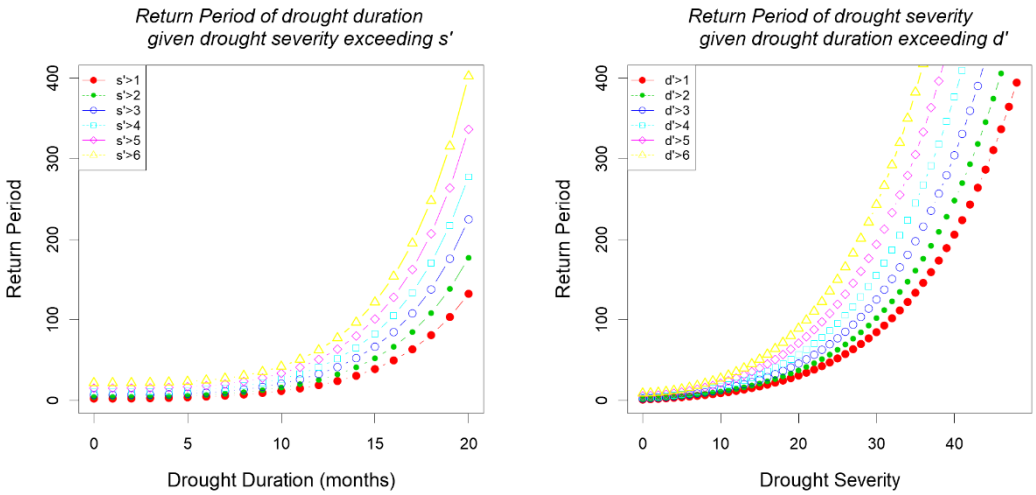

17355 SPI 6-month

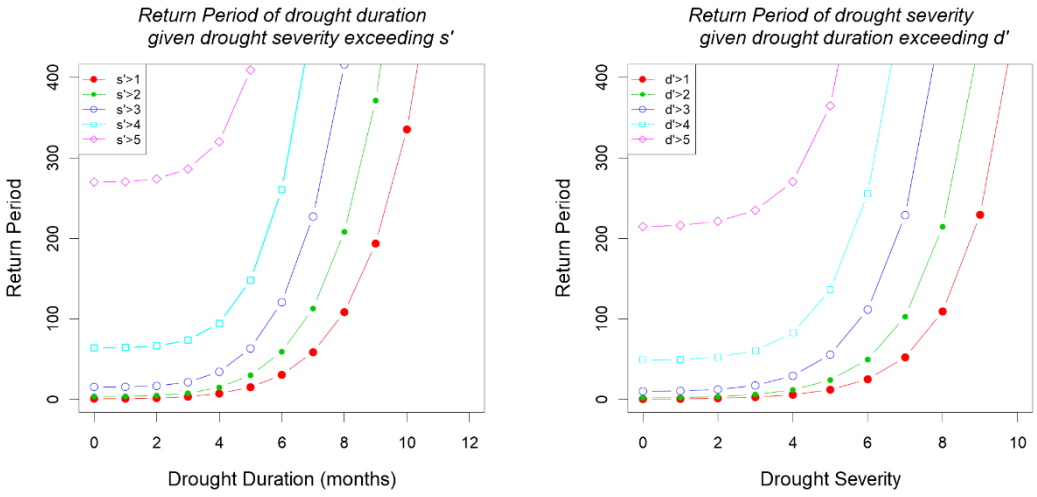

17866 SPI 1-month

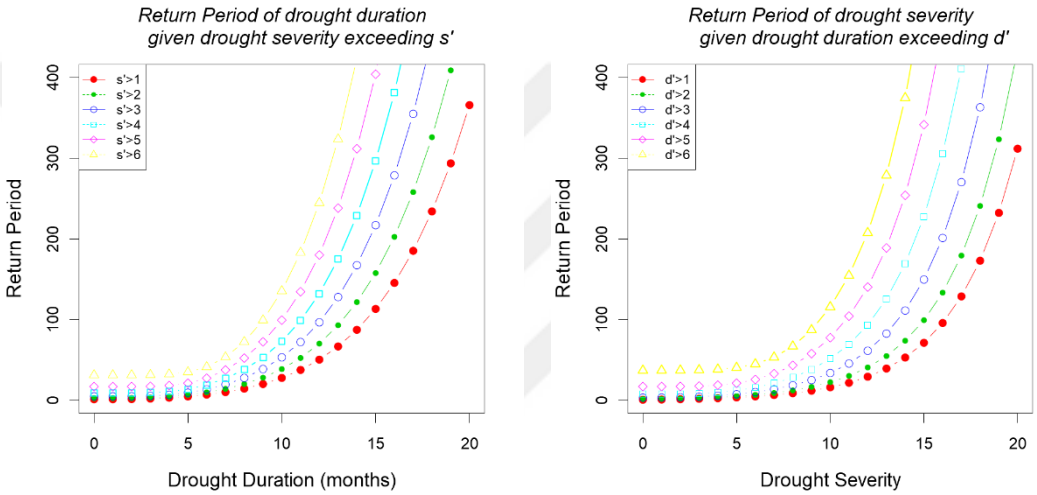

17866 SPI 3-month

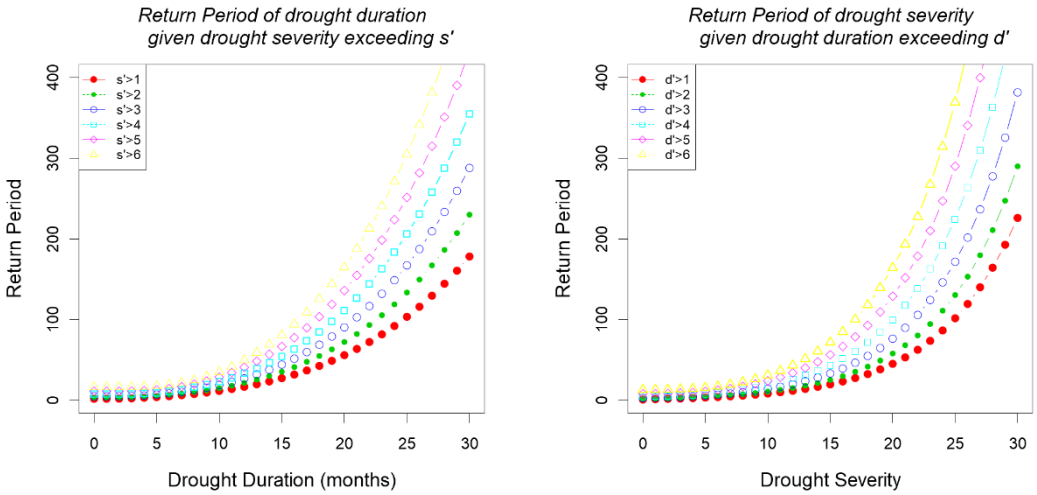

17866 SPI 6-month

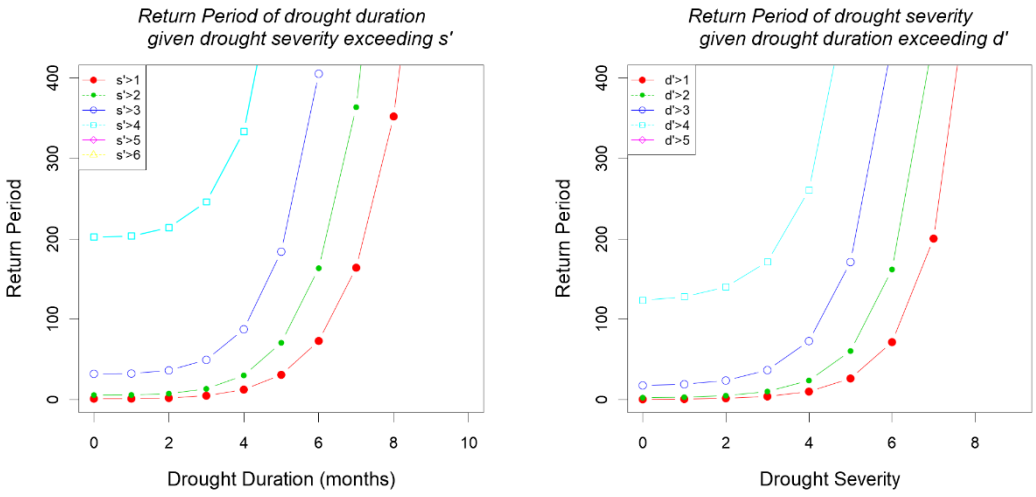

17868 SPI 1-month

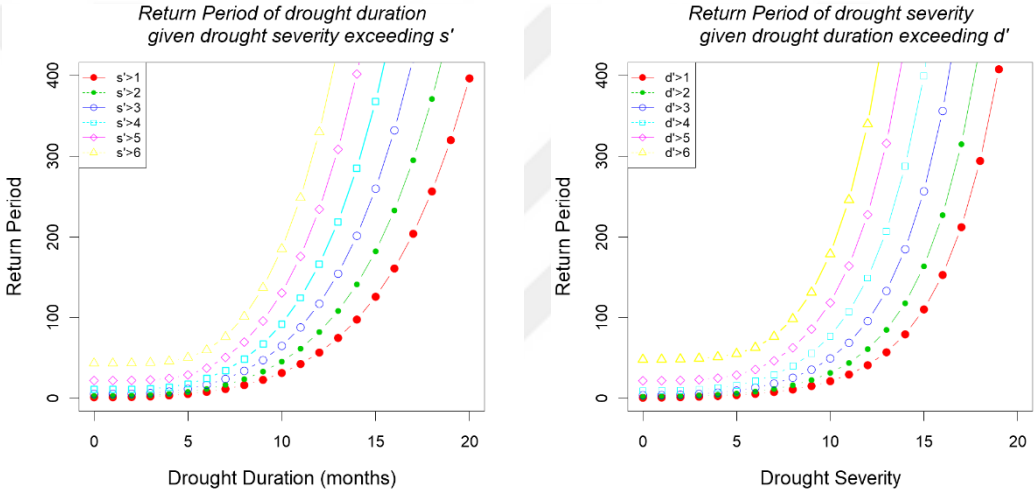

17868 SPI 3-month

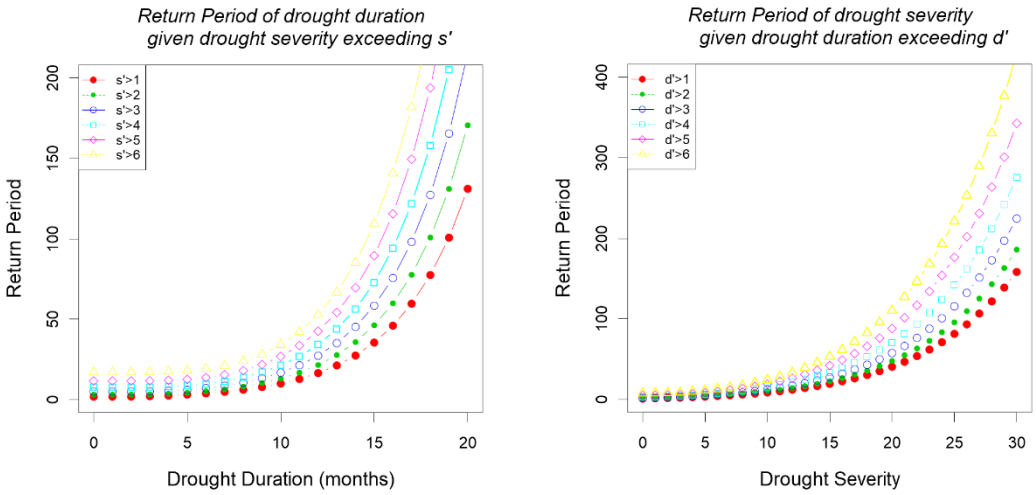

17868 SPI 6-month

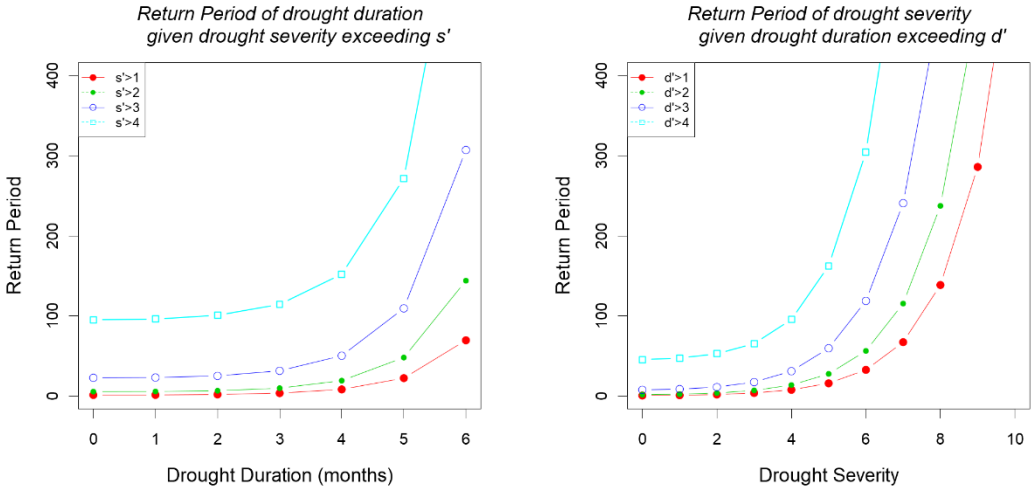

17870 SPI 1-month

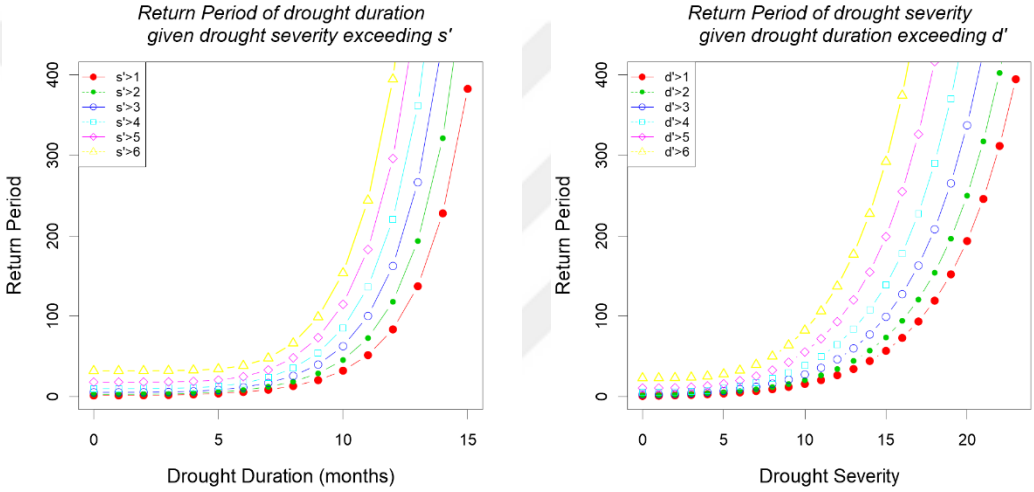

17870 SPI 3-month

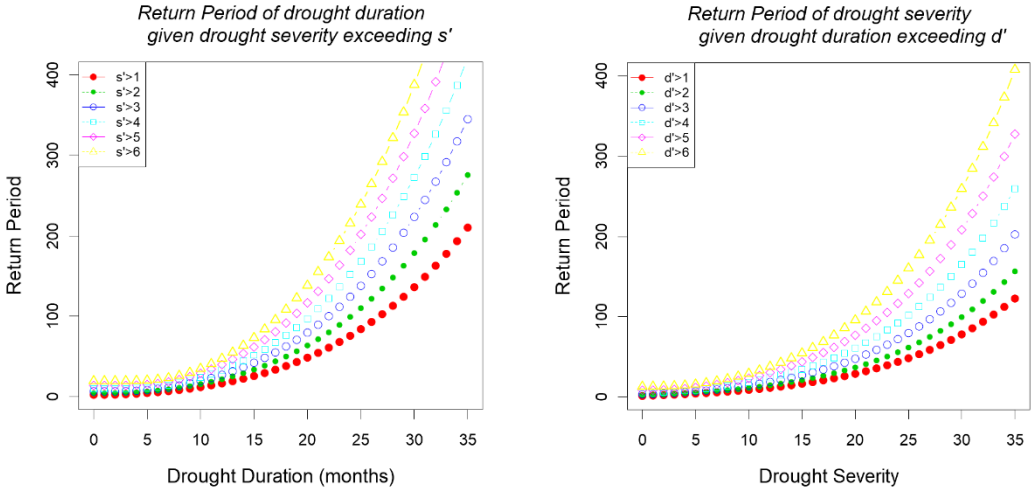

17870 SPI 6-month

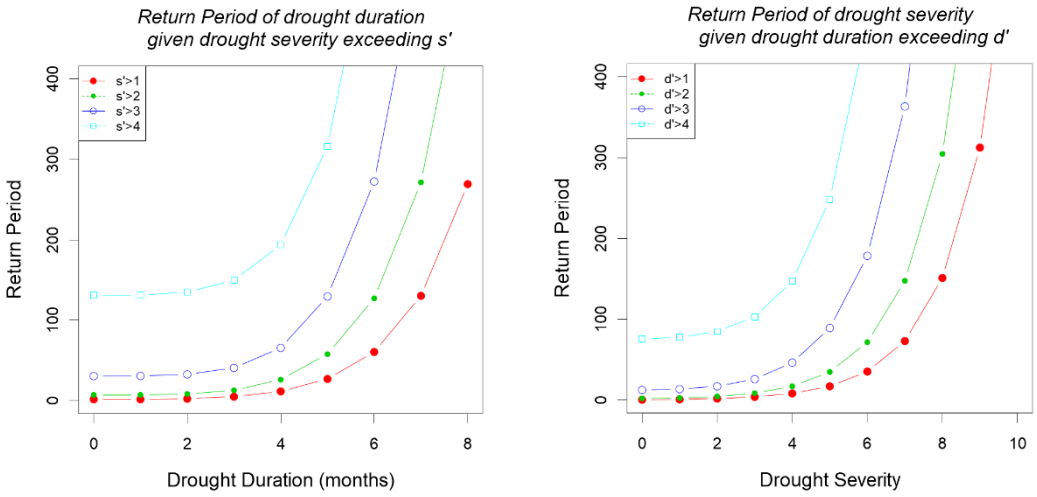

17871 SPI 1-month

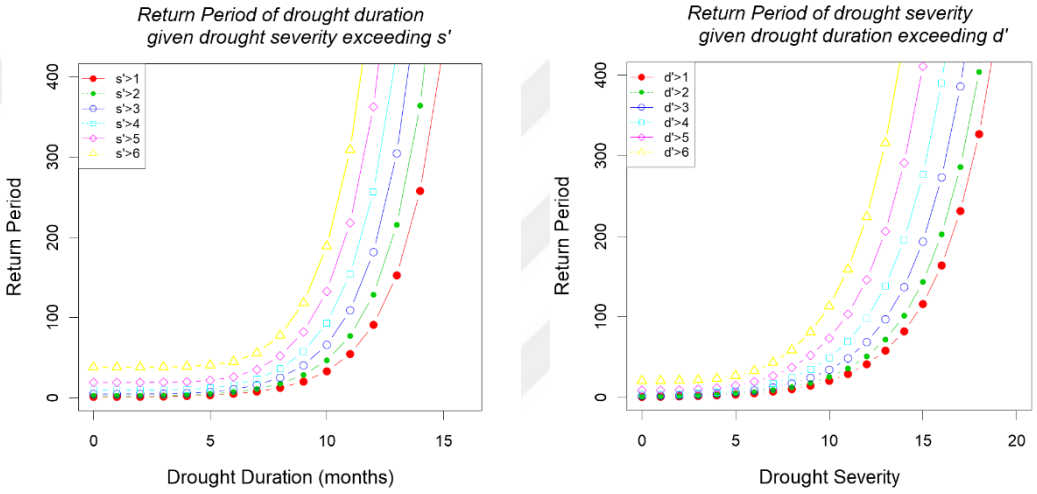

17871 SPI 3-month

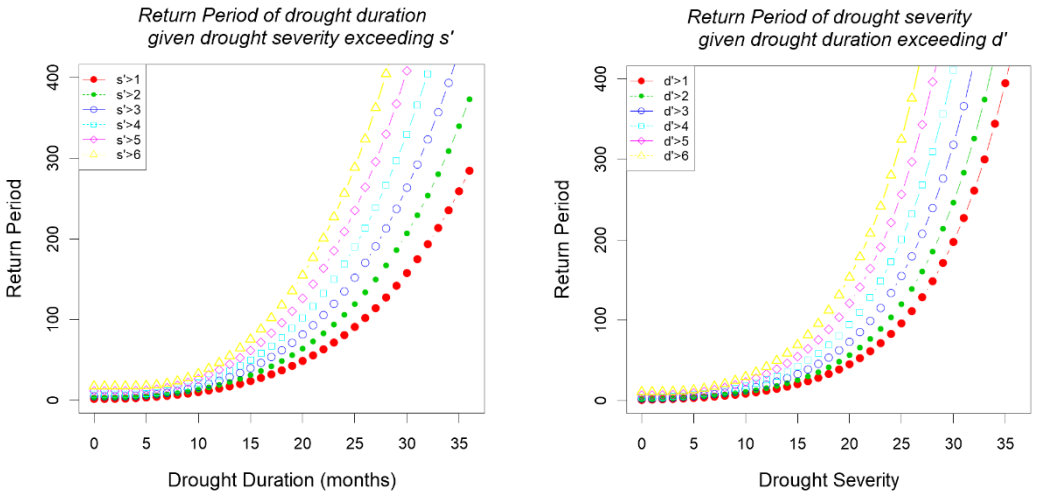

17871 SPI 6-month

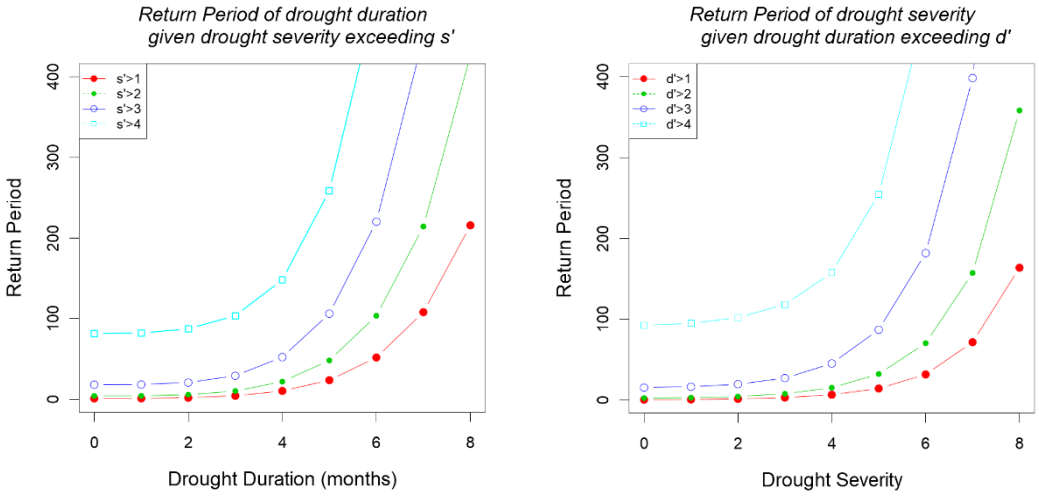

17908 SPI 1-month

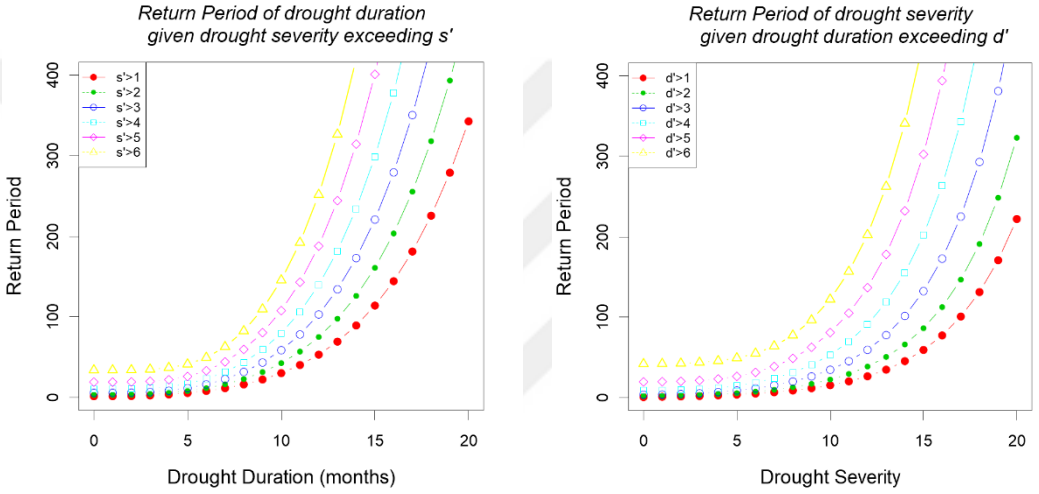

17908 SPI 3-month

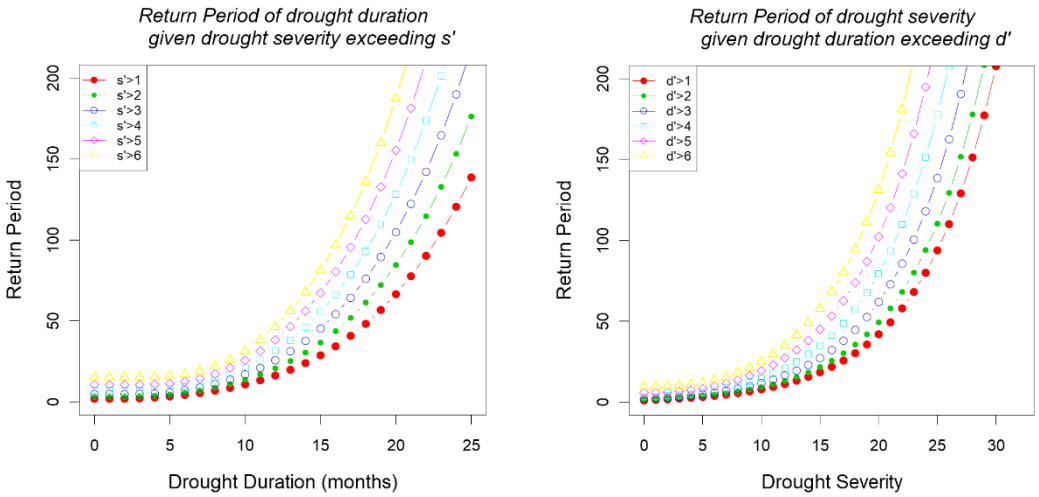

17908 SPI 6-month

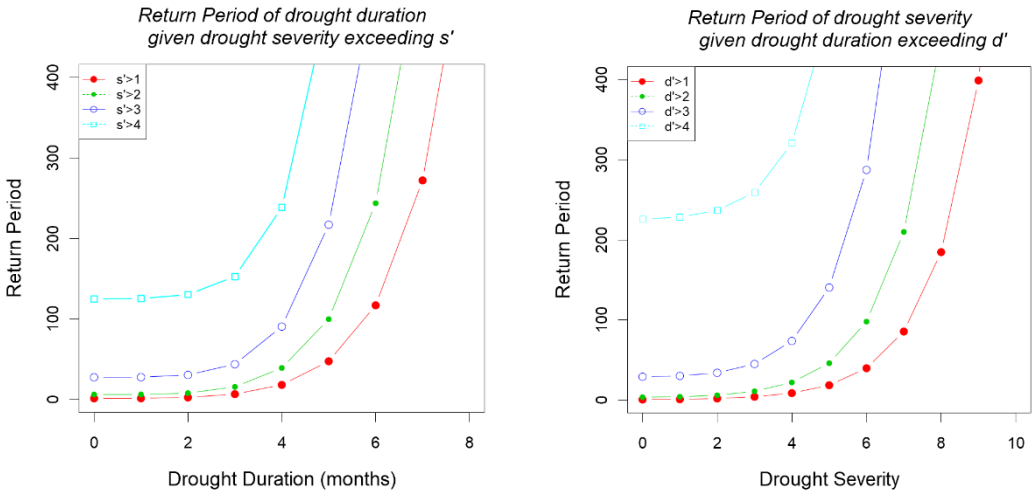

17960 SPI 1-month

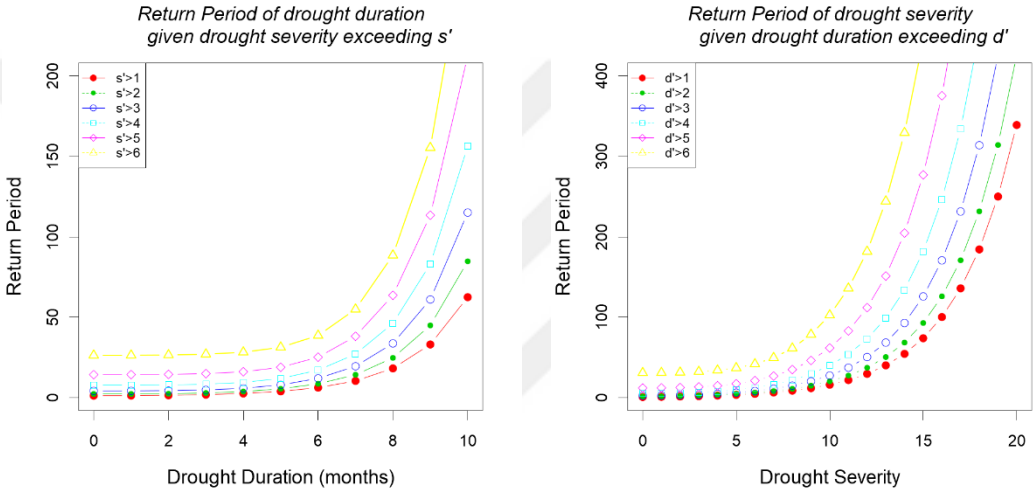

17960 SPI 3-month

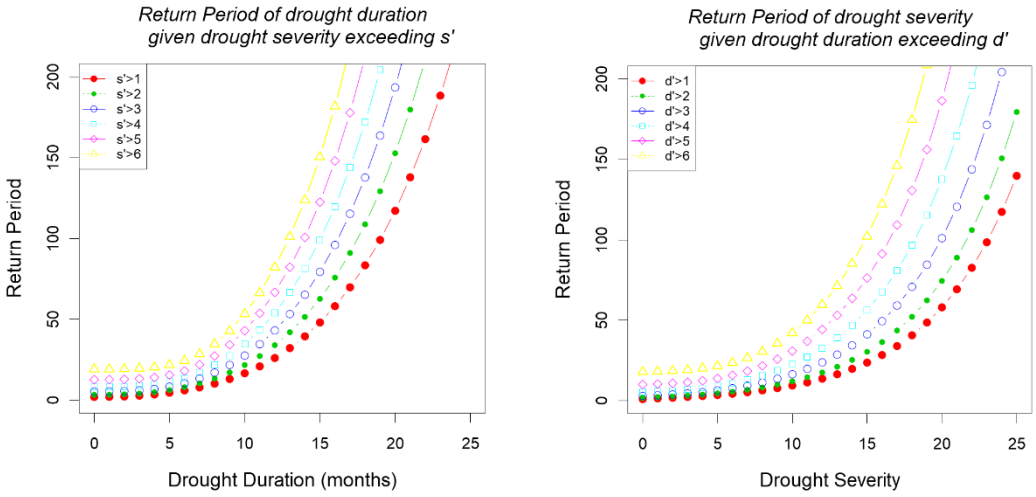

17960 SPI 6-month

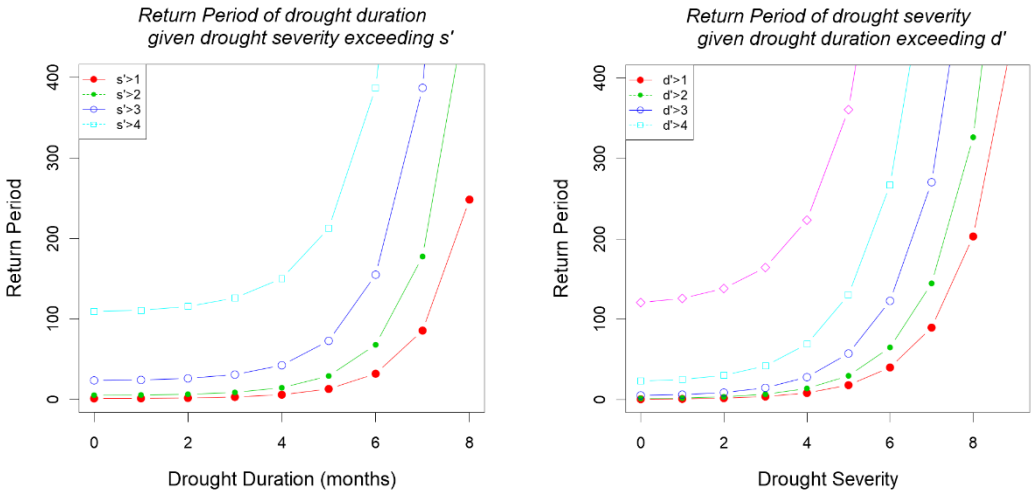

17979 SPI 1-month

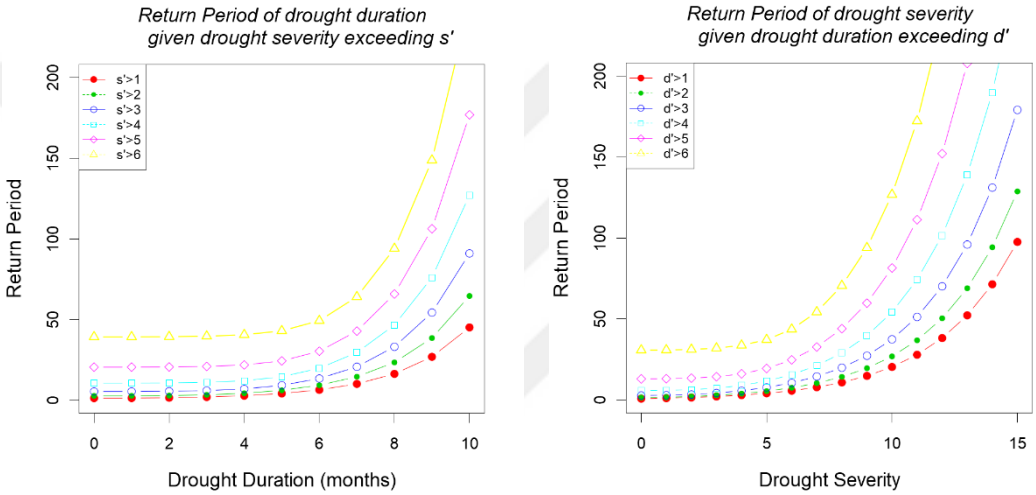

17979 SPI 3-month

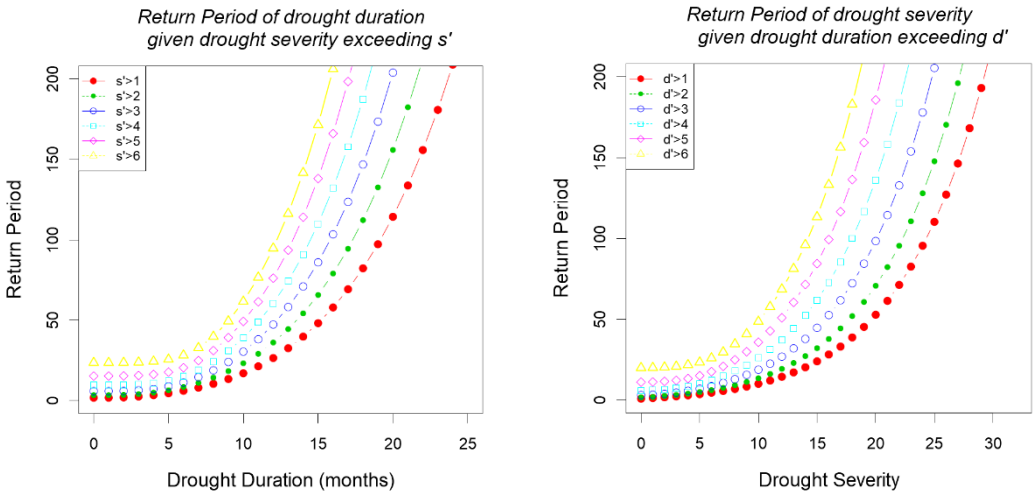

17979 SPI 6-month

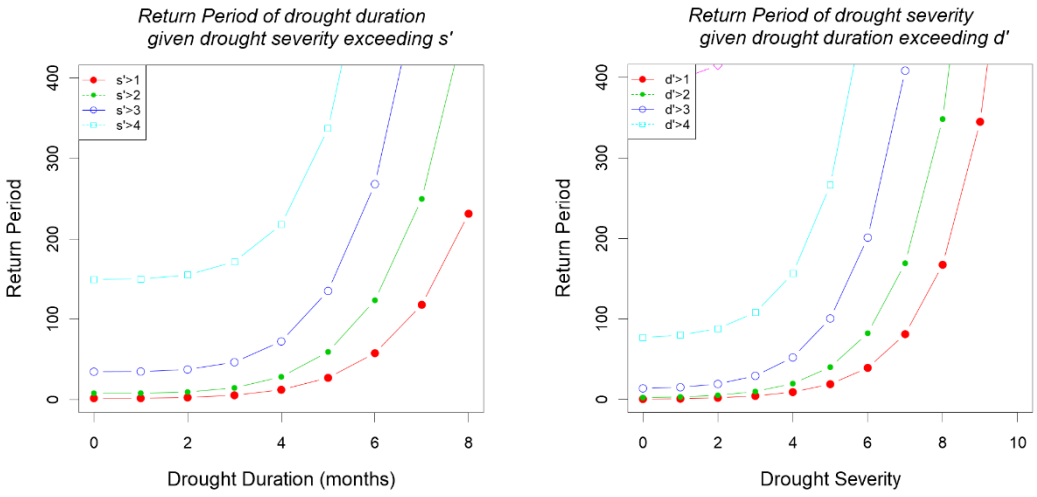

D20M001 SPI 1-month

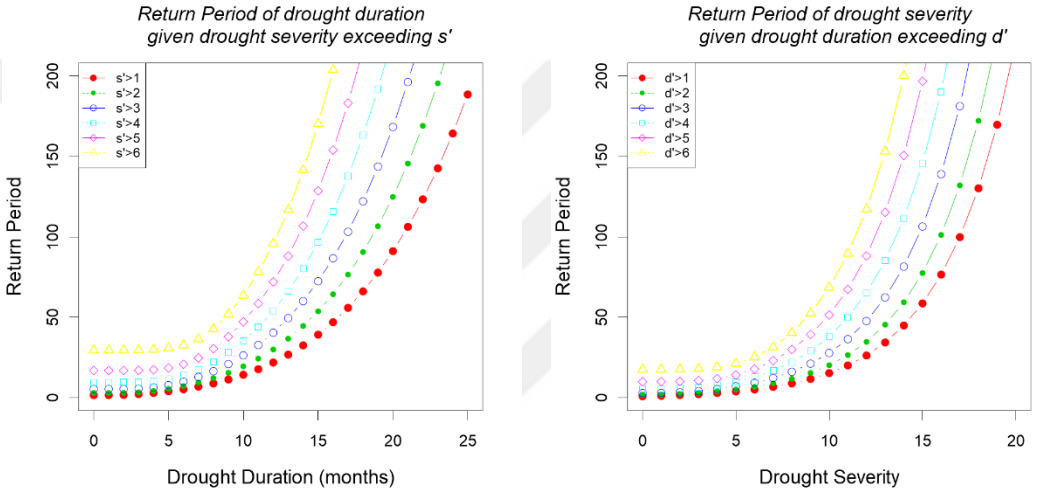

D20M001 SPI 3-month

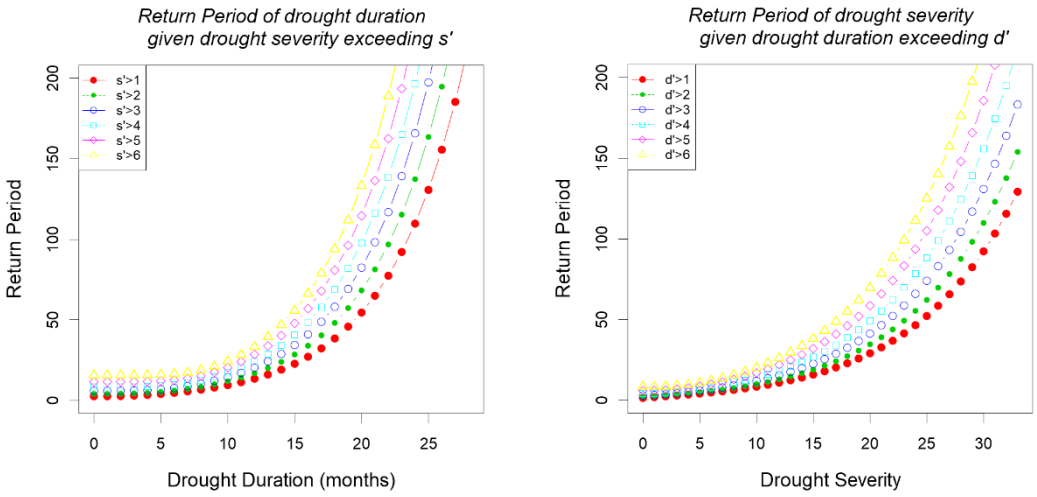

D20M001 SPI 6-month

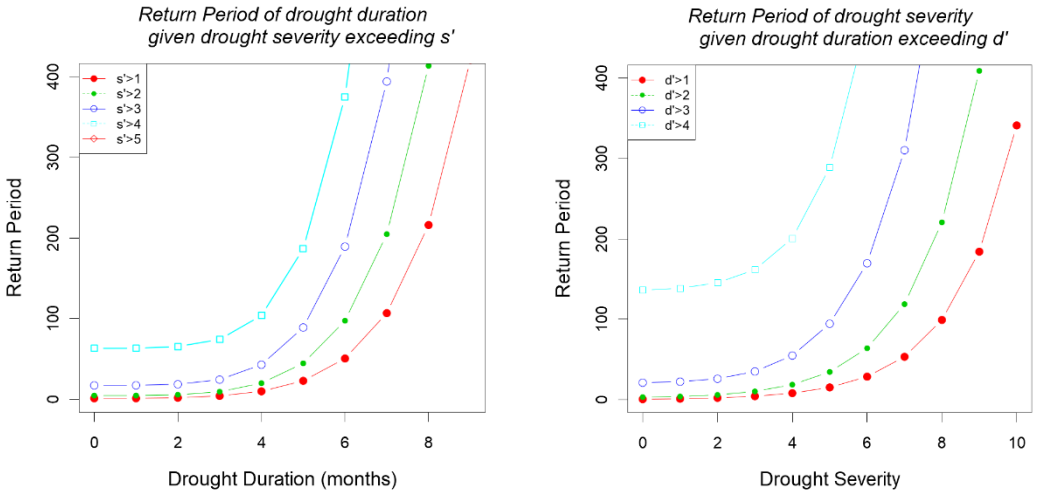

D20M002 SPI 1-month

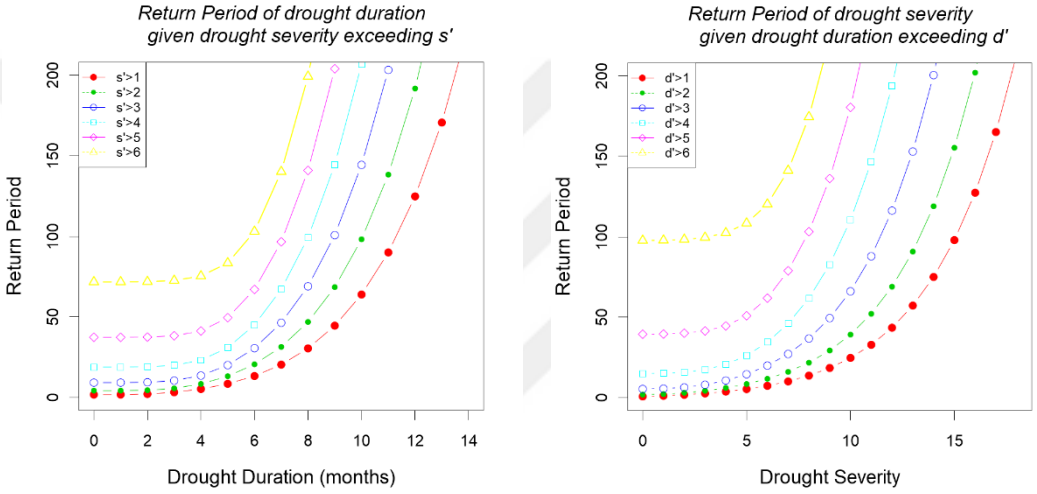

D20M002 SPI 3-month

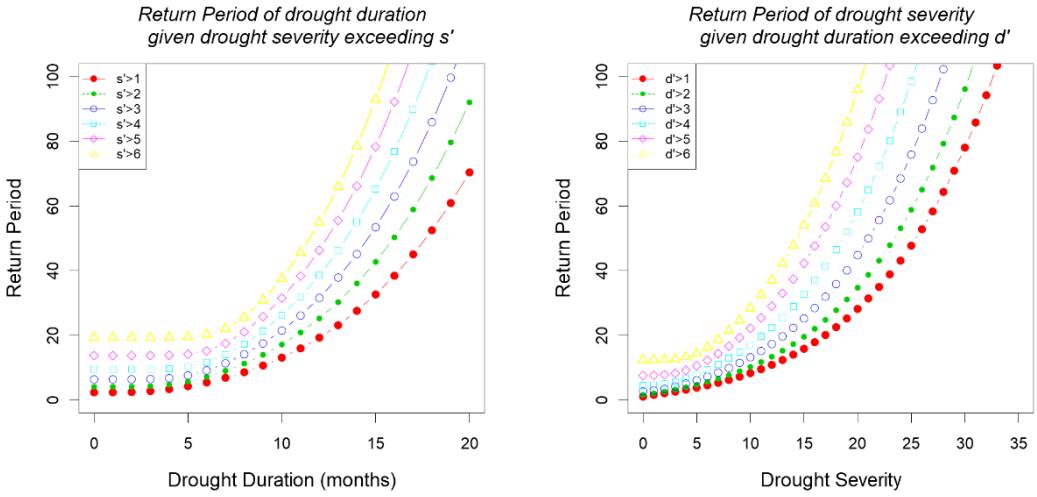

D20M002 SPI 6-month

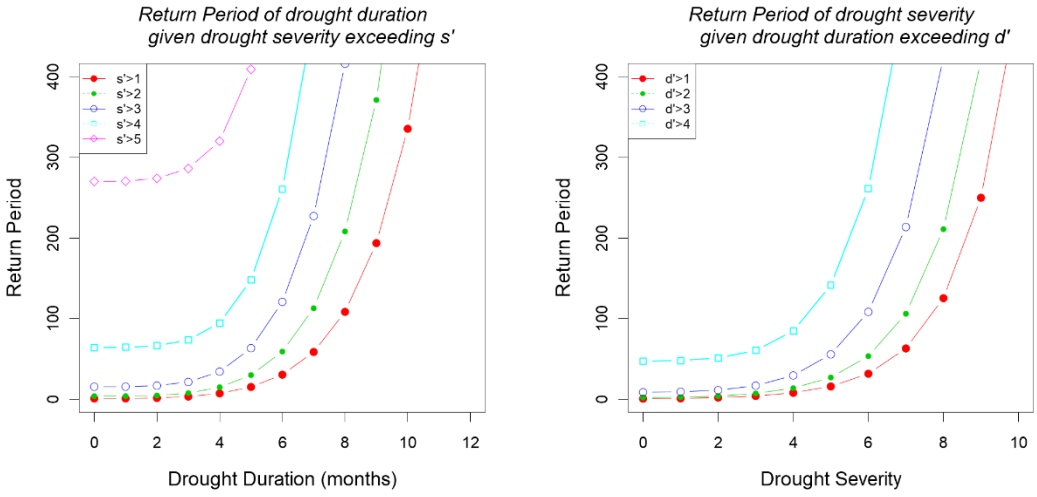

D20M004 SPI 1-month

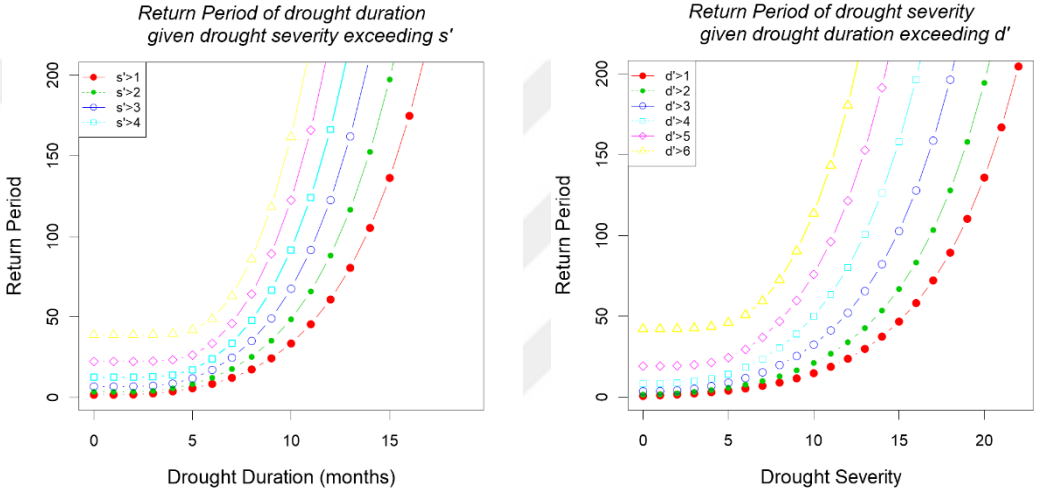

D20M004 SPI 3-month

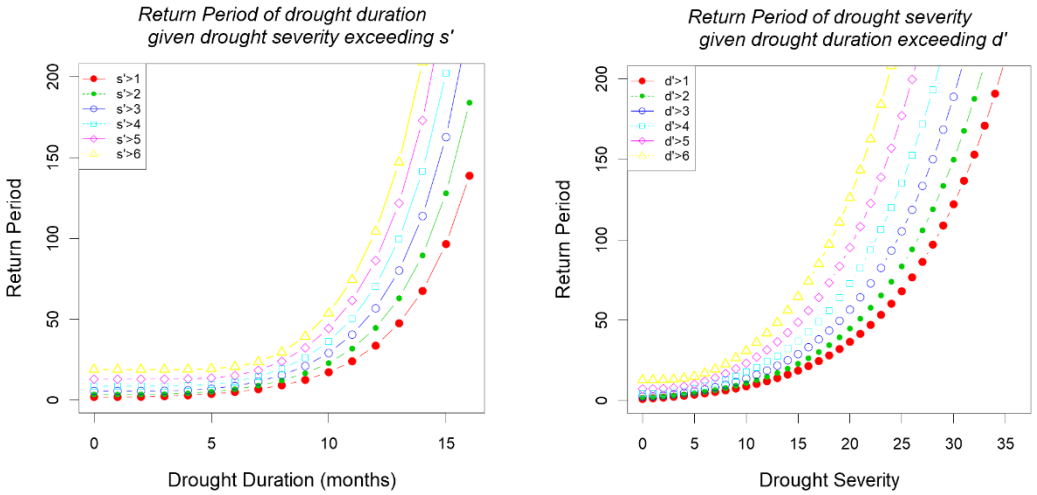

D20M004 SPI 6-month

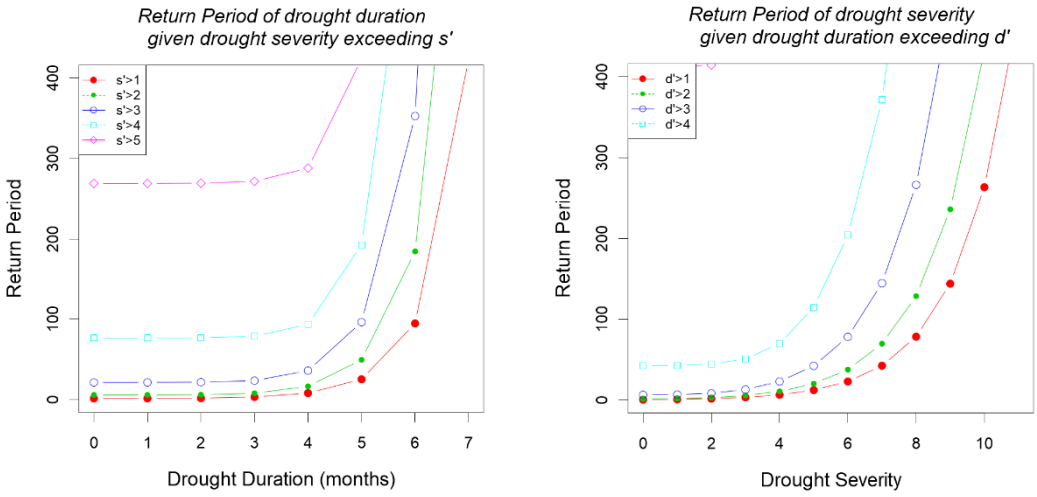

D20M006 SPI 1-month

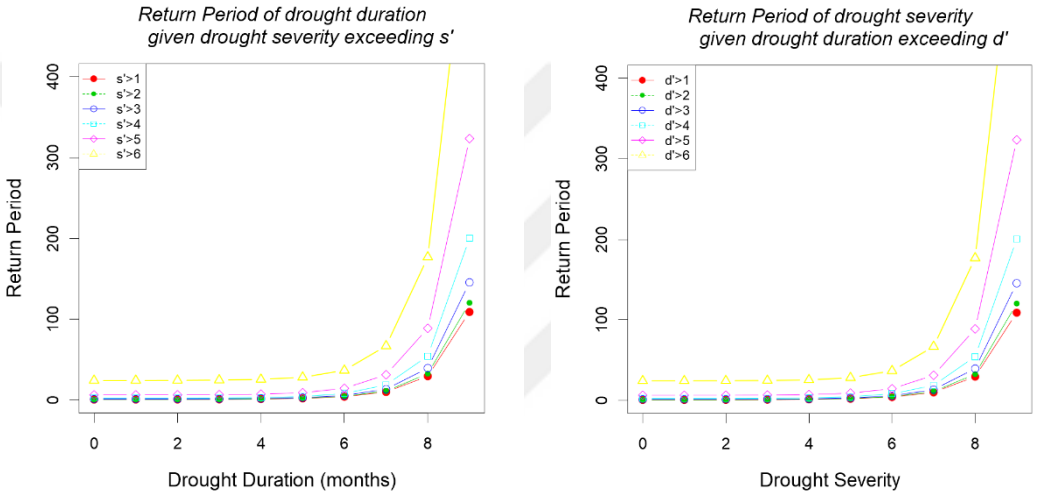

D20M006 SPI 3-month

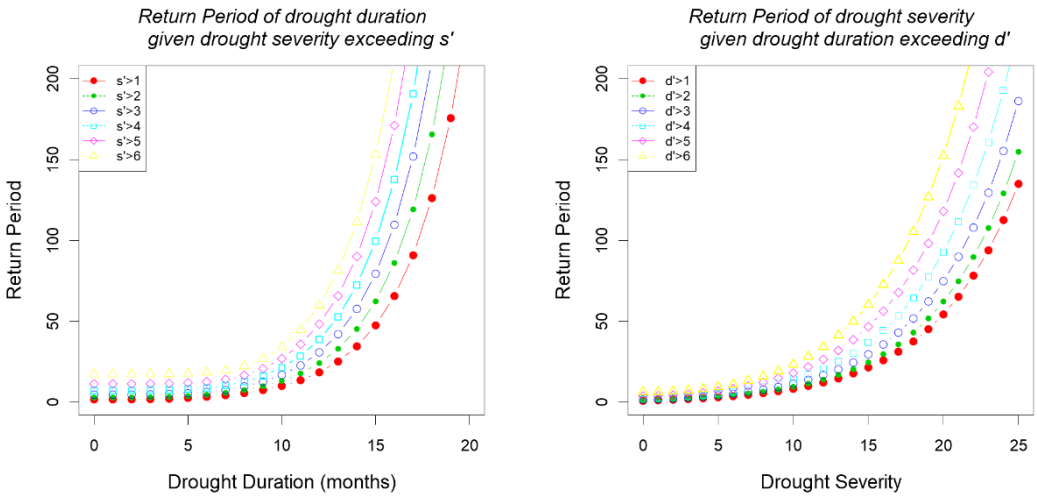

D20M006 SPI 6-month

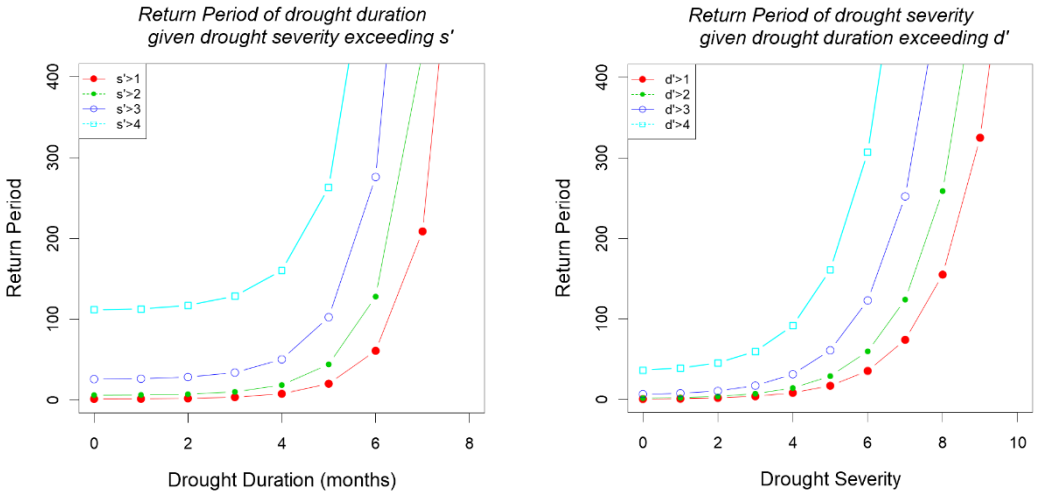

D20M009 SPI 1-month

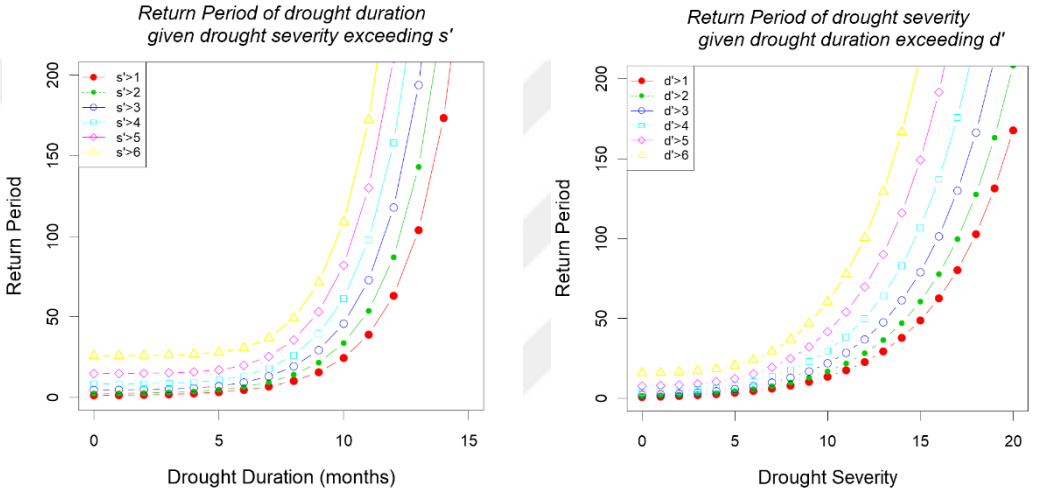

D20M009 SPI 3-month

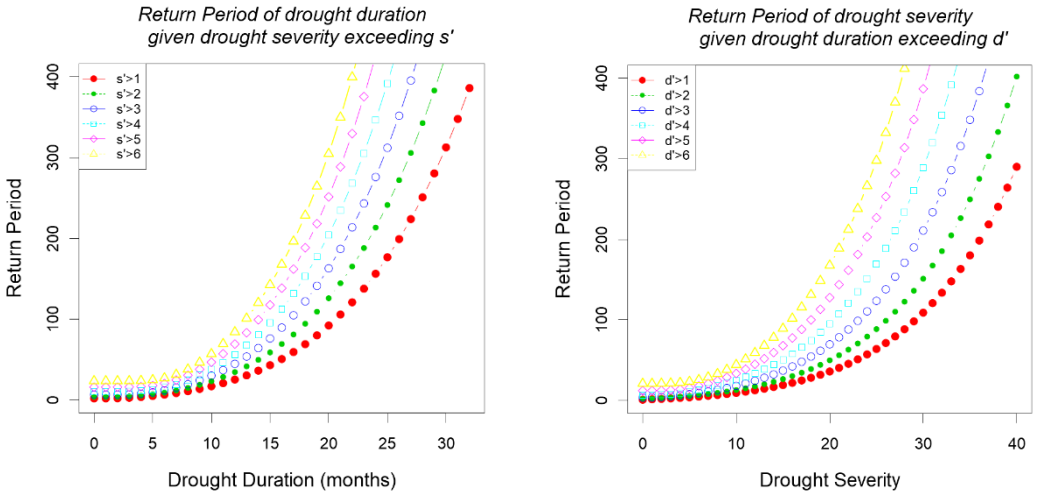

D20M009 SPI 6-month

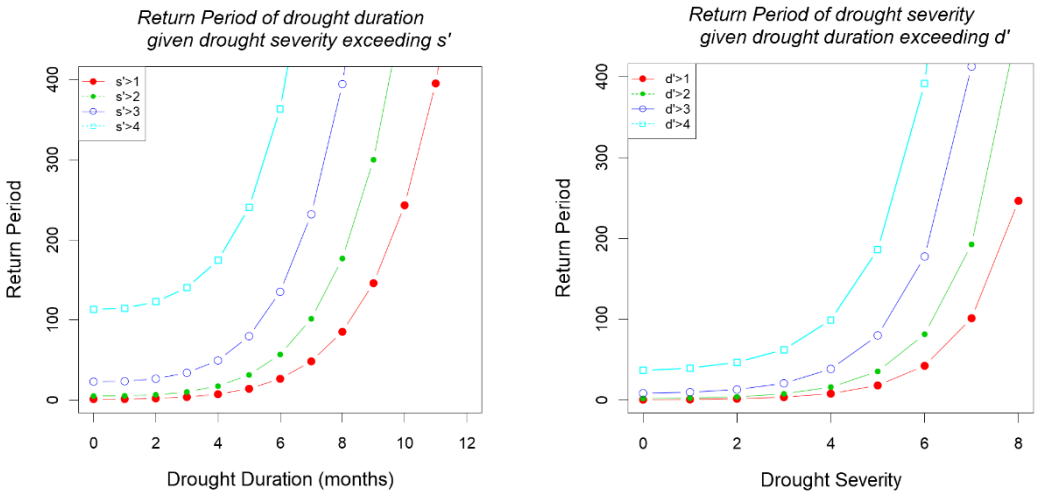

D20M011 SPI 1-month

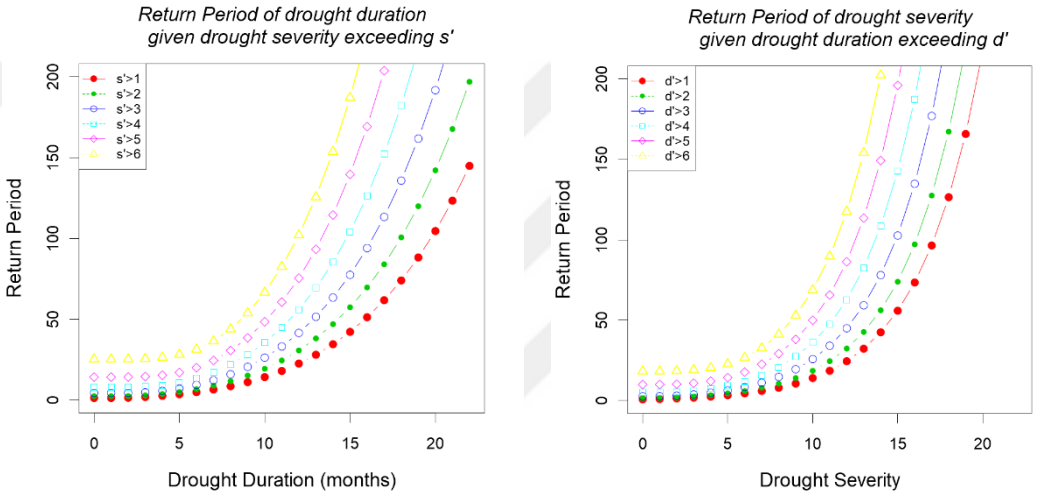

D20M011 SPI 3-month

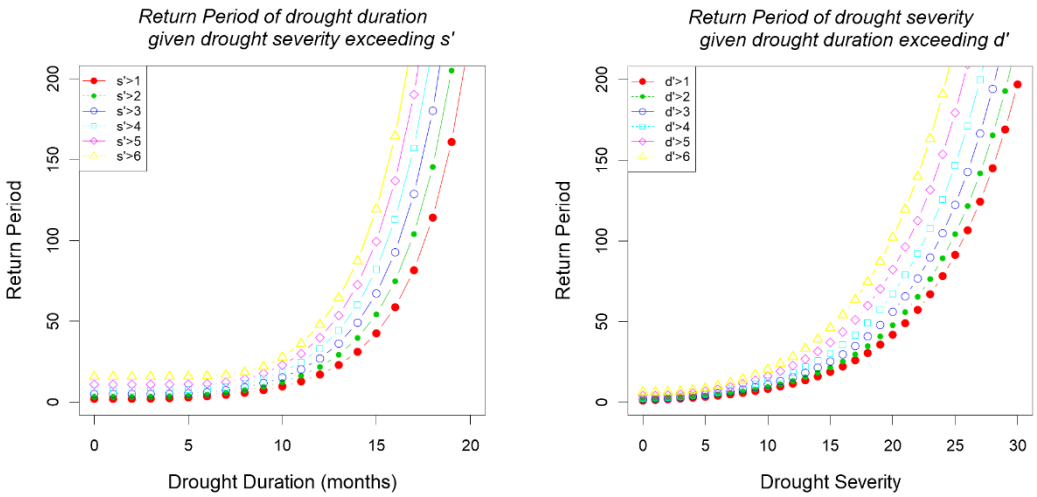

D20M011 SPI 6-month

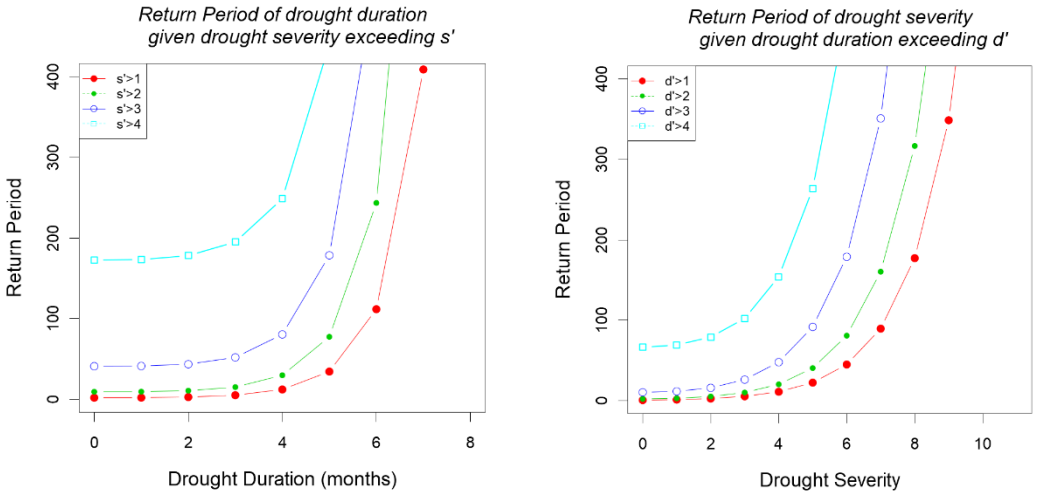

D20M013 SPI 1-month

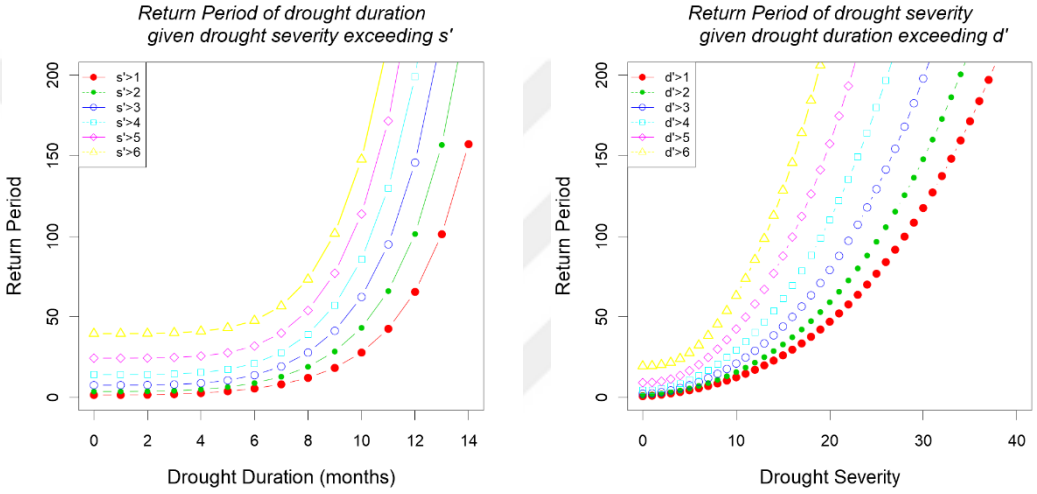

D20M013 SPI 3-month

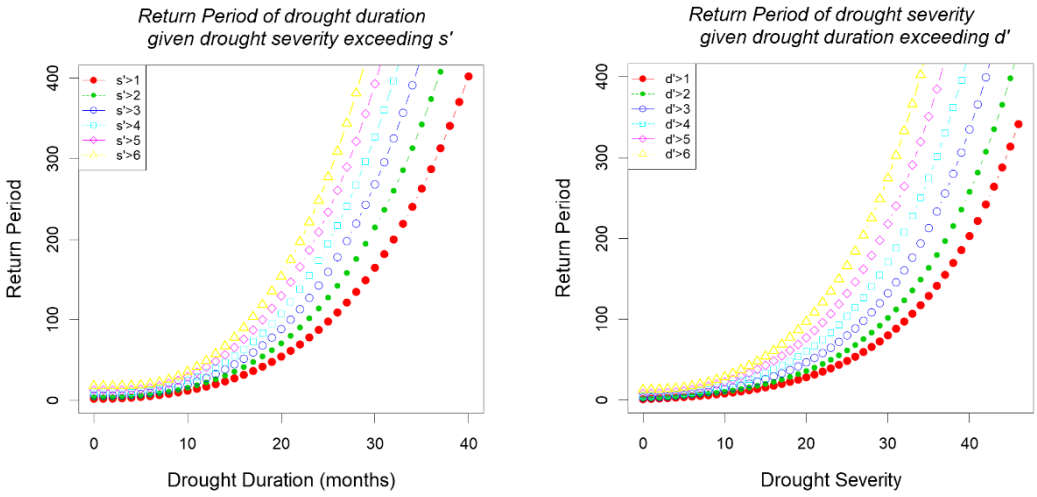

D20M013 SPI 6-month

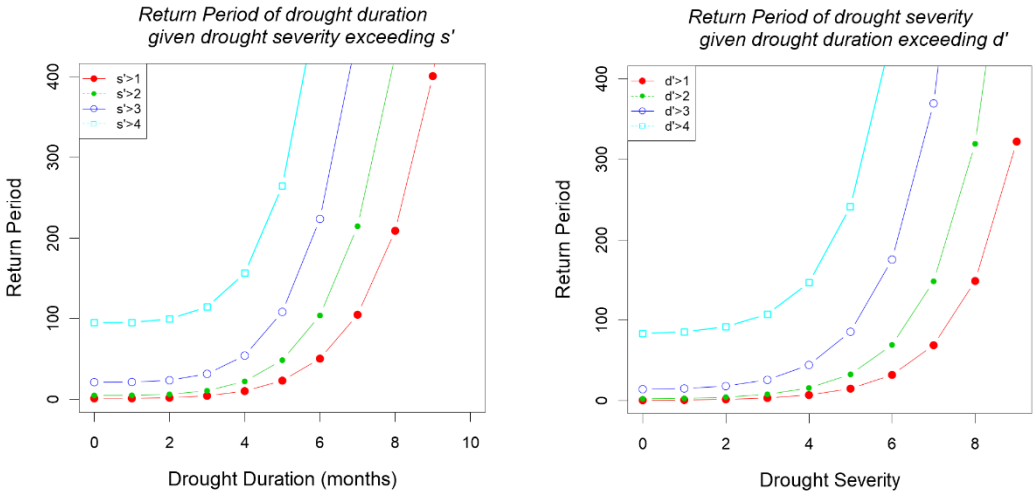

D20M014 SPI 1-month

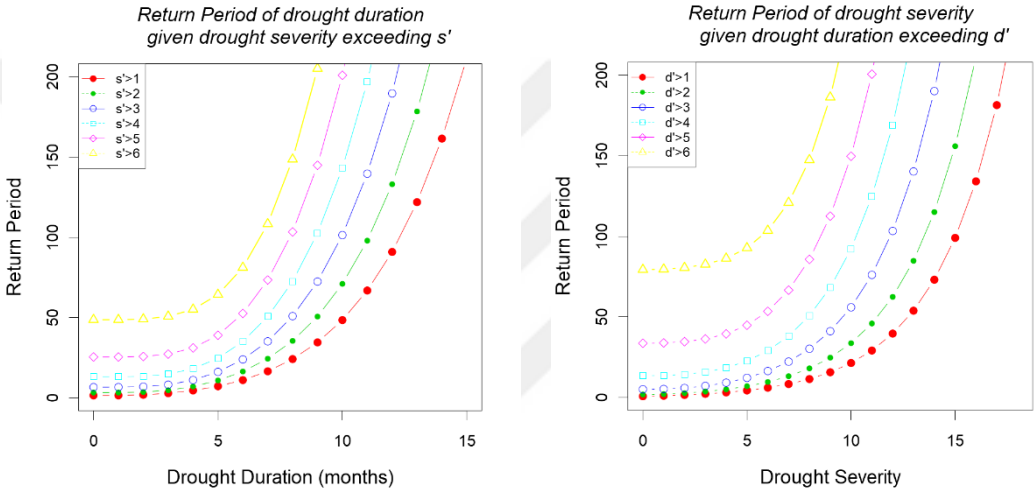

D20M014 SPI 3-month

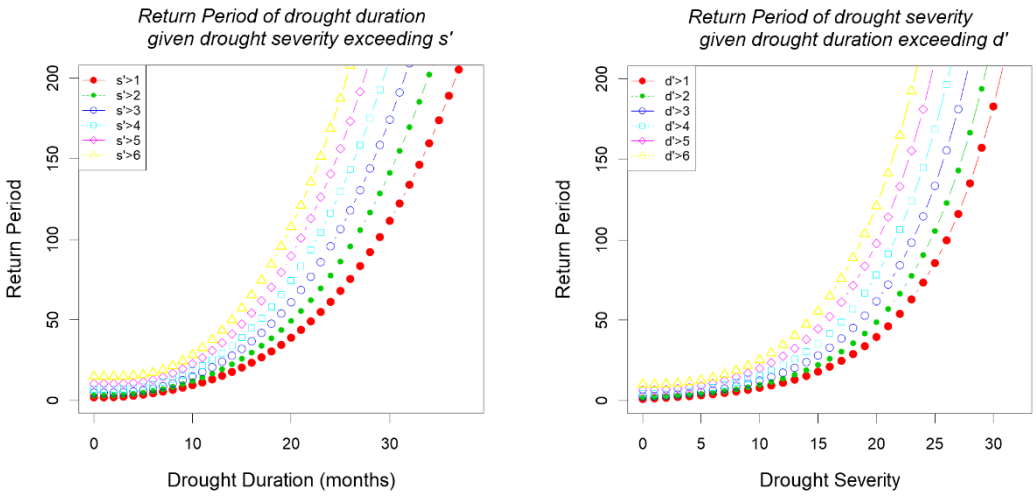

D20M014 SPI 6-month

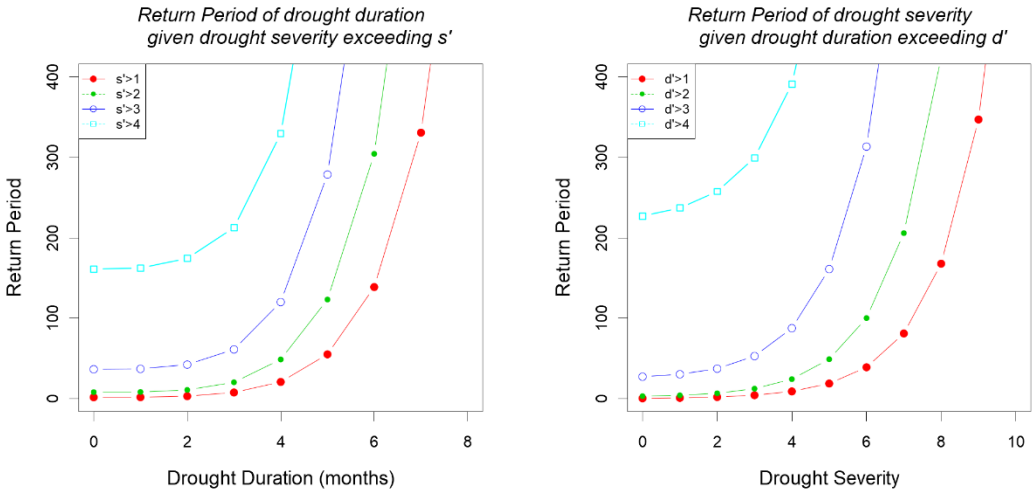

D20M015 SPI 1-month

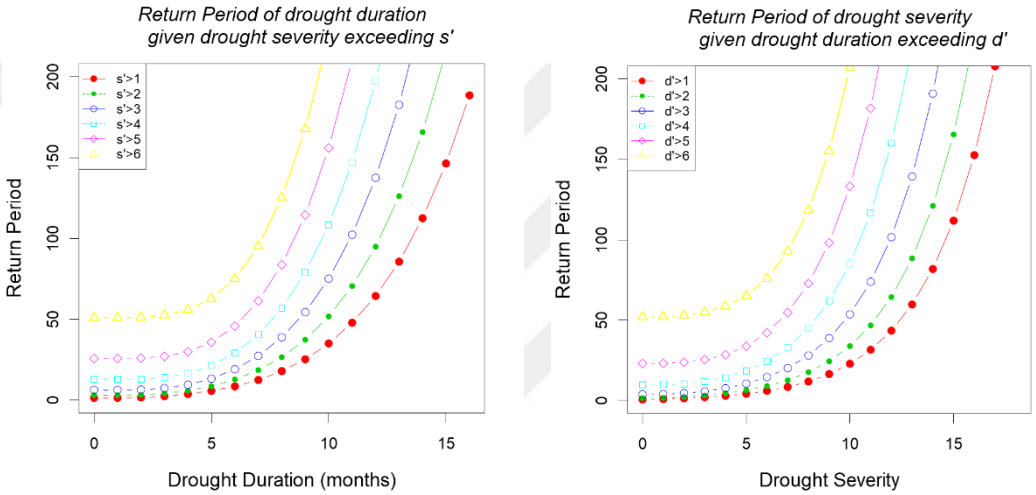

D20M015 SPI 3-month

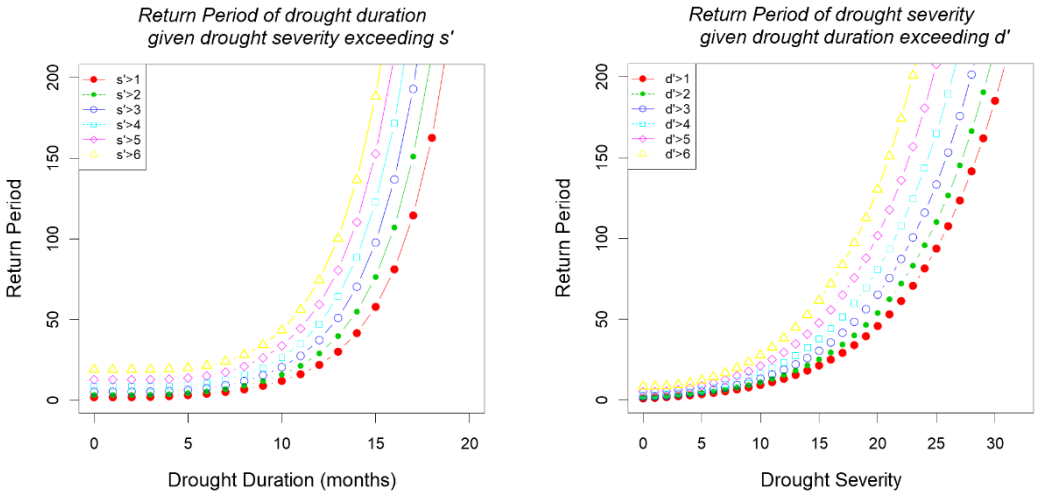

D20M015 SPI 6-month

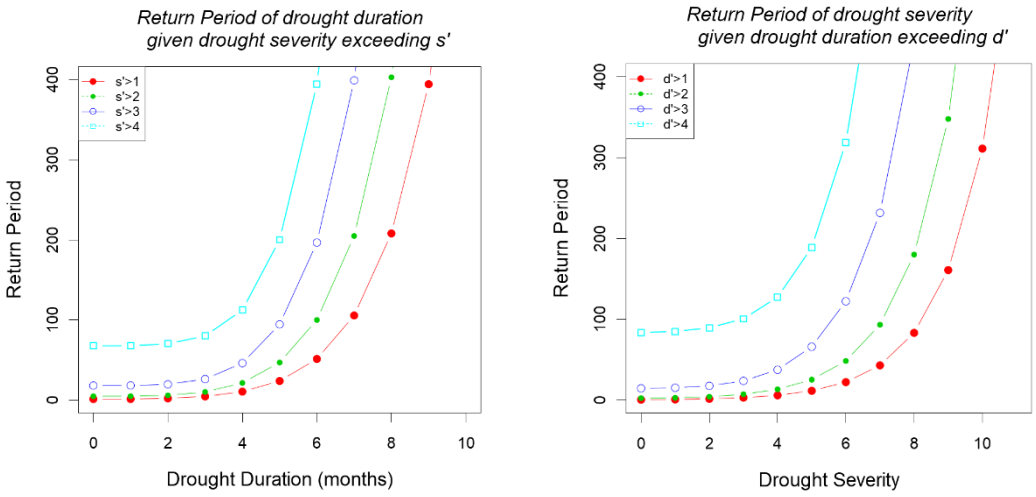

D20M016 SPI 1-month

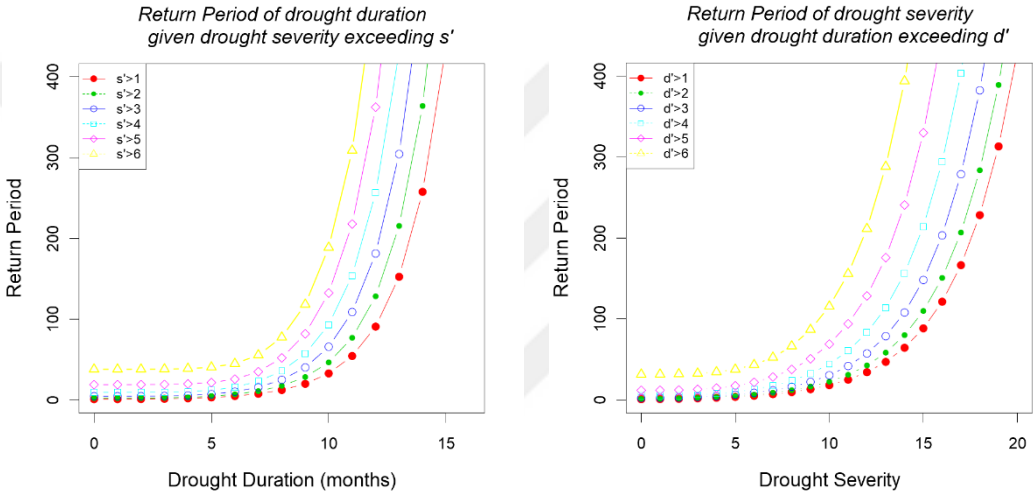

D20M016 SPI 3-month

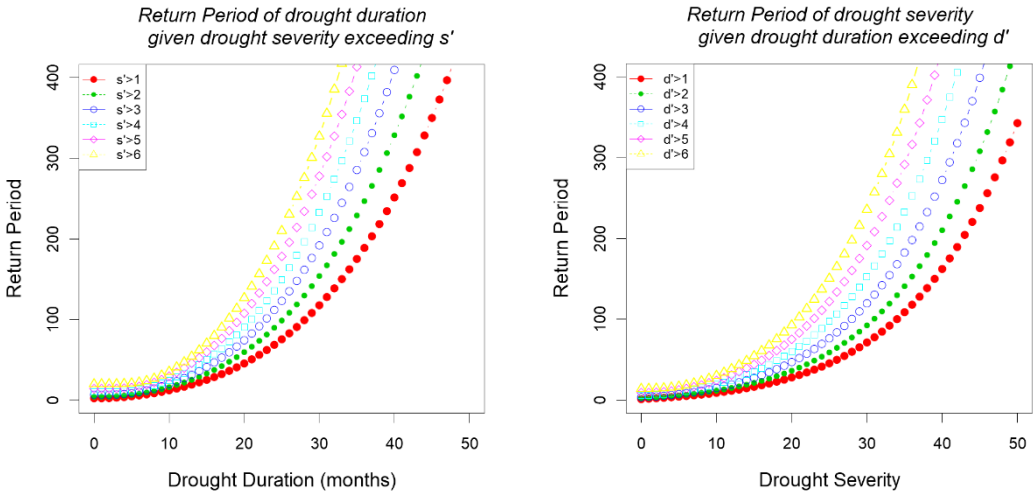

D20M016 SPI 6-month

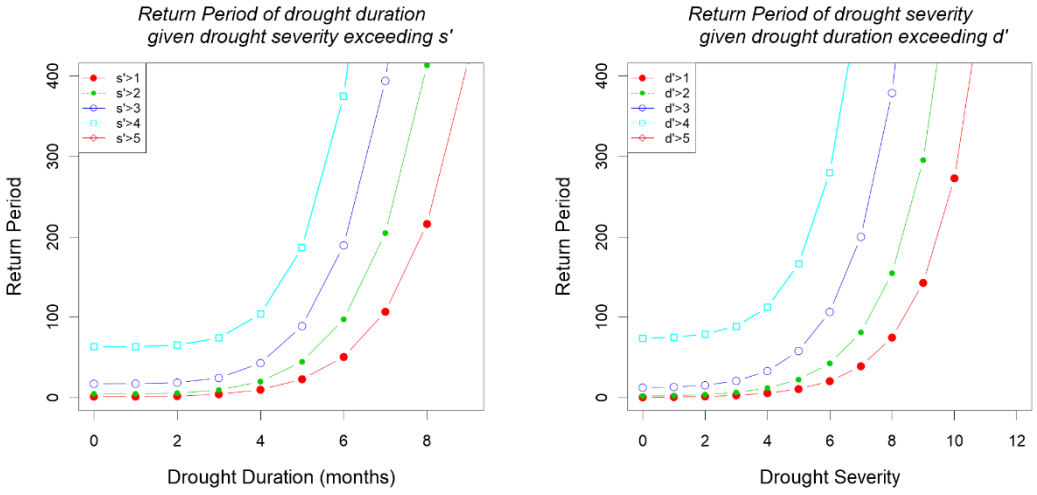

D20M017 SPI 1-month

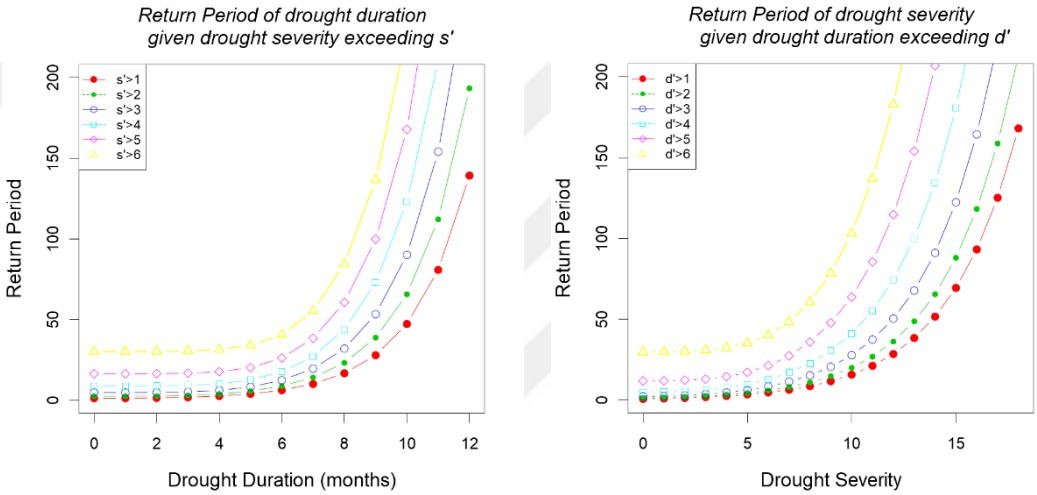

D20M017 SPI 3-month

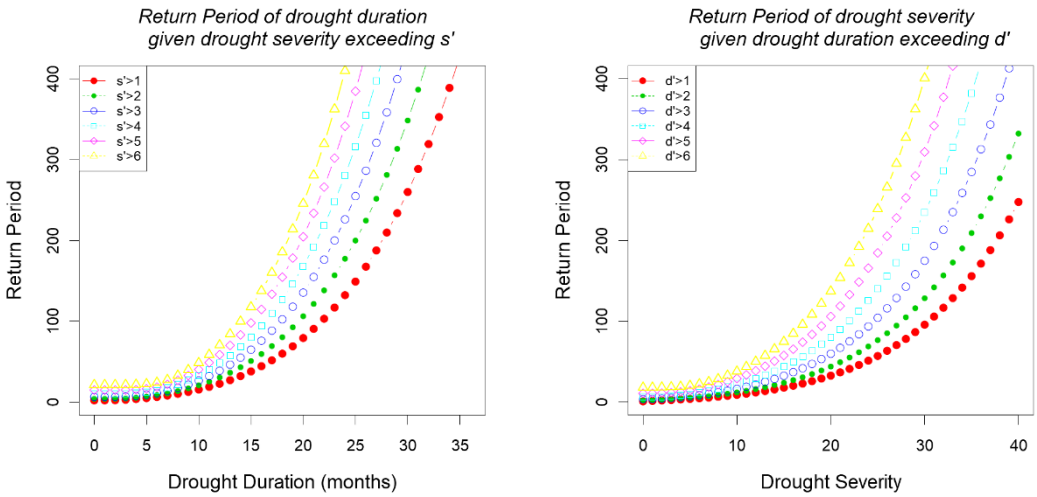

D20M017 SPI 6-month

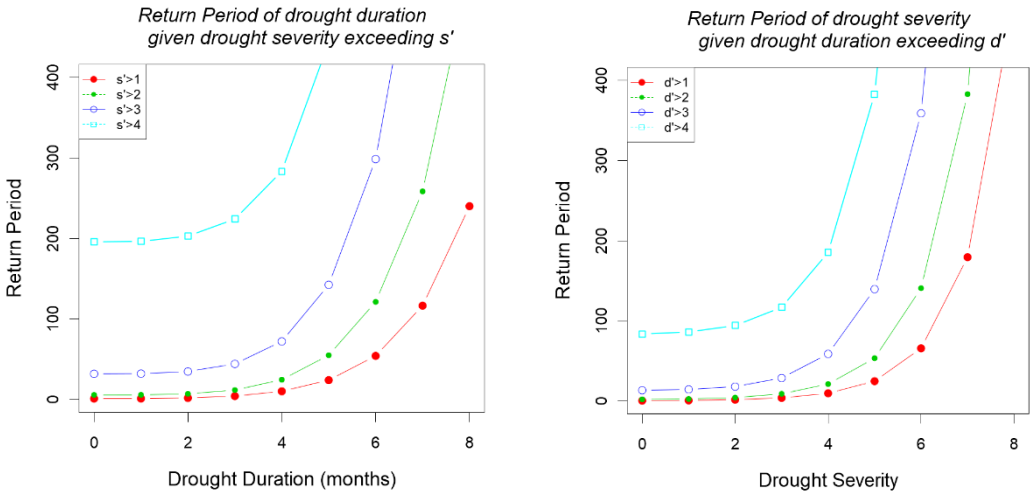

D20M018 SPI 1-month

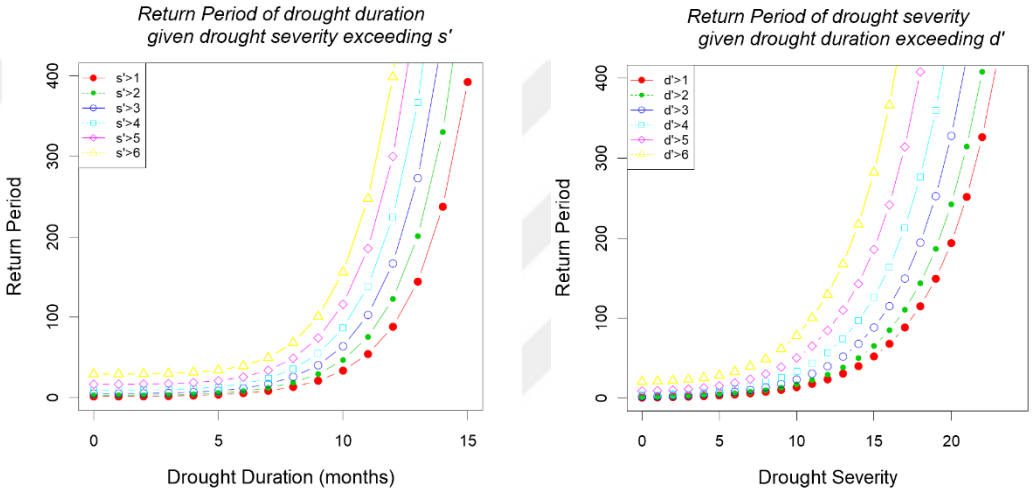

D20M018 SPI 3-month

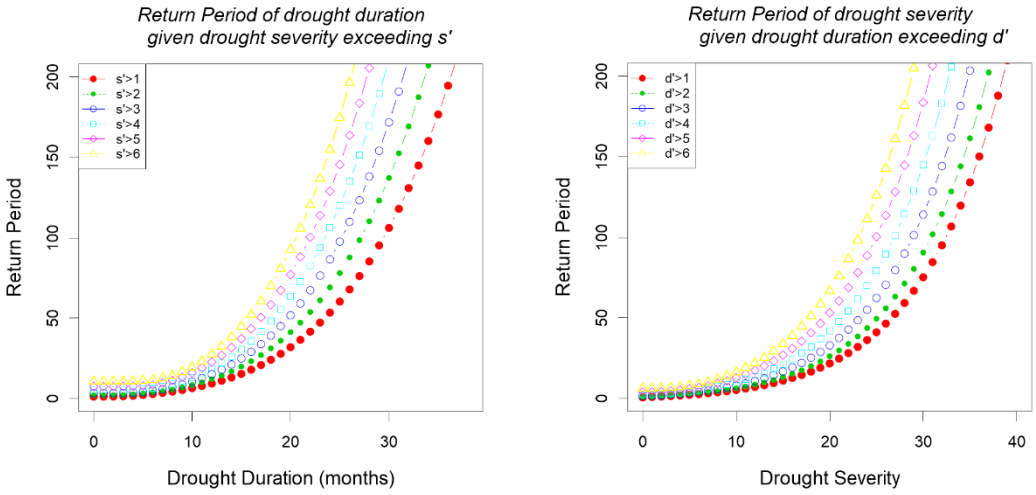

D20M018 SPI 6-month

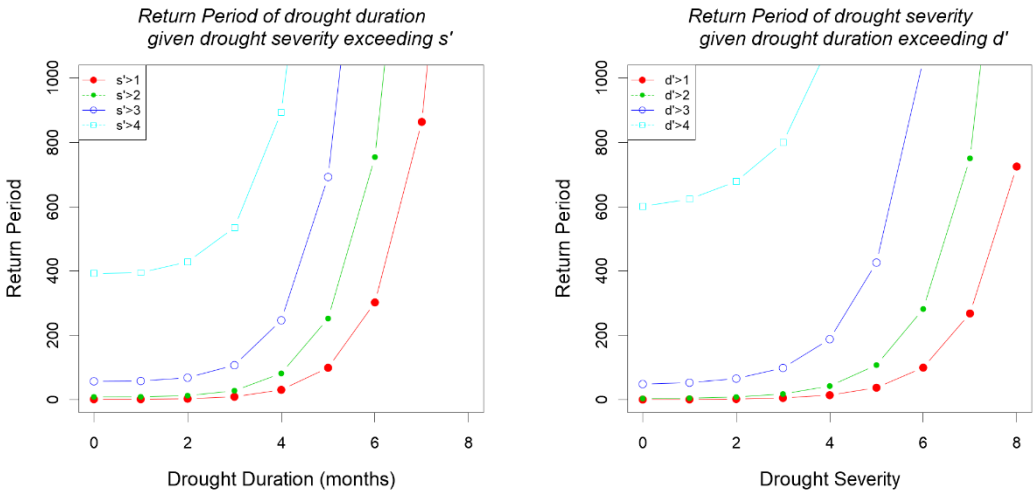

D20M020 SPI 1-month

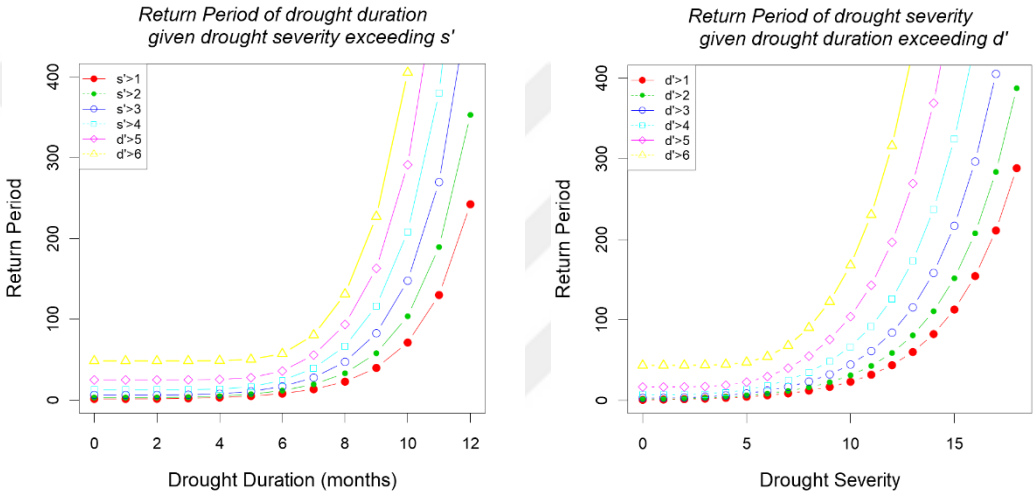

D20M020 SPI 3-month

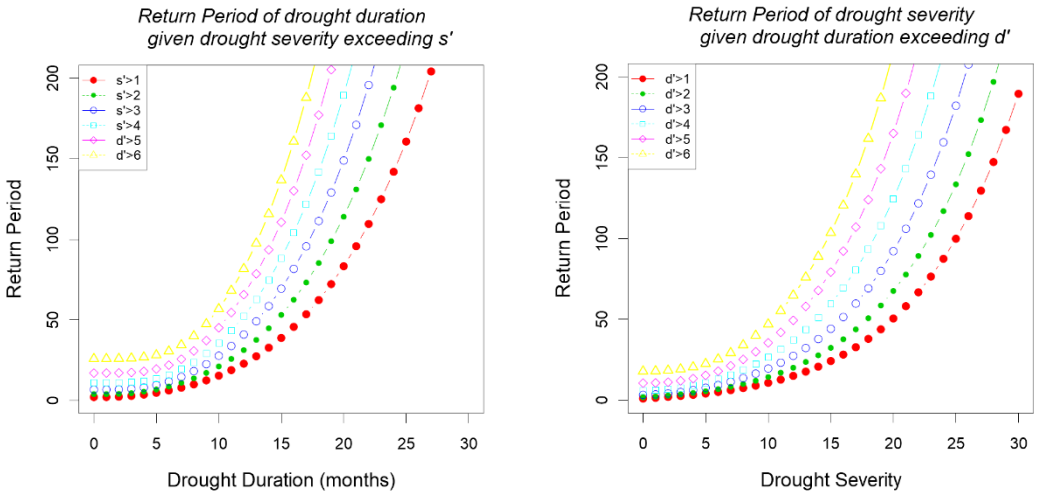

D20M020 SPI 6-month

Figure 7.9 The conditional return periods of drought severity/duration given that the duration/severity is greater than a certain value

7.8 Drought Risk Probability Assessments

After evaluating the joint return period of drought duration and severity for each station, the spatial distributions of T_{DS} and T'_{DS} for return periods under case 1 and case 2 (SPI 1, SPI 3 and SPI 6 month) are presented in Figure 7.10-12. Drought risk categories are described as light, moderate, severe and extreme droughts considering a specific threshold for drought duration and severity, respectively. (Chang et al., 2016). The percentile method (%25, %50, %75 and %95), which is mentioned Chang et al. (2016) in detail, was employed to the marginal distribution of drought duration and severity series considered to four drought risk categories.

First scenario for SPI 1 time scale, indicates that the eastern part is mostly dominated by relatively lower drought risk (maximum T_{DS} (left) and T'_{DS} (right)) at all categories, whereas southwestern region shows relatively higher drought risk, indicating lower T_{DS} and T'_{DS}. For all drought risk categories, the return periods of T_{DS} are generally longer than T'_{DS} and they show a good consistence except northern part. While the northern regions largely experience higher T_{DS} under all stated drought conditions, shorter return periods T'_{DS} (high-risk,) are exhibited at northern regions (Figure 7.10).

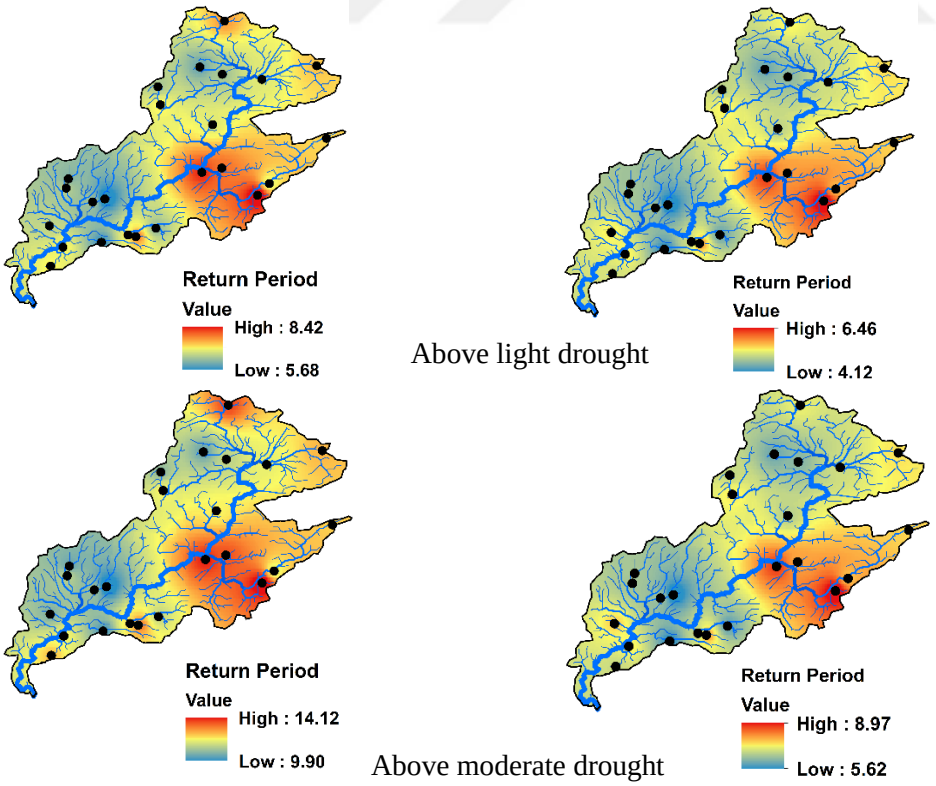

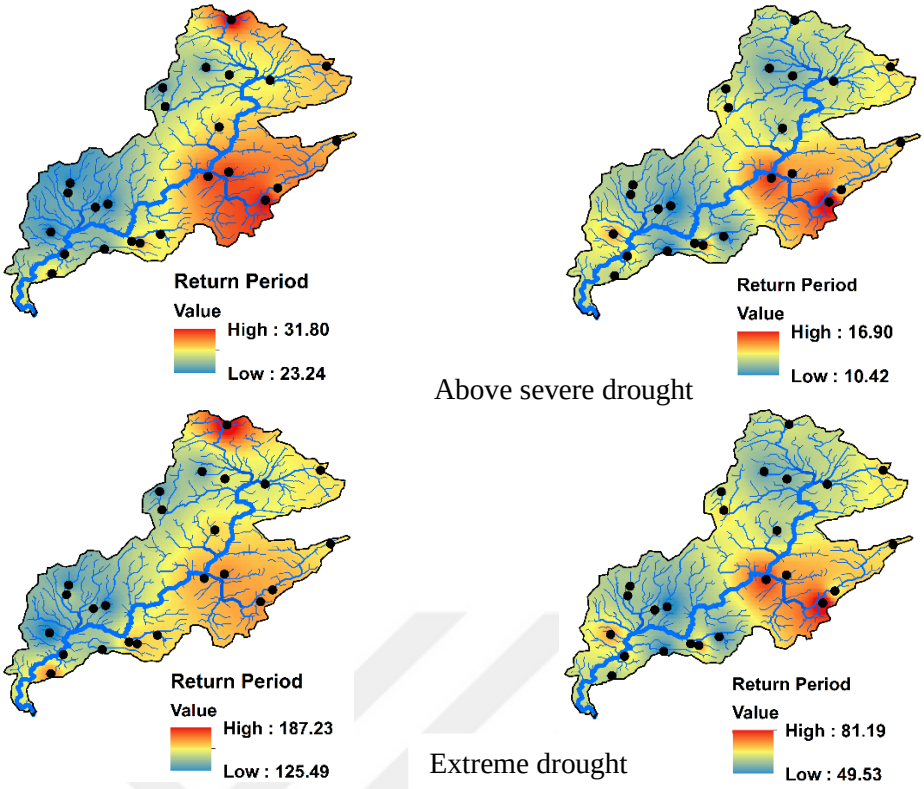

Figure 7.10. The spatial distribution of T_{DS} (left) and T'_{DS} (right) return period (month) based on SPI 1 when the drought duration and severity exceed their long-term average

Second scenario for SPI 3-time scale, when compared to the southern regions, the northern regions, under all drought categories, especially D20M001 and D20M011, higher return period T_{DS} and T'_{DS} (lower risk) are observed. But the western part shows a tendency to decrease the risk from light to extreme category for T_{DS}. T'_{DS} exhibits higher risk at this region. When examined the middle part of basin, high risks are observed for all T_{DS} and T'_{DS} under light drought categories.

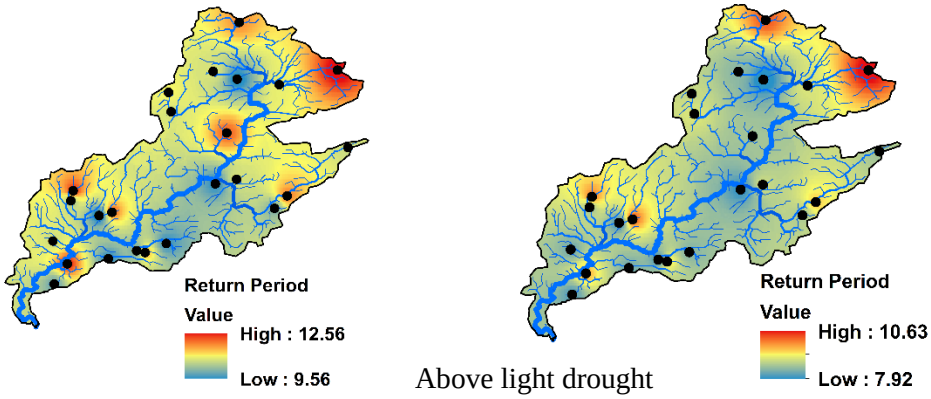

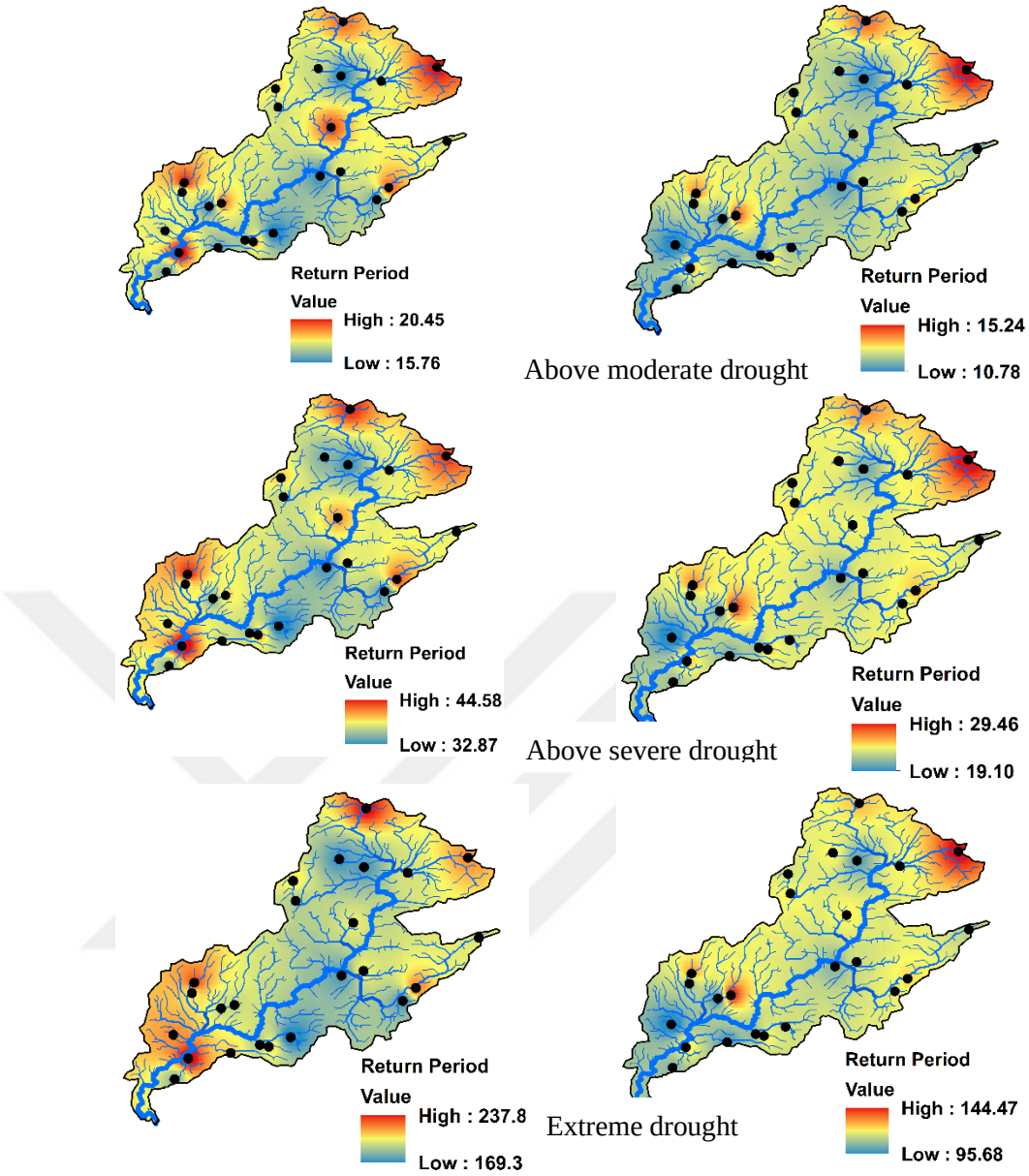

Figure 7.11 The spatial distribution of T_{DS} (left) and T'_{DS} (right) return period (month) based on SPI 3 when the drought duration and severity exceed their long-term average

Last scenario for SPI 6-time scale, under all drought risk conditions, the northeastern and slightly western regions generally indicate same conditions with higher return period of T_{DS} and T'_{DS}, while the northwestern regions exhibit lower return period of T_{DS} and T'_{DS} (high risk), except higher both return periods under all drought categories. Focusing on the outcomes of T'_{DS} on the light drought categories, D20M006 and 17868 stations show high risk due to lower return period.

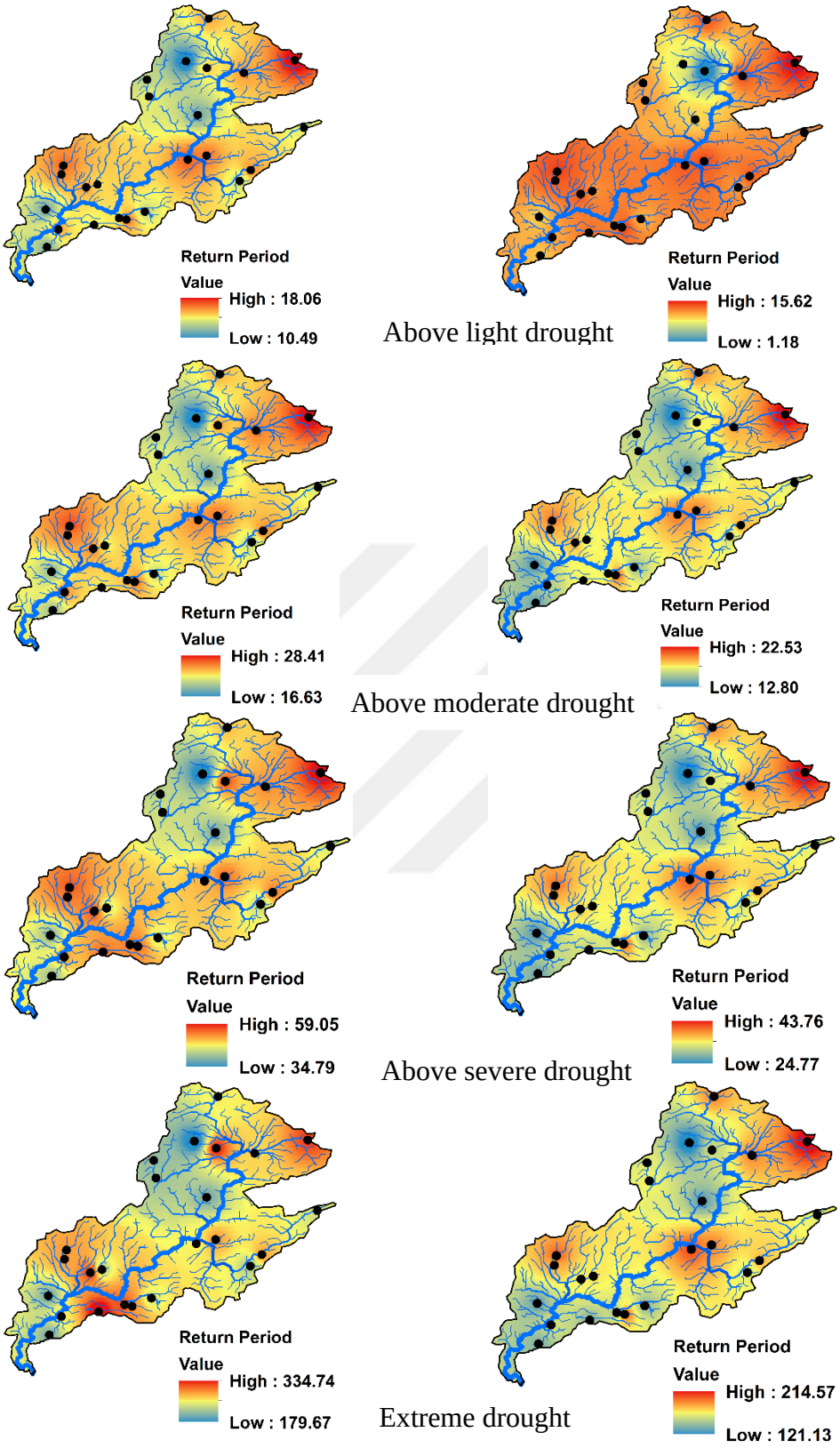

Figure 7.12 The spatial distribution of T_{DS} (left) and T'_{DS} (right) return period (month) based on SPI 6 when the drought duration and severity exceed their long-term average

CHAPTER EIGHT

CONCLUSION

8.1 Conclusion

In this study, first part, ten commonly utilized indices, namely; the SPEI, scPDSI, SPI, MCZI, CZI, RDI , RAI, PNI**,** DI and ZI, have been employed to monitor drought events in the Ceyhan River Basin, Turkey. While the RDI, SPEI and scPDSI require both precipitation and evapotranspiration, the other seven indices need only precipitation data to estimate the drought characteristics. The applicability of these indices and their performances corresponding to historical droughts were examined by employing data from eight meteorological stations.

As a result of the analyses, a significant increasing trend in annual maximum, annual minimum and annual average temperature time series have been detected in all seven stations at significance levels of above 95%. A decreasing trend was revealed in five stations and increasing trend in three stations, which indicates droughts, will inevitably take place in the Ceyhan Basin.

For 1-month time scale, apart from the scPDSI, the other indices have shown strong correlations with coefficients varying between 0.81-0.97 for all stations, while only the correlations between the SPI, SPEI and RDI were observed to be high at different time scales of 3-, 6-, 9- and 12-month. The SPI, SPEI and RDI have demonstrated a strong correlation in perceiving drought severity categories for 1-month time scale, whereas, for longer time scales of 3-, 6-, 9- and 12-month the correlation of the SPEI with the other two indices was noted to be low.

An empirical equation has been constructed between drought severity and duration in various climate types for multiple time steps. It is revealed that SPEI index revealed higher R^2 with increase time step and maximum drought event as compared to other indices for three climatic types, whereas, the maximum drought events identified in stations of Sub-humid, Humid and Dry-Sub-humid for 12-month SPI time step. These empirical equations will enable to predict drought severity for various time

scales directly based on drought duration and will also help to plan drought mitigation and preparedness strategies for the basin. Our results have a good agreement in previous studies.

Due to growing demand for water in agriculture, the need to provide acceptable discharge of water, sufficient and safe water supply, and increasing deterioration of its quality during periods of low water levels, the water resource management is becoming more complex. Therefore, one index cannot identify drought characteristics of a specific climatic region as being absolutely reliable. According to the results obtained in the study, SPI and RDI indices could be recommended for the Ceyhan Basin.

Second part, trends in the extreme drought events such as the annual maximum drought severity (AMDS) and the annual maximum drought duration (AMDD) time series, obtained from the SPI drought index of twenty-three stations in the Ceyhan River Basin, Turkey were investigated by employing Mann-Kendall (MK) and Spearman Rho tests. The AMDS and AMDD series are important extreme hydrological drought events in disaster preparedness and the regional management of water supplies. The homogeneity of the drought events was examined by utilizing Wallis-Moore and Wald-Wolfowitz methods, while the magnitude of trends was evaluated by employing the Sen's slope estimator and linear regression analysis methods, and the change point that signifies the start point of the trend was determined by applying the Standard Normal Homogeneity Test (SNHT), Buishand's Range Test (BRT) and Pettitt's test. The number of stations with the non-homogeneous data was perceived to increase as the SPI time scales increase, especially in the AMDS time series. Most of the stations seem to have homogeneous time series; however the data in a few stations was noted to be homogeneous by one of the methods and non-homogeneous by the other one with a significance level of 90%.

Results showed that generally increasing trends but insignificant at 95%, whereas, nine stations revealed statistically significant trend including stations 7767 (the increasing trend in AMDS series for 3-,6-,9-,12-month, decreasing trend in AMDD series for 6- and 9-month), 8275 (the increasing trend in AMDD series for 3-,6-,9-,12-month, decreasing trend in AMDS for 12-month), 17866 (increasing trend in AMDD series for 6-month), D20A009 (the increasing trend in AMDD series for 12-month),

D20A014 (the decreasing trend in AMDD series for 1-month), D20A016 (the increasing trend in AMDD series for 6- and 9-month, decreasing trend in AMDS series for 6-,9-and 12-month) and D20A018 (the increasing trend in AMDD series for 12-month). The trend results indicated that the AMDD series with higher time scales revealed an upward trend, while the AMDS series showed a downward trend, which was statistically important at the 90% confidence level. Possible change points started after the 1988s for D20A016 and D20A018, while stations 7767, 8275, 17866, D20A009 shifted after in the late 2000s, 1969s, 1981s and 1982s, respectively. Change point-detection tests captured different years at some stations. It should be possible due to climate type, topographic and hydrologic conditions, etc. However, it appears that further research is needed to determine whether climate variability began in that year or not. Also, the impact of precipitation, temperature, evapotranspiration, and groundwater level on agriculture, water and food security, energy production and security, economic growth, ecosystem sustainability, environmental health, and health security are all needed to be investigated.. The results of this paper is expected to provide valuable information to water resource management decision-makers in the Ceyhan River Basin for assessing drought variation and preparing for drought mitigation measures to avoid future drought risk.

Third part, since drought is a complex phenomenon, understanding drought variable is great of importance for water resource management. In this study, bivariate drought analysis was applied based on copula functions. Last studies mainly focused on that drought risk assessments are evaluated by using single variable. However, drought should be assessed employing multiple variables together due to affecting various parameters. Hence, bivariate copula functions are essential to construct a link between drought variables.

In this study, drought events were defined by standard precipitation index (SPI) series when the index below zero. After acquiring drought duration and severity, they are fitted separately by the different probabilistic distribution functions. 10 copula functions including Gaussian, Student t, Clayton, Gumbel, Frank, Joe, BB1, BB6, BB7 and BB8 copula are considered to determine the best fit copula for modeling the dependence between correlated drought duration and severity. Apart from employing several statistical tests (Akaike's Information Criterion (AIC), Bayesian Information Criterion (BIC) and Maximum likelihood methods), the performance of different

copula classes is evaluated in terms of upper tail dependence. After performing statistical and tail dependence tests for modeling best copula function for each station, based on the joint distribution function, the drought severity – duration – frequency (SDF) of various recurrence intervals for all stations are derived.

Spatial distribution joint return period of T_{DS} and T'_{DS} considering drought risk assessment based on percentile method (%25, %50, %75 and %95) are displayed at four different categories (light, moderate, severe and extreme drought). Based on categorizing drought return periods, their interpreting provides clearly information about drought analysis. According to results, lower return periods should be considered a high risk for drought occurrence that could negatively affect water quality, water suppliers and soil moistures. Hence, the southwestern region exhibits more drought risk when compared the other region under all categories at SPI 1-time scale. When considered SPI 3 and SPI 6-time scales, the high drought risk generally is expected to experience at middle part of basin. The higher drought risk is shown at the northwestern region for T_{DS} except extreme drought categories and any significant drought risk was detected under moderate, severe and extreme categories for T'_{DS} return period. However, the outcomes of T'_{DS} on the light drought categories, D20M018 and 17868 stations show high risk due to lower return period. The finding of this thesis may be helpful for planning of future water resource management and mitigation drought impact in Ceyhan Basin.

REFERENCES

Adarsh, S., Karthik, S., Shyma, M., Prem, G.D., Shirin Parveen, A.T., Sruthi, N., (2018). Developing Short Term Drought Severity-Duration-Frequency Curves for Kerala Meteorological Subdivision, India Using Bivariate Copulas. *KSCE J Civ Eng* **22**, 962–973.

AghaKouchak, A., Bárdossy, A., Habib, E., (2010). Conditional simulation of remotely sensed rainfall data using a non-Gaussian v-transformed copula. *Advances in Water Resources* **33**, 624–634.

Ahmadi, F., Radmaneh, F., Sharifi, M.R., Mirabbasi, R., (2018). Bivariate frequency analysis of low flow using copula functions (case study: Dez River Basin, Iran). *Environ Earth Sci* **77**, 643.

Ahmadi, S.H., Fooladmand, H.R., (2008). Spatially distributed monthly reference evapotranspiration derived from the calibration of Thornthwaite equation: a case study, South of Iran. *Irrig Sci* **26**, 303–312.

Akaike, H., (1976). "An information criterion (AIC)." *Math Sci* **14 (153)**, 5–7.

Alexandersson, H., (1986). A homogeneity test applied to precipitation data. *Journal of Climatology* **6**, 661–675.

Alhaji, U., Yusuf, A.S., Edet, C.O., Oche, C.O., Agbo, E.P., (2018). Trend Analysis of Temperature in Gombe State Using Mann Kendall Trend Test. *Journal of Scientific Research and Reports*, **20(1)**, 1-9.

Amirataee, B., Montaseri, M., Rezaie, H., (2018). Regional analysis and derivation of copula-based drought Severity-Area-Frequency curve in Lake Urmia basin, Iran. *Journal of Environmental Management 206*, 134–144.

Asfaw, A., Simane, B., Hassen, A., Bantider, A., 2018. Variability and time series trend analysis of rainfall and temperature in northcentral Ethiopia: A case study in Woleka sub-basin. *Weather and Climate Extremes* **19**, 29–41.

Ay, M., (2020). Trend and homogeneity analysis in temperature and rainfall series in western Black Sea region, Turkey. *Theor Appl Climatol* **139**, 837–848.

Azam, M., Maeng, S.J., Kim, H.S., Murtazaev, A., (2018). Copula-Based Stochastic Simulation for Regional Drought Risk Assessment in South Korea. *Water* **10**, 359.

Bárdossy, A., (2006). Copula-based geostatistical models for groundwater quality parameters. *Water Resources Research* **42 (11)**.

Barger, G.L., Thom, H.C.S., (1949). A Method for Characterizing Drought Intensity in Iowa1. *Agronomy Journal* **41**, 13–19.

Barnston, A.G., Lyon, B., (2016). Does the NMME Capture a Recent Decadal Shift toward Increasing Drought Occurrence in the Southwestern United States? *J. Climate* **29**, 561–581.

Barua, S., Ng, A.W.M., Perera, B.J.C., (2011). Comparative Evaluation of Drought Indexes: Case Study on the Yarra River Catchment in Australia. *Journal of Water Resources Planning and Management* **137**, 215–226.

Bayissa, Y., Maskey, S., Tadesse, T., Van Andel, S.J., Moges, S., Van Griensven, A., Solomatine, D., (2018). Comparison of the Performance of Six Drought Indices in Characterizing Historical Drought for the Upper Blue Nile Basin, Ethiopia. *Geosciences* **8**, 81.

Benesty, J., Chen, J., Huang, Y., Cohen, I., (2009). Pearson Correlation Coefficient, in: Cohen, I., Huang, Y., Chen, J., Benesty, J. (Eds.), Noise Reduction in Speech Processing, *Springer Topics in Signal Processing. Springer, Berlin, Heidelberg*, pp. **1–4**.

Benton, G.S., (1942). Drought in the United States Analyzed by Means of the Theory of Probability. *United States Department of agriculture* (No. 1488-2016-125010).

Beran, M.A., Rodier, J.A., (1985). Hydrological aspects of drought. *Etudes et Rapports d'Hydrologie (UNESCO)*.

Bonaccorso, B., Cancelliere, A., Rossi, G., (2003). An analytical formulation of return period of drought severity. *Stochastic Environmental Research and Risk Assessment* **17**, 157–174.

Bozkurt, D., Lutfi Sen, O., Utku Turuncoglu, U., Onol, B., Kindap, T., Nuzhet Dalfes, H., Karaca, M., (2010). Impacts of climate change on hydrometeorology of the Euphrates and Tigris Basins. *In EGU General Assembly Conference Abstracts* **12**, 14278.

Bozkurt, D., Sen, O.L., (2013). Climate change impacts in the Euphrates–Tigris Basin based on different model and scenario simulations. *Journal of Hydrology* **480**, 149–161.

Buishand, T.A., (1982). Some methods for testing the homogeneity of rainfall records. *Journal of Hydrology* **58**, 11–27.

Burn, D.H., Cunderlik, J.M., Pietroniro, A., (2004). Hydrological trends and variability in the Liard River basin / Tendances hydrologiques et variabilité dans le basin de la rivière Liard. *Hydrological Sciences Journal* **49**, 53–67.

Burnham, K.P., Anderson, D.R., (2002). Model Selection and Multimodel Inference: A Practical Information-Theoretic Approach, 2nd ed. *Springer-Verlag, New York.*

Calow, R., Robins, N., Macdonald, A., Nicol, A., (1999). Planning for groundwater drought in Africa. *Interdisciplinary international conference on integrated drought management* 20-22 September 1999.

Cancelliere, A., Salas, J.D., (2004). Drought length properties for periodic-stochastic hydrologic data. *Water Resources Research* **40 (2)**.

Chacon-Hurtado, J.C., Alfonso, L., Solomatine, D.P., (2017). Rainfall and streamflow sensor network design: a review of applications, classification, and a proposed framework. *Hydrology and Earth System Sciences* **21**, 3071–3091.

Chang, K.-H., (2015). Chapter 3 – Solid Modeling. *Computer-Aided Engineering Design* 125-167.

Chen, L., Singh, V.P., Shenglian, G., Hao, Z., Li, T., (2012). Flood Coincidence Risk Analysis Using Multivariate Copula Functions. *Journal of Hydrologic Engineering* **17**, 742–755.

Cheng, Y., Du, J., Ji, H., (2020). Multivariate Joint Probability Function of Earthquake Ground Motion Prediction Equations Based on Vine Copula Approach [WWW Document]. *Mathematical Problems in Engineering*.

Chow, V.T., (1919-, 1964). Handbook of applied hydrology.

Clayton, D.G., (1978). A Model for Association in Bivariate Life Tables and Its Application in Epidemiological Studies of Familial Tendency in Chronic Disease Incidence. *Biometrika* **65**, 141–151.

Dabanlı, İ., (2017). Climate Change Impact on Precıpıtatıon-Temperature in Turkey and Drought Analysis: Akarcay Case Study (PhD Thesis). I*stanbul Technical University*.

Dai, A., (2013). Increasing drought under global warming in observations and models. *Nature Clim Change* **3**, 52–58.

Danandeh Mehr, A., Vaheddoost, B., (2020). Identification of the trends associated with the SPI and SPEI indices across Ankara, Turkey. *Theor Appl Climatol* **139**, 1531–1542.

Demarta, S., McNeil, A.J., (2005). The t Copula and Related Copulas. *International Statistical Review* **73**, 111–129.

Demircan, M., Demir, Ö., Atay, H., Eskioğlu, O., Tüvan, A., Akçakaya, A., (2014). Climate Change Projections for Turkey with New Scenarios. Presented at the The Climate Change and Climate Dynamics Conference-2014 – *CCCD2014*, İstanbul, Türkiye.

Dodangeh, E., Shahedi, K., Shiau, J.-T., MirAkbari, M., (2017). Spatial hydrological drought characteristics in Karkheh River basin, southwest Iran using copulas. *J Earth Syst Sci* **126**, 80.

Dogan, S., Berktay, A., Singh, V.P., (2012). Comparison of multi-monthly rainfall-based drought severity indices, with application to semi-arid Konya closed basin, Turkey. *Journal of Hydrology* **470**–471, 255–268.

Dong, Q., Zhang, X., Lall, U., Sang, Y.-F., Xie, P., (2019). An improved nonstationary model for flood frequency analysis and its implication for the Three Gorges Dam, China. *Hydrological Sciences Journal* **64**, 845–855.

Dracup, J.A., Lee, K.S., Paulson, E.G., (1980). On the definition of droughts. *Water Resources Research* **16**, 297–302.

Dubrovsky, M., Svoboda, M.D., Trnka, M., Hayes, M.J., Wilhite, D.A., Zalud, Z., Hlavinka, P., (2009). Application of relative drought indices in assessing climate-change impacts on drought conditions in Czechia. *Theor Appl Climatol* **96**, 155–171.

Durocher, M., Burn, D.H., Mostofi Zadeh, S., (2018). A nationwide regional flood frequency analysis at ungauged sites using ROI/GLS with copulas and super regions. *Journal of Hydrology* **567**, 191–202.

Easterling, D.R., Kunkel, K.E., Arnold, J.R., Knutson, T., LeGrande, A.N., Leung, L.R., Vose, R.S., Waliser, D.E., Wehner, M.F., (2017). Precipitation change in the United States, in: Wuebbles, D.J., Fahey, D.W., Hibbard, K.A., Dokken, D.J., Stewart, B.C., Maycock, T.K. (Eds.), *Climate Science Special Report: Fourth National Climate Assessment, Volume I. U.S. Global Change Research Program, Washington, DC, USA*, pp. 207–230.

EL-Sagheer, R.M., (2018). Estimation of parameters of Weibull–Gamma distribution based on progressively censored data. *Stat Papers* **59**, 725–757.

Encyclopedia of Climate and Weather, (2011) . *Oxford University Press*.

Evans, J.P., (2009). 21st century climate change in the Middle East. *Climatic Change* **92**, 417–432.

Fauchereau, N., Trzaska, S., Rouault, M., Richard, Y., (2003). Rainfall Variability and Changes in Southern Africa during the 20th Century in the Global Warming Context. *Natural Hazards* **29**, 139–154.

Feng, G., Cobb, S., Abdo, Z., Fisher, D.K., Ouyang, Y., Adeli, A., Jenkins, J.N., (2016). Trend Analysis and Forecast of Precipitation, Reference Evapotranspiration, and Rainfall Deficit in the Blackland Prairie of Eastern Mississippi. *J. Appl. Meteor. Climatol.* **55**, 1425–1439.

Fischer, T., Gemmer, M., Lüliu, L., Buda, S., (2011). Temperature and precipitation trends and dryness/wetness pattern in the Zhujiang River Basin, South China, 1961–2007. *Quaternary International, Larger Asian rivers: climate, hydrology and ecosystems* **244**, 138–148.

Fırat, E., Yılmaz, K.K., Aydın, H., Kemeç, S., Sürer, S., Aras, M., Murat Özaltın, A., Bora, E., Deniz İtibar, M., Soyugür, B., (2018). Evaluation and Comparison of Drought Indices and Determination of Drought Events in Van Lake Basin, Turkey 20, 13773.

Frich, P., Alexander, L.V., Della-Marta, P., Gleason, B., Haylock, M., Tank, A.M.G.K., Peterson, T., (2002). Observed coherent changes in climatic extremes during the second half of the twentieth century. *Climate Research* **19**, 193–212.

Fu, G., Barber, M.E., Chen, S., (2010). Hydro-climatic variability and trends in Washington State for the last 50 years. *Hydrological Processes* **24**, 866–878.

Gao, X., Pal, J.S., Giorgi, F., (2006). Projected changes in mean and extreme precipitation over the Mediterranean region from a high resolution double nested RCM simulation. *Geophysical Research Letters* **33**.

Gao, X., Shi, Y., Zhang, D., Giorgi, F., (2012). Climate change in China in the 21st century as simulated by a high resolution regional climate model. *Chin. Sci. Bull.* **57**, 1188–1195.

Ge, Y., Cai, X., Zhu, T., Ringler, C., (2016). Drought frequency change: An assessment in northern India plains. *Agricultural Water Management* **176**, 111–121.

Genest, C., Favre, A.-C., (2007). Everything You Always Wanted to Know about Copula Modeling but Were Afraid to Ask. *Journal of Hydrologic Engineering* **12**, 347–368.

Gibbs, W.J., Maher, J.V., Meteorology, A.B. of, (1967). Rainfall deciles as drought indicators. Melbourne : *Bureau of Meteorology*.

Giorgi, F., (2006). Climate change hot-spots. *Geophysical Research Letters* **33**.

Gocic, M., Trajkovic, S., (2013). Analysis of precipitation and drought data in Serbia over the period 1980–2010. *Journal of Hydrology* **494**, 32–42.

Goda, K., Tesfamariam, S., (2015). Multi-variate seismic demand modelling using copulas: Application to non-ductile reinforced concrete frame in Victoria, Canada. *Structural Safety* **56**, 39–51.

Great Britain Meteorological Office, (1951). The Meteorological Glossary by Office Meteorological - AbeBooks. URL https://www.abebooks.co.uk/book-search/title/the-meteorological glossary/author/office-meteorological/ (accessed 9.17.20).

Gumbel, E.J., (1960). Bivariate Exponential Distributions. *Journal of the American Statistical Association* **55**, 698–707.

Hansen, J., Ruedy, R., Sato, M., Lo, K., (2010). Global Surface Temperature Change. *Reviews of Geophysics* **48**.

Hayes, M., Svoboda, M., Wall, N., Widhalm, M., (2010). The Lincoln Declaration on Drought Indices: Universal Meteorological Drought Index Recommended. Bull. *Amer. Meteor. Soc.* **92**, 485–488.

Heathcote, R.L., (1988). Drought in Australia: Still a problem of perception? *GeoJournal* **16**, 387–397.

Heim, R.R., (2017). A Comparison of the Early Twenty-First Century Drought in the United States to the 1930s and 1950s Drought Episodes. Bull. *Amer. Meteor. Soc*. **98**, 2579–2592.

Helsel, D.R., Hirsch, R.M., (2002). Statistical methods in water resources (USGS Numbered Series No. 04-A3), Techniques of Water-Resources Investigations. U.S. *Geological Survey, Reston, VA.*

Hemming, D., Buontempo, C., Burke, E., Collins, M., Kaye, N., (2010). How uncertain are climate model projections of water availability indicators across the Middle East? Philosophical Transactions of the Royal Society A: *Mathematical, Physical and Engineering Sciences* **368**, 5117–5135.

Hesami Afshar, M., Sorman, A.U., Yilmaz, M.T., (2016). Conditional Copula-Based Spatial–Temporal Drought Characteristics Analysis—A Case Study over Turkey. *Water* **8**, 426.

Hui-Mean, F., Yusof, F., Yusop, Z., Suhaila, J., (2019). Trivariate copula in drought analysis: a case study in peninsular Malaysia. *Theor Appl Climatol* **138**, 657–671.

Hulme, M., Doherty, R., Ngara, T., New, M., Lister, D., (2001). African climate change: 1900-2100. *Climate Research* **17**, 145–168.

IPCC, (2018). Global Warming of 1.5 ºC. URL https://www.ipcc.ch/sr15/ (accessed 2.23.20).

IPCC, (2013). AR5 Climate Change 2013: The Physical Science Basis — IPCC. URL https://www.ipcc.ch/report/ar5/wg1/ (accessed 9.17.20).

IPCC, (2007). AR4 Climate Change 2007: The Physical Science Basis — IPCC. URL https://www.ipcc.ch/report/ar4/wg1/ (accessed 9.17.20).

Ismail, T., Alamgir, M.M., Noor, M., (2018). Bivariate frequency analysis of flood variables using copula in Kelantan river basin. *Malaysian Journal of Civil Engineering* **30**, 395–404.

J, K., Ngesa, O., Orwa, G., (2019). On Generalized Gamma Distribution and Its Application to Survival Data. International *Journal of Statistics and Probability* **8**, 85–102.

Jain, V.K., Pandey, R.P., Jain, M.K., Byun, H.-R., (2015). Comparison of drought indices for appraisal of drought characteristics in the Ken River Basin. *Weather and Climate Extremes* **8**, 1–11.

Jaiswal, R.K., Lohani, A.K., Tiwari, H.L., (2015). Statistical Analysis for Change Detection and Trend Assessment in Climatological Parameters. Environ. *Process*. **2**, 729–749.

Jamshidi, H., Khalili, D., Zadeh, M.R., Hosseinipour, E.Z., (2012). Assessment and Comparison of SPI and RDI Meteorological Drought Indices in Selected Synoptic Stations of Iran 1161–1173.

Jiang, R., Xie, J., He, H., Luo, J., Zhu, J., (2015). Use of four drought indices for evaluating drought characteristics under climate change in Shaanxi, China: 1951–2012. *Nat Hazards* **75**, 2885–2903.

Joe, H., (1997). Multivariate Models and Multivariate Dependence Concepts. CRC Press.

Kadioğlu, M., (1997). Trends in surface air temperature data over Turkey. *International Journal of Climatology* **17**, 511–520.

Kadıoğlu, M., (2012). Türkiye'de İklim Değişikliği Risk Yönetimi. Türkiye'nin İklim Değişikliği II. Ulusal Bildiriminin Hazırlanması. Projesi Yayını.

Kao, S.-C., Govindaraju, R.S., (2010). A copula-based joint deficit index for droughts. *Journal of Hydrology* **380**, 121–134.

Kao, S.-C., Govindaraju, R.S., (2007). A bivariate frequency analysis of extreme rainfall with implications for design. *Journal of Geophysical Research: Atmospheres* 112.

Karabulut, M., Gürbüz, M., Korkmaz, H., (2008). Precipitation and Temperature Trend Analyses in Samsun. *Journal International Environmental Application & Science*, **3(5)**, 399-408.

Kendall, M.G., (1975). Rank correlation methods. Griffin, London.

Kendall, M.G., Stuart, A., (1973). The Advanced Theory of Statistics. Griffin.

Keskin, M.E., Taylan, D., Aslanbaş, T., (2015). An Investigation of Water Potential of Lake Eğirdir, Turkey. Procedia Earth and Planetary Science, *World Multidisciplinary Earth Sciences Symposium*,**15**, 244–248.

Kifer, R.S., Stewart, H.L., (1938). Farming Hazards in the Drought Area. U.S. Government Printing Office.

Kim, T.-W., Valdés, J.B., Yoo, C., (2003). Nonparametric Approach for Estimating Return Periods of Droughts in Arid Regions. *Journal of Hydrologic Engineering* **8**, 237–246.

Kissell, R., Poserina, J., (2017). Optimal Sports Math, Statistics, and Fantasy. Academic Press.

Kitoh, A., Yatagai, A., Alpert, P., (2008). First super-high-resolution model projection that the ancient "Fertile Crescent" will disappear in this century. *Hydrological Research Letters* **2**, 1–4.

Klaus, M., (2013). Multivariate Dependence Modeling using Copulas.

Klemes, V., (1987). Drought prediction: A hydrological perspective. *Planning for Drought*: Toward a Reduction of Societal Vulnerability 81–94.

Kulik, M.S., (1962). Agroclimatic indices of drought. Compendium of abridged reports to the Second Session of CagM (WMO). *Hydrometeorological Publishing*. 75–81.

Kundzewicz, Z.W., Robson, A., (2000). WCDMP, 45. Detecting trend and other changes in hydrological data, *WMO/TD. WMO, Geneva*.

Kwak, J., Kim, D., Kim, S., Singh, V.P., Kim, H., (2014). Hydrological Drought Analysis in Namhan River Basin, Korea. *Journal of Hydrologic Engineering* **19**, 05014001.

Kwon, H.-H., Lall, U., (2016). A copula-based nonstationary frequency analysis for the 2012–2015 drought in California. *Water Resources Research* **52**, 5662–5675.

Kwon, H.-H., Lall, U., Kim, S.-J., (2016). The unusual 2013–2015 drought in South Korea in the context of a multicentury precipitation record: Inferences from a nonstationary, multivariate, Bayesian copula model. *Geophysical Research Letters* **43**, 8534–8544.

Kwon, M., Kwon, H.-H., Han, D., (2019). Spatio-temporal drought patterns of multiple drought indices based on precipitation and soil moisture: A case study in South Korea. *International Journal of Climatology* **39**, 4669–4687.

Lai, C.-D., Murthy, D.N., Xie, M., (2006). Weibull Distributions and Their Applications, in: Pham, H. (Ed.), *Springer Handbook of Engineering Statistics, Springer Handbooks. Springer, London*, pp. 63–78.

Laio, F., (2004). Cramer–von Mises and Anderson-Darling goodness of fit tests for extreme value distributions with unknown parameters. *Water Resources Research* 40.

Lawrence, D., S., (2007). Analytical derivation of at-a-station hydraulic–geometry relations. *Journal of Hydrology* **334**, 17–27.

Lee, T., Modarres, R., Ouarda, T.B.M.J., (2013). Data-based analysis of bivariate copula tail dependence for drought duration and severity. *Hydrological Processes* **27**, 1454–1463.

Lehmann, E.L., D'Abrera, H.J., (1975). Nonparametrics: Statistical methods based on ranks, Nonparametrics: Statistical methods based on ranks. *Holden-Day, Oxford, England*.

Li, Q., Chen, Y., Shen, Y., Li, X., Xu, J., (2011). Spatial and temporal trends of climate change in Xinjiang, China. *J. Geogr. Sci*. **21(6)**, 1007-1018.

Linsley Jr, R.K., Kohler, M.A., Paulhus, J.L.H., (1975). Hydrology for Engineers.

Liu, B., Xu, M., Henderson, M., Qi, Y., Li, Y., (2004). Taking China's Temperature: Daily Range, Warming Trends, and Regional Variations, 1955–2000. *J. Climate* **17**, 4453–4462.

Liu, X.-F., Wang, S.-X., Zhou, Y., Wang, F.-T., Yang, G., Liu, W.-L., (2016). Spatial analysis of meteorological drought return periods in China using Copulas. *Nat Hazards* **80**, 367–388.

Loukas, A., Vasiliades, L., Dalezios, N.R., (2003). Intercomparison of meteorological drought indices for drought assessment and monitoring in Greece. Presented at the *In Proceedings of the International Conference on Environmental Science and Technology*, pp. 484–491.

Lyon, A., (2014). Why are Normal Distributions Normal? *Br J Philos Sci* 65, 621–649.

Madsen, H., Lawrence, D., Lang, M., Martinkova, M., Kjeldsen, T.R., (2014). Review of trend analysis and climate change projections of extreme precipitation and floods in Europe. *Journal of Hydrology* **519**, 3634–3650.

Mahe, G., L'hote, Y., Olivry, J.C., Wotling, G., (2001). Trends and discontinuities in regional rainfall of West and Central Africa: 1951–1989. *Hydrological Sciences Journal* **46**, 211–226.

Mahmood, R., Jia, S., Zhu, W., (2019). Analysis of climate variability, trends, and prediction in the most active parts of the Lake Chad basin, Africa. *Scientific Reports* **9**, 1–18.

Manley, G., (1953). Reviews of modern meteorology—9: Climatic variation. *Quarterly Journal of the Royal Meteorological Society* **79**, 185–209.

Mann, H.B., (1945). Nonparametric Tests Against Trend. *Econometrica* **13**, 245–259.

Marsaglia, G., Marsaglia, J., (2004). Evaluating the Anderson-Darling Distribution. *Journal of Statistical Software* **9**, 1–5.

Marsh, T., (1994). The 1988-92 Drought. *Institute of Hydrology*.

Mason, S.J., Waylen, P.R., Mimmack, G.M., Rajaratnam, B., Harrison, J.M., (1999). Changes in Extreme Rainfall Events in South Africa. *Climatic Change* **41**, 249–257.

Masud, M.B., Khaliq, M.N., Wheater, H.S., (2015). Analysis of meteorological droughts for the Saskatchewan River Basin using univariate and bivariate approaches. *Journal of Hydrology* **522**, 452–466.

McKee, T.B., Doesken, N.J., Kleist, J., (1993). The relationship of drought frequency and duration to time scales. *In Proceedings of the 8th Conference on Applied Climatology* (Vol. 17, No. **22**, pp. 179-183).

McMahon, T.A., Mein, R.G., (1986). River and Reservoir Yield. *Water Resources Publications* (Vol 368).

MGM, (2015). Türkiye İçin İklim Projeksiyonları.
URL:(https://www.mgm.gov.tr/iklim/iklim-degisikligi.aspx?s=projeksiyonlar)

Middleton, N., Thomas, D., (1997). World atlas of desertification.. ed. 2. Arnold, Hodder Headline, PLC.

Mirabbasi, R., Fakheri-Fard, A., Dinpashoh, Y., (2012). Bivariate drought frequency analysis using the copula method. *Theor Appl Climatol* **108**, 191–206.

Mishra, A.K., Singh, V.P., (2010). A review of drought concepts. *Journal of Hydrology* **391**, 202–216.

Misra, V., (2003). The Influence of Pacific SST Variability on the Precipitation over Southern Africa. *J. Climate* **16**, 2408–2418.

Mo, K.C., Chelliah, M., (2006). The Modified Palmer Drought Severity Index Based on the NCEP North American Regional Reanalysis. *J. Appl. Meteor. Climatol.* **45**, 1362–1375.

Modarres, R., Sarhadi, A., (2009). Rainfall trends analysis of Iran in the last half of the twentieth century. *Journal of Geophysical Research: Atmospheres* 114.

Morid, S., Smakhtin, V., Moghaddasi, M., (2006). Comparison of seven meteorological indices for drought monitoring in Iran. *International Journal of Climatology* **26**, 971–985.

Mpelasoka, F., Hennessy, K., Jones, R., Bates, B., (2008). Comparison of suitable drought indices for climate change impacts assessment over Australia towards resource management. *International Journal of Climatology* **28**, 1283–1292.

Nabaei, S., Sharafati, A., Yaseen, Z.M., Shahid, S., (2019). Copula based assessment of meteorological drought characteristics: Regional investigation of Iran. *Agricultural and Forest Meteorology* **276**, 107611.

National Drought Mitigation Centre, 2020. Types of Drought.

Nelsen, R.B., (2006). An Introduction to Copulas, 2nd ed, *Springer Series in Statistics*. Springer-Verlag, New York.

New, M., Hewitson, B., Stephenson, D.B., Tsiga, A., Kruger, A., Manhique, A., Gomez, B., Coelho, C.A.S., Masisi, D.N., Kululanga, E., Mbambalala, E., Adesina, F., Saleh, H., Kanyanga, J., Adosi, J., Bulane, L., Fortunata, L., Mdoka, M.L., Lajoie, R., (2006). Evidence of trends in daily climate extremes over southern and west Africa. *Journal of Geophysical Research: Atmospheres* 111.

Nicolai-Shaw, N., Zscheischler, J., Hirschi, M., Gudmundsson, L., Seneviratne, S.I., (2017). A drought event composite analysis using satellite remote-sensing based soil moisture. *Remote Sensing of Environment, Earth Observation of Essential Climate Variables* **203**, 216–225.

NOAA, (2020). Did You Know? | Monitoring References | National Centers for Environmental Information (NCEI) . URL https://www.ncdc.noaa.gov/monitoring-references/dyk/drought-definition (accessed 11.25.20).

Ntale, H.K., Gan, T.Y., (2003). Drought indices and their application to East Africa. *International Journal of Climatology* **23**, 1335–1357.

Okpara, J.N., Tarhule, A., (2015). Evaluation of Drought Indices in the Niger Basin, West Africa. *J. Geogr. Earth Sci*, **3**, 1-32.

Palmer, W.C., (1968). Keeping Track of Crop Moisture Conditions, Nationwide: *The New Crop Moisture Index*. *Weatherwise* **21**, 156–161.

Palmer, W.C., (1965). Meteorological Drought. U.S. Department of Commerce, Weather Bureau.

Pandey, S., Kumar, M., Mahanti, N.C., (2014). Assessment of Drought Severity in Various Regions of Jharkhand State of India. *International Journal of Environmental Science*, **3**, 8-14.

Partal, T., Kahya, E., (2006). Trend analysis in Turkish precipitation data. *Hydrological Processes* **20**, 2011–2026.

Pathak, A.A., Dodamani, B.M., (2020). Comparison of Meteorological Drought Indices for Different Climatic Regions of an Indian River Basin. *Asia-Pacific J Atmos Sci* **56**, 563–576.

Pettitt, A.N., (1979). A Non-Parametric Approach to the Change-Point Problem. *Journal of the Royal Statistical Society: Series C (Applied Statistics)* **28**, 126–135.

Poulin, A., Huard, D., Favre, A.-C., Pugin, S., (2007). Importance of Tail Dependence in Bivariate Frequency Analysis. *Journal of Hydrologic Engineering* **12**, 394–403.

Rahmat, S.N., Jayasuriya, N., Bhuiyan, M., (2015). Assessing droughts using meteorological drought indices in Victoria, Australia. *Hydrology Research* **46**, 463–476.

Rahmat, S.N., Jayasuriya, N., Bhuiyan, M., (2012). Trend analysis of drought using Standardised Precipitation Index (SPI) in Victoria, Australia. *Hydrology and Water Resources Symposium* 2012 441.

Ramdas, L.A., (1961). Crops and weather in India. *Crops and weather in India.*

Reddy, M.J., Ganguli, P., (2012). Application of copulas for derivation of drought severity–duration–frequency curves. *Hydrological Processes* **26**, 1672–1685.

Reddy, M.J., Singh, V.P., (2014). Multivariate modeling of droughts using copulas and meta-heuristic methods. *Stochastic environmental research and risk assessment.* **28(3)**, 475-489

Salas, J.D., Fu, C., Cancelliere, A., Dustin, D., Bode, D., Pineda, A., Vincent, E., (2005). Characterizing the Severity and Risk of Drought in the Poudre River, Colorado. *Journal of Water Resources Planning and Management* **131**, 383–393.

Salehi, S., Dehghani, M., Mortazavi, S.M., Singh, V.P., (2020). Trend analysis and change point detection of seasonal and annual precipitation in Iran. International *Journal of Climatology* **40**, 308–323.

Salvadori, G., Michele, C.D., Kottegoda, N.T., Rosso, R., (2007). Extremes in Nature: An Approach Using Copulas, *Water Science and Technology Library. Springer Netherlands* (Vol. 56).

Schreck, C.J., Semazzi, F.H.M., (2004). Variability of the recent climate of eastern Africa. *International Journal of Climatology* **24**, 681–701.

Schwarz, C., (2011). Sampling, Regression, Experimental Design and Analysis for Environmental Scientists, Biologists, and Resource Managers. URL /paper/Sampling%2C-Regression%2C-Experimental-Design-and-for-Schwarz/332f836f3ad98bee6e77b734a8b81a2b331a8fc0 (accessed 9.22.20).

Seber, G.A.F., Lee, A.J., (2012). Linear Regression Analysis (Vol.329). John Wiley & Sons.

Sen, P.K., (1968). Estimates of the Regression Coefficient Based on Kendall's Tau. *Journal of the American Statistical Association* **63**, 1379–1389.

Şen, Z., Uyumaz, A., Öztopal, A., Cebeci, M., Küçükmehmetoğlu, M., Erdik, T., Sirdaş, S., Şahin, A.D., Geymen, A., Ceylan, V., Oğuz, S., Karsavran, Y., (2010). Final report on the impacts of climate change on Istanbul and Turkey water resources. *Istanbul:ISKI*.

Serinaldi, F., Bonaccorso, B., Cancelliere, A., Grimaldi, S., (2009). Probabilistic characterization of drought properties through copulas. Physics and Chemistry of the Earth, Parts A/B/C, *Recent developments of statistical tools for hydrological application* **34**, 596–605.

She, D., Xia, J., (2018a). Copulas-Based Drought Characteristics Analysis and Risk Assessment across the Loess Plateau of China. *Water Resour Manage* **32**, 547–564.

She, D., Xia, J., (2018b). Copulas-Based Drought Characteristics Analysis and Risk Assessment across the Loess Plateau of China. *Water Resour Manage* **32**, 547–564.

Sheffield, J., Wood, E.F., Roderick, M.L., (2012). Little change in global drought over the past 60 years. *Nature* **491**, 435–438.

Shiau, J.T., (2006). Fitting Drought Duration and Severity with Two-Dimensional Copulas. *Water Resour Manage* **20**, 795–815.

Shiau, J.-T., Feng, S., Nadarajah, S., (2007). Assessment of hydrological droughts for the Yellow River, China, using copulas. *Hydrological Processes* **21**, 2157–2163.

Shiau, J.T., Modarres, R., (2009). Copula-based drought severity-duration-frequency analysis in Iran. *Meteorological Applications* **16**, 481–489.

Shiau, J.-T., Modarres, R., Nadarajah, S., (2012). Assessing Multi-site Drought Connections in Iran Using Empirical Copula. *Environmental modeling and assessment*. **17(5)**, 469-482

Shiau, J.-T., Shen, H.W., (2001). Recurrence Analysis of Hydrologic Droughts of Differing Severity. *Journal of Water Resources Planning and Management* **127**, 30–40.

Shigang, Y., De-bao, Y., Gui-xiang, Z., Ya-ping, F.U., Jie, W.U., (2011). Comparision of three drought indices in drought of Shanxi province. *Plateau Meteorology* **30**, 1406–1414.

Sibuya, M., (1960). Bivariate extreme statistics, *I. Ann Inst Stat Math* **11**, 195–210.

Sklar, M., (1959). Fonctions de Répartition À N Dimensions Et Leurs Marges. Université Paris 8.

Smadi, M.M., Zghoul, A., (2006). A Sudden Change In Rainfall Characteristics In Amman, Jordan During The Mid 1950s. *American Journal of Environmental Sciences* **2**, 84–91.

Smakhtin, V.U., Schipper, E.L.F., (2008). Droughts: The impact of semantics and perceptions. *Water Policy* **10**, 131–143.

Smirnov, N., (1948). Table for Estimating the Goodness of Fit of Empirical Distributions. *The Annals of Mathematical Statistics* **19**, 279–281.

Smirnov, N., (1939). Estimate of deviation between empirical distribution functions in two independent samples. *Bulletin Moscow University* **2** (2).

Sneyers, R., (1990). On the statistical analysis of series of observations, *Technical Note*. WMO, Geneva.

Soltani, S., Saboohi, R., Yaghmaei, L., (2012). Rainfall and rainy days trend in Iran. *Climatic Change* **110**, 187–213.

Sonali, P., Nagesh Kumar, D., (2013). Review of trend detection methods and their application to detect temperature changes in India. *Journal of Hydrology* **476**, 212–227.

Song, S., Singh, V.P., (2010a). Frequency analysis of droughts using the Plackett copula and parameter estimation by genetic algorithm. *Stoch Environ Res Risk Assess* **24**, 783–805.

Song, S., Singh, V.P., (2010b). Frequency analysis of droughts using the Plackett copula and parameter estimation by genetic algorithm. *Stoch Environ Res Risk Assess* **24**, 783–805.

Spearman, C., (1961). The Proof and Measurement of Association Between Two Things, Studies in individual differences: The search for intelligence. *Appleton-Century-Crofts*, East Norwalk, CT, US.

Stephens, M.A., (1974). EDF Statistics for Goodness of Fit and Some Comparisons. *Journal of the American statistical Association 69,* no. **347** : 730-737.

Stone, M., (1979). Comments on Model Selection Criteria of Akaike and Schwarz. *Journal of the Royal Statistical Society. Series B (Methodological)* **41**, 276–278.

Sunday, R.K.M., Masih, I., Werner, M., van der Zaag, P., (2014). Streamflow forecasting for operational water management in the Incomati River Basin, Southern Africa. *Physics and Chemistry of the Earth, Parts A/B/C, Transboundary Water Cooperation: Building Partnerships*. **72**–75, 1–12.

Tabari, H., Grismer, M.E., Trajkovic, S., (2013). Comparative analysis of 31 reference evapotranspiration methods under humid conditions. *Irrig Sci* **31**, 107–117.

Tannehill, I.R., (1947). Drought, Its Causes and Effects. *Soil Science* 64, 83.

Tanrıverdi, Ç., Alp, A., Demirkıran, A.R., Üçkardeş, F., (2010). Assessment of surface water quality of the Ceyhan River basin, Turkey. *Environ Monit Assess* **167**, 175–184.

Tate, E.L., Gustard, A., (2000). Drought Definition: A Hydrological Perspective, in: Vogt, J.V., Somma, F. (Eds.), Drought and Drought Mitigation in Europe, *Advances in Natural and Technological Hazards Research. Springer Netherlands, Dordrecht*, pp. 23–48.

Tekten, D., (2016). Suggestıons for Sectoral Based Clımate Change Adaptatıon Practices for Turkey (Master's Thesis). Istanbul Technical University.

Thom, H.C.S., 1958. A Note on the Gamma Distribution. *Mon. Wea. Rev.* **86**, 117–122.

Thornthwaite, C.W., (1948). An Approach toward a Rational Classification of Climate. *Geographical Review* **38**, 55–94.

Tirivarombo, S., Osupile, D., Eliasson, P., (2018). Drought monitoring and analysis: Standardised Precipitation Evapotranspiration Index (SPEI) and Standardised Precipitation Index (SPI). *Physics and Chemistry of the Earth*, Parts A/B/C **106**, 1–10.

Tosunoglu, F., Can, I., 2016. Application of copulas for regional bivariate frequency analysis of meteorological droughts in Turkey. *Nat Hazards* **82**, 1457–1477.

Tosunoglu, F., Kisi, O., (2016). Joint modelling of annual maximum drought severity and corresponding duration. *Journal of Hydrology* **543**, 406–422.

Trenberth, K.E., Dai, A., Schrier, G. van der, Jones, P.D., Barichivich, J., Briffa, K.R., Sheffield, J., (2014). Global warming and changes in drought. *Nature Clim Change* **4**, 17–22.

Tsakiris, G., Pangalou, D., (2009). Drought Characterisation in the Mediterranean, in: Iglesias, A., Cancelliere, A., Wilhite, D.A., Garrote, L., Cubillo, F. (Eds.), Coping with Drought Risk in Agriculture and Water Supply Systems: Drought Management and Policy Development in the Mediterranean, Advances in Natural and Technological Hazards Research. *Springer Netherlands, Dordrecht*, pp. 69–80.

Tsakiris, G., Pangalou, D., Vangelis, H., (2007). Regional Drought Assessment Based on the Reconnaissance Drought Index (RDI). *Water Resour Manage* **21**, 821–833.

Tsakiris, G., Vangelis, H., (2005). Establishing a Drought Index Incorporating Evapotranspiration. *European water*, **9(10)**, 3-11.

Tunalıoğlu, R., Durdu, Ö.F., (2012). Assessment of future olive crop yield by a comparative evaluation of drought indices: a case study in western Turkey. *Theor Appl Climatol* **108**, 397–410.

Turan, F., (2002). Türkiye'nin Su ve Toprak Kaynaklari Potansiyeli ve Gelişimi. *Su Kaynaklarının Geliştirilmesi ve Yönetimi*. pp 4-6.

Türkeş, M., Erlat, E., (2018). Variability and trends in record air temperature events of Turkey and their associations with atmospheric oscillations and anomalous circulation patterns. *International Journal of Climatology* **38**, 5182–5204.

Unganai, L.S., Mason, S.J., (2001). Spatial characterization of Zimbabwe summer rainfall during the period 1920-1996. *South African Journal of Science*, **97(9)**, 425-431

Uzunkol, M., Kızılelma, Y., (2016). Ceyhan Havzasi'nin Kuraklik Durumu ve Eğilimlerinin Belirlenmesi. *ASOS* **29**, 503–503.

Van Lanen, H.A.J., Peters, E., (2000). Definition, Effects and Assessment of Groundwater Droughts, in: Vogt, J.V., Somma, F. (Eds.), Drought and Drought

Mitigation in Europe, *Advances in Natural and Technological Hazards Research. Springer Netherlands*, Dordrecht, pp. 49–61.

Van Rooy, M.P., (1965). A Rainfall Anomally Index Independent of Time and Space, *Notos* **14**, 43–48.

Vazifehkhah, S., Tosunoglu, F., Kahya, E., (2019). Bivariate Risk Analysis of Droughts Using a Nonparametric Multivariate Standardized Drought Index and Copulas. *Journal of Hydrologic Engineering* **24**, 05019006.

Vezzoli, R., Pecora, S., Zenoni, E., Tonelli, F., (2012). Data Analysis to Detect Inhomogeneity, Change Points, Trends in Observations: An Application to Po River Discharge Extremes (SSRN Scholarly Paper No. ID 2195345). Social Science Research Network, Rochester, NY (138).

Vicente-Serrano, S.M., Beguería, S., López-Moreno, J.I., (2009). A Multiscalar Drought Index Sensitive to Global Warming: The Standardized Precipitation Evapotranspiration Index. *J. Climate* **23**, 1696–1718.

Vicente-Serrano, S.M., Beguería, S., Lorenzo-Lacruz, J., Camarero, J.J., López-Moreno, J.I., Azorin-Molina, C., Revuelto, J., Morán-Tejeda, E., Sanchez-Lorenzo, A., (2012). Performance of Drought Indices for Ecological, Agricultural, and *Hydrological Applications. Earth Interact*. **16**, 1–27.

Vose, R., Easterling, D., Kunkel, K., Wehner, M., (2017). Temperature changes in the United States. Publications, Agencies and Staff of the U.S. Department of Commerce.

Wald, A., Wolfowitz, J., (1943). An Exact Test for Randomness in the Non-Parametric Case Based on Serial Correlation. *The Annals of Mathematical Statistics* **14**, 378–388.

Walker, J.C.G., (1977). Evolution of the atmosphere. *Macmillan, New York*.

Wallis, W.A., Moore, G.H., (1941). A Significance Test for Time Series and Other Ordered Observations. *In A Significance Test for Time Series and Other Ordered Observations* (pp. 1-67). NBER

Wang, B., Zhang, M., Wei, J., Wang, S., Li, S., Ma, Q., Li, X., Pan, S., (2013). Changes in extreme events of temperature and precipitation over Xinjiang, northwest China, during 1960–2009. *Quaternary International*, **298**, 141-151..

Wang, C., (2016). A joint probability approach for coincidental flood frequency analysis at ungauged basin confluences. *Natural Hazards* **82(3)**, 1727-1741.

Wang, F., Wang, Z., Yang, H., Zhao, Y., Zhang, Z., Li, Z., Hussain, Z., (2019). Copula-Based Drought Analysis Using Standardized Precipitation Evapotranspiration Index: A Case Study in the Yellow River Basin, China. *Water* **11(6)**, 1298.

Wang, H., Pan, Y., Chen, Y., (2017). Comparison of three drought indices and their evolutionary characteristics in the arid region of northwestern China. *Atmospheric Science Letters* **18**, 132–139.

Wang, H., Zhang, M., Zhu, H., Dang, X., Yang, Z., Yin, L., (2012). Hydro-climatic trends in the last 50years in the lower reach of the Shiyang River Basin, NW China. *CATENA* **95**, 33–41.

Wang, W., Shao, Q., Peng, S., Zhang, Z., Xing, W., An, G., Yong, B., (2011). Spatial and temporal characteristics of changes in precipitation during 1957–2007 in the Haihe River basin, China. *Stoch Environ Res Risk Assess* **25**, 881–895.

Wang, W., Shao, Q., Yang, T., Peng, S., Yu, Z., Taylor, J., Xing, W., Zhao, C., Sun, F., (2013). Changes in daily temperature and precipitation extremes in the Yellow River Basin, China. *Stoch Environ Res Risk Assess* **27**, 401–421.

Wells, N., Goddard, S., Hayes, M.J., (2004). A Self-Calibrating Palmer Drought Severity Index. *J. Climate* **17**, 2335–2351.

Whipple, W., (1966). Regional Drought Frequency Analysis. *Journal of the Irrigation and Drainage Division* **92**, 11–32.

Wilhite, D.A., (2016). Droughts : A Global Assesment. *Routledge*.

Wilhite, D.A., (2009). Drought Monitoring as a Component of Drought Preparedness Planning, in: Iglesias, A., Cancelliere, A., Wilhite, D.A., Garrote, L., Cubillo, F. (Eds.), Coping with Drought Risk in Agriculture and Water Supply Systems: Drought

Management and Policy Development in the Mediterranean, *Advances in Natural and Technological Hazards Research. Springer Netherlands, Dordrecht*, pp. 3–19.

Wilhite, D.A., (2000). Drought: A Global Assessment. *Routledge*.

Wilhite, D.A., Glantz, M.H., (1985a). Understanding: the Drought Phenomenon: The Role of Definitions. *Water International* **10**, 111–120.

Wilhite, D.A., Glantz, M.H., (1985b). Understanding: the Drought Phenomenon: The Role of Definitions. *Water International* **10**, 111–120.

Wilhite, D.A., Svoboda, M.D., Hayes, M.J., (2007). Understanding the complex impacts of drought: A key to enhancing drought mitigation and preparedness. *Water Resour Manage* **21**, 763–774.

Wilson, E.B., Hilferty, M.M., (1931). The Distribution of Chi-Square. *Proc. Natl. Acad. Sci. U.S.A.* **17**, 684–688.

WMO, (2006). Drought Monitoring and Early Warning: Concepts, Progress, and Future Challenges. World Meteorological Organization. URL https://public.wmo.int/en/resources/library/drought-monitoring-and-early-warning-concepts-progress-and-future-challenges (accessed 2.23.20).

Wu, H., Hayes, M.J., Weiss, A., Hu, Q., (2001). An evaluation of the Standardized Precipitation Index, the China-Z Index and the statistical Z-Score. *International Journal of Climatology* **21**, 745–758.

Xu, Y.-P., Booij, M.J., Tong, Y.-B., (2010). Uncertainty analysis in statistical modeling of extreme hydrological events. *Stoch Environ Res Risk Assess* **24**, 567–578.

Xu, Z.X., Takeuchi, K., Ishidaira, H., (2003). Monotonic trend and step changes in Japanese precipitation. *Journal of Hydrology* **279**, 144–150.

Yavuz, H., Erdoğan, S., 2012. Spatial Analysis of Monthly and Annual Precipitation Trends in Turkey. *Water Resour Manage* **26**, 609–621.

Ye, J.-S., (2014). Trend and variability of China's summer precipitation during 1955–2008. *International Journal of Climatology* **34**, 559–566.

Yevjevich, V.M., (1966). Objective approach to definitions and investigations of continental hydrologic droughts, *An (Doctoral dissertation, Colorado State University. Libraries).*

Yoo, J., Kim, D., Kim, H., Kim, T.-W., (2016). Application of copula functions to construct confidence intervals of bivariate drought frequency curve. *Journal of Hydro-environment Research* **11**, 113–122.

You, Q., Kang, S., Aguilar, E., Yan, Y., (2008). Changes in daily climate extremes in the eastern and central Tibetan Plateau during 1961–2005. *Journal of Geophysical Research: Atmospheres* 113.

Yu, M., Li, Q., Hayes, M.J., Svoboda, M.D., Heim, R.R., (2014). Are droughts becoming more frequent or severe in China based on the Standardized Precipitation Evapotranspiration Index: 1951–2010? *International Journal of Climatology* **34**, 545–558.

Yu, Y.-S., Zou, S., Whittemore, D., (1993). Non-parametric trend analysis of water quality data of rivers in Kansas. *Journal of Hydrology* **150**, 61–80.

Yuce, M.I., Esit, M., Ercan, B., 2015. A Relationship between Flow Discharge, Sediment Discharge and Sub-Basin Areas in Ceyhan Catchment. Presented at the 13th International Congress on Advances in Civil Engineering, 12-14 September 2018, Izmir/TURKEY.

Yuce, M.I., Esit, M., Karatas, M.C., (2019). Hydraulic geometry analysis of Ceyhan River, Turkey. *SN Appl. Sci*. **1**, 763.

Yuce, M.I., Muratoglu, A., (2012). Determining the Downstream Channel Geometry Parameters of Tigris River. *Presented at the International Conference, Sediment transport modeling in hydrological watersheds and rivers*, pp. 14–16.

Yusof, F., Hui-Mean, F., Suhaila, J., Yusof, Z., (2013). Characterisation of Drought Properties with Bivariate Copula Analysis. *Water Resour Manage* **27**, 4183–4207.

Zar, J.H., (2005). Spearman Rank Correlation, in: Encyclopedia of Biostatistics. *American Cancer Society*.

Zhai, P., Zhang, X., Wan, H., Pan, X., (2005). Trends in Total Precipitation and Frequency of Daily Precipitation Extremes over China. *J. Climate* **18**, 1096–1108.

Zhang, L., Singh, V.P., (2006a). Bivariate Flood Frequency Analysis Using the Copula Method. *Journal of Hydrologic Engineering* **11**, 150–164.

Zhang, L., Singh, V.P., (2006b). Bivariate Flood Frequency Analysis Using the Copula Method. *Journal of Hydrologic Engineering* **11**, 150–164.

Zhang, Q., Liu, C., Xu, C., Xu, Y., Jiang, T., (2006). Observed trends of annual maximum water level and streamflow during past 130 years in the Yangtze River basin, China. *Journal of Hydrology* **324**, 255–265.

Zhang, Q., Peng, J., Xu, C.-Y., Singh, V.P., (2014). Spatiotemporal variations of precipitation regimes across Yangtze River Basin, China. *Theor Appl Climatol* **115**, 703–712.

CV

MUSA EŞİT

EDUCATION

PhD	Gaziantep University / Civil Engineering & Hydraulic Department (09/2015-)
Thesis	Copula Based Bivariate Drought Frequency Analysis in the Ceyhan Basin, Turkey
Postgraduate	Gaziantep University / Civil Engineering & Hydraulic Department (09/2012 - 06/2015)
Thesis	Determining hydraulic geometry of Seyhan River
University	Gaziantep University /Civil Engineering 09/2007 - 06/2012
High School	Batman Fatih High School (09/2002 - 06/2005)

WORK EXPERIENCE

Auburn University/USA	
Visiting Scientist	09/2019-09/2020
Adiyaman University / Turkey	12/2013- Working
Research Assistance	
Gazikent Building Audit	07/2012 - 012/2013
Controller	

Projects

- Kopula Fonksiyonları Kullanılarak Orta Fırat, Kızılırmak ve Yeşilırmak Havzalarının Kuraklık Risk Haritalarının Çıkarılması (Doç. Dr. Mehmet İshak YÜCE TUJJB-TÜMEHAP-2020-02) /01-11-2020- Ongoing

-Analysis of low flow and drought in hydrological watersheds (Prof. Dr. Hafzullah AKSOY TUJJB-TUMEHAP-2015-1) / 01-11-2015-Completed

- Analysis of seasonal to decadal soil moisture predictability in Community Earth System Model-Decadal Prediction Experiments (Completed)

Articles

1-Yuce, M. I., & **Esit, M.** (2021). Drought monitoring in Ceyhan Basin, Turkey. *Journal of Applied Water Engineering and Research*, 1-22. https://doi.org/10.1080/23249676.2021.1932616

2-Esit, M., & Kumar, S. (2020, December). Effects of the land-atmosphere coupling on drought predictability. In *AGU Fall Meeting 2020*. AGU.

3-YUCE, Mehmet İshak, and **ESIT, Musa** (2020). "Ceyhan Havzasının Kuraklık Risk Haritasının SPI ve SPEI Metotları İle Belirlenmesi." *Su Kaynakları* 5.2: 24-33.

4-Esit, M., Kumar, S., Pandey, A. et al. Seasonal to multi-year soil moisture drought forecasting. npj Clim Atmos Sci 4, 16 (2021). https://doi.org/10.1038/s41612-021-00172-z

5-Yuce, M.I., **Esit, M.** and Karatas, M.C. (2019) Hydraulic geometry analysis of Ceyhan River, Turkey, SN Applied Sciences, Vol.1, Issue 7, https://doi.org/10.1007/s42452-019-0800-1

6-Eris, E., Aksoy, H., Onoz, B., Cetin, M., Yuce, M. I., Selek, B., Aksu, H., Burgan, H. I., **Esit, M**., Yildirim, I. and Karakus, E. U. (2019) Frequency analysis of low flows in intermittent and non-intermittent rivers from hydrological basins in Turkey, *Water Science and Technology: Water Supply*, Vol. 19, Issue 1, pp. 30-39, https://doi.org/10.2166/ws.2018.051

7-Yuce, M. I., **Esit, M**. and Muratoglu, A. (2015) Determining the Hydraulic Geometry Parameters of Seyhan River, *American Journal of Engineering, Technology and Society*, Vol. 2 No. 4, pp. 77-84

8-Cetin, M., Aksoy, H., Onoz, B., Eris, E., Yuce, M. I., Selek, B., Aksu, H., Burgan, H. I. and **Esit, M.,** Cavus, Y. and Orta, S. (2018) Deriving Accumulated Precipitation Deficits from Drought Severity-Duration-Frequency Curves: A Case Study in Adana Province, Turkey, *1st International, 14th National Congress on Agricultural Structures and Irrigation*, 26-28 September, Antalya, Turkey

9-Aksoy, H., Eris, E., Onoz, B., Cetin, M., Yuce, M. I., Selek, B., Aksu, H., Burgan, H. I., **Esit, M.,** (2018) SPI-based Drought Severity-Duration-Frequency Analysis**,** *13th International Congress on Advances in Civil Engineering*, 12-14 September, Izmir, Turkey

10-Aksoy, H., Eris, E., Onoz, B., Cetin, M., Yuce, M. I., Selek, B., Burgan, H. I., Ucan, M. **Esit, M.**, Kayan, G., Caylak, E. and Aksu, H., (2017) Frequency Analysis of Low Flows, *IWA 2nd Regional Symposium on Water, Wastewater and Environment,* 22-24 March, Çesme-Izmir, Turkey.

11-Yuce, M. I., Muratoglu, A., Yuce, S. and **Esit, M.** (2016) Gaziantep İlinin Gelecekteki İhtiyacını Karşılamak üzere Göksu Havzasından Su Temini, *International Symposium of Water and Wastewater Management (ISWWM), October 26-28, Malatya, Turkey*

12-Muratoglu, A., Yuce, M. I. and **Esit, M.** (2016) Foil Generation Inspiring from Nature, *International Conference on Natural Science and Engineering* (ICNASE'16), March 19-20, Kilis, Turkey, pp. 3611 – 3623

13-Yuce, M. I., **Esit, M.** and Muratoglu, A. (2016) A relationship between basin area and average discharge A case study for Turkey, *ISTEC, International Science and Technology Conference*, 13 - 15 July Vienna, Austria, pp. 48 – 57

14-Yuce, M. I., **Esit, M.** and Muratoglu, A. (2015) Assessment Hydraulic Geometry of Seyhan River for Downstream Modelling, 3rd International Symposium on Innovative Technologies in Engineering and Science, June 3-5, Valencia – Spain pp. 1318 – 1325

15-Yuce, S., Ercan, B., **Esit, M.,** Unsal, M. and Yuce, M. I. (2018) Seyhan Havzasi Yağiş Verilerinin Eğilim Analizi*, İklim Değişikliği ve Çevre* Vol. 3, No.2, pp. 47–54

16-Aksoy, H., Eris, E., Onoz, B., Cetin, M., Yuce, M. I., Selek, B., Aksu, H., Burgan, H. I., **Esit, M.,** Yildirim, I. and Karakus, E. U. (2018) Düşük Akımların Frekans Analizi ve Çevresel Akış ile İlişkisi, *DÜMF Mühendislik Dergisi Cilt 9 No. 1, pp. 503-514*

17-Aksoy, H., Cetin, M., Onoz, B., Yuce, M. I., Eris, E., Selek, B., Aksu, H., Burgan, H. I., Cavus, Y., **Esit, M.** and Orta, S. (2019) Frekans Analizi İle Kritik Kuraklik Şiddet-Süre-Frekans Eğrilerinin Elde Edilmesi, *10. Ulusal Hidroloji Kongresi* 09-12 Ekim, Mugla, pp 641-649

18-Yuce, M. I., Aksoy, H., Onoz, B., Cetin, M., Eris, E., **Esit, M.,** Burgan, H. I., Oguz, A. and Kalaci, V. (2019) İklim Değişikliğinin Yağişlar Üzerine Etkisi: Kahramanmaraş ve Osmaniye Örneği, *10. Ulusal Hidroloji Kongresi* 09-12 Ekim, Mugla, pp 375-388

19-Aksoy, H., Onoz, B., Cetin, M., Yuce, M. I., Eris, E., Selek, B., Aksu, H., Burgan, H. I. and **Esit, M.** (2018). Edirne için Kuraklık Siddet-Süre-Frekans Egrileri. *Ulusal Hidrojeoloji ve Su Kaynakları Sempozyumu (HIDRO'xx2018)*, 27-29 Eylul pp 42-47, Ankara, Turkiye

20-Aksoy, H., Eris, E., Onoz, B., Cetin, M., Yuce, M. I., Selek, B., Aksu, H., Burgan, H. I., **Esit, M.,** (2018) Gediz Havzasinda Kuraklik Analizi, *Turkiye Ulusal Jeodezi ve Jeofizik Birligi Bilimsel Kongresi* 30 Mayıs - 2 Haziran, İzmir, Turkiye, pp. 28 – 31

21-Aksoy, H., Eris, E., Onoz, B., Cetin, M., Yuce, M. I., Selek, B., Aksu, H., Burgan, H. I., Yildirim, I., **Esit, M.** and Unsal, E. K. (2017) Kuruyan Akarsularda Düşük Akımların Frekans Analizi, *IX. Ulusal Hidroloji Kongresi* 04-06 Ekim, Diyarbakır, Turkiye